IAEA-TECDOC-1060

LMFR core and heat exchanger thermohydraulic design: Former USSR and present Russian approaches

INTERNATIONAL ATOMIC ENERGY AGENCY

January 1999

LMFR CORE AND HEAT EXCHANGER THERMOHYDRAULIC DESIGN:
FORMER USSR AND PRESENT RUSSIAN APPROACHES
IAEA, VIENNA, 1998
IAEA-TECDOC-1060
ISSN 1011–4289

FOREWORD

All fast reactor fuel assemblies and heat exchangers have rod bundle geometry. Fluid flow and heat transfer in a rod bundle and complex phenomena and basic understanding of these phenomena is essential for developing designs that optimize performance during normal operating conditions and that maintain structural integrity during abnormal operation.

Extensive experimental and analytical studies on liquid metal fluid flow distribution and heat transfer in fuel pin and heat exchanger rod-bundles have been performed in several countries with fast reactor programmes (notably in France, Germany, India, Japan, the Russian Federation, the United Kingdom and the United States of America) over the past decades. The validity of the computer codes and design approaches was proven by comparison of code results with measured velocity, pressure and temperature distributions in rod-bundles cooled/heated by liquid metal, usually sodium.

Considerable experimental and theoretical studies on various aspects of LMFR thermohydraulics have been done at the Institute of Physics and Power Engineering (IPPE), Obninsk, Russian Federation. The IAEA's International Working Group on Fast Reactors (IWGFR) recommended that IPPE should generalize its thermohydraulic studies as well as other countries' results that have been published in journals and in proceedings of international meetings.

This report was prepared in response to the recommendation from IWGFR and includes the methodology and philosophy of the analytical and experimental investigations in their application to the core and heat exchanger thermohydraulic design of LMFRs.

The IAEA officer responsible for this work was A.A. Rinejski of the Division of Nuclear Power.

EDITORIAL NOTE

CONTENTS

INTRODUCTION

The information given in this report is concerned with liquid metal fast breeder reactors, some of which are in operation (France, Japan, Russian Federation), others under construction. Comprehensive thermal hydraulic research applied to such reactors has been carried out in the SSC IPPE.

It should be noted that liquid metal reactors can now be considered as the most safe and promising type of reactor in nuclear power engineering. However, in order for fast reactors to be widely used in industry it is necessary to improve their economic indicators, as well as to make their performance more reliable. This requires analysis of the problems of the reactor performance under deviations of the subassembly geometry from nominal (deformation), as well as under the transient conditions to be resolved, as well as various accident situations.

The problems noted above can be resolved by both experiments and predictions. The information accumulated must be processed, firstly for steady state operating conditions with the ensuing extension to the transient behavior.

The authors believe that the material given below will be useful for the further advanced thermal hydraulic analysis of fast reactors in the situations closely approximating the in-pile conditions.

The codes developed up to now are rated in order of governing equations, calculation procedures, system of closing relations and their accuracy. However, all modern codes use the momentum and energy transport factors, heat transfer coefficients, pressure drop and others to close relation between velocity and temperature fields. These factors should be evaluated with the use of relationships presented here, so they have been derived on processing the data gained in the special experiments.

Detailed analysis and rating of the thermal hydraulic codes which have been developed in the IPPE, as applied to reactor subassembly and heat exchanger, are given in this publication. Also, results of experimental investigations and numerical modelling of velocity and temperature distribution are illustrated. Experience of fast reactor performance (Russian Federation, France, Kazakhstan) suggests that subassemblies are subject to great deformation in campaigns associated with swelling and creeping. The authors have obtained considerable experimental data on temperature behaviour in deformed bundles, that have allowed this data to be generalized and used in the complex code TEMP-MIF. Considerable attention has been given to the problems of the equalization of temperature behaviour in the fast reactor subassembly, for which purpose an influence of various parameter is analysed.

On the whole, the authors demonstrate advanced approaches, new experimental techniques and numerical procedures, hydraulic and thermal constants required for the thermal physical validation of liquid metal reactor core and heat exchanger.

1

Chapter 1

THERMAL HYDRAULIC ANALYSIS OF FAST REACTOR CORE AND HEAT EXCHANGERS. EXPERIMENTS AND PREDICTIONS

1.1. SOME FEATURES OF FAST REACTOR THERMAL HYDRAULICS

The need to improve fast reactor performance (in particular of reactor core and intermediate heat exchangers) is a vital problem, resolution of which depends largely on the quality thermal physic validation. Features of fast reactor performance (high neutron flux, great pressure of gas fission products inside of fuel pins, high levels of fuel and pin clad temperatures), uncertainties in some parameters have resulted in a special attention to be given to in-depth analysis of thermal physic processes and investigations of a new phenomena that are adequate for the modern knowledge. Inter-channel hydrodynamic and thermal exchange, variable power production, entrance thermal region, deformation of pin bundle, non-standard geometry, thermal loads far from symmetric and availability of spacer structures, regular and stochastic temperature non-uniformity and ensuing hot spots is far not a whole list of the problems posed recently by practice and being of a great importance in thermal physic validation of fast reactor core. Conceivable boiling of sodium within reactor core and inherent emergency problems have assumed a great significance.

The necessity of knowledge of the local hydrodynamic and thermal parameters in the combined axial-transverse flows in the IHXs with the object of their efficiency validation is not lesser currently central. To take into account the factors mentioned above makes its a very complex problem in the thermal hydraulic analysis. Among the requirements to thermal hydraulic analysis there are a large volume of information, a reliability of the results including, above all, the local hydrodynamic and thermal characteristics: on the one hand - high temperatures are not allowable (the power and efficiency of the facility are limited), on the other hand - local temperature should not be over acceptable limits, that can result in failure.

The necessary conditions for ensuing reactor safety are restrictions on maximum temperatures of pin wall and nuclear fuel. Respectively, the heavy demands are imposed on the thermal physic validation of fast reactors. To satisfy the limitations not only for the average parameters, but for those representing deviations from the nominal values, invites the study of their influence on the temperature behaviour in subassembly, their contributions in reactor core thermal physics and normal fast reactor subassembly performance.

Reliable operation of modern fast breeder reactors has called for the combined study of thermal hydraulics (experiments & predictions), development of a new analytical methods on the local characteristics in subassemblies and heat exchangers, that has allowed the data (constants) to be derived for nominal and accident operating conditions, the effects of various factors on temperature behaviour to be analysed.

The mechanisms for inter-channel exchange and the combined axial-transverse flow in reactor units, hydrodynamics and heat transfer features in the system of parallel channels, as well as in non-standard channels (near to the wrapper tube), temperature fields in regular and deformed bundles under uniform and variable power production (including heterogeneous variant), in steady-state and transient flow have formed the basis for calculation.

The points mentioned above concern a wide range of the problems and define in essence the further evolution of reactor thermal physics, in general. For example, analysis of pin bundle under deformation including the pin's displacements, local temperature rises, blockages, pin bending is of a great importance in reactor core design.

Such characteristics as the pin clad temperature and temperature non-uniformity around the pins arising under the local distortion of the pin arrangement (shifting and bending of one or two pins), elevated power production in the separate pins, rises in clad temperature behind the wire or behind the blockage are of different value. Sensible overheating, and the temperature non-uniformity, respectively, ($\sim$20% of $\Delta \bar{t}$ and more) can take place in the event of the fuel pins are displaced a one-half the inter-pin clearance and more, and in the event of the blockage of subassembly cross section.

The hot spots can be of local character and involve a small number of pins (2, 3, 7), and of global character covering the sizeable part of the pin bundle. Pin temperature can exceed the average level due to specific construction of subassembly; with the exceed flow rate in the edge channels leading to the coolant becomes subcooled in the edge channels and the wall temperature elevated in the internal area of subassembly. At the linear power production across the subassembly positioned at the periphery of reactor core ($q^{max}/\bar{q} = 12$), the additional elevation of the clad temperature by $\sim 10 \div 15$% of $\Delta \bar{t}$ is observed in the area of maximum power production.

In the compact pin bundle when pins are in contact with each other the clad temperature is much more than in statistic arrangement. The rise in coolant temperature behind the blockage in the internal area of subassembly can be of 50% of $\Delta \bar{t}$, and in the edge area $\sim$100%. Also a significant changes can be observed in the wrapper tube temperature. To reduce clad temperature irregularities and non-uniformities in coolant temperature, so called counter-directed wire wraps on the pins can be used. The random arrangement of fuel pin in subassembly sets the problem of the choice of justified geometrical model. As for statistic model, it estimates the subassembly geometry and improves ideas how the hot spot factors would be predicted. Temperature deviation due to hot spot factor can be defined by two ways. First (analytical) calculates the known temperature function depending on many random parameters (factors), provided their distributions are given. Second is the method of statistical iterations (Monte-Carlo approach). Analytical method is faster and more mobile than Monte-Carlo procedure, but it restricts the functional dependence of temperature on a various parameters. Monte-Carlo procedure would be appropriate for use, when temperature effect on governing parameters is multidimensional and non-linear and provided a random deviations are great and follow the arbitrary distribution laws. It allows the more approximate analytical method to be corrected. Also, it is advantageous to use the superposition of these methods, when temperature deviations caused by the local factors are defined with the use of Monte-Carlo procedure, and the general deviations are predicted by analytical method.

As a fast reactor core is a large and combined system of subassemblies representing bundle of fuel pins, which, in its turn, being of a complex structure, the thermal hydraulic analysis can be performed in some steps. In the first step - at the design stage - the coolant flow rates through subassemblies and average coolant temperatures are defined. Then, thermal hydraulic characteristics of individual subassembly and fuel pin are predicted. This step, in its turn, assumes determining the subassembly geometry, the coolant flow distribution

throughout the subassemblies taking into account inter-channel momentum exchange, the coolant temperature in the channels taking into account inter-channel thermal exchange, the wall-liquid temperature difference and maximal temperature irregularities around the pin, the contribution of various factors into temperature behaviour, and maximum clad temperatures. Inasmuch as coolant overheating in fast reactor subassembly are quite large (~200 °C), an accuracy in definition of the maximum pin clad temperature is appreciably specified by the correct calculation of coolant temperature distribution over the subassembly channels.

Velocity and temperature fields in subassembly representing a system of interconnected channels, between which the mass, momentum and heat exchanges take place, are formed unlikely those in insulated channels. Inter-channel mass exchange being more strong than in insulated channels, an influence of casual deformations (bending, displacements and others) on flow distribution, impact of helical wire wrap on mixing and degree of turbulence, non-uniform flow distribution though the channels of a different form (internal, edge ones) - all these factors define hydrodynamics in the interconnected channels. The use of the methods and relationships for insulated channels in hydrodynamic and thermal predictions causes the great errors to appear, that results in the special approaches having regard to the features of interconnected channels to be developed.

Interchannel heat and mass transfer is a very important factor in generation of temperature and flow behaviour in fast reactor core. Caused by helical wire wrap, it reduces temperature in hot spots and in so doing it can serve to enhance subassembly power. By using none of the modern approach of thermophysic prediction of reactor, you can not do away with the inclusion of this factor, an importance of which is reflected when the processes are considered, as inside of the pin bundle and in reactor core, as in whole (inter-subassembly interaction). Account of heat and mass transfer in the framework of so called subchannel approaches can be considered as a significant contribution into development of thermohydraulic prediction of fast reactor core.

According to the approach mentioned the pun bundle is divided into a parallel channels, for which the system of mass, momentum and energy conservation equations is solved with the resulting derivation of velocity and temperature distributions. Systems of governing equations written by other authors are distinguished by a degree of completeness. Respectively, the codes realising solution of balance equations are rated in a classes of the problem under consideration and in the validity of hydrodynamic description. Analysis performed have allowed the correct statement of subchannel approach to be developed and resulted in the development of the codes TEMP, TEMP-M and MIF.

Much attention in thermohydraulic analysis has to be given to the edge area of subassembly being a serious hazard in terms of temperature irregularity. The edge pins are surrounded by the channels of a different geometry, that is why conditions of their performance are far from symmetric. Due to different amounts of coolant passing through the channels surrounding the edge pins, coolant temperature varies significantly around the edge pins.

Liquid metals have a larger heat conductivity, smaller volumetric heat capacity. Great temperature differences and great heat transfer coefficients result in that the temperature of pin surface cooled by liquid metal is defined in general by the local temperature of coolant, but not local heat transfer coefficients. This is largely concerned with the edge pins, where the great differences in coolant temperature take place.

Tolerances for the sizes of fast reactor subassembly that involves pins of a small diameter arranged with a relative small pitch are comparable with the size of the channel surrounding pins, with a consequent sensible effect of bending and shifting of the pins appearing even in the wire wrapped bundles. Of prime importance is such a problems for the edge pins wrapped by the half as many wire as those at the internal pins. Due to this the edge pins have a chance of shifting along the subassembly cover.

Heat transfer in the edge channel is, as a rule, of a transient nature and depends on the equivalent thermal conductivity, relative pitch of the bundle, displacers' diameter, gap between pins and wrapper tube and others. Features of liquid metal heat transfer in the wrapped pin bundle are determined by the facts that, on the one hand, wire wrap is favourable for mixing, that improve heat transfer, on the other hand, wire or fin causes the local pin wall temperature to enhance.

Thus, features of hydrodynamics and heat transfer in fast reactor subassembly are connected, in general, with the near wall area and the use of sodium as a coolant. New problems caused by the features mentioned in comparison with an infinite pin bundle can be summarised as follows:
- greater temperature nonuniformities around the edge pins as compared with internal pins;
- greater flow non-uniformities around the edge pins;
- noticeable effect of inter-channel mixing on the temperature and velocity behaviour;
- influence of pin bundle deformation on the temperature and velocity behaviour;
- transient heat removal in the edge channels.

Thermal hydraulics of fast reactor intermediate heat exchangers has been investigated by as experimental and numerical modeling of velocity and temperature fields with the use of the modern measurement techniques and computer codes, such as: electromagnetic technique to measure local liquid metal velocity in transverse and axial directions, local measurements of thermal characteristics in tube bundle, advanced numerical procedures based on the quasi homogeneous and subchannel approaches. New data gained in the last few years for various geometry of tube bundle (triangular, square, combined) at low velocities and under conditions of mixed convection testifies that a possibility of reversal circulation occurs. Criteria were derived that describe the processes under consideration, time and space limits of transients were defined, recommendations for designing heat exchanger equipment were proposed.

Correlation made between the local data and the results of common integral experiments has allowed a revealing reasons and an order of the distinction of heat transfer coefficients, determining their variation over the heat exchanger zones and advising means for the heat transfer surface optimisation. Variation in the height of the inlet and outlet windows of heat exchanger is of significance in equalising coolant flows across the bundle section and possible decreasing heat transfer surface, that says the inlet and outlet structures are of a great importance.

Material discussed below is a result of long-term investigations into reactor core and intermediate heat exchanger thermal hydraulics and is a foundation for the modern approaches to thermal hydraulic analysis of fast breeder reactor.

Brief information on the subjects under discussion. Fig. 1.1 presents the view of the integral fast breeder reactor. Positions 3, 4 and 7 indicate reactor core breeder and heat exchanger, respectively, being the object of present thermal hydraulic analysis.

6
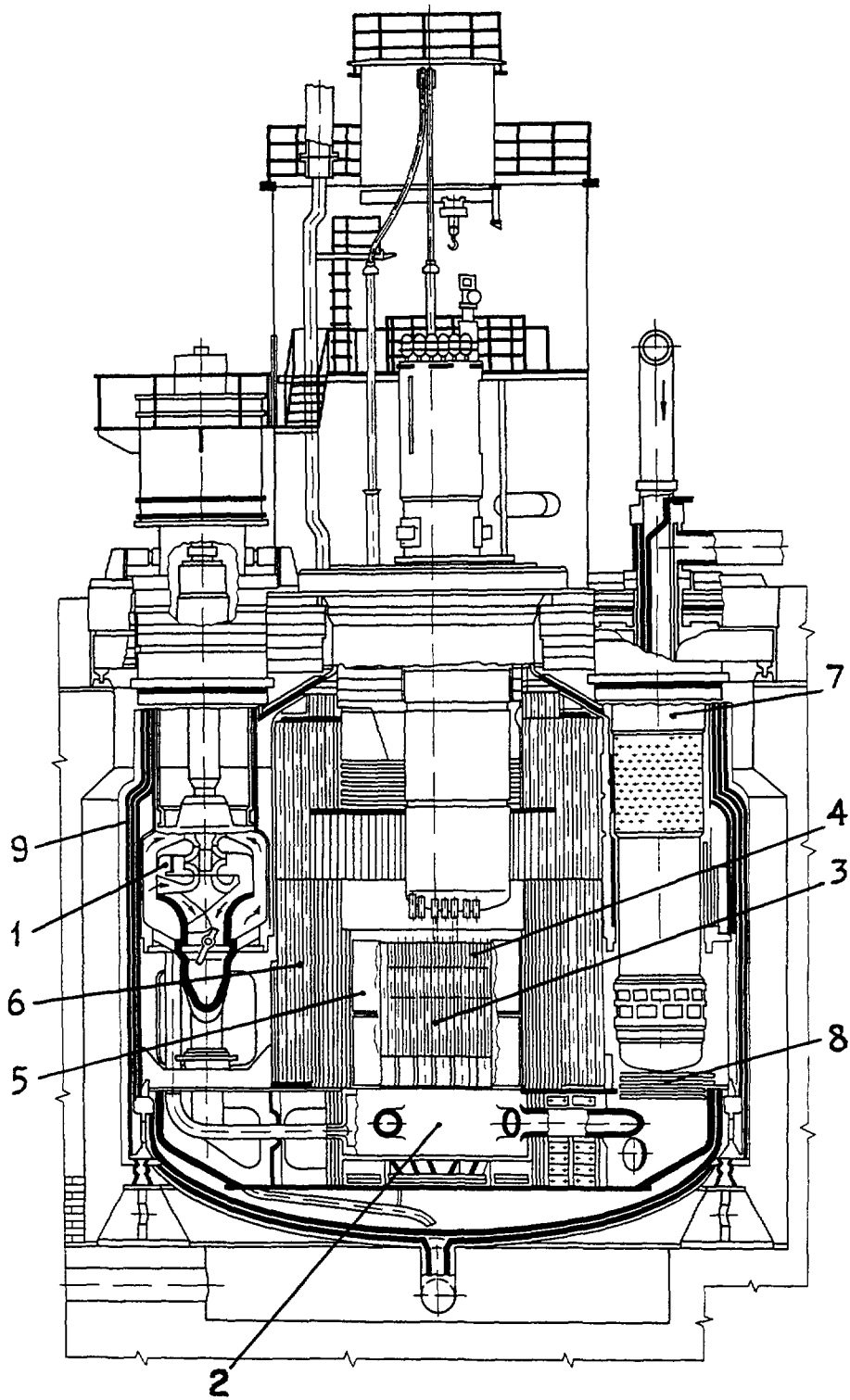
Fig 1 1   Integral fast reactor block
1 - pumps,   2- high pressure header,
3 - core,   4 - blanket zone,   5 - spent
assemblies storage,   6- in-vessel neu-
tron shield,   7- heat exchanger,
8 - dumps,   9- reactor vessel

Fig. 1.2. BN-600 core:

◯ ⎫
   ⎬ — fuel subassembly
⊛ ⎭

◎ ⎫
   ⎬ — blanket subassembly
⬡ ⎭

⊕ — spent fuel storage

◉ — regulation rod

○ — safety rod

⬣ — compensation rod
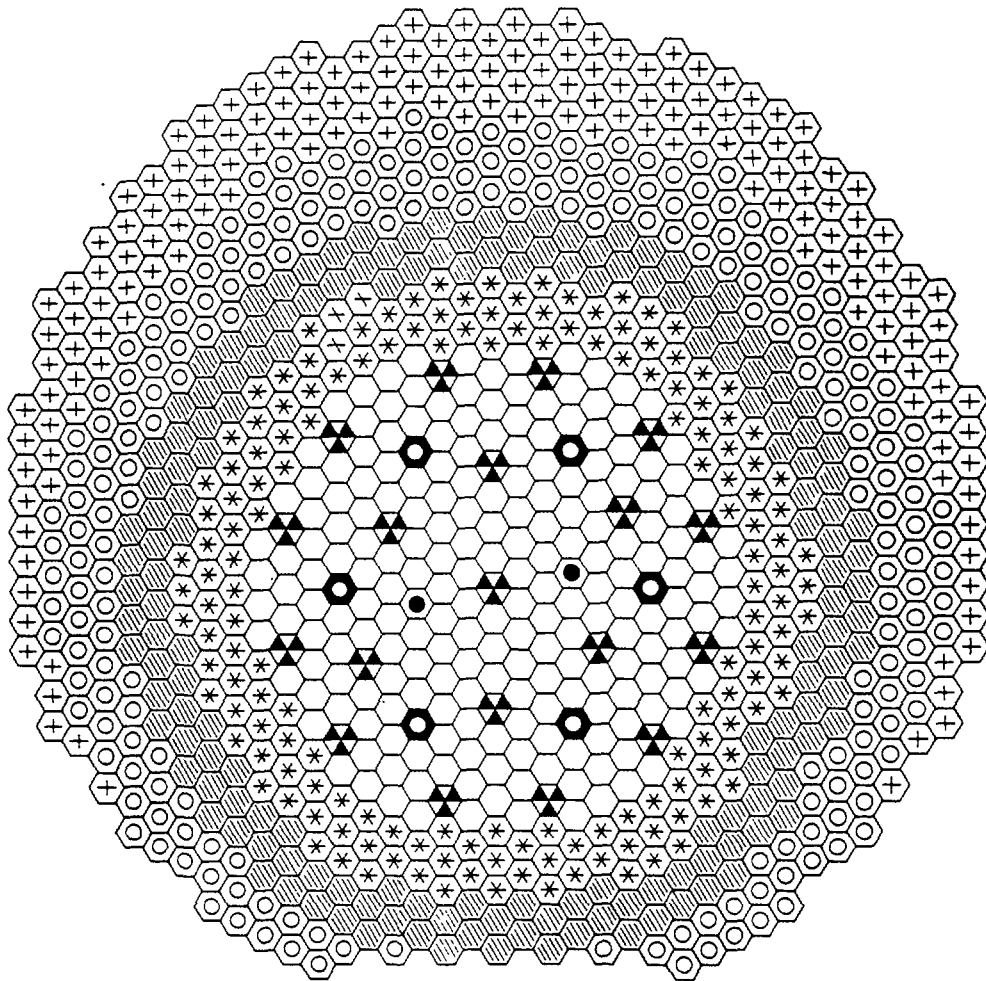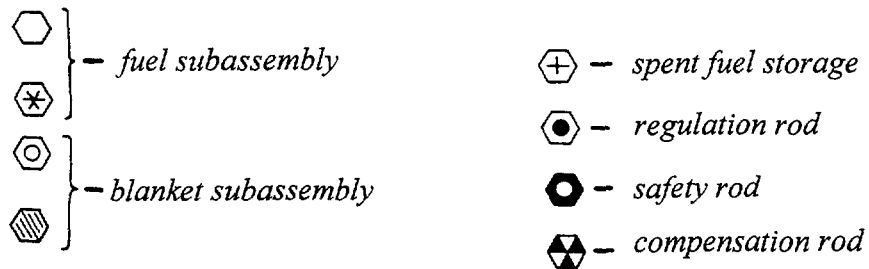
Views of reactor core and breeder , as well as radial distribution of power production are shown in Fig. 1.2 and 1.3, respectively. Subassembly geometry is presented in Fig. 1.4 and 1.5. Specific features of the structures under discussion are the smaller pin diameter ($d = 6.9$ mm), but the larger pitch of the pin arrangement ($s/d = 1.17$) in reactor core as compared with those in breeder ($d = 14.1$ mm, $s/d = 1.04$) with the considerably greater amounts of fuel pins in the core subassembly.

Fig. 1.6 and 1.7 show schematics of the axial view and cross sections of intermediate heat exchanger providing the foundations of experimental and analytical modeling of heat exchanger thermal hydraulics.

8
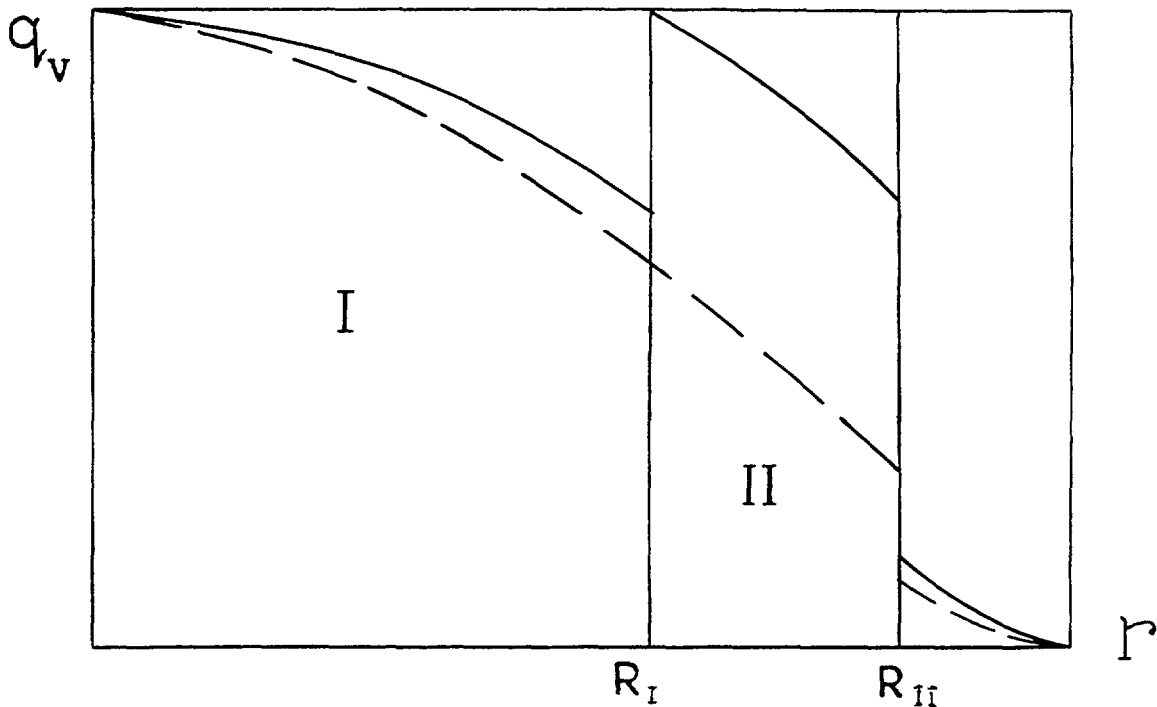
Fig. 1.3. Heat production with reactor core radius:
‒ ‒ ‒ ‒ *- without levelling,* ‒‒‒‒ *- two-zone levelling.*

1.2. CLASSIFICATION AND BRIEF OVERVIEW

Let us take a look at the thermal hydraulic approaches applied to fuel subassemblies. This will allow the problems of subchannel analysis and its potentialities to be inspected for the more general points of view, as well as its place among the thermal hydraulic approaches having regard to an interchannel exchange to be defined.

Thermal hydraulic analysis of reactor subassembly implies that mass, momentum and energy conservation equations are solved in association with initial and boundary conditions. Mathematical modeling concerning hydrodynamics and heat transfer in fast breeder reactor have been analyzed in [1-4].

Fuel pins in combination with the subassembly wrapper and displacers form the channel of complex shape with essentially variable thermal and hydraulic characteristics across of the channel, resulting in 3-D coolant flow. That is why, researcher fails to find thermal hydraulic characteristics with a required accuracy by the methods based on an idea of "equivalent channel" determining average parameters of subassembly.

Three lines in thermal hydraulic analysis of pin bundle (Fig.1.8) can be currently recognised, with each of them having its own advantages and disadvantages:
• prediction of local velocities and temperatures;
• prediction of average characteristics in the framework of a porous body model;
• prediction of lumped parameters (coolant velocity and temperature averaged across the subassembly), that is subchannel analysis.

9

A-A

40
400
750
400
794

3500

I
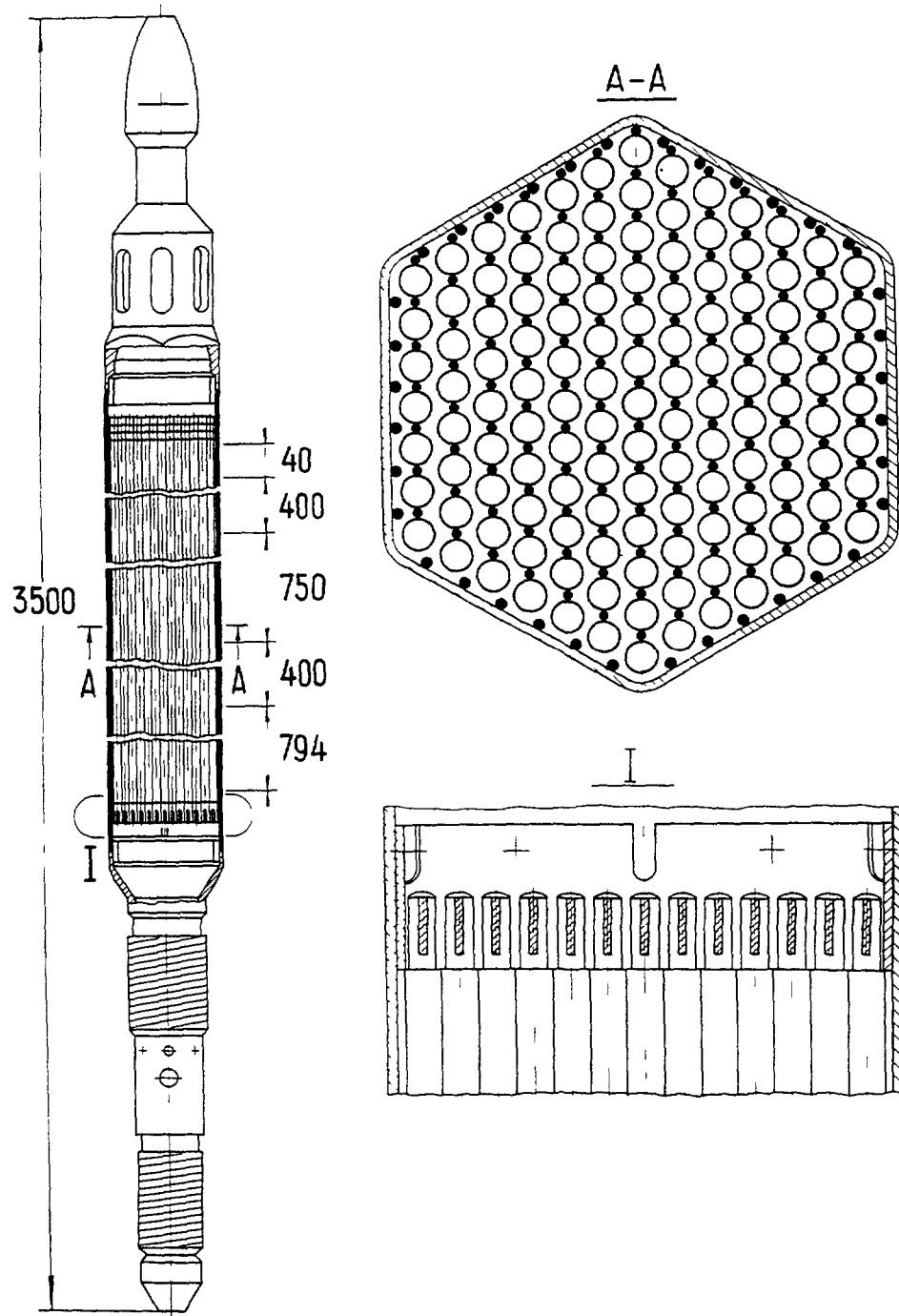
Fig 1.4. Fast reactor core fuel subassembly.
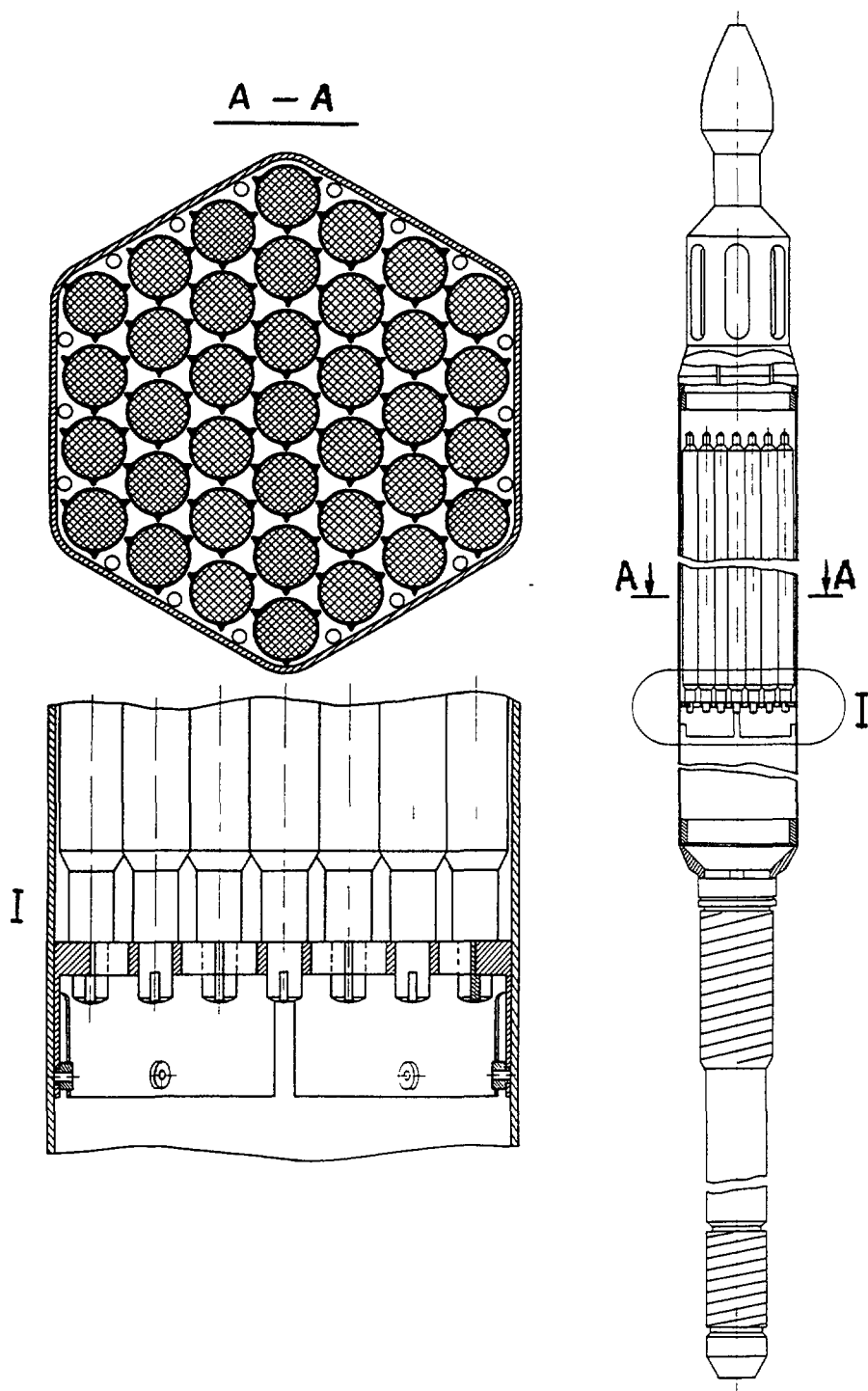
Fig. 1. 5. Blanket assembly.
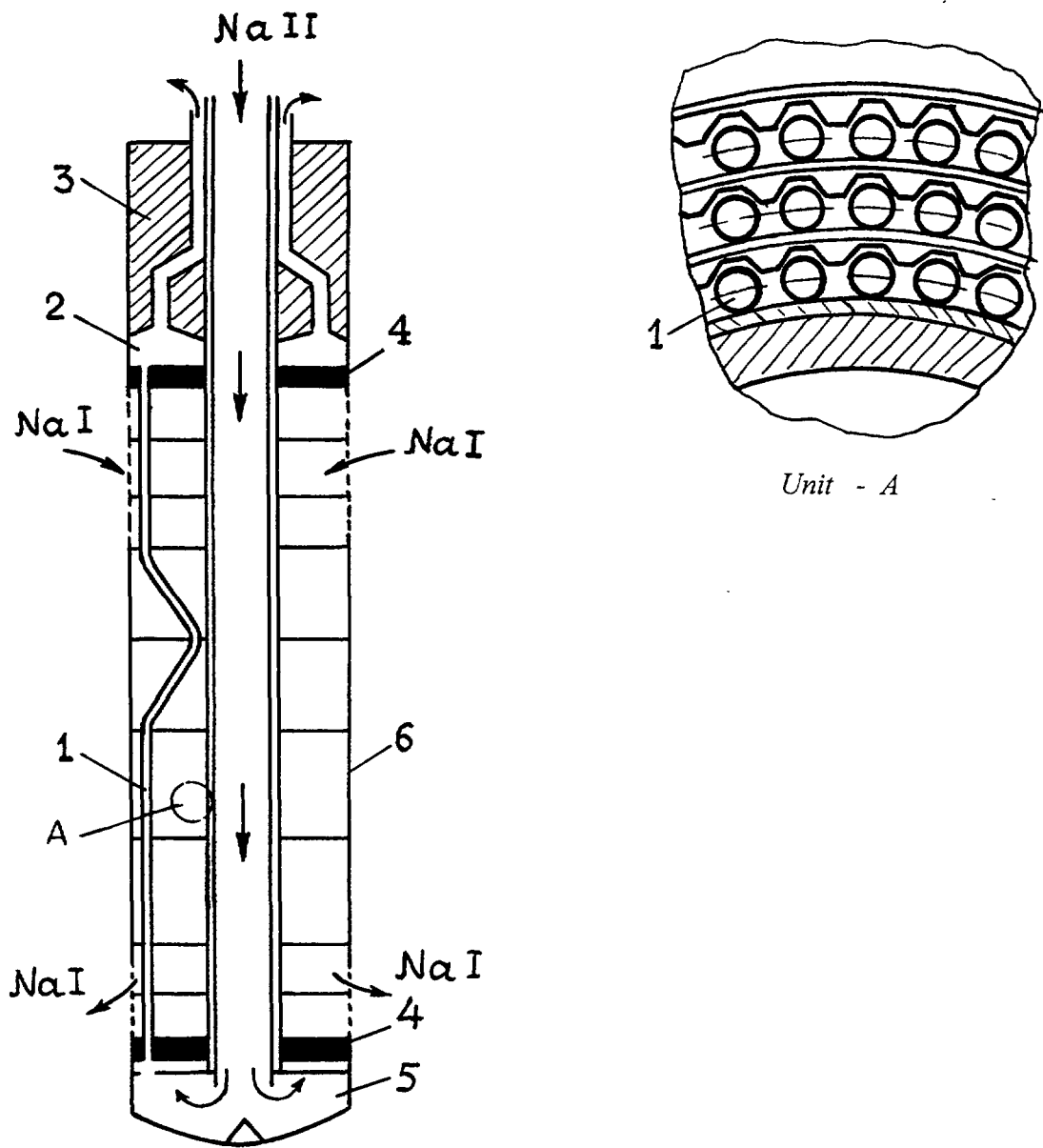
Fig. 1.6. BN-600 intermediate heat exchanger:
1 - pipe, 2 - secondary coolant outlet header,
3 - biological protection, 4 - pipe panels,
5- secondary coolant inlet header,
6 - heat exchanger vessel.
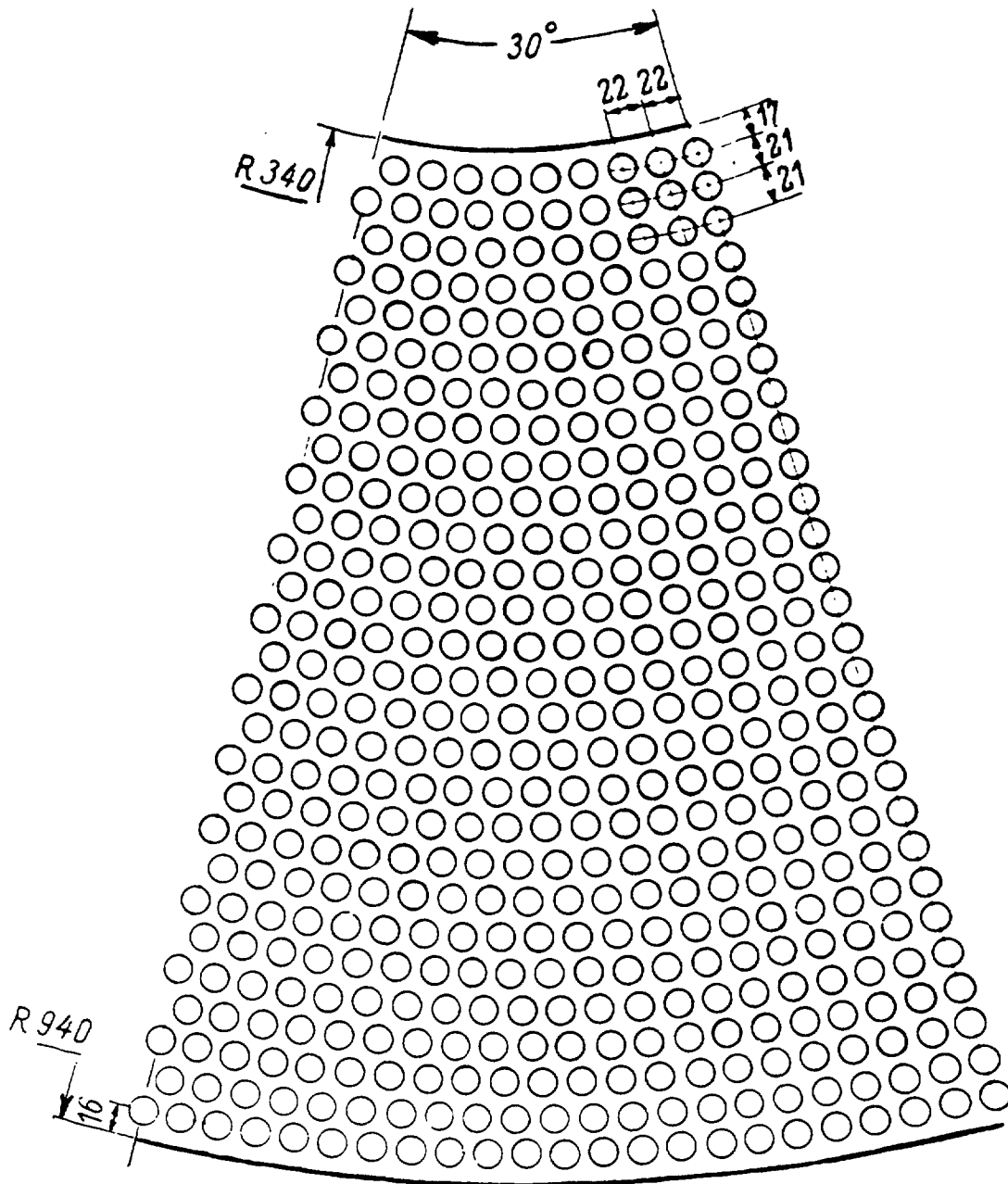
Fig. 1.7. Fast reactor heat exchanger pipe bundle.

The main difficulties in application of mathematical models to thermal hydraulic analysis are complex geometry and large length of pin bundle.

Local methods based on the system of differential equations allow the local flow characteristics to be predicted and starting from them an integral parameters (factors of friction, heat transfer, maximum non-uniformity of temperature at the pin cladding) to be evaluated. Moreover, the complexity of the bundle geometry (especially in the event of deformation), a tedious procedure of solution of the heat and mass transfer equations give no way of taking into account an influence of various factors on temperature behaviour in subassembly. The problem is considered in general as steady state coolant flow in the bundle of smooth pins. The procedure, provided uses a similar mesh, requires a time of calculation being several orders greater than those in subchannel approaches.

Governing equations

Local differential equations:
- *diffusion* (concentration of component),
- *momentum* (velocity, pressure),
- *energy* (enthalpy, temperature)

Averaging

| Over time (local characteristics) | Over channels (subchannel model) | Over space (porous body model) |

Mathematical model

Differential equations (Reynolds approximation)

Macro transport equations

Constants

| Molecular and turbulence diffusion | Inter-phase exchange | Inter-channel exchange | Hydraulic resistance |

Approximations

Transient   Steady state

Axial diffusion   Boundary layer   Stable

Numerical procedures

Finite differences   Finite elements   Analytical methods

Explicit scheme   Semi-explicit scheme   Implicit scheme

Fig. 1.8. Classification of approaches to thermal hydraulic analysis

14

To find average flow parameters on the basis of averaged momentum and energy equations (a porous body model and subchannel analysis) extends calculation domain, allows an influence of various factors to be taken into account. But, such a methods involve an additional procedure, from which a temperature of subassembly structure to be defined.

A porous body model, which implies that an averaging is carried out with the greater scale, and in some cases, the vastly greater, than the size of the channel in bundle, which uses the mesh being not coincident with the bundle channels allow us to gain solution being less detail. This method reflects an effects being much more extended than the channel in bundle, whereas subchannel analysis covers phenomena with inherent scale being equal to the distance between the pin axises. Thus, a porous body model describes macro parameters, and subchannel approach can be considered as macro-micro approximation in the sense that it describes macro effects in reference to the phenomena occurring in the channel, and yet describes micro effects in reference to the bundle size.

In spite of a commonness for setting up a problem, similarity of equations, and respective calculation procedure, there is distinction between them associated with the evaluation of the constants (transport factors and others). These methods are followed to be mutually relative. The use of the local methods allows the constants to be defined as input parameters for solving transport equations with averaged flow approximation.

Single phase steady state flow. The methods of local characteristics calculation have been developed as applied to solving the momentum and energy equations in a differential form. They includes analytical methods, finite differential, finite elements, variable differential procedures. Some works are concerned with the analytical solution of the problem of stable heat transfer in pin bundle [5,6]. The drawbacks are complexity of calculations and approximations required taking account the structure of velocity field and turbulence characteristics.

The most widely used among the local methods are a finite differences [7] and finite elements [8]. A limitation of these approaches is that, due to the calculated area is confined, the need for its division into multipointed pattern, and, besides, these methods, as a rule, take into account an approximate local flow structure, turbulence characteristics and do not account transverse convective exchange produced by helical wire wrap on fuel pins. Variable differences allow us to predict velocity and temperature in areas with arbitrary boundary [9]. Approximating heat transfer in pin bundle having regard to the transverse convective flow have been based on a porous body model. Method of pointed source being under development for an appreciable length time invites definition of so called «functions of influence», which are not universal and by virtue of this the method approximates temperature behaviour under conditions of combined heat transfer [10].

Subchannel analysis consists on solution of mass, momentum and energy conservation equations written for elementary channels, which a subassembly is divided on [11] (Fig. 1.9). It allows us to determine the thermohydraulic characteristics of coolant everywhere over the subassembly taking into consideration all mechanisms of interaction between channels, as well as taking into account heat exchange between subassemblies. There are a lot of codes in which the subchannel approach is realised as applied to steady state and non-stable hydraulics in subassembly. Their analysis is given in [11]. Drawback of these codes is connected with the difficulty of inclusion of inter-channel exchange in subassemblies, the approximations
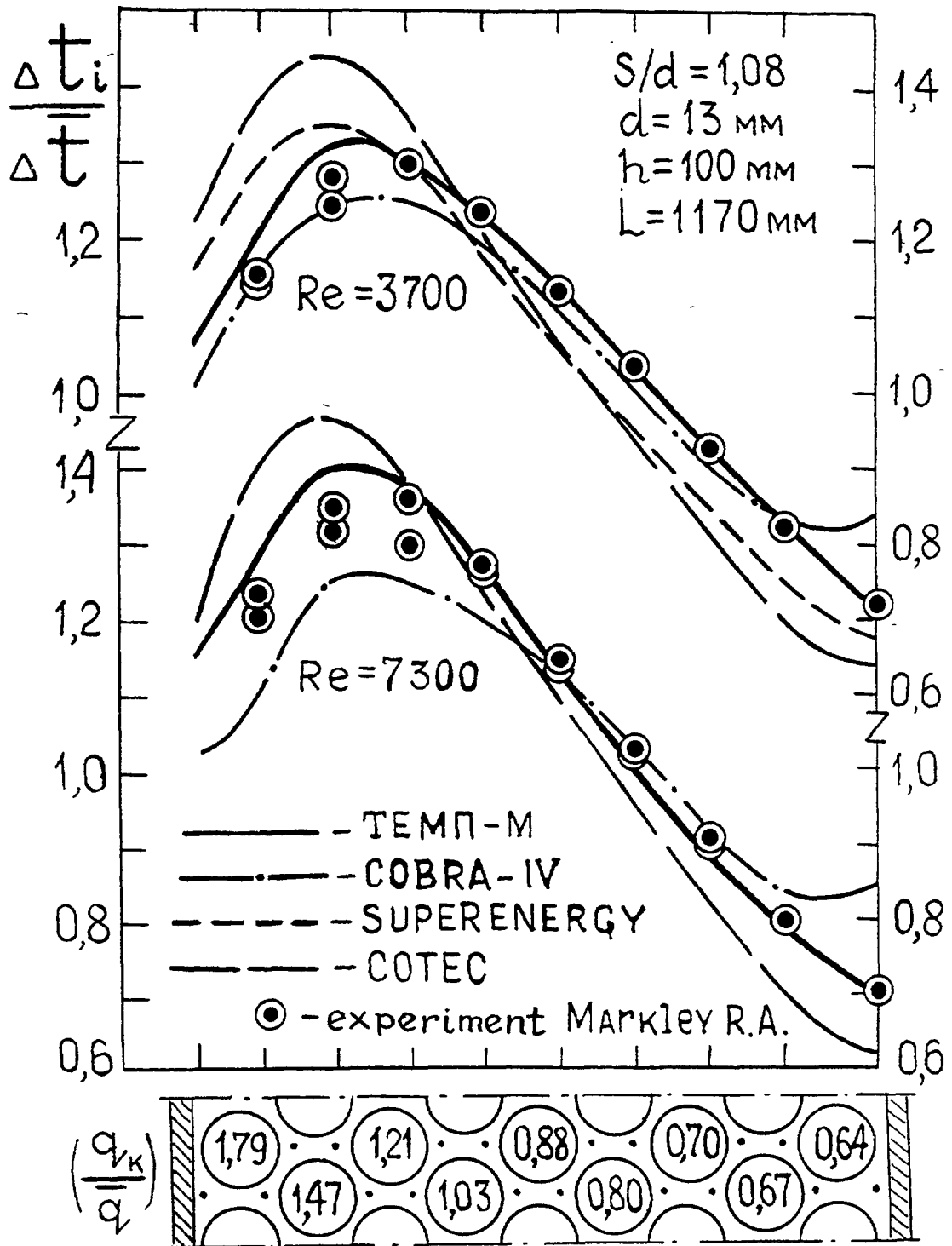
Fig. 1.9. Comparison coolant temperature over the model
section: ⊙ *- experiment Markley R.A.*
————— *- prediction TEMP-M*
—·— *- COBRA-IV*
—— *- COTEC*
— — — *- SUPERENERGY*

required to take into account the subassembly deformation and the difficulty connected with the longitudinal momentum and mass exchange.

Accordingly, predictions by various codes appreciably differ even for such the commonly used versions, such as COBRA-IV [12], COTEC [13], SUPERENERGY [14] and TEMP-M [15] (Fig. 1.9). A complete and precise system of interchannel exchange coefficients have been written as a result of systematic experiments performed in the State Scientific Centre of Russian Federation «Institute of Physics and Power Engineering» (Obninsk) and was realised in the codes TEMP-M and MIF [16]. It has allowed us to improve predictions as compared with the foreign codes mentioned above (Fig. 1.9). Also calculation approach of statistic thermal characteristics of fast reactor subassembly [15] was developed. Code MIF is the only code making possible predictions of local temperature in subassembly in the event of deformation of both fuel pins and subassembly cover. It is the code TEMP-M around which the procedure of probability analysis of "hot spots" factors was improved.

A porous body model describes the fields of elementary unit-averaged coolant velocity and temperature values and is based on solution of momentum and energy equations with volumetric friction and heat production [5]. It only approximately takes into account the local flow structure, peculiarities of subassembly geometry (periphery, deformation) and is effective at temperature behaviour calculation in highly disturbed flows, for example, of a partial solid flow blockade. Based on the mathematical models of transport in anisotropic porous body the codes PROTVA and UGRA were developed [5]. In single phase flow a porous body model was realised, in particular, in such codes as SABRE -1, UZU, COMMIX-1, COMMIX 1a which can be used to predict transients associated with the loss of coolant, enhancement of subassembly power, blockades.

Dynamic approaches in two phase liquid metal coolant. The analysis of transient coolant flows in pin bundle has become especially urgent in connection with investigating transient operating conditions of reactor and the analysis of various emergency situations as well. The first models for calculating sodium boiling in the reactor channel were based on consideration of a single bubble expansion [17]. It was due to sodium tendency to superheating, which was initially estimated as very high, and also due to very fast transition to slug and annular flow pattern. Further development of calculation models were carried out towards increasing the number of bubbles generated in the channel. In this case, in modern model the sodium superheating above the saturation temperature is, as a rule, taken to be no more than 20°C.

It should be noted that these models are in good agreement with experimental data. Up-to date codes for calculating the ULOF and UTOP type accidents- SAS 4A, SAS 3D, EAC-1, FRAX. CAPR-1, CARMEN - most often represent boiling with the use of version of well known multi-bubble models as SAS-2A (USA) and BLOW-3 (Germany). Later the models were made more complicated due to improvement in an account of friction, liquid film motion and its separation, and due to an added criterion of pin dryout. In the framework of such a models the initial thickness of liquid film is taken, on the base of the liquid fraction over the channel cross section, as equal to, and crisis occurs when 1/3 of its initial thickness remains. The first code developed in Russia for fast reactor channel dynamic calculations, taking into account sodium boiling, was also based on a single-bubble model.

The main content of up-to-date models is conservation equations for mass, energy and momentum for the two-phase non-equilibrium flow, the closing relations and inherent

boundary conditions. A delay in the development of such models for sodium is concerned with large great non-linearity and a discontinuities of derivative at the liquid-steam interface, as for sodium the ratio between liquid density to steam density is larger than for water. Of fundamental importance is also the relationship between the absolute pressure of the medium and pressure drop over the channel .

A 3D two-liquid model has been obtained by using temporal or statistical averaging.. The model is expressed in terms of two sets of conservation equation governing the mass, energy and momentum balance in each phases. However, since the averaged fields of one phase are not independent on the other phase, the interaction term appear in the field equations as source term. For the most general dynamic problems such models were developed previously [18].

A similar system of governing equations can be used also in subchannel analysis of nuclear reactor core. In this case, a surface of the control volume is determined by the presently accepted subdivision of reactor core into elementary channels. For doing so, as a rule, an additional equation of momentum balance in transverse direction, as well as respective modeling notions on substance transport between the channels. Ignoring these effects and also analysing the process going on in simply connected domain a system assume the terms mentioned to be left out.

Interphase exchange terms are derived from the balance conditions at the interface. It requires the local phase parameters on each side of the interface to be averaged, with the mixture satisfying the mutual exchange conditions. Initial and boundary conditions, relationships for turbulence transport of heat and momentum should be amplified by governing relationships for each of interaction terms in two-fluid model. At present, technical difficulties restrict obtaining experimental information, as the established relations under development are defined by the significant uncertainties.

It should be marked that the system of equations is neither the only possible nor the totally validated. The local transient equations are being derived and studying in a number of R&D centres.

Two-liquid model is a very powerful procedure and is best capable of describing the two-phase phenomena, where the flow areas are available with the «loosely» held phases. Flow stratification (in particular, in horizontal channels), including those under counter-current motion of the phases, as well as sudden mixing (one phase injects into another), two phase flow under acceleration are an examples. Let us notify that phenomena mentioned is far of the whole list of events attendant on loss of coolant accidents. That is why the two-fluid model is a basis of the majority of developments in this direction. In practice, due to a high level of generality of the equations and a large amount of closing relations, a simplifications are needed to define numerical results, in particular. The first way to simplify equations is connected with the reduction of dimensions (number of space coordinates), the second assumes the abandonment of the two-liquid description (reduction of phase number).

Two-phase non-equilibrium flows. In order to have analysed transient and accident flow in 1D approximation a large amounts of codes were developed, basically concerned with steam generators design [19-21].

Those not numerous works involving analysis of a quality and efficiency of codes developed are of prime interest for practice. Reference [22] can be presented as an example, although it is based on the traditional, simple «homogeneous» slip model, but containing detailed analysis of numerical efficiency of the models. The algorithm TRANS [23] uses a "hybrid" approach introduced by combining a finite difference implicit process (for mass and momentum balances) and the method of characteristics (for energy balance).

The use of the formal averaging of conservation equations is a reasonable expedient to the transition to the 1D description, this results in the appearance of averaged factors (C=0,1, ...) referred to as distribution parameters. Representation of 1D equations containing distribution parameters which are equal to 1 is appropriate to the assumption on the plane profiles of phase parameters to be accepted. Forms and number of distribution parameters depends on the kind of two-fluid model. Analytical relationships for averaged factors were gained in [24].

Subchannel two-phase codes. A great variety of subchannel codes is conditioned by, on the one hand requirements on researches for the specific reactor cores, and on the other hand by an attempts to develop specific codes capable of processing as various structures, and different performances. Accepted description of two-phase flows can be classified by types of the model, namely: homogeneous, of separate flow and drift flow.

A very important feature of two-phase models is the description of the following exchange mechanisms between the adjacent channels:
1. Microtransport referred to as turbulent mixing, which arises from the random turbulence in the inter-channel gaps. Energy transport direction in this event is set so that the enthalpy gradient between channels reduces. Analysis of the data available is presented in [11], for example.
2. Macrotransport referred to as transverse (or convective) flow is governed by the difference in axial pressure gradients in the channels under consideration, which arise from the change in the channels geometry, dissimilar heat fluxes and other irregularities. Physical prerequisites accepted in deriving mathematical models, empirical relationships as well as native and abroad codes are discussed in [11].
3. Drift (or diffusion) of steam phase which is taken as proportional to gradient of mass velocity in adjacent channels. By the use of mechanism indicated it has become possible to explain the observed during experiments tendency to the steam runs into the high-velocity channels of subassembly.

Two-phase codes taking into account an axial diffusion. Recently, a number of codes has been developed on the basis on solution of 3D macrotransport equations in terms of an axial diffusion (momentum and energy) partially in the framework subchannel analysis and, basically in the frame of a porous body model [25-27]. The main group of the codes was developed to analyse two-phase thermal hydraulics, but some of them have a single-phase versions, including those applied to reactor fuel subassemblies cooled by liquid metal. Two-phase flow is simulated, as a rule, by homogeneous model. To solve liquid dynamic equations the methods ICE [28], SIMPL [29] and their modifications are used, basically. The codes applied to fast breeder reactors have been developed, for the most part, to analyse loss of flow accidents, blockades of subassembly cross section, subassembly warming up.

Three-liquid models (heat transfer crisis). To analyse heat transfer crisis in disperse-annular flow the three-liquid models are currently used [26], in which three

interacting phases are under consideration, namely: liquid film, vapour core and disperse (drop) flow. In this case, as a rule, the following assumptions are allowed: the phase temperatures is equal to saturation temperature, velocities of vapour and drops are equal.

A considerable gain in physics and mathematics of three-liquid models turns into a serious problems associated with a rich variety (in comparison with two-liquid models) of closing relations and difficulties in their numerical realisation.

1.3. TECHNICAL MODELING OF FAST REACTOR SUBASSEMBLIES AND HEAT EXCHANGERS

The need to have the reliable data on fast reactor core and heat exchangers thermal hydraulics has required that the principles of thermal modeling to be adhered to.

The basis for technical simulation of fast reactor subassembly and heat exchanger is the developed and introduced in practice methods applied to design the fuel pin simulators and the models of subassembly and heat exchanger, to develop the heater of a larger power with the uniform or variable power production, to choose amount of pins and tubes, to measure temperature and so on [30].

The principles, among theoretical grounds of thermal modeling of fuel pins developed previously [31,5], are usefully employed now. They are presented below.

Fuel pin simulators. Let us consider a general construction of cylindrical fuel pin being composed of «n» claddings with the contact thermal resistance between fuel and cladding (or between claddings - Fig. 1.10-a), and let us have changed a relative pitch of the pin arrangement. In this case, criterion equation for dimensionless temperatures in the pin and coolant can be written as:

$$T_i = f_1\left(\xi, z, \varphi, x, \xi_1, \xi_2, \ldots \xi_n, \Lambda_o, \Delta_1, \ldots \Lambda_n, \sigma_1, \sigma_2, \ldots \sigma_n, Re, Pe\right) \qquad (1.1)$$

$$T_f = f_2\left(\xi, z, \varphi, x, \xi_1, \xi_2, \ldots \xi_n, \Lambda_o, \Delta_1, \ldots \Lambda_n, \sigma_1, \sigma_2, \ldots \sigma_n, Re, Pe\right) \qquad (1.2)$$

Here $T_i = t_i \lambda_f /\left(\overline{q} R_{n+1}\right)$, $T_f = t_f \lambda_f /\left(\overline{q} R_{n+1}\right)$ - dimensionless pin and coolant temperatures, respectively; $\xi = r/R_{n+1}$, z, φ - dimensionless coordinates in radial, axial and azimuthal directions; $x = s / 2 R_{n+1}$ - pitch-to-diameter ratio (s is the distance between the pins axises), n - amount of claddings on the pin, $\xi = R_i / R_{n+1}$ $(i=1 \div n)$ - dimensionless thickness of the cladding; $\Lambda_i = \lambda_i / \lambda_f$ $(i=0 \div n)$ - dimensionless thermal conductivity of fuel (Λ_o) and claddings ($\Lambda_1 \div \Lambda_n$); $\sigma_i = \phi_i \lambda_{i-1} / R_{n-1}$, $(i=1 \div n)$ - dimensionless contact resistance between fuel and cladding (σ_1) and between claddings ($\sigma_2, \sigma_3 \ldots \sigma_n$), ϕ_i -thermal resistance, $\overline{q} = q_v R_1^2 / 2 R_{n+1}$ - mean heat flux at the pin surface ($\xi=1$); $Re = \overline{w} d_h / v$ - Reynolds number, $Pe = \overline{w} d_h / a$ - Peclet number, $\overline{w}$ - mean coolant velocity, d_h - hydraulic diameter of the channel. The otherwise is specified in the Fig. 1.10,a.

Equations (1.1 and 1.2) follow from the analysis of the heat conduction equations in a pin and the thermal transport in liquid written in dimensionless form. They assume that heat transfer is stable, coolant and pin have the invariant properties, volumetric heat production in

20
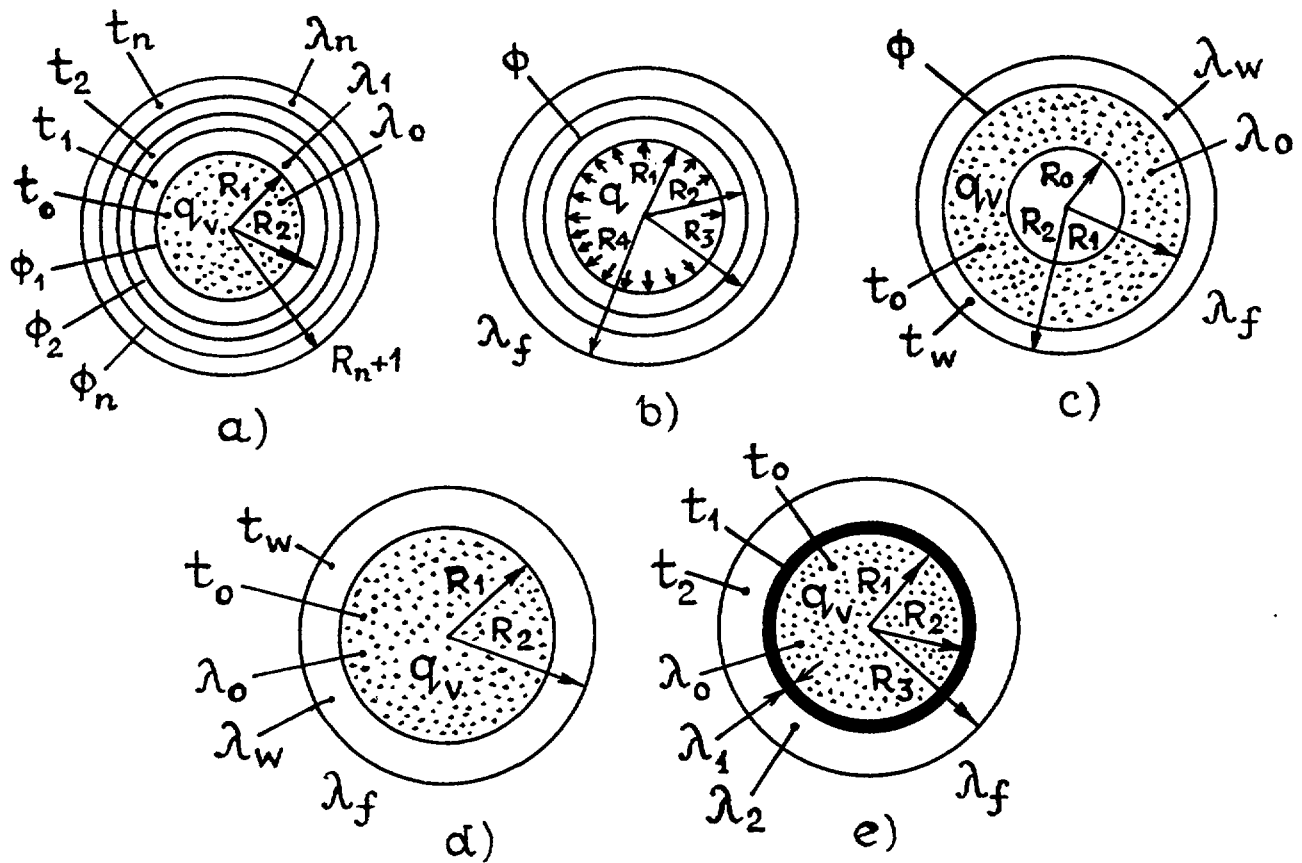
Fig. 1.10. Cross section of fuel pin (a, c, d, e) and pin simulator (b).

pin is isotropic, the pin is of symmetric structure in its properties and geometry, the second temperatures derivation with respect to axes z is negligible, turbulence characteristics of coolant flow are defined by the channel geometry, properties and coolant velocity only.

In modeling fuel pins the parameters $x, \Lambda_1 \div \Lambda_n, Re, Pe$ are easy to be reproduced. Difficulties arise when the pin simulator is made with volumetric power production (modeling Λ_o) and contact thermal resistance (σ_i). If even the fuel pins are considered as free of the contact thermal resistance, it is difficult to provide an ideal thermal contact between the claddings. Attempts to reproduce the relative thickness of the cladding are not necessarily successful.

The essence of the thermal modeling of fuel pins [31,5] consists in the integration of the parameters responsible for azimuthal thermal conductivity of the pin, namely Λ_o, $\Lambda_1 \div \Lambda_n$, $\xi_1 \div \xi_n$, $\sigma_1 \div \sigma_n$, into a single parameter of equivalent thermal conductivity $\left(\varepsilon_k\right)$ and in the fulfillment of equality of parameters ε_{k_o} for the natural structure and for the model. This parameter is calculated on the basis of the main temperature harmonics in Fourier - series expansion. The possibility of such an integration was approved by the analytical solution of the equation of fuel pin heat conduction. N.I. Buleev was the first who solved this problem in application with cylindrical pin containing the fuel and one cladding. The general solution of the problem on cylindrical pin embedded in «n» claddings and having the contact interlayers was performed by P.A. Ushakov, that has allowed the relationship of ε_{k_o} to be derived.

$$\mathcal{E}_K = \left\{ \frac{\lambda_W}{\lambda_f} \cdot \frac{1 - m\left(\frac{d_1}{d}\right)^{2K}}{1 + m\left(\frac{d_1}{d}\right)^{2K}} \right\}_T = \left\{ \frac{\lambda_W}{\lambda_f} \cdot \frac{1 \mp \left(\frac{d_1}{d}\right)^{2K}}{1 \pm \left(\frac{d_1}{d}\right)^{2K}} \right\}_M$$

$$m = \frac{\lambda_W - \lambda_0}{\lambda_W + \lambda_0} : \begin{cases} \lambda_0 \ll \lambda_W, & m = +1 \\ \lambda_0 \gg \lambda_W, & m = -1 \end{cases}$$
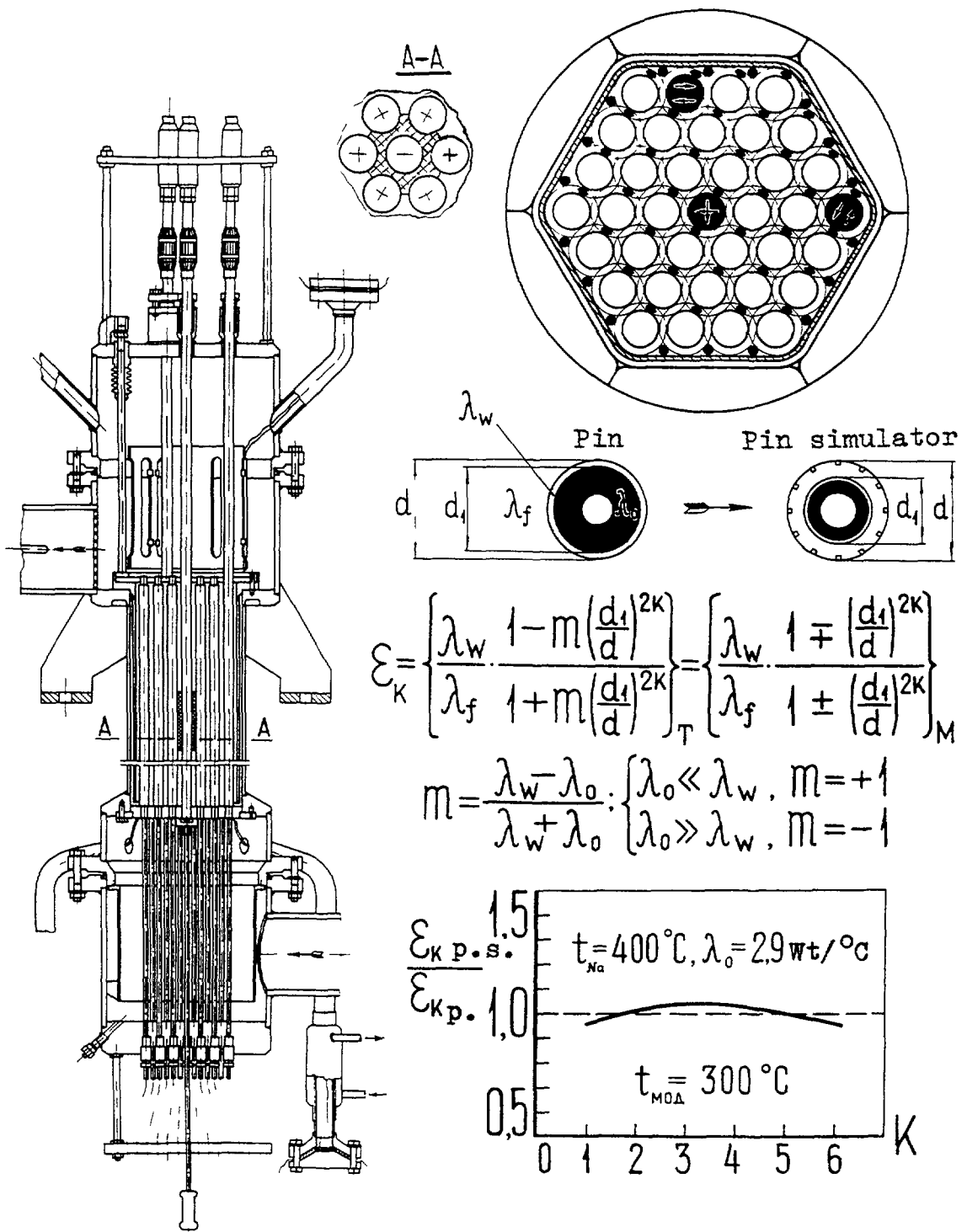
Fig. 1.11. Fast reactor assembly model.

The graphs show:

$$\frac{q}{q_{max}}$$

$$q = q_{max} \cos \beta \left(\frac{z}{H} - 0.5\right)$$

$$\delta_z = \frac{\delta_{\text{ц}}}{\sqrt{\cos \beta \left(\frac{z}{H} - 0.5\right)}}$$

$$q \cdot 10^{-5} \frac{Wt}{m^2}$$
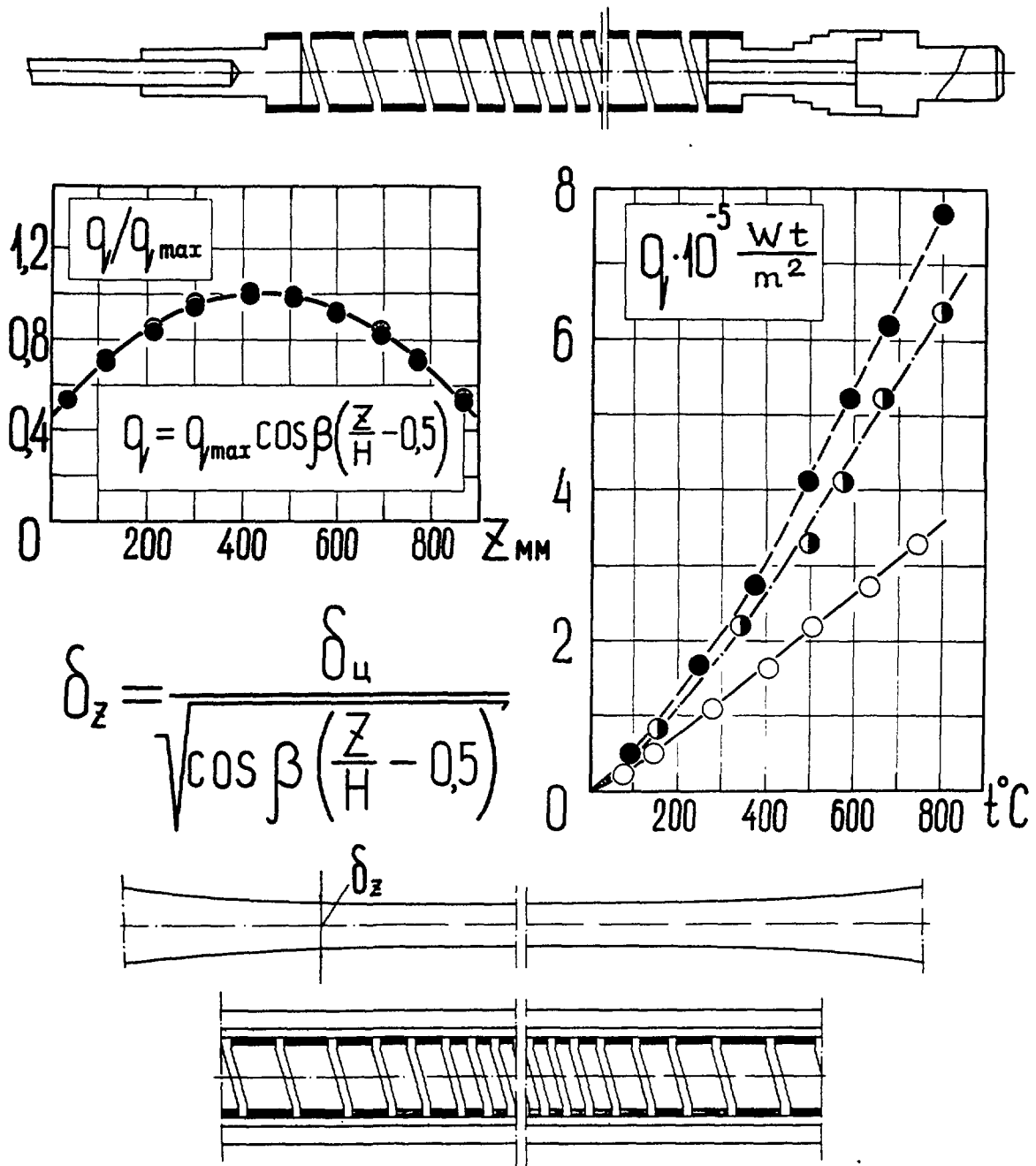
Fig. 1.12. Pin simulator.

The use of ε_{k_o} allows us to obtain criterion equations:

$$\tilde{T}_f \approx \Psi_1\left(\varphi, \xi, z, \varepsilon_{ko}, Pe, Re\right) \qquad (1.3)$$

$$Nu \approx \Psi_2\left(z, \varepsilon_{ko}, Pe, Re\right) \qquad (1.4)$$

Having regard to these equations, the technical concepts of thermal modeling presented below were developed.

The pin simulator (Fig. 1.11, 1.12) is a grooved pipe, inside of which the helical wire heater manufactured from a high-temperature material (chromel) or nichrom strip (wire).

23

Electric heater is insulated from the wall by the casting wrapper with a subsequent annealing. Finishing the wrapper by reamer ensures the inter diameter of the pipe to the helix size with a high accuracy. The heater helix is filled with the silicon organics, and a free volume of the pipe with aluminium dioxide. The heater is designed so to provide a rather great heat flux at the pin surface ($\sim 8 \cdot 10^5$ w/m^2) at temperature $\sim 850°C$. To produce non-uniform over the pin length power production the helixes of formed strip are used. Fig. 1.12 shows the heater with resulting cosine power production inherent for fast reactor core.

The heaters discussed above are simple to manufacture, reliable to maintain and low in cost. They ensure the uniform power production around the periphery of a pin with a high accuracy, being primarily responsible for that we can gain reliable data using approximate thermal modeling of fuel pins. Allowing for various (warranted) shape of length-variation in the power production and giving great heat fluxes at the pin surface at the reasonable great pipe diameter (12÷25mm), the heaters represent a very feasible structures.

The major practical issue is how to evaluate an accuracy of approximate thermal modeling of fuel pin. Examples of well simulated fuel pins are found in fast reactors (BN-350, BOR-60, BN-600, BM-800) being of a small thermal conductivity of fuel ($\lambda_o \sim 1.8 \div 2.9$ W/m^{2}K). At the inner surface of the pin the condition q=const should be met. Dependence of parameter ε_k on thermal resistance or on number of harmonics for such a pins and their simulators are similar in kind. Values of ε_k are little different (not more by 5%) from each other (Fig. 1.11).

To calculate ε_k for fast reactor pins the following relations can be used:

$$\varepsilon_k = \frac{\lambda_w}{\lambda_f} \cdot \frac{1 + x_1 + \left(\sigma + \dfrac{x_1 + x_o}{x_1 - x_o}\right) \cdot (1 - x_1) - m\left[1 + x_1 + \left(\sigma + \dfrac{x_1 + x_o}{x_1 - x_o}\right) \cdot (1 - x_1)\right]}{1 - x_1 + \left(\sigma + \dfrac{x_1 + x_o}{x_1 - x_o}\right) \cdot (1 + x_1) - m\left[1 - x_1 + \left(\sigma + \dfrac{x_1 + x_o}{x_1 - x_o}\right) \cdot (1 + x_1)\right]} \qquad (1.5)$$

where $x_o = \xi_o^{2k}$; $\xi_o = R_o/R_2$; $x_1 = \xi_1^{2k}$; $\xi_1 = R_1/R_2$; $m = (\lambda_w - \lambda_o)/(\lambda_w + \lambda_o)$; $\sigma = k\lambda_w \Phi / R_1$

The remainder are explained in Fig. 1.10-c. Number of the main harmonics in Fourier series is accepted to be equal $k=k_o=6$ for the regular part of bundle and $k=k_o=1$ for the edge pins.

The value of the contact thermal resistance originated between the stainless steel and dioxide of uranium may be defined in accordance with [32], and those between the helix and insulation was defined in experiments [30] $R_f=1.3 \cdot 10^{-2}$(m^{2}K)/W.

An internal structure of the pin has no effect on the value of ε_k for the most part, as shown in [30]. Therefore, ε_k can be predicted with the single pipe formula:

$$\varepsilon_k = \frac{\lambda_w}{\lambda_f} \cdot \frac{1 - (R_3/R_4)^{2k}}{1 + (R_3/R_4)^{2k}} \cdot \qquad (1.6)$$

See nomenclature in Fig 1.10.b.

24
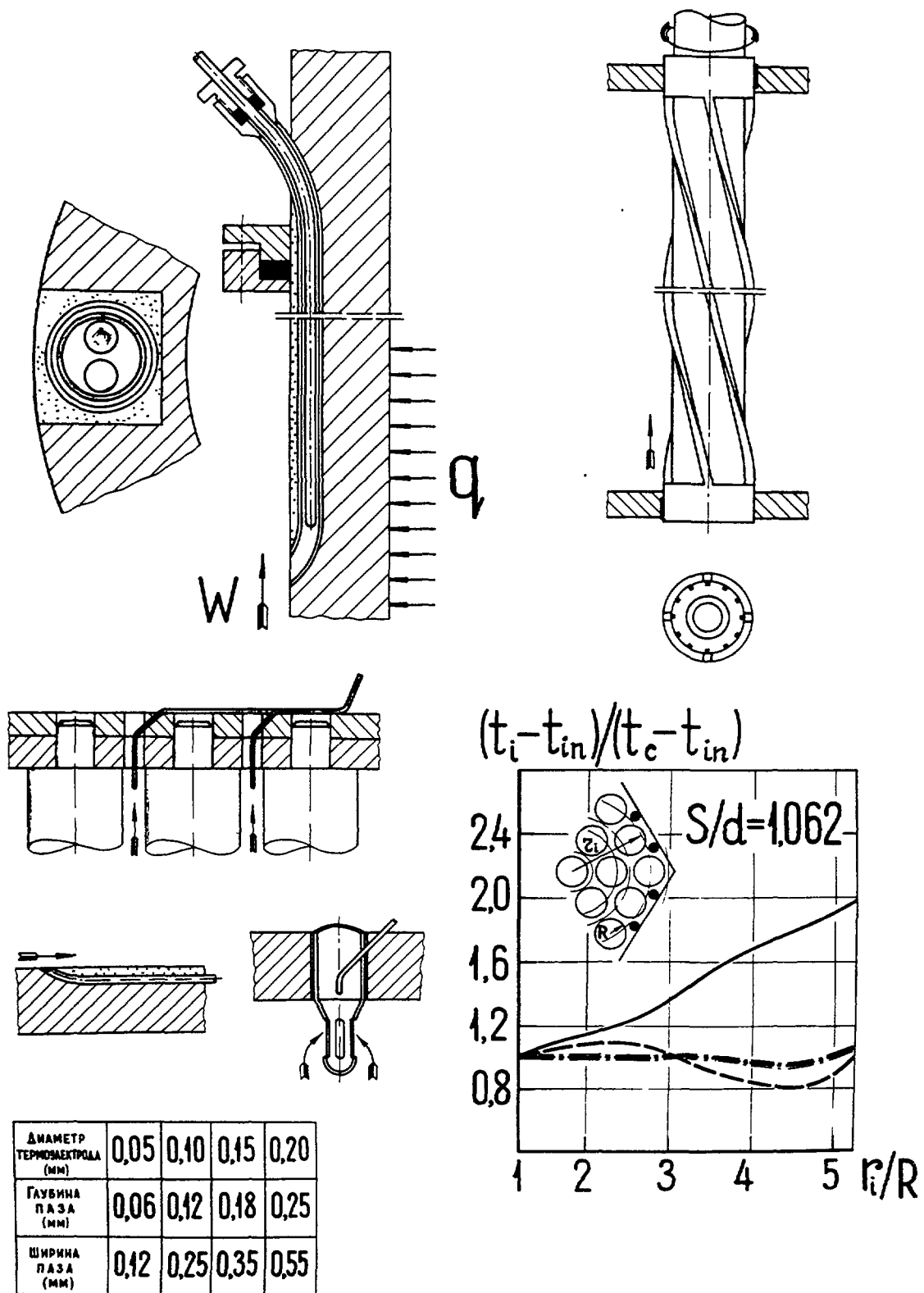
Fig. 1. 13. Measurement technique of wall and coolant temperature: t_i *- local temperature,* t_{in} *- inlet temperature,* t_c *- central channel temperature.*
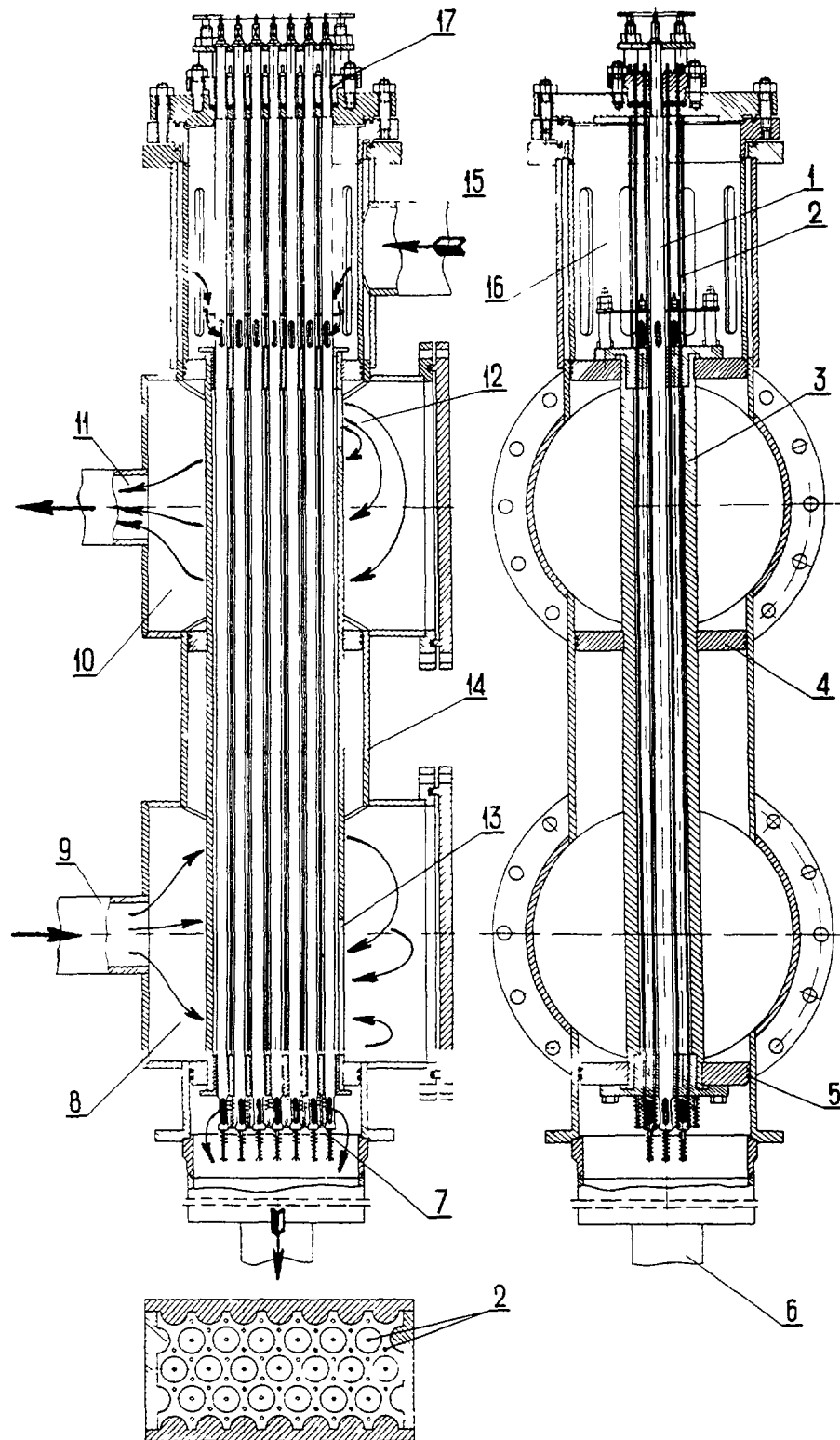
Fig. 1.14.   Experimental model:

1 - measurement pipe,   2 - mobile thermocouple,   3 - pipe bundle
wrapper tube,   4, 5 - diagrids,   6, 15 - inlet of outlet of coolant,
7 - spring to tension capillars,   8, 9 - inlet and outlet hot
headers,   9, 11 - hot coolant supply leadaway,   12, 13 - pipe bundle
mindows,   14 - case,   17 - seal, (coolant flows   from bottom to top).
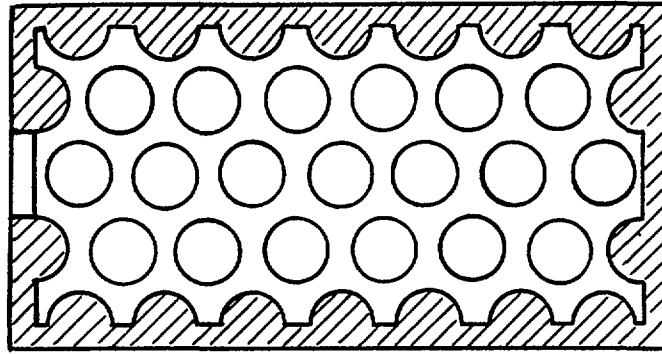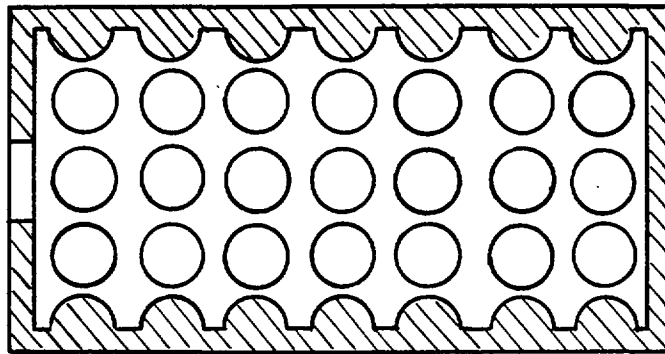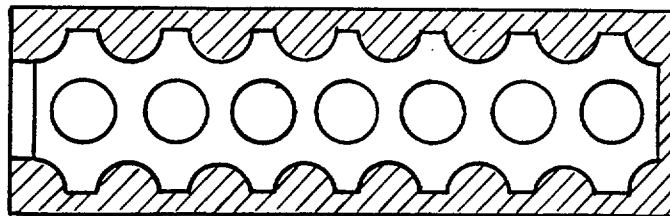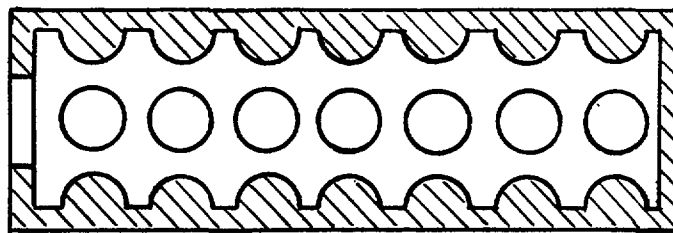
Fig. 1. 15. Models of triangular (a, c) and square (b, d) pipe bundles.

The model (Fig.1.11) measures the mean mixed outlet temperatures in every channel. The thermocouples are fixed in the special grids attached to the flange of the header, which allows the thermocouples to be inserted into the channels during the flange mounting. Fig. 1.13 presents also an additional information on the micro thermocouples construction, their sizes and the measurement technique.

On thermal hydraulic modeling of fast reactor intermediate heat exchangers. Into the housing-piping heat exchanger (Fig. 1.6) an uniform, over perimeter, the coolant supply has been designed, that is a non-symmetric flow distribution is realised in the inter-pin space. In cylindrical bundle the pins are positioned on a circle with a given pitch and the regular triangular or square channels are formed (Fig. 1.7). Replacing the isolated sector of cylindrical bundle by a rectangular area, we can study (to a certain approximation) the coolant flow in a sector using «planar» model , as flow through such a model does not differ noticeably from those through the cylindrical bundle. For this purpose the thermal hydraulic experiments for intermediate heat exchanger have been carried out on liquid metal planar models (Fig. 1.14, 1.15, a-d) involving one or three rows of tubes and displacers attached to the wrapper (structure in detail see in [30].

The local modeling of thermal hydraulics have received detailed attention, defining finally a competence to use the data found in the full-scale systems (heat exchangers involving large number of tubes, long tubes and so on). The main questions of thermal hydraulic modeling of the multi-tube heat exchanger are concerned with the number of tubes in the model, length of experimental bundle, velocity and temperature measurement techniques.

It has been established that the single-row hydraulic model (7 pipes, together with displacers attached to the planar walls) simulates hydrodynamics in general terms, whereas in order to simulate a thermal processes the model is needed involving three rows of the tubes, at least (modeling governed by the internal tubes of the central row); the length of the model bundle is sufficient to simulate a full-scale heat exchangers, as an experiments have shown the stable velocity and temperature difference between the hot and cold coolants.

The fact that results gained are reliable and can be converted to the full-scale heat exchanger is suggested that the local, not averaged, velocity and temperatures are measured in the models mentioned above. Hydrodynamics is studied with the use of electromagnetic technique, which allows a longitudinal and lateral components of liquid metal velocity to be measured in each point of the volume under consideration. In studying characteristics a specially developed technique is used to measure temperature of hot and cold coolants by mobile thermocouples (method of local thermal modeling).

1.4 ELECTROMAGNETIC TECHNIQUE AS A BASIS OF DATA SECURING IN THERMAL HYDRAULIC ANALYSIS OF FAST REACTOR CORE AND HEAT EXCHANGERS

General insights into the technique. Traditional measurement techniques based on the Pitot tubes and thermal anemometer is difficult to be used in liquid metal flows. Experiments with coolants of a moderate Prandtl numbers (water, air) generate often a need for the models of a large size (as compared with in-pile bundles), that is of great expense and it does not give an appropriate consistency between the experimental and standard reactor technology.

Thermal hydraulic model of fast reactor fuel subassembly. As shown in Charter 1.1, the reactor core consists of hexagonal subassemblies, in every of which the cylindrical fuel pins are arranged by a triangular manner with the given pitch-to-diameter ratio (Fig. 1.4, 1.5). Fuel is uranium dioxide or plutonium dioxide, the pin cladding is stainless steel. Spacer structure is performed by wire wrap. Edge pins are offset by the inter-pin gap (or half of gap) from the cover. To equalize coolant temperature across the bundle, displacers are incorporated in the structure. Power production along the core follows a cosine.

The thermal hydraulic model (Fig.1.11) simulates the power part of subassembly at the scale 2.5:1. It involves 37 fuel pin simulators, that, in certain cases, is equal to the number of pins in in-pile subassembly (BOR-60), and less for other types (BN-350, BN-600, BN-800). 37 pins are best suited in number, because not only internal area of subassembly, but the close to wrapper area are strictly specified (in terms of thermal hydraulics). When assembled together as triangular bundle with the given pith-to-diameter ratio, the pin simulators (wire wrapped) are arranged inside of the hexagonal cover. Cylindrical displacers mounted at the periphery are secured in the top and bottom aligning grids. Pins equipped with the thermocouples are positioned in the specific areas of the model (internal, edge, corner). They are made as turning ones and allow the temperature behavior in specific areas of subassembly to be studied. The relative length of simulator tends to be little less than those in-pile. It permits extrapolating the data gained to the whole length of in-pile pin, which is of great importance in the near wrapper areas, where there is no hydraulic stabilization, as usual. The internal area of subassembly comes into steady state rather steeply and the question does not raised about the choice of relative length of simulator.

The fact that the edge pins are positioned in the immediate vicinity of the wrapper complete with displacers results in an additional parameters, in comparison with the internal pins, influence the temperature behavior of the pins, among them: geometry of wrapper and displacers, clearances between the wrapper and the pins, boundary conditions and so on. Of particular importance is the reproduction of the edge area's characteristics and the choice of the main harmonics in Fourier series. A thermal interaction between subassemblies is simulated by heat removal using a controlled coolant flow in the clearance between the wrapper and the model body (inter-subassembly flows).

Temperature measurement technique. Micro thermocouples (covered by the capillary of stainless steel $\varnothing 0.8 \times 0.6$ mm, 0.5×0.3 mm, 0.3×0.2 mm; thermoelectrods: chromel-alumel, cooper-constantan $\varnothing$ 0.1, $\varnothing$ 0.05 mm) are embedded in longitudinal grooves (Fig. 1.13), which displaced an angle of 30° (12 points) from each other. Micro thermocouples are applied a metal coating. Also the mobile micro thermocouples are used to measure temperature distribution with the pin length.

In studying the pin overheating caused by the helical wire the technique for rotating the smooth pin inside of the immobile structure was developed. In accordance with the spacer type (either a fin touches an adjacent pin cladding or a fin touches a fin of adjacent pin) the structure mentioned above is made either from wire helix or from the pipe having been put through a milling. The last is slipped over the pin with a slide fit and its wall thickness is equal to the fin height. The structure is welded on the spacer grids. Inspected tension of the structure over the pin yields that the fin is tight against the pin surface.

In addition, without minimising the importance of hydrodynamic modeling, it should be noted that a precise knowledge of local in-pile hydrodynamic characteristics is of

paramount importance in thermal hydraulic validation of liquid metal reactor, that defines temperature behaviour in reactor core. The need for studying the local hydrodynamic characteristics in three main types of flows achieved in reactor units - axial flow (local flow distribution over fuel pin perimeter), transverse flow (mass exchange in the inter-pin space), combined axial-transverse flow in heat exchangers - has required an universal technique to be developed as applied to any mentioned type of flow.

Hydrodynamics is conveniently studied using the model bundles, those geometry is close to the in-pile subassembly, provided the same liquid is used as a coolant (liquid metal). The advisability of pursuing such a researches is evident, as experiments provide near the natural hydrodynamic conditions, and the conduction of the experiments is found to be economical. Once hydrodynamic measurements have been amplified by thermal ones, a full information for thermal hydraulic validation of nuclear reactor is derived.

Electromagnetic technique developed in the Institute of Physics and Power Engineering allows a local hydrodynamic characteristics to be measured in the immediate mock-up liquid metal bundles [33-34]. This enables using the mock-up assemblies manufactured in accordance with the standard practice and conforming reactor design specifications, except that fuel material is lacking.

Analytical and experimental researches in the framework of the technique were carried out, the local magnetic sensors were constructed (sensors are used with the magnets in size 5×3×2mm, which are mounted in the pin cladding of 6mm in diameter), concepts of calibrations and transformation of the sensors' findings into the local flow rate (velocity) were developed, as applied to liquid metal flows.

As of now , the technique is used to measure both longitudinal [34,41] and transverse [11,35-38] liquid metal flows in the bundle of smooth and wire wrapped pins (in the last case the technique was validated to two types of helical wrap: fin-to-cladding [11,37,38] and fin-to-fin [11,39]. It is used also in studying the combined axial-transverse flow in the intermediate heat exchanges [40,41]. Technique is found to be suited in measuring the local flow distribution over the pin perimeter arranged in distorted manner (shifting, bending), in non-regular channels, beyond a subassembly (stream flow in the headers), along the channels [42] and so on.

Performance and construction of the local electromagnetic sensors. If the permanent magnet is located inside of the tube, a distributed e.m.f. arises in the magnet, as well as difference in potentials at the surface of the tube as it is turned in the channel [33]. Problem is associated with the development of such a construction that assures the findings converted to reliable local flow (velocity) within the specified part of flow cross section, which hereinafter we shall designate as «the fundamental contribution part». The reason of discrepancy between the measured signal and the desired flow rate (velocity) can lies in the magnetic field which follows distinct paths at the magnet ends, that is responsible for the stray (being beyond the fundamental contribution part) areas of coolant flow can contribute into the fundamental signal. From this viewpoint a construction of sensor has to assure the local magnet field in specified part of flow section being adjacent to electrodes. The resolution of the issue was derived during combined analytical & experimental investigations resulting in the constructions presented in Fig. 1.16.

$$\frac{W_i}{W} = \frac{k e_i \Omega}{\sum k e_i \omega_i}$$

a)

b)

c)

d)
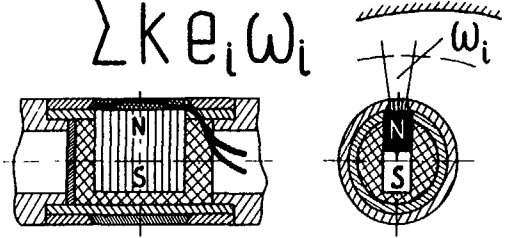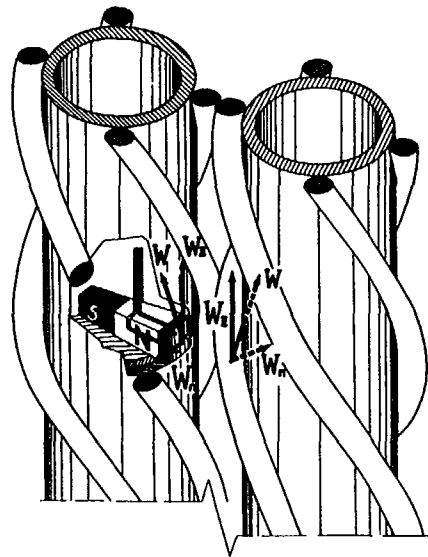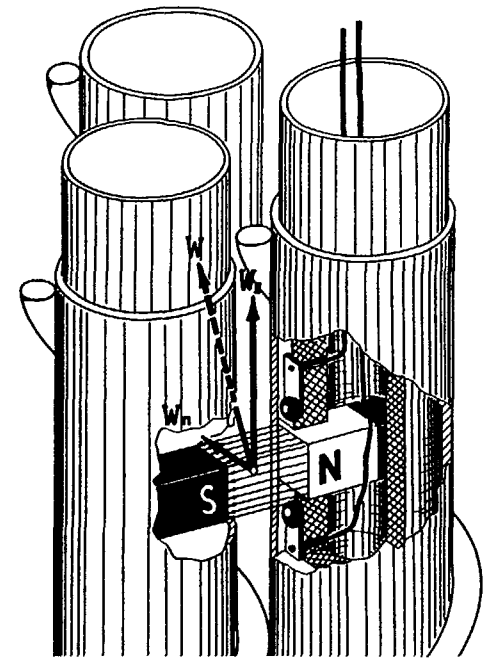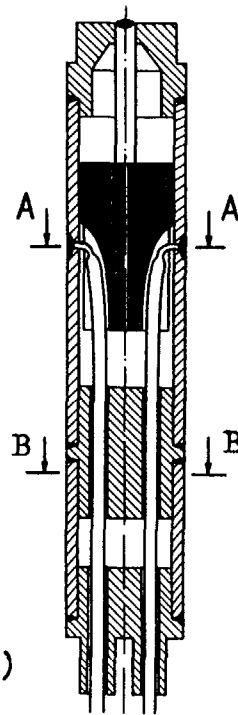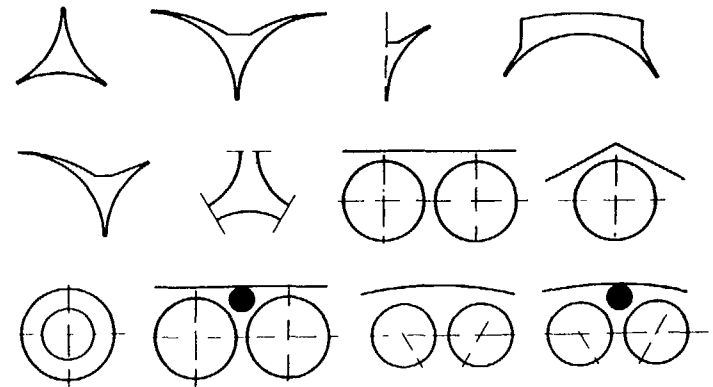
e)

Fig. 1.16. *Local action electromagnetic sensors and channels used to develop sensors, construction.*

Permanent magnet is entered into the tube of stainless steel surrounded by by-pass ring of armco steel (Fig.1.16, a). The magnet axis is coincident with the tube diameter being at right angles to the flow (we are dealing with the axial direction). At the external surface of the tube the neck is made where the cooper shield ring enclosing the magnet is fitted to. The ring has the cut filled with insulator, in which two electrodes being in contact with the coolant and reading longitudinal component of velocity are fixed. Central angle between electrodes ($2\Delta\varphi$) equal to $3\div7°$. Distance between electrodes axises is 0.7 of the cut width ($2\Delta\alpha$).

Based on the experimental [11, 34-42] and analytical [5, 11, 34, 43] validations of electromagnetic technique, it has been shown that difference in potentials resulting from the electrodes in liquid metal passing through the bundle (longitudinal flow) can be associated with the mean coolant velocity within the elementary area formed by radial rays drawing through the electrodes and the line of maximum velocity. In a great number of cases the length of the elementary area is chosen equal to the distance between the tube surface and the channel wall. Signal distribution around the tube measured in the rotating tube should be in conformity with the hydrodynamics of the channel under consideration.

To convert a signal into velocity is performed in dimensionless form on the assumption that the proportion factor k in relationship

$$W = k \cdot e \qquad\qquad (1.7)$$

is the same within the areas under consideration and can be counselled in processing data as:

$$\frac{W}{\overline{W}} = \frac{e}{\sum e\omega \ \Omega} \qquad\qquad (1.8)$$

where Ω - channel cross section area, ω - surface element that defines velocity, $\overline{w}$ - mean velocity within the channel.

To define velocity distribution along the model the electromagnetic sensor is moved along the tube axis (commonly either together with the tube or inside of the tube). A tube rotation allows the azimuthal distribution of velocity to be measured. In order to measure variation in the integral flow rate around pipe the sensors are used, where electrodes is positioned along the tube diameter (Fig. 1.16, b). Electrodes are in contact with the internal surface of the tube and are moved integrally with the magnet in axial and azimuthal directions. The use of such a sensors is very attractive in the bundle of thin-walled tubes of a small diameter ($\sim5\div6$ mm), when we does not succeed in positioning the electrodes in the immediate vicinity of a magnet end [39,43]. To replace the sensor from one tube to another opens the ways for detecting subchannel flow rates . Attempts to arrange sensors in the in-pile subassembly of (BOR-60) led to the appropriate data were gained.

Electromagnetic sensor designed to measure a transverse flow in subassembly with the «fin-to-cladding» spacer consists in the two magnets placed in to adjacent tubes, with the permanent magnetic field produced between the tubes (Fig. 1.16, c) [11, 35-38]. Magnets are concurrently moved inside the tubes. Using the sliding contacts an e.m.f. due to transverse flow of liquid metal throughout the clearance between the contacts is measured. For the transverse flow in the bundle of the pins wrapped by «fin-to-fin» type of wire spacer to be

measured [36, 37, 40, 47), when an opposite in directions flows occur between the pins, the sensor with one magnet is used (Fig.1.16,d) which operates in the area covering not more than half a gap between the pins (appropriate magnet to be chosen).

To investigate a combined axial-transverse flow, the sensors equipped by two pairs of electrodes are used, with the electrodes located near to magnet end (azimuthal and axial directions) (Fig. 1.16, d). Such a sensors allow the concurrent measurement of axial and transverse components of velocity [35, 36, 40, 41].

Theoretical notions on electromagnetic technique. To find the best construction to be followed, some variously of the sensors constructed were investigated, which differ in shape and in size of the magnet, in material and number of electrodes, in technique of the electrodes embedded into the tube surface, in an angle between the electrodes, in extent to which a magnetic field to be located at the magnet end (the availability or the absence of shield rings) and so on. Experiments were carried out in the channels of various sharp, (Fig. 1.16, e), including regular triangular bundle ($1.0 \leq$ s/d ≤ 1.2) and non-standard edge channels (hexagonal models are extensively used). As the most simple channel a concentric annular channel is used. Separable tubes of a different diameters ensure a change in the width of annular channel.

Hypothesises on the constancy of the factor k in (1.7) and on the possibility to confine the fundamental contribution element by the lines passing through the electrodes are true in the sensors mentioned. As empirical data have been derived from the hypothesis, they are approved in solving some problems of magnetic hydrodynamics followed by quantitative estimations. Let us consider some examples.

Sensors containing no shield rings. An analytical solution for the most simple model of the uniform flow in annuli, with the internal cylinder containing permanent magnet (Fig. 1.17, a) [35, 43, 45], shows that difference in potentials originated at the surface of internal cylinder between two points $\Delta U(r_o)$ varies in proportion to the coolant velocity (W), electrical conductance of the wall (σ_w) and liquid (σ_f) and sum of magnetic fluxes $\sum_m \Phi(2\Delta\varphi)$ over separate harmonics m involved through the weight function f_m, as

$$\Delta U(r_o) = \sum_{m=1,3,5}^{\infty} u_m = 0.5 \cdot W \cdot \Psi \cdot \sum_{m=1,3,5}^{\infty} f_m(R/r_o, \gamma)\Phi_m(2\Delta\varphi) \qquad (1.9)$$

$$\text{where } f_m = \frac{1 + (r_o/R)^{2m}}{1 - (r_o/R)^{2m}\gamma}$$

$$\gamma = 1 + \frac{1 - \sigma_w/\sigma_f}{1 + \sigma_w/\sigma_f}; \quad \Psi = 1 + \gamma; \quad f_m = \frac{1 - (r_o/R)^{2m}}{1 - (r_o/R)^{2m}\gamma} \qquad (1.10)$$

33
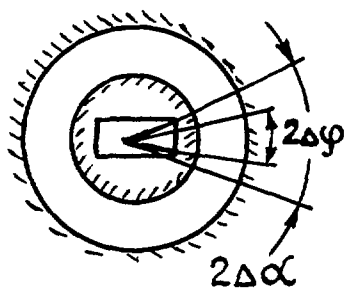
$$\Delta U(r_o) = \sum_{m=1,3,5}^{\infty} U_m = \frac{1}{2} W\psi \sum_{m=1,3,5}^{\infty} f_m\left(\frac{R}{r_o}, \gamma\right) \Phi_m(2\Delta\varphi);$$

$$\gamma = \frac{1 - \mathfrak{S}_w/\mathfrak{S}_f}{1 + \mathfrak{S}_w/\mathfrak{S}_f}; \quad \psi = 1 + \gamma; \quad f_m = \frac{1 + (r_o/R)^{2m}}{1 - (r_o/R)^{2m}\gamma}.$$

a)
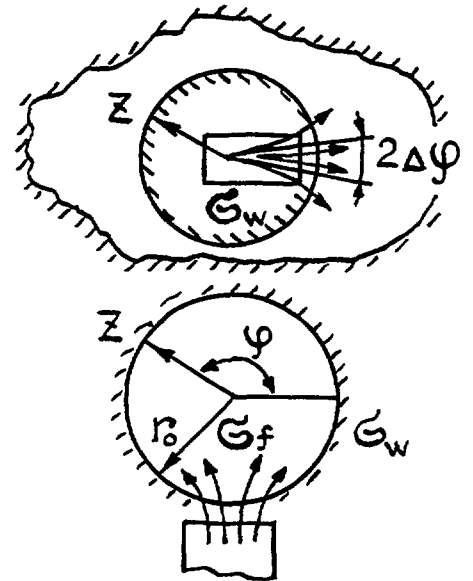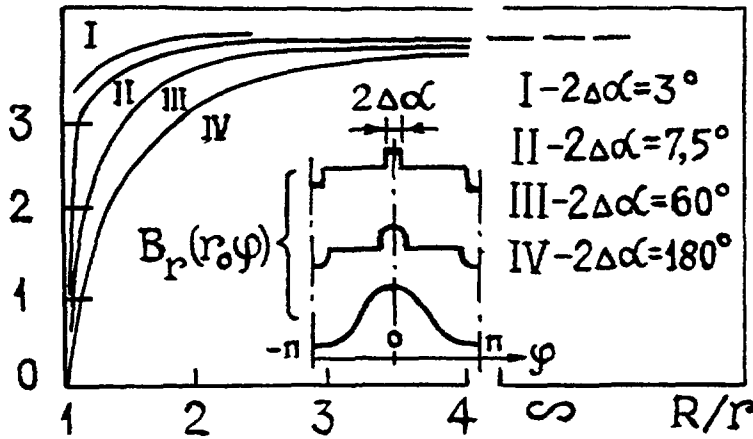
$$\Delta U(2\Delta\varphi) = \iint W(z)\, G(\Delta\varphi, z)\, dX\, dY$$

$$Z = X + iY$$

c)
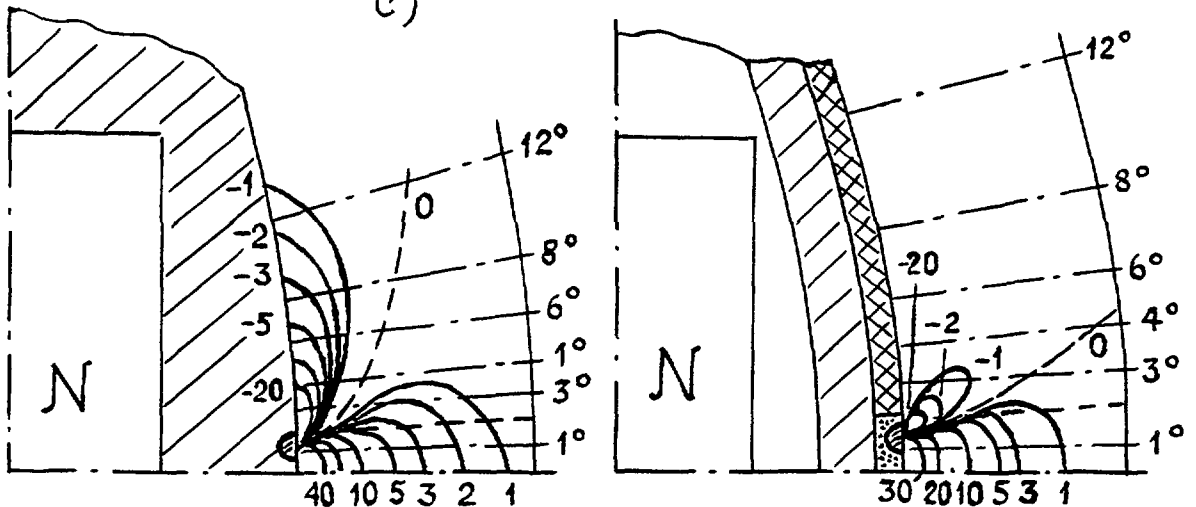
Fig. 1.17.   Theoretical foundation of electromagnetic technique to measure liquid metal local velocity.

where R, r_o - external and internal radii of annuli, respectively. Values f_m appears to approximate asymptotically an unity with the width of annular clearance, making up a series of functions $f_m(r/r_o)$, which converge to the Θ-function, as $m \to \infty$:

$$\Theta(R/r_o - 1) = \begin{cases} 1 & at \quad R/r_o - 1 \geq 0; \\ 0 & at \quad R/r_o - 1 < 0. \end{cases} \tag{1.11}$$

As the function f_m increases with R/r_o, signal also rises with R/r_o. Magnets possessing the concentrated field (top harmonics of m) give the faster signal saturation, then ones of lesser concentrated field (low harmonics of m).

The preceding is illustrated in Fig. 1.17-a as a dependence of $\Delta U/r_o Bw$ (that is inversely related to factor k in (1.17)) on R/r_o (here, B - induction at the liquid-wall boundary). Rectangular magnets having a field concentration angles $2\Delta\alpha$ equal to 3, 7, 5, 60° and cylindrical magnets with $2\Delta\alpha=180°$ are considered.

As the picture suggests, the condition $k=idem$ is complied with a greater order of accuracy for the concentrated magnets but an influence of 'side' areas of the flow on the signal generation is reflected to a lesser degree. For angles $2\Delta\alpha$ equal to 3 and 7.5 the hypothesis that $k=idem$ is rigorously fulfilled in a wide range of $1.1 \leq R/r_o \leq \infty$, and only in the narrow annular clearances the hypothesis breaks down due to impact of sensor mounted at the opposite wall.

Sensor with shielding rings. To detect operating features of the electromagnetic sensors equipped by the shielding rings the more common problem not restricted by the channel shape has been resolved Fig. 1.17 b. Cylindrical pin contains an infinite (in axial direction) magnet of arbitrary profile, that produces magnetic field at the pin surface. At the magnet end there is an insulation area, the remainder perimeter is the cooper ring. The pin is flowed by the electrical conductive liquid, with the conductance of the liquid being equal to conductance of the channel wall.

An assumption, that velocity is of arbitrary profile in the problem under consideration, is of principle importance, because it is the assumption which allows analysing the sensor location (it should be noted that in analysing combined channel in the form of pin bundle the velocity value must be considered as equal zero in the places of the pins location.

Definition of fundamental contribution area. Field of the values for weight function (Fig.1.17 c) is exemplified by a positive and negative contributions (central and side areas relative to the electrodes, respectively). The full signal is determined by the signals' sum. Ratio between the areas of positive and negative contributions into signal depends on the character of magnetic field. Magnetic field narrowing in angle direction results in reduction of the negative areas' proportion.

In dependence of the weight function the area of fundamental contribution can be detected. In the sensor with cooper ring the area mentioned is less than fundamental contribution area in the free of ring sensor by a factor of 2. Thus, the availability of cooper ring at the cylinder surface results in the more concentrated distribution of weight function in an area close to electrodes as compared with variant where ring is lacking.
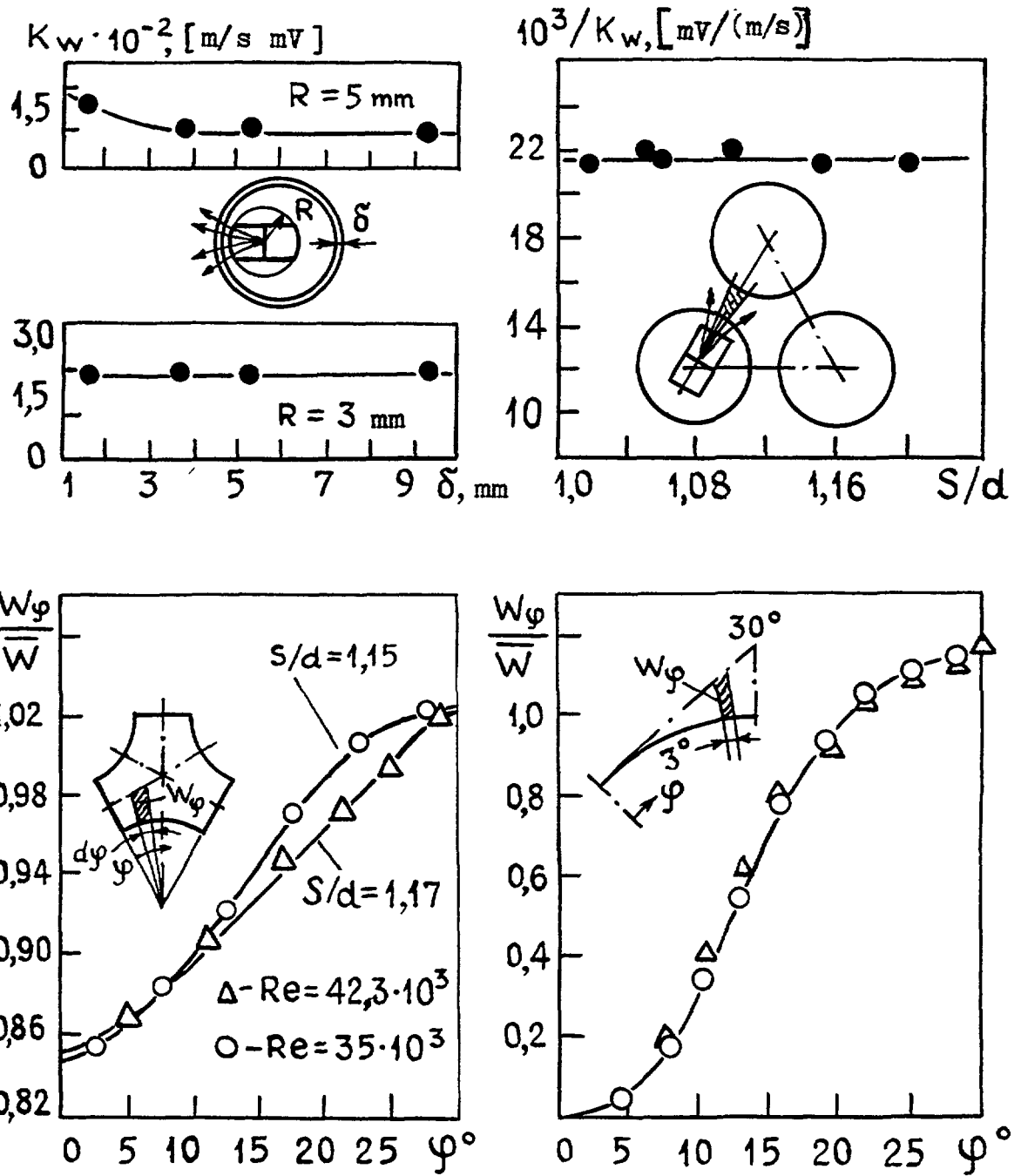
Fig. 1.18. Experimental validation of electromagnetic
technique.

A knowledge of weight function allows an approximation due to limitation on the fundamental contribution area to be estimated. In particular, it has been shown that the magnet of definite properties and under conditions of uniform velocity if angle between the electrodes is $2\Delta\varphi=6°$, forms the area which account for $11°$ without cooper ring and $7°$ with cooper ring. The availability of the ring of armco steel (Fig.1.16 a) exerts additional action on the weight function field. Although the problem did not resolved, experiments have indicated that limitation on the fundamental contribution area by the angle $2\Delta\varphi=3\div5°$ allows an accuracy of the final results to be not worse than 1% for the most practical part.

The extent of fundamental contribution in radial direction is much superior to the thickness of near wall layer, within the which the main velocity varies. Then, variation in fundamental contribution area in radial direction does not change the mean velocity. For convenience the fundamental contribution area can be assumed to be equal to the distance between the wall and the maximum velocity line or, in specific cases, between the walls of the channel.

On an influence of the opposite wall on the sensor signal. The greatest influence of adjacent wall on signal appears in the event, when the wall surrounds sensor (annuli), and the minor one when the wall has a curvature. In all cases an influence of the wall on the signal generation sharply decreases with the distance between the sensor and the wall, as well as the magnet becomes smaller (the «wall effect» disappears practically when magnets of definite size is used). The wall effect sharply decreases as cooper ring is used (magnetic field in the area close to electrodes becomes more local): in bundle with s/d =1.02 this effect does not exceed some percents, whereas the sensor without cooper ring gives ~ 15%. The availability of additional armco ring results in the effect is completely eliminated.

Experimental validation of the hypothesis that proportional factor between e.m.f. and coolant velocity is constant. Sensors with the magnet of length 10,8 and 6mm (Fig. 1.18 a) were tested in axial flow. Proportional factor k has been realised to be independent on the width of annular.

On checking hypothesis $k=idem$ in axial flow through the various bundle are shown in Fig.1.18 b. As the figure indicates, value of k does not depend on pith-to-diameter ratio. The hypothesis of the combined axial-transverse flow has been checked in the model of heat exchanger BN type [40,41] (see Fig. 1.14). The local coolant velocity distribution along the tube was measured by electromagnetic sensors which were moved in axial and azimuthal directions. Flow balance in every cross section (i) between the inlet and outlet windows:

$$V_i = \Omega\left(\sum k\overline{e_n}\right)_i = 7\Omega\overline{W} = V = const \qquad (1.12)$$

converged to better than 0.5%, and proportional factor k in (1.12) written for simplicity for 7-pipe modes was defined as constant value. Here $\overline{e_n}$ - averaged over perimeter signal of the n-pipe, Ω - coolant flow section around the n - pipe, $\overline{w}$ - averaged over the model cross-section coolant velocity .

Inherent velocity measured in test.

Axial flow. Fig.1.18-c shows velocity fields in the channels of regular triangular bundles produced by cylindrical smooth pins positioned with the pitch-to-diameter ratio s/d=1.0 and s/d=1.15. Electromagnetic measurements are in agreement with the other authors' data, which have been obtained by traditional techniques based on Pitot tubes, as well as with the predictions by well-known procedures.

Fig. 1.19 presents the axial velocity distribution over perimeter of near wall pins in fast reactor subassembly model (smooth pins). Data gained in the various combined channels (shape of the channels see in Fig. 1.16 e) is analysed below in Chapter 4. The results mentioned have been generalised and now used in thermal hydraulic analysis of reactors.

Transverse flow patterns within the gap between the wire wrapped pins (fin-to-cladding) follow approximately a sine function (Fig. 1.20), that reflects a mechanism of convective interchannel mass exchange. Electromagnetic technique has allowed the processes of interchannel exchange in reactor core to be studied in detail and appropriate constants to be derived (see Chapter 3).

Combined axial-transverse flow in the model of intermediate heat exchanger is demonstrated in Fig. 1.21 and 1.22. From the data presented it follows an important practical conclusions descriptive the heat exchanger performance in terms of hydrodynamics (see Chapter 5).

1.5. LIQUID METAL FACILITY 6B

The main functions. Experimental facility 6B (Fig.1.23) is designed for studying hydrodynamics and heat transfer in the models of reactor core and heat exchangers metal-metal (coolants: Na, NaK). Detail description of the loop is given in [45].

The general fundamental problems of liquid metal heat transfer and hydrodynamics, and in particular, fields of velocity and temperature are studied by local measurements of coolant and wall temperatures using micro thermocouples, and local velocities (flow rates) by electromagnetic sensors. Based on the results gained in experiments the in-pile fuel pin temperature behaviour is established, as well as operating efficiency of the heat exchanger equipment.

The main parameters are as follows: coolant flow rate (Na or NaK) up to 150 m³/h, temperature 20÷450°C, pressure up to 1.0 MPa, reference power ~ 1.2 MW, liquid metal volume - 1 m³.

Facility engineering. The rig 6B includes three circuits: first - NaK, second -Na, third -NaK, with the first and second circuits being the main. They are intended for performing experiments on the models simulating reactor core and liquid metal heat exchangers. The third circuit is designed for cooling the cold catchers in the first and second circuits.

Electromagnetic pumps (Fig. 1.24) are intended to produce liquid metal circulation. The operation of the pump is based on interaction of rotary alternating magnetic field in stator with the induced magnetic field in liquid metal. The pump involves stator and core (rotor). The space between stator and core representing annular clearance is packed in liquid metal.
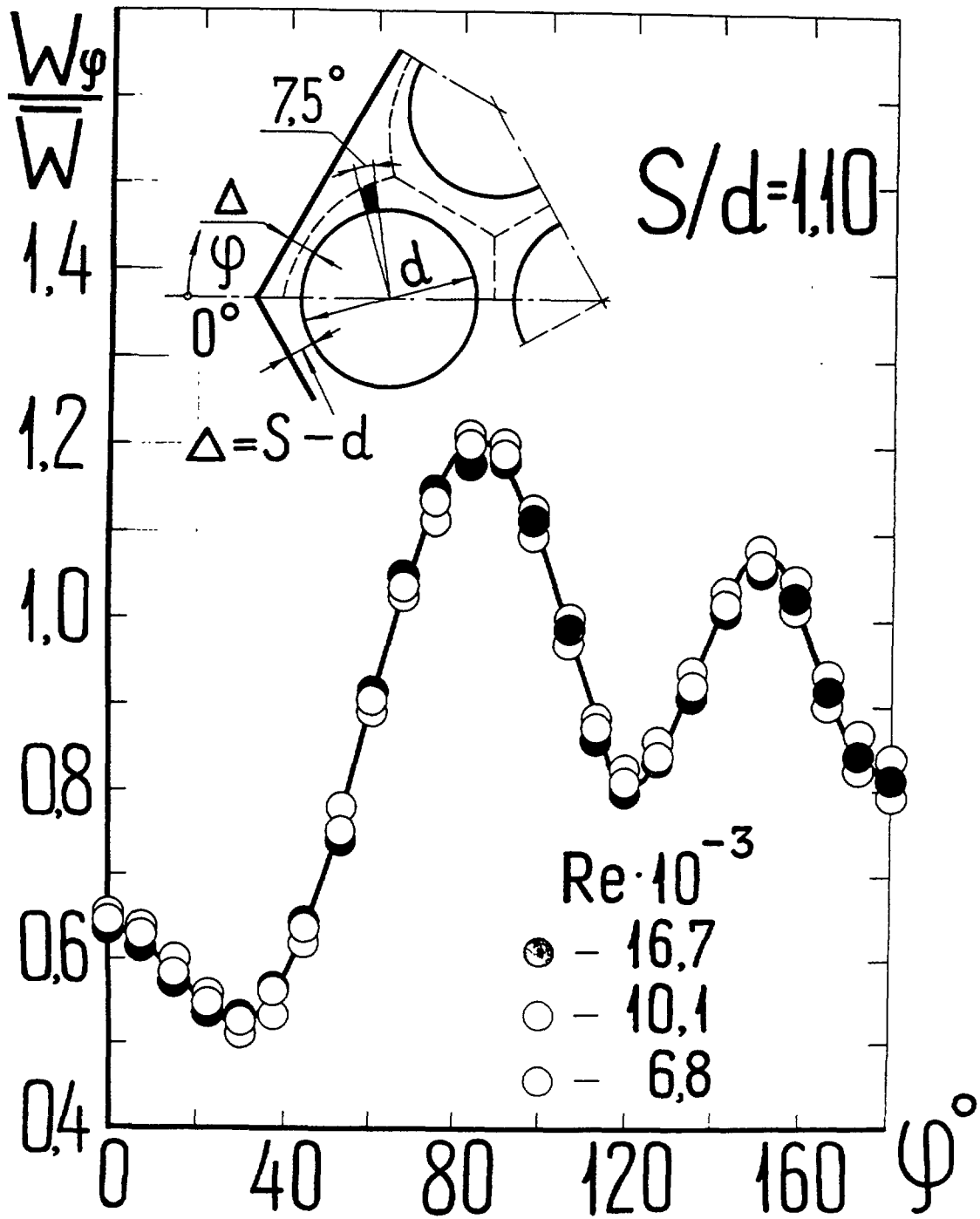
Fig. 1.19. Dimensionless velocity along the smooth corner pin perimeter.

$$d = 19 \cdot 10^{-3} \, m$$
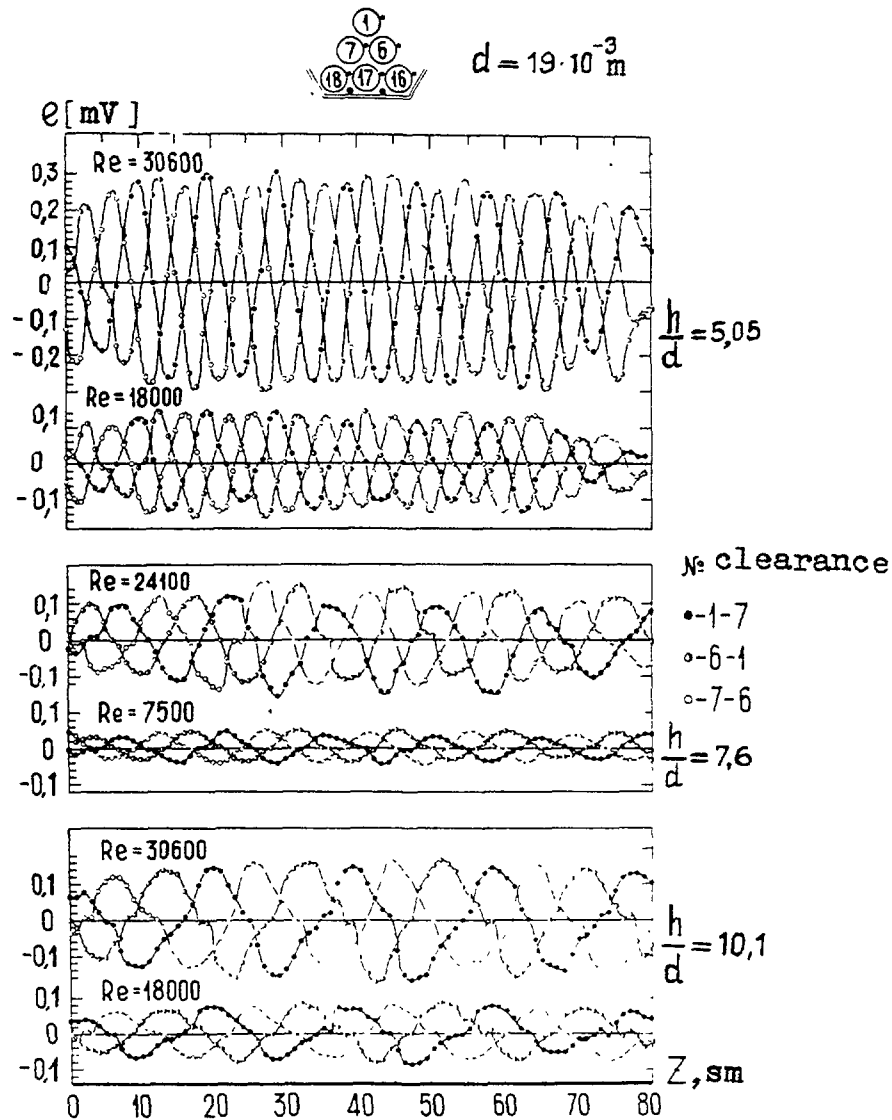
Fig. 1.20. Sensor signal with the channel length at various wire wrap pitches and Re numbers.

The stator slots receive a three-pass winding that induces an alternating magnetic field shorted to the core. In response to the interaction of magnetic field with induced in liquid metal currents a magnet rotates within the clearance. Three-pass fins welded to the wall impose directional motion. Heat given out by the stator windings is removed by the water flowing in a jacket. The winding temperature is measured by thermocouples.

The pumps mounted in the first and second circuits have the following characteristics coolant flow rate (NaK and Na) ~150 m^3/h, pressure head 6 kg/cm^2, power consumed ~ 170kW, maximum coolant temperature ~500°C, allowable temperature of winding ~ 180°C, maximum allowable current ~ 250 A.

Electromagnetic pump in the third circuit is of the following parameters: coolant flow ~ 10 m^3/h, pressure head ~ 10 kg/cm^2, electrical power ~14 kW, maximum coolant temperature ~300°C, temperature of winding ~ 180°C, allowable current ~ 40 A.

40
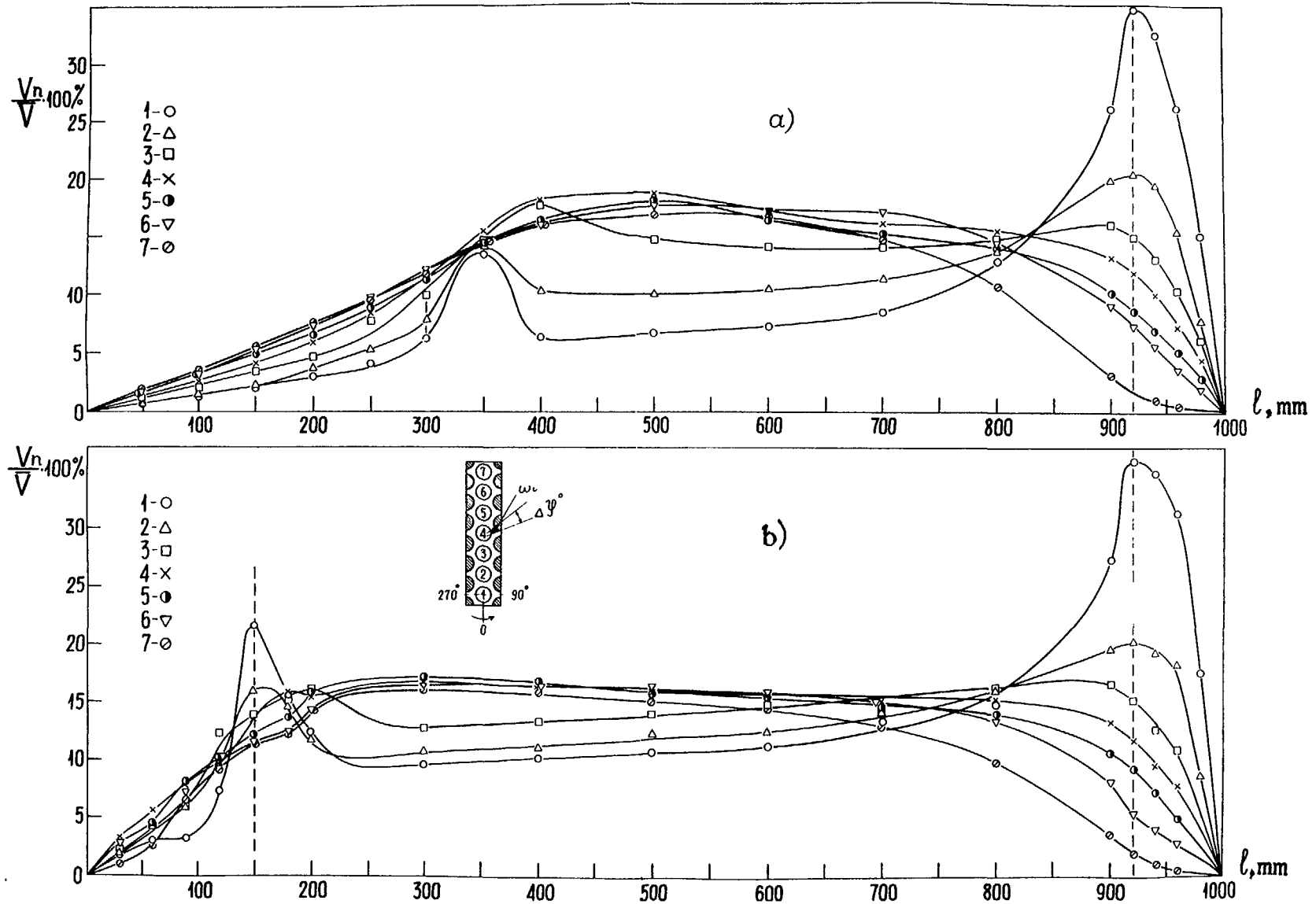
Fig. 1.21. Axial coolant flows (V_n) in sections around pipes «n» (n = 1÷7) with the pipe length. Inlet window height: 350mm (a) and 150mm (b).
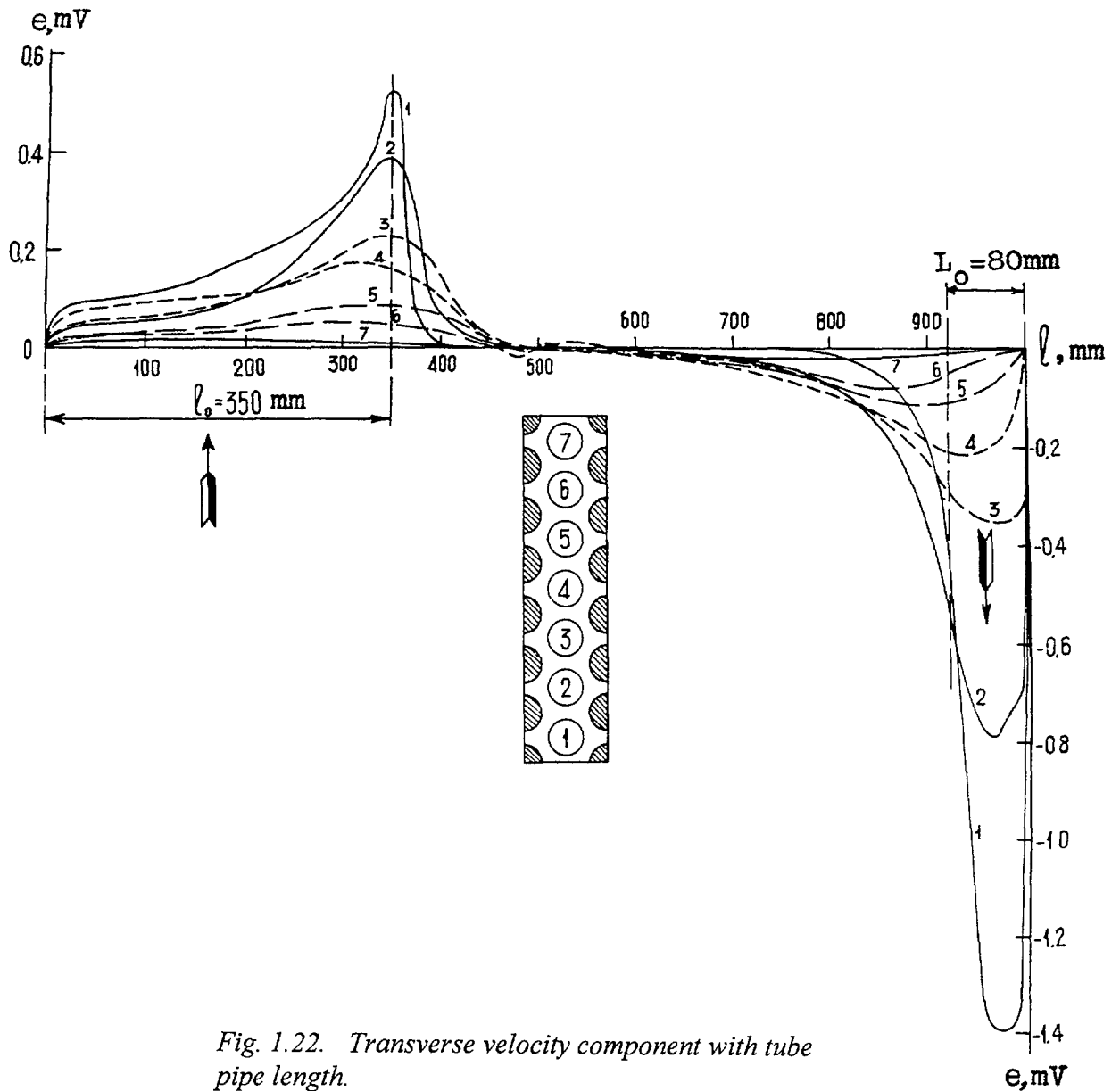
Fig. 1.22. Transverse velocity component with tube pipe length.

Carbon heaters (Fig. 1.25) serves to produce appropriate temperature of sodium coolant. From the pump 2 a part of metal is sampled for the carbon heaters, with the heating up to needed temperature, and is directed to the chamber where it is mixed with the main flow of sodium.

The heater consists of the carbon tube enclosed by cylindrical wrapper where vacuum or filled in inert gas. The tube has longitudinal slits allowing the tube to be of needed resistance. To reduce the end losses the carbon tube has the bottom thermal shields. Cylindrical wrapper is enclosed the heater body. In the space between body and wrapper a sodium flows from the top down. Guide fins create rotation, that produces an uniform heat removal from the wrapper surface. Power is applied through the water cooled a cooper current feeds. The feeds are in a contact with the carbon tube by the natural fall. Design characteristics of the carbon heater are follows: power -180 kW, voltage -94 V, current - 2000 A, mean temperature ~ 800°C, maximum coolant flow ~ 10 m³/h, surplus pressure of inert gas -0.3÷0.5 kg/cm².

42
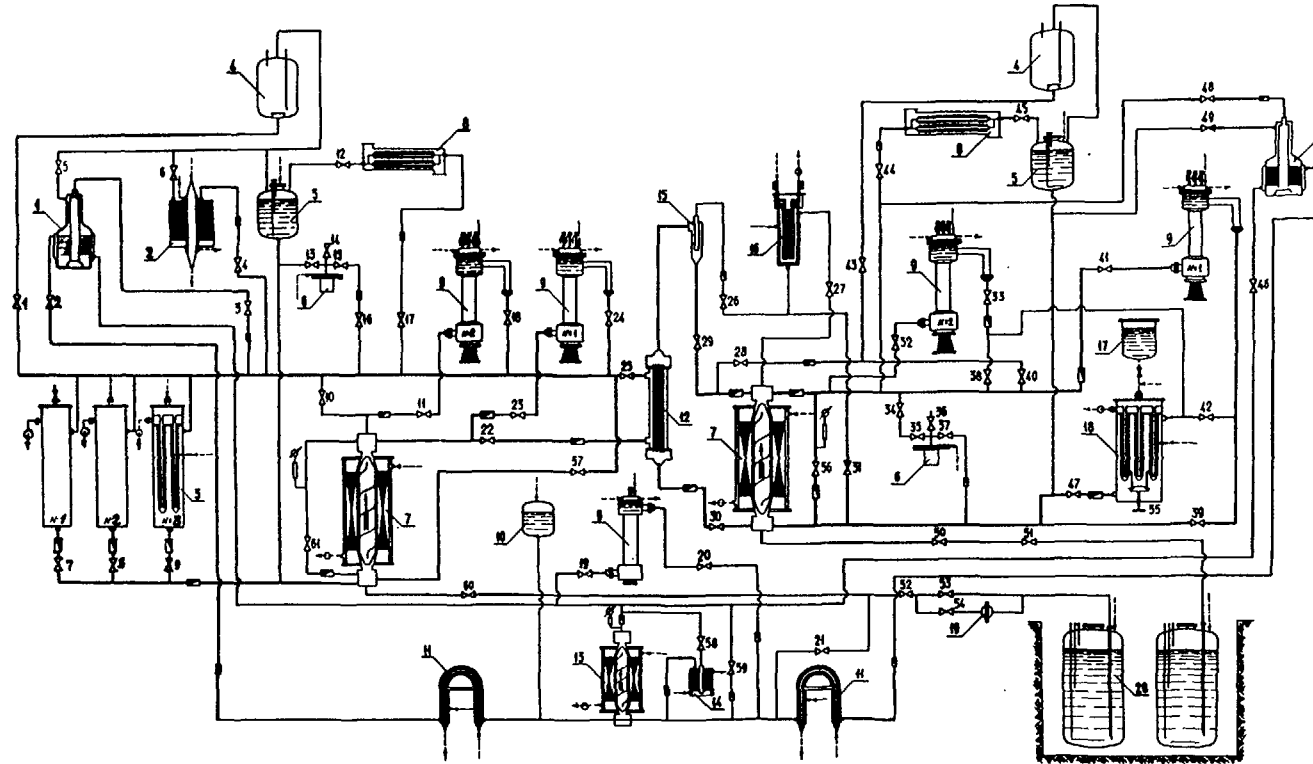
Fig. 1.23. Schematic diagram of three-lop contour: 1. 2 - cold catcher, 3. 11, 18 - cooler 4, 5, 10, 20 - tank, 6 -sampler, 7 - electromagnetic pump, 8 - air cooler, 9 - test section, 12 - recuperator, 13 - electromagnetic pump, 14 - cold catcher, 15 - mixer, 16 - carbon heater, 17 - water heating tank, 19 - filter

: ——— - the main loop, ⊸⋈⊢ - valve, magnetic flow-meter, ∅ - manometer,

- - - - -flown relay, — — —¯ -water line, — · — · — gas line.

Coolers (Fig.1.26) in first and second circuits are designed to remove a heat released in the models. The third circuit cooler is meant for heat removal in the catchers of first and second circuits. Coolers 1 and 2 have the same structures. They involve 30 triangularly arranged cylindrical elements, with every element representing three pipes (internal, intermediate, external) mounted one inside the other. Water comes into the internal pipe, flows from the top down and leaves for the pocket between internal and intermediate pipes. Another pocket between the intermediate and external pipes is vacuumed or filled in inert gas. The elements are flowed by liquid metal on the outside, thus, the cooler design excludes the possibility that water be in contact with liquid metal in the event of loss of pressure. Contact can be caused just concurrent water and metal leaks. However, the such an event is almost incredible. An intermediate pocket is controllable with vacuum or inert gas pressure by electromagnetic vacuum-meters.

Pipes are welded overhead together with the plats of the cooler or the upper flange, whereas in the lower part they are free to be spaced by the grid . Internal pipes are withdrawn together with the cooler's flange. It allows the pipes to be cleaned at regular intervals. Vertical arrangement of the coolers made the mounting much easier. The cooler in the second circuit (sodium coolant) has six internal elements separated from the other elements by the curly cover, which equipped with the sodium valve. Thus, in this cooler , apart from the control of heat removal due to change in water flow through the cooler, we can regulate heat removal by redistribution of sodium flow between the internal and edge areas of the cooler.

Characteristics of the coolers in circuits I and II are as follows: water flow $-0 \div 6 \cdot 10^{-3}$ m^3/h, water pressure - 6 kg/cm^2, water inlet temperature -20°C, water outlet temperature - 30°C, water velocity -0.36 m^3/s, sodium flow $-0 \div 27.8 \cdot^{-3}$ m^3/s, pressure -10 kg/cm^2, velocity - $0 \div 1.15$ m^3/s, inlet temperature ~300°C, outlet temperature ~ 290°C, allowable sodium temperature in the cooler II ~600°C.

To remove heat flow the first circuit at low temperatures the cooler are designed here, with the sodium alloy running through the internal pipes arranged in regular triangular manner, and external pipes being flowed by water. The spaces between the internal and the external pipes are united into the header and filled with the Wood alloy having melting temperature in 60°C.

Oxide catchers (Fig. 1.27, 1.28) are designed for purification of liquid metal from oxygen. The operation of the catcher is based on oxide precipitation in a catchers space filled with the stainless steel chip and cooled by a water (low temperature catcher - Fig. 1.27) or by NaK alloy (high-temperature catcher- Fig. 1.28).

Water cooled catchers are designed in the circuits I and III of the 6B facility. They have either internal or external cooling. In one case or another, a heat from liquid metal is conveyed to water through the cooper wall. Operating conditions of low-temperature catcher are as follows: circulation velocity -up to 4mm/s, inlet temperature- up to 250°C, water pressure - up to 3 kg/cm^2. NaK catchers are designed in the circuits I and II . Any one of these catcher consists of internal pipe which receives coolant to be chained (flow from top to bottom), the main space filled with stainless steel chip (flow from bottom to top and external cooling space with NaK (flow from bottom to top). Operating conditions of the main coolant
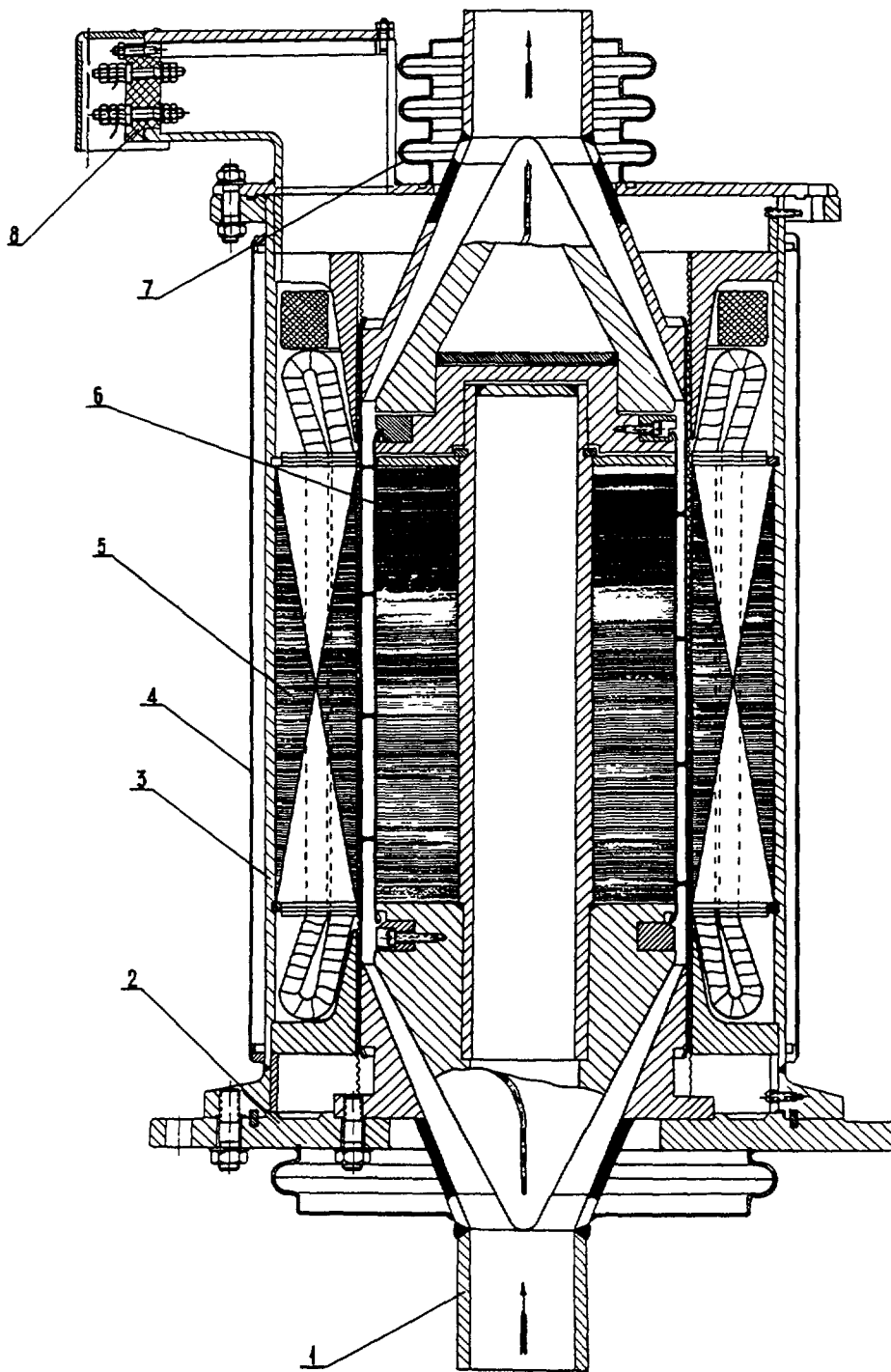
Fig. 1. 24. Electromagnetic pump: 1 - inlet connection,
2 - base, 3 - body, 4 - cooling shell, 5 - wrap, 6 - stator
7 - compensator, 8 - supply box.
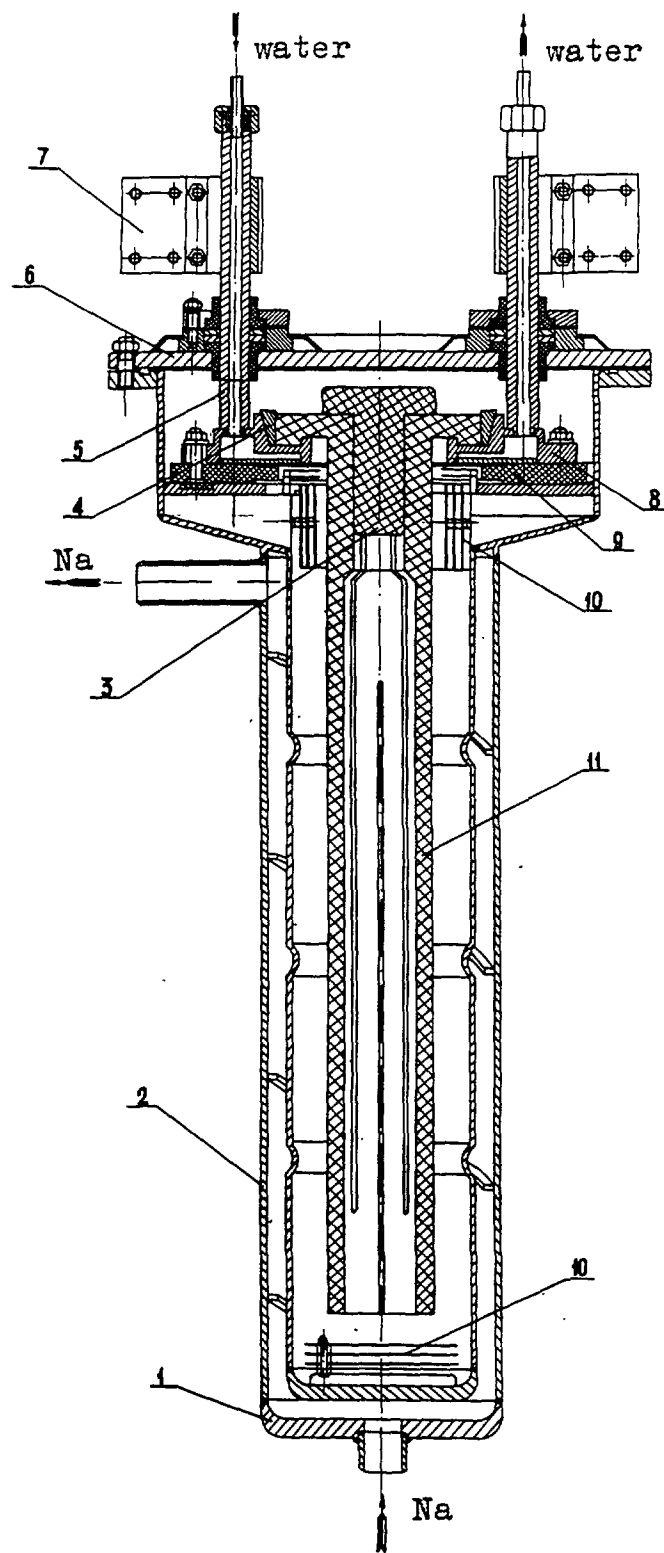
Fig. 1.25. Carbon heater: 1 -bottom, 2- body, 3 - plug,
4 - wedge, 5- current supply, 6- cover, 7- wire, 8 - current supply,
9- ring, 10 - shield, 11 - heater.
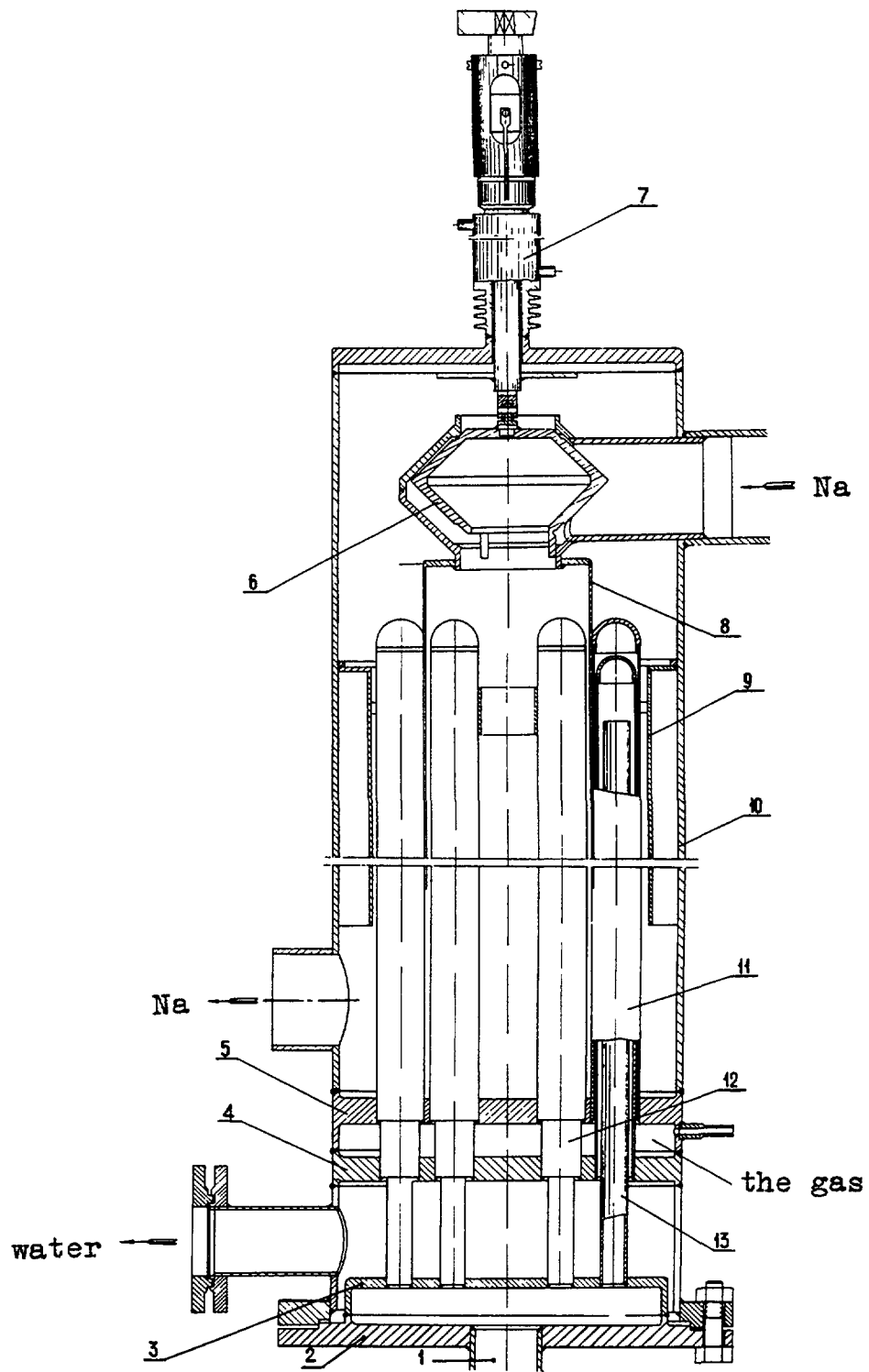
*Fig. 1.26. Sodium-water heat exchanger: 1 - inlet connection,
2 - flange, 3, 4, 5 - pipe grids, 6 - valve disc, 7 - valve,
8 - shell, 9 - displacer, 10 - body, 11 - pipe 50×3,
12 - pipe 42×2, 13 - pipe 27×2.*

Fig. 1.27. Cold catcher:

1 - bottom, 2 - grid, 3 - wrapper tube, 4 - packing of stainless steel chip, 5 - displacer, 6 - cover, 7 - thermocouple, 8 - shell, 9 - wrapper tube.
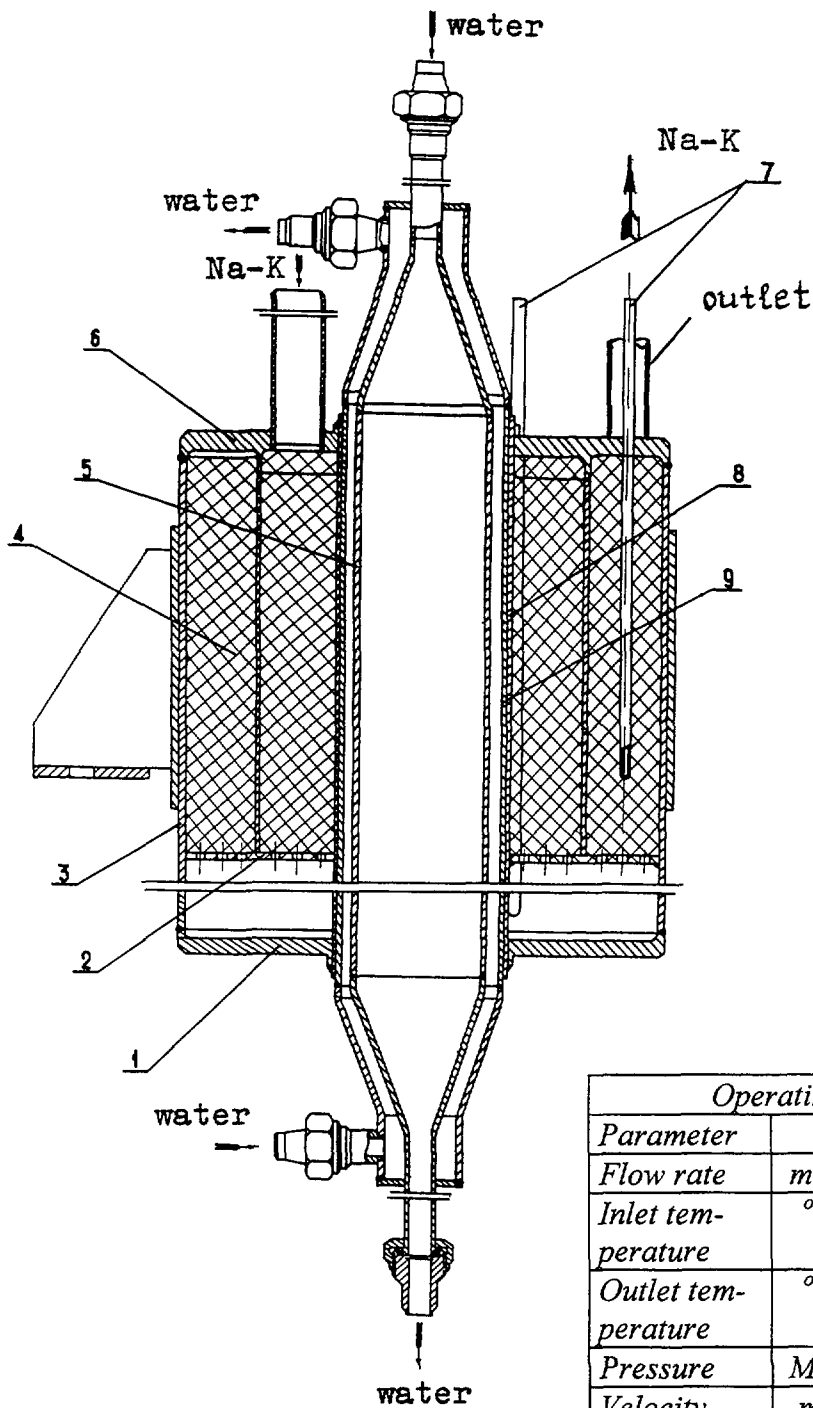
Operating condition			
Parameter		Na-K	water
Flow rate	m^3/h	0.83	3.0
Inlet temperature	^{o}C	100	20
Outlet temperature	^{o}C	80	23
Pressure	MPa	1	0.3
Velocity	m/s	0.04	0.028
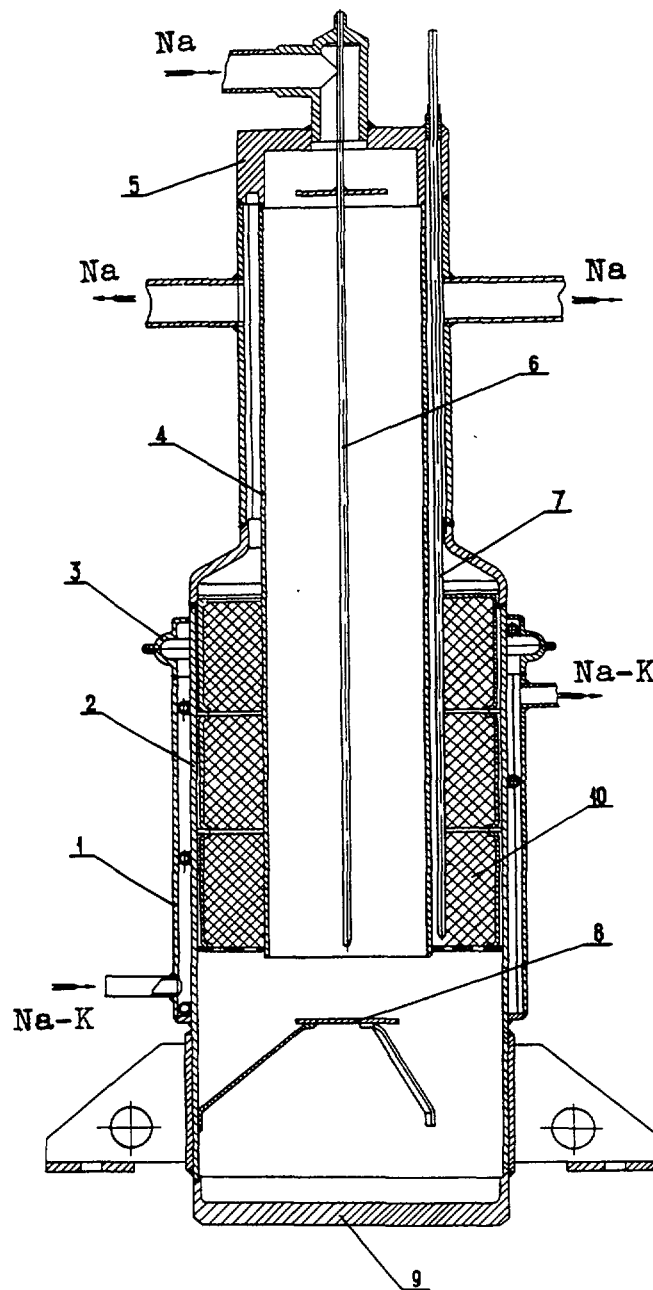
Fig. 1.28. Cold catcher :
1 - shell, 2 -body, 3 -compensator, 4 -wrapper tube
5 - cover, 6, 7 - thermocouple, 8 - canopy, 9 - bottom,
10 - stainless steel chip.

Operating condition		
Parameter	Na	Na-K
Inlet tempera-ture, °C	400	40
Outlet tempera-ture, °C	280	90
Pressure, MPa	10	3
Flow rate, m³/h	0.77	3.5
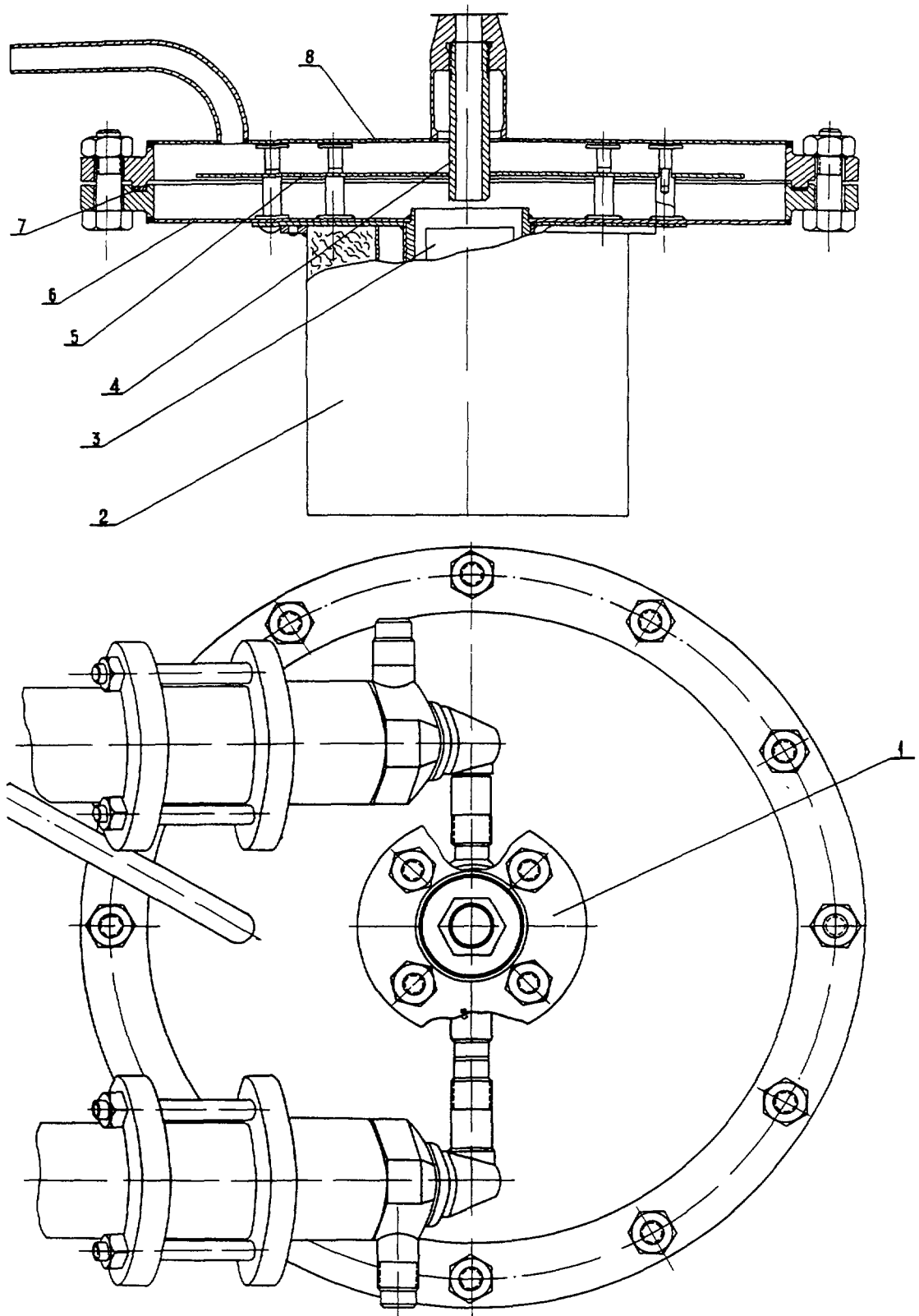
Fig. 1.29. Sampler - distiller:
1 - central valve, 2 - furnace, 3 - barrel, 4 - drain,
5 - reflector, 6 - bottom flange, 7 - gasket, 8 - top flange.
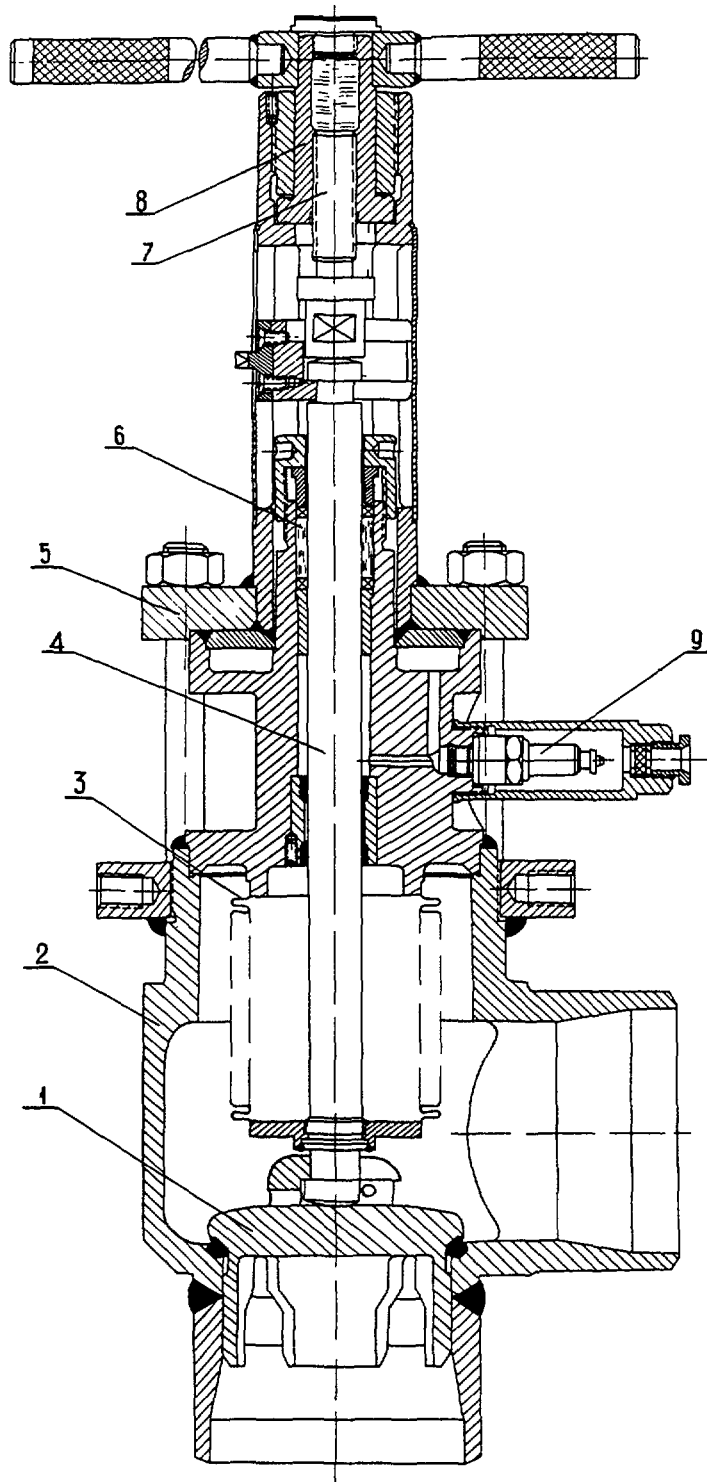
Fig. 1.30. Sylphon valve:
1 - valve, 2 -body, 3 - sylphon, 4 - rod, 5 - flange,
6 - seal, 7 - screw, 8 - nut, 9 - sensor.
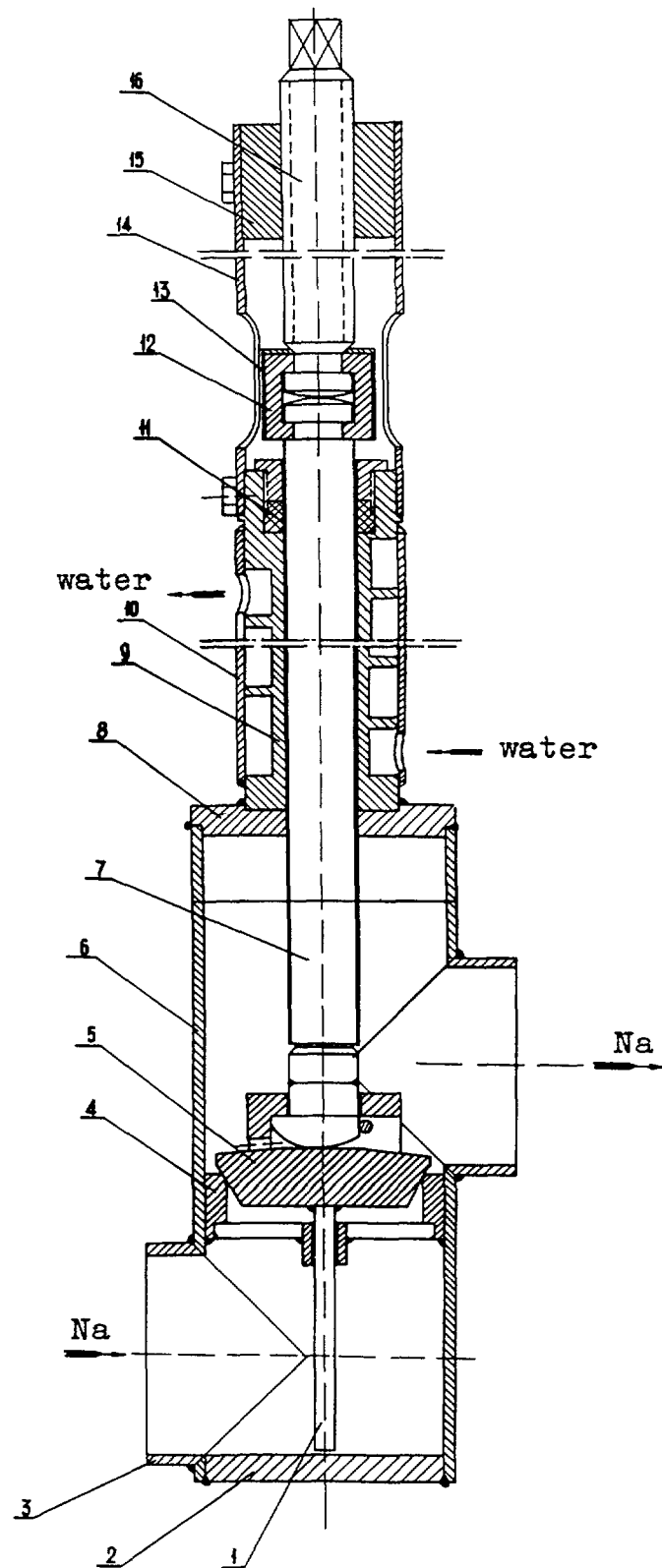
Fig. 1.31. Valve of cooling seal:
1 - guide rod, 2 - bottom, 3 - connection, 4 - ring, 5 - valve,
12 - split sleeve, 13 - cap, 14 - barrel.

(NaK in the circuit I, Na in the circuit II): flow ~0.8 m³/h, pressure -up to 6 kg/cm², inlet temperature - up to 400°C. The same of the cold coolant: flow -3.5 m³/h, pressure -up to 10 kg/cm², inlet temperature - 40°C, outlet temperature -90°C.

Sampler-distillators (Fig. 1.29) are designed for sampling sodium and NaK alloy (weight 100g), and ensuing distillation in vacuum and determination of the oxygen in oxides. Sampler consists of the vacuum chamber and three valves. The space chopped off by the valves is that from which the sampling is performed. In order that metal should not be splashed around during period the sample is drained into the barrel designed within the vacuum chamber, a special pipe is provided. To improve washing the pipe is made as removed one. Given temperature of distillation is supported with use of the furnace of variable power. Temperature is measured by thermocouples. Vapour of Na and NaK condenses at the surface of the bottom flange and the breaker that keeps the liquid metal vapour from entering the vacuum line. To extract barrel with remaining after the distillation the sampler is disassembled.

6B facility is completed with the **sylphon sealing** (Fig. 1.30) and **seal of frozen sodium** (Fig.1.31), as well as devices to measure temperature, flow and pressure of coolant. Among the ancillary structure are tanks, mixers, catchers, filters and so on.

Water service is from the main water header, where the pressure valves connected with the associated units are mounted in. **Gas-vacuum service** is designed to evacuate loop and to feed inert gas into the units.

Electric design provides the current supply through the following voltage controller:
- electromagnetic pumps - through the automatic transformators ATMKT-250/0.5,
- electrical heaters - through the automatic transformators AOMKT-250/0.5 or inductive controller MA-195.750 kVA,
- carbon heaters -through the inductive voltage controller MA-195 and step down transformator OCY-80.

6B loop incorporates the working place for operator equipped by sensor reading panel and distributing frame to control thermal and electric equipment.

CONCLUSIONS

1. Analytical analysis of fast reactor thermal hydraulics is based on two main approaches: subchannel analysis and a porous body model. The first is based on solution of governing momentum, mass and energy conservation equations written for channels formed by the adjacent pins. In the framework of the second the pin bundle is represented as anisotropic porous body with distributed volumetric power production. The possibility for prediction of non-nominal performance due to diabatic conditions at the subassembly wrapper, accidental deviations of parameters, deformation of subassembly in campaign, transient conditions and others receive primary attention in development of modern codes.

2. The following experimental techniques serve as a basis for gaining thermohydraulic constants:
    - approximate thermal modeling of fuel pins including development of the heaters which produce uniform or variable power distribution;
    - technical modeling of reactor core and heat exchangers;

- local measurement technique using special miniature sensors (electromagnetic flow meters, micro thermocouples);
- high powered liquid metal facilities allowing for a great coolant flow and wide range of temperature variation, on which large-scale experiments can be carried out with as "natural" coolant (sodium) and simulating (sodium-potassium alloy) one.

3. Electromagnetic technique intended for measurement of local velocity of liquid metal in combined channels allows the mock-up subassembly manufactured with a standard technology, except that fuel is absent, to be used. The method was validated by predictions and experiments, with the design of miniature local sensors and calibration principles developed. This method is used to measure as longitudinal (axial) and transverse components of liquid metal local velocity (flow rate) in bundles of smooth or wire wrapped pins. It was been shown that the method is very effective as applied to combined flow. The method is convenient to use for studying distributions of local flows around and along the pins arranged in deformed bundles (stream flow, pin bending, blockages and so on), in non-standard channels, at the bundle outlet (headers and chambers) and so on.

REFERENCES

[1] Zhukov A.V., Kirillov P.L., Matjukhin N.M., et al. Thermal Hydraulic Calculation of LMFBR. M., Energoatomizdat, 1985 (in Russian).

[2] Recommendations on Thermal Hydraulic Calculation of Fast Reactor Core. PTM 1604. 008-88. State Committee on Nuclear Energy. M., ONTI IPPE, 1989 (in Russian).

[3] Zhukov A.V., Sorokin A.P., Matjukhin N.M. Interchannel Exchange in Fast Reactor Subassemblies. M., Energoatomizdat, 1991 (in Russian).

[4] Sha W.T. An Overview on Rod Bundle Thermal-Hydraulic Analysis. Nucl. Eng. and Des., 1980, v. 62, p. 3-21.

[5] Subbotin V.I., Ibragimov M.H., Ushakov P.A.. Hydrodynamics and Heat Transfer in Nuclear Power Plants. M., Atomizdat, 1975 (in Russian).

[6] Yeung M.R., Wold L. Multi-Cell Slug Flow Heat Transfer Analysis for Finite LMFBR Bundles. Nucl. Eng. and Des., 1980, v. 62, p. 101-121.

[7] Zhukov A.V., Kirillova G.P. Temperature Behavior at Entrance Section of Pin Bundle in Turbulent Liquid Metal Flow. Preprint IPPE-715, Obninsk, 1976 (in Russian).

[8] Milbauer P. Application of Finite Elements Method for Calculating Turbulent Flow through the Non-round Tube. Hydrodynamics and Heat Transfer in Core and Steam Generator of Fast Breeder Reactors, v.1, Prague, 1984, p.104-105.

[9] Trevgoda V.M. Numerical Calculation of Laminar Velocity and Temperature Behavior in Combine Geometry. Problems of Nuclear Science and Engineering. Physics and Eng., 1980, 4, p. 89-95 (in Russian).

[10] Sholochov A.A., Zasorin I.P., Minashin V.E.. Calculation of Temperature Behavior in Nuclear Reactor Fuel Elements. M., Atomizdat, 1978 (in Russian).

[11] Zhukov A.V., Sorokin A.P., Matjukhin N.M. Interchannel Exchange in Fast Reactors. M., Energoatomizdat, 1989 (in Russian).

[12] Stewart C.W., Rowe D.S. Advanced Continuous Fluid Eulerian Computation Scheme for Flows with Large Density Gradients. TANS, 1976, v. 24, p. 178.

[13] Novendstern E.H. Mixing Model for Wide Fuel Assembly. TANS, 1972, v. 15, p. 866-867.

[14] Chen B.C., Todreas N.E. Prediction of Coolant Temperature Field in the Breeder Reactor Including Interassembly Heat Transfer. Nucl. Eng. and Des., 1975, v. 35, p. 423-440.

[15] Bogoslovskaya G.P., Zhukov A.V., Sorokin A.P. et al. Code TEMP-M for Thermal Hydraulic Analysis of Fast Reactor Subassemblies. Preprint IPPE-1401, Obninsk, 1983.

[16] Kazachkovski O.D., Sorokin A.P., Zhukov A.V. et al. Lumped Parameters in Problems on Temperature Behavior in Deformed Subassemblies of Fast Reactors under Diabatic Boundary Conditions. Preprint IPPE-1672, Obninsk, 1985.

[17] Cronenberg A.W. et. al. A Single-Bubble Model for Sodium Expulsion from Heat Channel. Nucl. Eng. and Des., 1971, v. 16.

[18] Ishii M. Two-Fluid Model Hydrodynamic Constitutive Relations. Nucl. Eng. and Des., 1984, v. 82, p. 107-126.

[19] Spasskov V.P. et al. Complex of Programs to Predict Transient Thermal and Hydraulic Processes in Designing WWER. Problems of Nuclear Science and Engineering. Physics and Eng., 1981, 7 (20), p.72 (in Russian).

[20] Kolev N.I. Comparision of the RALIZA-2/02 Two-Phase Flow Model with Experimental Data. Nucl. Eng. and Des., 1985, v. 5, p. 217-237.

[21] Bogoslovskaya G.P., Bogatyrev I.L., Zhukov A.V. et al. Two-Liquid Model of Two-Phase Flow Prediction. Preprint IPPE-1991, Obninsk, 1991 (in Russian).

[22] Gerliga V.A., Kirillov V.V. Conservative Difference Scheme for Steam Generating Channel Dynamic Equations. Problems of Nuclear Science and Engineering. Physics and Eng., 1982, 6(19), p.43 (in Russian).

[23] Mironov Yu.V., Razina N.S., Fomicheva T.I. et al. Analysis of Transients in Nuclear Reactor Contours. Atomic energy, 1986, v.60, p.255-260.

[24] Kornienko Y.N., Kuzevanov V.S., Sorokin A.P. The Technique of Calculation of Non-equilibrium Two-Phase Flows in Pin Bundles Using Quasi-Two-Dimensional Approaches and Subchannel Approximation. Advanced in Gas-Liquid Flows, Winter Annular Meeting of ASME, Dassal, Texas. 1990, FED-vol 99, p. 321-330.

[25] Macdougall J.D., Lillington J.N. The SABRE Code for Fuel Rod Cluster Thermohydraulics. Nucl. Eng. and Des.. 1984, Vol. 82, p. 171-190.

[26] Ninokata H., Okano T. SABENA: Subassemby Boiling Evolution Numerical Analysis. Nucl. Eng. and Des.. 1990, Vol. 120, p. 349-367.

[27] Kumaev V.Y., Leonchuk M.P., Dvortsova L.I. Numerical Procedure for Calculating 3-D Coolant Flow in Pin Bundles. Preprint IPPE-1733, Obninsk, 1985 (in Russian).

[28] Karlow F.H., Amsden F.F. A Numerical Fluid Dynamics Method for All Flow Speeds. J. of Comp. Physics, 1974, v. 8, p. 197-213.

[29] Patankar S. Numerical Solution of Liquid Heat Transfer and Hydrodynamics. M., Energoatomizdat, 1984.

[30] Zhukov A.V., Sorokin A.P., Sviridenko E.Y. et al. Experimental and Numerical MODELING of Heat Exchanger Thermohydraulics. Models, Sensors, Techniques. Textbook, ONPEI, Obninsk, 1992 (in Russian).

[31] Ushakov P.A. Approximate Thermal MODELING of Cylindrical Fuel Elements. Liquid metals, M., Atomizdat, 1967 (in Russian).

[32] Lastman B. Radiation in Uranium Dioxide. M., Atomizdat, 1964, p.196-208.

[33] Subbotin V.I., Ibragimov M.H., Loginov N.I. Measurements of Velocity and Temperature in Liquid Metal. Atomic energy, 1968, v.25.

[34] Subbotin V.I., Zhukov A.V., Sviridenko E.J. et al. Experimental and Theoretical Validation of Electromagnetic Technique. Heat Transfer and Hydrodynamics in Reactor Core and Steam Generators, Nove Mesto, Czech Republic, 1973.

[35] Zhukov A.V., Sviridenko E.J., Sorokin A.P. Electromagnetic technique to measure velocity and temperature fields in combined geometry. Proc. of Int. Conf. "Thermal Physics-96", Obninsk, IPPE, 1996, p.48-56 (in Russian).

[36] Zhukov A.V., Sviridenko E.J., Sorokin A.P. Sensors to Measure Liquid Metal Local Velocity and Flow Rate in Pin Bundles. Proc. of IPPE "Thermal Physic Measurement Techniques", ONTI IPPE, 1996, p.150-166.

[37] Zhukov A.V., Sviridenko E.J., Matjukhin N.M. et al. Measurement of Local Hydraulic Inter-channel Characteristics. Preprint IPPE-665, Obninsk, 1976 (in Russian).

[38] Zhukov A.V., Sviridenko E.J., Matjukhin N.M. et al. Study of Combined Flow in Bundle of Wire Wrapped Pins. Preprint IPPE-867, Obninsk, 1978 (in Russian).

[39] Zhukov A.V., Sviridenko E.J., Matjukhin N.M. et al. Study of Local Mixing Characteristics in Pin Bundles (Spacer Fin-to-Fin). Preprint IPPE-908, Obninsk, 1979 (in Russian).

[40] Ushakov P.A., Zhukov A.V., Yuriev Yu.S. et al. Local Hydraulic Characteristics in Fast Reactyor Heat Exchangers. Thermal Physical Investigations, M., VIMI, 1977.

[41] Zhukov A.V., Sorokin A.P., Sviridenko E.J. et al. Experimental and Numerical MODELING of Heat Exchangers. Hydrodynamics. Overview IPPE-0270-M., CNIIAtominform, 1995.

[42] Zhukov A.V., Sorokin A.P., Ushakov P.A. et al. Thermal Physic Validation of Temperature Behavior in Fast Reactor Subassembly Having Regard to Hot Spot Factors. Preprint IPPE-1816, Obninsk, 1986 (in Russian).

[43] Zhukov A.V. et al. Theoretical Validation of Magnetic Measurement Technique. Preprint IPPE-406, Obninsk, 1973 (in Russian).

[44] Catalogue of Facilities, Mock-up Reactors and Experimental Models. CEMR, KNTS-2, 1978, p.20-22 (in Russian).

56

Chapter 2

THERMAL HYDRAULIC SUBCHANNEL ANALYSIS

2.1. DEVELOPMENT OF SUBCHANNEL APPROACH

The first subchannel codes, which take into account a heat and mass inter-channel exchange, were developed for single-phase flows as applied to the detection of the hottest channel in the reactor subassembly (THINC-1,USA[1]; JOYO, *Japan* [2]; MISTRAL, *Germany* [3], TEMP, *USSR* [4] and others), and for two-phase flows (light water reactors) in order to evaluate a critical margins and to calculate temperature behavior under critical conditions (HAMBO, *Great Britain* [5,6], COBRA, *USA* [7], FLICA, *France* [8], POUCHOK, *USSR* [9] and others). Boundary conditions were written at the bundle inlet, with the macro-transport equations solved step by step along the channel. The codes' rating is presented in the Tables 2.1-2.3.

The need to study a blockades generated in the liquid metal fast reactor core has called for the development of the codes simulating the combined coolant circulation and strong transverse flow. Since the main challenge of the code is to provide means for prediction of non-standard structures, the code had to involve consideration of all types of subassembly flow deformation occurring in campaign (bending, blockades, coolant boiling, natural convection and so on). It should be noted that a large transverse coolant flows, as well as an availability of recirculation areas are possible in such an events.

Widening the class of the problems under consideration has resulted in the more combined statements of subchannel codes and has required recent advances in computation to be used for solution of source equations. Development of the completely governing codes (supercodes) are conditioned by the up-date methods intended to solve problems of continuous medium hydrodynamics such as MAC, ICE, SIMPLE and others.

Some generations of subchannel codes have been currently developed in different countries (*Russia, USA, Germany, UK, France, Japan* and others), which vary in a completeness of governing equations, numerical procedure of their solution and, respectively, are intended for the different problems. Although the main group of the codes have been developed in order to predict velocity and temperature fields in a separate subassembly with the smooth or wire wrapped pins, there are thermal hydraulic codes which allow the reactor core temperature behavior to be analyzed taking into account heat transfer and coolant interflow between subassemblies. A considerable number of the codes permits analysing a transient behavior in parallel with the study of steady state processes. A lot of codes have been developed to calculate two-phase characteristics, as well as an efforts have been made to develop liquid metal boiling codes. In all instances the more important factor is the inclusion of inter-channel exchange.

The difficulties associated with programming cause a number of codes to use the square mesh in the area under consideration, that is a porous body model is applied.

The most expanded and successive studies on development of subchannel codes were carried out in versions of COBRA, COMMIX, THI-3D (USA), SABRE (UK), POUCHOK, TEMP (Russia). So, among the versions of SABRE: the SABRE-1 and SABRE-2 were developed to predict single-phase steady or transient flows in subassemblies; SABRE-3 and SABRE-3D are used to predict two-phase flows in pin bundles.

Table 2.1 Rating of the codes predicting stabilised coolant flow

Code	Heat exchange							Momentum exchange		
	Convective			Molecular-turbulent	Heat conduction of the pin	Inter-subassembly	Molecular turbulent	Convective		
	Local	Integral	Periphery					Local	Integral	Periphery
EMP	+	+	+	+	+	+	+	+	+	+
CODE [10]; HECTIC [11]	–	–	–	+	–	–	–	–	–	–
JOTO [2]	–	+	–	–	–	–	–	–	–	–
MISTPAL [3]; ENERGY-11 [12]	–	+	–	+	–	–	–	–	–	–
FULMIX [13]; PACT [14]	+	–	–	–	–	–	–	–	–	–
COTEC [15]; SWEEP [16]	+	–	–	+	–	–	–	–	–	–
HEPA [17]	–	+	–	+	–	–	+	–	+	–
CORA [18]	–	+	+	+	–	–	–	–	+	–
CHANG; MORENO [19]	–	+	–	–	–	+	–	–	–	–
SUPERENERGY [20]	–	+	+	–	–	+	–	–	–	–
MONICAN [21]	–	–	–	+	–	+	–	–	–	–

Table 2.2. Rating of the codes to predict transient flows

N°	Codes	Heat exchange						Momentum exchange							
		Convective				Molecular	Fuel pin	Molecular	Convective			Flow divergence			
		Local	Integral	Periphery	Flow divergence	turbulent	heat conduction	turbulent	Local	Integral	Periphery	Axial	Transvers	Pressure drop	Friction
1	TEMP-MIF [22, 23]	+	+	+	+	+	+	+	+	+	+	+	+	+	+
2	THINC-II [24]	-	-	-	+	+	-	+	-	-	-	-	+	-	-
3	ENERGY-1 [25]	-	+	-	+	+	-	+	-	+	-	-	+	-	-
4	ORRIBLE [26]	+	-	-	+	+	-	-	+	-	-	-	+	-	-
5	SAMOVAR [27] THINC [1] HAMBO [5,6] MATTEO [28]	-	-	-	+	-	-	+	-	-	-	-	-	+	+
6	COBRA-KFKI [29] COBRA-II [7] TURMIX [30] DIANA [31] RETSAC [32]	-	-	-	+	+	-	+	-	-	-	-	-	+	+
7	POUCHOK-2 [9]	-	-	-	+	+	-	+	-	-	-	-	+	-	-
8	THI-3 [33]	-	+	-	+	+	-	+	-	+	-	+	-	+	+
9	HOTRAN [34]	-	-	-	+	+	-	+	-	-	-	-	+	-	-
10	COBRA-IIIC [35] COBRA-IY [36]	-	+	-	+	+	-	-	-	+	-	+	-	+	+
11	COBRA-IIIM [37]	-	+	-	+	+	-	-	-	+	-	+	-	+	+

Table 2.3. Rating of the reactor thermal hydraulics codes

Reference	Code	Approach	Single-phase	Two-phase		Transient	Procedure	Country
				Homogeneous	Heterogeneous			
[38]	SABRE-1	PBM	+	-	-	+	ICE	UK
	SABRE-2	PBM	+	-	-	+		
	SABRE-3	PBM	-	+	-	+	IMPL based	
	SABRE-3B	PBM/SUB	-	+	-	+	on SIMPLE	
[39]	BACCHUS	2D PBM	-	+	-	+	Implicit, Newton iteration	France
[40, 41]	TOPFRES	SUB	+	-	+	+	ICE	Japan
[42]	UZU	PBM	+	-	-	+	ICE	Japan
[36]	COBRA-IY	SUB	-	+	-	+	ICE	USA
[43, 44]	COMMIX-1	PBM	+	-	-	+	ICE	USA
	COMMIX-1a	PBM	+	-	-	+		
	COMMIX-2	PBM	-	+	+	+	IMF	
[45]	PORTER	PBM	+	-	-	+	Semi-implicit, iterative	Russia
[46]	BACCHUS-3D/TP	2D PBM	-	-	+	+	ICE	Germany
[47]	COMMIX-2/KFK	SUB	-	-	+	+	iterative, overrelaxation	Germany
[48]	SABENA	SUB	-	-	+	+	Semi-implicit, Newton iteration	Japan
[49]	TEMP-MIF	SUB	+	-	+	+	Semi-implicit, iterative	Russia

PBM - porous body model;   SUB - subchannel analysis

Modes of the code TEMP include predictions of single-phase flow in nominal subassembly under adiabatic (TEMP) and diabatic (TEMP-T) boundary conditions taking into account stochastic deviations of parameters from the nominal values (TEMP-M), in the event of counter directed helical wire wrapped on the fuel pins (TEMP-R), in the event of subassembly deformation (TEMP-MIF), under conditions of liquid metal boiling (TEMP-MF).

The use of the codes based on the simplified statements of subchannel approach is often justified, because allowing the wide class of thermophysical problems to be solved without the loss in accuracy and in a reasonable time, and inter-subassembly heat transfer to be taken into account, that requires the calculation domain be extended considerably. References [50-54] illustrate the possibility for using subchannel codes in the combined prediction of neutron, thermohydraulic and thermomechanical processes in reactor core, as well as in reactor design optimization [55].

2.2. MACRO-TRANSPORT EQUATIONS

What followed the completion of the first step including the statement of calculation procedure (differential equations and boundary conditions) was a development of numerical procedure for macro-transport equations which meet the wanted stability, convergence and accuracy.

In [49] an analogy between a subchannel approach (as well as between a porous body model) and continuos medium equations was stated. Thus, in solving a macro-transport momentum, mass and energy equations the procedure of solution of continuous medium equations is appeared to be applicable. The finite difference procedure is the most effective. The spectrum of block designs developed by different researchers is very wide - from completely explicit to completely implicit. Basic distinctions between approaches lies in the degree of momentum equation implicity with respect to time. The completely explicit block scheme at every time width is realized more simply, but a limitation of stability requires a very small time width that results in a great calculation time. In the completely implicit design, which is perfectly stable, the time width limitation is determined by a wanted accuracy.

In predicting fast reactor subassembly the time width has to be $\sim 10^{-6}$ s for explicit scheme and $\sim 10^{-3}$ s for semi-implicit one. The last is applied to fast transient processes, but requires an abundance of time steps for slow processes wherein the implicit scheme is preferable to be used. In subchannel approach the completely implicit schemes result in a very complex system of non-linear equations of a high order, with more tedious solution than in using an explicit procedure. An optimum scheme is to suppose a reasonable time step and has not-too-complex algorithm. It is of value to describe correctly effects being properly accounted in the equations and relative to the various time scales:

- propagation of sound, at high liquid velocity the pressure impulse time scale is about $10^{-6} \div 10^{-5}$ s;
- local transport effects (inter-phase, at channel wall);
- convective mixing with the greater time scale that is connected with lower velocity;
- diffusive mixing being of the same scale as convective one.

It should be noted, that many researchers apply the conservative difference approximation that gives the more precise results. An explicit procedures for solving

momentum equation with the direct time differences, central differences for the diffusive terms and opposite differences for the convective terms have gained a wide-spread acceptance [56]. In doing so, disturbance imposed on functions is transferred only in flow direction. The semi-implicit design is used in MAC approach (implicit a pressure and momentum designs), where the pressure field is first defined, then velocity profiles [57]. Subsequent modes of the approach mentioned received the names SMAC, ICE [58], SOLA, SOLA-ICE. For example, approach ICE is involved in SABRE code [38,59]. The pressure solution must be more accurate. Code SABRE uses the variable relaxation directions in axial planes, as well as the block correction between the axial planes that hastens an iterative convergence.

The semi-implicit approach restricts the time step by Courant conditions. In order to the design would be more stable the time width is to be less than the time of liquid passing over the mesh with the velocity of the main flow. The limitation on the time step can be removed when using implicit design for energy and momentum equations. Such approach as SIMPLE [60,61] enjoys a wide application. Every iterate in this case includes the sequential solution of momentum equation with the further correction of pressure, the mass balance to be satisfied. To design the completely implicit procedure, the algorithms of semi-implicit ones are often used. The completely implicit procedure IMPL based on the idea of SIMPLE is presented in [38].

2.3. VARIOUS FACTORS IN THERMAL HYDRAULIC ANALYSIS OF REACTOR CORE

General insights. Thermal hydraulic analysis of reactor core is performed in three steps (Fig. 2.1) [62] , we find:
- coolant flow distribution over the core;
- flow rate and coolant temperature over subassembly cross section and with the length;
- temperature distribution in separate pins.

The input data are geometry, variation in power production with the core length and across the core, flow rate through the core, coolant and structure properties. The main factors controlling temperature behavior (deformation of pins and subassembly cover, power production in reactor core), in their turn, depend on temperature behavior in the reactor core. Thus, the problem on reactor core temperature behavior is conjugate to the problem of deformation of the core units and power distribution (neutron-physical calculation). Predicting reactor core deformation is a very combined problem that, as a rule, also is divided into the stages determining deformation of the cover, pin bundle and separate pins. The ensuing iterative procedure is possible to predict temperature behavior in fast reactor elements taking into account their deformation (Fig. 2.2).

The first approximation of the input data may be taken as that of nominal geometry. The main block involves neutron-physical part, prediction of coolant flow distribution over the core, thermal hydraulic analysis of separate subassembly, estimation of pin and wrapper deformation. Using the data found, the thermal stress in the wrapper and pins are determined. The procedure is repeated until the convergence conditions to be met, for example, for criterion of normal performance. Predictions based on the pattern outlined allow the changes in subassembly geometry, in temperature behavior and in performance of the core units to be followed in campaign.

Selection of throttling zones

Total power production in SA

Total subassembly pressure drop

Flow rate through the separate SA

Coolant temperature in subassembly

Fuel pins power

Wrapper tube temperature

Headers pressure drop

Subassembly path pressure drop

Subassembly geometry

Coolant temperature distribution over the channels

Pin bundle pressure drop

Velocity distribution over the channels

Thermal mixing factors

Subassembly performance

Spacing grids pressure drop

Hydraulic mixing factors

Fuel pins geometry

Internal and edge channels pressure drop

Inlet velocity distribution

Local temperatures of pin cladding and fuel

Velocity distribution over the channel

Local heat transfer

Local temperature irregularities

Fig. 2.1. Thermal hydraulic analysis of reactor core of an assembly type.

| Total power of reactor core | | Total coolant flow through the core | | Properties of structure and coolant |

```
┌──────────────────┐   ┌──────────────────┐                                        ┌──────────────────────┐
│  Total power     │   │ Total coolant flow│                                        │ Properties of structure│
│ of reactor core  │   │  through the core │                                        │    and coolant        │
└────────┬─────────┘   └─────────┬────────┘                                        └──────────┬───────────┘
```

┌─────────────────────┐   ┌──────────────────┐   ┌──────────────────┐   ┌──────────────────────┐   ┌──────────────────┐   ┌──────────────────┐
│ Nominal geometry   │──▶│ Neutron-physical │──▶│ Flow rate through│──▶│ Thermal hydraulic   │──▶│ Wrapper tube   │──▶│ Deformation   │
│ of subassembly   │   │   analysis   │   │ the subassembly │   │ analysis of subassembly,│ │ deformation   │   │ of pin bundle   │
└─────────────────────┘   └──────────────────┘   └──────────────────┘   │ wrapper tube, pins   │   └──────────────────┘   │ and individual │
                                                                         └──────────────────────┘   │   pins   │
                                                                                                                           └──────────────────┘

no

if converging to

yes

┌──────────────────────────┐
│ Stresses in wrapper tube, │
│ fuel pins and subassembly │
│   performance   │
└──────────────────────────┘

end

Fig.2.2.   Scheme of combined analysis of reactor core taking into account fuel pins deformation in campaign

Flow distribution over reactor core based on the statistic estimation of temperature behavior taking into account mixing and deformation. The main input parameters in predicting flow distribution over reactor core are power and geometrical characteristics of subassembly and their variations in campaign. In fast reactor design, as a rule, the problem on maximum coolant temperature is solved with the nominal performance of reactor core in mind. The most simple approach is the flow distribution based on the uniform temperature distribution through the subassembly. The drawback to the approach is an incomplete using a thermal possibilities of subassembly of a lesser power. Another procedure starts from the same margin till to allowable value of determining parameter, for example till to maximum pin wall temperature [62-66]. If the power production varies in campaign, so called distribution with envelope is used [63]. This procedure assumes that coolant flow through the subassembly does not change in campaign. The common limitation of the procedures indicated is an incomplete consideration of engineering and operating parameters' variation.

Prediction of flow distribution based on the estimation of maximum pin temperature, with regard to so called hot spot factors, ignores inter-channel and inter-subassembly exchange, as well as mutual correlation of parameters, with the random deviations being small as compared with the nominal ones [67-69]. In doing so, temperature is estimated in one point, where the maximum temperature occurs. But, to provide a reliable design of reactor core, all areas with high temperature have to be considered at least. In this event, inter-channel and inter-subassembly heat transfer in reactor core has to be taken into account.

Subassembly performance is limited by that the maximum pin temperature (having regard to hot spot factors) should not exceed value prescribed for various steels. It is well to bear in mind, that this criterion do not completely reflect conditions of nominal performance of the pins. It is evident, that such a factors as maximum azimuthal non-uniformity of pin temperature, as pressure of fission gas, level of pin wall swelling, deformation of the subassembly wrapper and pins and so on should be taken into account. In general case, the criterion has to be combined.

Thus, an allowable temperature of the pin is expressed as a function of other limiting parameters:

$$t_{limit} = f(steel\ properties,\ \Delta t_{\varphi},\ p...) \tag{2.1}$$

where Δt_{φ} - maximum azimuthal non-uniformity of pin temperature, p - fission gas pressure.

Thermal reliability is governed by the number of allowable failures (pin's destructions) occurring in a separate subassembly. If the possibility of pin failure does not exceed p_o, that the possibility the pin temperature in separate subassembly does not exceed P_o:

$$P(t_w^{max} > t_{limit}) \le P_o \tag{2.2}$$

Statistic evaluation of temperature in the i-th subassembly allows the values t_i not exceeding allowable value to be calculated, and the factor k_i to be found:

$$k_i = \frac{t_i - t_{\alpha}}{\Delta t_i} = f\left(\Gamma, q^{max} / \bar{q}, \bar{Pe}, \bar{i}\right), \tag{2.3}$$

where t_{inlet} -core inlet temperature, Δt_i - mean coolant overheating in the i-th subassembly, Γ- geometry, Pe - Peclet number based on the mean velocity, $\bar{t}$ - mean coolant temperature, $\left(q^{max}/\bar{q}\right)$ - non-uniformity in power production over the subassembly cross section.

It should be noted that statistic analysis allows an inter-channel heat and mass transfer being responsible for the temperature behavior in the subassembly, to be taken into account. It also allows for various deviation of parameter from nominal distribution [70].

Coolant flow rate through the subassembly at the given inlet temperature is limited by the following relationship:

$$G_\Sigma \geq \frac{max\left[\sum_i \frac{\beta_i}{\alpha_i} \frac{K_i^0 K_{Q_i}}{K_{G_i}} Q_i N_i\right]}{\Delta t_{limit}^{ud}},$$ (2.4)

where N_i -number of subassemblies in the i- th zone ; Q_i -maximum power production in the i- th zone; $K_{Q_i} = (Q_i^{max} / Q_i^0)$ - factor describing the rise in power production in campaign (index «o» means the beginning of operation); $K_{G_i} = (G_i^{min} / G_i^O)$- factor describing the reduction of coolant flow through the subassembly in the i-th zone; $\alpha_i = (t - t_{inlet}) / (t^{id} - t_{inlet})$ - factor which accounts the change in allowable pin temperature as compared to the temperature under ideal conditions; $\beta_i = K_i / K_i^0$ -factor which shows how K_i varies in campaign.

Maximum overtemperature of the coolant can be found as follows:

$$\Delta t_{core}^{max} = \frac{\sum_i \sum_j (Q_j)_i}{max\left\{\sum_i \left[\frac{\beta_i}{\alpha_i} \frac{K_i^0 K_{Q_i}}{K_{G_i}} Q_i N_i\right]\right\}} \Delta t_{limit}^{id},$$ (2.5)

where j -subassembly number in the i -th zone.

Relationships (2.4) and (2.5) indicate that changes in power production and coolant flow thought the subassembly cause an increase in the temperature non-uniformity, that results in the lesser possible coolant temperature in the zone under consideration.

If an allowable value of pin temperature t_{allow} is given as less than limit temperature t_{limit}, the optimal reactor flow distribution is calculated as follows on the basic of the maximum thermal reliability of the most loaded subassembly:

$$G_i = \frac{\beta_i \frac{K_i^0 K_{Q_i}}{K_{G_i}} Q_i}{\sum_i \left[\beta_i \frac{K_i^0 K_{Q_i}}{K_{G_i}} Q_i N_i\right]} G_\Sigma,$$ (2.6)
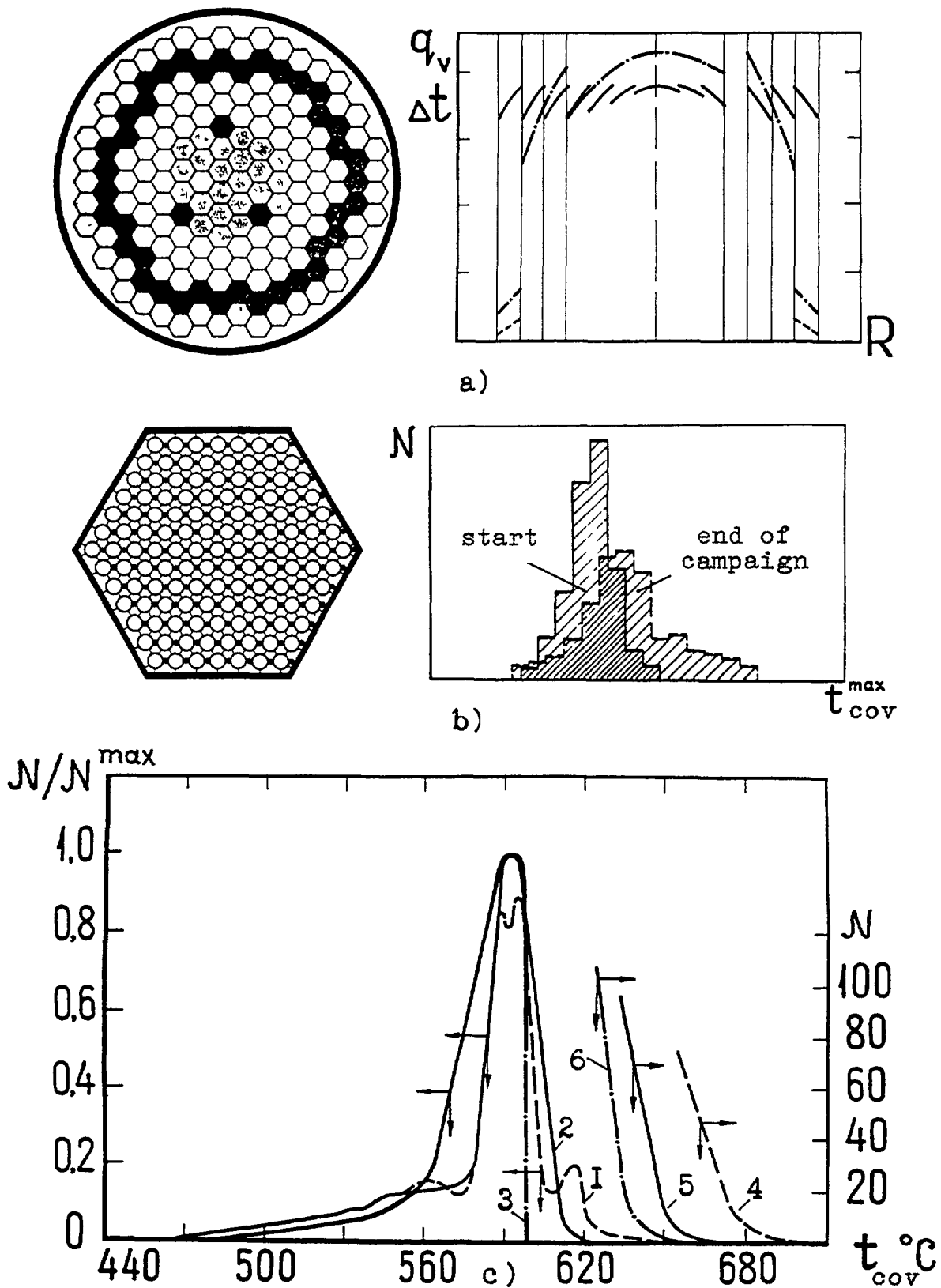
Fig. 2.3. Power production and radial temperature behaviour (a) and
distribution of pins over subassembly (b) and over core (c) having no
regard "hot spot" factors; 1 -mixing is absent, 2 - mixing available,
3 - optimal throttling having regard "hot spot" factors, 4÷6 - similar to 1÷3.

where

$$G_\Sigma = \frac{max\left[\sum_i \beta_i \dfrac{K_i^0 K_{Q_i}}{K_{G_i}} Q_i N_i\right]}{\Delta t_{allow}},$$ (2.7)

here $\Delta t_{allow} = t_{limit} - t_{inlet}$.

Average coolant heating in various zones is calculated as:

$$\Delta t_i = \frac{\sum_i \beta_i \dfrac{K_i^0 K_{Q_i}}{K_{G_i}} Q_i N_i}{\beta_i \dfrac{K_i^0 K_{Q_i}}{K_{G_i}} G_\Sigma}.$$ (2.8)

At the given total flow rate the optimization of flow distribution (2.6) allows the thermal reliability of the reactor zone to be enhanced. In this event, the pin temperature compatible with the condition $P(t_w^{max} > t_{limit}) \leq P$ can be found as:

$$t_{limit} = t_{inlet} + \frac{max\left[\sum_i \beta_i \dfrac{K_i^0 K_{Q_i}}{K_{G_i}} Q_i N_i\right]}{G_\Sigma}.$$ (2.9)

As statistic estimations of pin temperature behavior in reactor, taking into account inter-channel and inter-subassembly heat and mass transfer, has shown the optimization of flow distribution over reactor carried out in the procedure mentioned above could result in the more flat temperature profile than those based on the condition when maximum temperatures of the most loaded pins are the same in various zones of reactor (Fig.2.3).

Statistic estimation of temperature field implies that a series of the temperature field elements is defined using stochastic distribution of input parameters followed by statistic processing (to find mathematical expectation, variance and distribution function).

The stochastic distribution of parameters in the specific case can be found from the distribution functions deduced from experiments or analytical studies (for example, [68, 71]). In calculating the global parameters, such as flow rate throughout the subassembly, total power production, sizes and local parameters, such as pitch-to-diameter ratio, pin diameter, pin wall thickness, power production of the pin are distributed in random manner. It should be noted, that in the event of subassembly deformation in campaign the distributions of input geometrical parameters have the significantly greater variance than those in nominal bundle [72].

Thermal hydraulic analysis involves the subchannel procedure. The end of calculation means the convergence of mathematical expectations of coolant temperature, maximum pin temperature and non-uniformity of pin temperature. As a result of analysis, distributions of temperature characteristics are determined, too.

Code **TEMP-M** (regular flow throughout the reactor core) [73] allows securing stochastic and averaged temperature characteristics to be defined in fast reactor subassembly. Since the reactor core follows the sizable shield and gas space, the coolant flow in reactor core is regular under nominal operating conditions. Distributions of coolant velocity and temperature over the channels result from the solving the system of momentum and enthalpy equations which (once a pressure has been exclude, that is possible in regular flow) appear as (see [74, 75]):

in internal channels

$$\left(\frac{1}{\sum\limits_{i=1}^{N}\Omega_i}\sum_i^{N}\varepsilon_i\frac{W_i^{7/4}}{D_{h_i}^{5/4}}\Omega_i - \varepsilon_i\frac{W_i^{7/4}}{D_{h_i}^{5/4}}\right)\frac{\xi_o}{2}\Omega_i = \sum_{j=1}^{3}\left(\mu_{MT}^M + \mu_C^M\right)d_{ho}\frac{\Delta s_y}{\Delta s_0}\frac{W_i + W_j}{2}\left(W_i - W_j\right), \quad (2.10)$$

$$\frac{d}{dZ}\left(T_iW_i\Omega_i\right) = \sum_{k=1}^{3}Q_k + \sum_{j=1}^{3}\left[\left(\mu_{MT}^T + \mu_C^T\right)\frac{W_i + W_j}{2}\frac{\Delta s_y}{\Delta s_0} + \mu_\lambda\right]L\left(T_j - T_i\right); \quad (2.11)$$

in edge channels

$$\left(\frac{1}{\sum\limits_{i=1}^{N}\Omega_i}\sum_i^{N}\varepsilon_i\frac{W_i^{7/4}}{D_{h_i}^{5/4}}\Omega_i - \varepsilon_i\frac{W_i^{7/4}}{D_{h_i}^{5/4}}\right)\frac{\xi_0}{2}\Omega_i =$$

$$= \left(\mu_{MT}^{Mp} + \mu_C^{Mp}\right)d_{ho}\frac{\Delta s_{i3}}{\Delta s_0}\frac{W_i + W_3}{2}\left(W_i - W_3\right) +$$

$$+ \mu_C^{Mp}d_{ho}\left(\frac{\Delta s_{i2}}{\Delta s_0}\frac{W_i + W_2}{2}W_i - \frac{\Delta s_{i1}}{\Delta s_0}\frac{W_i + W_1}{2}W_1\right) + \quad (2.12)$$

$$\sum_{j=1}^{2}\mu_{MT}^P d_{ho}\frac{\Delta s_y}{\Delta s_0}\frac{W_i + W_j}{2}\left(W_i - W_j\right);$$

$$\frac{d}{dZ}\left(T_iW_i\Omega_i\right) = \sum_{k=1}^{2}Q_k + \mu_k^{Tpc}\frac{W_i + W_3}{2}\left(T_3 - T_i\right)\frac{\Delta s_{i3}}{\Delta s_0}L +$$

$$+ \mu_C^{Tp}L\left(\frac{W_i + W_1}{2}T_1\frac{\Delta s_{i1}}{\Delta s_0} - \frac{W_i + W_2}{2}T_i\frac{\Delta s_{i2}}{\Delta s_0}\right) + \mu_{i_\xi}^T L\left(T_\xi - T_i\right) + \quad (2.13)$$

$$+ \sum_{j=1}^{3}\left(\mu_{MT}^T\frac{W_i + W_j}{2}\frac{\Delta s_y}{\Delta s_0} + \mu_\lambda^T\right)L\left(T_j - T_i\right);$$

for the cells in the inter-subassembly gap

$$\frac{d}{dZ}\left(T_\xi W_\xi\Omega_\xi\right) = \sum_{i=1}^{2}\mu_{i\xi}^T L\left(T_i - T_\xi\right) + \sum_{l=1}^{2}\frac{8}{\pi}\frac{\delta/s}{Pe}\left(T_l - T_\xi\right)\frac{L}{d}, \quad (2.14)$$

where

$$D_{h_i} = d_{h_i} / d_{h0}; \quad \Omega_i = \omega_i / \omega_0; \quad \varepsilon_i = \xi_i / \xi_0; \quad W_i = w_i / \overline{w};$$

$$\xi_0 = 0.316 / Re^{0.25}; \quad Z = z / L;$$

$$Q_k = \frac{q_k}{\overline{q}} \frac{\Pi_{k_i}}{\Pi_0}; \quad T_i = \frac{t_i \rho w d_{ho} c_p}{4 \overline{q} L};$$

d_{h0}, w_0, w, q, Π - typical scales for hydraulic diameter, channel area, coolant velocity, heat flux, heat removal perimeter, respectively; Δs_{ij} - gap between the channels i and j; L - subassembly length; $\mu_{i\xi}^T$ - heat mixing factor; μ_λ - mixing factor due to fuel pin thermal conductivity.

Mixing factor μ_{MT}, μ_C, μ_λ, $\mu_{i\xi}$ are defined as presented in [49]. The fuel pin wall temperature is calculated using procedure indicated below. Temperature of subassembly wrapper as viewed from the edge channels is predicted as follows:

$$t_1 = t_i + \left(t_\xi - t_i\right)\left[1 + \frac{\lambda_f}{\lambda} \frac{\delta}{d_{hp}} Nu_P + \frac{Nu_P}{Nu_\xi} \frac{\delta'}{d_{hp}}\right]^{-1}, \quad (2.15)$$

where t_i - coolant temperature in the edge channel, t_ξ - coolant temperature between subassemblies; Nu_P, Nu_ξ - Nusselt numbers in the edge channels and between subassemblies, respectively; λ_f, λ - thermal conductivity of coolant and wrapper tube, d_{hp} - hydraulic diameter of the edge channel; δ - inter-subassembly gap, δ' - thickness of the subassembly wrapper.

Temperature difference on the wrapper can be written as:

$$t_1 - t_2 = \frac{t_i - t_\xi}{\frac{\lambda}{\lambda_f} \frac{d_{h_E}}{\delta} \frac{1}{Nu_P} + 1 + \frac{\lambda}{\lambda_f} \frac{\delta'}{\delta} \frac{1}{Nu_\xi}}. \quad (2.16)$$

System of the macro-transport equations for momentum (2.10), (2.12) is solved by introducing the time term ($\partial W_i / \partial Fo$, where Fo - Fourier parameter) in explicit procedure. Also, explicit procedure is applied for solving energy macro-transport equations (2.11), (2.13) and (2.14). The code is built up on the block principle. The subroutine RNDM (generator of random numbers uniformly distributed between 0 and 1) is used, distribution of power over the pins is governed by normal law [76].

Predictions on TEMP-M were compared with the data gained in the fast reactor out-of-pile experiments with a good agreements between velocity and temperature distribution over the subassembly radius (Fig. 2.4). Velocities and temperatures in the edge channels are agree with an accuracy of 10% (Fig. 2.5). Here, an influence of inter-channel exchange is very noticeable. When predictions on TEMP-M are compared with experimental data [79] for the pin bundle with non-uniform power distribution in subassembly cross section, it is apparent that variance is about 0,8%. As good as this result is connected with the more full
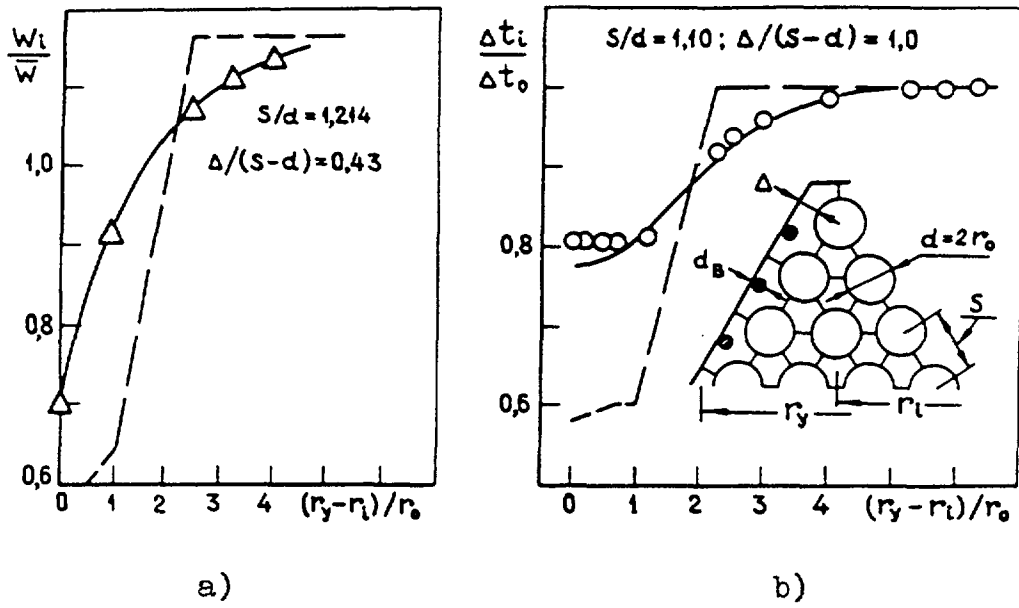
Fig 2.4. *Radial distribution of coolant velocity (a) and temperature (b):*
Δ -, O - *experiments,* ——— - *mixing is available,*
— — — - *mixing is absent.*
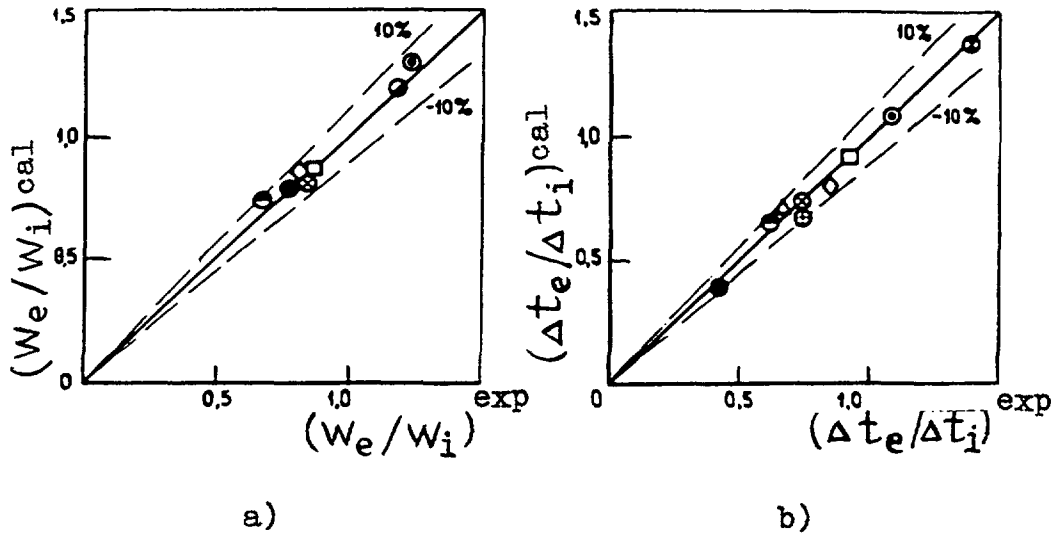
Fig. 2.5 *Comparison of predictions and experiments for velocity (a) coolant temperature (b) in edge and internal channels of the model.*

71
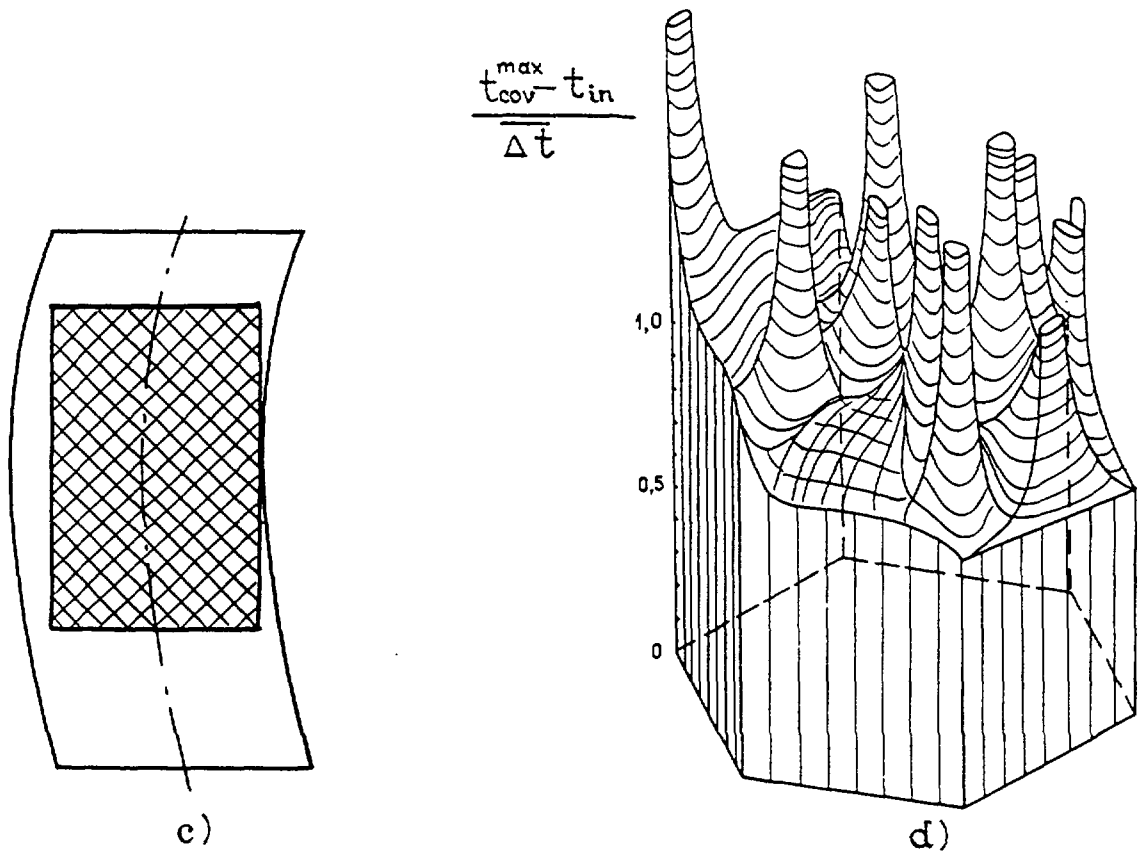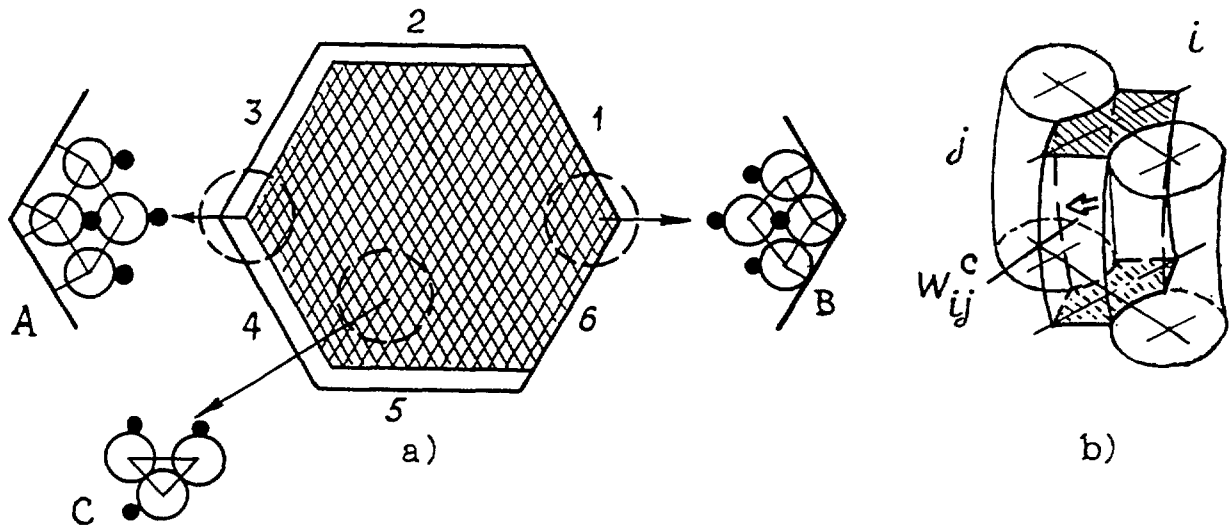
Fig. 2.6. Schematic diagram of lateral (a) and axial section of deformed subassembly (b, c) and distribution of maximal temperature of pin cladding in the middle cross section of PHENIX reactor (d).

mathematical statement in comparison with other codes (see Table 2.2), as well as with the careful analysis of input constants.

Predictions of temperature behavior in BN-600 core subassembly in the event of non-uniform power distribution over the cross section have shown that variance estimated having regard to inter-channel exchange is found to be in order less than those evaluated without regarding for inter-channel exchange (variance procedure).

Code TEMP-MIF to predict thermal hydraulics in deformed subassemblies. In the special case that subassembly is subjected to deformation in campaign a coolant flow is of irregular character, with the bundle flow being practically longitudinal (quasi-stable). Predictions have shown that even in case of large deformation (when pins bending is so great that compact channels are formed) the transverse component of velocity does not exceed about 30% of axial component and pressure out-of-balances for a length not more than (0.1 ÷ 0.2) d_h. Thus, macro-transport equation of momentum in transverse direction can be approximately written as $p_i - p_j = c_{ij}$ *w_{ij} or substituted by the relationship $p=idem$ (hypothesis of isobaric flow), with the value w_{ij} being determined from the mass equation.

The feature of thermal hydraulic analysis in deformed subassemblies is also that the transverse mass transfer due to centrifugal effect is taken into account in the channel when bending. By assuming that transverse flows due to centrifugal effect are in balance in central channels, it is easy to verify that specific momentum and energy fluxes (Fig. 2.6) are in proportion with the transverse flow:

$$\left. \begin{aligned} P_{ij} &= \rho_{ij} w_{ij}^C w^{**} \Delta s_{ij} \\ Q_{ij} &= \rho_{ij} w_{ij}^C h^{**} \Delta s_{ij} \end{aligned} \right\}$$

(2.17)

where ** - index of the donor-channel .

$$w^{**} = \begin{cases} w_i, & if \ w_{ij}^C > 0 \\ w_j, & if \ w_{ij}^C < 0 \end{cases} \qquad h^{**} = \begin{cases} h_i, & if \ w_{ij}^C > 0 \\ h_j, & if \ w_{ij}^C < 0 \end{cases}$$

Having performed the needed transformations for the purpose to exclude pressure and assuming $p=const$ in subassembly cross section [22], we find the macro-transport equations in isobaric approximation:

$$\frac{d(w_i \omega_i)}{dz} = \frac{1}{2w_i - w_i^*} \left\{ w_i^2 \frac{d\omega_i}{dz} - \xi_i \frac{w_i^2}{8} \Pi_i + \sum_{j=1}^{3} \mu_{ij}^M \frac{w_i + w_j}{2} \left(w_j - w_i \right) \overline{\omega} + \right.$$

$$+ \mu_c^M \frac{w_i + w^{**}}{2} \left(w^{**} - w_i \right) \overline{\omega} - \frac{\omega_i}{\sum_{i=1}^{\Lambda} \frac{\omega_i}{2w_i - w_i^*}} \sum_{i=1}^{\Lambda} \frac{1}{2w_i - w_i^*} \left[w_i^2 \frac{d\omega_i}{dz} - \right.$$

(2.18)

$$\left. \left. - \xi_i \frac{w_i^2}{8} \Pi_i + \sum_{j=1}^{3} \mu_{ij}^M \frac{w_i + w_j}{2} \left(w_j - w_i \right) \overline{\omega} + \mu_c^M \frac{w_i + w^{**}}{2} w^{**} \overline{\omega} \right] \right\};$$

$$\frac{d}{dz}\left(w_i\omega_i t_i\right) = \frac{1}{\rho c_p}\sum_{k=1}^{3}q_{ki}\,\Pi_{ki} + q_{vi}\omega_i + t_i^* \frac{d\left(w_i\omega_i\right)}{dz} +$$

$$+ \sum_{j=1}^{3}\left(\mu_{ij}^T\,\frac{w_i + w_j}{2} + \mu_\lambda^T\,\overline{w}\right)\left(t_j - t_i\right)\overline{\omega} + \mu_H^T\,\frac{w_i + w^{**}}{2}\,t^{**}\overline{\omega};$$

(2.19)

$$w_i^* = \frac{1}{2}\sum_{j=1}^{3}\left[\left(w_i + w_j\right)\left|w_{ij}\right| + \left(w_i - w_j\right)w_{ij}\right]\Delta s_{ij}\bigg/\sum_{i=1}^{3}w_{ij}\Delta s_{ij};$$

$$t_i^* = \frac{1}{2}\sum_{j=1}^{3}\left[\left(t_i + t_j\right)\left|w_{ij}\right| + \left(t_i - t_j\right)w_{ij}\right]\Delta s_{ij}\bigg/\sum_{j=1}^{3}w_{ij}\Delta s_{ij}.$$

(2.20)

In (2.18) and (2.19) the hydraulic and thermal mixing factors due to centrifugal effects can be expressed as:

$$\left.\begin{array}{l}\mu_C^M = \dfrac{P_{ij}}{\dfrac{\rho\left(w_i + w_j\right)}{2}w^{**}\overline{\omega}} \approx \dfrac{w_{ij}^U}{\dfrac{w_i + w_j}{2}}\dfrac{\Delta s_{ij}}{\overline{\omega}}, \\[4mm] \mu_C^T = \dfrac{Q_{ij}}{\dfrac{\rho\left(w_i + w_j\right)}{2}h^{**}\overline{\omega}} = \mu_C^M \cdot \beta\end{array}\right\}$$

(2.21)

Local mixing factors due to convective exchange and molecular - turbulent diffusion are in the forms, respectively

$$\left.\begin{array}{l}\mu_{ij}^M = \mu_{C_{ij}}^M + \alpha \cdot \mu_{MT_{ij}}^M; \\[2mm] \mu_{ij}^T = \mu_{C_{ij}}^T + \mu_{MT_{ij}}^T,\end{array}\right\}$$

(2.22)

where α - coefficient considering mutual relation between convective exchange and molecular - turbulent diffusion. Three parameters μ_{ij}^M, μ_{ij}^T, α are defined on the basic of [76, 74, 81].

From momentum balance written for the gap between channels we can write the following relationship for the mixing factor due to centrifugal effect, $1/m$:

$$\mu_{ij}^M = 1.58\,Re^{0.143}\left[\frac{s/d - 1}{\dfrac{2\sqrt{3}}{\pi}\left(s/d\right)^2 - 1}\right]^{1.143}\left(\frac{s}{R_{ij}}\right)^{0.57}\frac{1}{d},$$

(2.23)

where R_{ij} - curvature radius.

Coefficient of non-equivalence between heat transfer and momentum transport β may be thought of as being about 0.7 in deformed geometry. Then, on the basic of (2.21) we have

$$\mu^T = 0.7\mu^M$$

(2.24)

74

As it was evaluated, the thermal and hydraulic mixing factors due to centrifugal effect can achieve some unites.

In the event of pin out-of-roundness, that may be responsible for the significant decrease in the width of inter-pin clearance, the transverse convective flows is more intensive than those evaluated with the averaged parameters of pin bundle. For example, the limiting degree of the out-of-roundness attended with the pins touch each other results in the value of 40% of that defined using averaged parameters:

$$\overline{w_{ij}\Delta s_{ij}} = 0.4\overline{w_{ij}}\,\overline{\Delta s_{ij}}. \tag{2.25}$$

Once you have decided upon the averaged parameters of subassembly as the reference one, it should be introduce correction on the out-of-roundness:

$$\mu_{ij} = \mu(s/d)\beta' \tag{2.26}$$

where correction factor β' is determined as follows:

$$\beta' = \overline{w_{ij}\Delta s_{ij}} \big/ \left(\overline{w_{ij}}\,\overline{\Delta s_{ij}}\right). \tag{2.26a}$$

Macro-transport equations are also supplemented by the equations for the cells chosen in the gap between subassemblies. Velocity and temperature boundary conditions are given at the bundle inlet. System (2.18) and (2.19) is resolved with the use of the explicit finite difference approach.

Code TEMP-MIF was verified on experimental data on temperature behavior in the model bundle being exposed to deformation in the edge area under conditions of uniform power distribution over the cross section, as well as under conditions of strong coolant flow through the clearance between subassemblies. There is a good agreement of coolant temperature distribution over the outlet cross section.

Let us demonstrate the possibilities of the code on the example of PHENIX subassembly deformation (Fig. 2.6), when the pin bundle and subassembly wrapper are bended (Fig. 2.6 - 2.6a). First of all, the rearrangements of collant flow and temperature are observed. Coolant passing close to the sides with the lesser distance from the edge pins becomes more heated and significantly subheated near the opposite sides. Predictions show the large temperatures of pin wall and enhanced azimuthal pin temperature non-uniformity in the event of the channels are formed close to compact ones (Fig. 2.6-a,d).

Comparison of mathematical description of the TEMP-MIF and those for other well known codes indicates the more complete account of mechanisms of momentum and energy exchange (see Table 2.2) and the more plausible predictions on this code.

CONCLUSIONS

1. Subchannel analysis being the most effective procedure for predicting thermohydraulics in fast reactor subassembly has received much attention of the authors. Recently analysis of the codes available was performed; spectrum for use was

determined; the most promising codes that answer modern needs were selected, with the rating. It has been shown that subchannel codes have gained a wide-spread acceptance in practice not only in predicting single-phase flows, but under boiling conditions. Some generations of subchannel codes developed in such countries as Russia, USA, Germany, UK, France, Japan differ in governing equations, methods of their solution, and, respectively are intended to different problems to be tackled.

2. At the SSC RF IPPE some versions of subchannel codes GID and TEMP were developed to predict thermal hydraulics in fast reactor subassembly. Complex TEMP includes prediction of single phase flow in nominal bundle geometry under adiabatic (TEMP) and diabatic (TEMP-T) conditions at the wrapper, having regard to accidental deviation of parameters from nominal values (TEMP-M), in the event of the pins are spaced by counter-directed wire wrap (TEMP-R), in deformed subassembly (TEMP-MIF), under transient conditions accompanied by liquid metal boiling (TEMP-MF).

3. The validity of the versions of TEMP has been demonstrated in predicting flow distribution over the reactor core based on statistical determination of temperature field having regard to interchannel exchange and subassembly deformation. Statistical analysis causes the temperature field to be more smooth, than those predicted from the criterion on equality of maximum wall temperature at maximum loaded pins (taking into account hot spot factors) in various zones of reactor core. The potentialities of code TEMP-M are illustrated in predicting distributed and averaged temperature characteristics of several adjacent subassemblies. The more complete mathematical description of TEMP-M and more careful analysis of closing correlations leads to more accurate predictions as compared with experimental data. The advantages of the code TEMP-MIF is shown by the example of temperature distribution in deformed subassembly of PHENIX.

REFERENCES

[1] Zernick W., Currin H. B., Elyath E., Previti G. THINC – A Thermal Hydraulic Interaction Code for a Semi-Open or Closed Channel. WCAP – 3704, 1962.

[2] Okamoto Y., Hishida M., Akino N. Hydraulic Performance in Rod Bundles of Fast Reactor Fuel Pressure Drop Vibration and Mixing Coefficient. Progress in Sodium-Cooled Fast Reactor Engineering. Monako, IAEA / SM-130/5.1970.

[3] Baumann W., Hoffman H. Coolant Cross Mixing of Sodium Flowing in Line through Spacer Arrangements. International Heat Transfer Seminar. Trogir. Yugoslavia, 1971.

[4] Zhukov A.V., Mouzanov A.B., Sorokin A.P. et al. Inter-Channel Mixing in Cylindrical Pin Bundles. Preprint IPPE-413, Obninsk, 1973 (in Russian).

[5] Bowling R. W. HAMBO - A Computer Programme for Subchannel Analysis of the Hydraulic and Burnout Characteristics of Rod Bundles (Pt. 1). General Description. AEEW-R524. London, 1967.

[6] Bowling R. W. HAMBO - A Computer Programme for the Hydraulic and Burnout Characteristics of the Rod Clusters (Pt. 2). The Equation. AEEW-R582. London 1968.

[7] Rowe D. S. Thermal-Hydraulic Analysis for Rod Bundle Nuclear Fuel Elements. Heat Transfer Conference, Paris – Versailles, 1970, v.3. Fc 7.13.

[8] Plas E. Programme FLICA-III Pour l'Etude Thermohydraulic de Reacteurs et de Boucles d'Essees. Report on the France-Soviet Seminar. Moscow, 1974.

[9]   Mironov Y.V., Shpanski S.V. Distribution of Two-Phase Flow Parameters over the Pin Bundle. Atomic energy, 1975, v.39.

[10]   Polianin L.N. Heat and Mass Transfer in Pin Bundle Turbulant Flow. Atomic Energy, 1969, v.26.

[11]   Kovacs L. M. HECTIC-II, Computer Program for Heat Transfer Analysis of Gas or Liquid Cooled Reactors. KFKI-70-33 RPT. 1970.

[12]   Khan E. V., Rosenow W. E., Sonin A. A. et. al. A Porous Body Model for Prediction Temperature Distribution in Wire-Wrapped Fuel Rod Assemblies. Nucl. Eng. and Des., 1975, v. 35.

[13]   Maggee P. M. Modelling of Flow Sweeping Effects in Wire-Wrapped Rod Bundles. TANS, 1972, v. 15.

[14]   Wei J. P., Stephen J. D. PACT: A Probabilistic Method for Analysis of LMFBR Coolant and Cladding Temperature Distribution. TANS 1976, v. 24.

[15]   Novendstern E. N. Mixing Model for Wire-Wrap Fuel Assemblies. TANS 1972, Vol. 15.

[16]   Ginsberg T. Forced-Flow Interchannel Mixing Model for Fuel Rod Assemblies Utilizing a Helical Wire-Wrap Spacer System. Nucl. Eng. and Des.. 1972, Vol. 22.

[17]   Nijsing R., Eifler W. A Computer Method for Steady State Thermo-hydraulic Analysis of Fuel Rod Bundles with Phase Cooling. Nucl. Eng. and Des.. 1974, v. 30.

[18]   Pecha P. Hydrodynamicand Statistic Estimetion of Uncertainty Factors in Combined Bundles. Thermal Physics and Hydrodynamics of Reactor Core and Steam Generators for Fast Reactors. Prague, CzCNE, 1978, v.1.

[19]   Chen B. C., Todreas N. E. Prediction of the Coolant Temperature Field in a Breeder Reactor Including Interassembly Heat Transfer. Nucl. Eng. and Des.. 1975, v. 35.

[20]   Wolf L., Fisher K., Herkenrath H. et. al. Comprehensive Assessment of the Ispra BWR and PWR Subchannel Experiments and Code Analysis with Different Two-Phase Model and Solution Schemes. Nucl. Eng. and Des., 1987.

[21]   Carelli M. D., Bach N. W. Thermal-Hydraulic Analysis for CRBRP Core-Restraint Design. TANS 1975, v. 21.

[22]   Kazachkovski O.D., Sorokin A.P., Zhukov A.V. et al. Lumped Parameters in the Problem on Temperature Behavior in Deformed Fast Reactor Subassemblies under Diabatic Boundary Conditions. Preprint IPPE-1672, Obninsk, 1985 (in Russian).

[23]   Kazachkovski O.D., Sorokin A.P., Zhukov A.V. et al. Stohastic Non-Uniformities of Temperature Fields in Deformed Bundles. Preprint IPPE-1678, Obninsk, 1985 (in Russian).

[24]   Chelemer H., Weisman J., Tang N. S. Subchannel Thermal Analysis of the Rod Bundle Cores. Nucl. Eng. and Des., 1972, v. 21.

[25]   Zhukov A.V., Sorokin A.P., Titov P.A. et al. Calculation Procedure for Determining Mixing Effect on Temperature Distribution in Wire-Wrapped Bundles. Preprint IPPE-512, Obninsk, 1974.

[26]   Wantland J. L. ORRIBLE – A Computer Program Flow and Temperature Distribution in 19-Rod LMFBR Fuel Assemblies. Nucl. Technology, 1974, v. 24.

[27]   Svitak F. Code SAMOVAR-1 for Subchannel Stationary Thermal Hydraulic Analisys of Steam-Water Flow. Seminar Thermal Physics-74 "Study of Critical Heat Flux in Pin Bundles". M., IAE, Moscow, 1974.

[28]   Forti G., Gonsales-Santalo J. A Model for Subchannel Analysis of BWR in Steady State and Transient. Reactor Heat Transfer, Karlsruhe, 1973.

[29]   Betten P. B. Bowing of Element and Changes in Radial Coolant Temperature Profile over Subassembly Life Time. TANS 1986, v. 53.

[30]   Kovacs L. C., Szabados L. TURMIX - Computer Program to Determine Single-Phase Interchannel Mixing in Reactor Fuel Rod Bundles. KFKI-73-16. 1973.

[31]   Hirao S., Nakao N. DIANA - A Fast and High Capacity Computer Code for Interchannel Coolant Mixing in Rod Arrays. Nucl. Eng. and Des., 1974, v. 30.

[32]   Van der Ros. A Two-Phase Flow Exchange Between Interacting Hydraulic Channels. WWO15-R. 1970.

[33]   Sha W. T., Schmitt R. C., Huebotter P. R. Boundary-Value Thermal-Hydraulic Analysis of a Reactor Fuel Rod Bundle. Nucl. Science and Eng. 1976, v. 59.

[34]   Zhukov A.V., Kornienko Y.N., Sorokin A.P. et al. Methods and Codes of Subchannel Analysis of Pin Bundles Having Regard to Coolant Mixing. Analitical Overview - 107, Obninsk, 1980 (in Russian).

[35]   Mingaleeva G.S., Mironov Y.V. Thermal Hydraqulic Analusis of Multi-Pin Bundles in Single-Phase Flow. Atomic Energy, 1980, v.48.

[36]   Wheller C. L. COBRA-IV-I: An Interim Version of COBRA for Thermal-Hydraulic Analysis of Rod Bundle Fuel Elements and Cores. BNWL-1962. Battelle-Pacific Northwest Laboratories. Richland, Washington, 1976.

[37]   Marr W. W. COBRA-III M: A Modified Version of COBRA for Analysing Thermal-Hydraulics in Small Pin Bundles. Nucl. Eng. and Des., 1979, v. 53.

[38]   Macdougall J. D., Lillington J. N. The SABRE Code for Fuel Rod Cluster Thermohydraulics. Nucl. Eng. and Des., 1984, v. 82.

[39]   Basque G., Delapierre L., Grand D. et. al. BACCHUS. A Numerical Code to Two-Phase Flow in a Rod Bundle. Nucl. Eng. and Des., 1984, v. 82.

[40]   Arai M., Hirata H. Numerical Calculation For Two-Phase Flow Analysis in Pin Bundles. Nucl. Eng. and Des., 1984, v. 82.

[41]   Arai M, Hirata H. Analysis of the Central Blockage Wake in a LMFBR Subassembly. Nucl. Eng. and Des., 1978, v. 45.

[42]   Miyaguchi K. Analytical Studies on Local Flow Blockages in LMFBR Subassemblies Using the UZU Code. Nucl. Eng. and Des., 1980, v. 62.

[43]   Domanus H. M., Shan V. L., Sha W.T. Applications of the COMMIX Code Using the Porous Medium Formulation. Nucl. Eng. and Des.. 1980, v. 62.

[44]   Miao C.C., Baumann W.L., Domanus H.M. et. al. Two-Phase Thermal-Hydraulic Simulations with COMMIX-2. Nucl. Eng. and Des.. 1984. v. 82.

[45]   Kumaev B.J., Leonchuk M.P., Dvortsova L.I. Numerical Calculation of 3D Flow in Pin Bundles. Preprint IPPE-1733, Obninsk, 1985 (in Russian).

[46]   Dorr B., Homann Ch., Struwe D. State of Development of the Computer Programme BACCHUS-3D/TP for the Description of Transient Two-Phase in LMFBR Fuel Pin Bundles. Nucl. Eng. and Des.. 1987, v. 100.

[47]   Bottom M., Willerding G. Advanced Solution Algorithms for Transient Multidimensional Thermohydraulic Flow Problems in Complex Geometries with the Programme COMMIX-2/KfK. Nucl. Eng. and Des.. 1987, v. 100.

[48]   Ninokata H. Analysis of Low-heat-flux Sodium Boiling Test in a 37-Pin Bundle by the Two-Fluid Model Computer Code SABENA. Nucl. Eng. and Des., v. 97.

[49]   Zhukov A.V., Sorokin A.P., Matjukhin N.M. Interchannel Exchange in Fast Reactor Subassemblies: Theoretical Foundations and Physics of the Process, M., Energoatomizdat, 1989 (in Russian).

[50]   Walter A. E. MELT-III: A Neutronics-Thermal-Hydraulic Program for Fast Reactor Safety Analysis. HEDL-TME-74-47. 1974, Vol.2.

[51]   Doi K. Nuclear–Thermal–Hydraulic Characteristics of BWR Fuel Bundles. J. of Nucl. Science and Technology. 1975, v.12.

[52]   Parks C. V., Mandlin P. J. Application of Differential Sensitivity Theory to Neutronic–Thermal–Hydraulic Reactor Safety Code. Nucl. Technology, v. 54.

[53]   Hsiech T.C.-S., Billone M.C. LIFE-GCFR: A Computer Code for Prediction Gas-Cooled Fast Reactor Fuel Performance. Nucl. Eng. and Des.. 1981, v. 68.

[54]   Tanabe F., Matsumoto K., Yoshida K., Shimooke T. Post-Facta Analysis of the TMI Accident (II): Analysis of Fuel Rod Behavior and Core Damage Estimation by Use TOODEE-2-J. Nucl. Eng. and Des.. 1982, Vol. 69.

[55]   McCandless R. J., Neil G. V., Johnson D. D., Freerick B.T. LMFBR Core Dosing Optimization Method. TANS. 1976, v. 24.

[56]   Rouch P. Numerical Hydrodynamics, M., Mir, 1980.

[57]   Harlow F. H., Welch J.E. Numerical Calculation Time-Dependent Viscous Incompressible Flow of Fluid with Free Surface. Physics Fluids. 1971, v. 8.

[58]   Stewart C. W., Rowe D. S. Advanced Continuous-Fluid Eulerian Computation Scheme for Flows with Large Density Gradients. TANS 1976, v. 24.

[59]   Rose S. D., Dearing J. F., Clapp N. E. et. al. Experimental and Numerical Thermal-Hydraulic Results from a 61-Pin Simulated LMFBR Subassembly. TANS 1980, v. 34.

[60]   Patankar S. V., Spalding D. B. A Calculation Procedure for Heat, Mass and Momentum Transfer in Three–Dimensional Parabolic Flow. International J. of Heat and Mass Transfer. 1972, v. 15.

[61]   Patankar S.V. Numerical Solution of Heat Transfer and Hydrodynamics, M., Energoatomizdat, 1984.

[62]   Zhukov A.V., Sorokin A.P., Ushakov P.A.. Thermal Physic Validation of Fast Reactor Subassembly Temperature Fields Having Regard to Hot Spot Factors.Preprint IPPE-1778, Obninsk, 1986 (in Russian).

[63]   Kramerov A.J., Shevelev A.V. Nuclear Reactor Engineering, M., Energoatomizdat, 1984.

[64]   Mikhan I.J., Solonin B.I. et al. Nuclear Reactor Designing, M., Energoizdat, 1982.

[65]   Usynin G.B., Kusmartsev E.V. Fast Breeder Reactors, M., Energoatonizdat, 1985.

[66]   Waters A., Reynolds A. Fast Breeder Reactors, M., Energoatomizdat, 1986.

[67]   Kleomin A.N., Polianin L.N., Strigulin M.M. Thermal Hydraulic Calculation and Technological Realibility of Nuclear Reactors, M., Atomizdat, 1980.

[68]   Kurbatov I.M., Tikhomirov B.B.. Estimation of Random Temperature Deviations in Reactor Core. Preprint IPPE-1090, Obninsk, 1980 (in Russian).

[69]   Carelli M.D. Hot Channel Factor for Rod Temperature Calculations in LMFBR Assemblies. Nucl. Eng. and Des.. 1980, v. 62.

[70]   Zhukov A.V., Sorokin A.P., Ushakov P.A., et al. Statistic Estimation of Fast Reactor Core Having Regard to Deformation in Campaign. Preprint IPPE-1845, Obninsk, 1987 (in Russian).

[71]   Bogoslovskaya G.P., Zhukov A.V., Sorokin A.P. et al. Calculation of Statistic Temperature Characteristics in BN-600 Subassembly Using Monte-Carlo Procedure. Preprint IPPE-1376, Obninsk, 1985 (in Russian).

[72]   Tikhomirov B.B., Savitskaya L.V., et al. Models of Statistic Estimetion of Radiative Deformations. Paper on French-Soviet Seminar "Problems of Reactor Core Thermal Hydraulics", Cadarache, 1986.

[73]   Bogoslovskaya G.P., Sorokin A.P., Tikhomirov B.B. et al. Code TEMP-M for Thermal Hydraulic Analysis of Fast Reactor Subassemblies. Preprint IPPE-1401, Obninsk, 1983 (in Russian).

[74] Recommendations on Thermal Hydraulic Calculation of Fast Reactor Core. PTM 1604. 008-88. State Committee on Nuclear Energy. M., ONTI IPPE, 1988 (in Russian).

[75] Zhukov A.V., Kirillov P.L., Matjukhin N.M. et al. Thermal Hydraulic Analysis of Liquid Metal Fast Breeder Reactors, M., Energoatomizdat, 1985.

[76] Knut D. Art of Programming, M., MIR, 1977, v.2.

[77] Zhukov A.V., Sorokin A.P., Ushakov P.A. et al. Influence Interchannel Exchange on Velocity and Temperature Fields in Pin Bundles. Preprint IPPE-1062, Obninsk, 1980 (in Russian).

[78] Sorokin A.P., Ushakov P.A., Yuriev Yu.S. Influence of Interchannel Exchange on Velocity and Temperature Fields in Pin Bundles. Problems of Nuclear Science and Engineering. Physics and Eng., 4 (41), 1984 (in Russian).

[79] Markley R. A., Engel F. C. LMFBR Blanket Assembly Heat Transfer and Hydraulic Test Data Evaluation. Thermodynamics of FBR Fuel Subassemblies under Nominal and Non-nominal Operating Condition. Summary Report, Vienna, 1979.

[80] Kirillov P.L., Zhukov A.V. Modern Methods of Thermal Hydraulic Analysis of Reactor Subassemblies. Text-Book, Obninsk, OINPE, 1988 (in Russian).

NOMINAL SUBASSEMBLY THERMAL HYDRAULICS

3.1. FRICTION FACTORS

Bundles of smooth pins.
Laminar flow. Friction factor is defined as:

$$\lambda = \frac{64}{Re} K \tag{3.1}$$

where the values of the form factor K are indicated in the Table 3.1 in accordance with the data [1]; $Re = (w \cdot d_h)/v$ is the Reynolds number based on the mean velocity and hydraulic diameter of "infinite" pin bundle.

Table 3.1.Values of factor K_{lam} **in laminar flow through the smooth bundle**

Type of bundle	Relative pitch , s/d								
	1.0	1.02	1.05	1.10	1.20	1.30	1.40	1.5	2.0
Triangular	0.407	0.663	0.966	1.274	1.56	1.715	1.834	1.940	2.46
Square	0.406	0.518	0.679	0.913	1.264	1.510	1.699	1.858	2.51
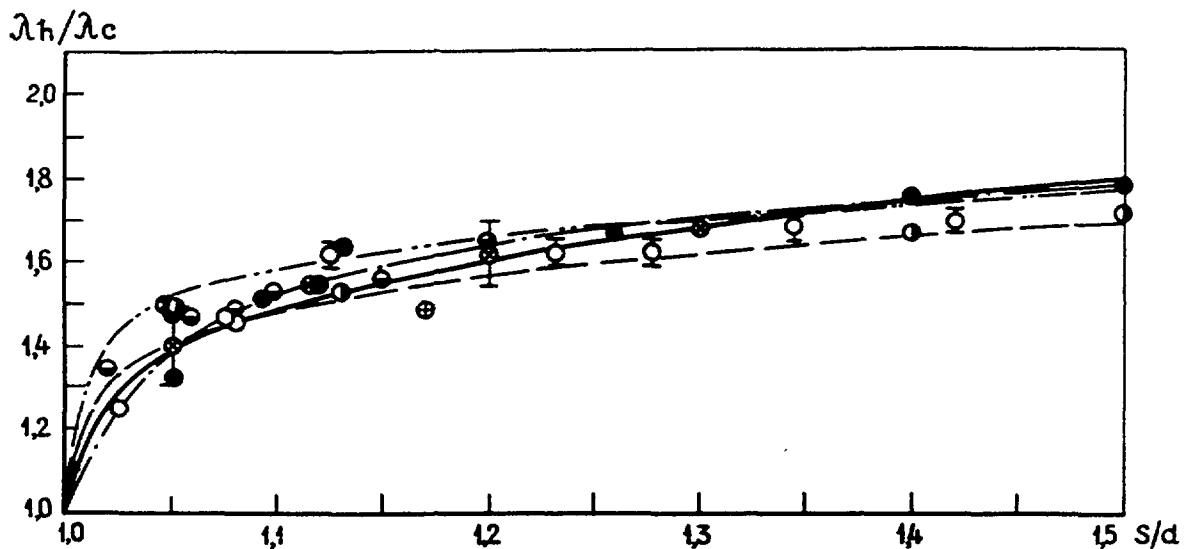
Fig. 3.1. Relative hydraulic resistance in the bundle of smooth pins with the pitch-to-diameter ratio:

———— *- relationship by the authors,* ⊜ , ○, ⊖ , ●, ◐ , ⊕ *-experimental data,* —— — , — · — , — ·· — *- predictions of other authors (*λ_c *- hydraulic resistance in compact bundle (S/d = 1.0)*

Turbulent flow. Considerable recent attention has been focused on the analysis of a rich variety of the data accumulated on the friction factors in "infinite" bundles of smooth pins that results in the following simple relationship [2]:

$$\lambda = \frac{0.210}{Re^{0.25}}\left[1+\left(\frac{s}{d}-1\right)^{0.32}\right]$$

(3.2)

$$1.0 \le s/d \le 1.5; \quad 6\cdot10^3 \le Re \le 2\cdot10^5.$$

The relationship (3.2) is in a good agreement with the results of experimental and numerical investigations into hydraulic resistance of multi-pin bundle (Fig. 3.1).

Transition from laminar to turbulent flow. The following relation can be recommended:

$$lg\,\lambda = 5.2\,Re^{-0.22+0.145(s/d-1)}-2.35$$

(3.3)

The same formula describes friction factor over a wide range of parameters ($10 \le Re \le 2*10^5$; $1.0 \le s/d \le 1.5$), with an accuracy being $\pm 20\%$.

When arranged in square bundle the pins produce resistance in accordance with the well known relationship:

$$\frac{\lambda}{0.316Re^{-0.25}} = 0.59+0.19\left((s/d)-1\right)+0.52\left\{1-exp\left[-10\left((s/d)-1\right)\right]\right\}$$

(3.4)

$$1.0 \le s/d \le 2.,0\,; \quad 10^4 \le Re \le 5\cdot10^5.$$

Wall channels and subassembly as a whole.

Friction factors in laminar and turbulent flow can be expressed through the geometrical parameters χ_L and χ_T, respectively [3]:

$$\lambda = \frac{64}{Re}\chi_L^2$$

(3.5)

$$\sqrt{\frac{\chi_T}{\lambda}} = 2\,lg\,\frac{Re\sqrt{\lambda}}{\chi_T^{1.5}}-0.8$$

(3.6)

Experiments have shown that parameters χ_L and χ_T are related to each other as:

$$\chi_T = \frac{1+3\chi_L}{4}$$

(3.7)

$$0.25 < \chi_L < 1.25;\ 0.45 < \chi_T < 1.2$$

Fig. 3.2, 3.3 show the values of parameters concerning fast reactor subassembly. The wall channels are considered here and an influence of the pin number on these parameters is demonstrated.
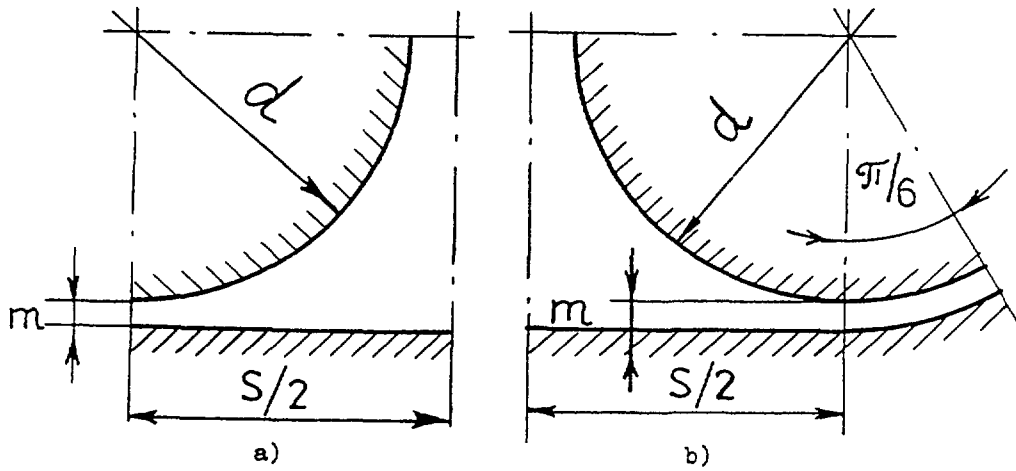
*Fig. 3.2 Coefficient and schematic elements of BN-600 subassembly
(S/d =1.166, m/d =0.1045):*

$$\chi_L = 1.030; \quad \chi_T = 1.023 \qquad (a)$$

$$\chi_L = 0.603; \quad \chi_T = 0.703 \qquad (b)$$

№ ряда
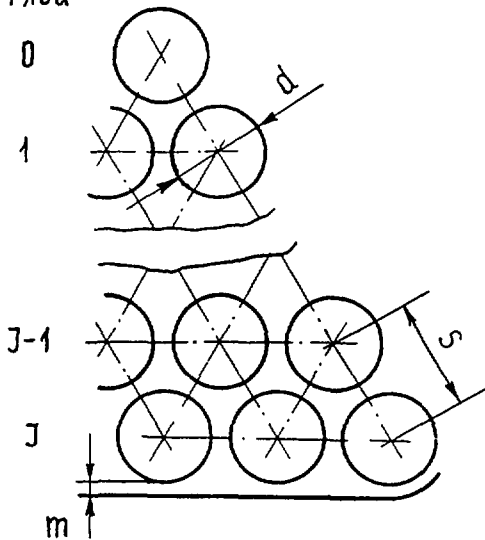
$$d_r = d \; \frac{4,719 \, J^2 + 7,501(J-1) + 5,810}{9,425 \, J^2 + 16,425(J-1) + 23,365}$$

J	n	$\mathscr{æ}_L$	$\mathscr{æ}_T$
1	7	0,774	0,830
2	9	0,982	0,987
3	37	1,059	1,044
4	61	1,098	1,073
5	91	1,120	1,090
6	127	1,135	1,101
7	169	1,145	1,109
8	217	1,152	1,114
9	271	1,158	1,119
10	331	1,163	1,122
11	397	1,166	1,125

*Fig. 3.3. Coefficients $\mathscr{æ}_L$ and $\mathscr{æ}_T$ for pin bundle of BN-600 type:
J - number of rows, n - number of pins, S/d = 1.166; m/d = 0.1045.*

Bundles of wire wrapped pins.

When in **laminar flow** in the bundle of wire wrapped pins, friction factor can be evaluated as:

$$\lambda_P = \frac{64}{Re}\left(0.407 + 2.0\sqrt{(s/d)-1}\left[1 + \frac{17.0\big((s/d)-1\big)}{(h/d)}\right]\right) \tag{3.8}$$

$1.125 \leq s/d \leq 1.417 \; ; \; 10^2 \leq Re \leq 2\cdot10^3 \; ; \; 8.3 \leq h/d \leq 50.$

In **turbulent flow** analysis of the data on friction factor in triangular bundle of the pins spaced by the helical wire of the type "fin touches the pin wall" has caused the following formula for the infinite pin bundle [2]:

$$\lambda_P = \frac{0.210}{Re^{0.25}}\left\{1 + \frac{124}{(h/d)^{1.65}}\big[1.78 + 1.485(s/d-1)\big]\cdot(s/d-1)\right\} \tag{3.9}$$

$1.0 \leq s/d \leq 1.5 \; ; \; 10^4 \leq Re \leq 2\cdot10^5 \; ; \; 8.0 \leq h/d \leq 50.$

The formula is simple in structure, with passing on to (3.2), if s/d = 1.0. It is in agreement with the experimental data [4,5] with an accuracy of ± 15%.

To predict friction factor exactly, but in the lesser range of parameter h/d, the following formula is recommended [2]:

$$\frac{\lambda_P}{\lambda} = 1 + f(h/d)\cdot(s/d-1)\,Re^{0.038} \tag{3.10}$$

where

$$f(h/d) = 30.3956 - 4.5911(h/d) + 0.24308(h/d)^2 - 0.0042955(h/d)^3$$

$1.0 \leq s/d \leq 1.5 \; ; \quad 8.0 \leq h/d \leq 25; \quad 6\cdot10^3 \leq Re \leq 2\cdot10^5.$

λ is defined by the (3.2).

Relationship (3.10) agrees with the experiments [4.5] with an accuracy ± 10%, but improves formulas recommended in [5,6] (Fig. 3.4). It, as relation (3.9), makes possible going to the compact bundle of smooth pins. It is interesting to notice that experimental data generalized by the well-known Novendstern's formula [6]:

$$\lambda_P = \frac{0.3164}{Re^{0.25}}\left[\frac{1.034}{(s/d)^{0.124}} + \frac{29.7(s/d)^{6.94}\,Re^{0.086}}{(h/d)^{2.239}}\right]^{0.885} \tag{3.11}$$

$1.06 \leq s/d \leq 1.42 \; ; \quad 2.6\cdot10^3 \leq Re \leq 2\cdot10^5 \; ; \; 8.0 \leq h/d \leq 96$

lie in the range ± 30% (at least at great Re), that is worse than ± 15% indicated by the author of publication [6].
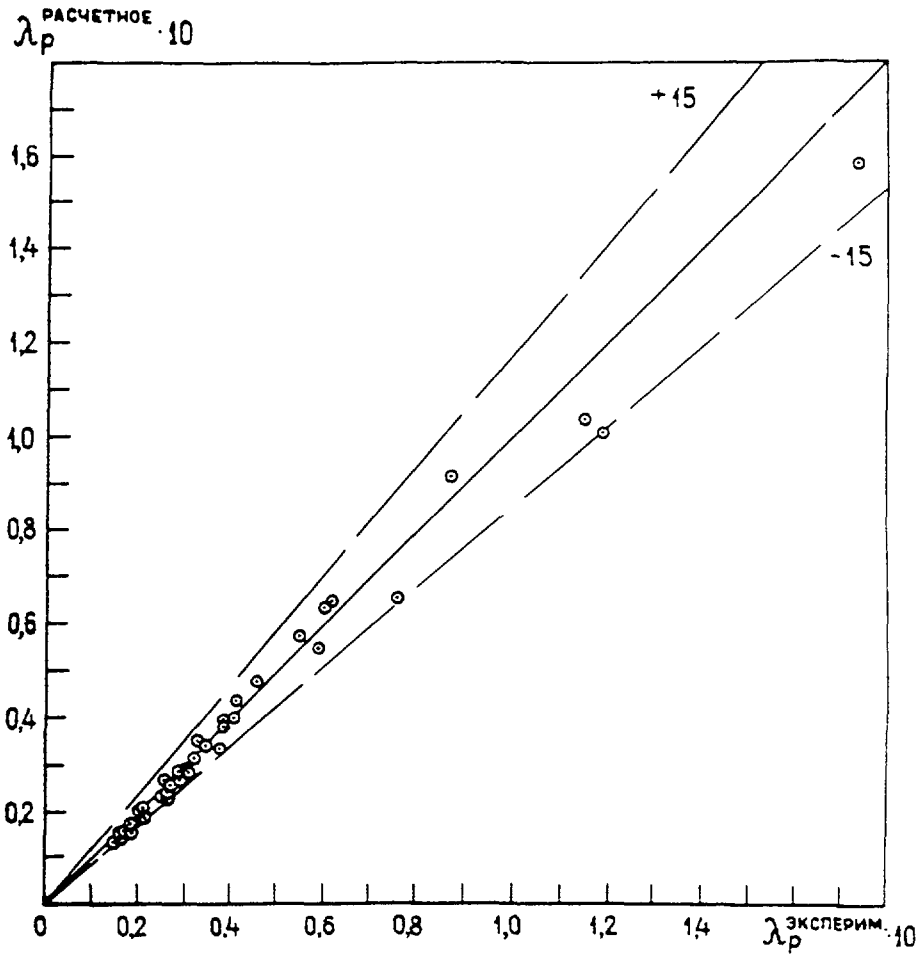
Fig. 3.4. Comparison of predicted hydraulic resistance '
with experimental data by different authors.

Markley R.A. presented the following relations:

laminar flow

$$\lambda_P = \frac{110}{Re}$$
(3.12)

$(2 \le Re \le 400; \quad 1.067 \le s/d \le 1.32; \quad h/d \approx 8);$

transition flow

$$\lambda_P = \frac{110}{Re}\sqrt{1-\psi} + \frac{0.48}{Re^{0.25}}\sqrt{\psi}$$
(3.13)

$(2 \le Re \le 500; \quad 1.067 \le s/d \le 1.32; \quad h/d \approx 8);$

where $\psi = 0.22 \cdot 10^{-3}(Re - 400)$
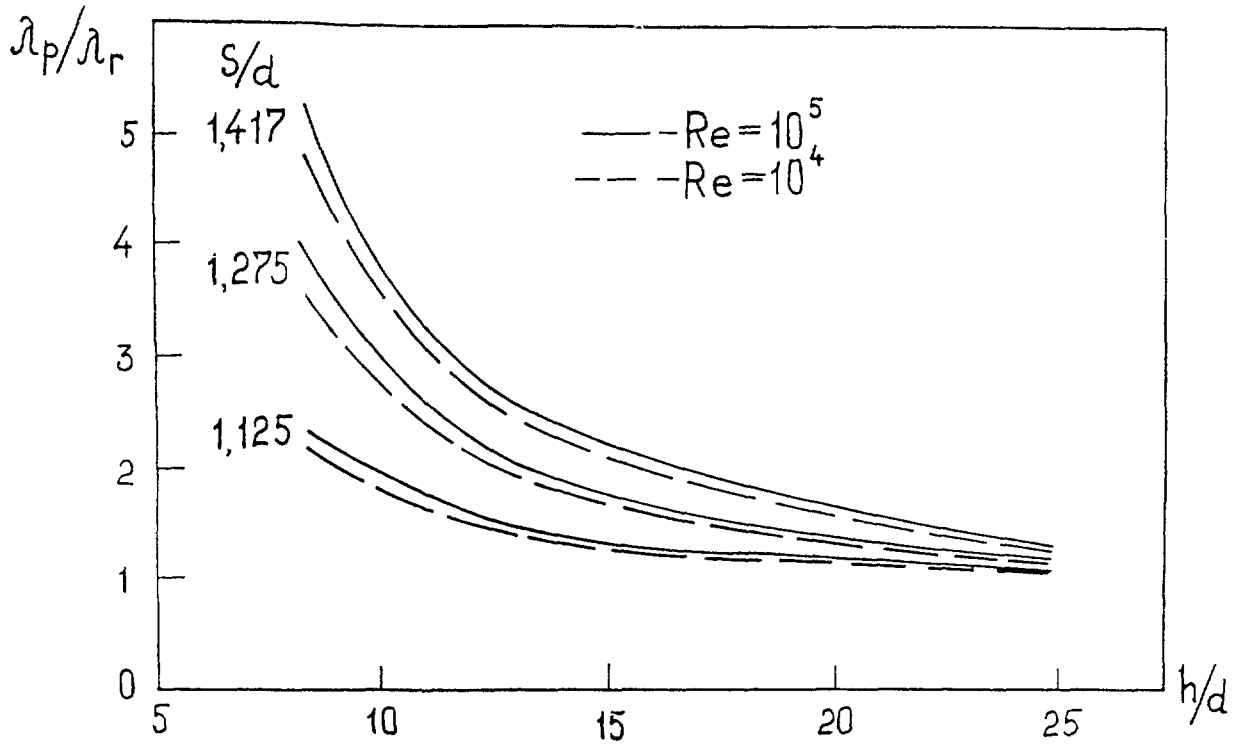
Fig. 3. 5. Relative hydraulic resistance in the bundle of wire wrapped pins.

turbulent flow

$$\lambda_P = \frac{0.48}{Re^{0.25}} \tag{3.14}$$

(Re > 5000; 1.067 ≤ s/d ≤ 1.32; h/d ≈ 8).

For the BN-600 fuel subassembly the following formula was derived by the authors from the in-pile measurements:

$$\lambda_P = 0.117\left(\frac{\Delta}{d_h} + \frac{68}{Re}\right)^{0.25} \tag{3.15}$$

where Δ - is the roughness of the pin surface. Ratio λ_p/λ is shown in Fig.3.5.

Also in the transition flow it is recommended that the following relationship be used:

$$\lambda'_p = \lambda_{Plam}\varepsilon + \lambda_p(1 - \varepsilon) \tag{3.16}$$

where λ_{Plam} - friction factor in the bundle of wrapped pins in laminar flow defining by (3.8), λ_p - friction factor in accordance with (3.9).

86

Parameter ε can be determined as:

$$\varepsilon = 0.5\left\{1 - th\left[0.80\left(\frac{Re}{1.45\cdot 10^3} - 1\right)\right]\right\}$$ (3.17)

An accuracy of the relationship (3.16) is about 20%.

In the event the pin spacer is performed by the "fin-to-fin" type of wire wrap, the friction factor adheres to the relations [1]:

laminar flow

$$\lambda_p/\lambda \approx 1 + \left[1.8/(h/d)\right]$$ (3.18)

(s/d varies from 1.13 to1.15);

turbulent flow

$$\left(\lambda_p/\lambda\right) \approx 1 + \frac{600(s/d - 1)}{(h/d)^2}$$ (3.19)

$10^4 \leq Re \leq 20\cdot 10^4$; $1.05 \leq s/d \leq 1.25$; $h/d \geq 5$; $2 \leq n \leq 4$;

where *n* is the number of entries of the fin.

Inclined flow throughout the bundle.

In triangular bundle the friction factor depends on the slope:

$$\frac{\lambda_\varphi}{\lambda_{90^o}} = sin^2\,\varphi + \left(\frac{\lambda_z}{\lambda_r}\right)cos^2\,\varphi$$ (3.20)

where

$\lambda_z = \dfrac{\Delta p d_h \cdot 2}{l\rho\,\overline{w}^2}$ is the friction factor in longitudinal flow,

$\lambda_r = \dfrac{\Delta p d_h \cdot 2}{l\rho\,\overline{w}^2}$ is the friction factor in transverse flow,

$\overline{w} = \overline{v}/\varepsilon$ - velocity averaged over the bundle, $\overline{v}$- free flow velocity, ε- porosity.

U⁺

25

$e = 17,2\,mm\ \ Re_b^{\infty} = 185\ 700$

TYČ č	φ	
4	90°	+
	150°	X
	180°	O
5	240°	□
6	300°	λ
7	0°	Y
	60°	△

20

15

$U^+ = 5,75\ \log y^+ + 5,5$

$e = 20,4\,mm\ \ Re_b^{\infty} = 187\ 000$

TYČ č	φ	
4	300°	+
	210°	X
5	225°	O
	261°45'	□
6	240°	λ
	300°	Y
	325°15	△

U⁺

25

20

15

4 5 6 8 10²   2   3 4 5 6 8 10³   2   3 4 5 6   y⁺
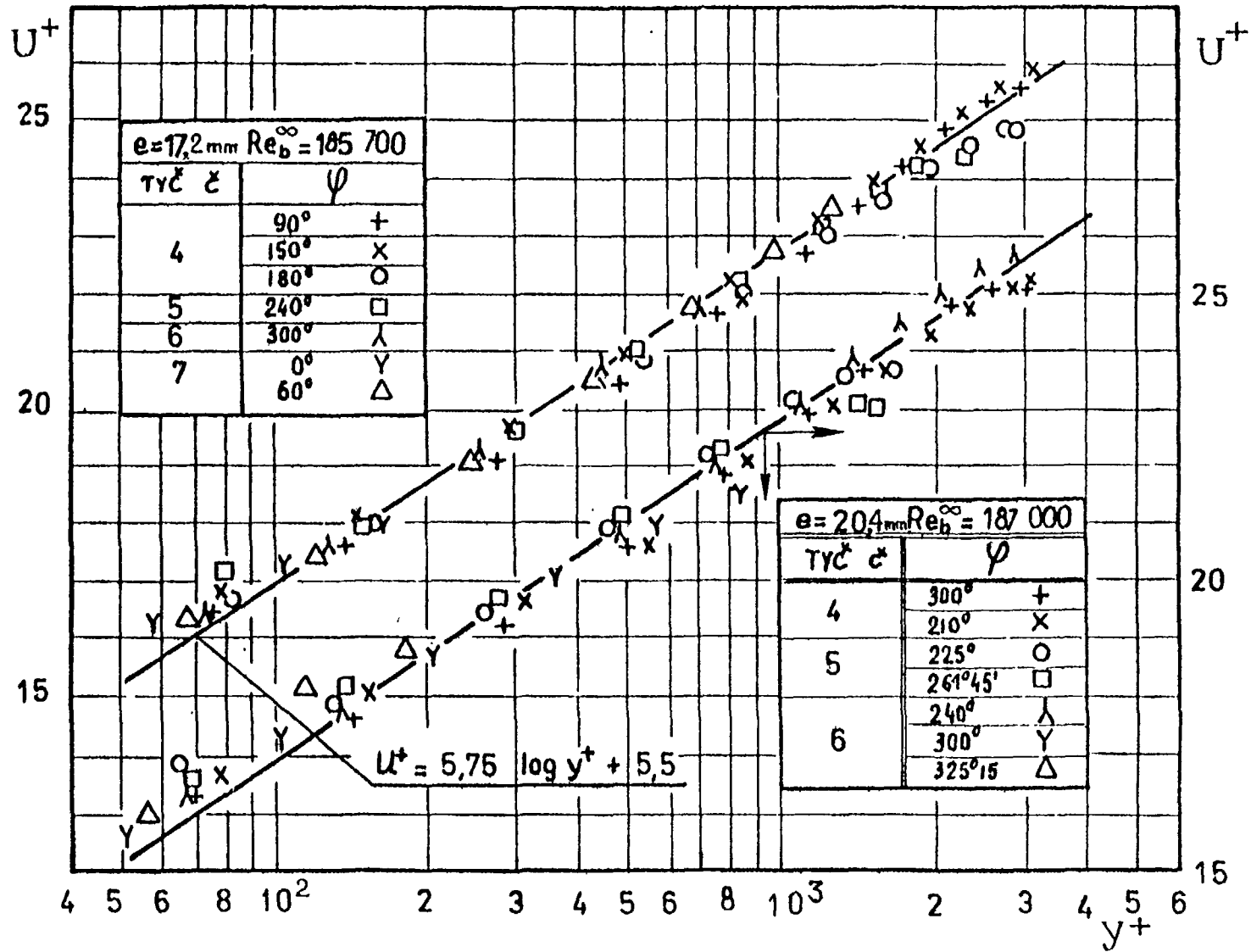
Fig. 3.6. Comparison of experimental data with predicted on universal Prandtl velocity in deformed bundle.

Transverse flow in triangular bundle. Friction factor is determined with an accuracy $\pm$ 20% as:

$$\lambda_r = \left(s/d - 1\right)^{-0.125} K_p \cdot 10^{\left(3.14 Re^{-0.22} - 0.42\right)}$$ (3.21)

where parameter K_P accounts for an influence of the I -entries of wire wrap with the pitch h; $x = s/d$ - relative pitch of the bundle.

$$K_p = \left[I - \frac{I}{\pi}\sqrt{\left\{\left(2 - \frac{1}{x}\right)^2 - 1\right\} \cdot \left\{1 + \left(\frac{\pi x d}{h}\right)^2\right\}} \right]^{-2}$$ (3.22)

Distribution of local velocity over the bundle (smooth pins). The basis for the calculation of velocity in turbulent flow is distribution of shear stress around the pin which is used when universal velocity profile is defined (for the bundle of smooth pins at least). The use of universal velocity profile for the bundles of as nominal and deformed geometry was warranted by experiments [8,9].

For use in practice the most simple and rather precise relation by Prandtl can be recommended:

$$\left. \begin{array}{l} U^+ = y^+ \quad for \ 0 \le y^+ \le 11.5 \\ U^+ = 2.5 ln\, y^+ + 5.5 \quad for \ y^+ > 11.5 \end{array} \right\}$$ (3.23)

Fig. 3.6 compares relation (3.23) with experimental data [10] gained in the internal channel of the fast reactor subassembly model under deformation.

3.2 CLASSIFICATION OF INTER-CHANNEL EXCHANGE PROCESSES AND EXPERIMENTAL TECHNIQUE

Inter channel exchange (mixing) is the process when the coolant flowing in the parallel channels exchanges by liquid portions, that causes the temperature difference between the channels to reduce. Clearances between the pins joining the channels into a unified system assure generally an exchange by mass, momentum and energy. Among the main mechanisms are convective transport, turbulence diffusion and molecular transfer (electronic one in liquid metal).

Classification of inter-channel exchange processes. Natural and forced mixing are recognised. In its turn process of natural mixing can be subdivided into turbulent exchange and lateral diversion flow, induced by the pressure gradient when flowing under not steady

conditions (entrance section) or by departure of geometry from the nominal. Forced mixing is associated with the coolant flow due to special mechanical means (wire wrap, spacer grid and so on). It can be subdivided into dissipation flow and spin one. The first mechanism is governed by the means not responsible for a directional flow, but the enhancement of turbulence (spacer grid, end pieces and so on). Spin flow is due to means setting up directional flow (helical wire wrap).

Non-uniform temperature distribution over the pin brings into existence the heat flux be redistributed over the pin perimeter defining one more mechanism of inter-channel energy exchange due to heat conduction within the pin. In the event of the coolant passing the clearance between subassemblies, the heat exchange due to wrapper heat conduction occurs.

Mixing factor can be identified in a accordance with the transported substance.

Having considered the mass transfer, let as define mass mixing factors, m^{-1}, as the ratio between transverse mass flow, accounted for by the unit length of the slot channel, and the full axial flow.

$$\mu^M = G_{ij} / G_I.$$ (3.24)

where G_{ij} is the transverse coolant flow from the channel i to the channel j per the unit length, $m^3/m*s$; G_I is the axial coolant flow throughout the channel i, m^3/s. In such a definition the mixing factor has hydrodynamical meaning.

Having written a quantity of the heat transferred from one channel to another in the from $Q_j = G_{ij} \Delta z (\overline{h} - \overline{h_{ij}})$, we obtain the thermal mixing factor:

$$\mu^T = \frac{Q_{ij}}{G_I \Delta z (\overline{h}_I - \overline{h}_J)}.$$ (3.25)

that shows what fraction of the enthalpy difference between the adjacent channels the transverse heat flux will be.

When solving momentum equation, it is important to know the value of momentum mixing factor determining as follows:

$$\mu^M = \frac{\int_{\omega_{ij}} [\rho(v + v_T) \partial W/\partial n - \rho \overline{W'V'}] d\omega}{\rho \overline{W}(W_J - W_I) \omega_I \Delta z}$$ (3.26)

where $\rho(v + v_T) \partial W / \partial n$ is the momentum transferred by gradient mechanism due to molecular friction and small-scale eddies; $\rho \overline{W'V'}$ is the momentum transfer due to large-scale eddies (W'- velocity pulsation in axial direction, V'- large eddies velocity pulsation around the channel perimeter); ω_{ij} - area of the clearance between the channels i and j; ω_I -

the channel cross section area; $\overline{W} = \left(W_i + W_j\right)/2$ - mean velocity in the channels i and j. It should be noted that (3.26) is written for the bundle of smooth pins. The mixing factor, obtained by this means, shows what a fraction of momentum difference between the adjacent channels represents the transverse momentum flow.

So, we can speak about the mass, momentum and energy (heat) mixing factors. In general, these factors vary in value. It is essential that mass and heat mixing factor can be measured in experiments, but techniques for momentum mixing factor are unavailable. From here on we assume that the mass mixing factor is equal to the momentum mixing factor ($\mu_m = \mu_h$) and use hydrodynamic and thermal mixing factors.

The specific mixing factor representing ratio between the transverse and axial mass velocity is:

$$\beta = \frac{w_{\Pi}}{w_z} = \frac{G_{ij}}{s-d}\frac{\omega_i}{G_i} = \mu^{\Gamma}\frac{\omega_i}{s-d}. \tag{3.27}$$

As for the local and average mixing factor [11,12], it should be noted that periodical (for example sinusoidal) variation in local mixing factor (wire wrap on the pin) [12] the average over the pin length factor is defined as ($z \gg h$):

$$\mu_k^+ = \mu_k^- = \frac{1}{2}\,A\,\frac{1}{h/2}\int_o^{h/2}\sin\frac{2\pi z}{h}dz = \frac{A}{\pi}, \tag{3.28}$$

where: A is the amplitude of the local mixing factor variation, h is the wire wrap pitch. Result is divided to 2 because the suggestion was made about the uniform exchange along the clearance between pins (discrete rectangles resulting from the averaging sinusoid half-periods are replaced by equivalent continuous rectangle).

Generally dimensionless mixing factor depends on the relative pitch (s/d), pitch of helical wrap (h/d), Reynolds and Prandtl criteria, number of fins (l) and their geometry:

$$\mu L = f\left(s/d, h/d, Re, Pr, \Gamma p, J\right), \tag{3.28a}$$

where L is a some linear dimension, Γ_p is the criterion involving geometrical features of the fins. The most essential parameters effected the mixing factor (at the chosen type of the wrap) are: pitch of the bundle, pitch of the wrap and Reynolds number. An influence of these parameters are discussed in detail below.

Mixing factors are required to close system of mass, momentum and energy conservation equations. An accuracy of the predictions performed is appreciably defined by an accuracy of the numerical relations on the mixing factors. Being correct in evaluating mixing factors we met one of the necessary conditions for fast reactor subassembly thermal hydraulics.

Effective (combined) mixing factor represents the sum of components. When momentum exchange considered, these are convective and turbulence transport

$$\mu_{ef}^M = \mu_C^T + a\mu_T^M ,$$

(3.29a)

when heat exchange considered including convective, molecular, turbulence exchange and heat transfer due to pin heat conduction:

$$\mu_{ef}^T = \mu_C^T + a\mu_T^T + \mu_{\lambda fluid}^T + \mu_{\lambda pin}^T .$$

(3.29b)

where $\alpha \leq 1$ is the factor allowing for influence of the convective component on the turbulence one. This influence can be estimated as follows:

$$\mu_T = \mu_T^0 \left[1 - \frac{\mu_C}{2\mu_T^0} + \frac{1}{4} \cdot \left(\frac{\mu_C}{2\mu_T^0} \right)^2 \right], \text{ if } \mu_C / \mu_T^o \leq 4;$$

$$\mu_T = 0, \text{ if } \mu_C / \mu_T^o > 4,$$

(3.29c)

where μ_T^0 - mixing factor in the bundle involving smooth pins.

The use of the effective mixing factor is convenient for the concrete reactor, as allowing the temperature behaviour to be calculated (if the value of this factor is given). Also the knowledge of the components of the effective heat mixing factor is of practical importance. As applied to fast reactors, measurements the effective (total) mixing factor and its separate components were carried out.

Factor of non-equivalent heat and mass transfer. The "flat" model of mixing holds that an uniform temperature distribution takes place inside of the parallel channels, but temperature step is obtained in the clearance between the channels. In this case, transverse mass flow transfers the greatest possible quantity of heat due to convection and thermal mixing factor is equal to hydrodynamical one ($\mu_c^T = \mu_c^M$)

Any disagreement with the flat model (account for the molecular and turbulent diffusion, heat conduction) results in the non-uniform temperature distribution across the channel and is responsible for the fact that convective heat transfer is lesser than those under the uniform temperature conditions. This allows entering the non-equivalence factor between energy and mass transfer:

$$\beta = \mu_c^T / \mu_c^M .$$

(3.29d)

which varies in the range $0 < \beta < 1$ and depends on Pr. In liquids with $Pr \approx 1$ (water, gas) $\beta \approx 1.0$. As a first approximation, the non-equivalence factor may be through of as the same for the pins with the various types of wire wrapping.

The effective mixing factor μ_{ef}^T measured in thermal experiment is responsible for not only convection, but heat transfer due to turbulence diffusion and heat conduction of coolant

and pins, that is why the difference $(\mu_{ef}{}^{T} - \beta * \mu^{M})$ corresponds to conduction and turbulence diffusion.

Theoretical analysis of the non-equivalence factor is performed in [14], with experimental validation of its value presented by the authors in [12, 15, 16]

Experimental techniques. An overview of methods available to detect the mixing factors with reference to an accuracy performed by the authors is presented in [9]

Tracer technique starts from recording transverse mass flow of some transmitted substance (salt, paint, freon and so on) and falls in the category of indirect methods. If tracer is entered into the channel i bordering three channels j, the mixing factor can be recognised from the variation in tracer concentration over the channel length (φ_i, φ_j).

$$\mu = -\frac{1}{\varphi_i - \varphi_j} \frac{d\varphi_i}{dz}.$$ (3.30)

The mixing factor defined by this means includes the components being responsible for convection, turbulence and molecular diffusion. But it should be noted that tracer technique is not sufficiently sensitive (expect the freon technique), because a large quantity of tracer needs to be injected into the flow under study, that may cause the coolant flow to be distorted. This technique furnishes information on the mean mixing factors and is in common for controlling the small Prandtl number coolant.

Thermal trace technique. As a peculiar kind of tracer in studying process of inter-channel exchange the heat is supplied to the coolant. Modifications of the method vary in way of energy supplying.

So, in **injecting coolant at higher temperature into the main flow**, a knowledge of the heat released and liquid temperature behaviour along the channels allows the mixing factor to be estimated in integral form. Dissipation of hot spot from the flow injected is a transient process going on from the "entrance thermal section" law, with the strong heat dissipation into the adjacent channels. This version is applied in studying mixing under conditions of great temperature differences. An accuracy of the data obtained depends on the inlet structure (hydraulic instability), on the edge region influence and others. To improve accuracy is favoured by the enhancement of the pin number, at least up to 37. The effective mixing factor is measured, as studing the local characteristics becomes more complicated. As usual, liquids with the moderate Prandtl number are used as coolants.

To study an integral mixing characteristics the technique can be used involving **the power production only in the internal pin**, with the radial temperature distribution being measured over the bundle. The mixing factor is determined from the heat balance equation:

$$G_i C_p \frac{d\bar{t}_i}{dz} + \sum_{j=1}^{3} \mu^{\mathrm{T}} G_i \left(\bar{t}_i - \bar{t}_j \right) = q_i \Pi_i$$ (3.31)

where Π_i is the heat removal perimeter.

This method is used in viewing the sections far removed from the subassembly inlet, where considerable temperature difference between channels take place. The measurements are performed, as usual, under the stabilised hydraulic conditions. An influence of the edge regions and inlet structure on the readings shows itself as the more slight effect than in injecting.

The modified thermal trace technique involving the measurements of local temperature distributions over the length and radius, when only one internal pin is heated, was developed by the authors applied to liquid metal reactors [17]. The main objective of the modification is to provide for measuring the local characteristics of inter-channel mixing. Mobile thermocouples to measure pin wall temperatures are embedded into the surface of turning pin simulator. On having solved thermal problem the coolant temperature distribution along the channel is defined. The local mixing factors are put in calculation, and when varying values of mixing factors we can gain good agreement between prediction and experiment. Coolant temperatures measured at the outlet allows an integral (effective) mixing factors to be determined.

This technique was developed also as applied to the bundle of pins with spacing "fin-to-fin". In this case, temperatures are measured by the mobile thermoprobes moved inside of the pin simulator as in axial and in azimuthal directions.

Electromagnetic technique. The problem of evaluation of a "pure" convective component of mass exchange providing the local measurements is of great importance. Separating out the convective components from the total mixing factor allows the process of interchannel exchange to be expanded, an influence of this component on the main parameters to be defined in experiments. The local character of the measurements permits a nature of the process to be studied, departure of integral characteristics from the local readings to be defined. Electromagnetic technique is capable of meeting the requirements mentioned above as in the model and in-pile experiments [16, 18].

As noted above, the technique is built upon the use of electromagnetic sensors involving one or two magnets inside of the pin simulator. Voltage between electrodes varies in proportion to the local mass flux. Electromagnetic technique gives the measurements being in not more 2-3% error, that is more precise than techniques mentioned above. This technique is very simple, low in cost, economic and effective, that places it among the most advanced experimental technique in studying inter-channel exchange.

3.3. INTER-CHANNEL EXCHANGE IN THE INTERNAL AND EDGE AREAS OF WIRE WRAPPED PIN BUNDLE

Mass exchange. In practice, to guard against any possible bendings the pins are spaced by the helical wire.

The main component of inter-channel exchange when in bundle of wrapped pin is a convective mixing. The object of systematic researches using electromagnetic technique is to get reliable data on mass mixing factor, to study influence of the component on defining parameters, recommend relationship on hydraulic mixing factor.
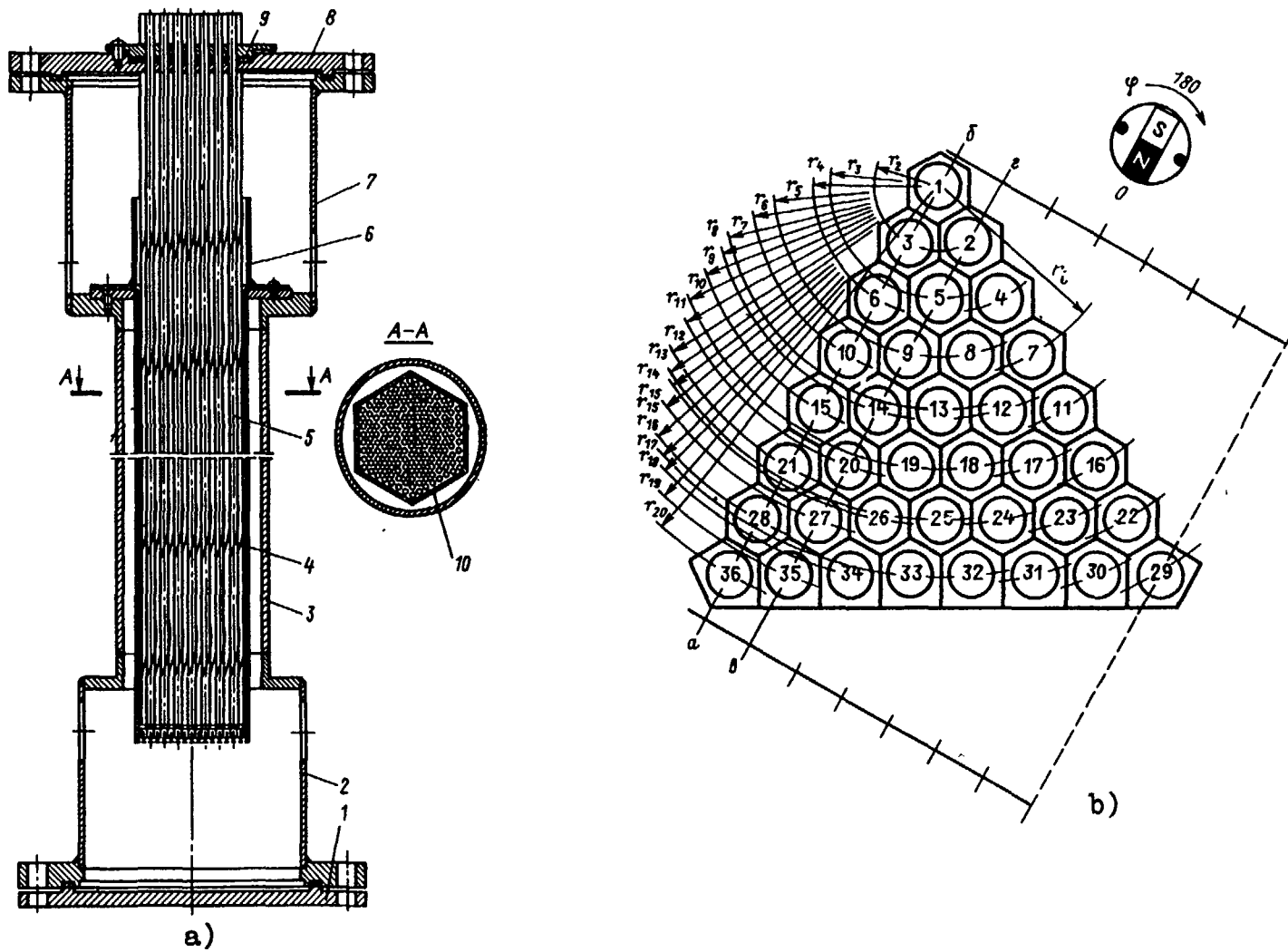
Fig. 3.7. In-pile subassembly of BN-350 (a) and positions of sensors (b):

a) 1 - bottom flange, 2 - bottom header, 3 - body, 4 -fins, 5 - pipes, 6 - barrel, 7 - top header,
   8 - top flange, 9 - seal, 10 - wrapper tube:

b) 1÷36 - pin number, r_2 ÷r_{20} - radii of the pins axises.
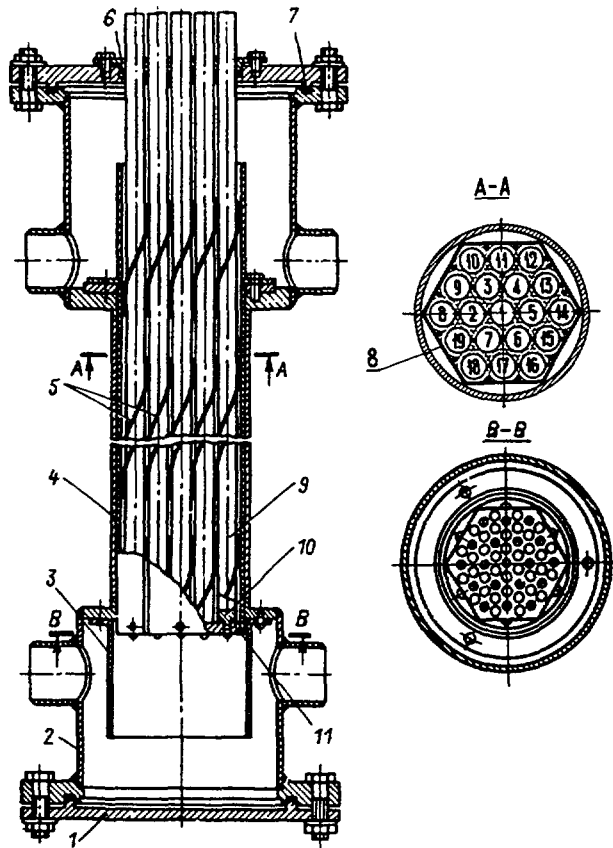
Fig. 3.8. Subassembly model to study interchannel exchange: 1 - flange, 2 - header, 3 - barrel, 4 - body, 5 - fins, 6 - gland, 7 - gasket, 8 - pipes19 0.5mm,9 - wrapper tube, 10 - tail, 11 - supporting grid.
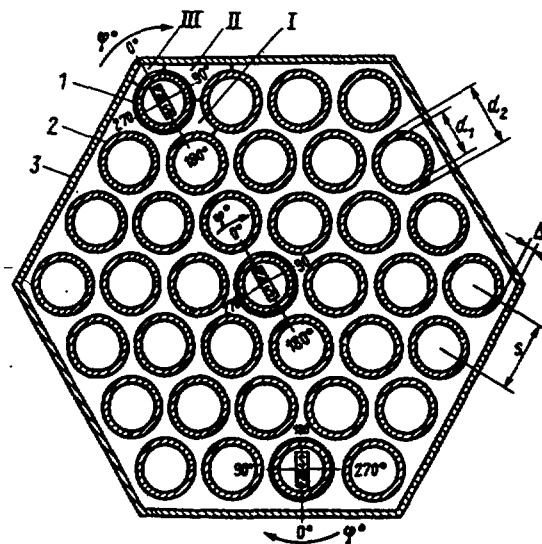
Fig. 3.9. Model cross section:
1 - turning pin with electromagnetic sensor inside,
2 - fuel pin simulator, 3 - wrapper tube, I÷III - specific channels.

96
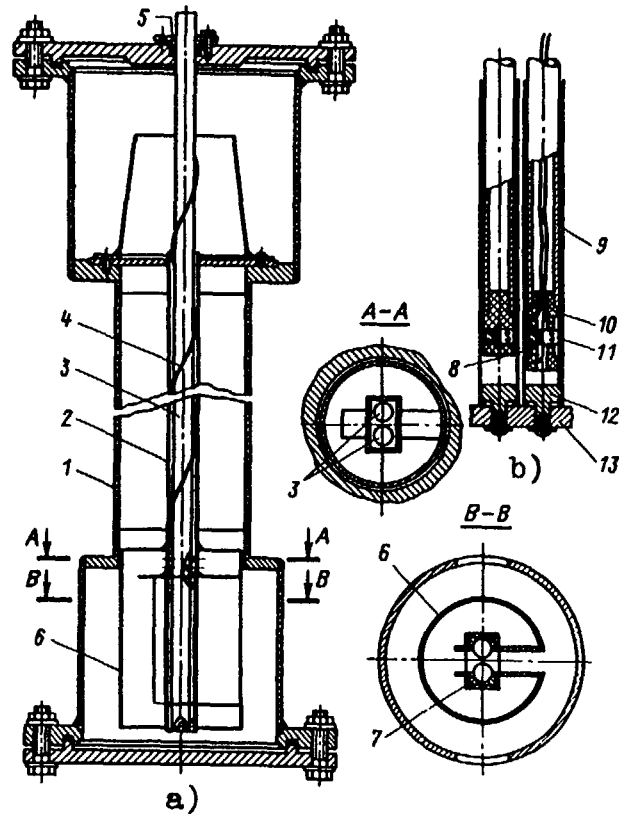
Fig. 3. 10.   Calibration model (a) and sensor (b):
1 - model body, 2 - wrapper tube, 3 - pipes
, 4 -wire wrap, 5 - gland,6 - guide barrel,
7 - displacers,8 - mobile contacts, 9 - guide rod,
10 - sleeve holder, 11 - permanent magnet,
12 end plugs, 13 - pipe spaces.
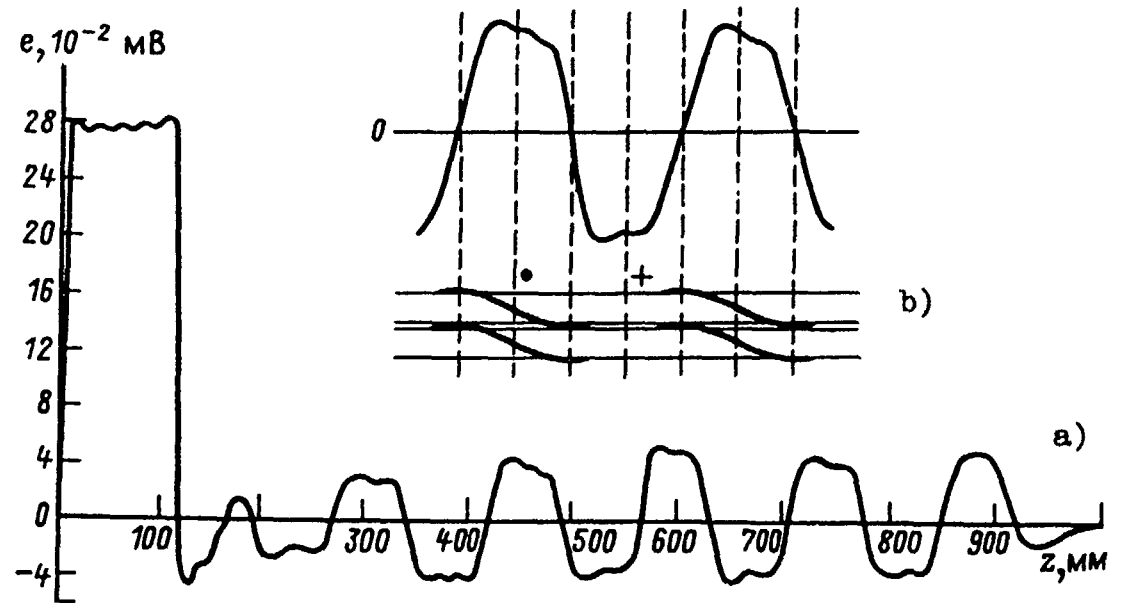
Fig 3.11.   Signal of sensor with the length of the calibration
model (a) and measurement scheme for lateral flows in the
clearance (b), • , + - directions of lateral flows.
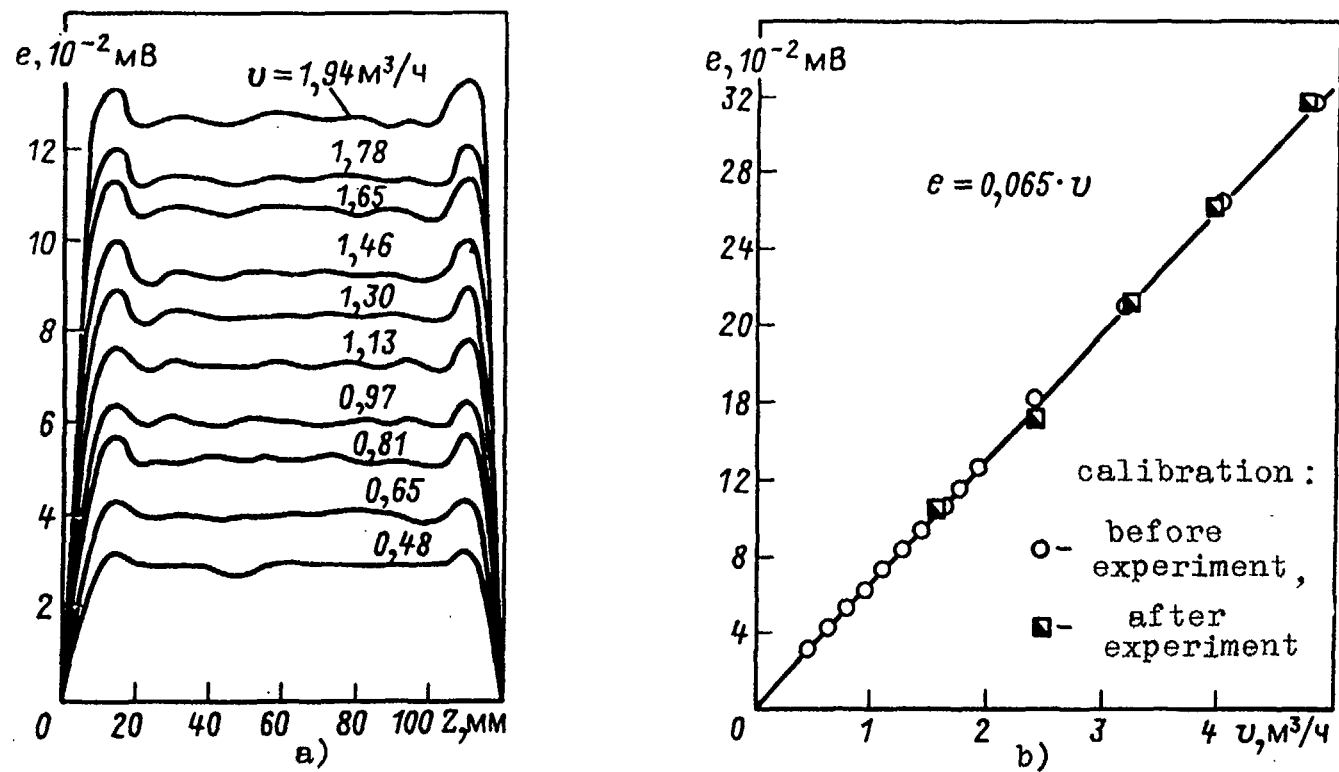
Fig. 3.12. Sensor signal with the length of calibration section (a) and signal value with the flow through the model (b)
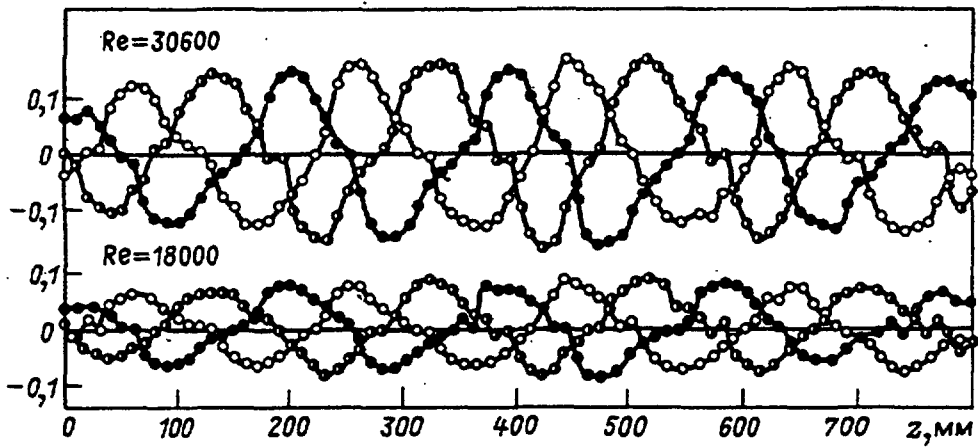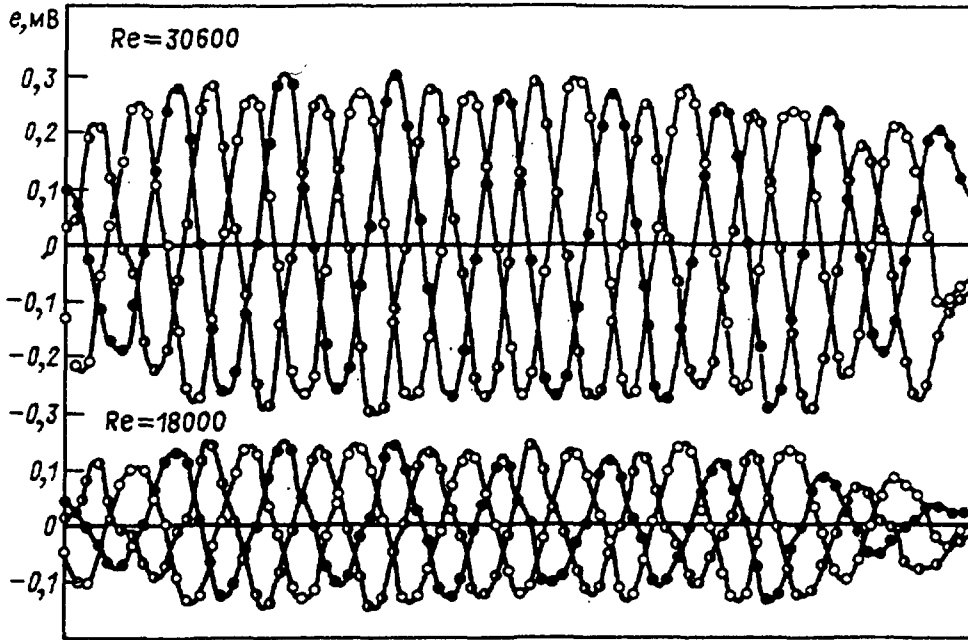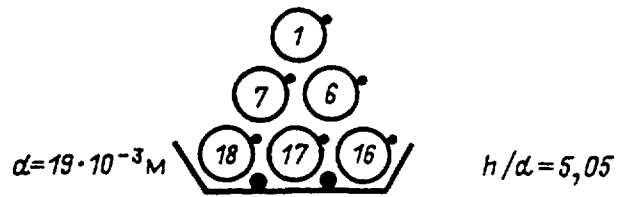
Fig. 3.13. Lateral mass flow with length of clearance in the internal channel of fast reactor subassembly model.

e, point EP-09

e/ē
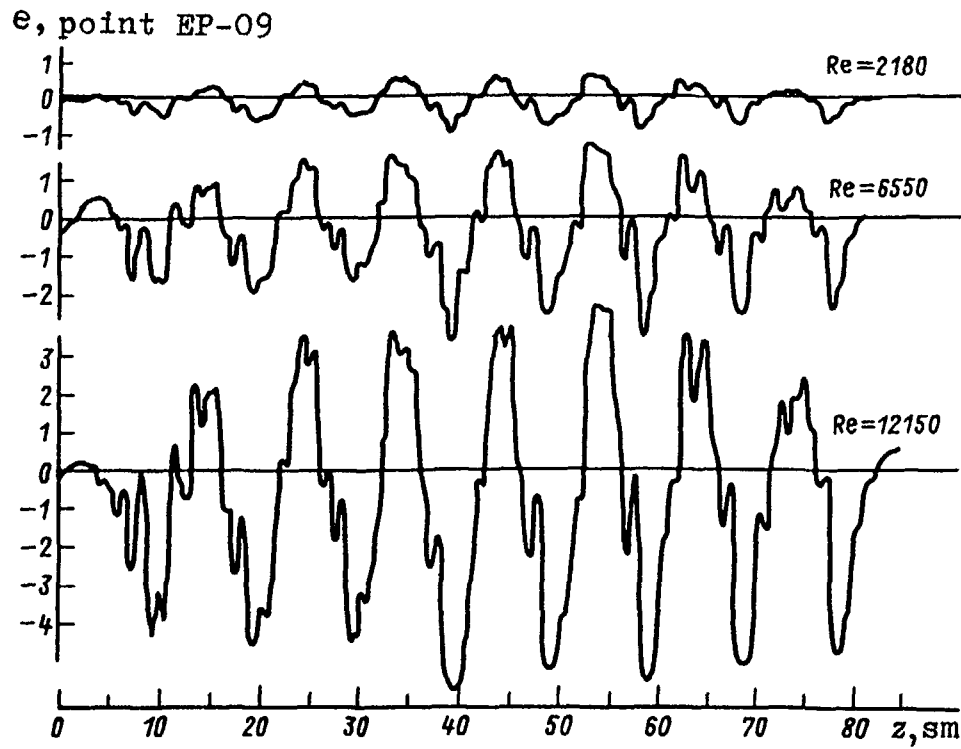
Fig. 3.14. Signals of sensor with the length of clearance in internal channel of BN-350 subassembly.
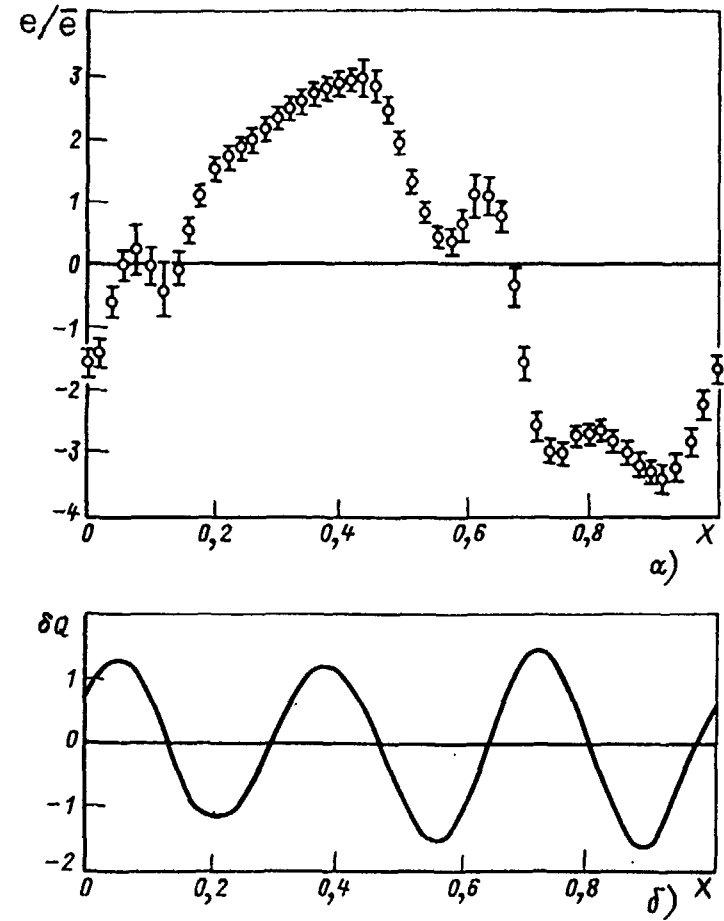
Fig. 3.15. Average lateral mass flow (in dimensionless form) through one clearance (a) and through three clearances (b) of internal channel (S/d =1.062, Pe =8400, number of averaging procedures - 24), x=z/h.

Experiments were carried out on the models of LMFBR subassembly with pitch-to-diameter ratio changing in the range s/d = 1.062 ÷ 1.17 (Fig. 3.7, 3.8). Electromagnetic sensors were positioned inside of the typical simulators (internal, edge, corner - Fig.3.9) or inside of any other simulator that allowed measuring local velocity distribution around the pin simulator. In order to measure an axial and transverse components of velocity simultaneously the sensor involving two normally arranged pairs of electrodes were used.

Sensors were calibrated on the two-pin models (Fig.3.10). Area under the curve representing dependence of the sensor's reading on the length $e = f(z)$ shows the full coolant flow throughout the model at the calibration section (Fig. 3.11a) and an area under the curve at the other sections is in proportion to the coolant flowing through the inter-pin clearance due to wire wrap (Fig. 3.11b). It is obvious from Fig. 3.12, that the sensor's readings are linear with the coolant flow.

Features of inter-channel exchange in wire wrapped bundle are as follows:
Transverse coolant flows though the inter-pin clearances vary with the length as a sine function (Fig. 3.13), with the period being equal to the wire wrap pitch;
Maximum transverse velocity falls to the sections arranged halfway between the points the wire touches the adjacent pin;
velocity component is equal to zero in the points of contact;
exchange intensity increases with the wire pitch reduction, with Reynolds number and relative pitch of the bundle.

When a small bundles are considered (small pin diameters, small pitches), an influences of the local pulsation's of flow arise and curves do not hold their smooth character (Fig. 3.14). Procesing of statistic data becomes more important [13].

It has been revealed (Fig. 3.15a) that the main very intensive flow (first harmonics) is complemented by the local flow in the regions of wire (harmonics of a higher order). Thus, the mass mixing factor is basically determined by the first harmonics. The expansion of the inter-channel exchange curve into trigonometric series [13] shows that:

$$A = \frac{\int_0^1 b_1 |sin 2\pi X| dX}{\int_0^1 |v(X)| dX} = \frac{1}{2} \int_0^1 b_1 |sin 2\pi X| dX = \int_0^{1/2} b_1 sin 2\pi X dX = 0,967 \approx 1. \qquad (3.32)$$

Here, $X = z/h$ is the dimensionless axial distance.

Inter-channel exchange curves are some non-symmetric as relative to zero, that indicates that the flow balance through the selected clearance is distributed. Full flow balance is in agreement with a high degree of accuracy, when considered through three clearances. The local balances agree only in separate sections, in general there are transverse flows (Fig. 3.15b), that causes the axial coolant flow to vary along the channel. An axial flow amplitude ΔV_m (Fig. 3.15b) is:

$$\Delta V_m = \frac{1}{6} \int_0^h |\delta Q| dz = \frac{h}{6} \int_0^1 |dQ| dX,$$ (3.33)

where δQ - total transverse flow.
By definition:

$$\mu = \frac{1}{2h} \int_0^h |v(z)| dz.$$ (3.33a)

Thus, it can be written as:

$$\frac{\Delta V_m}{V} = \frac{\mu h}{6} \frac{2|\overline{\delta Q}|}{|\overline{v}|},$$ (3.33b)

where

$$|\overline{\delta Q}| = \int_0^1 |\delta Q| dX; \quad |\overline{v}| = \int_0^h |v(z)|.dz$$

In the bundle with $s/d = 1.062$ the value $2|\overline{\delta Q}| / |\overline{v}| \approx 1;$; experimental value of $\mu h \sim 0.3$, thus, $\Delta V_m /V \approx 0.05$, that is maximum variation in axial flow lies in the range 5%.

In every cross section there is coolant flow directed from one side of the wrapper to another in accordance with the type of oriented wire wrap (Fig. 3.16). But also there is a turning movement of the coolant, because the wire changes its location in accordance with helical line. Along the wrapper tube the coolant flows in one direction (Fig. 3.17).

Mass exchange is governed by periodic (sine) law (Fig. 3.13), that defines the local mixing factor varies periodically with the length. The local mass mixing factor representing the ratio between mass flux from the i-th to the j-th channel through the unit clearance and axial flow can be described by only one harmonics:

$$\mu_{ij}^M = v / V_c = -\mu_{ij}^M = A \sin\varphi_{ij},$$ (3.34)

where V_c - axial flow through the central channel, m³/h; $\varphi_{ij} = [(2\pi z /h) - \alpha_{ij}]$, α_{ij} - phase the wire wrap appears in the j-th channel from the i-th one. For example, $\alpha_{i1} = 0$, $\alpha_{i2} = (2/3)\pi$, $\alpha_{i3} = (4/3)\pi$; h -wire wrap pitch. Amplitude A, m⁻¹, is taken from [13, 15]:

$$A = (1.047 / h)\Phi^{\Gamma}(s / d)\Psi(Re),$$ (3.34a)

where

$$\Phi^M(s / d) = 2.57 s / d - 3.57 e^{\left[-119(s/d-1)^2 \, 12\right]}$$ (3.34b)

$$\left(1.01 \leq s/d \leq 1.4; \quad 2 \leq h/d \leq 50\right);$$

$$\Psi(Re) = 1.085 - 0.754e^{-0.132 \cdot 10^{-3}Re}$$

(3.34c)

$$\left(2.10^3 \leq Re \leq 2.10^5\right)$$

are the experimentally found functions.

The mixing factor averaged over the length and derived from (3.28) using (3.34) - (3.34c) is

$$\mu_c^M = \frac{1.047}{\pi h} \Phi^M(s/d)\Psi(Re) = \frac{1}{3h}\left[2.57 s/d - 3.57e^{-119(s/d-1)^{2.12}} + 1\right] \cdot$$

$$\left(1.085 + 0.754e^{-0.132 \cdot 10^{-3}Re}\right)$$

(3.35)

with the range of use being $1.01 \leq s/d \leq 1.4$; $2*10^3 \leq Re \leq 2*10^5$; $2 \leq h/d \leq 50$, accuracy is 10% . Function $\Phi^f(s/d) = 3\mu_c^M *h$ represents the averaged mixing factor (with respect to three clearances) multiplied by the wrap pitch (Fig. 3.18). Function $\psi(Re)$ obtained from the analysis of experimental data presented in (Fig. 3.19). The most strong dependence on Reynolds number is observed to be at $Re \leq (20 \div 25) *10^3$.

It should be noted an importance of determining correctly the coolant flow through the channel where the mixing factor is predicted using an uniform velocity distribution and those obtained from experimental data. The difference is evident to be significant.

In spite of the mixing factor increases with Reynolds number (Fig. 3.19), in liquid metal there exist independence of thermal mixing factor on Reynolds number [17,20]. It is connected with the component being responsible for the liquid metal heat conduction, that varies in inverse proportion to Reynolds number. If added to the convective component, it can cause the mixing factor not depend on Re [21].

Relationships presented allow reliable predicting the mixing factors for the bundles of the wire wrapped pins. Universal relations (3.34), (3.35) can be used in wide ranges of relative pitch, wrap pitch and Reynolds number.

Inter-channel thermal exchange. Many experiments were performed by the thermal technique [20-34]. Analysis of these studies presented in [35] shows, that the bundles under investigations differ greatly in length ($1 \leq l/h \leq 18$), in pin number ($7 \leq n \leq 217$), in relative pitch ($1.06 \leq s/d \leq 1.35$), in the wrapper's shape (hexahedral, round), in wrap pitch ($12 \leq h/d \leq 50$), in kind of coolant (water, air, sodium) and so on. Different experimental conditions result in the wide scatter of the experimental data, that causes the values of mixing factor to be open to questions and this makes correlation between experimental data hard. In a number of cases, we can notice that a dependence of the mixing factor on the defining parameters is far from natural [28,33]. Random scatter of the experimental points (Fig. 3.19) does not enable a single-valued function of mixing factor to be found (Fig. 3.16). This problem is dramatised by the fact that in experiments with different coolants, being of a various thermal conductivity

just effective (integral) mixing factors were measured. Only several works [20, 24-26] can be used in the data generalisation.

To get the local mixing factors the thermal experiments were carried out on the sodium models, with the wrap pitch varying [17]. Experimental model (Fig.3.21-a,b) is the triangular bundle of the wire wrapped pins. Four pins are made as rotating ones (the shaded in Fig. 3.21-b). Internal pin is heated, with the heat flux at the outer surface being about $1.2*10^6$ W/m^2. Wall and coolant temperatures are measured by thermocouples (enumeration see in Fig.3.21-b).

Experimental results on local temperature distribution over subassembly length [17] permit revealing information supplementing our view of the process of inter-channel exchange in the bundle of wrapped pins:

- Due to helical wire wrap the hot and cold streams of liquid are forced out from the channels and come into adjacent channels, where coolant temperature either increases or decreases;
- Temperature distribution over the channel length has maximum and minimum, with the period of temperature non-uniformity being equal to the wrap pitch;
- The wall temperature averaged over perimeter has the same character (Fig. 3.22)

Authors have shown [11] that when the pins are spaced by helical wire wrap the convective mass exchange is followed to (3.34) and convective heat exchange between channels can be presented as:

$$Q_{ij}\Delta z = \int_{\omega_{ij}} \int \rho W_i d\omega = \mu_{ij}^T \rho \frac{W_i + W_j}{2} h^* \varpi \Delta z, \tag{3.36}$$

where

$$\mu_{ij}^T = \beta \frac{W_{ij}}{\left(W_i + W_j\right)/2} \left(\frac{s-d}{\varpi}\right)\left(cos_{ij}\right) = \left(\mu_{ij}^T\right)cos\varphi_{ij} \tag{3.37}$$

is the local thermal mixing factor,

$$\varphi_{ij} = 2\pi z / h + \alpha_{ij} + \Delta\alpha; \qquad h^* = \begin{cases} h_i, & if \ \varphi_{ij} > 0; \\ h_j, & if \ \varphi_{ij} < 0. \end{cases}$$

Here $\Delta\alpha$ - the phase shift between the mass flow harmonics effected in the section z and actual mass flow; β is the non-equivalence factor between mass and energy transport; ω_{ij} is an area of inter-channel cross section; ϖ - mean statistic area of internal channel.

Local thermal mixing factor (convective component), m^{-1}, for one-directional wrap is determined by:

$$\mu_{ij}^T = \beta\mu_{k_{ij}}^M = \frac{1.047\beta}{h} \Phi^M(s/d)\Psi(Re) sin\left(\frac{2\pi z}{h} - \alpha_{ij}\right), \tag{3.38}$$

where $\beta \approx 0.7$.
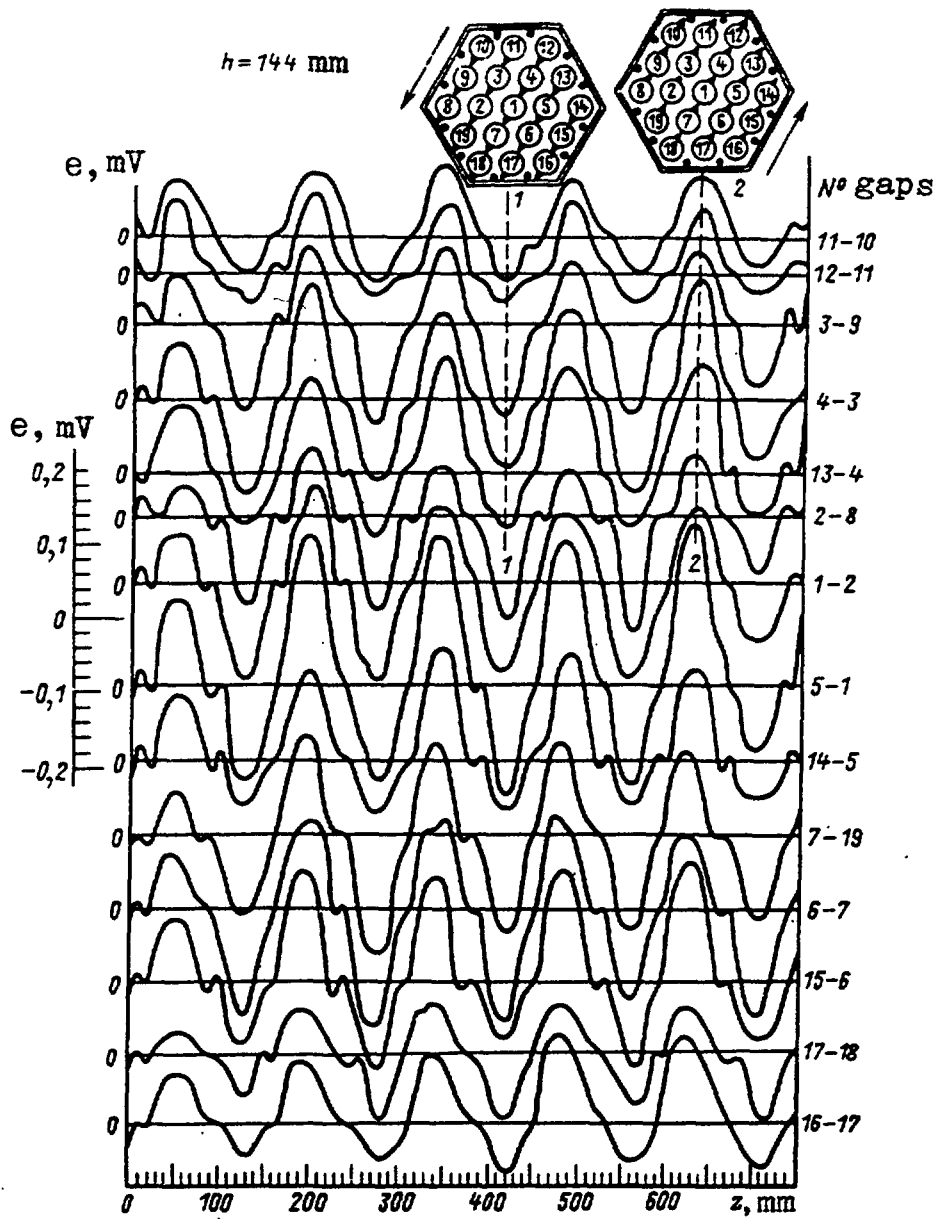
Fig. 3.16. Lateral mass flow with length of different channels (arrows show directions of lateral flow in cross sections 1-1, 2-2).
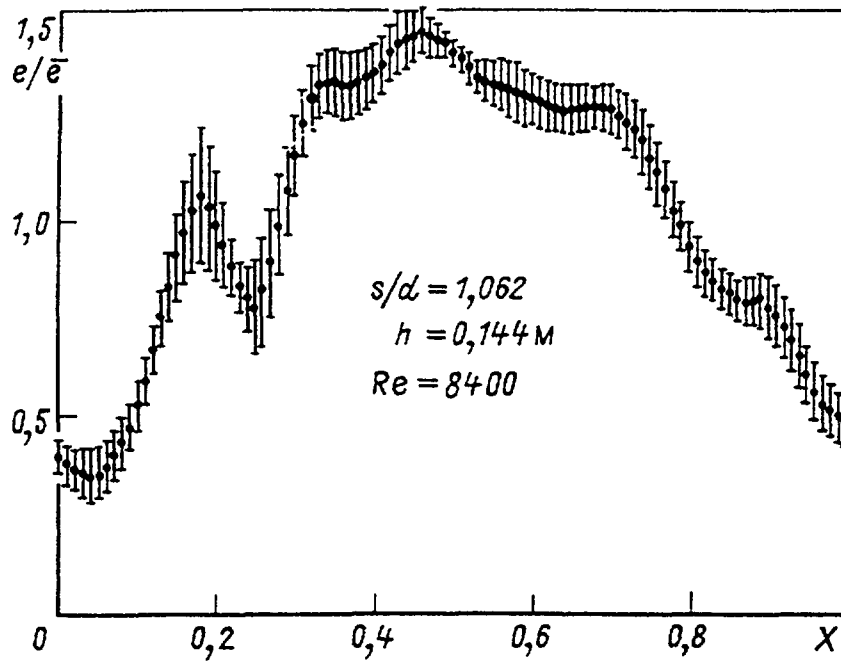
Fig. 3.17. Averaged lateral mass flow (in dimensionless form) with the axial axis in the clearances between wrapper tube and pins (number of averaging procedures 16), x = z/h.
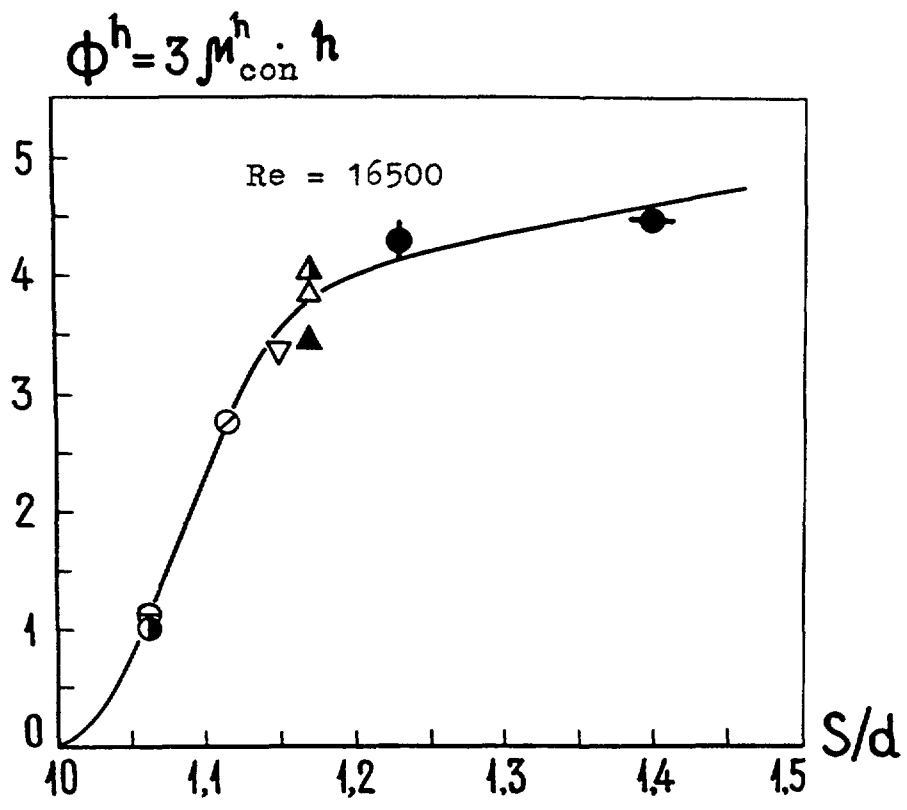
Fig. 3.18. Experimental (symbols) ands averaging (solid line) of Φ^h parameter on relative pitch of bundle.
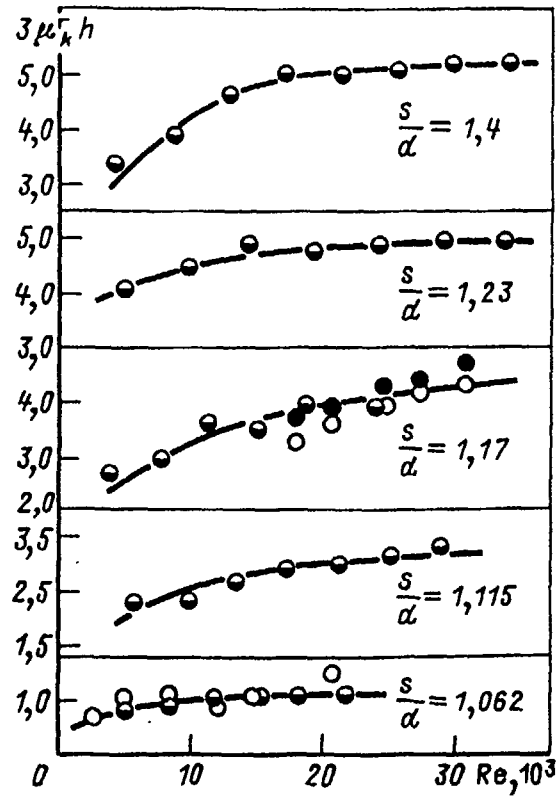
Fig. 3.19. Mass transfer factors with Reynolds number.
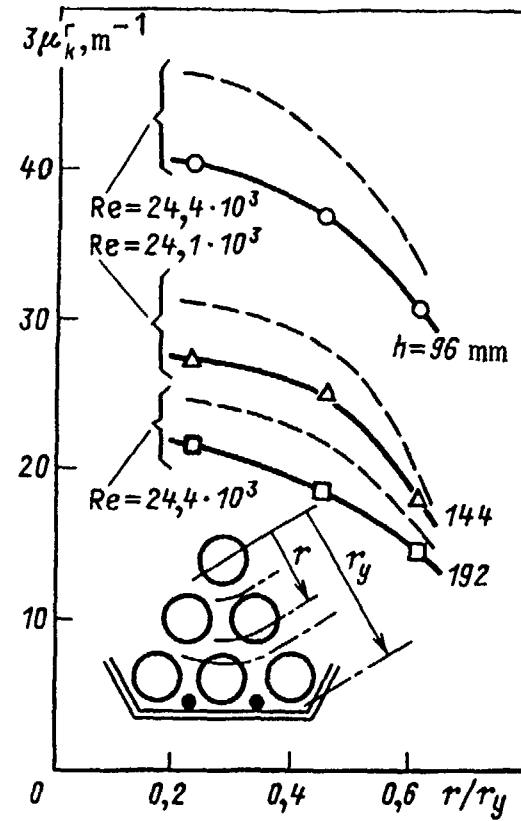
Fig. 3.20. Mixing coefficient with the model radius (S/d = 1.17): — — - in assumption of uniform velocity distribution across the model, taking -O -, -△-, -□- - taking into account cross section velocity profile.
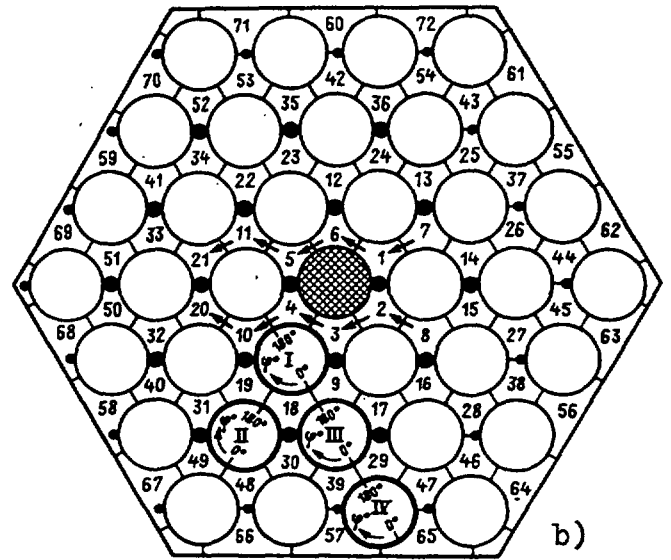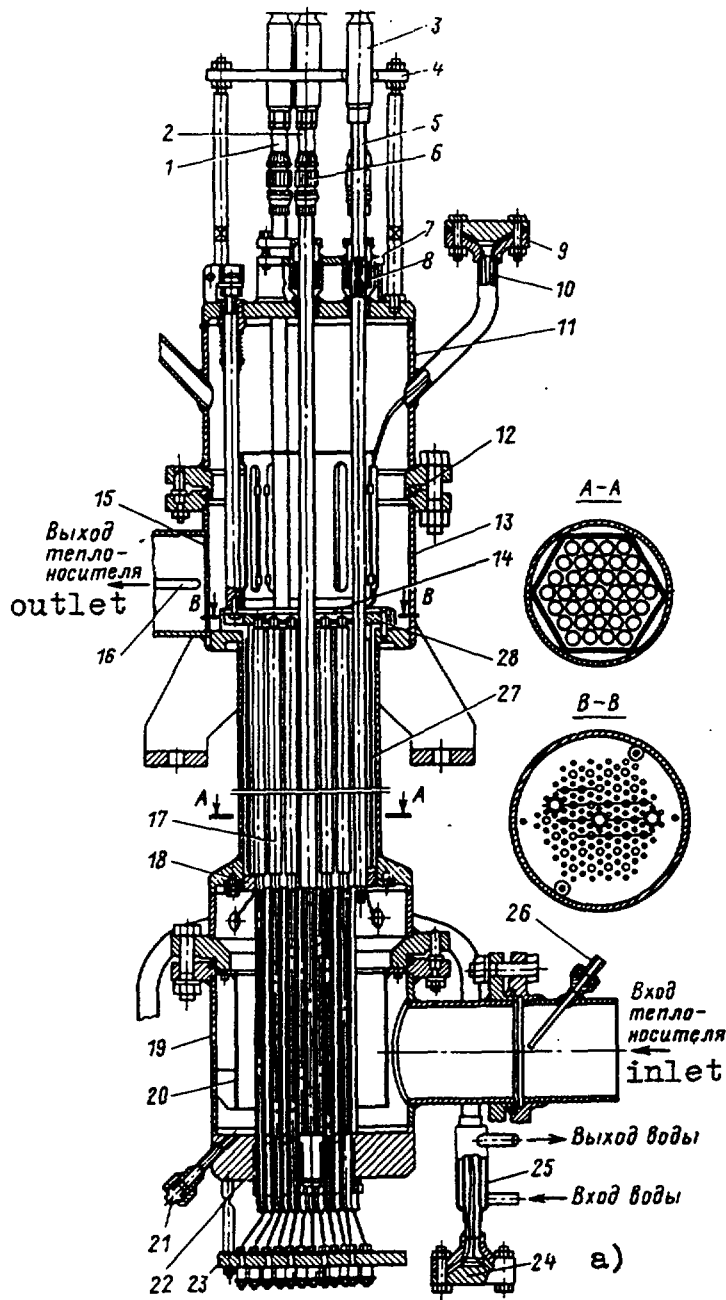
Fig. 3.21.   General view of fast reactor sub-assembly model (a) and the model cross section (b):

1, 2, 5 edge, internal and corner turning simulators,
3 - current supply to heater, 4 - spacing grid, 6 - thermocouples faxing arm, 7, 8 - gland, 9,24 - thermocouple seals, 10 - thermocouples, 11, 13 - to header, 12 - gasket, 14 - grid holding thermocouples, 15 - mixing chamber, 16, 26 - thermocouple covers, 17 - pin simulator, 18, 28 - bottom and top aligning grids, 19 - bottom header, 20 - distributive barrel, 21 - drainage, 22 - gland, 23 - insulation, 25 - cooler, 27 - hexagonal wrapper tube. I -IV - turning pin simulators, 1 ÷ 72 - thermocouples.
Arrows indicate directions of lateral flow of coolant, heated pin is in centre of the model.

108

Having averaged inter-channel heat flux over the wire wrap phase, we can obtain the following integral relation:

$$Q_{ij} \Delta z = \frac{1}{2\pi} \int_0^{2\pi} \left[\iint_{\omega_{ij}} W_i d\omega \right] d\alpha = \mu_k^T \frac{W_i + W_j}{2} \left(h_i - h_j \right) \varpi \Delta z,$$ (3.39)

where

$$\mu_c^T = \left(\mu_{c_{ij}}^T \right)_{max} / \pi.$$ (3.40)

Pulsating character of the forced convective exchange in subassembly with wrapped pins cause the coolant temperature to pulsate, that appears in a distance two-three pitches of wire wrap from the beginning of power production [36].

Heat balance equation for the i-th channel [14,18]:

$$\frac{dt_i}{dz} = \frac{\pi q d}{2 c_p G} - \sum_{j=1}^{3} \left(\beta \mu_{ij}^M \Psi_{ij} + \mu_\lambda^T + \mu_T^T \right) \left(t_i - t_j \right) + \beta t_i \sum_{j=1}^{3} \mu_{ij}^M,$$ (3.41)

where μ_{ij}^M is the local hydraulic mixing factor defined by (3.34 - 3.34c); μ_λ^T, μ_T^T - mixing factors due to heat conduction and turbulent diffusion, respectively; ψ_{ij} (φ_{ij}) - periodic function taking the values:

$$\Psi_{ij}\left(\varphi_{ij}\right) = \Psi_{ij}\left(\varphi_{ij} + 2\pi\right) = 1 - \Psi_{ij}\left(\varphi_{ij}\right) = \begin{cases} 1 & \text{for } 0 \leq \varphi_{ij} < \pi; \\ 0 & \text{for } \pi \leq \varphi_{ij} < 2\pi. \end{cases}$$

Here $\varphi_{ij} = [(2\pi z/h) - \alpha_{ij}]$, phase the wire enters into the j-th channel from the i-th one.

In deriving (3.41) the fact was taken into account that resetting the indexes changes the sign into opposite.

Numerical solution of (3.41) has shown that predictions are in a good agreement with experimental data (Fig. 3.22) at $\beta = 0.7$. Thus, the value of non-equivalence heat and mass transport factor was found and the values of local mixing factors determined in experiments with the use electromagnetic technique were validated. For the edge channels

$$g_i \frac{dT_i}{dZ} + L\mu_c^{Tp}\left(T_i - T_3 \right) + L\mu_c^{Tp}\left(T_i - T_1 \right) +$$

$$+ \sum_{j=1}^{3} L\left(\mu_T^T + \mu_\lambda^T \right)\left(T_i - T_j \right) = \sum_{k=1}^{2} Q_{ki} \left(k = 1,2,...,M \right),$$ (3.42)

where μ_c^{Tp} is the convective mixing factor between internal and edge channels; g_i - relative flow rate through the edge channel. Equations (3.42) are equal to the edge channels in number.

Mixing factors are determined with the highest accuracy in the channels surrounding the heated pin (Fig. 3.23) [35]. Data of hydrodynamic measurements multiplied by the non-equivalence factor β = 0.7 are in a good agreement with the data obtained in thermal experiments. The final relationship for the averaged thermal mixing factor is of the form:

$$\mu_c^T = \frac{\beta}{\pi h} \Phi^M (s/d) \Psi(Re) = \frac{0.234}{h} \left[2.57 \, s/d - 3.57 e^{-119(s/d-1)^2 \, 12} + 1 \right] \cdot$$

$$\left(1.085 + 0.754 e^{-0.132 \, 10^{-3} Re} \right)$$

(3.43)

$$1.01 \le s/d \le 1.4; \quad 2 \cdot 10^3 \le Re \le 2 \cdot 10^5; \quad 2 \le h/d \le 50; \quad \beta = 0.7.$$

Thus, it was found from the correlation made between experimental data obtained by thermal and electromagnetic technique that the non-equivalence factor in liquid metal β is equal to 0.7.

Convective inter-channel exchange in the edge area.

Mass exchange. Relationship for the convective mass exchange in the clearance between wrapper and edge channels was found from processing of hydraulic data [13, 37-42] (Fig. 3.24):

$$\mu_c^{Mp} = G_{ij} / G_{cent} = (1/h) \left[17.34(\Delta/d) + 144(\Delta/d)^2 - 373.4(\Delta/d)^3 \right] \cdot \Psi'(Re)$$

(3.44)

where

$$\Psi'(Re) = 1 - 0.694 \, exp\left(-0.132 \cdot 10^{-3} Re \right),$$

(3.45)

Δ is the clearance between subassembly wrapper and the edge pins

Results of experiments on convective thermal mixing between the edge channel [39, 41, 42, 45-50, 51] is described as (Fig. 3.25):

$$\mu_c^{Tp} = \frac{Q_{ij}}{\left[\rho\left(W_i - W_j \right) / 2 \right] h_j \varpi \Delta z} = 0.5 \mu_c^{MP}$$

(3.46)

$$1.0 \le (d + \Delta) / d \le 1.25; \quad 7.6 \le h/d \le 52; \quad 0.6 \cdot 10^3 \le Re \le 7 \cdot 10^4.$$

Mass mixing factor μ_c^{MP} is calculated by (3.42).

It is well to bear in mind that an enthalpy in donor-channel appears in denominator of (3.46) but not enthalpy difference as in the central area of subassembly, considering that here we are dealing with directed heat transfer. Mass and heat mixing factors reduce with the wire wrap pitch (approximately in inverse proportion) and increase with Reynolds number and clearance between the wrapper and edge pins.
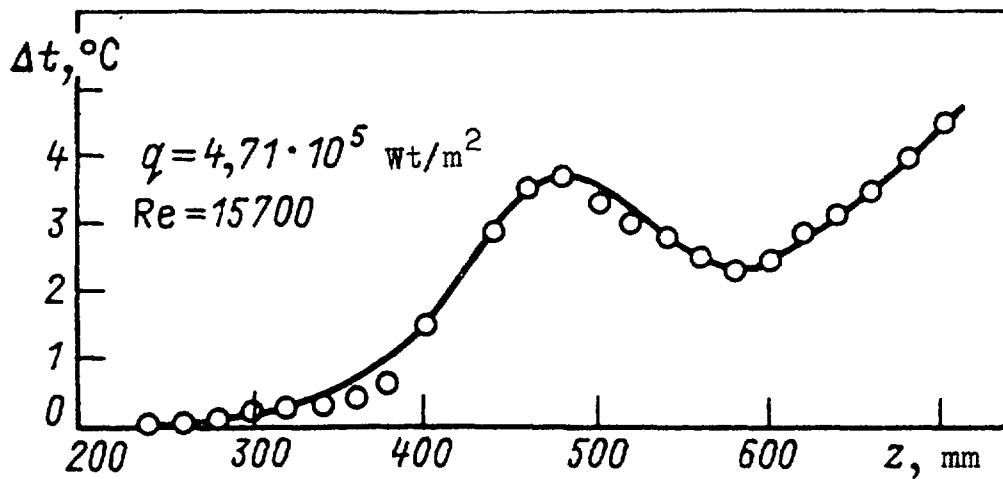
Fig. 3.22. Coolant temperature along the channel:
O - measurements by mobile thermocouple,
—— - prediction on the basis of local mixing coefficients.
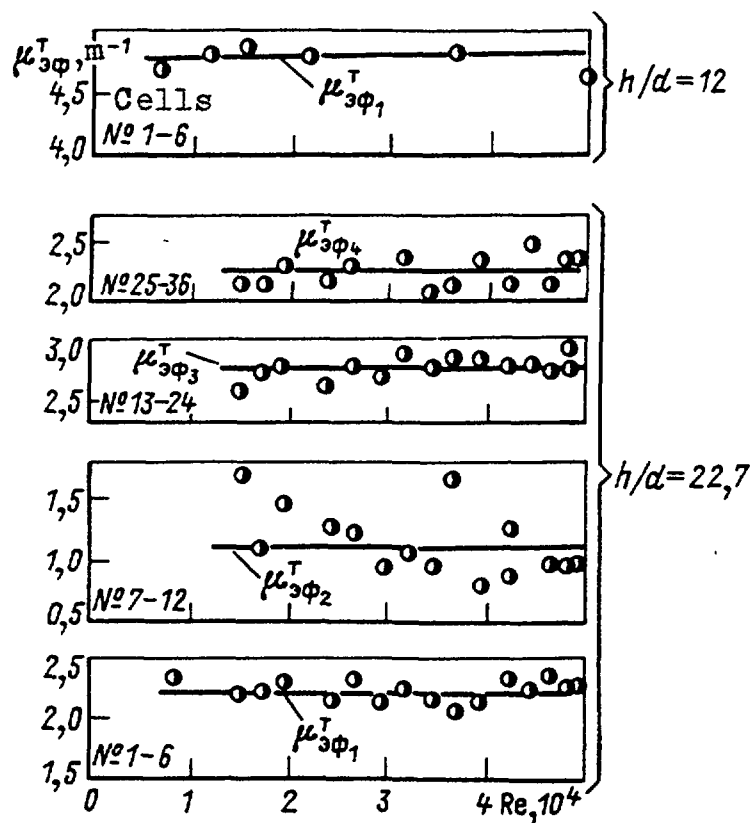
Fig. 3.23. Experimental effective mixing coefficients, number of channels see fig. 3. 21b.
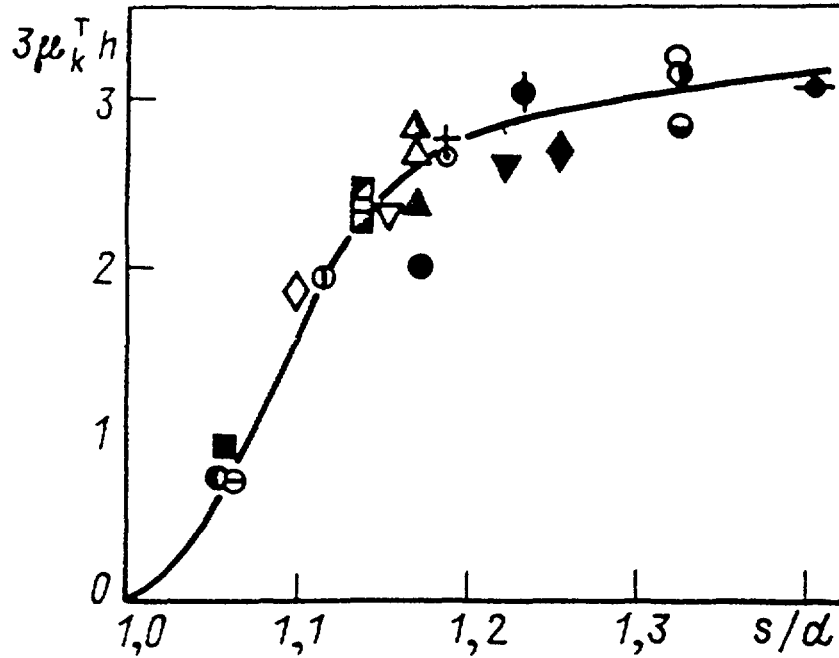
Fig. 3.24. Thermal mixing coefficients with the relative pitch of bundle: $\bullet,\ominus$ *- S/d = 1.062 (h/d = 5.1, 7.6);* $\oplus$ *- S/d = 1.115 (h/d = 7.6);* ∇ *- S/d = 1.15 (h/d = 16.4);* $\triangle$, $\blacktriangle$, $\blacktriangle$ *- S/d = 1.17 (h/d = 5.1, 7.6, 10.1);* $+$, $\odot$ *-S/d = 1.185 (h/d = 12, 22.7); experimental data of other authors:* $\square$, $\square$, $\square$, *- S/d = 1.14 (h/d = 14.3, 21.4, 27.4);* $\blacksquare$ *- S/d=1.06 (h/d = 19.5);* $\circ$, $\circleddash$, $\ominus$ *- S/d = 1.32 (h/d = 16.7, 33.3, 50);* $\bullet$ *- SD/d = 1.17 (h/d = 16.7);* $\blacklozenge$ *-S/d = 1.25 (h/d =51.4);* $\lozenge$ *- S/d =1.10 (h/d =14.8);* $\blacktriangledown$ *- S/d = 1.22 (h/d =40,4).*

3.4. MOLECULAR AND TURBULENCE EXCHANGE IN SMOOTH BUNDLE EXCHANGE DUE TO HEAT CONDUCTION OF THE PINS

To estimate mixing factor components due to turbulence and molecular diffusion in liquid metal the experiments were carried out on smooth bundles with sodium and NaK alloy, as a coolants [52].

Having expressed a heat flux due to turbulence diffusion as

$$Q_{T_{ij}} = \lambda_T \frac{\left(\bar{t}_i - \bar{t}_j\right)}{\Delta_{r_{ij}}}(s-d)\cdot 1 = G_{ij}C_p\left(\bar{t}_i - \bar{t}_j\right), \tag{3.47}$$

the turbulence mixing factor can be written:

$$\mu_T^T = \lambda_T(s-d) / GC_p\Delta r_{ij}.$$

112

Having expressed a quantity of heat transferred from one channel to another due to molecular heat conduction:

$$Q_{\lambda_y} = \frac{\lambda_f (\bar{t}_i - \bar{t}_j)}{\Delta r_y}(s-d)\cdot 1 = \frac{\lambda_f}{C_p G}\frac{s-d}{\Delta r_y} C_p G (\bar{t}_i - \bar{t}_j)$$

(3.48)

the molecular mixing factor is

$$\mu_\lambda^T = \frac{\lambda_f}{C_p G}\frac{s-d}{\Delta r_y} = \frac{8}{\pi}\frac{1}{Pe}\frac{s/d-1}{\Delta r_y}.$$

(3.49)

where Δr_y is the inherent path of interaction.

Suggesting an analogy occurs between heat and momentum transfer $\left(a_T = \nu_T\right)$ and using one or other expression for ν_T and Δr_y, we can calculate μ_T^T and μ_λ^T. Since there is the great diversity of relations, estimations available in literature [53-62] differ widely from one another. The great distinction has been demonstrated also in water and air experiments. The same picture can be seen in respect of mixing factor due to heat conduction [53, 63, 64].

The all mentioned above and even that the liquid metal data are entirely lacking is mainly responsible for the performing experiments on liquid metals. Experimental models (Table 3.2.) were the bundles of smooth pins arranged by triangular manner with relative pitch $s/d = 1.13, 1.15, 1214, 1.32$. Local coolant flows were measured by electromagnetic sensors.

Experimental data on effective thermal mixing factor, m^{-1}, are given by the formula (Fig.3.26-a)

$$\mu_T^T + \mu_\lambda^T = \frac{1}{Pe^{0.7}}\frac{\sqrt{s/d-1}}{s/d}\frac{1}{d}$$

(3.50)

$$\left(1.10 \le s/d \le 1.35;\ 70 \le Pe \le 1600\right).$$

If the contribution of molecular component evaluated by the formula [64]:

$$\mu_\lambda^T = \frac{67}{Pe}\frac{s/d-1}{s},$$

(3.51)

is eliminated from the effective mixing factor, that turbulence component will be consistent with the relationship:

$$\mu_T^T = \frac{1}{150\sqrt{s/d-1}\,Re^{0.2}\,d}$$

(3.52)

$$\left(1.10 \le s/d \le 1.35;\ 4.10^3 \le Re \le 50\cdot10^3\right)$$

Fig.3.26-b presents experimental data on turbulence component of mixing factor compared with those predicted by some relations [35, 62].

Table 3.2. Geometry of the smooth models

Parameter	Value Model		
	1	2	3
Pin number	19		
Outer diameter of pin, mm	14	24.7	15.8
Relative pitch, s/d	1.15	1.214	1.32
Bundle length, mm	1720	1300	
Heated section, l_o, mm	1620	1200	
Relative clearance, $\Delta/(s-d)$	0.75	0.43	0.52
Displacer diameter, d_d , mm	4	5	-
Cross section area of internal channels ω, mm^2	35.3	150.1	89.3
Hydraulic duameter, d_h , mm	6.4	15.5	14.4
Coolant	Na	NaK	
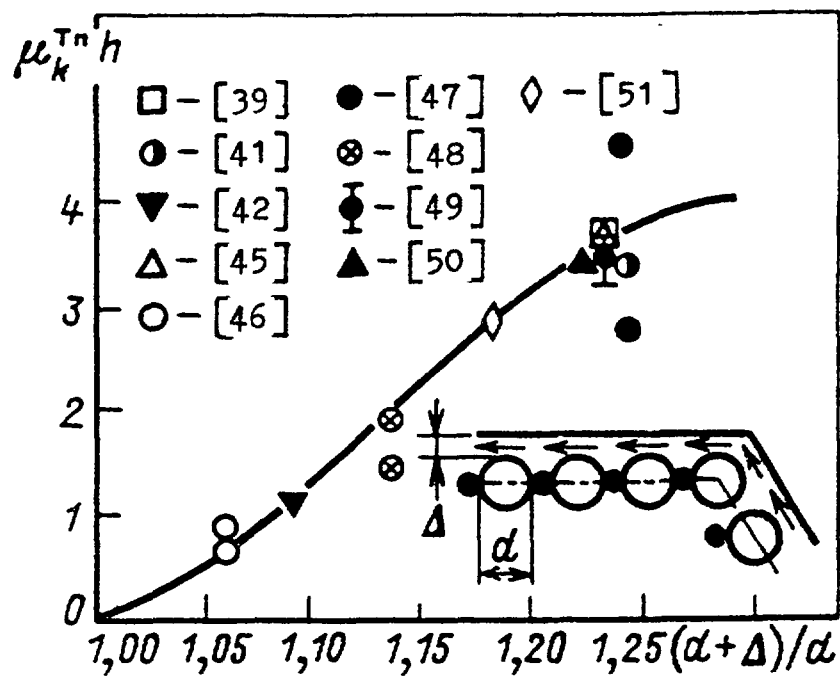
Fig. 3.25. Comparison of experimental data on convective mixing heat between subassembly wrapper tube and edge pins obtained by different authors.

114
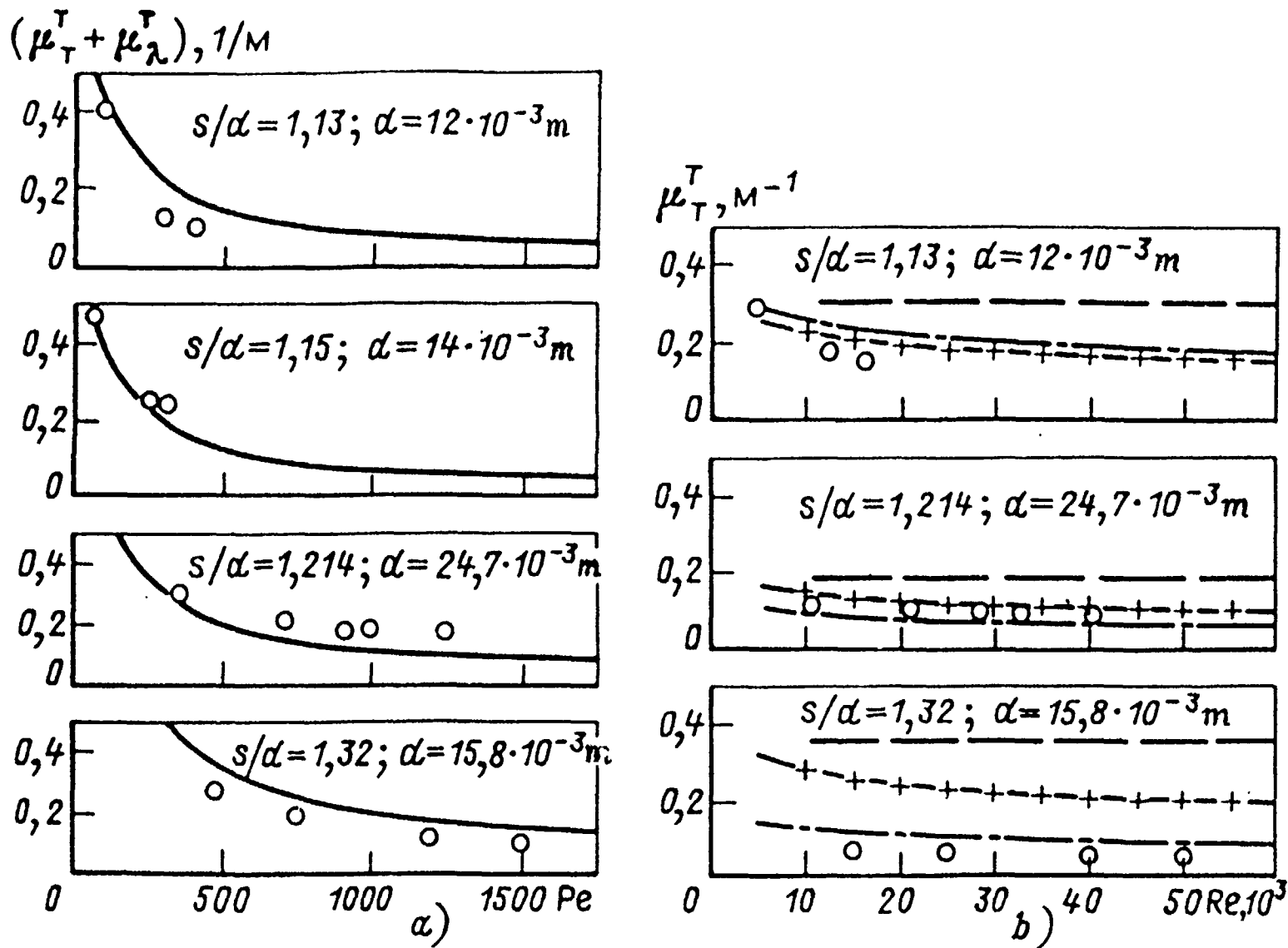
Fig. 3.26. Molecular-turbulence and turbulence mixing with Peclet and Reynolds number in the bundle of smooth pins:
O- experiment, ———' , —·— - empirical formulae's, ———, —+— - relationships

$(0.01 \cdot \sqrt{S/d - 1})/d$ and $\left[0.063(S/d-1)^{Q7} \cdot \sqrt{1+(S/d-1)^{0.2}} \right] / S \cdot Re^{0.2}$ [1],[62].

Thus, experiments have resulted in getting relations for evaluation of effective mixing factor and its components. It has been shown that component due to molecular heat conduction should be calculated by the formula (3.51). Analysis performed by the authors based on the notion that molecular and turbulence exchange is a sum of «gradient» transport, induced by molecular diffusion and small-scale turbulent eddies, and convective transport induced by the large-scale eddies (so called secondary flows) allows deriving formula for the thermal molecular - turbulent mixing in liquid metal [65]:

$$\mu_{MT}^{T} = \left\{ \frac{350}{Pe} \frac{s/d-1}{s/d} - \frac{0.318}{(s/d)\sqrt{s/d-1}} \times \right.$$

$$\times \left[1 - exp\left(0.62.10^{-4} \, Re \, Pr^{1/3}\right)\right] + \frac{0.38 \, Re^{0.1}}{\left(2\sqrt{3}/\pi\right)(s/d)^2 - 1} \left.\right\} \frac{10^{-2}}{d} \qquad (3.53)$$

$$\left(113 \le s/d \le 1.32; \; 70 \le Pe \le 1500\right).$$

and also relation for the hydraulic molecular - turbulent mixing in coolants of $Pr \approx 1$ [66].

$$\mu_{MT}^{M} = \frac{0.0293 - 0.051(s/d - 1)}{\left[\left(2\sqrt{3}/\pi\right)(s/d)^2 - 1\right]Re^{0.1}d} \qquad (3.54)$$

$$\left(10^4 \le Re \le 2.10^5; \; 1.05 \le s/d \le 1.6\right).$$

Really, based on the belief that the main axises of the small-scale turbulence diffusion tensor are arranged along the channel symmetric line, let us write «gradient» flux of the substance Ψ, trough the area $\Delta\omega_{ij}$ between the channels i and j as follows

$$\int_{\Delta\omega_{ij}} \left(j^{\Psi} + j_{T}^{\Psi}\right)d\omega_{ij} = \left(\varepsilon + \varepsilon_{T_{\phi=0}}\right)\frac{\Psi_j - \Psi_i}{\Delta r_{ij}^{\Psi}}\Delta\omega_{ij} , \qquad (3.55)$$

where j^{Ψ}, j_{T}^{Ψ} – specific molecular and turbulence flux of the substance Ψ, respectively; ε, ε_T - molecular and turbulence diffusivity; Ψ_i and Ψ_j - mean values of the substance Ψ in the channels i and j, respectively, Δr_{ij}^{Ψ} - effective path of interaction.

As the secondary flows carry substance from the internal areas of channel to the area between channels i and j, we can write:

$$\iint_{\Delta\omega_{ij}} \overline{\Psi' W'}d\omega_{ij} = \overline{W}_{ij}\Delta\omega_{ij}^{*}\Psi_i - \overline{W}_{ij}\Delta\omega_{ij}^{*}\frac{\Psi_i + \Psi_j}{2} = \frac{1}{2}\overline{W}_{ij}\Delta\omega_{ij}^{*}\left(\Psi_i - \Psi_j\right) \qquad (3.56)$$

Here, Ψ', W' - substance and velocity pulsation's in the clearance, respectively; $\overline{W}_{ij}$ - mean velocity of large - scale eddies; $\Delta\omega_{ij}^{*}$ - flow cross section.
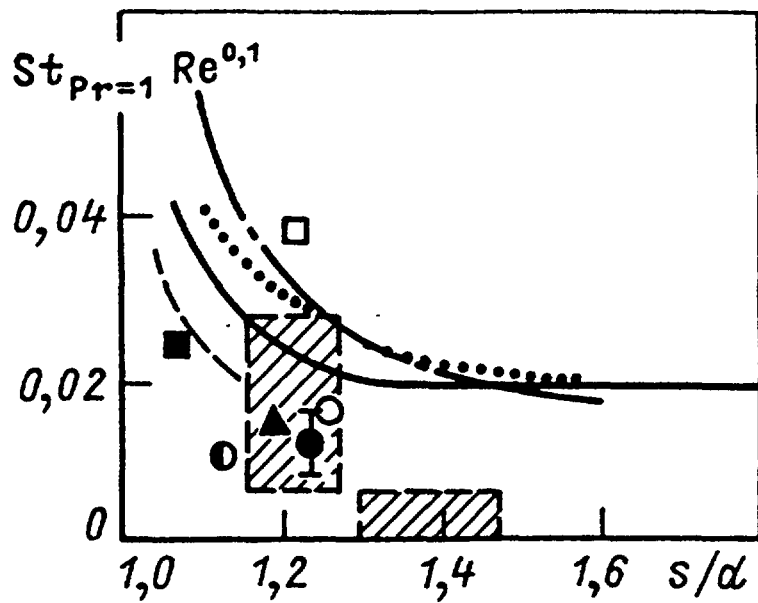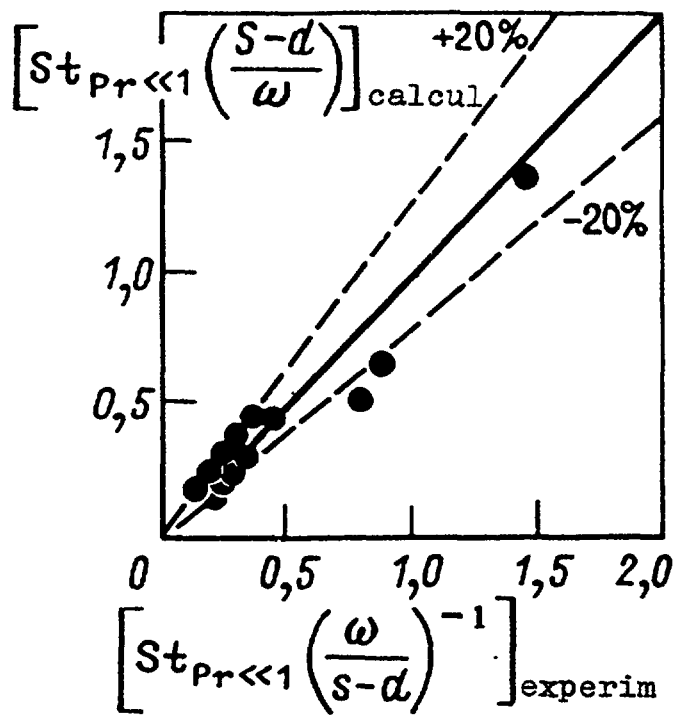
Fig. 3.27. Comparison of water, air (a) and liquid metal (b) mixing parameter:
Liquid metal: ● *- authors data.*
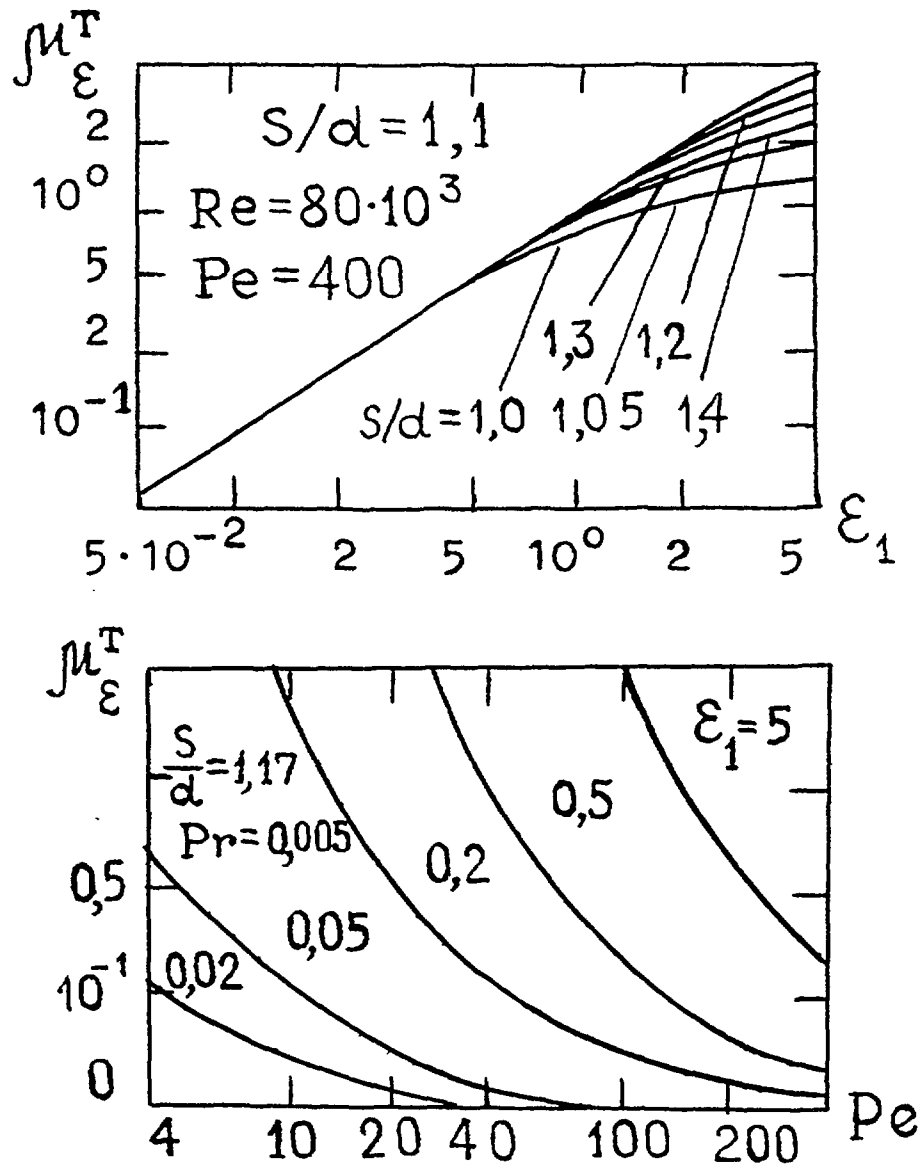
Fig. 3.28. Heat mixing coefficient due to heat conductivity of pin with the equivalent thermal conductivity and Peclet number.

Having regard to (3.56), molecular turbulence mixing factor in dimensionless form can be written as:

$$St^{\Psi} = \frac{\mu^{\Psi}\varpi}{\Delta s_y} = \left(1 + \frac{\varepsilon_{T_\varphi=0}}{\nu_{T_\varphi=0}} \frac{\nu_{T_\varphi=0}}{\nu} \frac{\nu}{\varepsilon}\right) \cdot \left(\frac{d_h/d}{Re\,Pr^{\Psi}\,\Delta r_y^{\Psi}} + \frac{\pi}{4} \frac{\overline{W_y}}{W_i + W_j} \frac{\Delta\omega_y^*}{\Delta\omega_y}\right) \qquad (3.57)$$

where, the first term describes gradient exchange and the second - large - scale one, ΔS_y - clearance between the channels i and j, $\overline{\omega}$ - averaged area of internal channel cross section.

Analysis of experimental data on inter-channel exchange in the bundles involving spacer grids has shown that, in first approximation, relationship for bundle being free from grids can be used (Fig. 3.27). But this can cause the transverse turbulence diffusion behind the grids to reduce.

Inter-channel exchange due to pin heat conduction. In the event of the coolant in the channels surrounding the pin is heated non-uniformity, the heat flux distribution around the pin is also non-uniformity, that causes the heat exchange between channels due to pin heat conduction to occur.

By assuming that temperature distribution around the pin can be described by Fourier series with harmonics being a multiple of - 6, we obtain the following expression for power production in the i-th channel:

$$\sum_{k=1}^{3} \overline{q}_{ki}\Pi_{ki} = \sum_{k=1}^{3} \overline{q}_k\Pi_{ki} +$$

$$+ \sum_{k=1}^{3} \frac{\lambda_f\Pi_{ki}(\overline{t} - t_i)}{\left[1/\varepsilon_1 + (1/Nu)(2d_\Gamma/d)\right]d/2}, \qquad (3.58)$$

where $\overline{q}_k$ - heat flux averaged over the k-th pin perimeter, $\overline{q}_{ki}$ - mean heat flux produced by the k-the pin in to the i-th channel, t_i - mean coolant temperature, $\overline{t}$ - coolant temperature averaged over the channels surrounding the k-th pin, λ_f - coolant thermal conductivity, ε_1 - equivalent thermal conductivity evaluated through the first harmonics, Nu - Nusselt number; d_h - hydraulic diameter.

Having performed the needed transformations, we obtain [71]:

$$\mu^T_{\lambda_{pin}} = \frac{16}{3} \frac{\varepsilon_1}{1 + (2d_h/d)(\varepsilon_1/Nu)} \frac{1}{Pe} \frac{1}{d} \qquad (3.59)$$

The relationship shows, that the thermal mixing factor due to pin heat conduction reduces with Peclet number and pin diameter and depends only weakly on the relative pitch of the bundle (Fig.3.28).

Homogeneous model. The distinguishing feature of the two-phase inter-channel exchange is that the local behaviour of the mixing has a maximum in transition region from nucleate to annual boiling (quality 5-10%), with the value depending heavily on pressure, mass velocity and relative pitch of the bundle.

An appreciable pressure pulsations under flow conditions compatible with those on maximum transport of liquid phase were pointed to the maximum amplitude is 0.05 - 0.07 bar at frequency 0.2Hz. Such an amplitude appears to be sufficient to educe an intensive mixing in the slug flow. In other flow patters maximum pressure amplitude is lesser, but frequency increases.

At great quality, corresponding to annular and disperse flow (x>0.1÷0.2) an intensity of transverse exchange decreases, with the great effect of inter-pin clearance.

Information on systematic researches of two-phase inter-channel exchange processed in the framework of the homogeneous model indicates that the flow parameters influence on the mixing intensity as in single-phase flow. It reduces with the coolant mass velocity (Fig. 3.29).

The lower the flow velocity, the greater is the molecular-turbulent mixing being the ratio between transverse molecular-turbulent transport and axial one. With increase in the clearance between the pins, the greater parts of stream-liquid mixture are forced through the clearance into adjacent channels. Reduction in pressure results in a decrease in the stream density and, respectively, in the earlier transition to the annular flow.
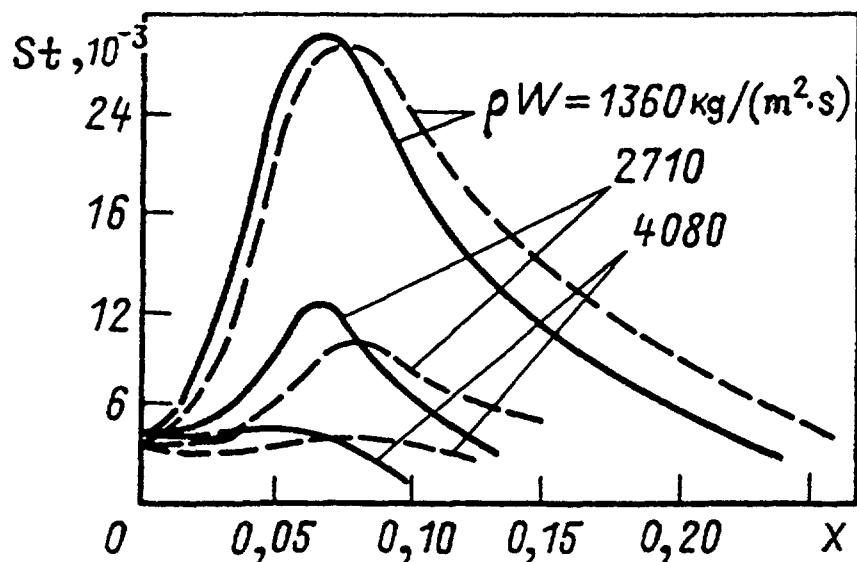
Fig. 3.29. Intensity of interchannel mixing (in the frame of homogeneous flow) with quality in two-phase flow with (solid line) and without (dash lime) spacing grids.

In the square or mixed bundle the value St^Ψ is somewhat above than those in triangular bundle. As the data [73] have shown the availability of spacers effects the inter-channel exchange, this relation can be approximated as:

in nucleate and plug flows $(0 \leq x \leq x^M)$

$$St^\Psi = St_I^\Psi + f(s/d) \, f(\rho W) \left(\rho_l / \rho_g\right)^n x;$$ (3.60)

in disperse and annular flows $(x^M \leq x \leq 1)$

$$St^\Psi = St_\Pi^\Psi + \left(St_M^\Psi - St_\Pi^\Psi\right) f(x).$$ (3.61)

where the pattern boundary is defined as:

$$x_M = \left\{ \frac{0.4 \rho_\Pi}{\rho_l} \left[g \frac{\rho_l}{\rho_g} d_\Gamma (\rho_l - \rho_g) \right]^{1/2} + 0.6 \right\} \Big/ \left\{ \left[\frac{\rho_l}{\rho_v} \right]^{1/2} + 0.6 \right\},$$ (3.62)

In the work [74] the following relations for the coefficients in (3.60) and (3.61) are suggested:

$$f\left(\frac{s}{d}\right) = \frac{0.0157}{s/d - 1}; \quad f(\rho W) = \frac{\beta - 1}{\beta}; \quad f(x) = \frac{1 - 0.17 Re^{0.417}}{x/x_M - 0.57 Re^{0.417}}.$$ (3.63)

The drawback to the formula (3.63) is that the limiting transition to St^Ψ at $x \to 1$ does not assert. The check has shown that relationships (3.60 - 3.63) describe experimental data [74, 75] poorly.

More exactly the data [74, 75] correspond to the following relations

$$f(\rho W) = 7.25 / (\rho W)^{0.745};$$ (3.64)

$$f\left(\frac{s}{d}\right) = 1 + \frac{0.0575}{s/d - 1};$$ (3.65)

$$f(x) = (1 - x) / (1 - x_M);$$ (3.65a)

$$x_M = \frac{\left(\rho_g / \rho_l\right) \left[g d_h (\rho_l / \rho_g)(\rho_l / \rho_g - 1) \right]^{1/2} + 1}{1 + 2.5 \left(\rho_l / \rho_g\right)^{1/2}}.$$ (3.66)

Data [76] show that mixing in subcooled boiling is close to the mixing in liquid flow. When quality approaches zero $(x > -0.1)$ the intensity of inter-channel exchange is observed to rise by a factor of three:

$$St^h = 3St^h_{x=0\,1}[1 + 6.66x] \quad \text{for } (-0.1 < x < 0).\tag{3.67}$$

In the corner channel of the square 9-pin bundle the enthalpy appears to be lesser than those in the internal channel, against the predictions on COBRA. Distinction is likely due to the availability of the thick liquid film at the unheated surface that was not considered in predicting, and also due to heterogeneous transfer in combined channels. The overwhelming stream entertainment occurs from the most loaded channel. To describe exactly this effect in the frame of homogeneous model have not met with success.

Two-liquid model. Experiments carried out in [75, 77, 78] to study inter-channel exchange for either of the two phases have shown that intensity of inter-channel exchanges in liquid and gas are dissimilar.

Dependencies St_l and St_g on quality is of complex character associated with rearrangement of two-phase flow (Fig. 3.3a, b). Peak of exchange intensity, well defined for liquid phase, have been suggested to fall on the transition area from plug to moist flow [77].

Data [75] show that at low mass velocity (60 ÷ 120 kg/m^2 s) each phase mixing is observed to depend on ρw, whereas at great velocity this dependence may be degenerate. In [75] the following relations were proposed:

$$St^2_l = St^1_l \varphi_1\left(\frac{1-d}{d_\Gamma}, x\right)\varphi_r(p,x)\gamma(x)\frac{1}{\theta(x)};\tag{3.68}$$

$$St^2_g = St^1_g \varphi_1\left(\frac{s-d}{d_\Gamma}, x\right)\varphi_r(p,x)\gamma(x)\tag{3.69}$$

$$\left(1.035 \le s/d \le 1.35; \quad 1500 \le \rho W \le 4000\left[\kappa z/\left(M^2.c\right)\ 0 \le x \le 1\right]\right);$$

where St^1_l and St^1_g are defined from the single-phase flow relations, functions φ_1, φ_2, γ, θ are presented in [75].

Having regard to the non-equilibrium flow, we obtain:

$$St^\Psi_k = \left(St^\Psi_k\right)_0\left(1 - K_M\frac{G_l - G_e}{G_l + G_e}\right)\tag{3.70}$$

$$\left[1.035 \le s/d \le 1.35; \quad 62 \le \rho W \le 8100\kappa z/\left(M^2.c\right); \quad 0 \le x \le 1\right].$$

3.6. TEMPERATURE BEHAVIOUR AND HEAT TRANSFER IN NOMINAL GEOMETRY

Information on heat transfer coefficient and pin temperature in the bundle cooled by liquid metal was extracted from a measurements in LMFBR core (1.04 $\le s/d \le$ 1.17), and also from the common physical notions in a wide ranges of defining parameters (1.0 $\le s/d \le$ 1.18;
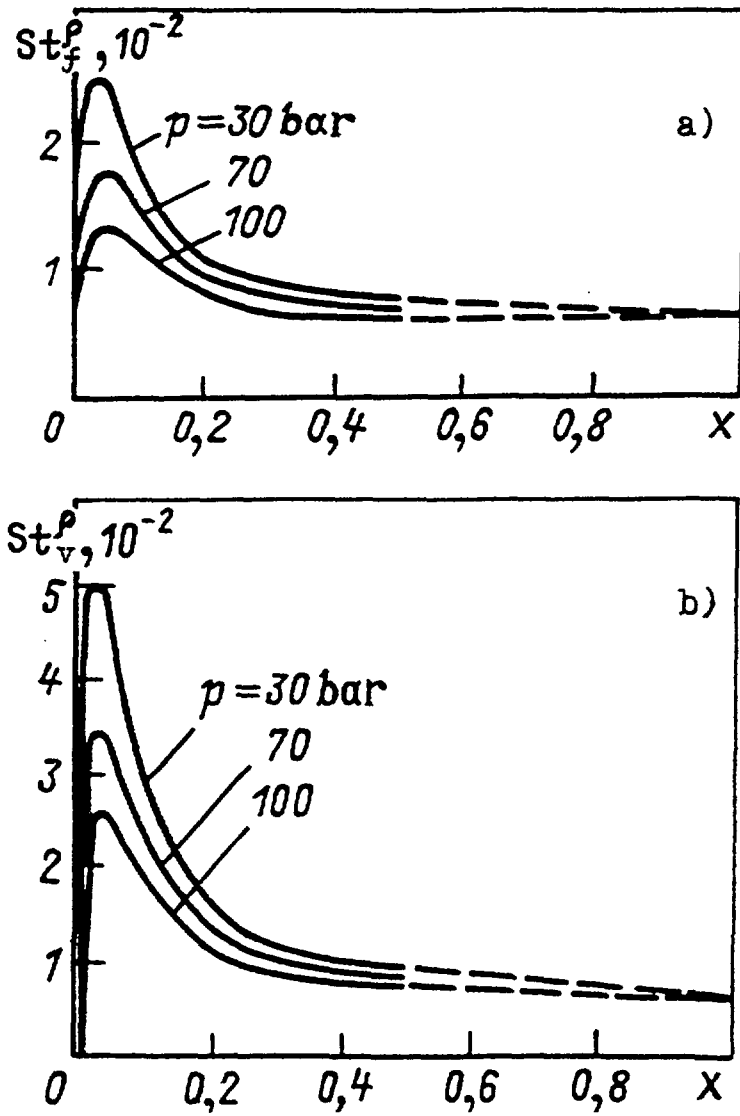
Fig. 3.30. interchannel exchange by liquid *(a)* and vapour *(b)* in two-phase flow *(model of separated flows)* with quality, as pressure changes.
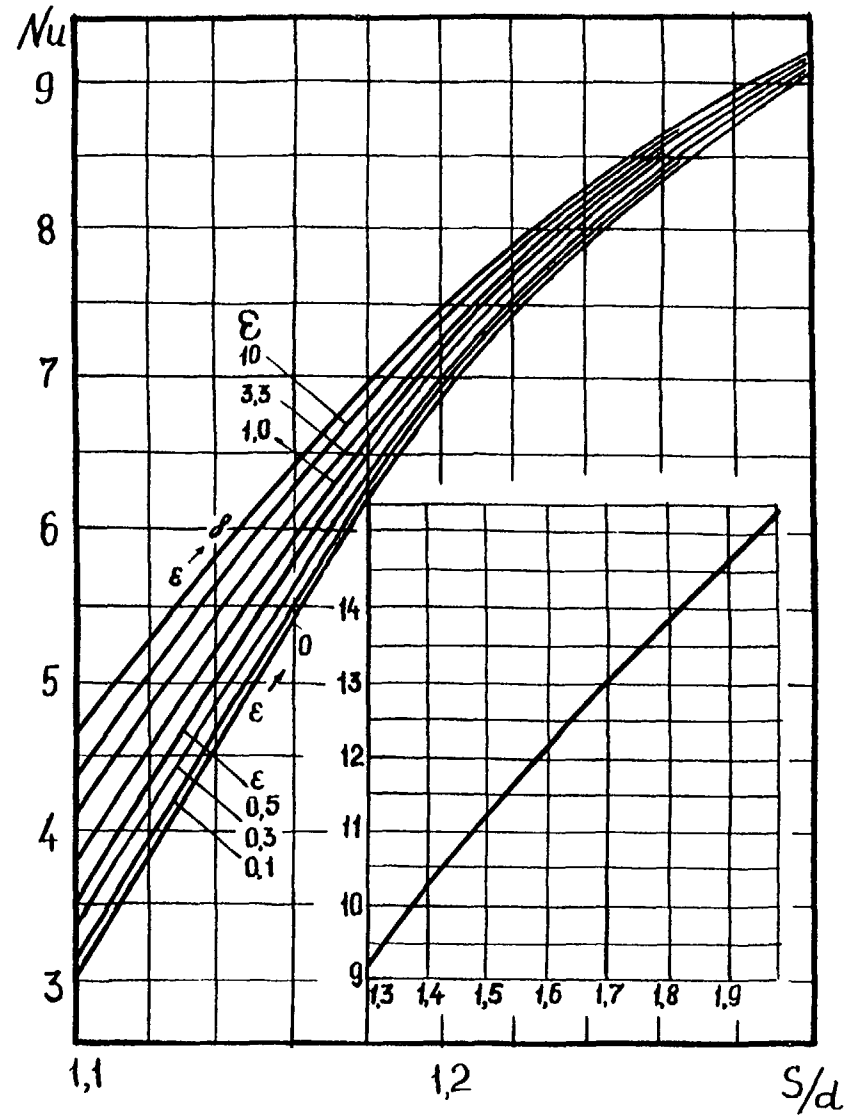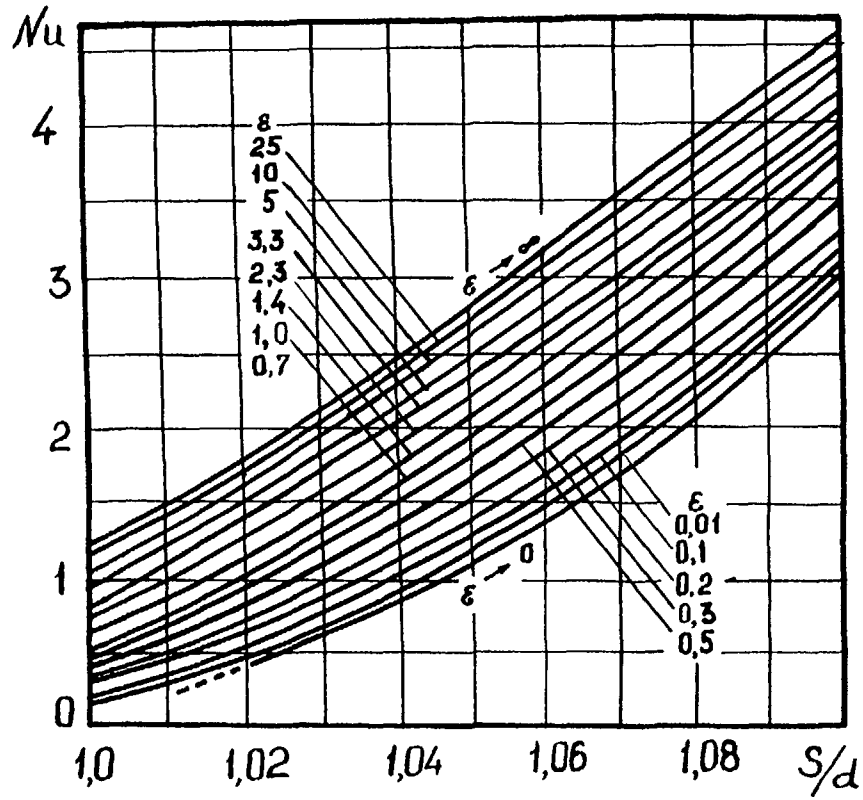
Fig. 3.31. Diagrams find Nusselt number in laminar flow of coolant through the bundle.
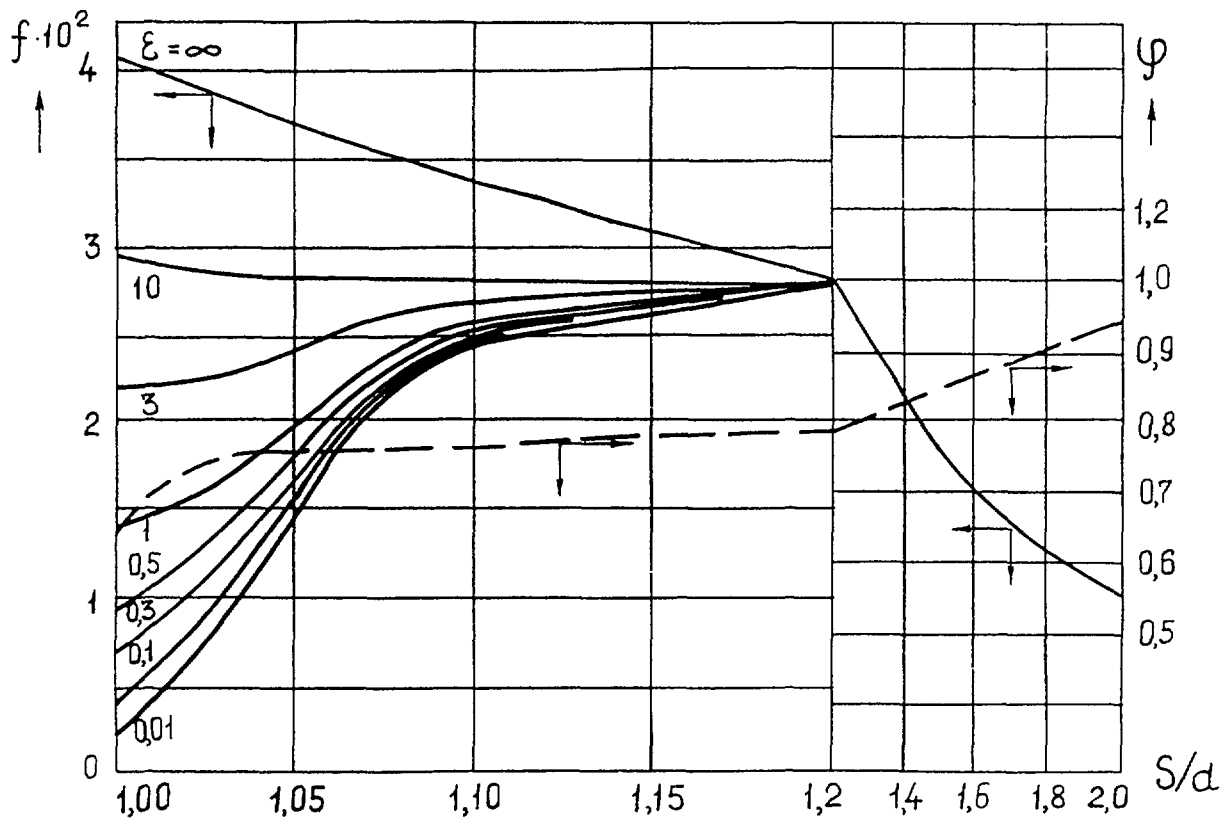
Fig. 3.32. Diagram to define «f» and «φ» in relation (3.)

Table 3.3. *Calculation relations for* Nu_{lam}, f, φ *in (3.71)*

	$s/d = 1.0$	$1 \le s/d \le 1.2$	$1.2 \le s/d \le 2.0$
Nu_{lam}	$1.25\left(1 - \dfrac{3.6}{4.2 + 2.5\varepsilon^{0.86}}\right)$	$\left[7.55\dfrac{s}{d} - \dfrac{6.3}{(s/d)^{17 s/d\left(s/d\frac{s}{d} - 0.81\right)}}\right] \cdot$ $\left[1 - \dfrac{3.6(s/d)}{(s/d)^{20}\left(1 + 2.5\varepsilon^{0.86}\right) + 3.2}\right]$	$7.55\dfrac{s}{d} - 20\left(\dfrac{s}{d}\right)^{-13}$
f	$0.041\left(1 - \dfrac{1}{\sqrt{124\varepsilon + 1.15}}\right)$	$\dfrac{0.041}{(s/d)^2} \cdot$ $\left[1 - \dfrac{1}{\dfrac{\left(s/d^{30} - 1\right)}{6} + \sqrt{124\varepsilon + 1.15}}\right]$	$\dfrac{0.041}{(s/d)^2}$
φ	0.65	$0.56 + 0.19(s/d) - \dfrac{1}{10(s/d)^{80}}$	$0.56 + 0.19\left(\dfrac{s}{d}\right)$

$4 \leq Pe \leq 3500$; $0.007 \leq Pr \leq 0.03$; $0.02 \leq \varepsilon \leq 16$) allowing the main features of heat transfer in liquid metal bundle to be revealed. Relationships are universal, as applied to any pins.

Central area of subassembly. Heat transfer in "infinite" pin bundle can be predicted as [5-8]:

$$Nu = Nu_l + f\left(\varepsilon_6, s/d\right) Pe^{\varphi(s/d)}, \tag{3.71}$$

$1 \leq s/d \leq 2$; $\quad 0.1 \leq \varepsilon_6 \leq \infty$; $\quad 1 \leq Pe \leq 4000$,

where Nu_l - Nusselt number in laminar flow, ε_6 - thermal modeling parameter calculated by the main harmonics $(k = 6)$ [79]; f and φ - empirical functions.

Values of Nu_l, γ and φ are determined as:

$$Nu_l = \left[7.55(s/d) - \frac{6.3}{(s/d)^{17(s/d)((s/d)-0.81)}}\right] \cdot \left[1 - \frac{3.6s/d}{(s/d)^{20}\left(1+2.5\varepsilon_6^{0.86}\right)+3.2}\right], \tag{3.72a}$$

$$f = \frac{0.041}{(s/d)^2}\left(1 - \frac{1}{\frac{(s/d)^{30}-1}{6}+\sqrt{1.24\varepsilon_6+1.15}}\right), \tag{3.72b}$$

$$\varphi = 0.56 + 0.19s/d - \frac{0.1}{(s/d)^{80}} \tag{3.72c}$$

or taken from nomograms (Fig. 3.31, 3.32). The formula view is conserved just in the range $1.0 < s/d < 1.2$.

In reference points the formula becomes simpler:

$$Nu = Nu_{lam} + 0.041\left(1 - \frac{1}{\sqrt{1.24\varepsilon_6+1.15}}\right) \cdot Pe^{0.65}, \tag{3.73}$$

where

$$Nu_{lam} = 1.25\left(1 - \frac{3.6}{4.2+2.5\varepsilon_6^{0.86}}\right) \text{; for } 1.20 \leq s/d \leq 2.0 \tag{3.73a}$$

$$Nu = Nu_{lam} + \frac{0.041}{(s/d)^2} Pe^{0.56+0.19s/d}, \tag{3.74}$$

where

126

$$Nu_{lam} = 7.55(s/d) - 20(s/d)^{-13}$$

(3.74a)

An accuracy is ±15%.

Table 3.3 presents relationships to predict Nu_l, f and φ in different bundles. In Fig. 3.33 predictions are compared with experimental data. In order to approximate Nusselt number the nomogram presented in Fig. 3.34 is conveniently used.

Maximum temperature non-uniformities around the pin can be predicted as follows:

$$\Delta T = \frac{t_w^{max} - t_w^{min}}{qR} \lambda_f = \frac{\Delta T_{lam}}{1 + \gamma(\varepsilon_6)Pe^{\beta(s/d)}} \ ,$$

(3.75)

where ΔT_l - those in laminar flow defined from the nomogram (Fig. 3.35),

$$\gamma(\varepsilon_6) = (1 + 0.03\varepsilon_6) \cdot 8 \cdot 10^{-3} \ ;$$

(3.76)

$$\beta(s/d) = 0.65 + \frac{51 lg(s/d)}{(s/d)^{20}}$$

(3.77)

The deviation of the temperature distribution from a cosine law can be evaluated using nomogram (Fig. 3.36) or by the formula:

$$Z = \frac{t_w^{max} - \overline{t_w}}{\overline{t_w} - t_w^{min}} = 0.9 + 0.1\left\{1 - exp\left[-10\left(\frac{s}{d} - 1\right)\right]\right\} +$$

$$+ 0.2 exp\left[-50\left(\frac{s}{d} - 1\right)\right] - 0.49 exp\left[-20\left(\frac{s}{d} - 1\right)\right] th\left[lg\varepsilon_6 + 0.6\left(1 - \frac{s/d - 1}{0.1}\right)\right] \ .$$

(3.78)

Fig. 3.37 compares predictions by (3.75) and experiment.

Edge areas. In the close bundles ($s/d = 1.04$, 1.062) free from displacers the temperature non-uniformity at the edge pins is conditioned by the subcooled coolant near the wrapper tube (Fig. 3.38) [82]. Periodical non-uniformity caused by the channel geometry is superimposed on the general non-uniformity, with the periodic behaviour being the most expressed at large Peclet numbers and small distances from the section of power production oneself, where azimuthal flows are not large. Even though the pin thermal conductivity may be increased (pin with cooper cladding), it does not cause the total non-uniformity to reduce significantly, although a periodic component disappears virtually. Displacers considerably decrease the temperature non-uniformity.

In the bundle with $s/d = 1.1$ and relative pitch between wrapper and edge pins $\Delta/(s-d)$ = 1.0, temperature field becomes more smooth (Fig. 3.39) [83]. The greatest temperature non-uniformity's are observed to be in the bundle of smooth pins free of displacers. Wire wrap, as well as displacers, produce the more filled temperature profile and non-uniformity reduces markedly.

127
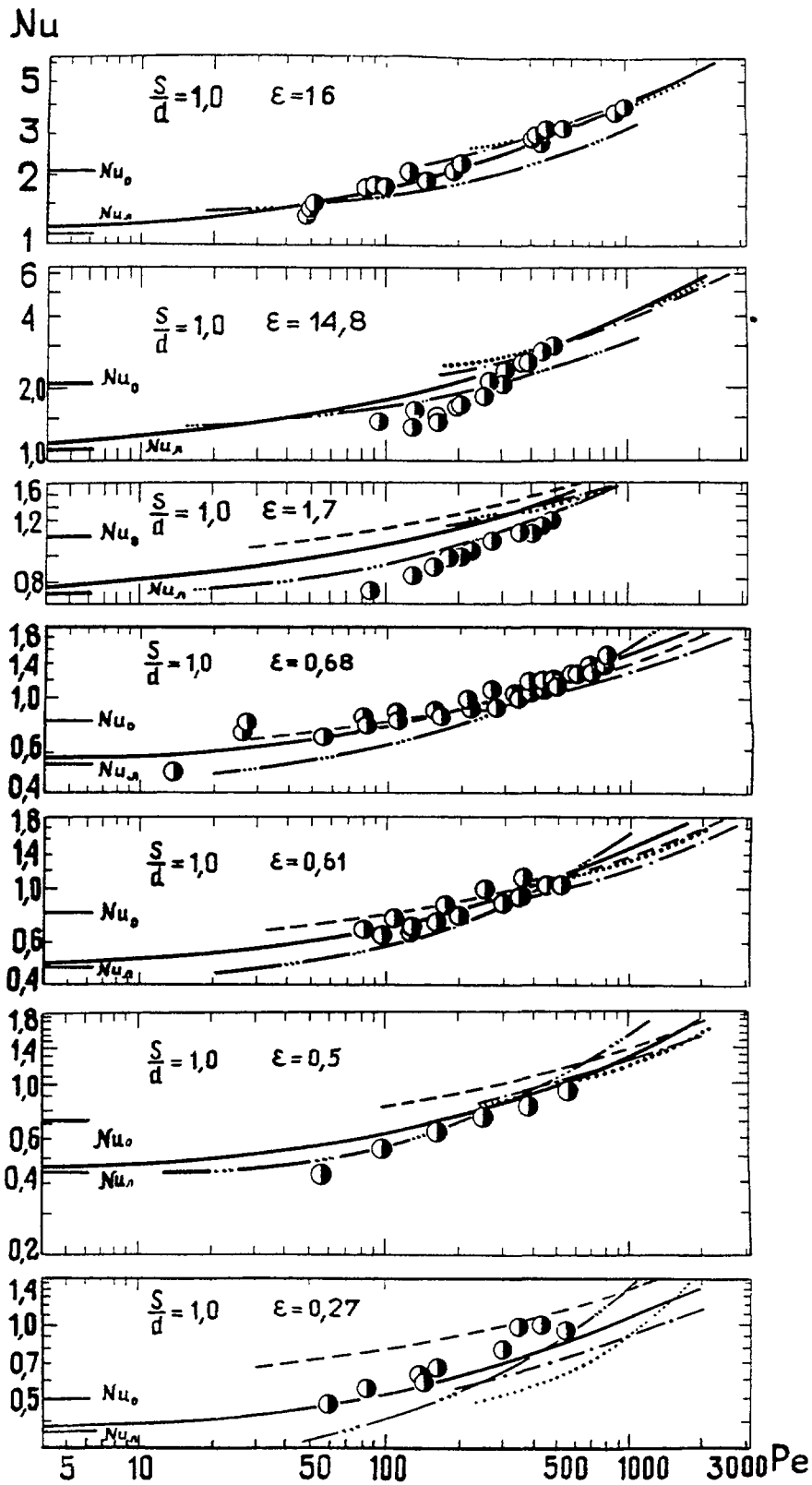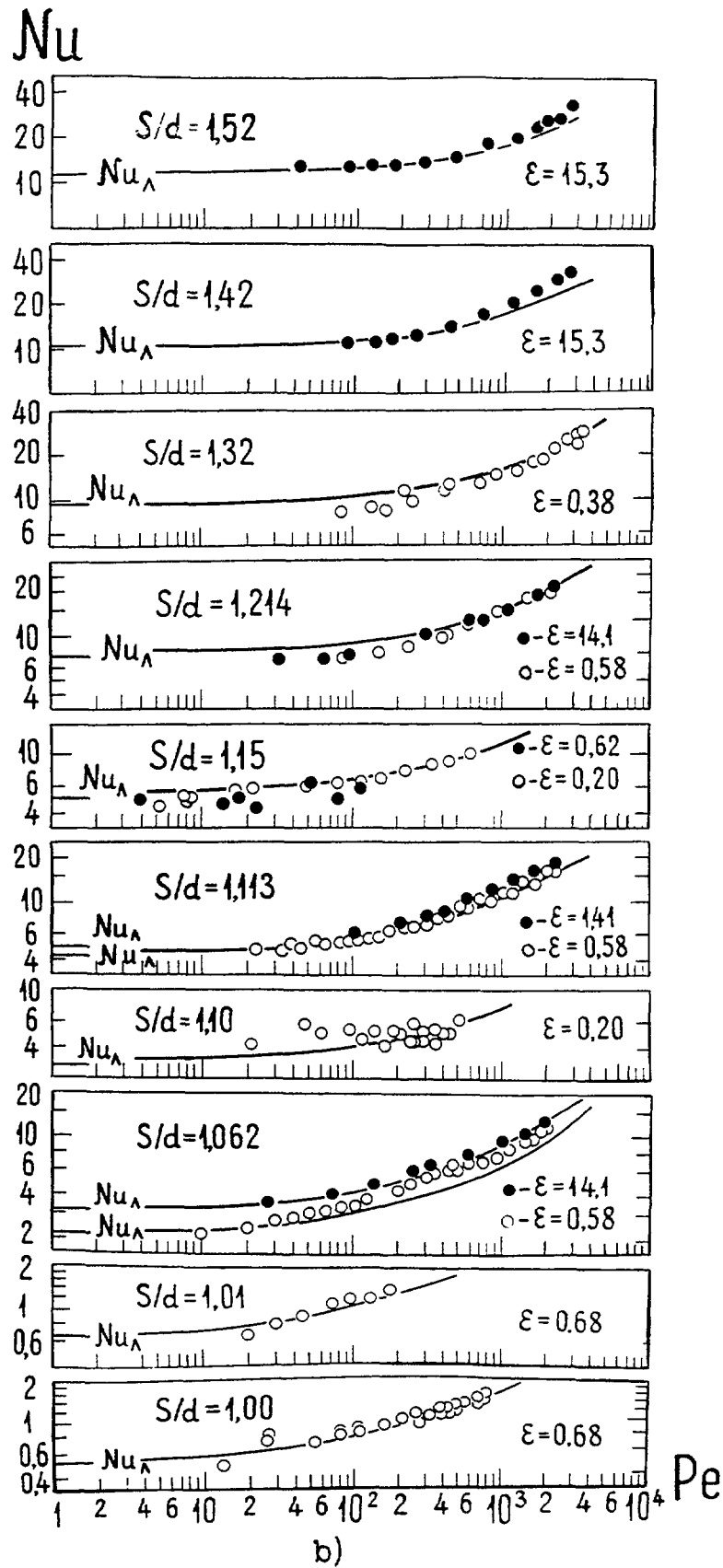
Fig. 3. 33.-a

Fig,. 3.33. Comparison of experimental data (◑, ○, ●)
with predicting relations on Nusselt numbers.

129
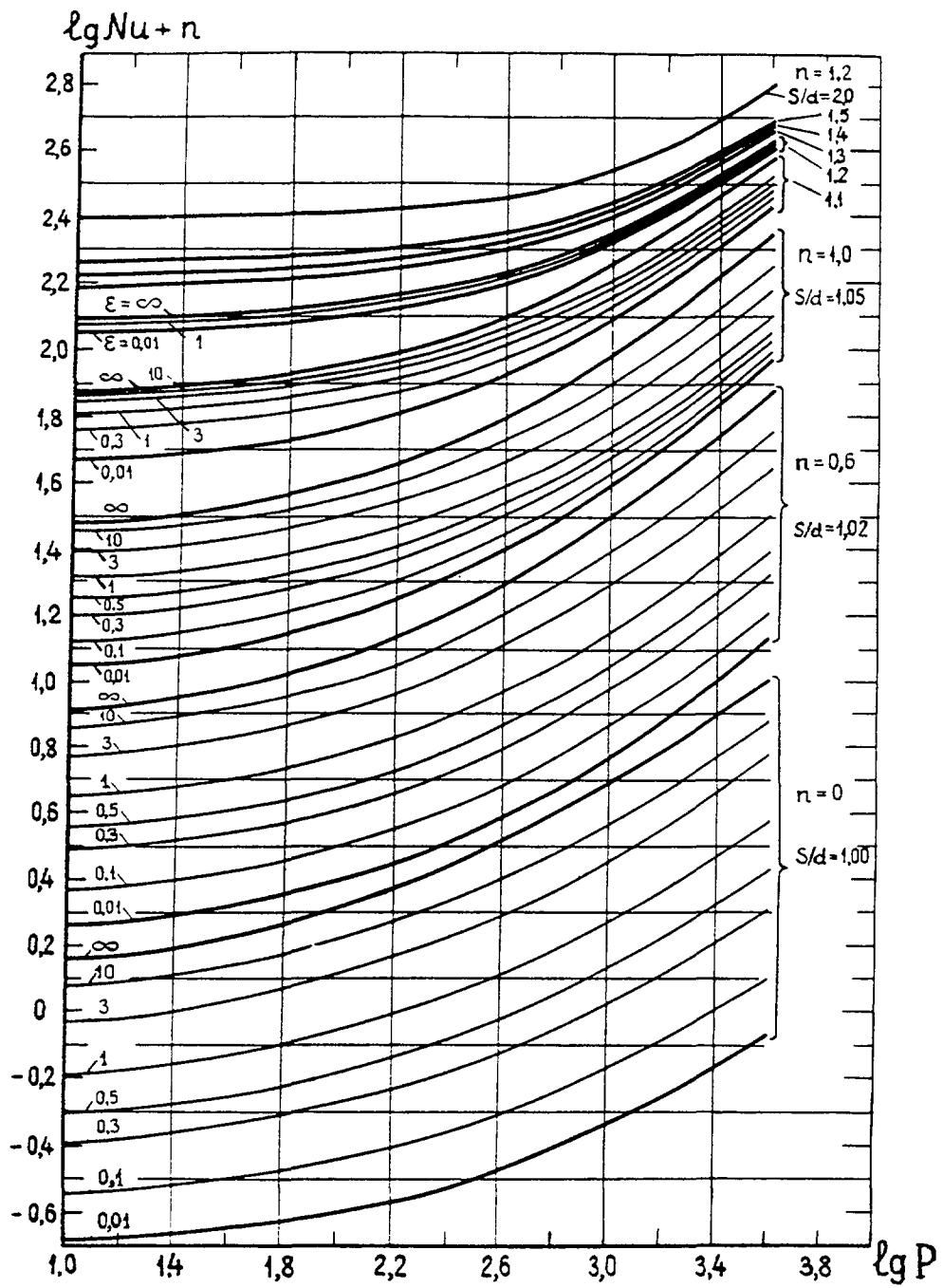
Fig. 3.34. Diagram to evaluate Nusselt numbers in pin bundle.
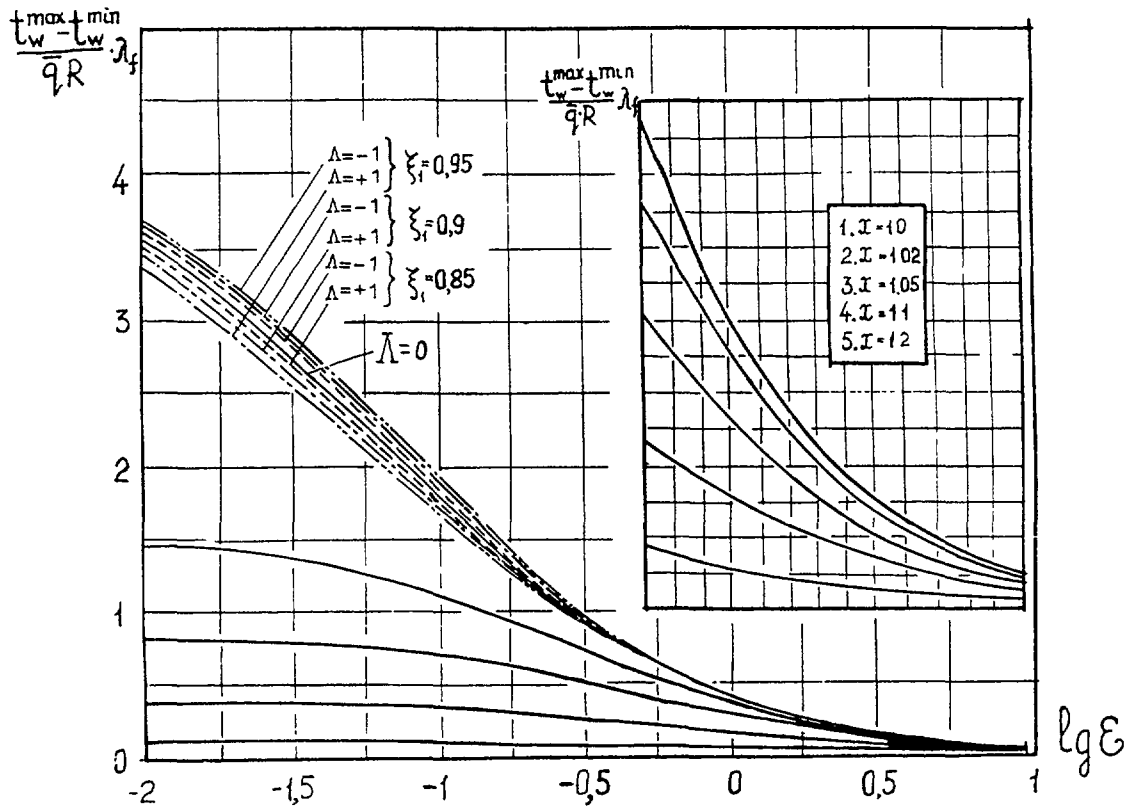
Fig. 3.35. Diagram to define maximal irregularities of pin temperature in laminar flow
$[\lambda = (\lambda_w - \lambda_0) / (\lambda_w + \lambda_0),\ \xi_1 = R_1 / R,\ \varepsilon = \varepsilon_6].$
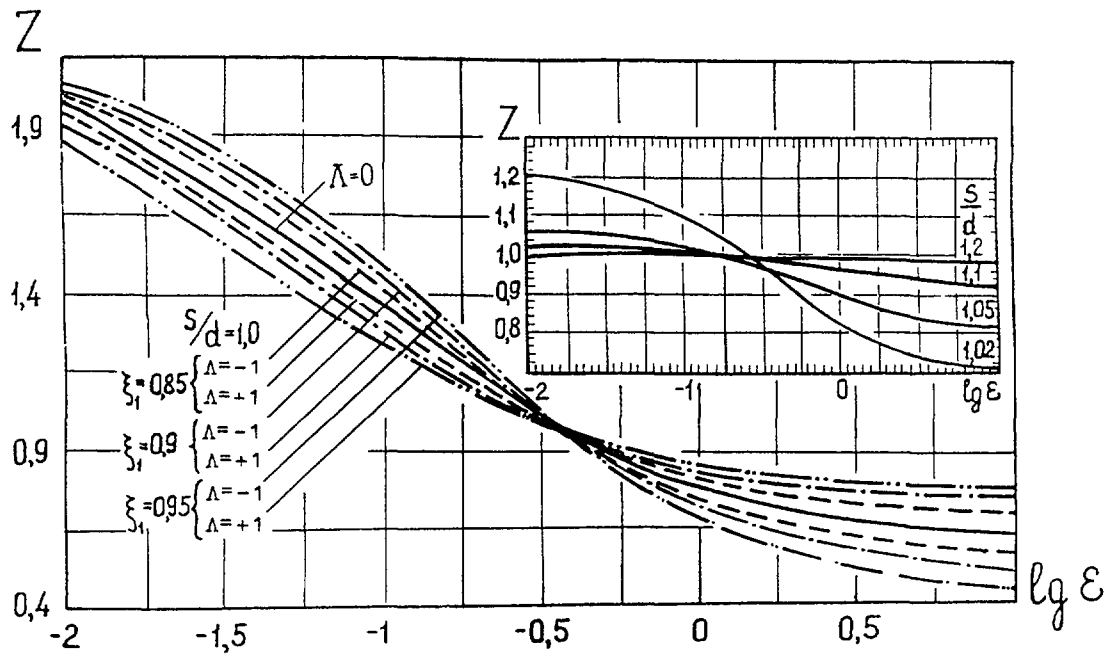
Fig. 3.36. The same to define parameter Z (see fig. 3.35).
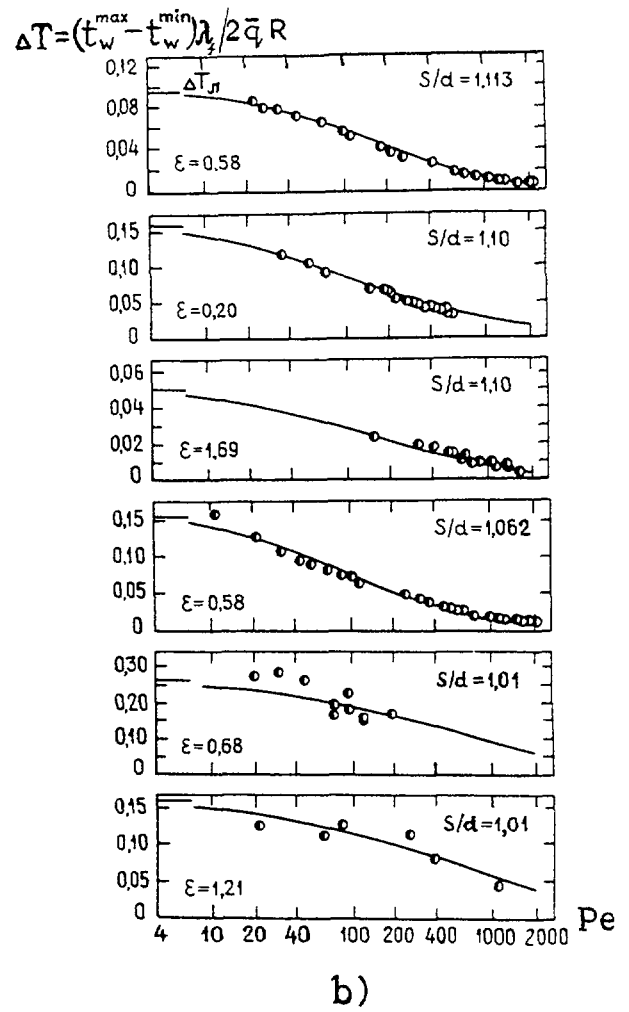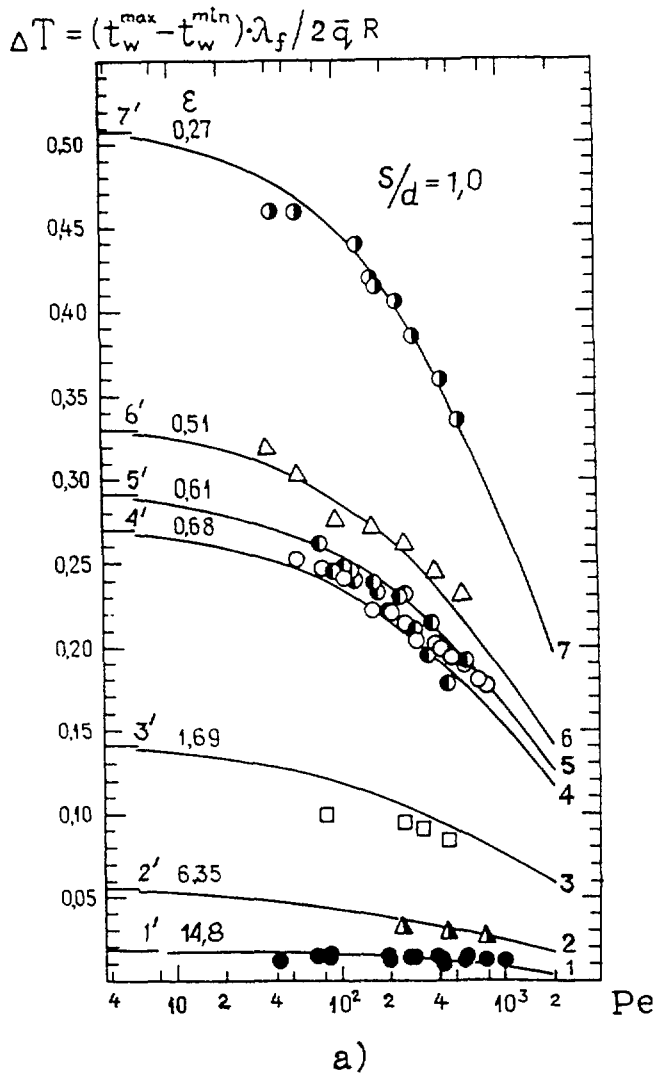
Fig. 3.37. comparison of experimental data IPPE with relationship for maximal irregularity of temperature pin in the compact bundle (a) and for pins arranged with various relative pitch S/d (b):

1÷7 - S/d = 1.0; 1'÷7' - laminar flow;

●,○, △, □, ◐, ▲, ◑ - experiments by IPPE.
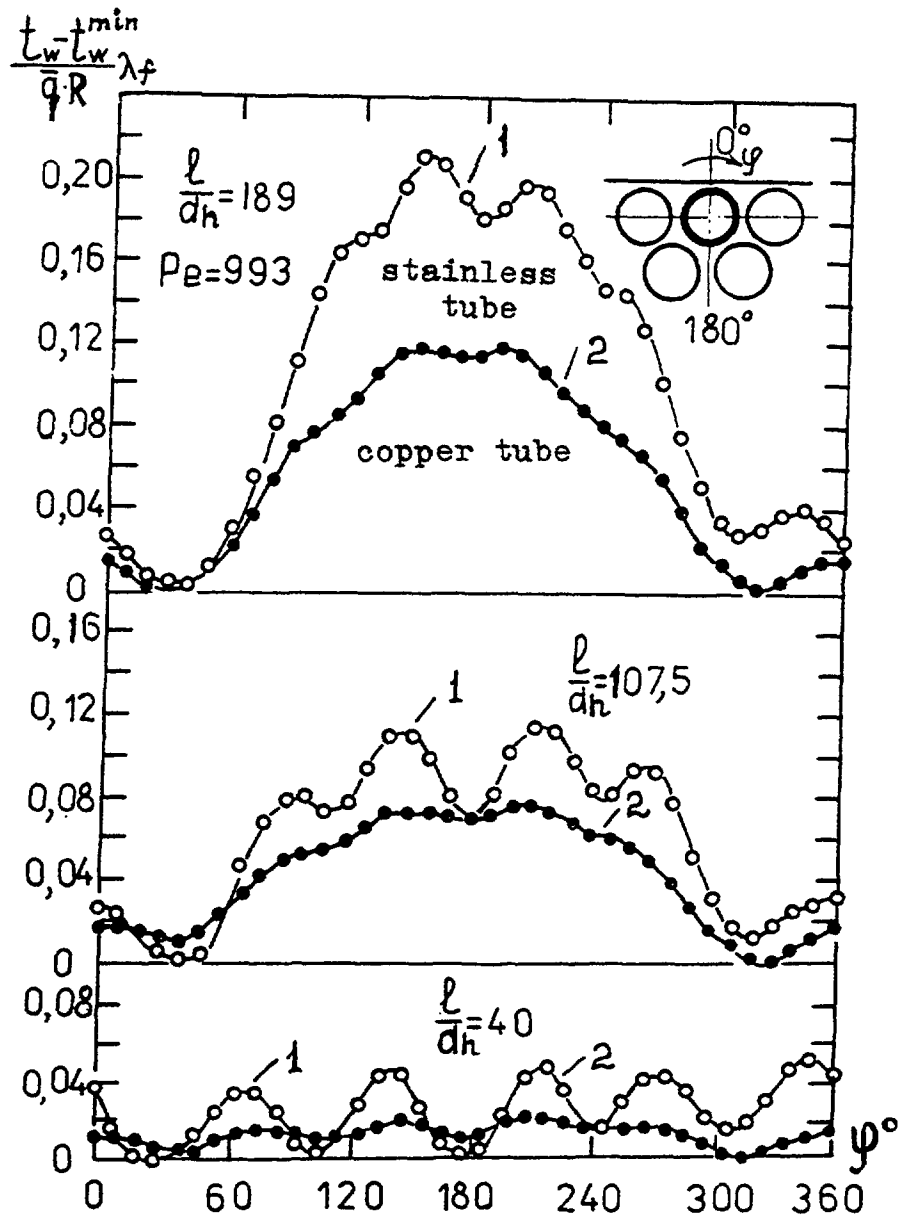
Fig. 3.38. Temperature behaviour of edge pin in the bundle with
S/d = 1.062 without displacers:
1 - simulator of stainless steel,
2 - copper simulator, O , ● - experiments
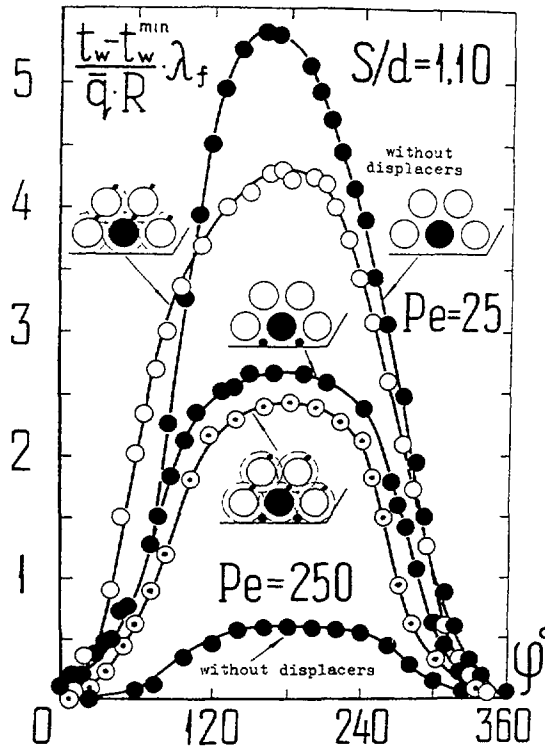
Fig. 3.39. Temperature behaviour in edge pins of BOR-60 reactor:

● - smooth pins without displacers,

● - smooth pins with displacers,

○ - wire wrapped pins without displacers,

⊙ - wire wrapped pins with displacers.
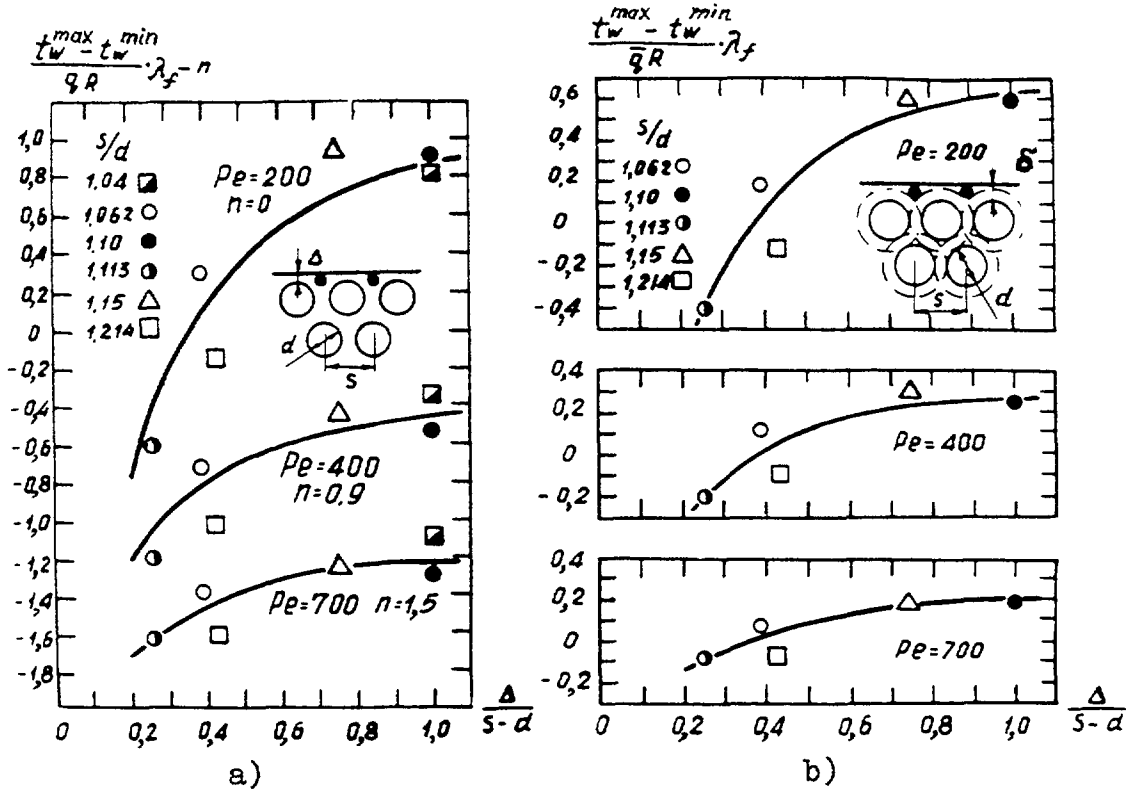
Fig. 3.40. Maximal irregularities of the edge pin temperature:
a) smooth pins,   b) wire wrapped pins.

134

Table 3.4. Factors A,B,C,D in (3.79)

Peclet number	A	B	C	D	β
Bundle of smooth pins without displacers ($1.06 \leq s/d \leq 1.15; 0 \leq \Psi \leq 1.05$)					
700	0.10	0.40	0.63	15	$5.4 \lg Pe - 7.52$
400	0.21	0.41	0.89	12.5	$(e = s\text{-}d)$
200	0.47	0.82	1.3	10	
Bundle of wire wrapped pins without displacers ($1.06 \leq s/d \leq 1.15; 0.3 \leq \Psi \leq 1.05$)					
700	0.02	0.48	0	0	$0.28 \lg Pe + 0.396$
400	0.27	0.31	0	0	$[e = 0,5\ (s\text{-}d)]$
200	0.52	0.62	0	0	
Bundle of smooth pins with displacers ($1.06 \leq s/d \leq 1.25; 0.25 \leq \Psi \leq 1.05$)					
700	0.214	0.083	1.03	4.15	$6.86 - 1.95 \lg Pe$
400	0.33	0.12	1.17	5.05	$[e = 0.5\ (s\text{-}d)]$
200	0.40	0.5	3.66	5.07	
Bundle of wire wrapped pins with displacers ($1.06 \leq s/d \leq 1.25; 0.25 \leq \Psi \leq 1.05$)					
700	0.0525	0.16	1.33	7.25	$0.34 \lg Pe + 0.783$
400	0.132	0.17	2.25	6.72	$[e = 0.5\ (s\text{-}d)]$
200	0.45	0.19	4.08	5.9	
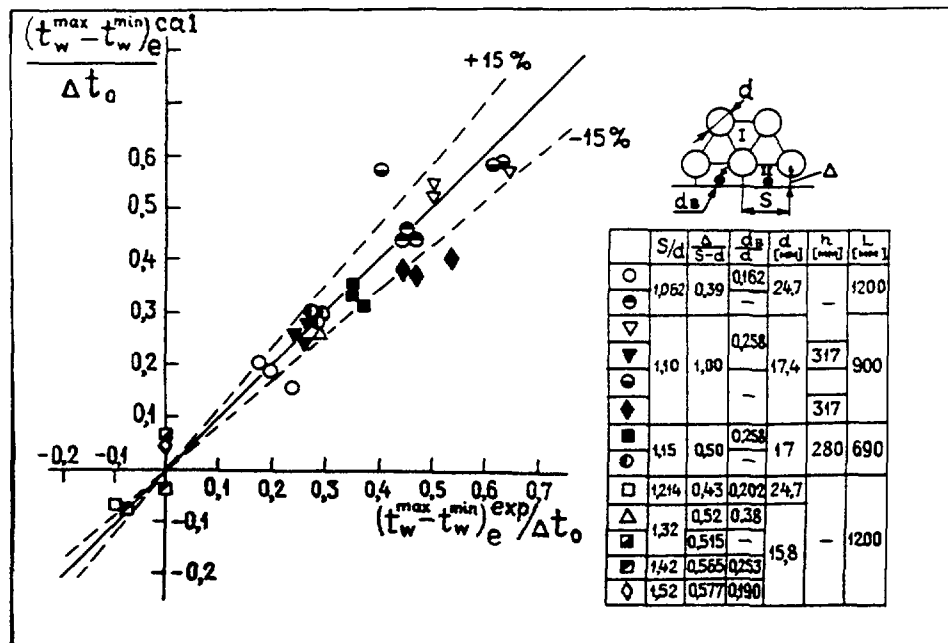
Fig. 3.41. Correlation between predictions and experimental data on temperature irregularities around the edge pins.

Temperature behavior of the edge pins, as a rule, is unstable. It is connected with the fact that the points of maximum and minimum temperature are diametrically opposite and this makes heat exchange difficult.

Unstable character of temperature distribution is most conspicuous in the bundles with the small relative pitch. Entering the displacers into such a bundles does not change temperature distribution along the bundle, provided that displacer diameter is not as great to generate high level of temperature in the edge channels.

Maximum temperature non-uniformity around the edge pin is generalized by the parameter $\psi = \dfrac{\Delta}{s-d} = \dfrac{\Delta}{d(s/d-1)}$, combining the bundle pitch (s/d) and the clearance between wrapper and pins (Δ) (Fig. 3.40).

Value ΔT is recognized as positive, if maximum temperature is observed as viewed from the internal channels (periphery is subcooled), and negative, if maximum temperature is observed from the wrapper (periphery is superheated) sing of ΔT is conventional, but helps the subcooled and superheated regions to be ascertained.

Maximum temperature non-uniformity around the edge pins can be evaluated as [84] recommends:

$$\Delta T = \frac{t_w^{max} - t_w^{min}}{qR}\lambda_f = A + B\psi - C\,exp\!\left(-D\psi\right) .$$

(3.79)

$200 \leq Pe \leq 700; \ \ l/d_h \geq 200$

Coefficients A, B, C, D are presented in the Table 3.4.

Also, approximately the maximum temperature non-uniformity around the edge pin can be estimated reasoning from the superposition of coolant temperature non-uniformity (Fig. 3.41) and local temperature non-uniformity for "infinite" bundle at the inherent parts of pin perimeter [85]:

$$\left(t_w^{max} - t_w^{min}\right)_{inf\,in} = t_{f1} - t_{f11} + \left(t_w^{max} - T_w\right)_{\infty}^{trian} + \left(t_w - t_w^{min}\right)_{\infty}^{square} .$$

(3.80)

Substituting expressions for the local non-uniformity in the "infinite" triangular and square bundle gives that:

$$\left(t_w^{max} - t_w^{min}\right)_{inf\,in} = \Delta t_o\left\{\left(1 - \frac{1}{g_{ef}}\right)\frac{1 - exp\!\left(-T_M\right)}{T_M} + \right.$$

$$\left. + \frac{Ped}{8L}\left[\frac{Z}{Z+1}\left(\Delta T_{\infty}^{max}\right)_{trian} + \frac{1}{Z+1}\left(\Delta T_{\infty}^{max}\right)_{square}\right]\right\} ,$$

(3.81)

where Δt_0 - overtemperature in the internal channels,

$$\Delta T_{\infty}^{max} = \frac{t_{w}^{max} - t_{w}^{min}}{q(d/2)} \lambda_{f}, \quad Z - \frac{t_{w}^{max} - \bar{t}_{w}}{t_{w} - t_{w}^{min}}$$

are calculated by (3.75 - 3.78) for triangular bundle [80, 81] and by the nomogram for square bundle at laminar flow [86], with the correction for the flow.

The correction is inserted from the relative parameters for triangular and square bundles are equal each other:

$$\left(\frac{\Delta T^{max}}{\Delta T_{lam}^{max}}\right)_{trian \ \infty} = \left(\frac{\Delta T^{max}}{\Delta T_{\pi}^{max}}\right)_{square\infty}$$

Statistic processing shows that experimental data [84, 87] are agree with the relationship (3.81) (Fig. 3.41).

Edge pin heat transfer. Considerable temperature non-uniformity around the edge pin reduces heat transfer intensity as compared with internal pins, and special relationship needs to be used in prediction [84, 87]:

$$Nu = \frac{\bar{\alpha} d_{h}}{\lambda_{f}} = a + bPe^{n}, \qquad (3.82)$$

$1.04 \le s/d \le 1.3; \quad 0.39 \le \Psi = \Delta/(s-d) \le 0.52; \quad 30 \le Pe \le 3000; \quad 0 \le d_{displacer} \le 0.32;$

$0.04 \le \varepsilon_{l} \le 0.14.$

Table 3.5. Calculation relations for factors a, b, n *(3.82)*

Type of pins	a	b	n
without displacers			
Edge	4.69 s/d − 4.131	0.577 s/d − 0.566	$3.53\left(\dfrac{s}{d}\right)^{2} - 8.71\dfrac{s}{d} + 5.97$
Corner	7.13 s/d − 6.972	0.331 s/d − 0.342	$5.27\left(\dfrac{s}{d}\right)^{2} - 13.12\dfrac{s}{d} + 8.83$
Displacers			
Edge	4.81 s/d − 3.348	1.381 s/d − 1.376	$1.26\left(\dfrac{s}{d}\right)^{2} - 3.35\dfrac{s}{d} + 2.74$
Corner	3.59 s/d − 3.189	1.324 s/d − 1.363	$14.88 - 3.35\dfrac{s}{d} + 25.43\left(\dfrac{s}{d}\right)^{2} - 6.57\left(\dfrac{s}{d}\right)^{3}$

Here d_h - hydraulic diameter of internal zone of subassembly, $Pe = \overline{w}d_2 / a$; $\overline{a} = \overline{q} / \left(\overline{t}_w - \overline{t}_f \right)$ - mean heat transfer coefficient under stable heat removal conditions (in the event when there is no stable temperature difference "wall - liquid", that is often observed at the edge pins, heat transfer coefficient is evaluated in top cross section of power production length); $\overline{q}, \overline{t}_w$ -- averaged heat flux and pin temperature, $\overline{t}_f$ - mean coolant temperature defined as arithmetic mean between temperatures in adjacent channels, ε_l - equivalent thermal conductivity based on the first harmonics in Fourier series, d_d - displacer diameter. Factors a, b, n are calculated in accordance with the Table 3.5.

Values of Nusselt number (Fig. 3.42) are segregated with relative pitch with decreasing and tend to limiting value internal in laminar flow Peclet number [88].

3.7. ENTRANCE THERMAL SECTION. VARIABLE POWER PRODUCTION

Hydraulically stable flow. In turbulent flow [89.90] the problem is resolved under the assumptions that power production is constant with length and across the pin, and physical properties do not depend on temperature. Mathematical description for the inherent channel in triangular bundle is of the form (Fig. 3.43a, b)

$\xi > 1$

$$\frac{1}{Pe'^2} \cdot f_1 \frac{\partial^2 \widetilde{T}}{\partial X^2} + \frac{1}{\xi} \frac{\partial}{\partial \xi} \left(\xi F_2 \frac{\partial \widetilde{T}}{\partial \xi} \right) + \frac{1}{\xi^2} \frac{\partial}{\partial \varphi} \left(f_3 \frac{\partial \widetilde{T}}{\partial \varphi} \right) = W \left(\frac{\partial \widetilde{T}}{\partial X} + \frac{4}{D_z} \right), \qquad (3.83)$$

$\xi_1 < \xi < 1;$

$$\frac{1}{Pe'^2} \frac{\partial^2 \widetilde{T}}{\partial X} + \frac{1}{\xi} \frac{\partial}{\partial \xi} \left(\xi \frac{\partial \widetilde{T}}{\partial \xi} \right) + \frac{1}{\xi^2} \frac{\partial^2 \widetilde{T}}{\partial \varphi^2} = 0, \qquad (3.84)$$

$\xi < \xi_1;$

$$\frac{1}{Pe'^2} \frac{\partial^2 \widetilde{T}}{\partial X^2} + \frac{1}{\xi} \frac{\partial}{\partial \xi} \left(\xi \frac{\partial \widetilde{T}}{\partial \xi} \right) + \frac{1}{\xi^2} \frac{\partial^2 \widetilde{T}}{\partial \varphi^2} + \frac{\lambda_f}{\lambda_o} \frac{2}{\xi_1^2} = 0. \qquad (3.85)$$

Boundary conditions:

$$\frac{\partial \widetilde{T}}{\partial n} \bigg|_{n=0} = 0;$$

$$\widetilde{T} \big|_{X=-\infty} = 0.$$

The following designations are used in (3.83 - 3.85):

$$Pe' = \frac{\overline{w}R}{a} = \frac{1}{2} \frac{d}{d_h} Pe, \quad \text{where} \quad Pe = \overline{w}d_h / a;$$

$$\widetilde{T} = T - \frac{4}{D_z} X; \quad T = \frac{2t\lambda_f}{q_v R_1^2} \text{ - dimensionless temperature}$$
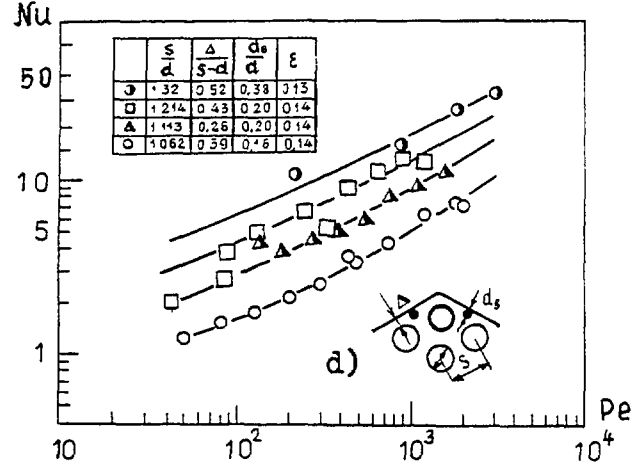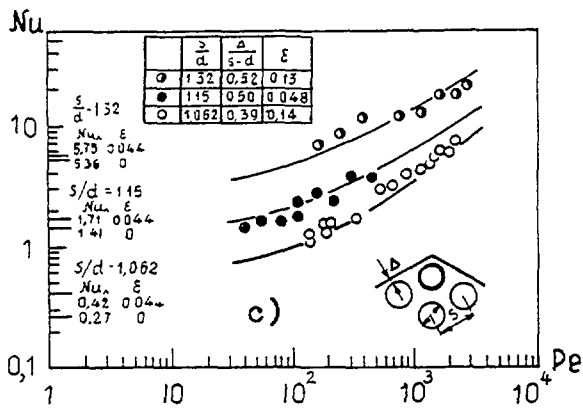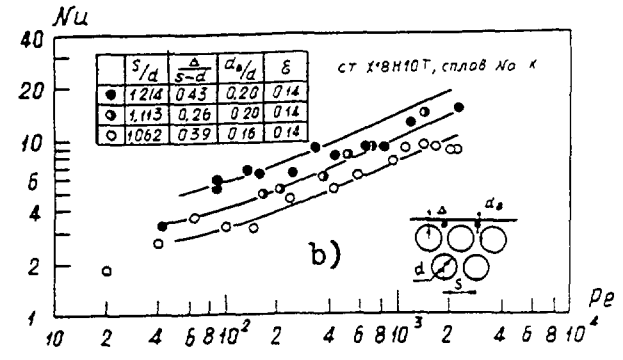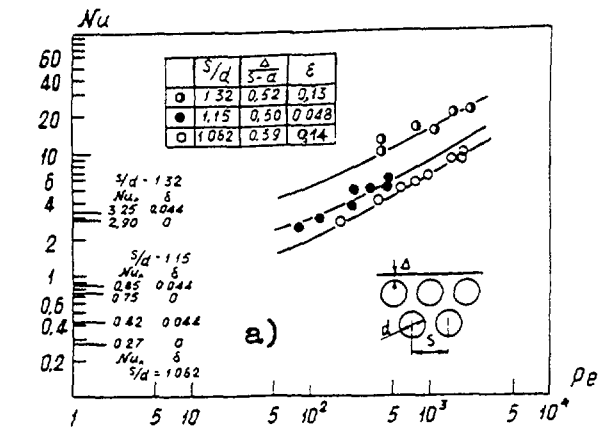
Fig. 3.42. Comparison experimental and analytical heat transfer for edge (a, b) and corner (c, d) pins.
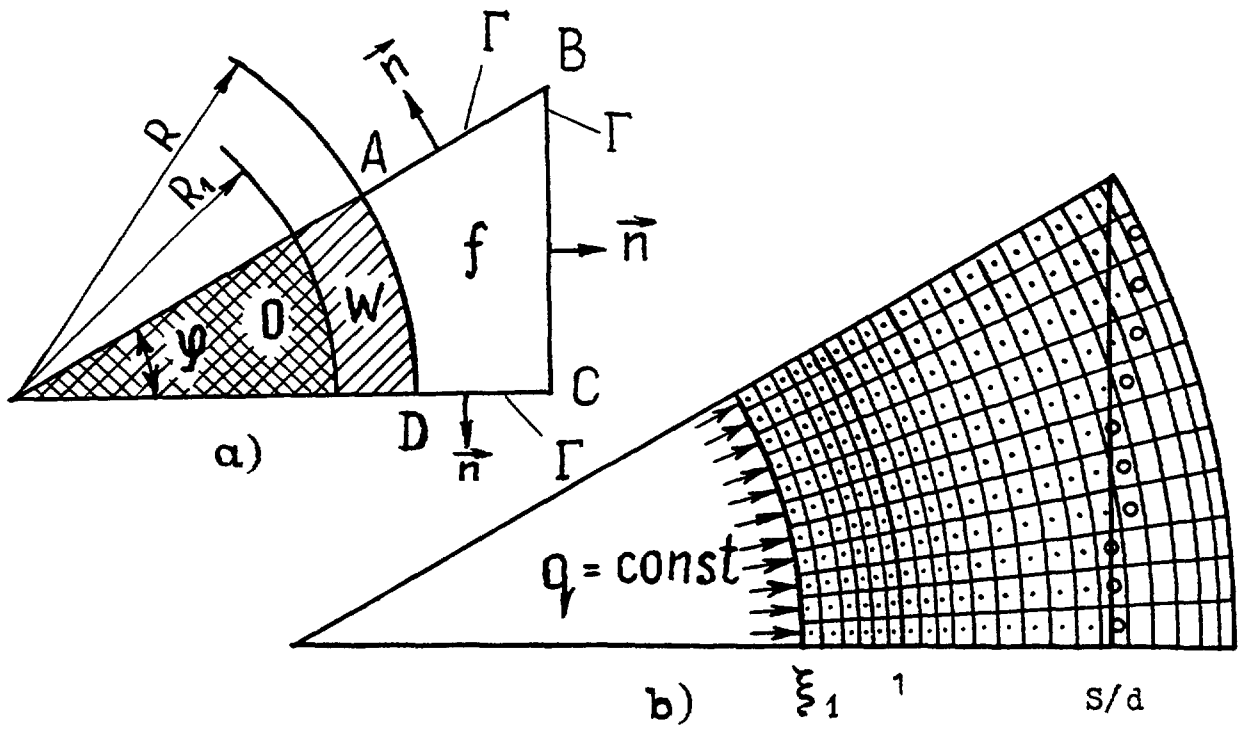
Fig. 3. 43. Specific element of pin bundle (a) and mesh (b):
● - nodes, ○ - boundary conditions.

$$f_1 = 1 + \frac{a_z^{turb}(r,\varphi)}{a}, \quad f_2 = 1 + \frac{a_r^{turb}(r,\varphi)}{a}, \quad f_3 = 1 + \frac{a_\varphi^{turb}(r,\varphi)}{a}$$

turbulence thermal diffusivity in different directions $(z, \ r, \ \varphi)$, $W = w / \overline{w}$.- dimensionless velocity, $X = \dfrac{z}{R \ Pe'}$ - dimensionless axial coordinate, $\xi = r / R$ - relative

thickness of pin cladding, t - temperature, . $q_v = \dfrac{2R\overline{q}}{R_1^2}$ - power production per unit volume, λ_f

, λ_0 -thermal conductivity of coolant and fuel, respectively, a - molecular thermal diffusivity, $,a_z^{turb}, a_r^{turb}, a_\varphi^{turb}$ - components of turbulence diffusivity in directions z, r, φ.

Entering $\widetilde{T}$, which is a difference between real temperature T in any point (with consideration for axial heat transport) and mean coolant temperature without considering axial

transport $\left(\widetilde{T}_{f_o} = \dfrac{4}{D_z} X \right)$ is convenient to make calculations more accurate, as well as an

influence of axial transport of heat to be estimated.

The problem is resolved by finite differences [90]. Sequential Yang-Frankel overrelaxation is used as iterative scheme [96, 97].

The length of entrance section is calculated on the assumption that the parameter under consideration (heat transfer coefficient, maximum temperature non-uniformity around the pin) differs from "stabilized" value $(z \to \infty)$ by not more that 2%.

To determine heat transfer coefficient and temperature behaviour at the entrance region in turbulent, laminar and plane flow the following formula is recommended

$$\frac{F(X)}{F_{stab}} = 1 - \left[p(50p)^{-X/X_{en.s.}} + (1-p) \ (50p)^{-4x/x_{en.s.}} \right] \qquad (3.86)$$

$1.02 \leq s / d \leq 2.0; \quad 0.01 \leq \varepsilon_6 \leq 10; \quad 100 \leq Pe \leq 2500,$

where $F(X)$ - is the value of functions $F_1(X) = 1 / Nu$ and

$F_2(X) = \Delta T = = \dfrac{t_w^{max} - t_w^{min}}{qR} \lambda_f$ at the entrance section, F_{stab} - is the value of functions $F_1(X)$

and $F_2(X)$ under the stable heat removal conditions, $X_{en.s. \ Nu} = l_{Nu}/R \ *Pe'$ - dimensionless length of Nucleate number entrance section, $X_{en.s.} = l_t /R*Pe'$ - dimensionless length of temperature non-uniformity entrance section, q - heat flux averaged around the pin perimeter.

Values of $X_{en.s.Nu}$ and $X_{en.st}$ are taken from Fig. 3.44 and 3.45, respectively. Functions are presented in Fig. 3.46, 3.47.

In the plane and laminar flows [90, 91] the temperature behaviour and heat transfer coefficients are governed by (3.86), with substituting inherent length and coefficients p (Fig. 3.48 - for plane flow, Fig. 3.49 - for laminar flow), with the ranges of application:
$1.01 \leq s/d \leq 2.0; \quad 0.01 \leq \varepsilon_6 \leq 10; \quad Pe \leq 100$.
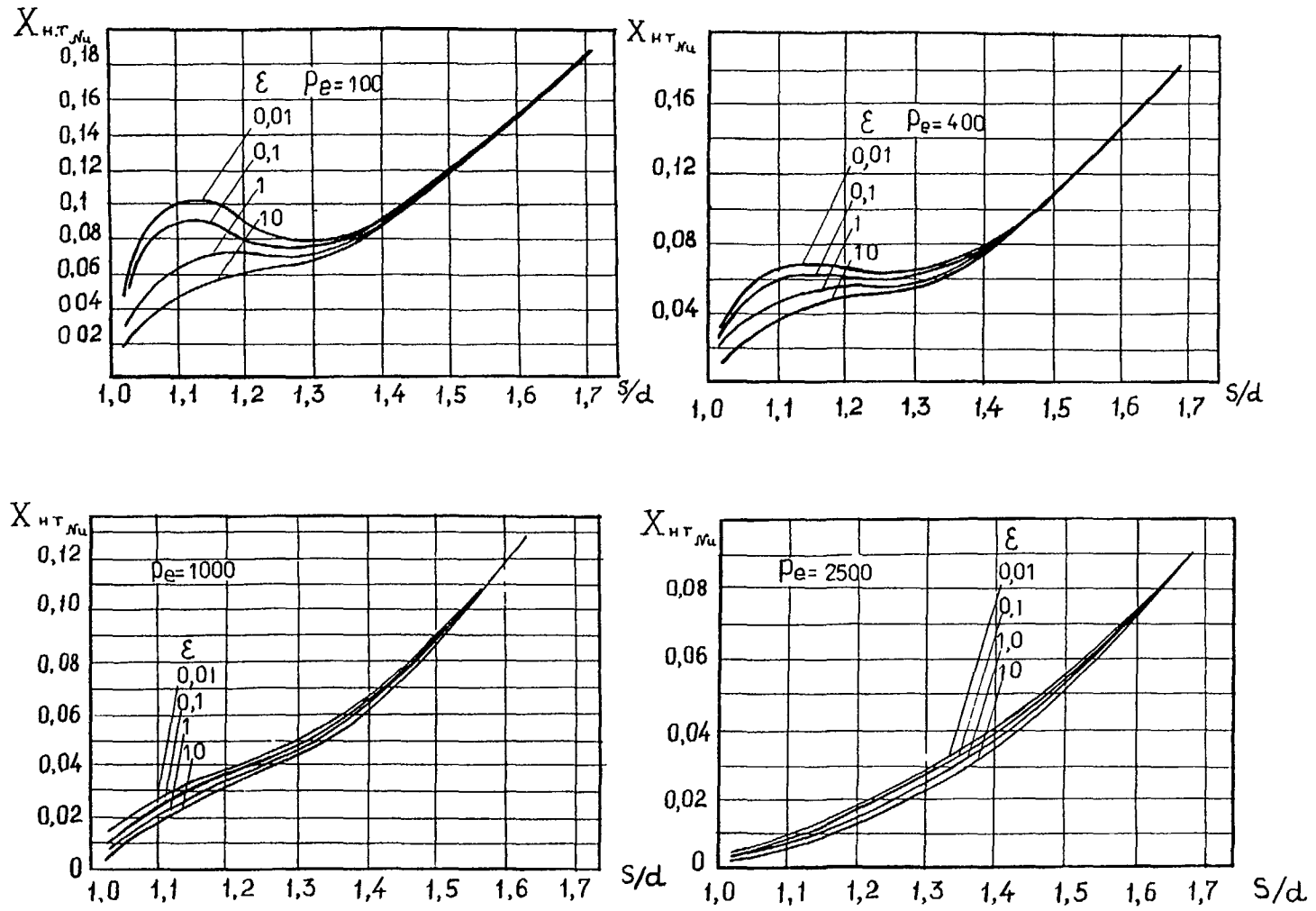
Fig. 3.44. Diagram to define the length of initial section when Nusselt number is set (turbulent flow).

$X_{H.T_t}$

0,30
0,25
0,20
0,15
0,10
0,05

ε
0,01
0,1
1,0
10

$p_e = 100$

1,0   1,05   1,1   1,13   1,2   1,25 S/d

$X_{H.T_t}$

0,16
0,12
0,08
0,04

ε
0,01
0,1
1,0
10

$p_e = 400$

1,0   1,03   1,1   1,15   1,2   1,25 S/d

$X_{H.T_t}$

0,08
0,06
0,04
0,02

ε
0,01
0,1
1,0
10

$p_e = 1000$

1,0   1,05   1,1   1,15   1,2   1,25 S/d

$X_{H.T_t}$

0,08
0,06
0,04
0,02

$p_e = 2500$

ε
0,01
0,1
1,0
10

ε
0,01
0,1

1,0   1,05   1,1   1,15   1,2   1,25 S/d
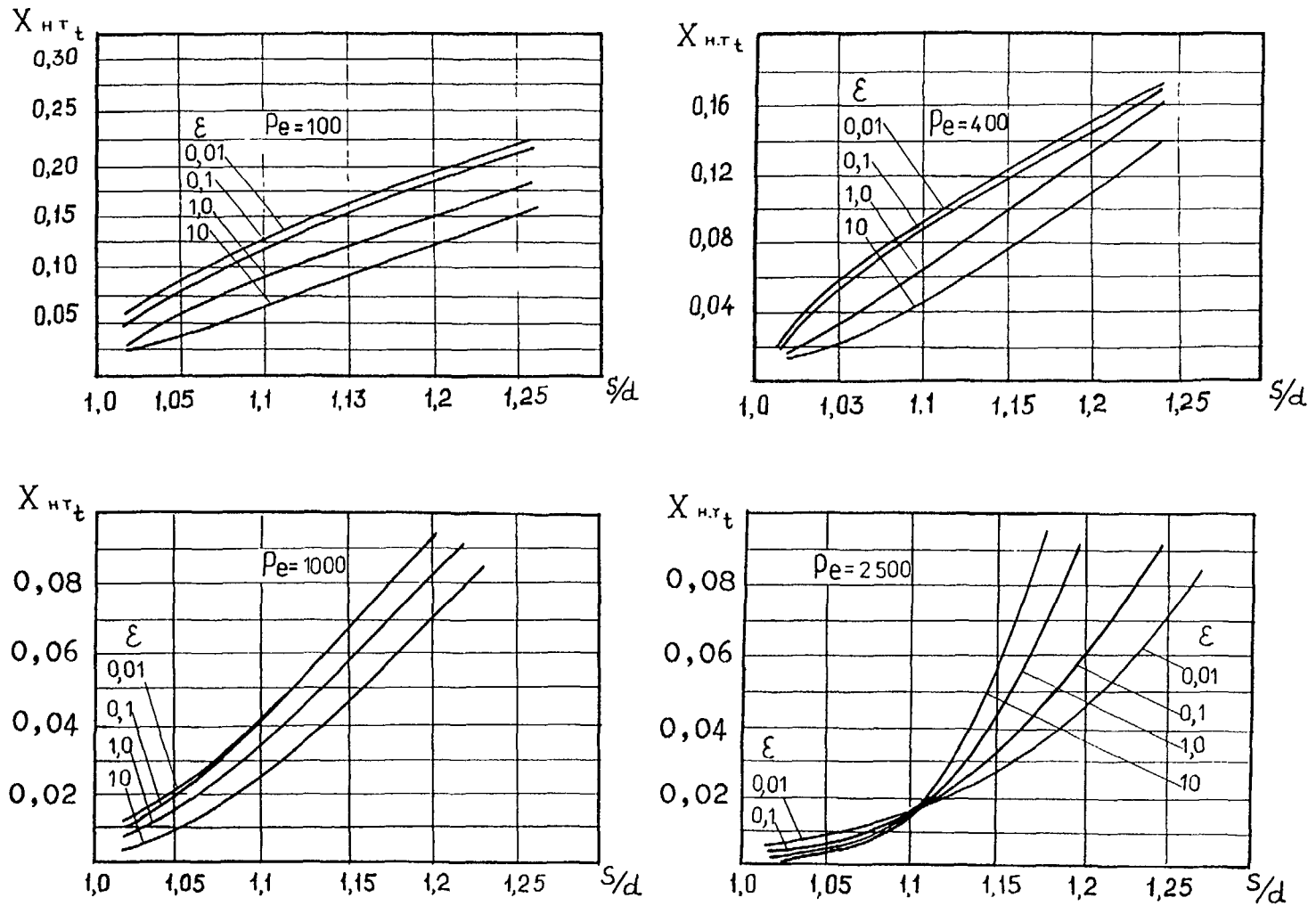
Fig. 3.45.   The same when maximal irregularity of temperature is set.
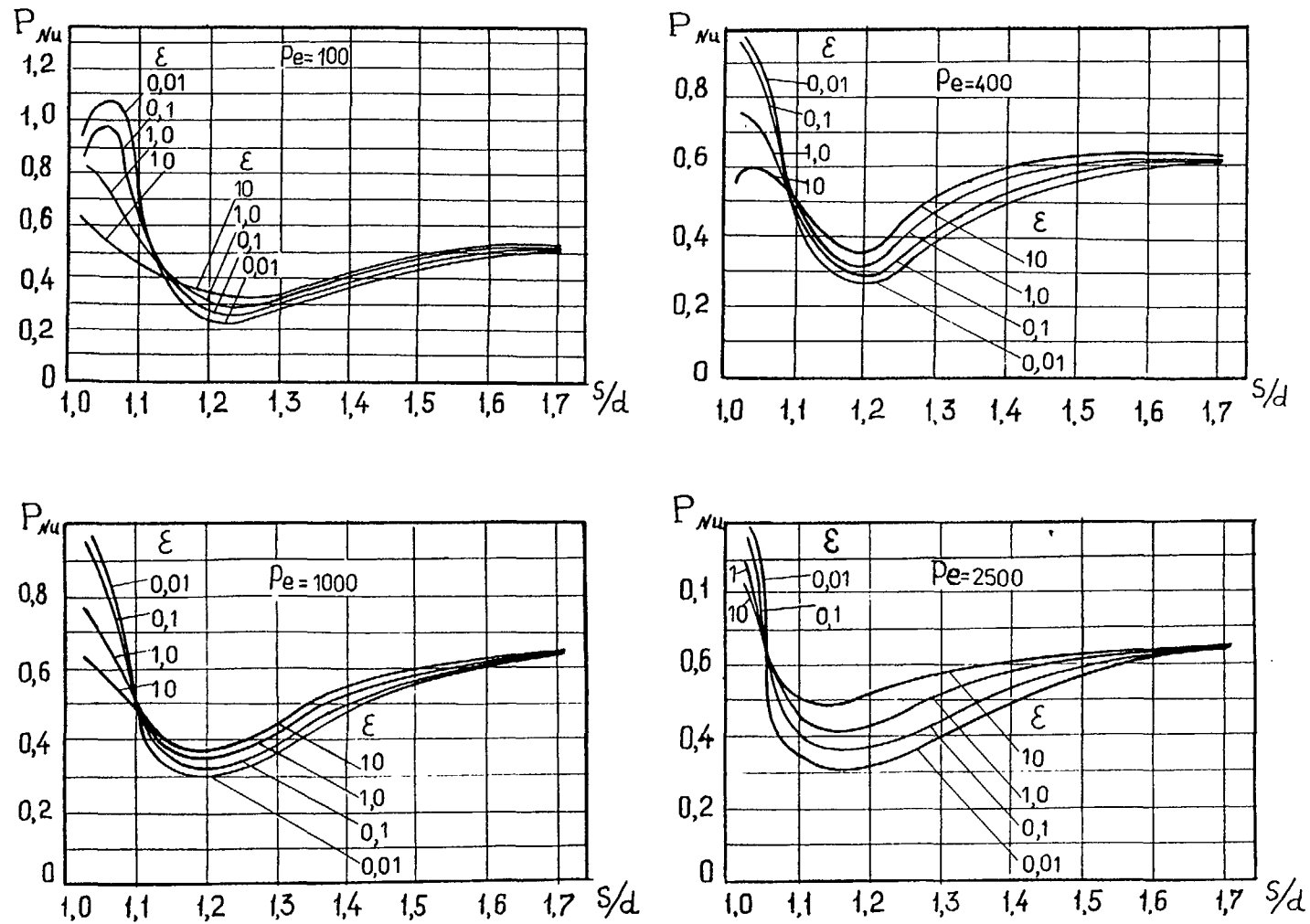
Fig. 3.46. Diagram to define coefficients p_{Nu} in relation (3.86) when Nusselt number is set (turbulent flow).
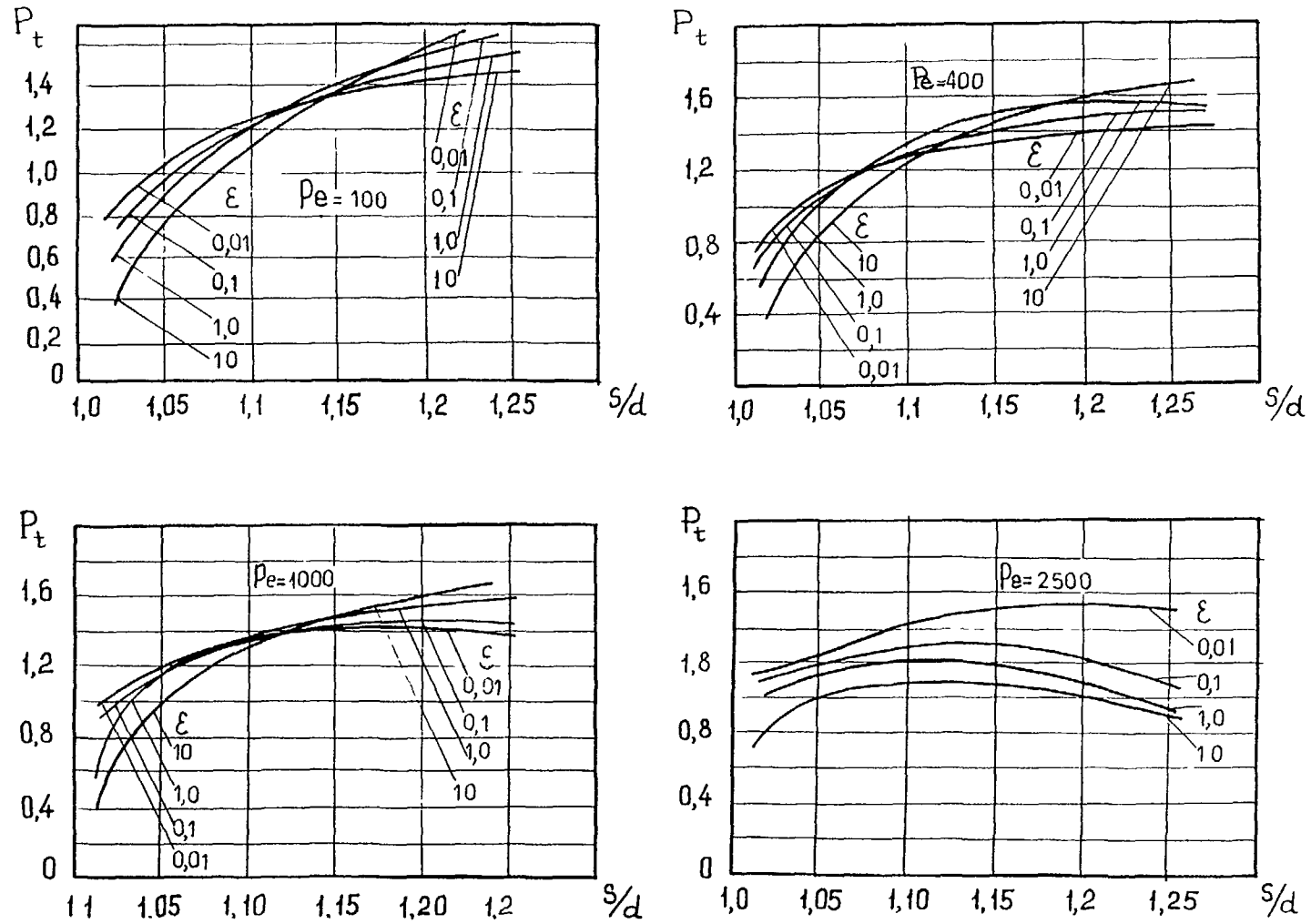
Fig. 3.47. The same for p_t in relation (3.86) when temperature irregularity is set.
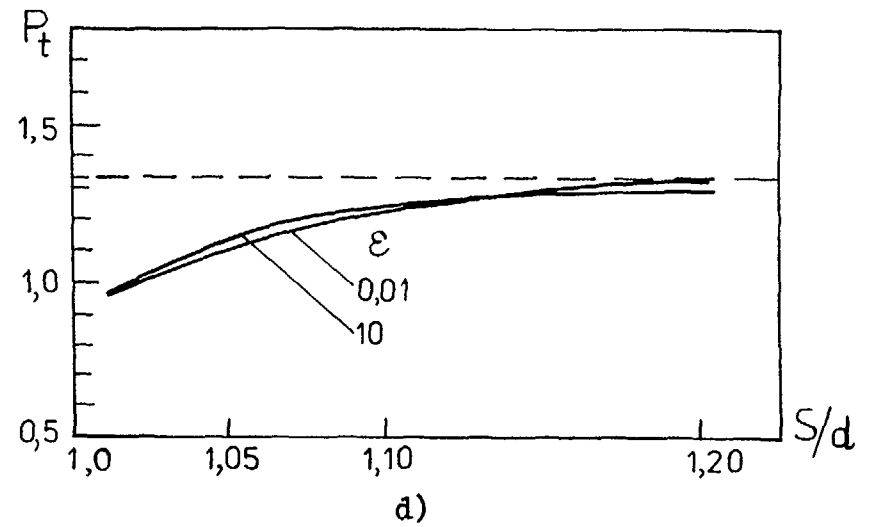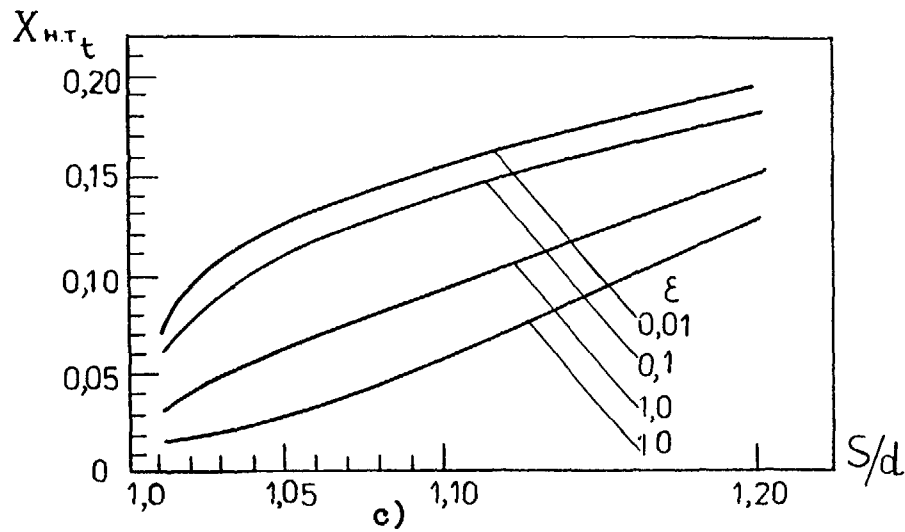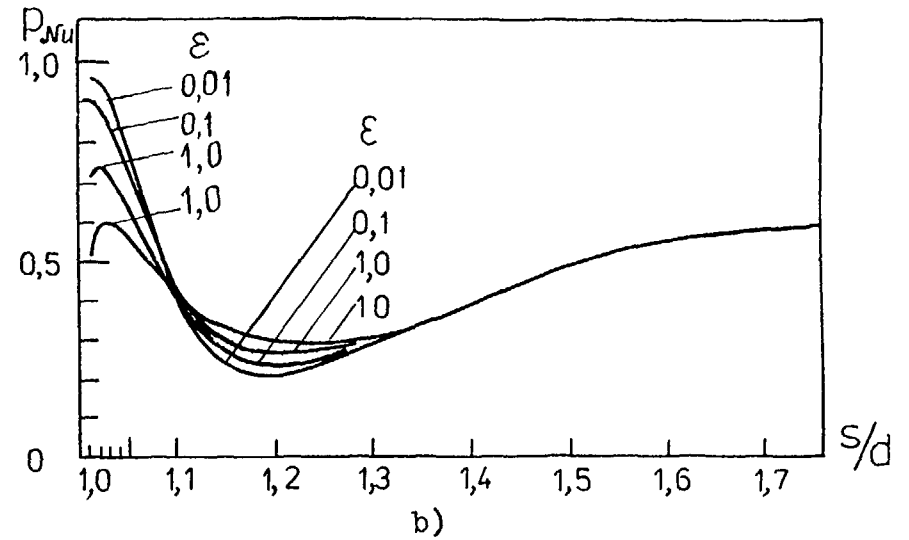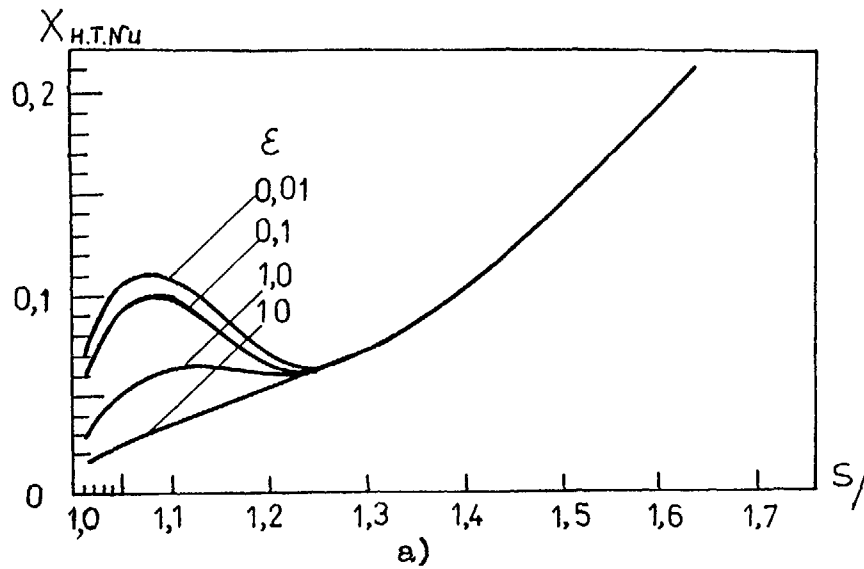
Fig. 3.48. Diagram to define the length of initial thermal sections (a, c) and coefficients
p_{Nu} *и* *(b) and* p_t *(d) in the flow with uniform radial distribution of velocity (rod flow).*
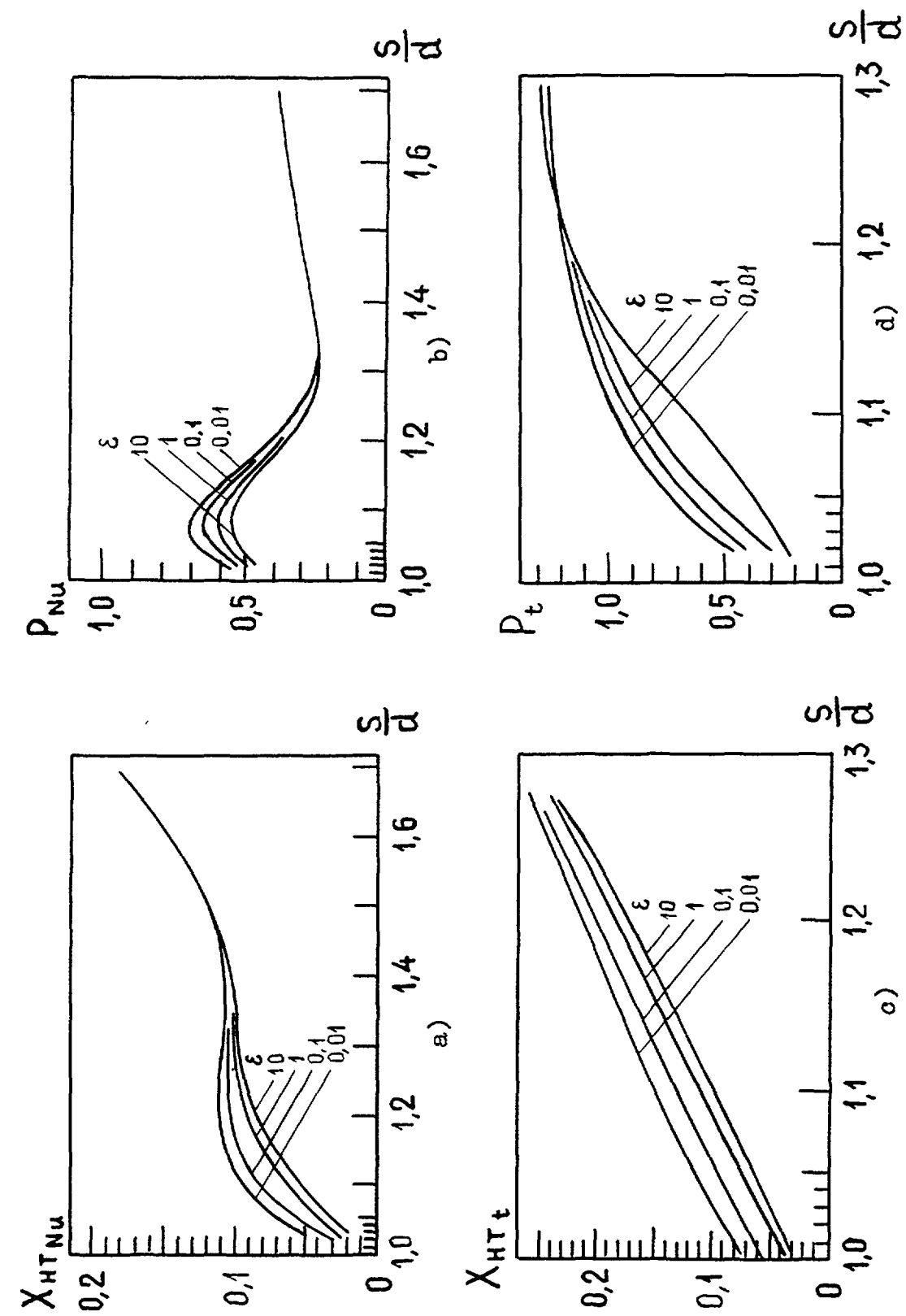
Fig. 3.49. The same in laminar flow (see fig. 3.48).

146
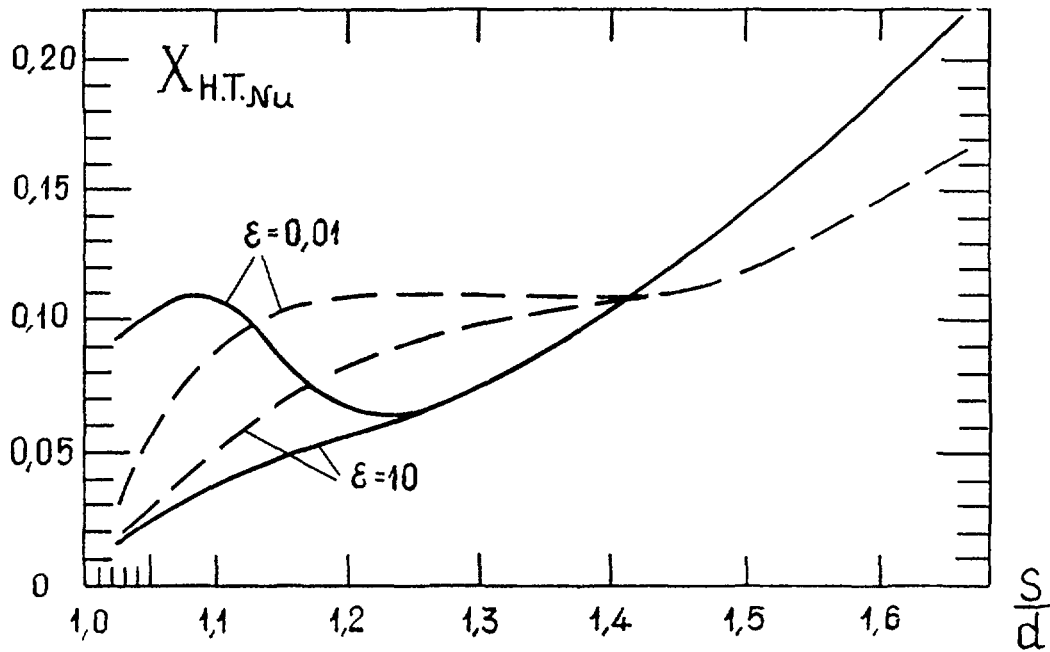
Fig. 3.50. The length of initial thermal section with relative pith of bundle in rod (————) and laminar (— — —) flows.

Comparison between the length of entrance sections in turbulent, laminar and plane flows (Fig. 3.50, 3.51) shows that in plane and laminar flows the length varies proportionally to Peclet number. In turbulent flow the length of entrance section has a peak. Such a behaviour is due to different transport processes in liquid metal: at low Peclet number the molecular heat conduction is dominated in heat transfer, at higher Peclet numbers the turbulence transport prevails. The longest entrance section at given Peclet number is observed to be in plane flow through the close bundle ($s/d = 1.02$).

Hydraulically instable flow. The length of heat transfer coefficient entrance section (Fig. 3.52) can be evaluated by empirical formula [93 -94]

$$\left(\frac{l}{d_h}\right)_{Nu} = A - \frac{B}{255 + Pe} \ , \tag{3.86a}$$

where

$$A = 156.2 - 102.4(s/d) \ ;$$
$$B = \left\{ 51 - 34.5s/d - 4\exp[-14.27(s/d - 1)] \right\}.10^3 \right\} \quad for \quad 1 \le s/d \le 1.2;$$

$$A = 95(s/d)^{-5.8},$$
$$B = 25.3(s/d)^{-5.6} \ .10^3 \right\} \quad for \quad 1.2 \le s/d \le 1.7;$$

$\ell_{HT}^{(Nu)}/d_h$
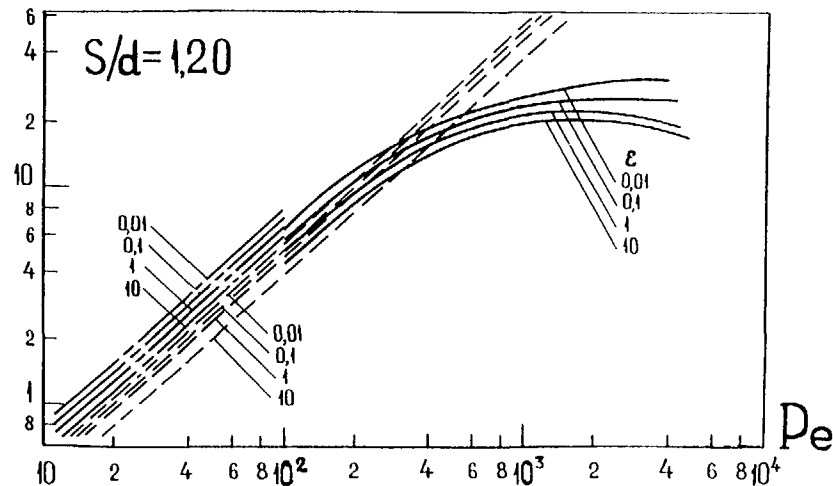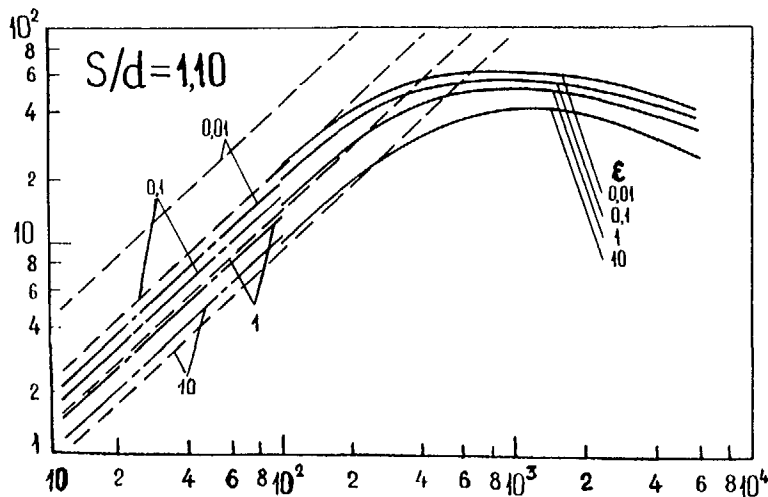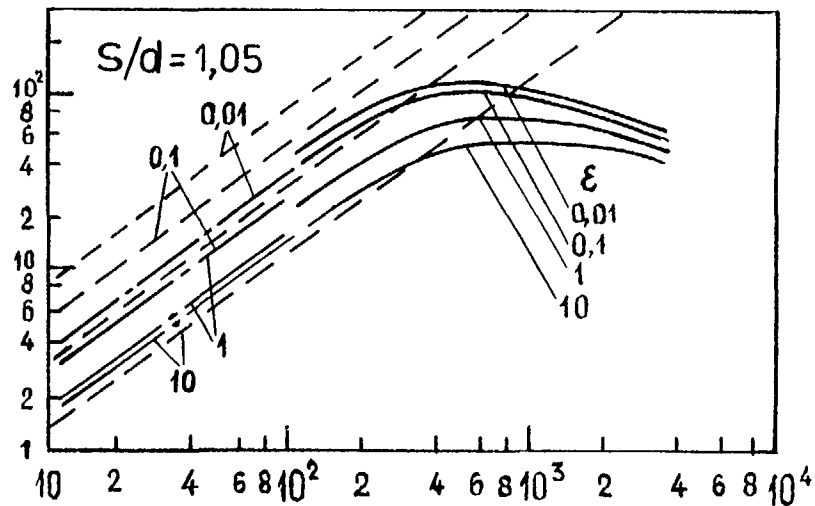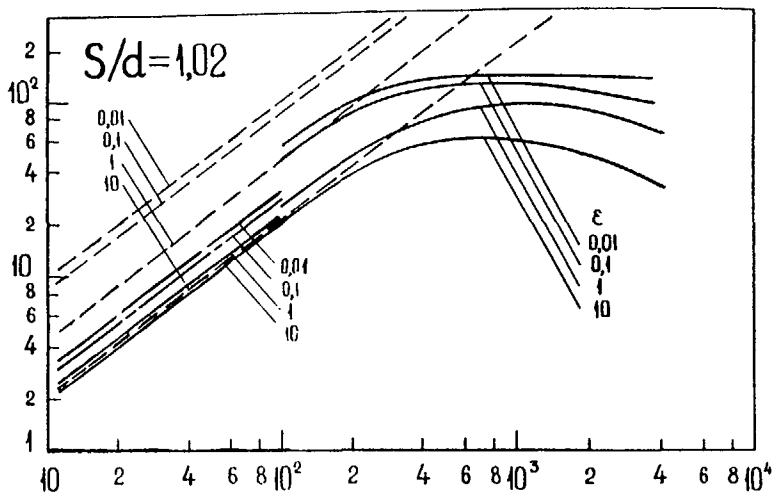
Fig. 3.51. Relative length of initial thermal sections in pin bundle with Peclet number

in turbulent (———), laminar (— · —) and rod (— —) flows.
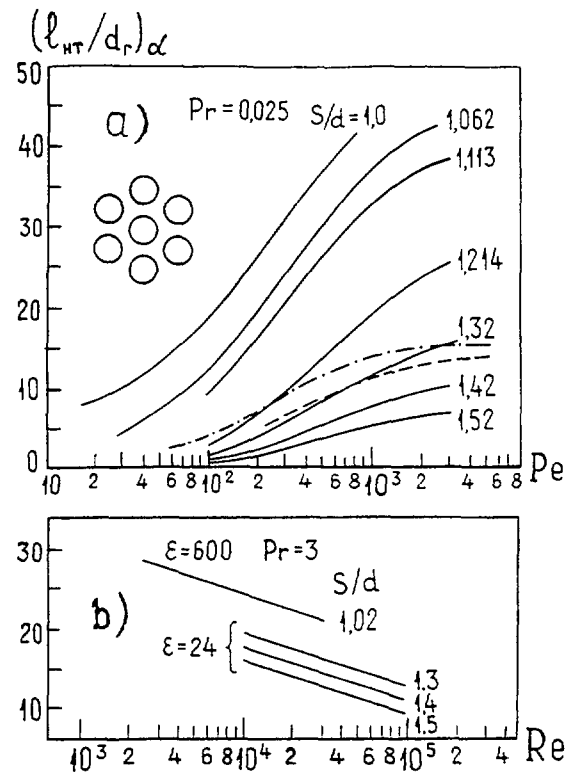
Fig. 3.52. Relative length of initial thermal sections in pin bundle with Peclet and Reynolds numbers for coolant of small (a) and large (b)Prandtl number, (— · —) ,(— —) round pipes.

The areas of application are:

$$0.4 \le \varepsilon_6 \le 1.0 \quad for \quad 1.0 \le s / d \le 1.10,$$

$$0.4 \le \varepsilon_6 \le 1.6 \quad for \quad 1.2 \le s / d \le 1.70,$$

for Peclet number:

$$15 < Pe < 800 \quad for \quad s / d = 1.0,$$

$$30 < Pe < 2500 \quad for \quad s / d = 1.06,$$

$$50 < Pe < 3000 \quad for \quad 1.10 < s / d < 1.7.$$

In close bundles of pins having high thermal conductivity ($s/d = 1.10$; $\varepsilon_6 \sim 10 \div 15$) the length of thermal entrance section defined by (3.86a) has to be reduced by $30 \div 40\%$.

The length of temperature non-uniformity entrance section can be evaluated by:

$$(l/d_h)_t \cong \left[(l/d_h)_{Nu} (18,1 - 4,5 lg\, Pe) \left(\frac{s}{d} - 1 \right) + 1 \right]$$

$$\tag{3.87}$$

$1.0 \le s/d \le 1.2;\quad 500 \le Pe \le 2000;\quad 0.4 \le \varepsilon_6 \le 1.0.$

Variable power production. If power production varies with the channel length, stabilization is lacking. Heat removal enhances, when heat flux gradient is positive and reduces, when it is negative.

Given the hydraulic stabilization, it is an easy to estimate an influence of variable power production on heat removal using so called Duhamel integral [98]

$$t(z) = \eta(0) t_{ql}(z) + \int_o^z \frac{d\eta(z')}{dz'} t_{ql}(z - z') dz'$$

$$\tag{3.88}$$

where $\eta(z)$ is the standardized to unit dimensionless heat flux; $\eta(0)$ - initial jump of heat flux, $t_{q1}(z)$ - temperature distribution at uniform heat flux being equal to unit (transition function defined by (3.86)).

In advanced approach the generalized Duhamel integral was proposed [92]. Instead of one transition function the system of such a function is established, with each function corresponding to specific part of length (Fig. 3.53):

$$t(z) = \eta(0) t_{yo}(z) + \int_o^z \frac{d\eta(z')}{dz'} t_{y'}(z - z') dz'$$

$$\tag{3.89}$$

where $t_{y'}(z - z')$ is the transition function corresponding to section from inlet to cross section z'.
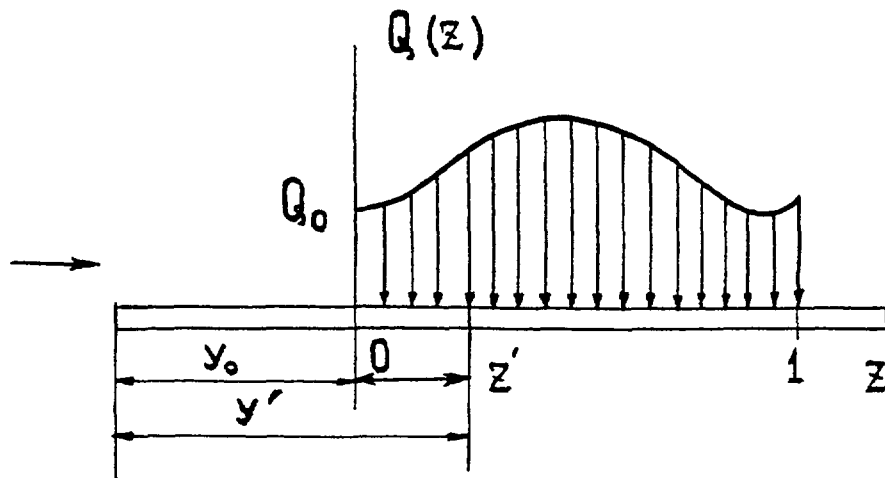

*Fig. 3.53. To generalised definition of Duhamel integral.*
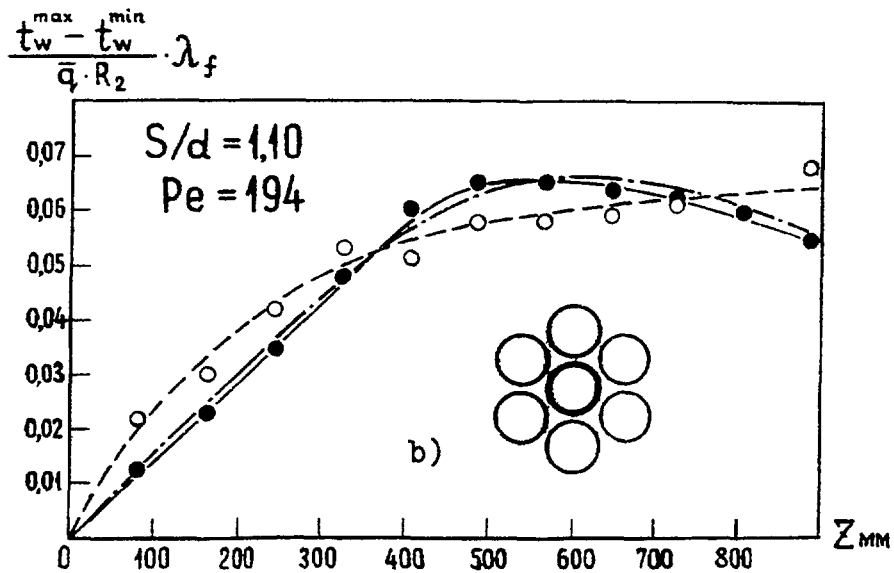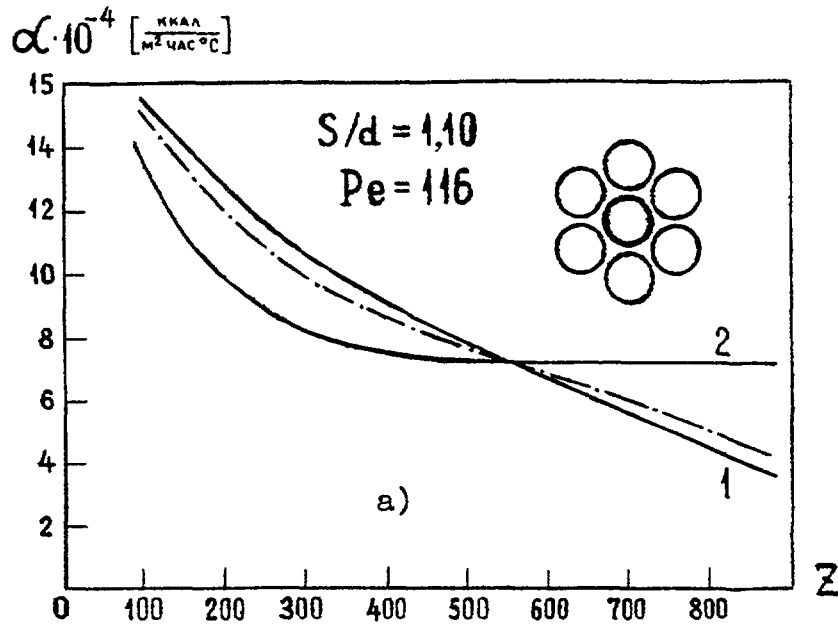
Fig. 3.54. Heat transfer (a) and temperature irregularity *b) along the central pin in the BOR-60 model:

$\bullet$ -, -$\mathbf{O}$ - - *experiments at* q_w =*const. and* $q_w = q_w^{max} \cos\left[2.19(z \,/\, H - 0.5)\right]$;

— $\cdot$— - *calculation on Duhamel integral.*

In many actual cases an influence of variable power production in second half of bundle can be estimated by the common Duhamel integral. It is supported by the experiments carried out on BOR-60 subassembly [100] (Fig. 3.54). Furthermore, to evaluate temperature difference "wall-liquid" it is possible to use a very simple formula [101]

$$\Delta t_o(z) = \frac{q\left(z - l_{en.s.} \,/\, 3\right)}{\alpha},$$

(3.90)

where α - heat transfer coefficient under conditions of uniform power production predicted by relations from Chapter 3.6; $l_{en.s}$ - entrance section length.

3.8. AN INFLUENCE OF SOME FACTORS

Calculation procedure in liquid metal reactor assumes that an influence of following factors on heat removal and temperature behaviour to be taken into account: wire wrap, diabatic conditions at the wrapper tube, power production of the pins.

Wire wrap. As noted above, wire on the pins cooled by liquid metal causes the local enhancement of pin temperature to appear. This is particularly true for pins of small equivalent thermal conductivity (fuel-uranium dioxide, cladding - stainless steel, coolant - sodium), defined by parameter ε. In fast reactors ε varies from 0.05 to 0.3.

In dependence of relative pitch of the bundle an influence of wire wrap shows up variously. In close bundles ($s/d \le 1.04$) temperature distribution around the pin depends, in general, on the channel shape:

$$\left. \begin{array}{l} \textit{for wire wrapped pins} \\[4pt] \dfrac{t_w^{max} - t_w^{min}}{\overline{q}d/2} \lambda_f = 1.5 Pe^{-0.32}, \\[10pt] \textit{for smooth pins} \\[4pt] \dfrac{t_w^{max} - t_{w1}^{min}}{\overline{q}d/2} \lambda_f = \dfrac{0.61}{1 + 8.10^{-3} Pe^{1.046}} \\[10pt] \left(s/d = 1.04; \varepsilon_6 = 0.27; 20 \le Pe \le 300 \right) \end{array} \right\} \tag{3.91}$$

In relatively free bundles ($s/d \sim 1.15$) the wire wrap is some larger and temperature distribution features the local wall temperature rises under the wire (Fig. 3.55). Such a rises under one-entry of a wrap and three-entries are approximately the same and can be evaluated as:

$$\frac{\Delta t^{max} \lambda_f}{\overline{q}d/2} = 1.86 Pe^{-0.44} \tag{3.92}$$

$$40 \le Pe \le 700, \quad 1.15 \le s/d \le 1.20$$

here Δt^{max} - temperature rise under the wire.

In the more close bundles ($1.08 \le s/d \le 1.1$) spaced by the wrap of "fin-to-fin" type:

$$\frac{\Delta t^{max} \lambda_f}{\overline{q}d/2} = 0.066 - 5 \cdot 10^{-5} Pe, \tag{3.93}$$

$$40 \le Pe \le 400.$$

Wire wrap has no practically influence on Nusselt number in the bundles when ($s/d \sim 1.15$) [82], if Nusselt and Peclet numbers are defined as:

$$Nu = \frac{\overline{q}d_\Gamma}{\left(\overline{t}_w - \overline{t}_f \right) \lambda_f}; \quad Pe = \frac{\overline{w}d_\Gamma}{a}, \tag{3.94}$$
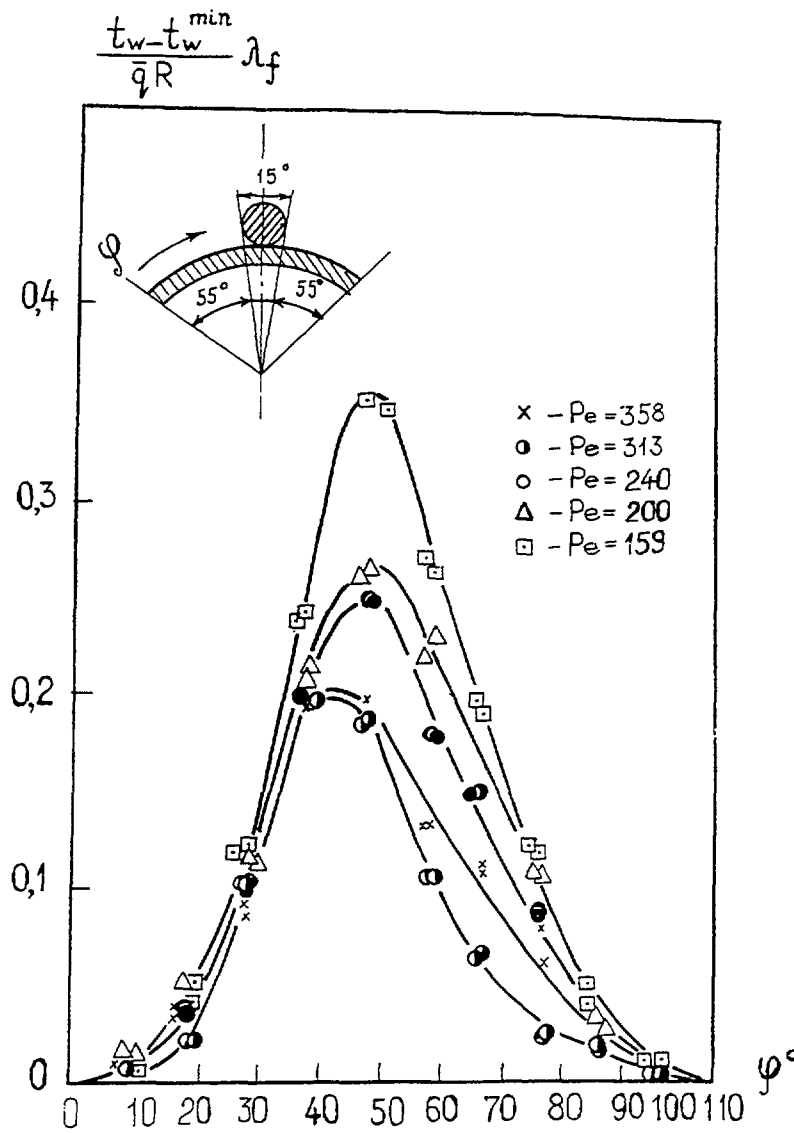
Fig. 3.55. Temperature behaviour around the pin in the area of wire location.

To calculate Nusselt number the relationship presented in Chapter 3.6 should be used.

In close bundles $(s/d = 1.04)$ the more strong dependence on Peclet number is observed [82]:

Pe	22	33	66	106	175
Nu (wire wrapped pins)	1,26	1,62	2,90	4,60	5,90
Nu (smooth pins)	1,53	1,64	1,95	2,27	2,79

Diabatic boundary conditions at the wrapper. In common case an influence of diabatic conditions is defined by subassembly geometry, by intensity of heat transfer inside of

153
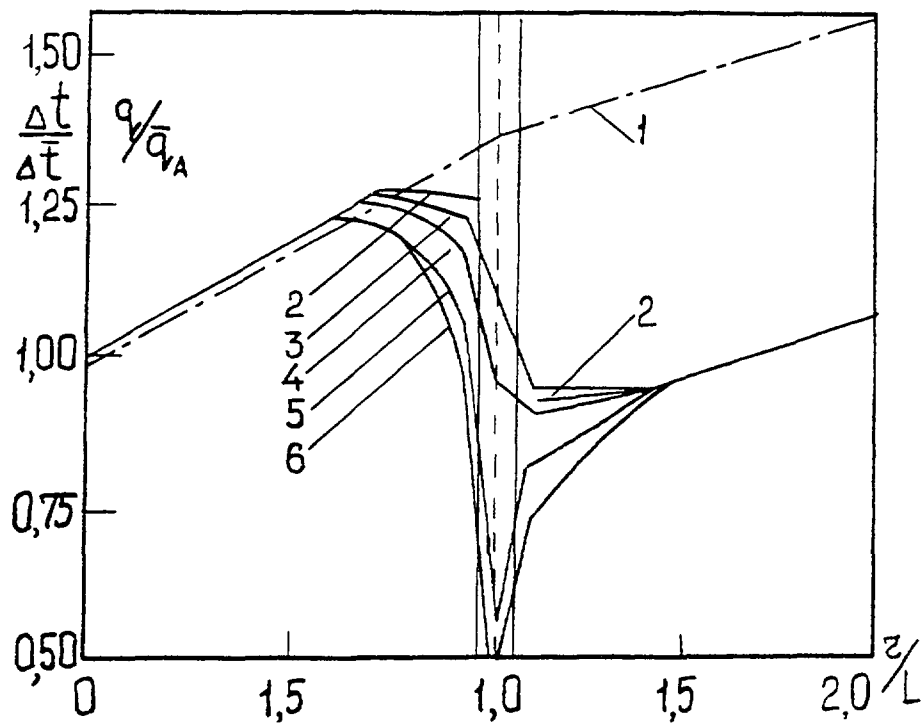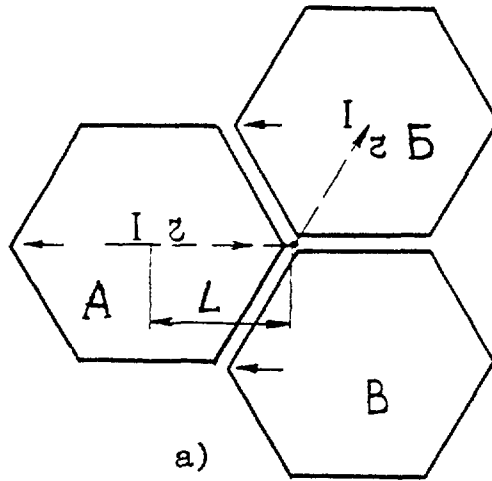
Fig. 3.56. Power production (1) and coolant temperature in the cross section
of two interacting subassembly:

1 - intersubassembly exchange is 0 ; 0.02;

2 - flow in the intersubassembly clearance is 0 ; 0.02;

0.4 and ∞ of coolant flow through the subassembly.
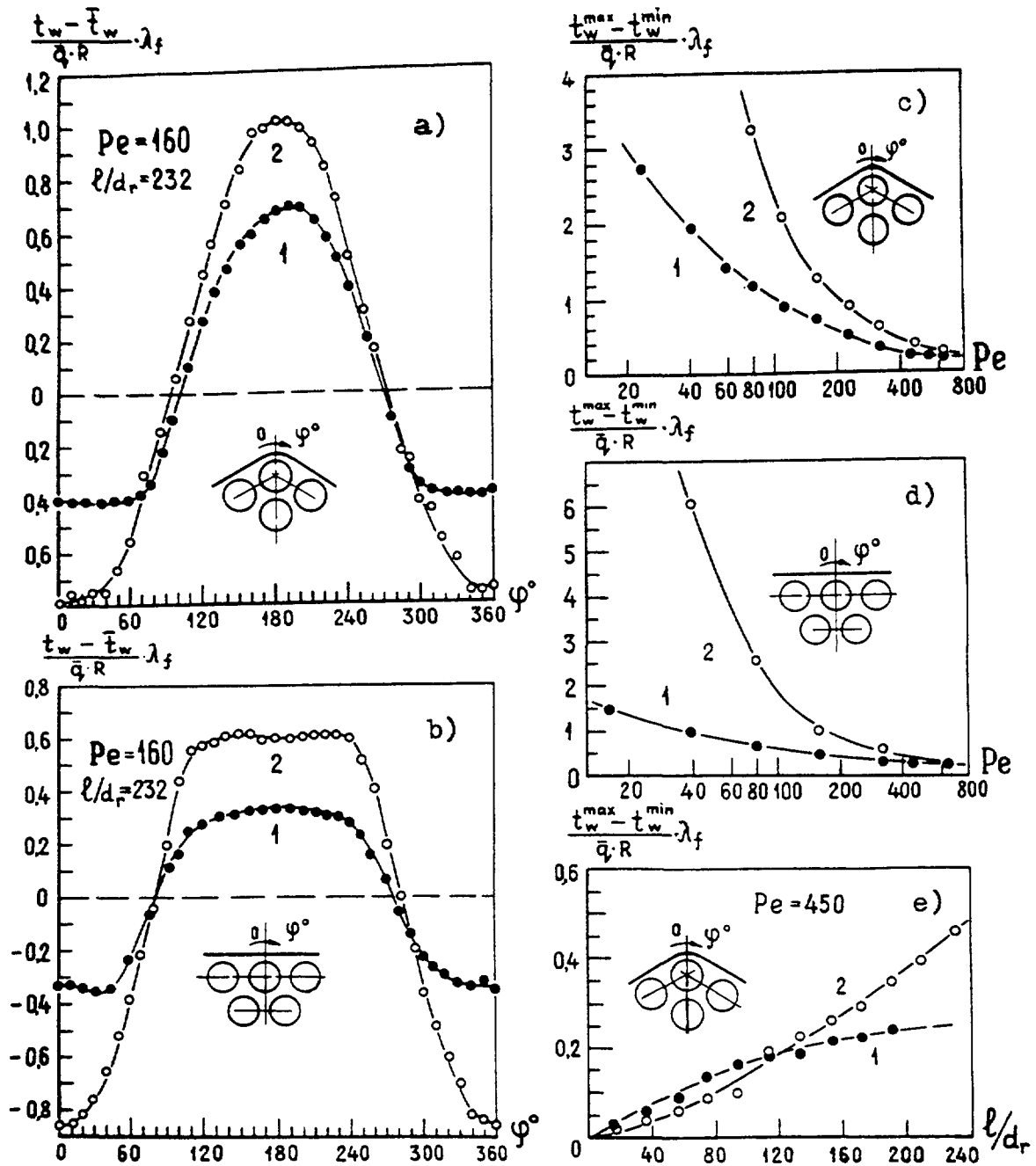
Fig. 3.57. Temperature behaviour in corner (a). edge (b) simulators under adiabatic (1) and diabatic (2) conditions at the wrapper tube and maximal temperature irregularities with Peclet number (c, d) and length of power production (e).
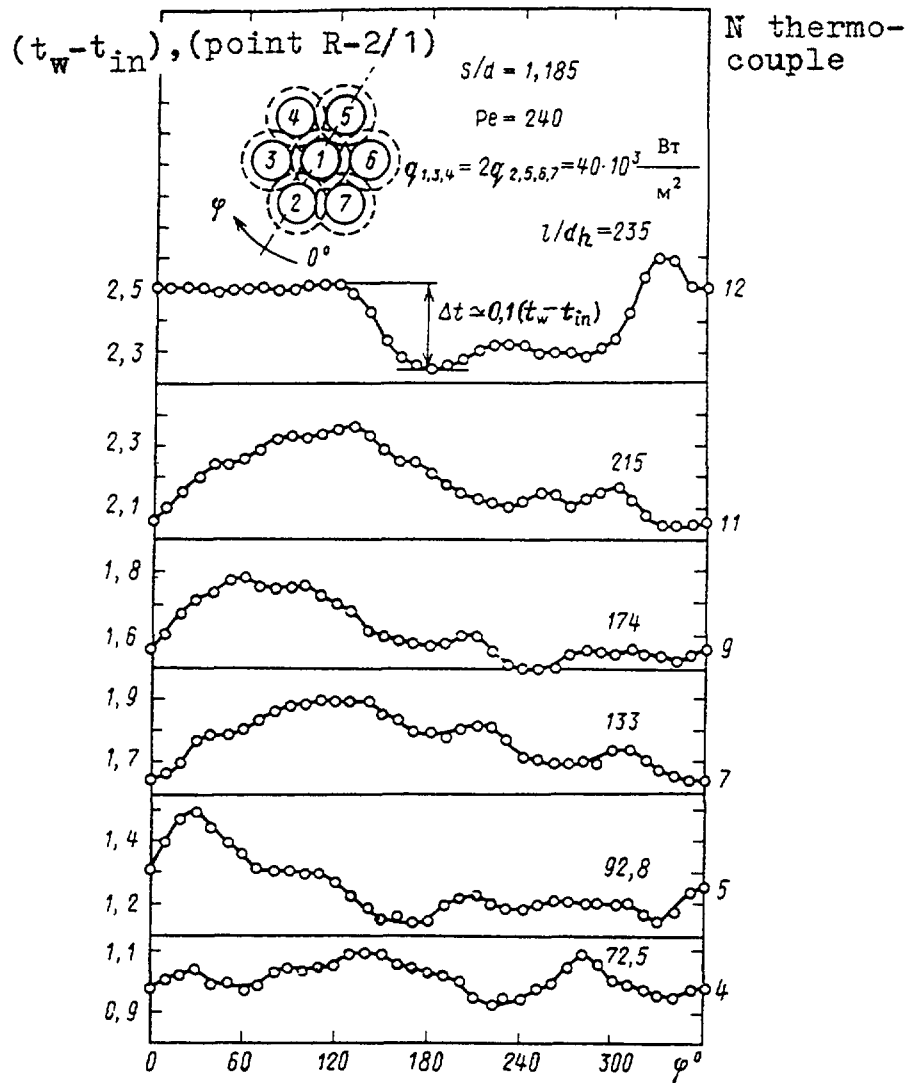
Fig. 3.58. Temperature behaviour around simulator (10 in the model subassembly when power of simulators 1, 3, 4 is twice as large as for power of other simulators.
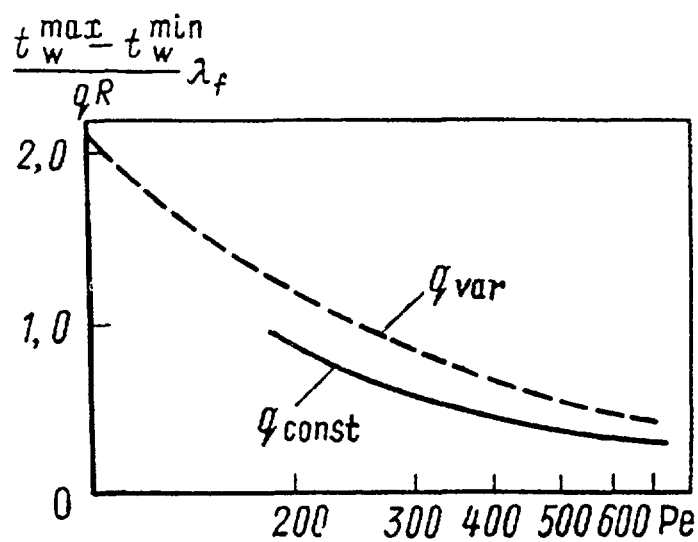

Fig. 3. 59. Dimensionless temperature irregularity of edge pin with Peclet number for uniform (———) and variable power (— —) across subassembly.

subassembly and inter-subassembly heat transfer, by inter-subassembly flow, by character of power production field.

Solution of the system of energy equations written for the group of interacting subassemblies shows that in the event of low inter-subassembly flow ($g_{i-s} \leq 2\%$) in parallel with some decrease in maximum temperature in the most powerful subassembly there also is a rise in coolant temperature in adjacent subassembly (Fig. 3.56). Heat removal through the wrapper effects the temperature behaviour near only three-four rows of pins adjacent to the wrapper and can be important in the subassembly involving small number of pins, as demonstrated by out-of-pile experimental data obtained on BOR-60 [21] and BN-350 models (Fig. 3.57).

Different power production of the pins. If power of one or three adjacent pins is *doubled (trebled) that temperature at the pin surface facing the "not" channel increases by 10 - 15%* [102] (Fig. 3.58). Approximately in a very similar manner the maximum temperature non-uniformity increases. In alternating power and empty wire wrapped pins in bundles simulating fast reactor subassembly there are no significant temperature variation from one channel to another, but dimensionless temperature non-uniformity can be doubled.

The experiments now under way [103] have shows that temperature non-uniformity around the pins in the bundle with non-uniform power production is more by 50-60% than those under uniform power production conditions (Fig. 3.59).

This raises the need for the further researcher on temperature variation around the pins under non-uniform power conditions in subassembly cross section.

CONCLUSIONS

1. Analysis of available experimental data on pressure drop in various channels allowed the hydraulic resistance factors to be determined in the bundles of smooth and wire wrapped pins (regular and near-wall areas) in laminar, transition and turbulent flows and recommendations to be granted reflecting influence of inherent parameters on hydraulic resistance and providing associated limiting transitions. The formulas recommended are true within the wide ranges of pitch-to-diameter ratio, wire wrap pitch, Reynolds number and *take into consideration diversity of the channels within fast reactor subassembly.*

2. Correlations for interchannel thermal and hydraulic characteristics were gained with the use of electromagnetic and thermal techniques. To conclude a problem of interchannel exchange in reactor subassembly the following remarks can be made:
   a) Physics of interchannel mass exchange in the bundle of wire wrapped pins is as follows:
      - convective component varies as sine with the length, if pins are wrapped by wires which touch the adjacent pin wall;
      - exchange intensity depends on pitch-to-diameter ratio, type and pitch of wire wrap, Reynolds number;
      - the directed flow occurs through the clearance between wrapper and pins along the hexagonal wrapper.
   b) Modified thermal track technique allows the local and integral thermal characteristics of interchannel exchange to be defined. As this technique shows a

temperature behavior in fast reactor subassembly corresponds to results of electromagnetic measurements: by the action of wire wrap the hot and cold portions of liquid leave for adjacent channels, where temperature either increases or decreases in dependence of inherent enthalpy; coolant temperature distribution over the channel length has maximums and minimums.

c) A joint use of electromagnetic and thermal track techniques allows dividing total interchannel exchange factor on components, correlating heat and mass exchange, defining non-equivalence factor between heat and mass exchange.

d) The main component of interchannel exchange in fast reactor core is convective one (due to wire wrap). The generalized relationship is recommended to predict convective component in wide range of defining parameters (s/d, h/d, Re).

e) Non-equivalence factor between heat and mass transfer was found in experiments on liquid metal bundles to be 0.7. This value needs to correlation of hydraulic and thermal characteristics in computer code development.

f) In order to calculate mixing factors due to turbulence diffusion and molecular heat conductivity the empirical and analytical formulas are recommended for the most important in designing reactor core and heat exchanger range of relative pitches $1.0 \le s / d \le 1.5$. The relationships for mixing factor due to pin heat conduction are presented , as well as mixing factors in homogeneous two-phase flow and in the framework of two-liquid model.

g) Experimental data on interchannel exchange are used as a basis for the methods developed to predict velocity and temperature behavior in reactor core and heat exchangers. Knowledge of thermal mixing factors allows revealing some factors' effects, such as the pin bundle deformation, variable power production, blockages, thermal interaction of adjacent subassemblies and so on. Notions of interchannel exchange inferred from theoretical analysis allows the calculation approaches for reactor core and heat exchanger thermal hydraulics to be developed.

3. Generalized correlations on Nusselt numbers and dimensionless temperature non-uniformities around the pins which are arranged in regular bundle represent a basic constants for performing thermal hydraulic calculations of liquid metal reactor core within the following ranges of defining parameters: Peclet number $1 \le Pe \le 3500$; relative pitch of the bundle $1.0 \le s / d \le 2.0$; equivalent thermal conductivity of pin $0.02 \le \varepsilon \le 16$. Correlations retain their complete structure (dependencies on three parameters mentioned) in fast reactor core and become more simple in intermediate heat exchangers ($s / d \le 1.3$), when Nusselt number does not depend on equivalent heat conduction of tubes and there is no regular temperature non-uniformity around the tube. Universal character of correlations is supported by the fact that they can be used in any axis-symmetrical pins cooled by liquid metal. In order to perform engineering estimations these correlations are presented as nomograms.

4. Thermal hydraulic constants for instable heat removal (variable power production, entrance thermal sections) were derived by a combination of analytical and experimental methods. The length of entrance section was estimated for two cases - hydraulically stable flow and transient flow.

In the first case, the heat transfer problem was resolved for the channel of "infinite" pin bundle in laminar, turbulent and plane flow taking into account the second derivative of temperature with respect to axial coordinate and influence of relative pitch and equivalent

thermal conductivity on temperature behavior have been analyzed, that is such a parameters, influences of which are of great importance in fast reactors.

In the second case, experimental data on temperature fields at the entrance sections were generalized. Thus, needed data were gained for predicting thermal hydraulics under variable power production as well as for deriving recommendations for the stable heat removal.

The fact deduced from experiments, that Duhamel's integral can be used in predicting flow under instable conditions, allows the experimental data on instable flow recalculated on variable power production to be used. In the event of stable flow the analytical data have to be used for recalculating.

Among the main physical features of entrance section there are as follows:
- Length of entrance section representing in scale of hydraulic diameter decreases with relative pitch and equivalent thermal conductivity of pin, but increases in proportion with Peclet number in laminar and plane flow (heat in transferred due to molecular heat conduction), in turbulent flow it has a peak.
- Temperature non-uniformity around the pin is stabilized over the length being more than those for stabilization of average heat transfer coefficients.
- Heat transfer coefficient in turbulent, laminar, plane flows varies with exponential law, that defines the relationships for temperature field and Nusselt number are universal in mentioned types of coolant flows.

5. The greatest temperature non-uniformities take place around the edge (wall) pins of subassembly, that is why much attention must be given to thermophysical validation of such type of pins. Relationships recommended for wall pins and relationships for "infinite" bundle comprise information that are needed for validation of temperature behavior liquid metal pin bundles.

The followings can be noticed as the main thermoophysical features of edge pins in fast reactor subassembly:
- Temperature non-uniformities around the edge pins are greater than those around the internal pins and can be generalized by the parameter $\psi = (\Delta/d)/(s/d - 1)$, including relative gap between pins and subassembly wrapper and pitch-to-diameter ratio. Relationships are presented for four types of subassemblies: with smooth or wire wrapped pins, with/without displacers in edge channels.
- Heat transfer coefficients in edge areas of fast reactor subassembly are less than those in the internal area by factor of 1.5 - 2.0.
- Maximum temperature non-uniformities at the wall pins occurring at small Peclet number (transition from turbulent to laminar flow) can be a serious hazard to reactor performance provided the power release is kept at high level. Maximum values can be estimated by graphical representations of experimental data.
- Heat transfer in edge channels of fast reactor subassembly is, as a rule, of instable character. Instability is defined by equivalent thermal conductivity and relafive pitch of the bundle, by shape and size of displacers, by width of the clearance between pins and subassembly wrapper.
- Coolant passing through the clearance between adjacent subassemblies reduces coolant temperature in the edge channels and causes the temperature non-uniformity to

enhance. Close to the wrapper area is acted upon by deformation, that also increases temperature non-uniformity and decreases the heat transfer intencity.

REFERENCES

[1]   Subbotin V.I., Ibragimov M.H., Ushakov P.A. Hydrodynamics and Heat Transfer in Nuclear Power Plants. M., Atomizdat, 1975 (in Russian).

[2]   Zhukov A.V., Sorokin A.P., Titov P.A. Analysis of Hydraulic Resistance of Fast Reactor Pin Bundles. Atomic Energy, 1986, v.60, p.317-321.

[3]   Malak J., Heina J., Schmid J. Pressure Losses and Heat Transfer in Non-circular Channels with Hydraulically Smooth Walls.. Ing. J. Heat Mass Transfer, 1975, v.18, p.139-149.

[4]   Rehme K. Widerstandsbeiwerte Von Gitterabstandshaltern fur Reactor - brennelementen.. Atomkernenergie, 1970, Bd.15, p.127-133.

[5]   Chiu C., Todreas N. Flow split measurements in a LMFBR radial blanket assembly. TANS, 1977, v.26, p.455-456.

[6]   Novendstern E.H. Pressure Drop Model for Wire-Wrapped Fuel Assemblies. TANS, 1971, v.14, p.660-661.

[7]   Markley R.A., Engel F.C. LMFBR Blanket Assembly Heat Transfer and Hydraulic Test Data Evaluation. Thermodynamics of FBR Fuel Subassemblies under Nominal and Non-nominal Operating Conditions. IWGFR/29, Vienna, 1979, p. 229-253.

[8]   Mantlik F., Heina J., Chervenka J. Results of Local Measurements of Hydraulic Chracteristics in Triangular Pin Bundle. UJV - 3778-R, Rzez, Czech Republic, 1976.

[9]   Heina J., Chervenka J. et al. Experimental Investigations on Hydrodynamics in Peripheral Area of Deformed Bundles. UJV - 7537-T, Rzez, Czech Republic, 1986.

[10]   Heina J., Chervenka J., Mantlik F. Results of Local Measurements of Hydraulic Chracteristics in Deformed Pin Bundle. UJV - 4156-T, part1. Rzez, Czech Republic, 1977.

[11]   Zhukov A.V., Sorokin A.P., Titov P.A. Influence of Mixing on Coolant Temperature Behavior in Wire Wrapped Bundles. Preprint IPPE-512, Obninsk, 1974 (in Russian).

[12]   Zhukov A.V., Kotowski N.A., Kudriavtseva L.K. Experiments on Interchannel Coolant Exchanger in Pin Bundles with Spacer Fins. Problems of Nuclear Science and Engineering. Reactor Design, Obninsk, 1977 (in Russian).

[13]   Zhukov A.V., Matjukhin N.M., Sviridenko E.J. Study of Mixing in Bundles with Small Relative Pitches. Preprint IPPE-799, Obninsk, 1977 (in Russian).

[14]   Mikhin V.I., Zhukov A.V. Theoretical Analysis of Influence of Mixing on Coolant Temperature Fields in Pin Bundles. Preprint IPPE-731, Obninsk, 1976 (in Russian).

[15]   Zhukov A.V., Kotowski N.A., Kudriavtseva L.K., et al. Mixing in Fast Reactor Subassembly. Thermal Physics and Hydrodynamics of Fast Reactor Core and Steam Generator, 1978, v.1 (in Russian).

[16]   Zhukov A.V., Sviridenko E.J., Matjukhin N.M. et al. Hydrodynamics of Combined Flow in Wire Wrapped Bundles (Electromagnetic Technique). Preprint IPPE-867, Obninsk, 1979 (in Russian).

[17]   Zhukov A.V., Kotowski N.A., Matjukhin N.M. et al. Experiments on Coolant Mixing In Wire Wrapped Pin Bundles. Preprint IPPE-556, Obninsk, 1975 (in Russian).

[18]   Ushakov P.A., Zhukov A.V., Yuriev Yu.S. Effect of Wire-Spaced Fuel Pins on Interchannel Heat and Mass Transfer. Rep. Sixth Int. Heat Transfer Conf. Toronto, Canada. 1978, v.5, p.5-9.

[19] Bolle L., Wauters P., Mestres J. et.al. Experimental Determination of the Lokal Transverse Mixing in a Rod Bundle with Helical Wire Spacer. Int. Meeting on Reactor Heat Transfer, 9-11 October 1973, Karlsruhe.

[20] Baumann W., Hoffmann H. Coolant Cross-Mixing of Sodium Fowing in Line Through Multirod Bundles with Different Spacer Arrangements. Int. Heat Transfer Seminar, Trogir, Yugoslavia, 1971.

[21] Griazev V.M., Aseev N.A., Markin S.A. et al. Experimentsand Predictions on Thermal Physics and Hydrodynamics of BOR-60 Core. Thermal Physics and Hydrodynamics of Fast Reactor Core and Steam Generators. Prague, 1978, v.1.

[22] Hoffmann M., Baumgartner E. Experimental Investigations of the Thermodynamic Behaviour of Fast Breeder Reactor Fuel Elements with Different Spacer Types. Fuel and Fuel Elements for Fast-Reactor/ Vienna: IAEA, 1974, v.1.

[23] Baumann W., Moller R. Experimental Study of Coolant Cross-Mixing in Multirod Bundles, Consisting of Unfinned, One-, Three- and Six-Fin Fuel Rods. Atomkernenergie, 1969, v.14.

[24] Skok J. Mixing of the Fluid Due in the Gelicoidal Wire of Fuel Pins in a Triangular Array. Paper Presented at Internat. Heat Transfer Seminar. Trogir, Yugoslavia, 1971.

[25] Okamoto Y., Hishida M., Akino N. Hydraulic Performance in Rod-Bundles of Fast Reactor Fuel-Pressure Drop, Vibration and Mixing Coefficient. Progress in Sodium-Cooled Fast Reactor Engng Monako, IAEA/SM-130/5, 1970.

[26] Collingham R.E., Thorne W.L., McCormack J.D. Coolant Mixing in a Fuel Pins Assembly Utilizing Helical Wire-Wrap Spacers. Nucl. Eng. Des., 1973, v.24.

[27] Bump T.R. Coolant Mixing in Fuel Subassemblies. TANS, 1966, v. 9, p.285.

[28] Marian V.R., Hines D.P. Transfer of Coolant Between Adjacent Subchannels in Wire-Wrap and Grid Spacer Rod Bundles. TANS, 1970, v. 13.

[29] Cushman R.A. Subchannel Coolant Mixing and Temperature Analysis in EBR-11 Insrumented Subassembly XX01. TANS, 1971, v. 14.

[30] Millhollen M.K., Sutey A.M. PNL-17. EBR.11 Instrumented Subassembly Test Interim Report. BNWL-1424. Battelle-Northwest Laboratories, 1970.

[31] Waters E.D. Fluid Mixing Experiments Wire Wrapped 7-Rod Bundle Fuel Assembly. HW-70178. Handford Laboratories, 1963.

[32] Shimazaki T.T., Freede W.J. Heat Transfer and Hydraulic Characteristics of the SRE Fuel Element. Reactor Heat Transfer Conf. 1956. TID-7529. US Atomic Energy Commission, 1957.

[33] Bishop A.A., Nelson P.A., Tong L.S. Coolant Mixing in a Nineteen-Rod Fuel Assembly. TANS, 1961, v. 4.

[34] Lane A.D. The Thermal and Hydraulic Characteristics of Power Reactor Fuel Bundle Design. Canadian J. Chemical Eng., 1963, v. 41.

[35] Zhukov A.V., Mouzanov A.B., Sorokin A.P. et al. Inter-channel Mixing in Cylindrical Pin Bundles. Preprint IPPE-413, Obninsk, 1973 (in Russian).

[36] Zhukov A.V., Kornienko Y.N., Sorokin A.P. et al. Methods and Codes of Subchannel Analysis of Pin Bundles Having Regard to Coolant Mixing. Analitical Overview - 107, Obninsk, 1980 (in Russian).

[37] Patch L. Experimental Studies of Flow Distribution in a Wire Wrapped LMFBR Blanket Assembly. Rep. Int. Meeting on Reactor Heat Transfer. 1979. Karlsruhe, Germany.

[38] Sha W.T. A Wire-Wrap Model. TANS, 1976, v. 24. p.344-346.

[39] Lorenz J.J. Coolant Mixing and Subassembly Velocities in an LMFBR Fuel Assembly. Nucl. Eng. Design., 1977, v.40.

[40] Lafay J. Local Pressure Measurements and Peripheral Rlow Visualisation in a Water 19-Rod Bundle Compared With FLJCA 11-B Calculations: Influence of Helical Wire-Wrapped Spacer System. CEA-CONF-3491. 1975.

[41] Chen Y.B. Velocity Measurements in Edge Channels of Wire-Wrapped LMFBR Fuel Assemblies. TANS, 1974, v. 19.

[42] Khan E.U. A.Porous Body Model for Predicting Temperature Distribution in Wire-Wrapped Fuel Rod Assemblies. Nucl. Eng. Design, 1975, v. 35.

[43] Zhukov A.V., Sorokin A.P., Ushakov P.A. et al. Subchannel Thermal Hydraulic Analysis in Nuclear Reactor Subassemblies. Atomic Energy, 1981, v.51.

[44] Bogoslovskaya G.P., Zhukov A.V., Sorokin A.P. et al. Prediction of Temperature Behavior in Fast Reactor Subassembly. Atomic Energy, 1983, v.55.

[45] Pedersen D.R. Cross Flow Mixing in a 91 Element Wire-Wrapped Bundle. TANS, 1974, v. 19.

[46] Chiu C. Turbulent Mixing Model and Supporting Experiments of LMFBR Wire-Wrapped Assemblies. Rep. Int. Meeting on Heat Transfer. 1979. Karlsruhe.

[47] Hanson A.S., Todreas N.E. Fluid Mixing Studies in a Hexagonal 61-Pin, Wire-Wrapped Rod Bundle. COO-2245-51TR, 1977.

[48] Skok J. Mixing of the Fluid Due to Helical Wire on Fuel Pins in a Triangular Arrays. Progress Heat Mass Transfer . N.-Y., 1973, v.7.

[49] Collinham R.S., Thorne W.L., Mc Cormack J.D. 217-Pin Wire-Wrapped Bundle Coolant Mixing Test. ME-TME71-146, 1971.

[50] Fontana M.H. Edge Channel Flow in a 19-Rod LMFBR Fuel Assembly. TANS, 1972, v. 15.

[51] Zhukov A.V., Matjukhin N.M., Rymkevich K.S. Interchannel Thermal Interaction in Periphery Area of Fast Reactor Subasembly. Preprint IPPE-1713, Obninsk, 1985 (in Russian).

[52] Zhukov A.V., Kotowski N.A., Kudriavtseva L.K. Liquid Metal Interchannel Thermal Exchange in Bundles of Smooth Pins. Preprint IPPE-757, Obninsk, 1977 (in Russian).

[53] Ingesson L., Hedberg S. Heat Transfer between Subchannels in a Rod Bundles. Heat Transfer, 1970, v.3.

[54] Rogers J.T., Todreas N.E. Coolant Interchannel Mixing in reactor Fuel Rod Bundles Single-Phase Coolants. Heat Transfer in Rod Bundles. ASME. Winter Meeting. N.-Y, 1968.

[55] Rogers J.T., Tarasuk W.R. Generalized Correlation for Natural Turbulent Mixing of Coolant in Fuel Bundles. TANS, 1968, v. 11.

[56] Polianin L.N. Heat- and Mass Transfer in Pin Bundle Turbulent Flow. Atomic Energy, 1969, v.26.

[57] Baumann W. Cross Mixing by Natural Turbulence in Fuel Element Bundles. Atomkernenergie, 1969, v. 14.

[58] Rowe D.S., Angle C.W. Experimental Study of Mixing Between Rod Bundle Fuel Element Flow Channels During Boiling. TANS, 1967, v. 10.

[59] Nijsing R., Eifler W.A Computation Method for the Steady State Thermohydraulic Analysis of Fuel Rod Bundles with Single Cooling. Nucl. Eng. Des., 1974, v. 30.

[60] Roidt, Pecherski, Markin et al. Determination of Turbulent Mixing Factor in Pin Bundles. Heat Transfer, 1972, v.96.

[61] Markoczy G., Huggenberger M. Virification of Subchannel Analysis Computer Codes by a Full-Scale Experiment. TANS, 1975, v. 20.

[62] Gabrianovich B.N., Roukhadze V.K. Study of Coolant Mixing by Freon Technique. Thermal Physic Investigations, VIMI, 1977.

[63] Fukuda A. Measurement of Shape Factors for Transferse Condition Between Rods. ORNL-TM. 1971.

[64] France D.M., Ginberg T. Evalution of Lumped Parameter Heat Transfer Techniques for Nuclear Reactor Applications. Nucl. Science and Eng., 1973, v. 51, p.41-51.

[65] Zhukov A.V., Sorokin A.P., Mantlik F. Thermal Physical Validation of Fast Reactor Subassembly Temperature Behavior Having Regard to Hot Spot Factors. Preprint IPPE-1778, Obninsk, 1986 (in Russian).

[66] Zhukov A.V., Sviridenko E.J., Matjukhin N.M. et al. Velocity and Temperature Distributions in Fast Reactor Subassembly. Thermal Physic Investigations, VIMI, 1977 (in Russian).

[67] Levchenko Yu.D. Study of Velocity and Temperature Distributions in Turbulent Longitudinal Flow, Obninsk, 1970.

[68] Bobkov V.P., Ibragimov M.H., Subbotin V.I. Heat Turbulence Transport Factor in Combined Channels. Simulating of Thermal Dynamics in reactor Core, Zbraslav, Czech republic, 1971.

[69] Ramm H. Single Phase Transport within Bare Rod Arrays at Laminal Transition and Turbulent Flow Conditions. Nucl. Eng. Des., 1974, v. 30.

[70] Nijsing R., Eifler F. Temperature Fields in Liquid-Metal Cooled Rod Assemblies. Rep. Internat, Heat Transfer Seminar, Trogir, Yugoslavia, EU/C-1C791/71. 1971.

[71] Zhukov A.V., Sorokin A.P., Ushakov P.A. Temperature Behavior in Fast Reactor Subassembly Having Regard to Hot Spot Factors. Preprint IPPE-1817, Obninsk, 1986 (in Russian).

[72] Rudzinski K.F., Singh K., St. Pierre C.C. Turbulent Mixing for Air-Water Flows in Simulated Rod Bundle Geometries. Canadian J. Chemical Eng., 1972, v. 50.

[73] Weisman J. Methods for Detailed Thermal and Hydraulic Analysis of Water-Cooled Reactors. Nucl. Science and Eng., 1975, v. 57.

[74] Rowe D.S. A Thermalhydraulic Subchannel Analysis for Rod Bundle Nuclear Fuel Elements. Heat Transfer, Paris-Versailles, 1970, v.3. FC7. 13.

[75] Singh K., St.Pierre C.C. Two-Phase Mixing for Annular Flow in Similated Rod Bundle Geometries. Nucl. Science Eng., 1973, v. 50.

[76] Castellana F.S., Adams W.T., Casterline E. Single-Phase Subchannel Mixing in a Simulated Nuclear Fuel Assembly. Nucl. Eng. Des., 1974, v. 26.

[77] V.P.Slutsker, E.P.Bolonov, N.V.Tarasov. Experiments on Turbulent Transport in Channels of Combined Form. Thermal Energetics, 1983.

[78] Tapucu F., Gencay S., Troche N. Mixing Between Two Laterally Interconnected Two-Phase Flows. TANS, 1980. v.35.

[79] Ushakov P.A. Approximate Thermal Modelling of Cylindrical Fuel Pins. Liquid Metals, M., Atomizdat, 1967, p.137-140.

[80] Zhukov A.V., Sviridenko E.J., Matjukhin N.M. Experiments on Temperature Behavior and Heat Transfer in Triangular Liquid Metal Pin Bundles. Preprint IPPE-800, Obninsk, 1978 (in Russian).

[81] Zhukov A.V., Kirillov P.L., Matjukhin N.M. Thermal Hydraulic Analysis of Liquid Metal Fast Breeder Reactors, M., Energoatomizdat, 1985.

[82] Zhukov A.V., Kudriavtseva L.K., Sviridenko E.J. et al. Experiments of Fuel Pin Temperature Distribution. Liquid Metal, M., Atomizdat, 1967, p.170-193 (in Russian).

[83] Subbotin V.I., Ushakov P.A., Zhukov A.V. et al. Temperature Fields in BOR-60 Core Subassembly. Atomic Energy, 1970, v.28, p.489-490.

[84] Zhukov A.V., Matjukhin N.M., Nomofilov E.V. Temperature Fields in Non-Standard and Deformed Fast Reactor Pin Bundles. Thermal Physics and Hydrodynamics of Reactor Core and Steam Generators, Prague, 1978, p.132-145.

[85] Sorokin A.P., Ushakov P.A., Yuriev Yu.S. Influence of Interchannel Exchange on Velocity and Temperature Fields in Pin Bundles. Problems of Nuclear Science and Engineering. Physics and Eng., M., 1984, 4(41), p.64-69 (in Russian).

[86] Ushakov P.A., Zhukov A.V., Matjukhin N.M. Temperature Fields in Regular Pin Bundles in Laminar Flows. Thermal Physics of High Temperatures, 1976, v. 14, p. 538-545.

[87] Zhukov A.V., Matjukhin N.M., Sviridenko E.J. Temperature Fields and Heat Transfer in Edge Areas of Hexagonal Subassemblies of Fast Reactors. Problems of Nucl. Science and Eng., 1977, 4(18), p.5-8 (in Russian).

[88] Hsu C.J. Laminar and Slug Flow Heat Transfer Characteristics of Fuel Rods Adjacent to Fuel Subassembly walls. Nucl. Science and Eng., 1972, v. 49, p. 398-404.

[89] Zhukov A.V., Kirillova G.P. Temperature Behavior at Entrance Section of Pin Bundle in Turbulent Liquid Metal Flow. Preprint IPPE-715, Obninsk, 1976 (in Russian).

[90] Sidelnikov V.N., Zhukov A.V. Calculation of Temperature Behavior at Entrance Section in Planar Flow. Preprint IPPE-414, Obninsk, 1974 (in Russian).

[91] Sidelnikov V.N., Zhukov A.V. Problems of Heat Transfer at Entrance Section in Pin Bundle. Proc. of Int. Sem., Nove Mesto, Czhech Republic, 1973, p.21.

[92] Zhukov A.V., Sidelnikov V.N., Titov P.A. Calculation of Temperature Behavior at Entrance Section in Laminar Flow. Preprint IPPE, Obninsk, 1974 (in Russian).

[93] Zhukov A.V., Matjukhin N.M., Kotowski N.A. et al. Experimental Study of Temperature Distribution at Entrance Section in Turbulent Flow of Liquid Metal. Preprint IPPE-781, Obninsk, 1977 (in Russian).

[94] Zhukov A.V., Matjukhin N.M., Kotowski N.A.. Temperature Fields at Entrance Sections and at Stabilized Area of Pin Bundles (Liquid Metal). Preprint IPPE-883, Obninsk, 1978 (in Russian).

[95] Zhukov A.V., Matjukhin N.M., Kotowski N.A.et al. Experimental and Numerical Study of Heat Transfer in Pin Bundles under Instabilised Conditions. Heat Transfer and Hydrodynamics of Single-Phase Flow in Pin Bundles, L., Nauka, 1979.

[96] Vasov V., Forsait D. Difference Methods in Solution of Partial Derivative Differential Equations, M., 1963.

[97] Fadeev D.K., Fadeeva V.N. Numerical Methods of Linear Algebra, Fizmatgiz, 1963.

[98] Minashin V.E., Sholochov A.A., et al. Calculation of Temperature Behavior in Reactor Core Under Arbitrary Power Production. Atomic Energy, 1967, v.22, p.362-366.

[99] Ushakov P.A., Sorokin A.P. Analysis of Generalized Duhamel Integral as Applied to Calculation of Temperature Behavior in Reactor Fuel Pins. Thermal Physics of High Temperatures, 1978, v.16, p.787-790.

[100] Dobrovolski V.F., Zhukov A.V., et al. Investigation into Temperature Behavior of Fast Reactor Fuel Pins under Non-Uniform Power Production. Atomic Energy, 1970, v.28, p.490.

[101] Gubarev V.A., Trofimov A.S. Determination of Temperature Difference Wall-Liquid in Reactor Design. Atomic Energy, 1974, v.3, p.251-252.

[102] Zhukov A.V., Matjukhin N.M., Sviridenko E.J. Temperature behavior in Deformed Pin Bundles under Unifor and Non-uniform Loads. Preprint IPPE-909, Obninsk, 1979 (in Russian).

[103] Kazachkovski O.D., Zhukov A.V., Matjukhin N.M. Intensification of Heat Tranfer in Fast Reactor Subassembly with Counter-Directed Wire Wraps and Non-uniform Power Production. Preprint IPPE-1306, Obninsk, 1983 (in Russian).

**NEXT PAGE(S)
left BLANK**

Chapter 4

EXPERIMENTAL AND NUMERICAL THERMAL HYDRAULICS OF FAST REACTOR CORE

4.1. VELOCITY FIELDS

Nuclear reactor subassembly represents the system of interacting channels. Mass exchange, more strong than in the insulated channels, influence of random geometrical deviations, effect of spacer structures, non-uniform distribution of the coolant over the channels of a different shape and other factors determine hydrodynamic features of the system under discussion. The use of methods and correlations for insulated channels in hydraulic predicting the interacting channels may cause the great error to appear.

Velocity fields in the bundles of smooth pins. Experiments were performed on the models involving 3, 7, 37 and 61 pins, with the electromagnetic sensors inserted into the measuring (rotating) pin (Fig. 4.1a, b). Rotation of the measuring pin about its axis made possible recording velocity distribution around the pin. The model design allowed the pin arrangement within triangular bundle to be varied ($1.01 \leq s/d \leq 1.31$). Tables 4.1 and 4.2 contain geometry of 3- and 7-pin models.

As for correlation between the values measured by electromagnetic technique and those measured by Pilot tube, it can be noted that velocity distributions over the channel perimeter are in agreement with the experimental data by authors [1, 2], as well as with the results of numerical analysis [3-5] (Fig. 4.2). When results were compared, the data are averaged through the area W_I enclosed by the wall, line of maximum velocity and radial axises, with the angle between them being $d\varphi$:

$$\frac{w_\varphi}{\overline{w}} = \frac{\int\limits_{r_o}^{R} wr\, dr \int d\varphi}{\overline{w} \int\limits_{o}^{R} r\, dr \int d\varphi} = \frac{\int\limits_{r_o}^{R} wr\, dr}{\overline{w}\left(\dfrac{R^2 - r_o^2}{2}\right)} = \frac{2\int\limits_{r_o}^{R} w(y + r_o)\, dy}{\overline{w}\left(R^2 - r_o^2\right)} =$$

$$= \frac{2\int\limits_{0}^{1} w\left(Y + \dfrac{r_o}{y_{max}}\right) dY}{\dfrac{\left(R^2 - r_o^2\right)}{y_{max}^2}} = \frac{2\int\limits_{0}^{1} \dfrac{w}{\overline{w}}\left[Y + \dfrac{1}{(s/d + \cos\varphi)}\right] dY}{\dfrac{s/d + \cos\varphi}{s/d - \cos\varphi}}, \tag{4.1}$$

where r - current radius, r_0 - pin radius, R - distance from the pin axis to the line of maximum velocity; $y = (r - r_0)$ - current distance from the wall; $y_{max} = (R - r_0)$ - distance from the wall to the line of maximum velocity; $Y = y/y_{max}$. Results of electromagnetic measurements and those in [6] are generally in agreement (Fig. 4.4), except for a small difference ($\sim 5\%$) in velocity amplitudes being due to variety of relative pitches in the bundles under investigation, as well as distinction between Reynolds numbers. It should be noted that velocity non-uniformity in a wide bundles (Fig. 4.5, 4.6) is some lesser than that in channel of "Palmer" type (simulating two adjacent channel by four smooth pins with the axial spacer [1, 2]). It seems likely that a number of hydrodynamical factors, such as secondary flows, inter-channel mixing and so on, appear in different manner in pin bundle and Palmer channel.

Table 4.1. Geometry of the 3-pin models

Parameter	Value
Number of pins, n, Outer pin diameter, d, mm Inner pin diameter, d_I, mm Pin lengh, L, mm L/d, . Inner diameter of the cover, D, mm	3 24.7 20 792 32.1 58.9
Distance from the bottom grid to $\quad l$, mm electromagnetic sensor $\quad\quad\quad l/d$ $\quad\quad\quad\quad\quad\quad\quad\quad\quad\quad\quad l/d_h$	686 27.8 55.7(withour displacers) 95.8(displacers)
Relative pitch of the bundle, s/d Displacer diameter, d_d, mm Hydraulic diameter of the model, d_h, mm Cross section area Ω, mm^2	1.01; 1.02; 1.05; 1.10; 1.15; 1.20 12 12.3(without displacers) 7.16(displacers) 1290(without displacers) 948 (displacers)

Table 4.2. Geometry of the 7-pin models

Parameter	Value
Number of pins, n, Outer pin diameter, d, mm Inner pin diameter, d_I, mm	7 24,7 20
Pin length between $\quad L$ mm the end grids $\quad\quad\quad L/d$	740 30
Distance from the bottom $\quad l$, mm to electromagnetic $\quad\quad l/d$ sensor $\quad\quad\quad\quad\quad\quad l/d_h$	560 21.9 154; 105; 68; 49.6; 38.6
Relative pitch of the bundle, s/d Hydraulic diameter, d_h, mm Cross section area Ω, mm^2	1.02, 1.05, 1.10, 1.15, 1.20 3.65, 5.34, 8.27, 11.3, 14.5 221, 310, 482, 658, 845

168

Table 4.3. Geometry and experimental techniques to study inter-channel exchanger in the edge area

Author	Pin number	d, mm	s / d	h / d	L, mm	Re, 10^4	Coolant	Technique
Lorenz J. e.a.	91	–	1,24	48	–	–	Water	Salt injection
Chen Y.e.a.	61	6,125	1,25	48 24	-	0,064 0,45	Water	LDA
Chiu C.e.a.	61	12,73	1,063	4 8	1524	0,2 1,7	Water	Salt injection
Pedersen D. e.a.	91	–	1,20	48	–	–	Water	Hot water injection
Fontana M.e.a.	19	5,75	1,24	52	–	0,1-7,0	Water	Pin heating
Skok J.	7	21	1,14	14 28	800	4,2	Water	Hot water injection
Collingham R.	217	5,84	1,24	51,3	1445	1,0-3,0	Water	Salt injection
Hanson A.S. e.a.	61	–	1,25	24	–	–	Water	Salt injection
Khan E.e.a	19 61	–	1,09 1,2	21 43	–	–	–	Pin heating

Table 4.4. Geometry of the model simulating fast reactorsubassembly

Parameter	Value
Outer pin diameter, d, mm Inner pin diameter, d_1, mm Relative pitch, s/d Length of heated section, l_o, mm	16 13 1.185 1720
Helical wire diameter d_d, mm	2.96 (all pins) 2.96 (inner pins) 1.48(edge pins)
Wire wrap pitch, h, mm Clearance between cover and pins, Δ, mm Relative clearance $\Psi=\Delta/(s-d)$ Pin number, n	192 2.96; 1.48 1.0; 0.5 37
Displacer diameter, d_d, mm	4.27
Hydraulic diameter of the inner channel Cross section area, ω, mm^2	6.94 48.67; 40.93
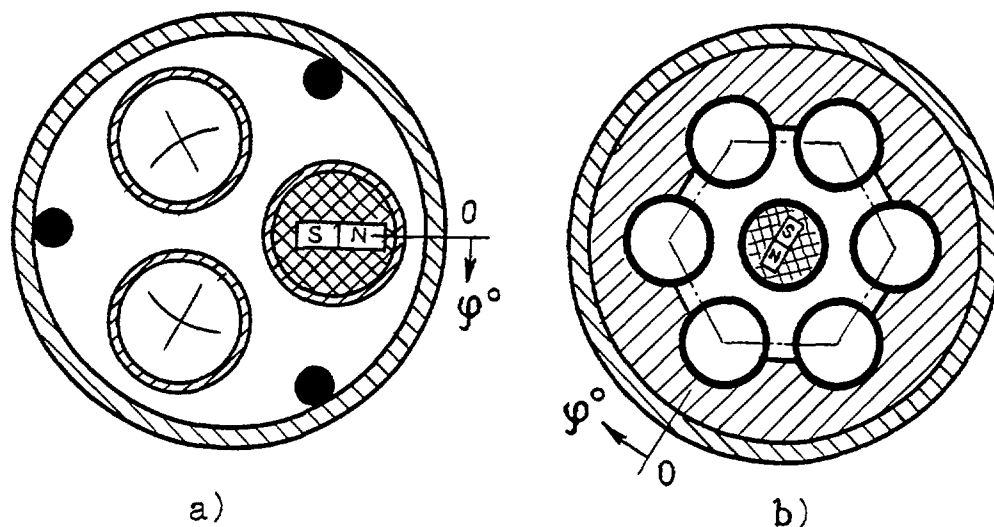
Fig. 4.1. Cross-sections of 3-pin (a) and 7-pin (b) models equipped
by electromagnetic sensors.
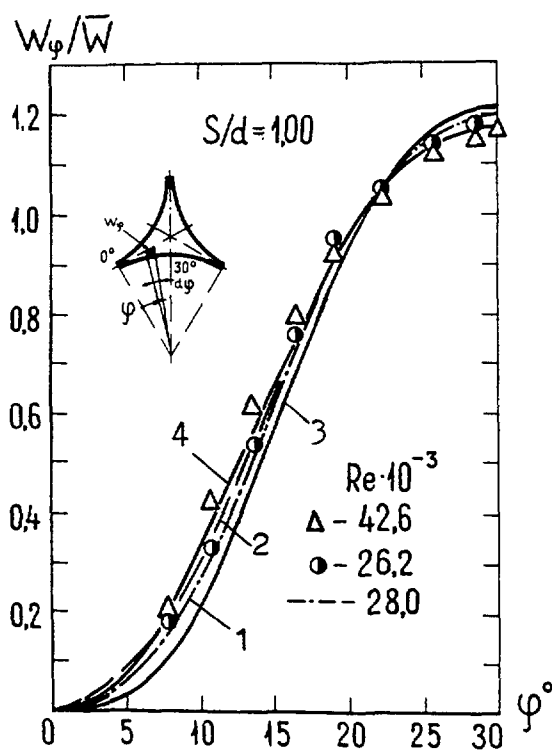
Fig. 4.2. Velocity distribution over the compact
arranged pin perimeter: ◑ - electromagnetic
measurement, △ - measurement by Pitot tube,
2-4 - predictions [4.3 - 4.5].
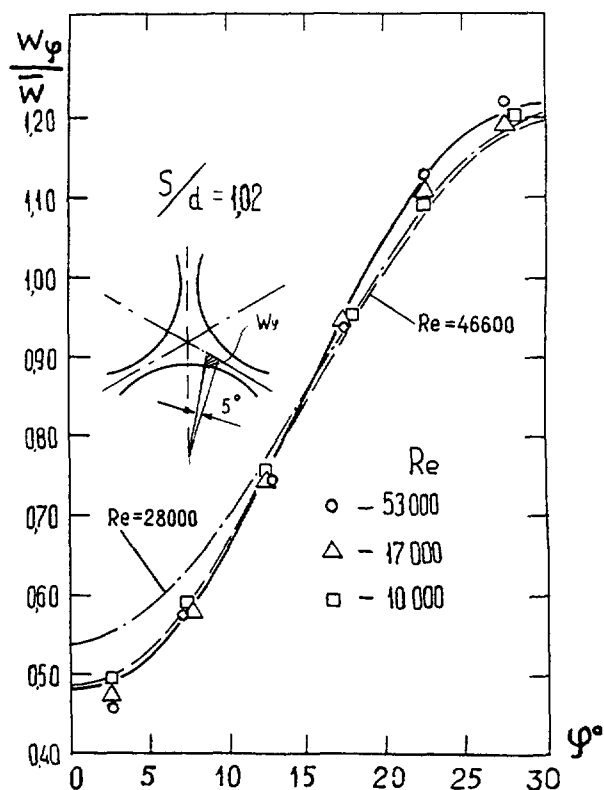
Fig. 4.3. Velocity distribution over the pin
perimeter at S/d = 1.02: : ○ , △ ,□- electromagnetic
sensors, — — , — · — - Pitot tubes.
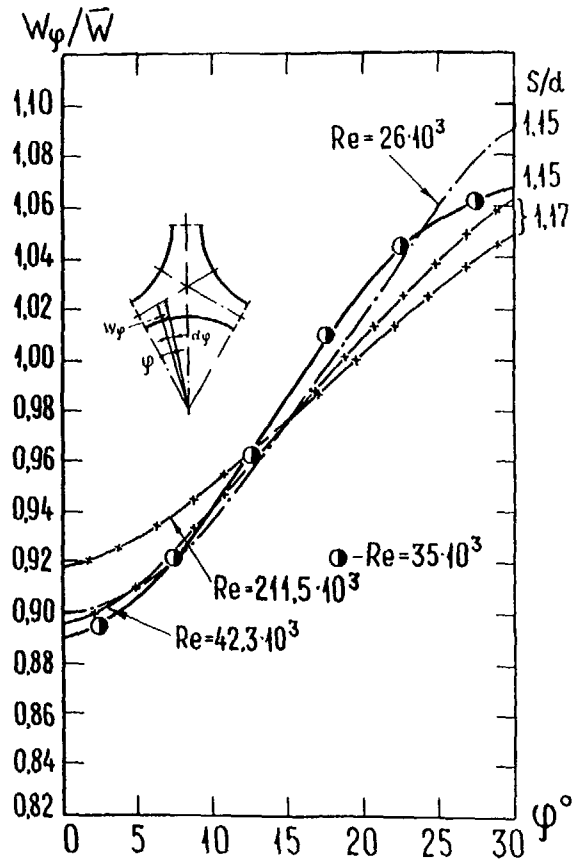
Fig. 4.4 Dimensionless velocity: ◑-electromagnetic sensors (7-pin bundle, S/d = 1.15), +, × - Pitot tubes (19-pin bundle, S/d = 1.17), —·— - Pitot tubes (Palmer channel, S/d = 1.15).
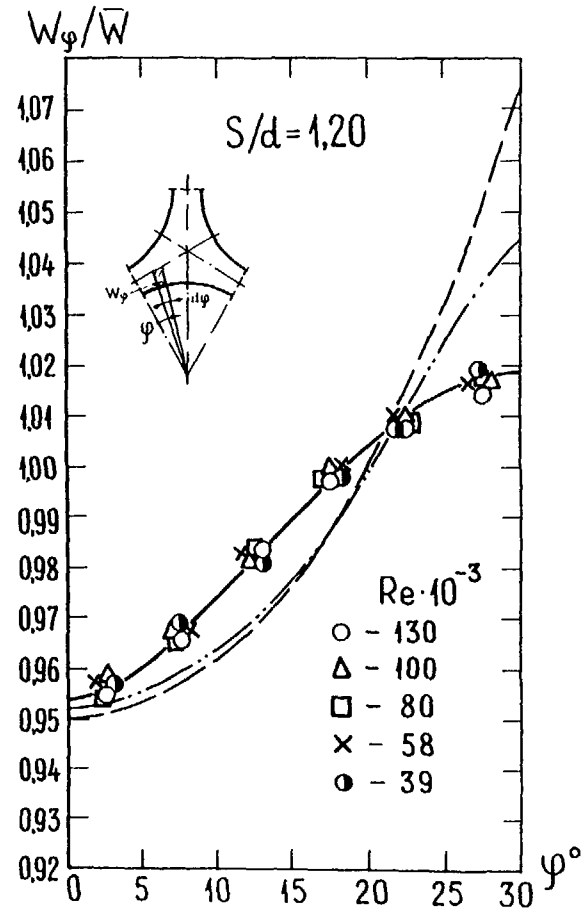
Fig. 4.5. Dimensionless velocity in the integral channel of triangular bundle (S/d = 1.2):
×, ○, ◑, △, □ - electromagnetic sensors,
— —, —·· — - Pitot tubes.
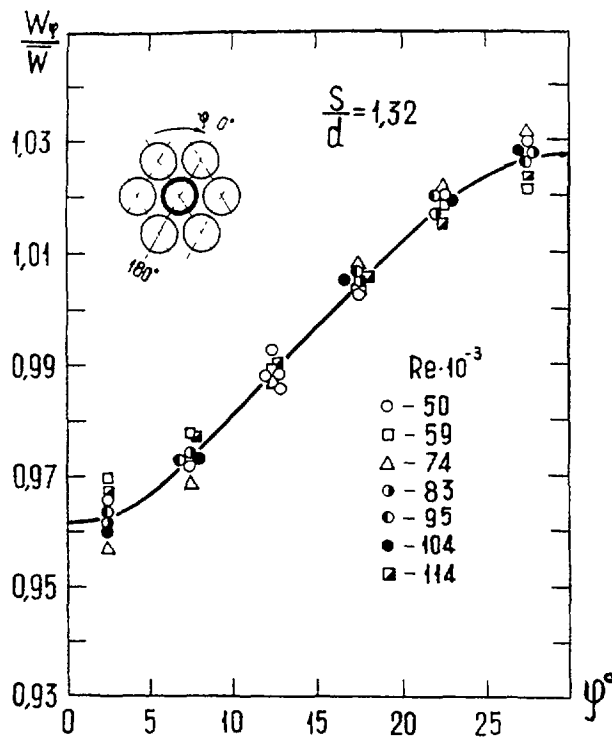
Fig. 4.6   Dimensionless velocity in the internal channel of triangular bundle S/d = 1.32;

O , □ , △ , ◐ , ◑ , ● , ◪   *- electromagnetic measurements,*
———— *- averaging relationship*
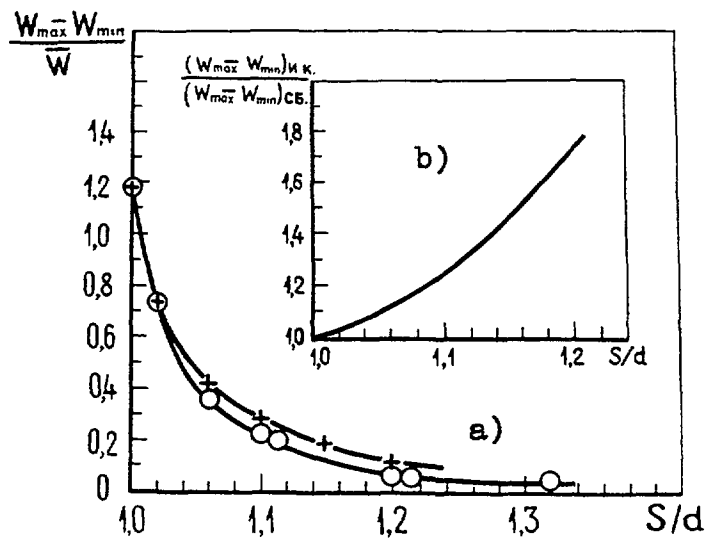
Fig. 4.7.   Maximum velocity irregularity in the «isolated» channel (—+—) and pin bundle (—o—) with the pitch-to-diameter ratio S/d.

172
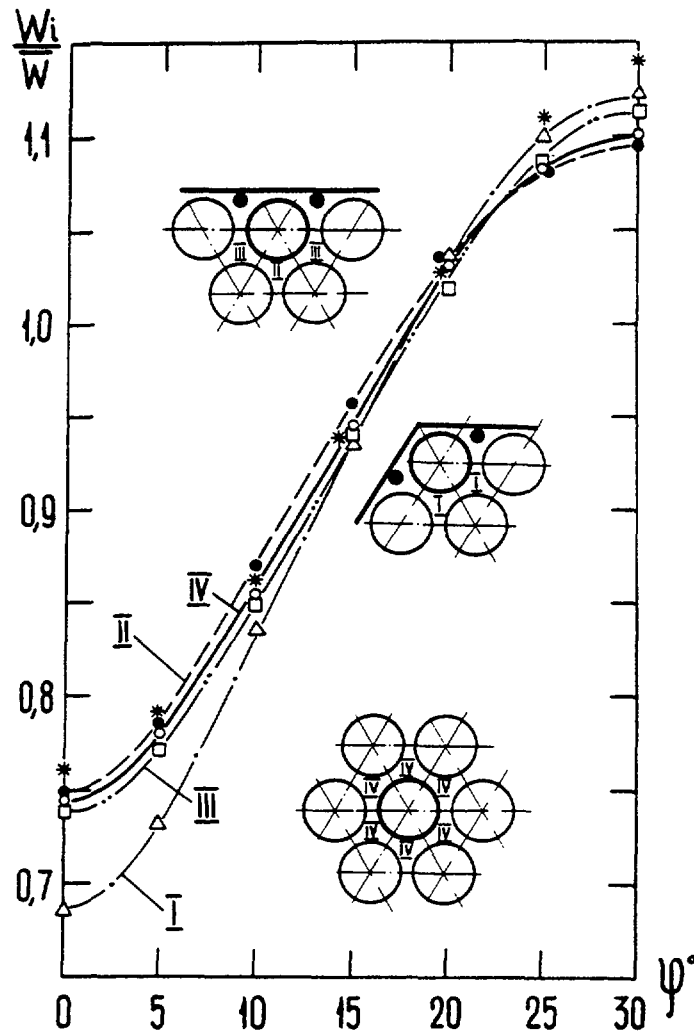
Fig. 4.8. Velocity distribution in the internal channel of pin bundle S/d = 1.062:

Δ , $\square$, $\bigcirc$, $\bullet$ - *electromagnetic measurements,*

$*$ - *data derived by interpolation* [6]

As relative pitch of the bundle is reduced, a difference between the velocity non-uniformities decreases in accordance with

$$\frac{(w_{max} - w_{min})_{palm}}{(w_{max} - w_{min})_{sub}} = 10(s/d)^2 - 18.4(s/d) + 9.4 \tag{4.2}$$

and dies away in the compact bundle (Fig. 4.7).

Velocity profile in the individual channel is formed under influence of adjacent channels. Even in the channels of the same geometry the different velocity profiles can take place depending on the features of flows in adjacent channels. So, velocity at the interface between the standard and edge channels in the corner area of subassembly is lesser than those in the side area (Fig. 4.8) [7]. This effect is most conspicuous in 3-pin bundle with /without displacers (Fig. 4.9, 4.10) . Detail measurements of velocity performed in the BN-600 model bundle with the smooth pins have allowed studying as nominal and deformed geometry [6, 8].
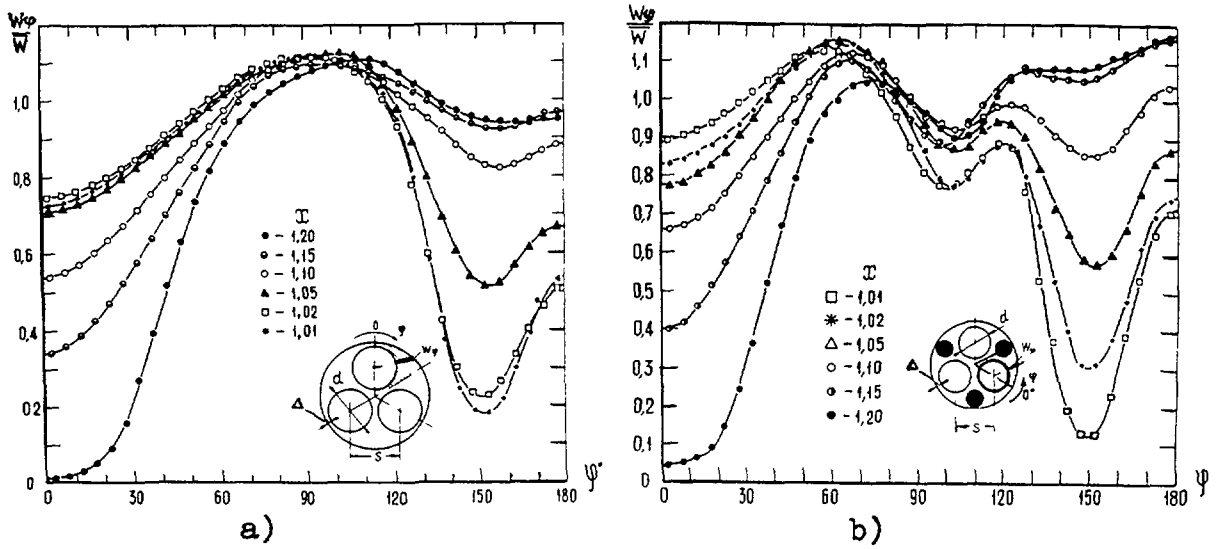
Fig. 4.9. Velocity in the 3-pin model involving displacers (a) and being free of displacers (b).
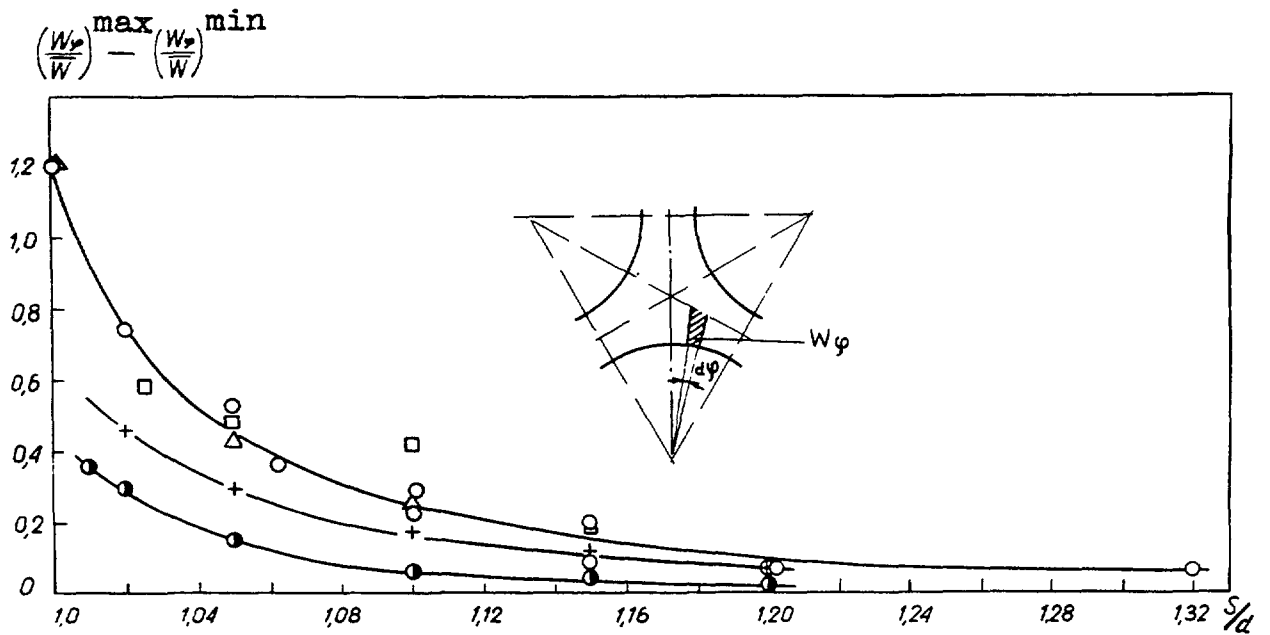
Fig. 4. 10. Maximum velocity irregularity within elementary channel:

O - electromagnetic measurements, Δ , □ - Pitot data [1,2] ,

◑ , + - pin model with and free of displacers, respectively.
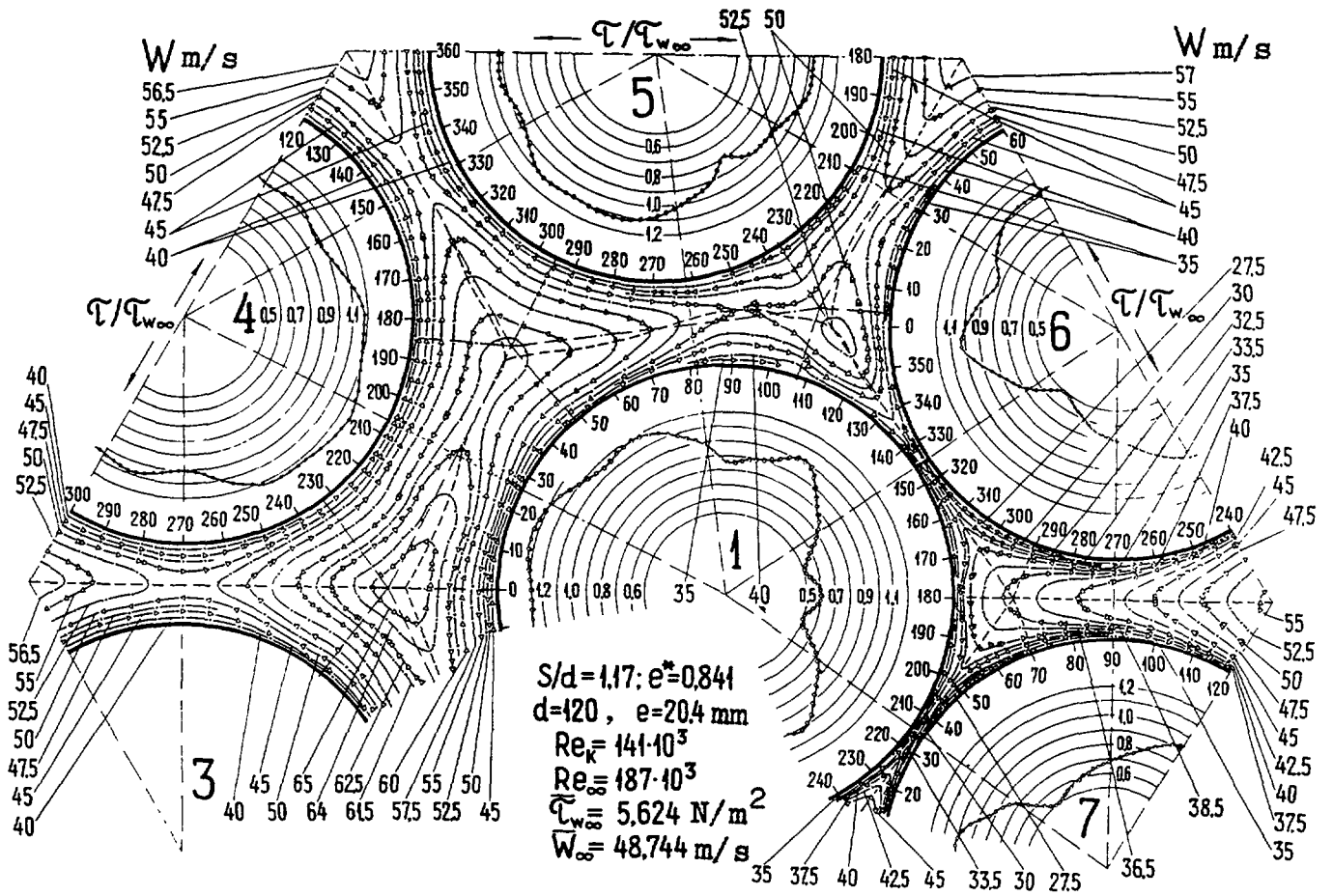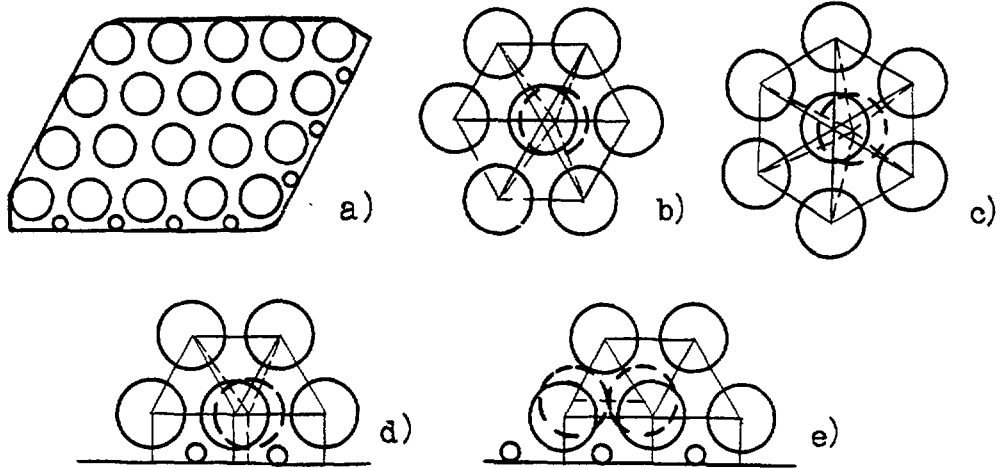
Fig. 4.11. Schematic diagram of the model bundle (a), various arrangements (b-e) and shear stresses τ and coolant velocity (w) in deformed bundle (f).
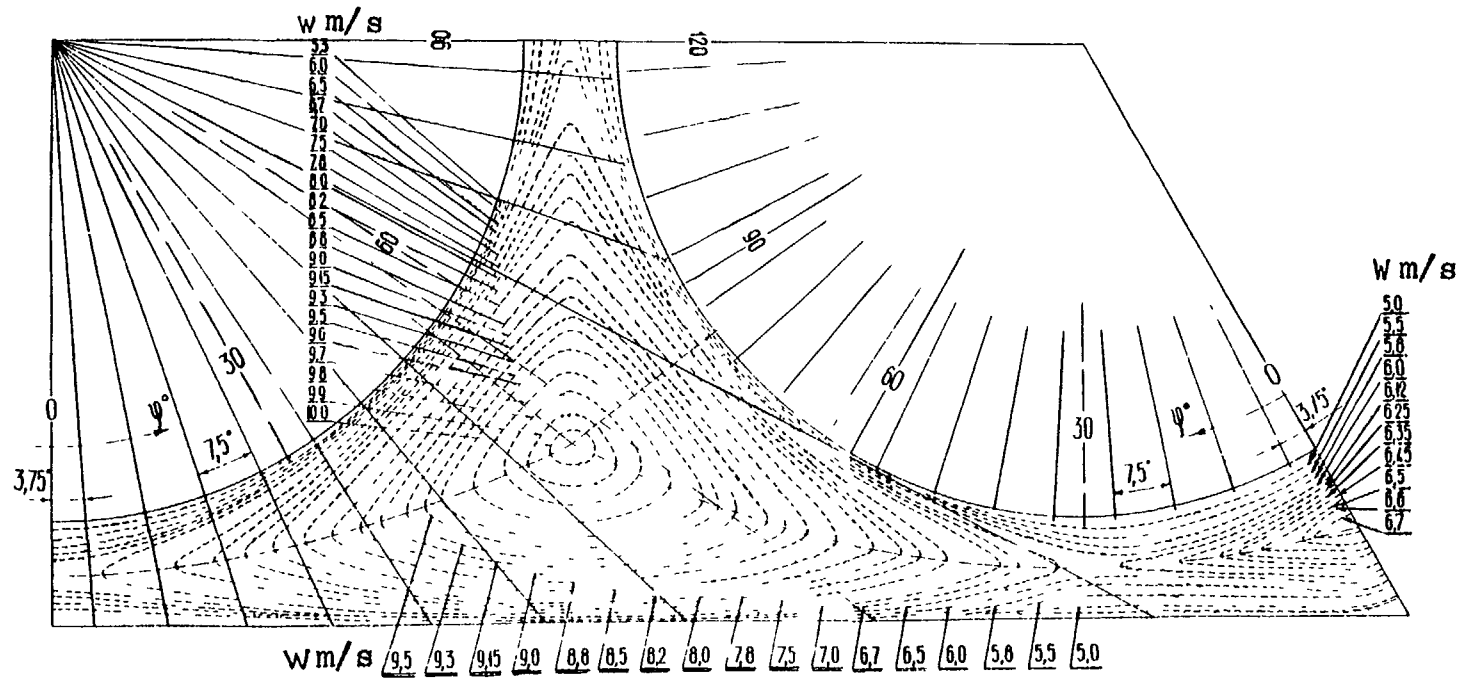
Fig. 4.12. Velocity distribution in the edge area of pin bundle calculated using procedure [3]
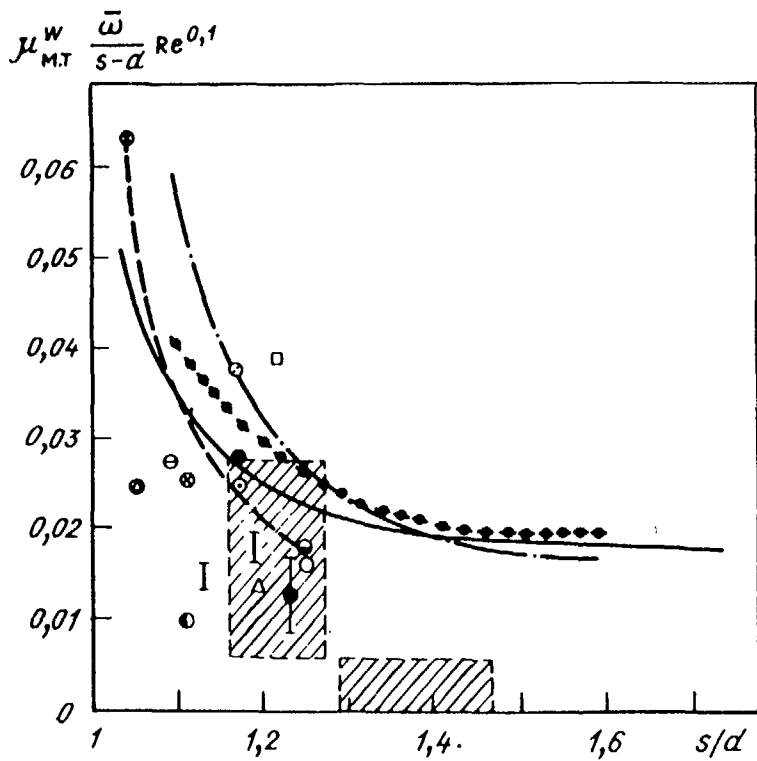
Fig. 4.13. Comparison experimental data and analytical relation
ship of molecular-turbulence exchange by momentum with the other
authors data :

⊖ , ⊗ , ◐ , ⊖ , ◑ , ● , ⊙ - experiments,

———— , - prediction, □ - Polyanin, ◕ -Rudzinsky ,

— — — - Ingesson, — — ·— - Rogers,

▨▨▨▨ Marcozy, O -Gabrianivich ,

◆ - Roidt, O - Voj, Δ - Pietralla, I -Rowe.
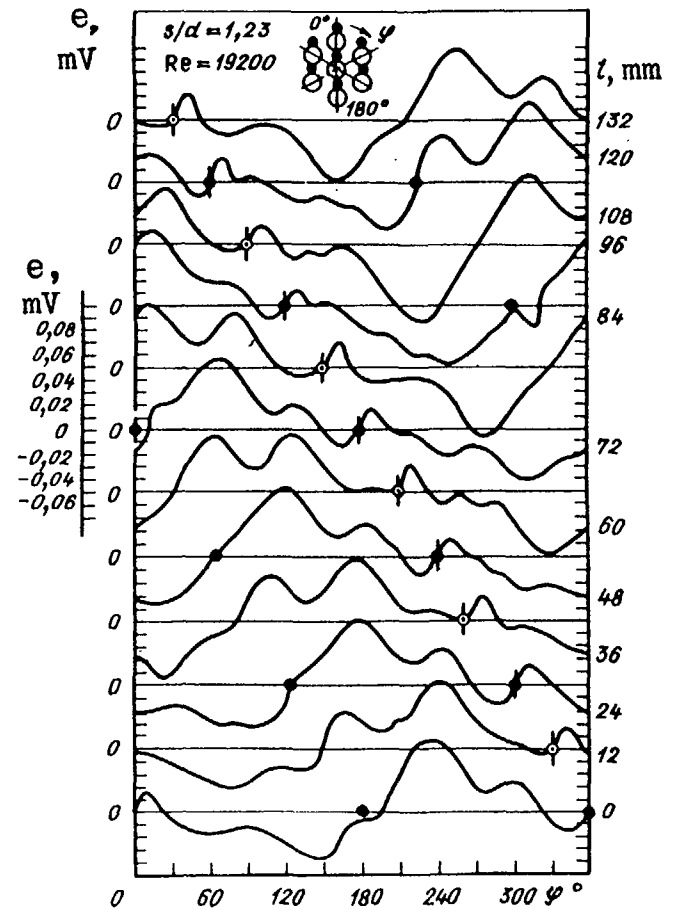
Fig. 4.14. Lateral flow around the pin in the places of fin
location in the narrow (● , ◖) and wide (◔) parts of the channel.

177

In last case, some pins were shifted from their nominal positions. Fig. 4.11 shows the model bundle, examples of pin shifting and velocity distributions in the internal and side areas of deformed bundle. The more detail information is available in [6, 8, 9]. Fig. 4.12 also illustrates velocity distribution in the nominal side area of hexagonal bundle predicted on the basis of procedure mentioned in [3].

Turbulent inter-channel momentum exchange. From the momentum macro-transport equation written in axial direction for the stable coolant flow, the momentum mixing factor between the channels i and j can be expressed through the difference between wall shear stresses and momentum flow throughout the other clearances [10]:

$$\mu_{ij}^{w} = \frac{(1/\omega_j)\sum_k \Pi_{k_j}\tau_{k_j} - (1/\omega_i)\sum_k \Pi_{k_i}\tau_{k_i} + \Delta P_{ij} - \Delta P_{ji}}{(1/\omega_j + 1/\omega_i)(w_i - w_j)\left[(w_i + w_j)/2\right]\overline{\omega}}$$

(4.3)

where ω_i, ω_j - areas of the channels; $l_{k_j}\Pi_{k_i}$ - perimeter of the k-th pin facing the

channels j and i, respectively, τ_{k_j}, τ_{k_i} -shear stresses.

$$\Delta p_{ij} = \frac{1}{\omega_i}\left[\sum_j \mu_{ij}^{w}(w_i - w_j)\frac{w_i + w_j}{2}\overline{\omega}\right];$$

$$\Delta p_{ji} = \frac{1}{\omega_j}\left[\sum_j \mu_{ij}^{w}(w_j - w_i)\frac{w_j + w_i}{2}\overline{\omega}\right];$$

(4.3a)

Relationship (4.3) indicates that momentum mixing factor can be found at the non-uniform velocity distribution (Fig. 4.12) or in the event of disturbed velocity, when one or several pins are shifted from their nominal position (Fig. 4.11a, c).

Processing the data mentioned above has allowed deriving the following formula for the bundle of smooth pins [10]:

$$\mu_{MT}^{M} = \frac{8.10^{-2}}{\pi d}\frac{\left[1.0744(s/d - 1) + 0.1864\right]}{\left[\left(\frac{2\sqrt{3}}{\pi}\right)(s/d)^2 - 1\right]Re^{0.1}}$$

(4.4)

at $1.035 \le s/d \le 1.25$; $6.5 \ 10^4 \le Re \le 18.1 \ 10^4$.

Values predicted by (4.4) are in agreement with an accuracy 15% with those predicted by the following formula derived by the authors:

$$\mu_{MT}^{M} = \frac{\left(8.10^{-2}/\pi\right)\left[2(s/d - 1) + 0.115\right]}{d\left[\left(\frac{2\sqrt{3}}{\pi}\right)(s/d)^2 - 1\right]Re^{0.1}}\cdot\left\{1 - exp\left[-80(s/d - 1)\right]\right\}$$

(4.5)

at $1.0 \le s/d \le 1.6$; $10^4 \le Re \le 2 \ 10^5$.

178
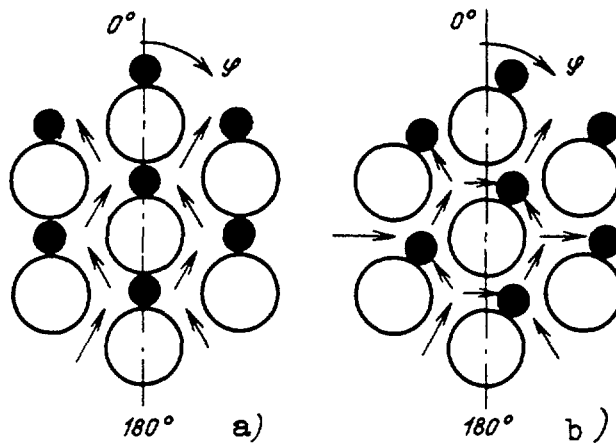
Fig. 4.15. The senses of lateral flows in narrow (a) and wide (b) parts of channel.
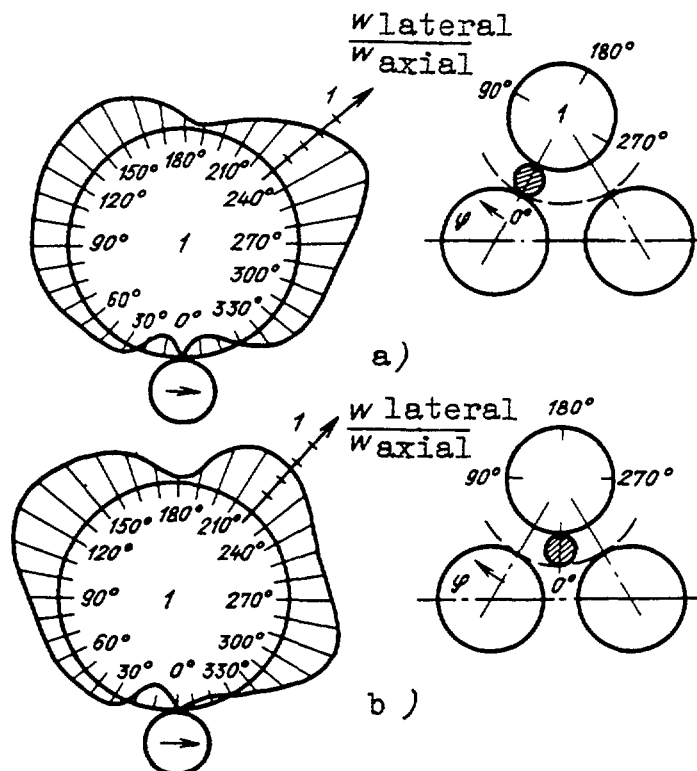

Fig. 4.16. Sketches of lateral velocity around the pin in narrow (a) and wide parts of the channel (b).
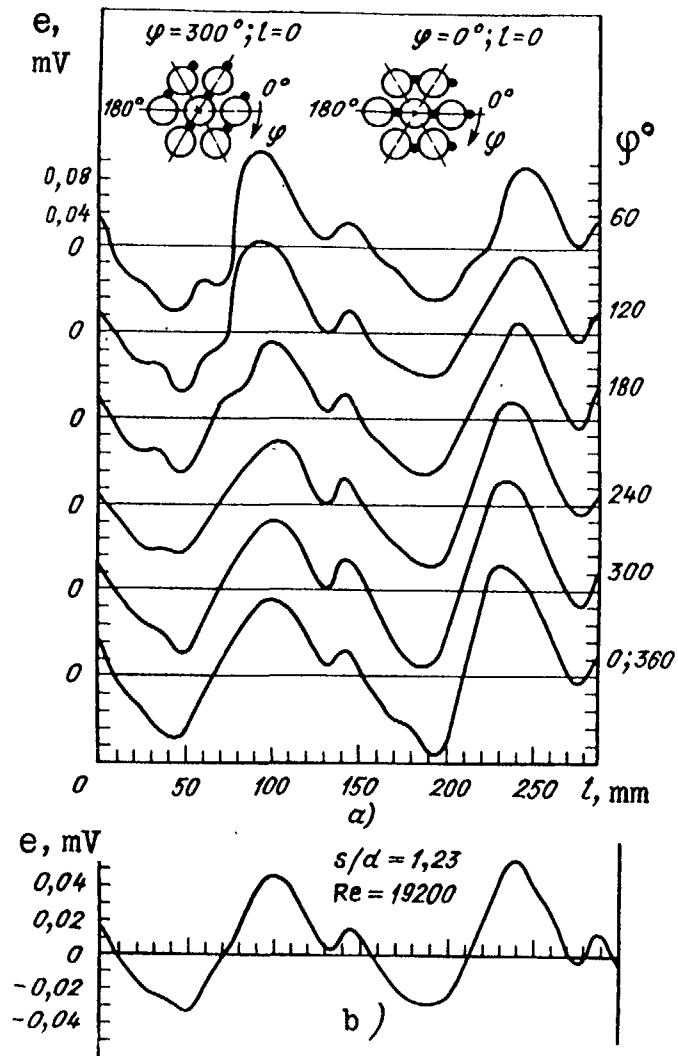
Fig. 4.17. Lateral flows in clearances between channels: in every clearance (a) and averaged over six clearances (b).
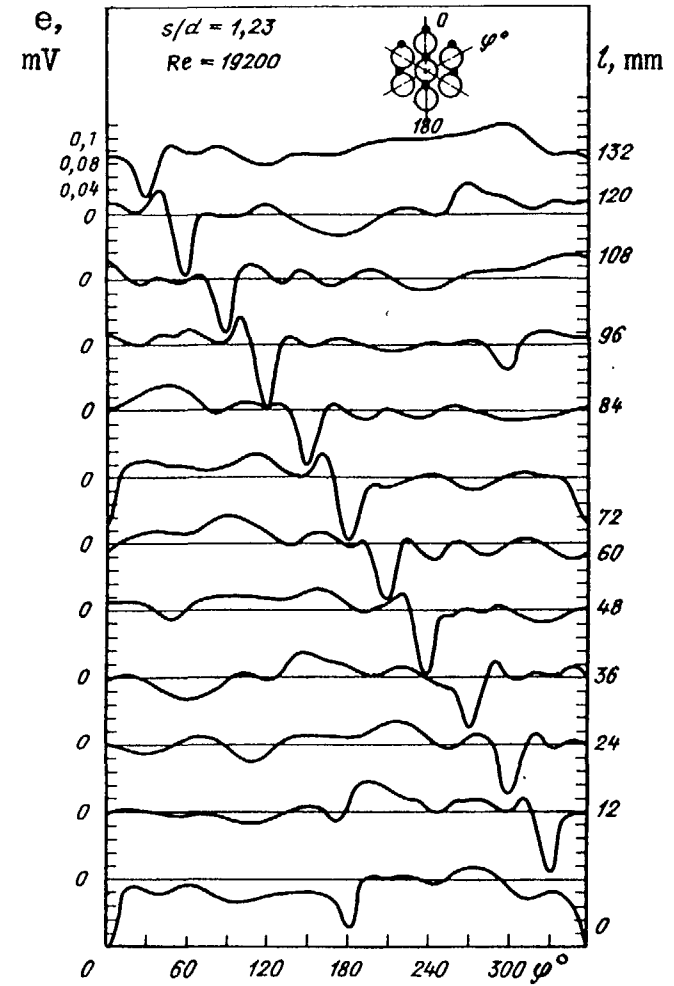
Fig. 4.18. Axial flows around the pin at a different levels:
l = 0, 24, 48, ... , 144mm - narrow part,
l=12, 36, 60, ..., 132mm - wide part.
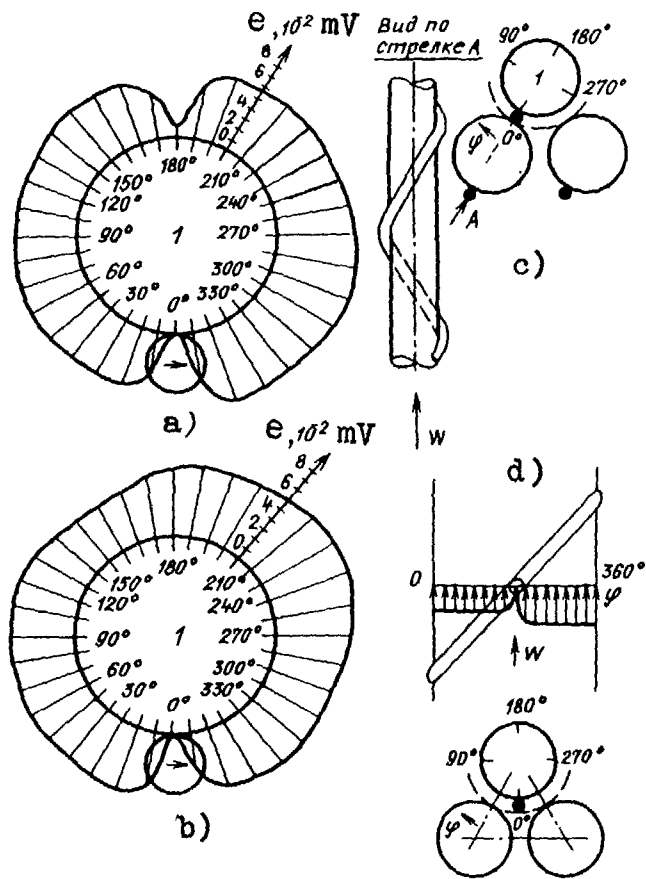
Fig. 4.19. Sketches of axial flows in narrow (a) and wide (b) parts of the channel, schematic views of arrangement of the wire on the pin (c) and velocity distribution ahead of and behind the wire (d).
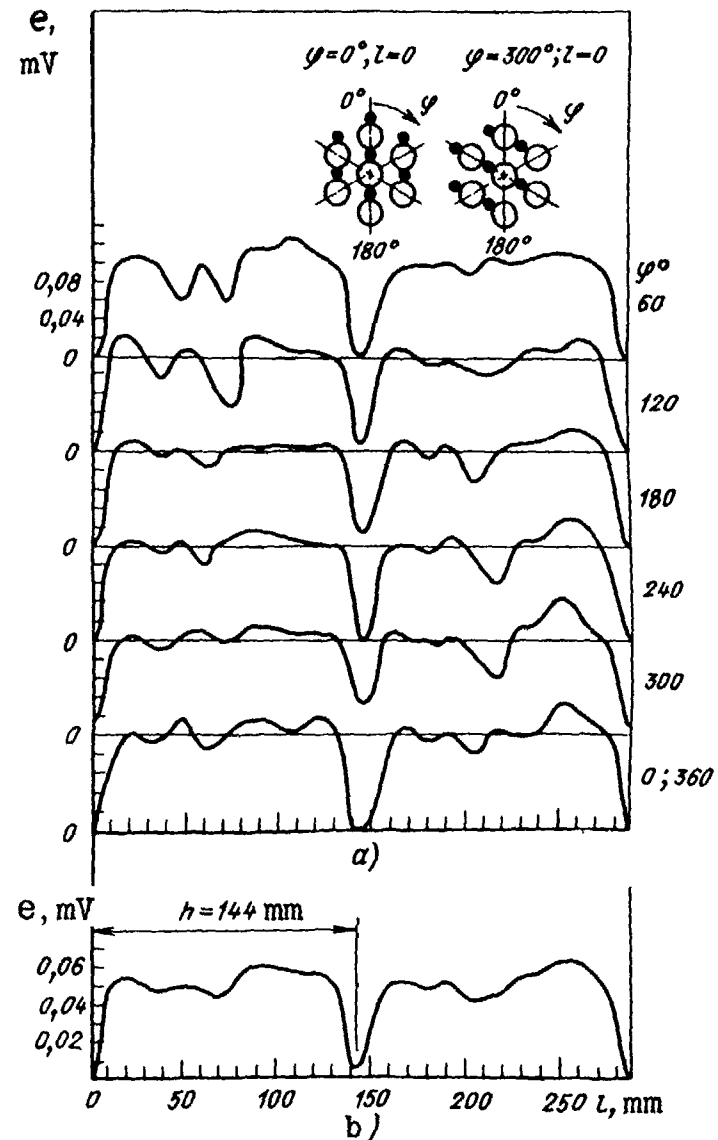
Fig. 4.20. Axial flows with the length of clearances (a) and averaged over six clearances (b).
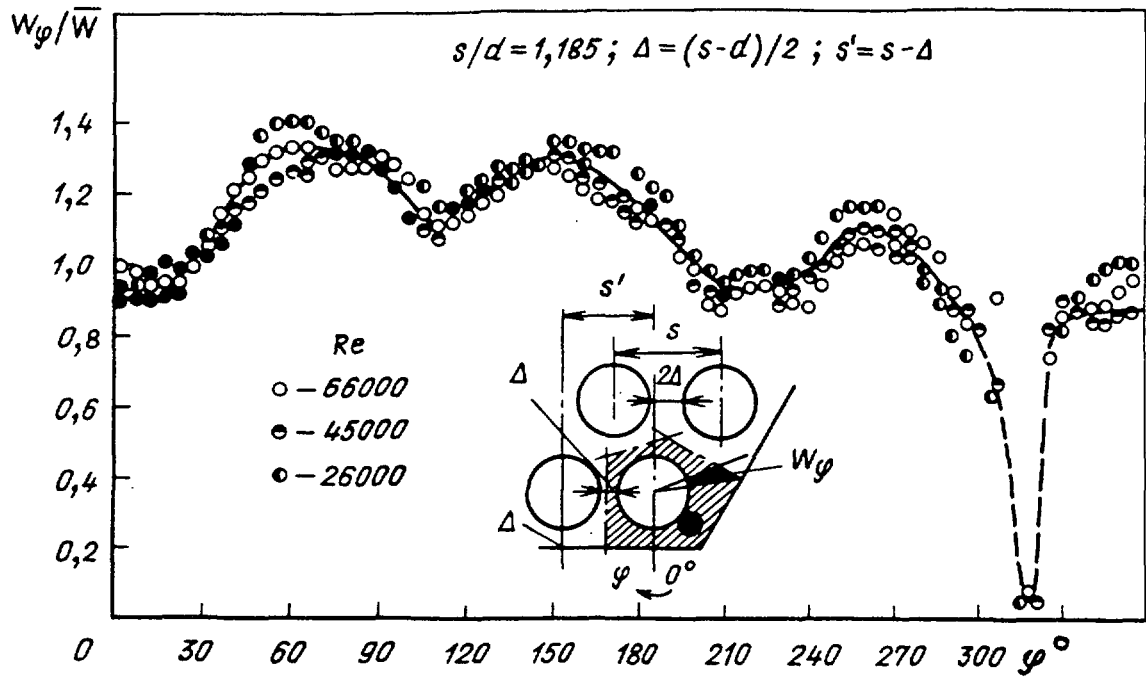
Fig. 4.21. Velocity distribution around the wire wrapped corner pin in the model bundle in shifting pin along the cover.
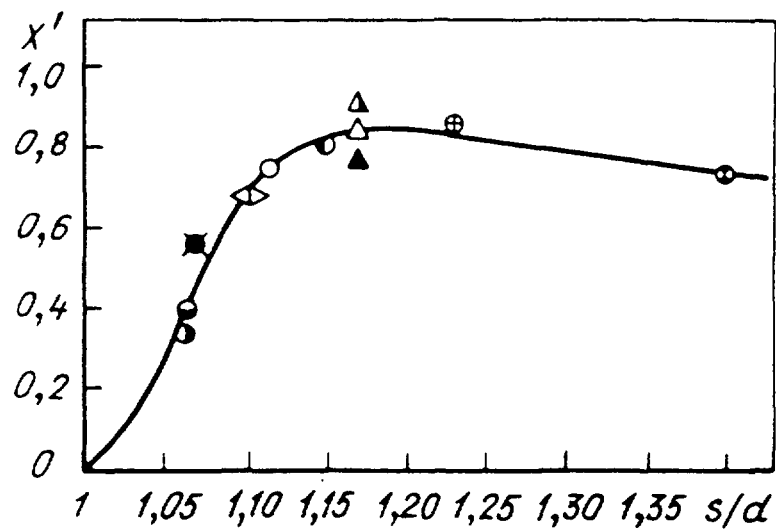

Fig. 4.22. Experimental data on convective interchannel mass exchange in the integral region of bundle:

◐ , ◑ , ◓ , △ , ▲, ▲ , ○ , ⊕ , ◐ - experimental data [16 ÷ 18] ,

- - - - generalising relationship , ◇ -Bolle, ✹ - Patch.

Velocity distribution in the bundle of wire wrapped pins. Physical picture of coolant flow through the bundle is as follows[15]:

In the points where the wire wraps are bridges the inter-pin clearance, transverse coolant flow is unavailable (Fig. 4.14). At the region between these points, the maximum transverse flows occur. Near the two sides of pin the coolant flows in the same directions, that is in the cross section under consideration a liquid flows from one bundle side to another in accordance with the wire orientation. (Fig. 4.15a, b). In going from the narrow part of the channel to the wide part and out of, the maximum value of transverse velocity is displaced from $\varphi = 120°$ to $\varphi = 240°$, that is for all time it falls on the wide part of the channel (Fig. 4.16a, b). Distribution of transverse velocity over the height of inter-channel clearance is of periodic character (Fig. 4.17a,b).

Axial component of velocity vanishes at the parts of pin perimeter engaged by the wire (Fig. 4.18), coolant velocity is greater over that half of perimeter to which the wire is tilted ($180° < \varphi < 360°$), Fig. 4.19a-d. The wire represents a "barrier" to the axial flow that defines the velocity behaviour before and behind the wire, Fig. 4.19d. Axial velocity distribution has minimum with the zeroth value in the points, where the wire is tight against the pin (Fig. 4.20a, b). Zeroth axial velocity under the wire, is naturally observed at the edge pins (Fig. 4.21).

Thus, velocity distribution over the pin height is non-uniform (has maximum and minimum), that is defined by the combined hydrodynamics. Variation in axial component of velocity is caused by the inter-channel mixing.

Analysis of inter-channel exchange. Intensity of transverse convective mass inter-channel exchange may be described by the ratio between the averaged values of transverse and axial velocities, that is Stanton criterion:

$$St^M = \mu_k^M \frac{\overline{\omega}}{s-d} = \frac{\overline{w}_{ij}}{\left(w_i + w_j\right)/2},$$

(4.6)

where $\overline{w}_{ij}$ - mean velocity of a directional transverse coolant flow through the clearance between the channels i and j; w_i, w_j - mean axial velocities in the channels i and j; ω - statistical area of the channel cross section.

To perform the subsequent analysis the parameter is to be introduced [18]:

$$X' = \frac{\left[\left|\overline{w}_{ij}\right| / \dfrac{\left(w_i + w_j\right)}{2} \right]}{tg\varphi}$$

(4.7)

describing the extent to which a liquid follows the wire wrap and the degree of the completeness of transverse velocity, here φ - the slope of wire wrap at the pin. If liquid follows strictly the wire wrap, with the velocity distribution over the clearance height being uniform, that $x' = 1$. When transverse velocity varies as cosine, with the vector of maximum velocity being coincident with the wire wrap direction, $x' = 2/\pi \approx 0.637$.

Experimental data [15, 16, 19, 20] show that x' rises up to 0.83 at $s/d = 1.17$ (Fig. 4.23), that correlates with $x' = 1.38$ at cosine variation of transverse velocity. Thus, maximum value of transverse component of velocity is found to be more by 38% than those predicted under the assumptions that liquid follows the wire wrap.

Transverse velocity through the clearance between the pins can be close to axial component of velocity [15] (Fig. 4.16, 4.19), that indicates the velocity vector departs from wire wrap toward an increase in φ.

Data [19, 20] are in agreement with the electromagnetic measurements [15 - 17] and reinforce the formula

$$St_k^M = \frac{0.478}{h}\left\{1.8\frac{s}{d} - 2.5exp\left[-119\left(\frac{s}{d} - 1\right)^{2\,12}\right] + 0.7\right\}\frac{\varpi}{s-d}\psi(Re)$$ (4.8)

where

$$\psi(Re) = 1.085 - 0.754\,exp\left(-0.132 \cdot 10^{-3}\,Re\right);$$

$$1.0 \leq s/d \leq 1.4; 7.6 \leq h/d \leq 52; 2.10^3 \leq Re \leq 2.10^5.$$

Inter-channel exchange in the bundle wall area . To know temperature behaviour in the bundle wall area of fast reactor being, as a rule , non-uniform is very important. Reliable values of transfer coefficients define authentic predictions with the use of thermal hydraulic codes. In its turn, the use of the codes for handling data on inter-channel exchange at the bundle periphery is the most effective techniques for predicting transfer coefficient in that areas of bundle.

Authors have performed experiments on the sodium model involving 37 wire wrapped pins arranged with relative pitch $s/d = 1.185$ (Fig. 4.24).One wall pin generated heat, with the length of heated section $(l_0 / d_h \approx 248)$ simulating the whole length of BN-600 core. The outlet coolant temperature measured in experiments were compared with those determined from the energy equation system:

for the internal channels (Fig. 4.25a)

$$\frac{d}{dz}(t_i w_i \omega_i) = \frac{1}{\rho c_p}\sum_{k=1}^{3}q_k\Pi_{k_i} + \sum_{j=1}^{3}\left[(\mu_{MT}^T + \mu_c^T)\frac{w_i + w_j}{2}\right.*$$

$$*\frac{\Delta s_{ij}}{\Delta s_o} + \mu_\lambda^T\,\overline{w}\left.\right](t_j - t_i)\omega;$$ (4.9)

for the wall channels (Fig. 4.25b)

$$\frac{d}{dz}(t_i w_i \omega_i) = \frac{1}{\rho c_p}\sum_{k=1}^{2}q_k\Pi_{k_i} + \mu_c^{Tp}\frac{w_i + w_3}{2}*$$

$$*(t_3 - t_i)\frac{\Delta s_{ij}}{\Delta s_o}\varpi + \mu_c^{Tp}\left(\frac{w_i + w_1}{2}t_1\frac{\Delta_{s_i1}}{\Delta_{s_o}} - \right.$$

$$\left.-\frac{w_i + w_2}{2}t_i\frac{\Delta_{s_i2}}{\Delta_{s_o}}\right)\varpi + \sum_{j=1}^{3}(\mu_{MT}^T + \mu_\lambda)\frac{w_i + w_j}{2}(t_j - t_i)\frac{\Delta_{s_{ij}}}{\Delta_{s_o}}\varpi,$$ (4.10)

where t, w - mean coolant temperature and velocity respectively; ω - channel cross-section area; q - heat flux; z - axial coordinate; Π - heat removal perimeter; Δs - the clearance between pins; λ_{pin} exchange due to heat conduction of the pin; ω_0, Δs_0 - mean cross-section area and mean clearance, respectively.

The system of energy equations is resolved by finite difference realized in the code TEMP-M. Thermal molecular-turbulent mixing factor (μ_{mt}^t) and that due to heat conduction (μ_{pin}^t) were calculated and assumed to be the same in all channels, convective mixing factor in the internal channels (μ_c^t) was also calculated and desired value of convective mixing factor between the edge channels varied.

Analysis experimental data performed invoking calculation results allows the value of thermal convective mixing factor to be evaluated in the edge area of the bundle. Fig. 4.26 presents calculated curves being distinct in value of μ_c^{tp}, that coinciding with experimental data gives required value.

Thus, features of heat transfer in the edge area of the bundle are as follows:
- by the action of coolant flow directed along the bundle wrapper the maximum temperature is displaced from the heated pin by $\Delta\varphi = 30 \div 40°$ (Fig. 4.27);
- a two-fold increase of the clearance ψ (in comparison with $\psi = 0.5$) causes an inter-channel exchange in the edge area to become more intensive (3 - 4 times) (Fig. 4.27);
- the hot spot produced by the heated pin is propagated through the approximately one-third of the bundle cross section and along the half the hexagonal wrapper (Fig. 4.24), that results from the more intensive heat transport along the wrapper than to the bundle depth (Fig. 4.28);
- dependence of mixing factor on Peclet number (Fig. 4.29) is exemplified by that it drastically increases at the small Pe and is invariant in the range of great Pe.

The data obtained are in a good agreement with the relationship:

$$\mu_c^{Tp} = \frac{\beta}{h}\left[17.34\left(\frac{\Delta}{d}\right) + 144\left(\frac{\Delta}{d}\right)^2 - 373.4\left(\frac{\Delta}{d}\right)^3\right]\Psi''(Re) \qquad (4.11)$$

at $1.0 \leq (\Delta + d) / d \leq 1.25; 7.6 \leq h / d \leq 48;$

$0.6 \cdot 10^3 \leq Re \leq 2.9 \cdot 10^4$

and non-equivalence heat and mass transport $\beta = 0.7$.

4.2. TEMPERATURE BEHAVIOUR IN FAST REACTOR FUEL SUBASSEMBLY (NOMINAL AND DEFORMED GEOMETRY)

Some general insights. In fast reactor subassembly there is a gap between wire wrap and adjacent pins, due to which pins can be shifted that causes the temperature behaviour to change. Also, a nominal geometry can be varied due to swelling, bending and other reasons. Some subassemblies come under an influence of great power, gradients, some fuel pins (or groups of pins) can produce energy more than predicted from the neutron field. Various blockages can prevent the coolant flowing through the subassembly.

As a result of the action of factors mentioned above, the temperature distribution over the subassembly becomes non-uniform. Equalizing the temperature behaviour is aided by the inter-channel exchange that is illustrated below by the examples of predictions performed for BN-350, BN-600, BN-800 and others.

The pin power, displacers' diameter, clearance between the edge pins and subassembly wrapper were varied in calculating. The effect of the three adjacent pins approach each other within tolerance (about 0.1 mm) was estimated. Under conditions of variable power across subassembly (Fig. 4.30) temperature behaviour in the internal area of subassembly follows the power variation. It should be noted, that inter-channel exchange does not overcome a general non-uniformity in the coolant temperature but has only a local effect on thermal processes. As pin power increases by 10 and 50%, the coolant temperature in adjacent channels rises by as low as 1 and 4%, respectively, whereas a neglect of inter-channel exchange is responsible for the temperature elevation by 10 and 50%, respectively.

When three internal pins approach each other till being in contact with their wire wrap, it causes the temperature to increase by 1.5%, although the coolant flow rate reduces by 15%. Shifting the edge pin to the half inter-pin clearance is found to act vigorously (about 13%) on temperature field, that may constitute a threat to fuel pin performance. Evaluation of the event without consideration of inter-channel exchange gives the temperature rise by more than 100% (Fig. 4.31). As the clearance between the wrapper and edge pins varies, the correlation between the coolant temperature in the internal channels and those in the edge ones changes. With the clearance being smaller (till $\delta = 0$), the inter-channel exchange reduces overtemperature from 40% to 8% (Fig. 4.32). Any sensors or devices inserted into the channel deforms the regular arrangement of the pins, that results in deformation of temperature fields (Fig. 4.33).

Thus, mass and energy inter-channel exchange is responsible for the more smooth temperature distribution and it follows, that maximal temperatures of pins and wrapper reduce. As this takes place, inter-channel exchange equalizes, to a large measure, a local temperature peaks and temperature non-uniformities (local hot spots) associated with the excess power of the pins, coolant superheating within a group of channels. But it should be noted, that inter-channel exchange equalizes a global non-uniformities not so intensively (Fig. 4.33, 4.30b, 4.32).

The extent to which the temperature reduces is a function of the following parameter (Fig. 4.34):

$$T_{\scriptscriptstyle M} = \mu_{\scriptscriptstyle \Sigma}^{m} \frac{z}{g},$$

(4.12)

where $\mu_{\scriptscriptstyle \Sigma}^{T}$ - total value of thermal mixing factor; z - length of heated section; g - variation in relative flow rate through the deformed channel.

Experience on fast reactor performance has shown that significant deformations take place in campaign associated with the creeping and swelling [22, 23], Fig. 4.35. The subassembly wrapper changes its from, also geometry of pin bundle is varied too.
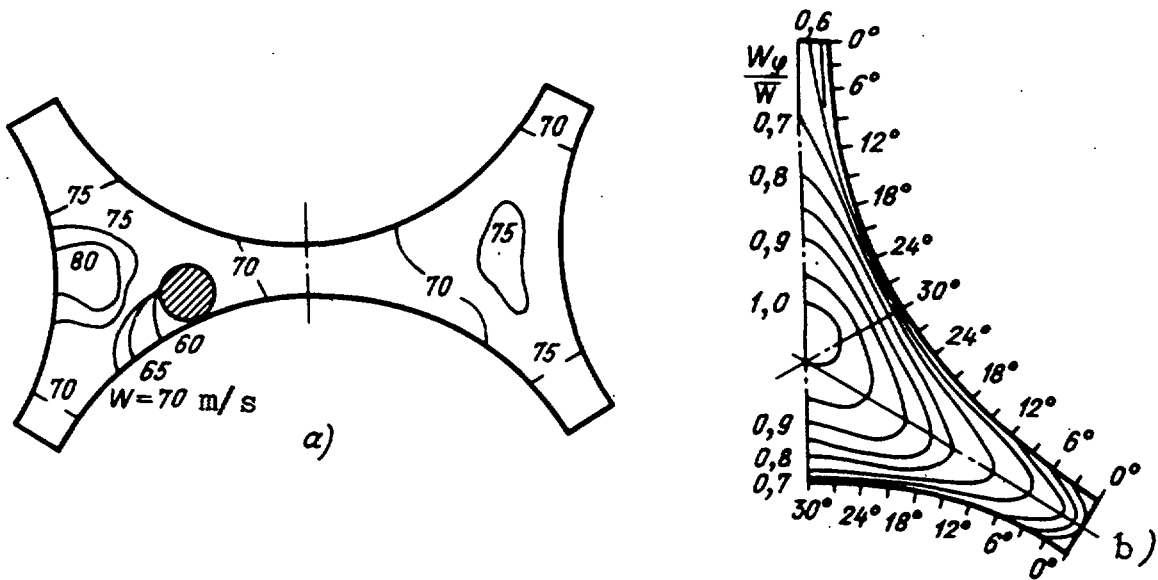
Fig. 4.23.   Axial velocity in the elementary cell formed by the wire wrapped pins
(a)smooth pins (b).
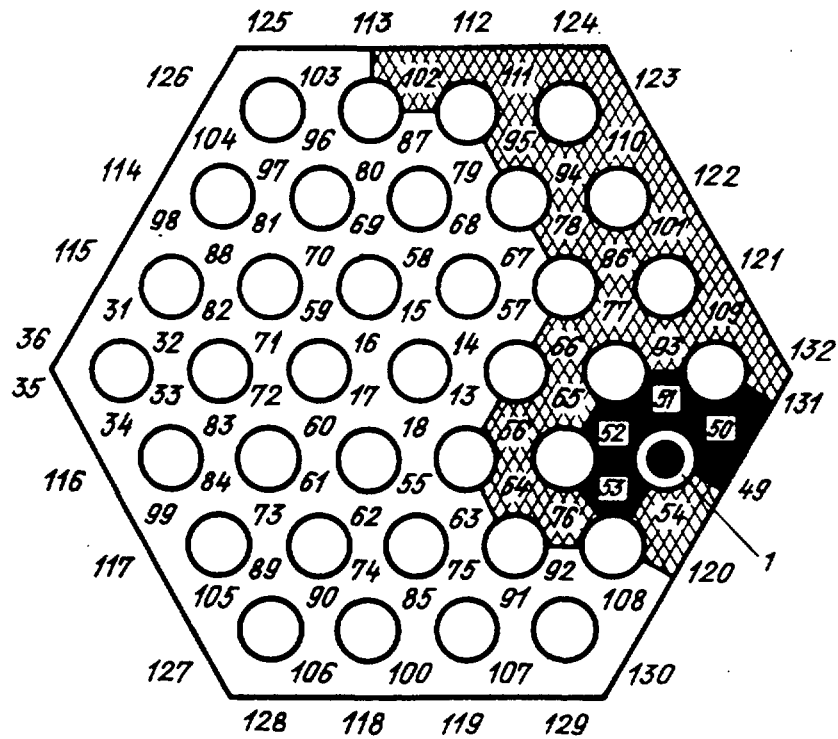
Fig. 4.24.   Model bundle cross section and outlet coolant temperature diagram:
1 - heat pin,   13÷132 - thermocouples, ☐▨■ - the darker the higher tempera-
ture.
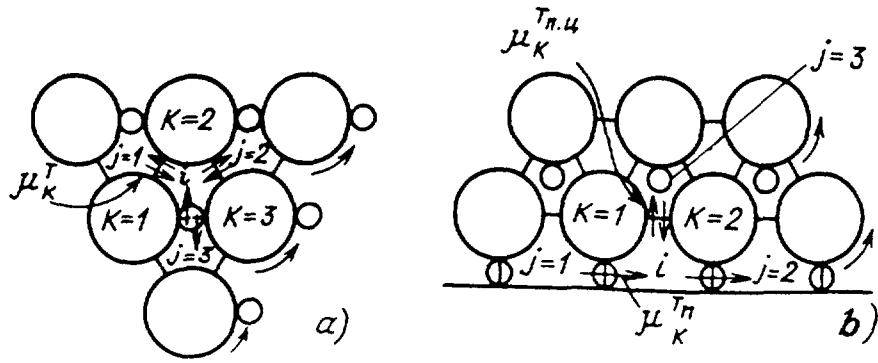
Fig. 4.25. Schematic diagram of internal (a) and edge (b) channels.
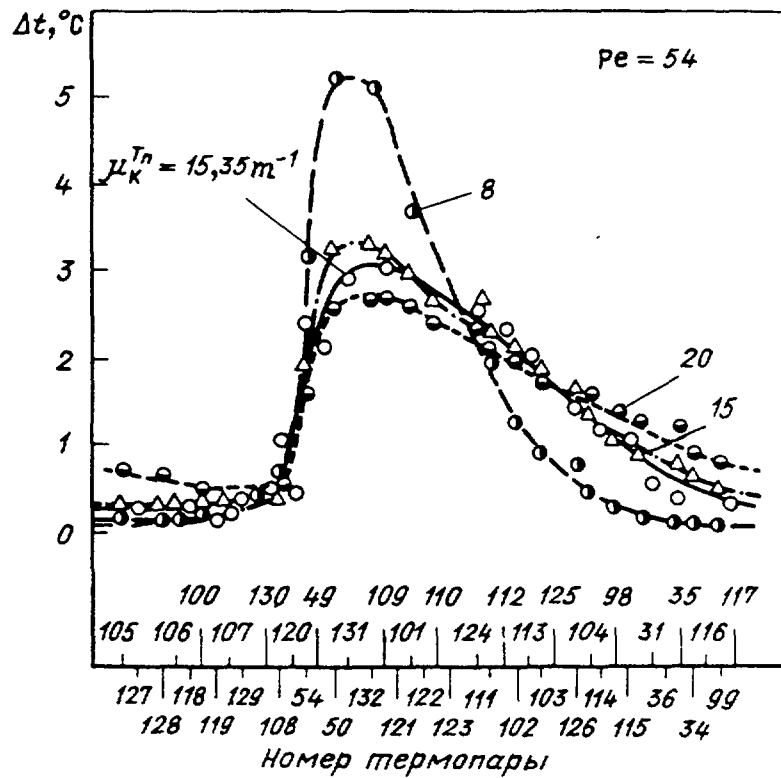
Fig. 4.26. Predicted coolant temperature along the cover for various mixing factors μ_c^t (lines) and comparison with the experiments (symbols).
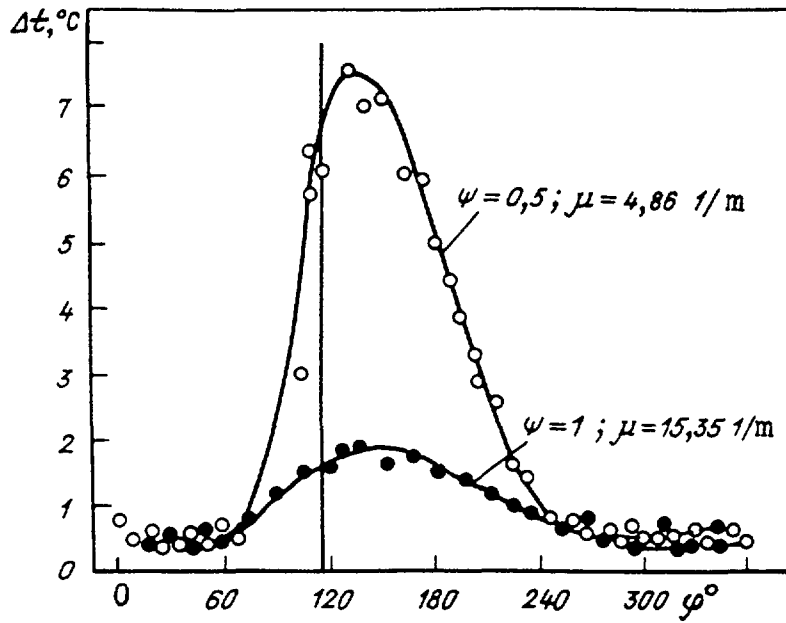
Fig. 4.27. Comparison of coolant temperature in the clearance between the pin and the model cover at Ψ = 0.5 and Ψ = 1.
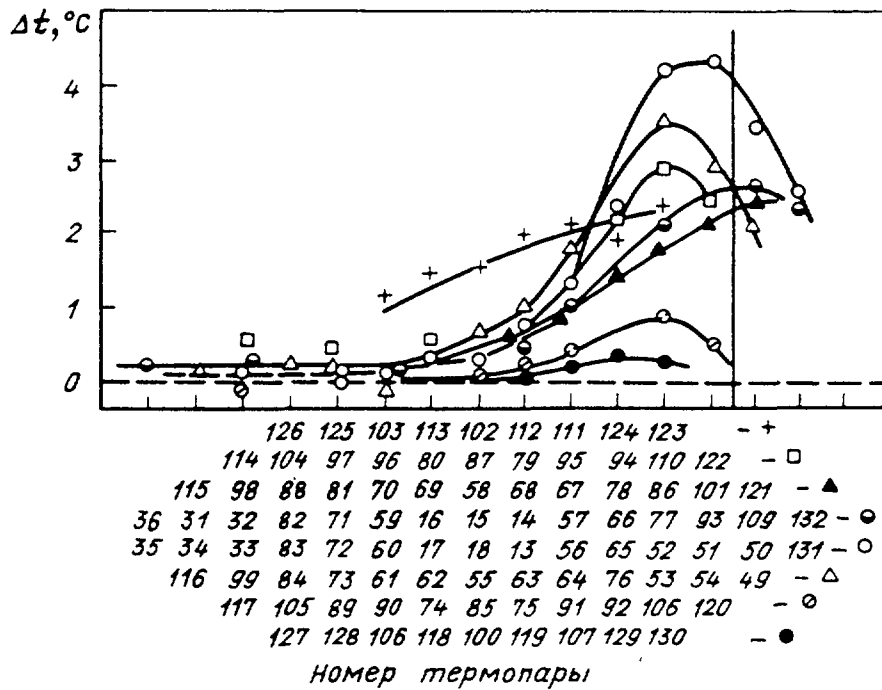

Fig. 4.28. Outlet coolant temperature along the pin rows.
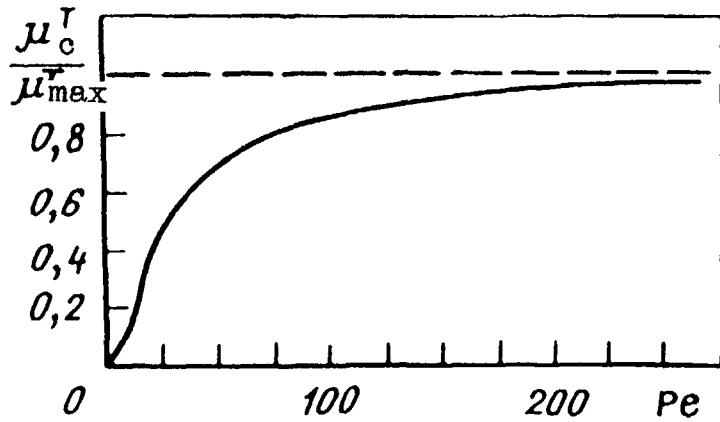
Fig. 4.29. Relative factor of interchannel convective exchange in the edge area of bundle (μ^t_{max} - maximum value of the factor being independent of Pe at great Peclet numbers.
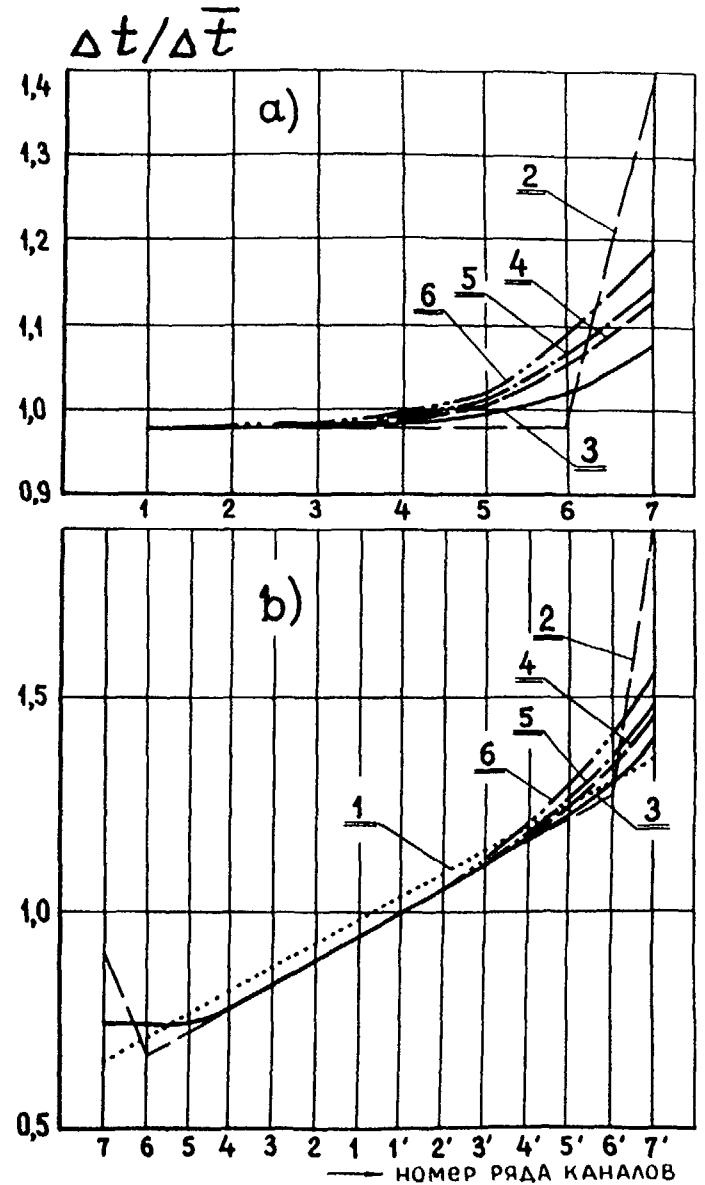

Fig. 4.30. Radial distribution of coolant temperature in the event of excess power production in the edge pin under conditions of uniform (a) and non-uniform ($q^{max} / \bar{q} = 1.35$) (b) power distribution over the subassembly cross section: 1 - power distribution, 2, 3 - nominal regime disregarding and regarding interchannel exchange, respectively; 4, 5 - excess power production 10 and 50%.
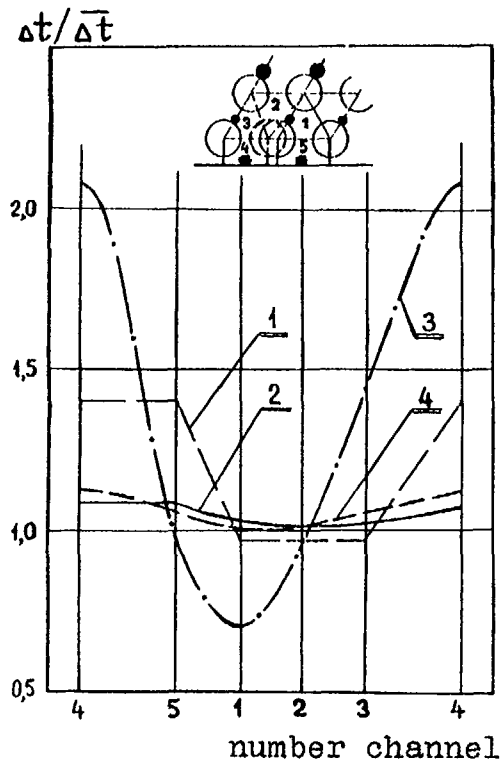
Fig. 4.31. Variation of coolant temperature around the edge pin: 1, 2 - nominal geometry disregarding and regarding interchannel exchange; 3, 4 - distorted geometry, the same.
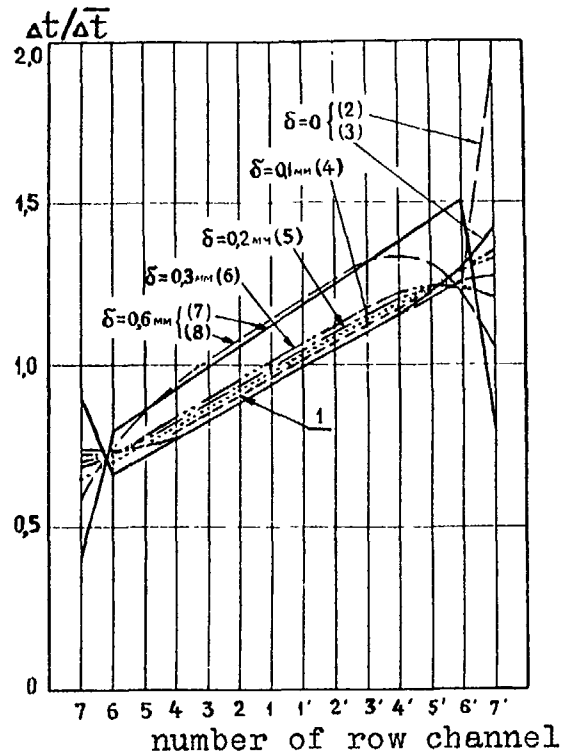
Fig. 4.32. Radial distribution of coolant temperature at a various clearances between edge pins and the cover q^{max} / $\bar{q}$ = 1.35 :

1 - power distribution; 2.7 - disregarding interchannel exchange; 3÷6, 8 - regarding interchannel exchange.
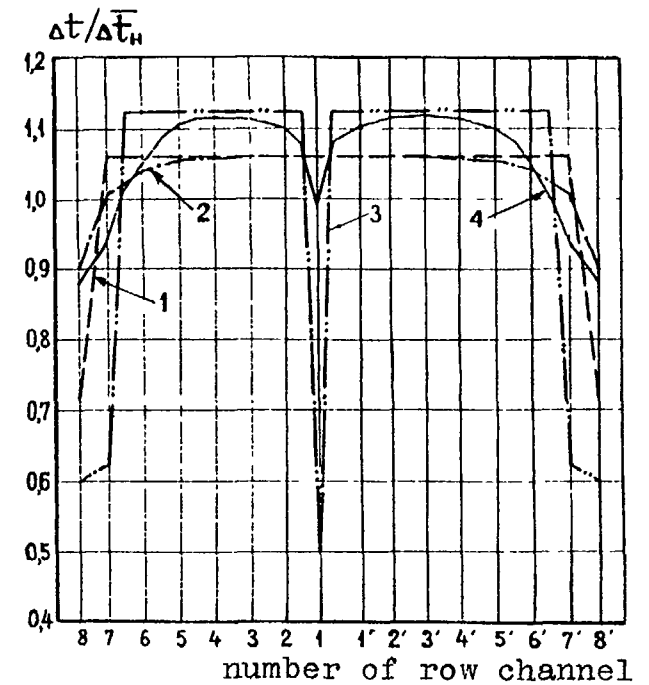
Fig. 4.33. Coolant temperature at the uniform power distribution in BN-350 subassembly: 1, 2 - subassembly without detector; 3, 4 - with detector.
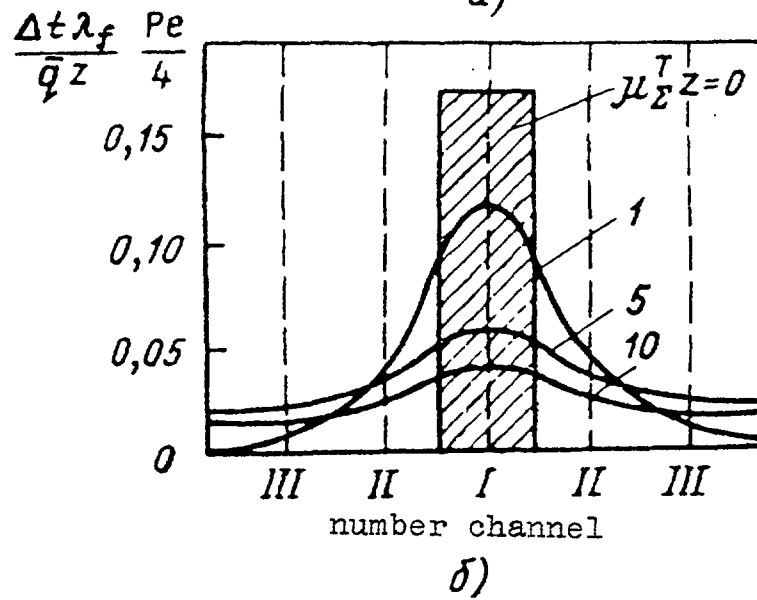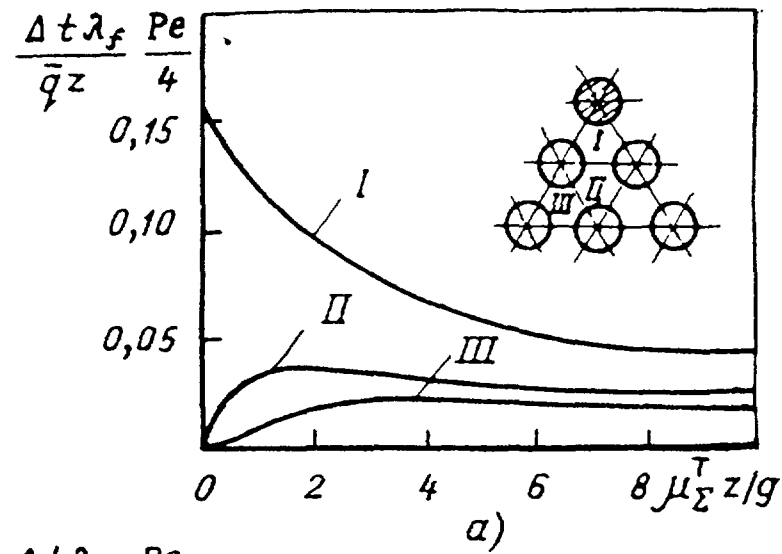
*Fig. 4.34.* *Variation of the dimensionless relative coolant temperature with the mixing factor (a) and with the subassembly radius (b) of the one pin produces heat:* I - III - *channel numbers.*

Loaded flanges

Subassembly bending
due to flanges

core

cold state | in campaing

a)

b)

c)

d)
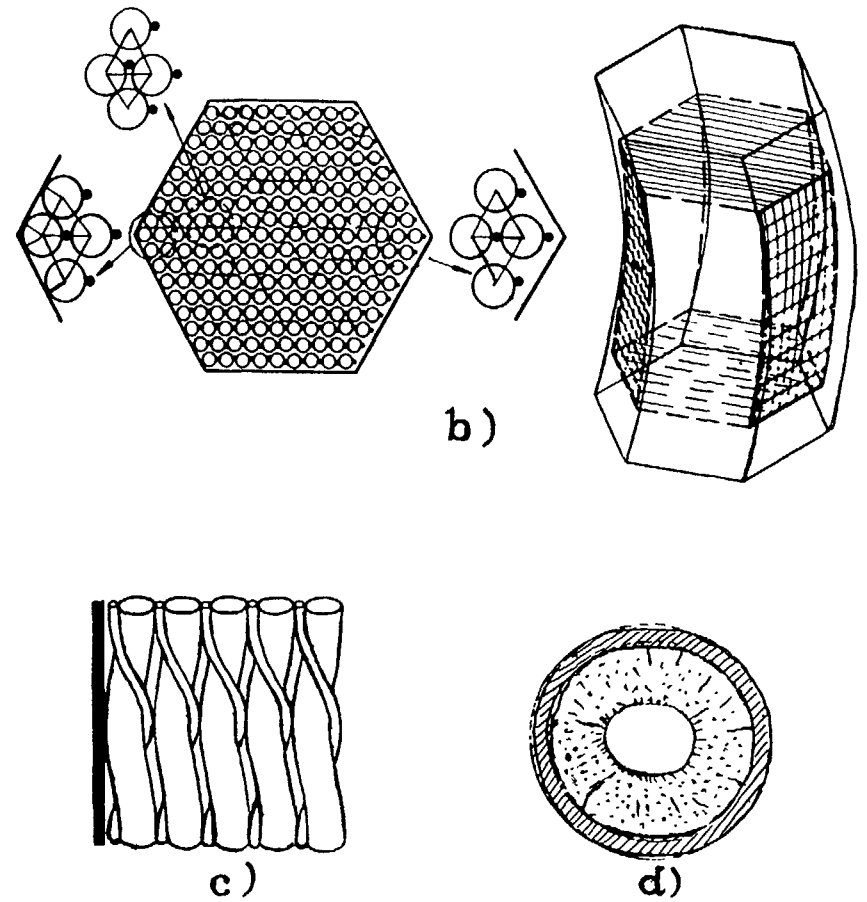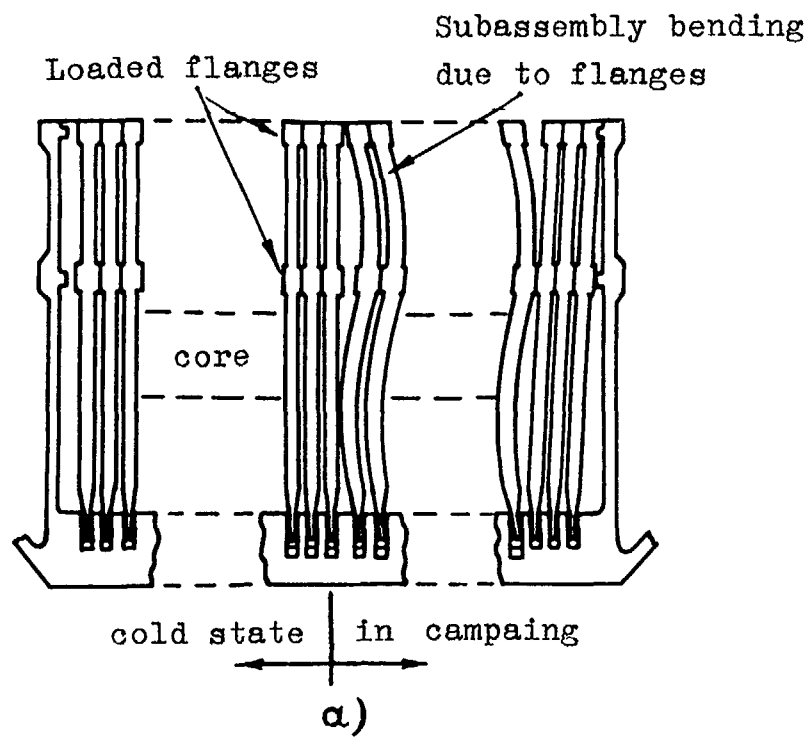
Fig. 4.35. Subassembly cover deformation (a), bending cover and bundle (b), twisting pins (c), swelling (d).

$$\Delta T_w = \left(t_w^{max} - t_w^{min}\right)\cdot\lambda_f / q\cdot R$$

7 $e = S-d$

$$\Delta T_w = 16 - 2{,}58(\lg Pe)^2 + 4{,}36(\lg Pe)$$

6 $e = S-d$

$$\Delta T_w = 107\cdot Pe^{-0{,}52}$$

5 $e = S-d$

$$\Delta T_w = 47\cdot Pe^{-0{,}47}$$

4 $e = 0{,}5(S-d)$

$$\Delta T_w = 150\cdot Pe^{-0{,}93}$$

3 $e = 0{,}5(S-d)$

$$\Delta T_w = 585{,}6\cdot Pe^{-1{,}22}$$

2 $e = 0{,}5(S-d)$

$$\Delta T_w = 60{,}9\cdot Pe^{-0{,}843}$$

1 $e = 0{,}5(S-d)$

$$\Delta T_w = 112{,}5\cdot Pe^{-1{,}028}$$

$e = 0,\ \Delta T_w = 0{,}18 + 1{,}67\exp(-1{,}0\cdot10^{-2}Pe)$
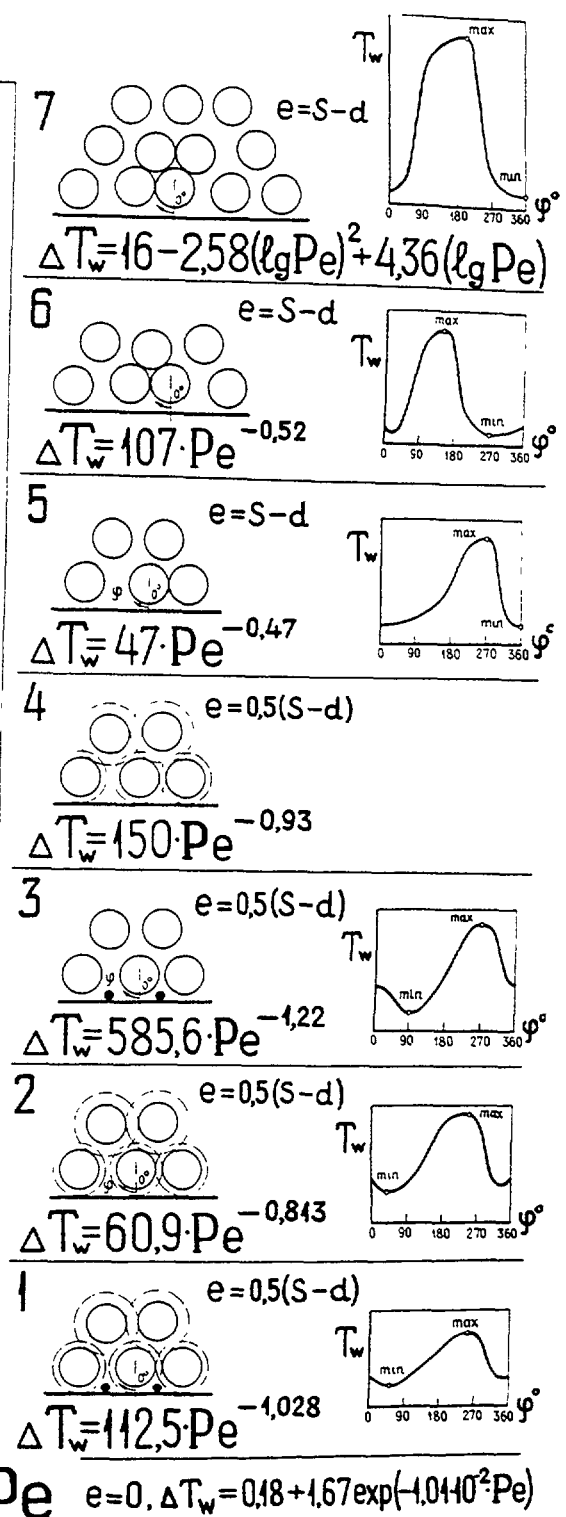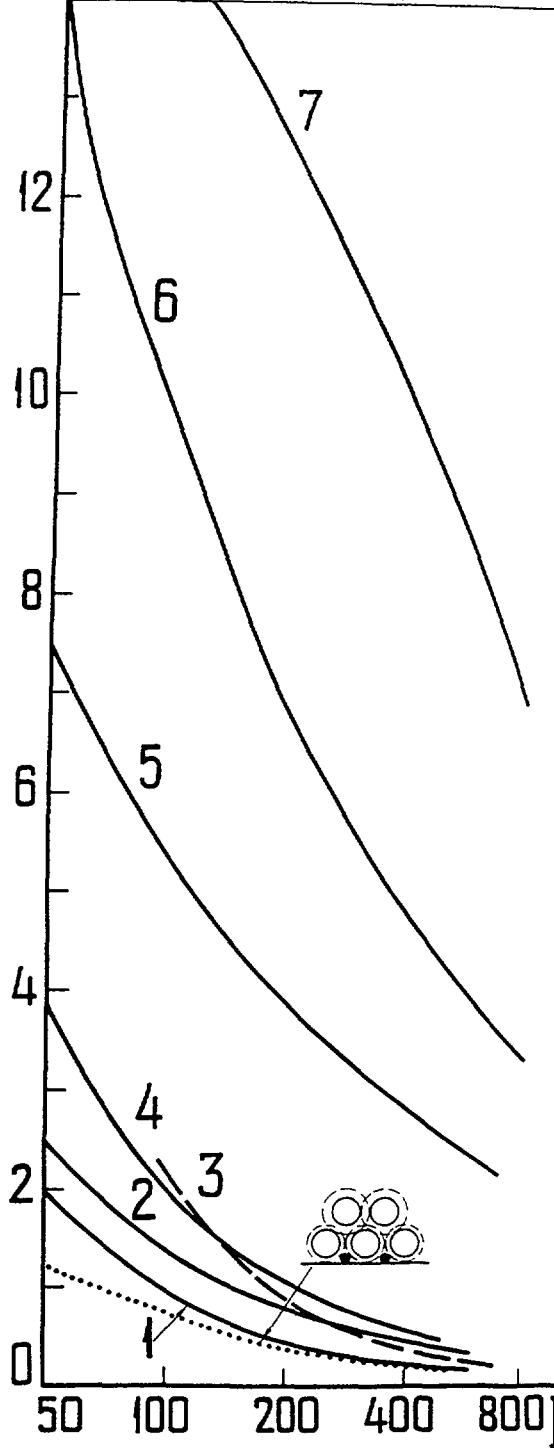
Fig. 4.36-a.

$$\Delta T_w = (t_w^{max} - t_w^{min})\lambda_f / qR$$
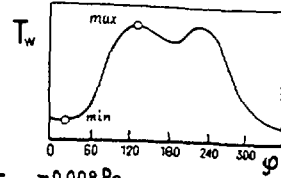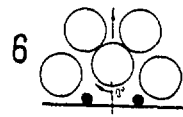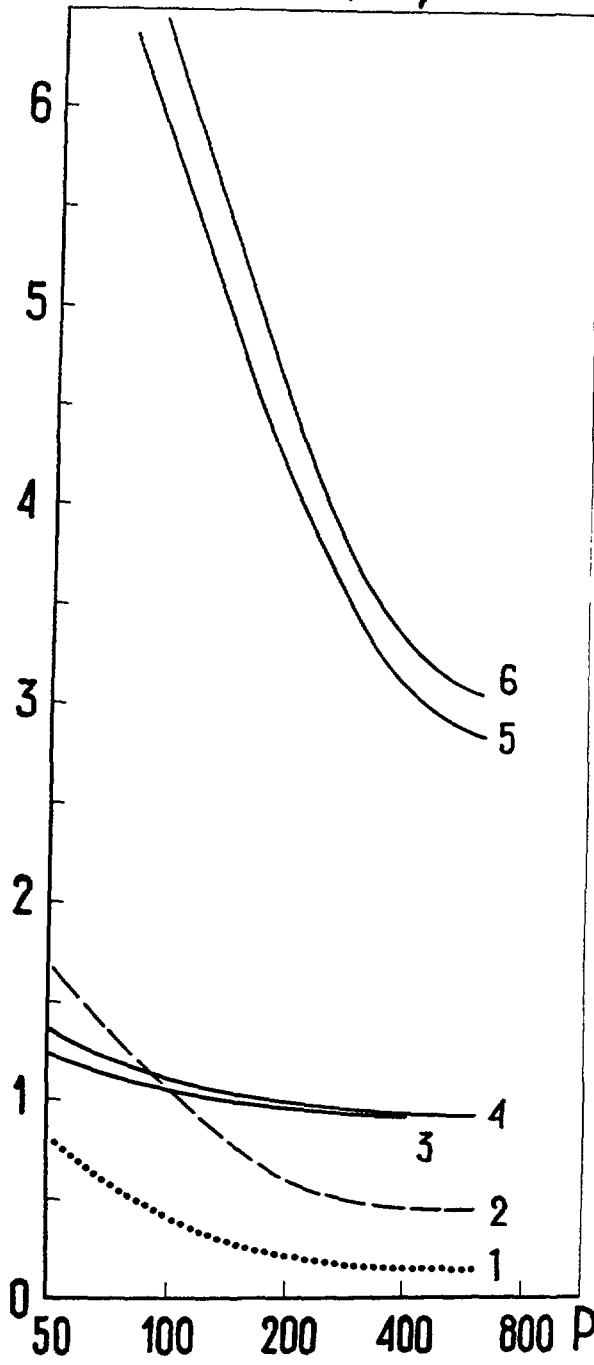
6    $\Delta T_w = 2{,}8 + 6{,}45\,e^{-0{,}008\,Pe}$
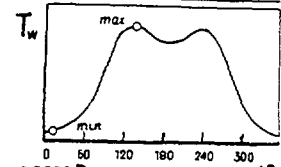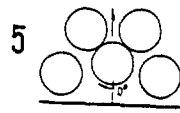
5    $\Delta T_w = 3 + 6{,}97\,e^{-0{,}0079\,Pe}$
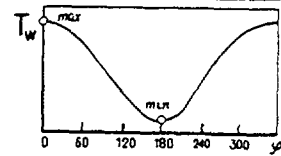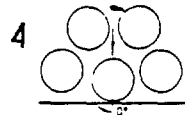
4    $\Delta T_w = 0{,}9 + 0{,}86\,e^{-0{,}014\,Pe}$
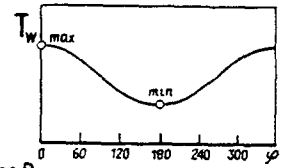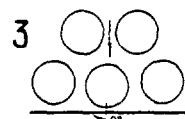
3    $\Delta T_w = 1{,}21\,e^{-0{,}0009\,Pe}$
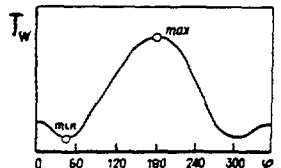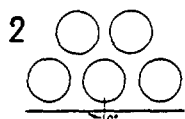
2    $\Delta T_w = 0{,}45 + 2{,}54\,e^{-0{,}014\,Pe}$
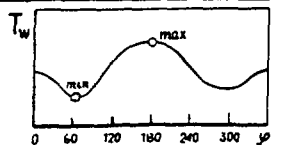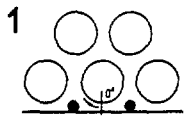
1    $\Delta T_w = 0{,}18 + 1{,}72\,e^{-0{,}02\,Pe}$

Fig. 4. 36-b.

$$\Delta T = (t_w^{max} - t_w^{min}) \cdot \lambda_f / q \cdot R$$

Fig. 4.36-c

7 — $\Delta T = 11,35 - 4,8(lgPe)^2 + 11,78\,lgPe$ e=S-d

6 — $\Delta T = 204 \cdot Pe^{-0,74}$ e=S-d

5 — $\Delta T = 573 \cdot Pe^{-0,97}$ e=S-d

4 — e=$\dfrac{S-d}{2}$

3 — $\Delta T = 100 \cdot Pe^{-0,708}$ e=$\dfrac{S-d}{2}$

2 — $\Delta T = 164 \cdot Pe^{-0,963}$ e=$\dfrac{S}{2}$

1 — $\Delta T = 112,5 \cdot Pe^{-1,028}$ e=0

$\Delta T = 92 \cdot Pe^{-1,00}$

$$\Delta T_w = \left(t_w^{max} - t_w^{min} \right) \cdot \lambda_f \big/ q R$$

5

$$\Delta T_w = 1072 \, Pe^{-1,09}$$

4

$$\Delta T_w = 185 \cdot Pe^{-0,75} \qquad e = S - d$$

3

$$\Delta T_w = 39,7 \, Pe^{-0,83} \qquad e = 0,5(S - d)$$

2

1

$$\Delta T_w = \frac{\Delta T_\pi}{1 + \beta(\varepsilon_o) \, Pe^{-m(S/d)}} \qquad e = 0$$

d)
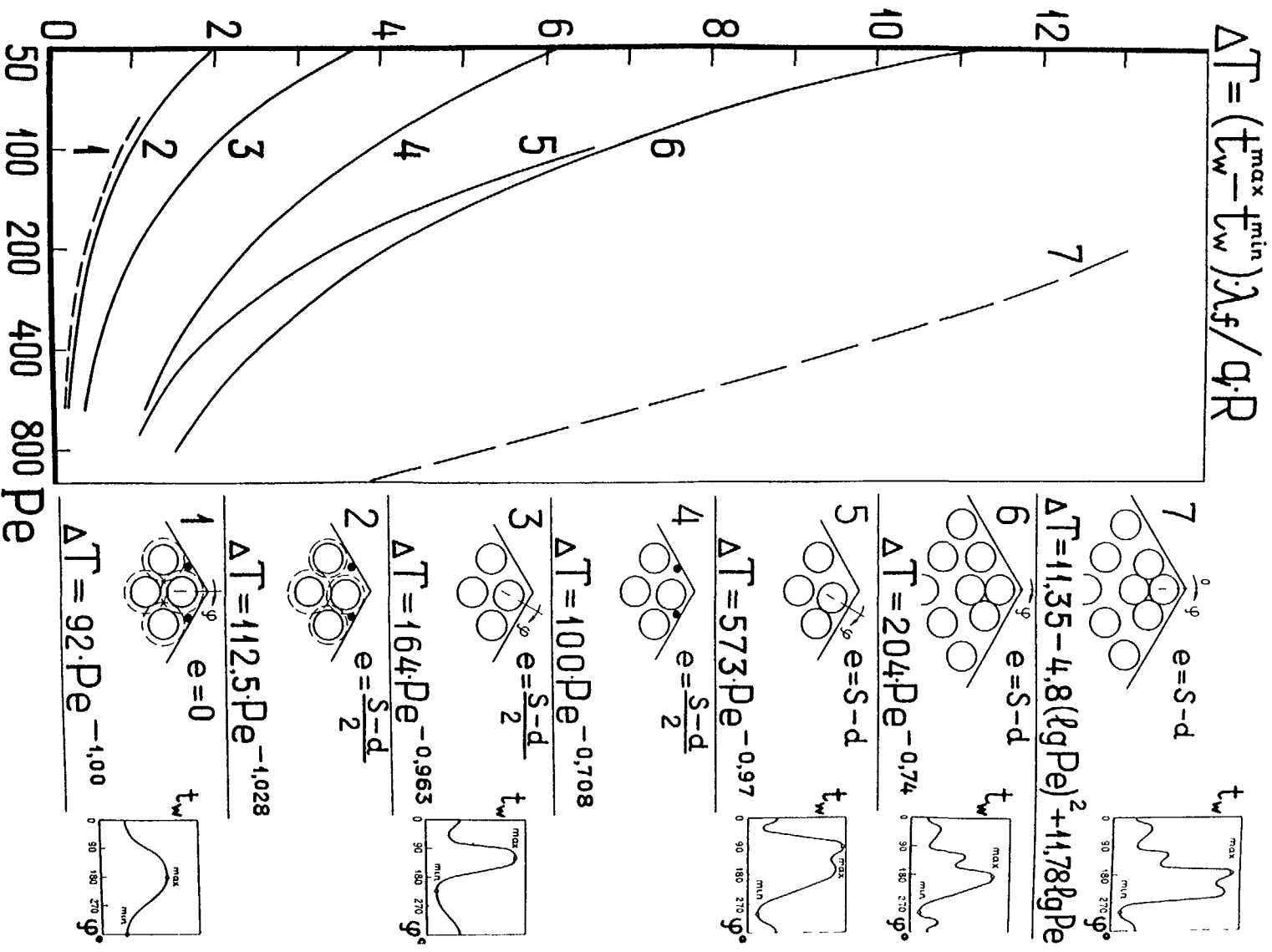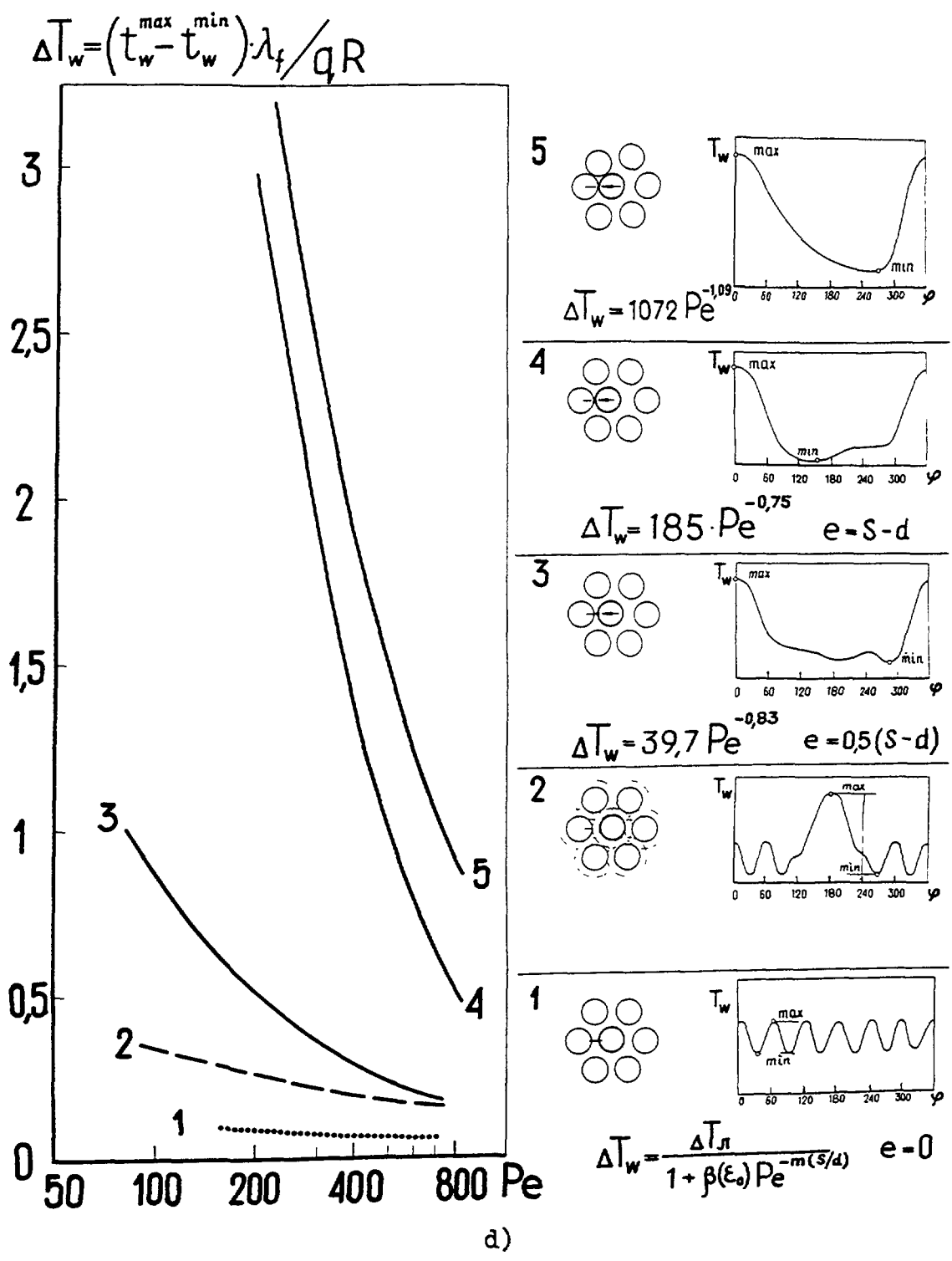
Fig. 4.36-d. Maximal azimuthal non-uniformity of pin temperature during various types of bundle deformation in the edge (a, b), corner (c) and internal (d) areas of subassembly.

197

In the last few years, a great interest has been expressed in studying temperature behaviour in deformed bundles. Experimental and analytical investigations have been carried in Russia (IPPE) [24 - 26], Czech Republic [27] and other countries [28 -30].

Systematic investigations performed in the IPPE have allowed having analyzed specific features of the formation of temperature fields under the effect of subassembly deformation and deriving the generalized relationship [31- 34]. Below is given the results of experimental and numerical investigations presented in [34 - 38]. A new data are presented also in the form of generalized approaches to temperature estimation taking into account an inter-channel exchange as a decisive factor of subassembly thermal hydraulics.

Temperature fields in different variants of pin shifting. Through the variant of the bundle deformation, when one pin or group of pins is shifted parallel with the pin axis is idealized, but it yields a very important information on the limiting temperature non-uniformities.

Temperature field of the pin shifted along the subassembly wrapper is non-symmetric: maximum temperature falls on the reduced cross section area. Values of temperature non-uniformity are significantly greater than those in nominal geometry. Temperature behavior is qualitatively the same in the bundles of wrapped and smooth pins, with and without displacers in the edge channels (Fig. 4.36 a-d).

From these figures it follows that:

• in reactors of BN-600 type (subassembly contains displacers, pins wrapped with helical wire) the maximum temperature non-uniformities around the edge pin, when it is displaced an half inter-pin clearance, is more, than expected in nominal geometry, by a factor of $1.3 \div 1.7$;

• fuel pins of BN-600 type, providing they have no wire wrap, induce significantly greater non-uniformities, that is responsible for the lesser inter-channel exchange.

Predictions of temperature non-uniformities on the single pin displacement. Temperature non-uniformities systematized in Fig. 4.36, a-d are generated in response to the inter-channel heat and mass exchange being inherent in every specific case and can be evaluated by the relationships presented in the same figures. Naturally, inter-channel exchange should be considered as a total (effective) process.

While on the subject of predictions, it should be noted that temperature distribution around the pin is determined in general case, from the conjugate problem of heat removal: heat conduction equations for the pin (with volumetric heat production for the fuel) and mass, momentum and energy conservation equations for the coolant, with the problem in irregular geometry a under conditions of non-uniform distribution of power over the subassembly cross-section being solved in sufficiently large (minimum two-there rows of interacting channels) combined domain taking account turbulence anisotropy and transverse convection due to wire wrap. The solution of the problem is fraught with a large body of calculations due to local structure of transverse coolant circulation, in particular, and is currently difficult to fulfill.

The use of the local heat transfer coefficients [39] makes the calculation procedure the more difficult to be realized, because of the need for local-coolant temperature averaged

198

through the local volumes and because of relationships available on the local heat transfer coefficients holding within the wide ranged of input parameters.

In view of the mentioned above, of particular interest is the development of approximate, but reliable, procedures for calculating temperature distribution around the pin (followed by definition of maximum pin wall temperature) based on the features of liquid metal heat removal. Among these features are a great coolant temperature ($\sim 200^0$C difference between inlet and outlet), high coolant thermal conductivity, strong inter-channel mixing due to helical wire on the pins.

In irregular areas of pin bundles a wide geometrical variations can be observed: some channels come into the compact shape, other ones are more separated. Calculations have shown, that the coolant flow rate through the compact channel falls by the order and more as compared with those in nominal channel. Respectively, the coolant temperature becomes higher (above $50 \div 100$ % of averaged coolant temperature). Thus, one of the most important problem is to determine the coolant temperature distribution having regard for mass, momentum and energy macro-transport. Such a predictions can be based on the subchannel approach. As indicated above, domain (subassembly) is divided on the cells within which the coolant temperature is defined from the mass, momentum and energy conservation equations.

Thus, we can specify that premises to approximate calculation of pin temperature distribution are as follows:
- the coolant temperature distribution over the channels surrounding the fuel pin is crucial in determining pin temperature;
- an inter-channel exchange exerts a primary control over equalization of the coolant temperature around the pin;
- heat removal in the clearance between pins is of a local nature;
- temperature in the inherent points of the pin cladding (narrow, wide parts of the channel) can be determined as superposition of local coolant temperature, temperature difference «wall-liquid» and wall temperature non-uniformity.

Numerical scheme (Fig.4.37) assumes the following operations:
- prediction of coolant temperature distribution over the channel surrounding the pin;
- the first harmonics is isolated from the coolant temperature distribution

$$t_f^{(1)}(\varphi) = \bar{t}_f + \alpha \cos\varphi + b \sin\varphi \qquad (4.13)$$

where

$$\bar{t}_f = \frac{1}{2\pi} \int_o^{2\pi} t_i d\varphi \ ; \quad a = \frac{1}{\pi} \int_o^{2\pi} t_i \cos\varphi \ d\varphi \ ;$$

$$b = \frac{1}{\pi} \int_o^{2\pi} t_i \sin\varphi \ d\varphi \ ;$$

- pin surface temperature in the narrow part of the channel is calculated as a sum of arithmetic mean coolant temperature between the channels i and j and temperature difference «wall-liquid»

$$t_{w_{ij}} = t_f^{(1)}\left(\varphi_{ij}\right) + \frac{q d_h}{Nu\lambda_f},$$ (4.14)

where

$$Nu = Nu\left[s_{ij}/d, Pe\left(w_{ij}, s_{ij}/d\right), \varepsilon\right]; \quad w_{ij} \approx \left(w_i + w_j\right)/2;$$

- the first harmonics in the pin temperature distribution (dotted line in Fig.4.37) is isolated:

$$\bar{t}_w^{(1)} = \bar{t}_w + c\ \cos\varphi + d\ \sin\iota\varphi,$$ (4.15)

where

$$\bar{t}_w = \frac{1}{2\pi}\int_o^{2\pi} t_{w_{i,i+1}} d\varphi \ ; \quad c = \frac{1}{\pi}\int_o^{2\pi} t_{w_{i,i+1}} \cos\varphi\ d\varphi \ ; \quad d = \frac{1}{\pi}\int_o^{2\pi} t_{w_{i,i+1}} \sin\varphi\ d\varphi \ ;$$

- temperature in the inherent points of the pin perimeter is defined as superposition of the first harmonies and local temperature difference

$$t_w = t_w^{(1)} + \Delta t_{w_j} \ ,$$ (4.16)

where it is in the clearances between the channels i and j that:

$$\Delta t_{w_j} = \frac{Z}{Z+1}\Delta\ t_\varphi^{loc},$$ (4.17)

Here,

$$Z = \frac{t_w^{max} - \bar{t}_w}{\bar{t}_w - t_w^{min}} = Z\left(s_{ij}/d, \varepsilon\right) \ ; \quad \Delta t_\varphi^{loc} = \frac{q(d/2)}{\lambda_f}\Delta T_\varphi\left[\frac{s_{ij}}{d}, Pe\left(w_{ij}, \frac{s_{ij}}{d}\right), \varepsilon\right] \ ;$$

in the wide part of the channels:

$$\Delta t_{w_j} = -\frac{\Delta t_\varphi^{eïê}}{Z+1},$$ (4.18)

where

$$Z = Z\left(\frac{s_{ij} + s_{jm}}{2d}, \varepsilon\right) \ ; \quad \Delta t_\varphi^{loc} = \frac{q(d/2)}{\lambda_f}\Delta T_\varphi\left[\frac{s_{ij} + s_{jm}}{2d} \ ; \ Pe\left(w_j, \frac{s_{ij} + s_{jm}}{2d}\right), \varepsilon\right]$$

- continuous pin wall temperature distribution is found by numerical interpolation (Lagrange's formula, for example):

$$t_w = \sum_{j=0}^{n} t_{w_j} L_j(\varphi),$$ (4.19)

where the functional has a form

$$L_j(\varphi) = \frac{(\varphi - \varphi_o)\ldots(\varphi - \varphi_{j-1})\ldots(\varphi - \varphi_{j+1})\ldots(\varphi - \varphi_n)}{(\varphi_j - \varphi_o)\ldots(\varphi_j - \varphi_{j-1})\ldots(\varphi_j - \varphi_{j+1})\ldots(\varphi_j - \varphi_n)},$$

The use of the spline approximation, for example a cubic spline-functions, is preferential. In this case, finding the interpolating spline-functions reduces to the solution of the system of linear equations. In each interval (φ_{j-1}, φ_j):

$$t_w(\varphi) = -s_{j-1}^2 \frac{(\varphi - \varphi_j)^3}{6\Delta_j} + s_j^2 \frac{(\varphi - \varphi_{j-1})^3}{6\Delta_j} +$$

$$+ \left(\frac{t_{w_j}}{\Delta_j} - \frac{s_j \Delta_j}{6} \right) (\varphi - \varphi_{j-1}) - \left(\frac{t_{w_{j-1}}}{\Delta_j} - \frac{s_{j-1}\Delta_j}{6} \right) (\varphi - \varphi_j),$$ (4.20)

where Δ_j interval of partition. Thus, we obtain the system of equations:

$$s_{j-1}^2 \frac{\Delta_j}{6} + s_j^2 \frac{\Delta_j + \Delta_{j+1}}{3} + s_{j+1} \frac{\Delta_{j+1}}{6} =$$

$$= \frac{t_{w_{j+1}} - t_{w_j}}{\Delta_{j+1}} - \frac{t_{w_j} - t_{w_{j-1}}}{\Delta_j}, \quad j = 1,2\ldots, \ n-1$$ (4.21)

derived with reference to (n+1) unknown variables $S_o^2, S_1^2, \ldots, S_n^2$. To define these variables identically, we add the equations resulting from the periodic temperature distribution:

$$s_o^2 = s_n^2, \quad s_1^2 = s_{n+1}^2.$$ (4.22)

In so doing, the first equation is substituted for the following

$$s_o^2 = s_n^2, \quad s_1^2 = s_{n+1}^2.$$ (4.23)

and new equation is added

$$s_1^2 \frac{\Delta_1 + \Delta_2}{3} + s_2^2 \frac{\Delta_2}{6} + s_n^2 \frac{\Delta_1}{6} = \frac{t_{w1} - t_{wn}}{\Delta_1} - \frac{t_{wn} - t_{wn-1}}{\Delta_n}$$ (4.24)

A curvature of interpolation curve is appears to be minimum. Values of Nu, ΔT_φ and Z in the correlations mentioned above are calculated in [34-36, 41] for regular pin bundles. Authors have derived the following generalized formula (regular bundle):

$$1.0 \leq s/d \leq 1.15; \quad 1 < Pe < 1200; \quad \varepsilon > 0.2)$$

$$\Delta T_\varphi = A(s/d)\frac{1 - exp(-X)}{X} \tag{4.25}$$

where

$$A(s/d) = exp\left[1.411 - \frac{6.93(s/d)\ln(s/d)}{\sqrt{s/d-1}}\right]; \tag{4.26}$$

$$X = B(s/d)\varepsilon^{C(s/d)} + \beta_1(\varepsilon)\beta_2(s/d)Pe^{\gamma_1(\varepsilon)\gamma_2(s/d)}; \tag{4.27}$$

$$B(s/d) = exp\left\{2.3026\left[1 - (s/d-1)^{0.272-0.6(s/d-1)}\right]\right\}; \tag{4.28}$$

$$C(s/d) = 0.71\left[exp\left(\sqrt{s/d-1}\right)\right]/\left[(s/d)0.71^{(s/d-1)/2}\right]; \tag{4.29}$$

$$\left.\begin{array}{l}\beta_1(\varepsilon) = 0.9815\varepsilon + 1.0923\varepsilon^2 - 0.0892\varepsilon^3; \\ \\ \beta_2(s/d) = 0.154\dfrac{1 - exp\left[-330(s/d-1)\right]}{330(s/d-1)} - 0.12\,exp\left[-750(s/d-1)\right];\end{array}\right\} \tag{4.30}$$

$$\left.\begin{array}{l}\gamma_1(\varepsilon) = exp\left[-\varepsilon/(1+1.68\varepsilon)\right]; \\ \\ \gamma_2(s/d) = 0.74\left(1 + \left\{(s/d-1)/[1-1.5(s/d-1)]\right\}\right).\end{array}\right\} \tag{4.31}$$

Correlation (4.25) describes ean xperimental data in a wide ranges of parameters (Fig.4.38).

The following expression on maximum pin temperature non-uniformity in the event of the pin is shifted in accordance with the Fig. 4.37 was obtained from the subchannel approach:

$$\Delta T_w^{max} = \frac{t_w^{max} - t_w^{min}}{qd/2}\lambda_f = \frac{8}{Pe_o}\frac{L}{d}\left(\frac{\Delta t_i}{\Delta t_o} - \frac{\Delta t_p}{\Delta t_o}\right) +$$

$$+\left(\frac{2d_{z_i}/d}{Nu_i} - \frac{2d_{z_p}/d}{Nu_p}\right) + \left(\frac{Z_i}{Z_i+1}\Delta T_{\varphi_i} + \frac{1}{Z_p+1}\Delta T_{\varphi_p}\right), \tag{4.32}$$

where Pe and Δt_o - Peclet number and coolant overtemperature in the internal standard channel, i - subscript of the maximum temperature channel; P - subscript of the minimum temperature channel.

Relative coolant temperature difference is found as:

$$\frac{\Delta t_i - \Delta t_p}{\Delta t_o} = \left(\frac{1}{g_i} - 1\right) f\left(T_{M_i}\right) + \left(1 - \frac{1}{g_p}\right) + \left(1 - \frac{1}{g_p}\right) f\left(T_{M_p}\right) ,$$ (4.33)

where

$$g_i = W_i\omega_i / \left(W_o\omega_o\right); \quad g_p = W_i\omega_i / \left(W_o\omega_o\right); \quad f\left(T_M\right) = \frac{1 - \exp\left(-T_M\right)}{T_M} ;$$

$$T_{M_i} = \frac{\left(\mu_{il}^m + \mu_{if}^m\right)z}{g_i}; \quad T_{M_p} = \frac{\left(\mu_{pl}^m + \mu_{pq}^m\right)z}{g_p} ,$$ (4.33a)

g_i, g_p – relative coolant flow in the i-th and p-th channels; Z - axial coordinate; $\mu_{il}^T, \mu_{if}^T, \mu_{pr}^T, \mu_{pq}^T$ - mixing factors in the clearances between the channels i and l, i and f, p and q respectively, calculated by relatioships from [34, 35]:

$$Z_{ip} = \left(t_w^{max} - \bar{t}_w\right) / \left(\bar{t}_w - t_w^{min}\right)$$ (4.34)

Fig.4.37 compares the predicted and experimental temperature distributions around the shifted pins. As it is evident, the use of reliable data on mixing factors offer good relation.

4.3. FUEL PIN TEMPERATURE DISTRIBUTION IN SOME VARIANTS OF DEFORMATION

Below is presented some variants of deformation when three or four smooth pins are displaced until touching one another (Fig.4.39, a-e). It seems likely that variant, when four smooth pins touch each other, involves the high temperature non-uniformities, as the area being close to infinite compact bundle and the area with subcooled liquid near the plane wrapper side are formed. Temperature field inherent at the shifting four pins is presented in Fig. 4.40.

The main effects and relationships. Temperature distribution is, in general, of a smooth character (the first harmonics in Fourier series dominates); local temperature splashes in the points of contact is reflected just at the beginning of the heated section, when coolant temperature is not so high.

The maximum temperature non-uniformities in deformed bundle produced by three shifted pins are followed the empirical correlations:

edge pins

$$\Delta T_w = \frac{t_w^{max} - t_w^{min}}{qR} \lambda_f = 107 Pe^{-0.52}, \quad 1 / d_h = 185; \quad 50 \le Pe \le 800;$$ (4.35)

corner pins

$$\Delta T_w = 204 Pe^{-0.74}, \quad 1/d_h = 185; \quad 50 \le Pe \le 800 \quad ; \tag{4.36}$$

internal pins

$$\Delta T_w = 1072 Pe^{-1.09}, \quad 1/d_h = 185; \quad 70 \le Pe \le 800. \tag{4.37}$$

Heat removal from the edge pins in the event of four shifted pins is less than those under nominal geometrical conditions:

edge pin (Fig.4.41):

$$Nu = 0.23 + 10^{-4} Pe^{1.28}, 20 \le Pe \le 800 \quad ; \tag{4.38}$$

corner pin:

$$Nu = 0.19 + 1.2 . 10^{-4} Pe^{1.28}, 20 \le Pe \le 800 \quad . \tag{4.39}$$

Fig.4.41 illustrates the effects of pin shifting.

Maximum temperature non-uniformities in the event of the four smooth pins come in to contact over the bundle length (without displacers) are evaluated as:

edge pins (Fig.4.39,d)

$$\Delta T_w = \frac{t_w^{max} - t_w^{min}}{qR} \lambda_f = 16 - 2.58 (\lg Pe)^2 + 4.36 \lg Pe, \tag{4.40}$$

$$1/d_h = 185; \quad 30 < Pe < 800 \quad ;$$

corner pins (Fig.4.39,e)

$$\Delta T_w = \frac{t_w^{max} - t_w^{min}}{qR} \lambda_f = 11.35 - 4.8 (\lg Pe)^2 + 11.78 \lg Pe \quad , \tag{4.41}$$

$$1/d_h = 185, \quad 30 < Pe < 800 \quad .$$

Predictions of temperature behaviour when three smooth pins come in to contact (subchannel approach) have allowed the following correlation to be derived:

$$\Delta t_c = \Delta t_o \frac{1 - \exp(-T_M)}{T_M} \left(\frac{1}{g_c} - 1 \right) (1 + 0.16 T_M) \quad , \tag{4.42}$$

where $\quad T_M = \dfrac{3 \mu_\lambda^m z}{g_c} ; \quad g_c = \left(\dfrac{\xi_c}{\xi_o} \right)^{4/7} \left(\dfrac{d_{z_c}}{d_{z_o}} \right)^{5/7} \dfrac{\omega_c}{\omega_o} \quad ,$

$\mu_{\lambda pin}^{T}$ – mixing factor due to pin heat conduction, z - distance from the beginning of the heated section, subscript «c» means compact arrangement of the pins..

Temperature non-uniformity of the pins producing the compact channel can be evaluated as:

$$t_w^{max} - t_w^{min} = \Delta t_o\left(\frac{\Delta t_c}{\Delta t_o} + \Delta T_c^{max}\frac{Z_c}{Z_c + 1}\frac{Ped}{8L}\right) .$$

(4.43)

with the maximum pin temperature being:

$$t_w^{max} = t_{ex} + \Delta t_o\left[\frac{\Delta t_c}{\Delta t_o} + \left(\frac{d_{hc}/L}{Nu_c} + \frac{Z_c}{Z_c + 1}\Delta T_c^{max}\frac{d}{2L}\right)\frac{Pe}{4}\right] ,$$

(4.44)

where Nu_{comp}, ΔT_{comp} are calculated in accordance with Chapter 3.

Relationships (4.42-4.44) show that high coolant temperature, due to the compact channel is formed, can result in the intolerable pin temperature at the inherent for fast reactor range (Pe = 100÷400).

Statistic evaluations. Universal relationship. Variation in the in-pile channel geometry is of statistic character. Under these conditions, relatioships mentioned above can yield only some limit values. At the same time, geometry of real subassembly are so widely diverse, that it is hardly probable their modeling and investigation under specific conditions. The temperature non-uniformities is required to be estimated for various kind of the bundle deformation (taking into account statistic nature of variation of the channel cross sections, for which the more universal, than the correlations discussed above, relationships should be derived.

These relationships can be generalized as a function of geometrical parameter in the form:

$$\Delta T_w = \frac{t_w^{max} - t_w^{min}}{\overline{qR}}\lambda_f = K + M\exp(-mPe) .$$

(4.45)

where the generalized geometrical parameter represents the relative area of deformed channel being of a maximum cross section.

$$f = \varpi / \omega_i^* ,$$

(4.46)

where $\varpi = \sum_{i=1}^{h}\omega_i/n$ - area of the averaged channel (Fig.4.42); ω_i^* – area of the largest channel Factor K, M and m are the functions of f (Fig.4.42)/ The sum of factors K and M represents the value ΔT_w in laminar flow thorough the channel under consideration. Three domains can be separated:
1. 0.5 < f <0.65 - large temperature disturbances;
2. 0.65 < f < 0.92 - moderate temperature disturbances;
3. 0.92 < f < 1.0 - disturbances being opposite in sign to 1 and 2.
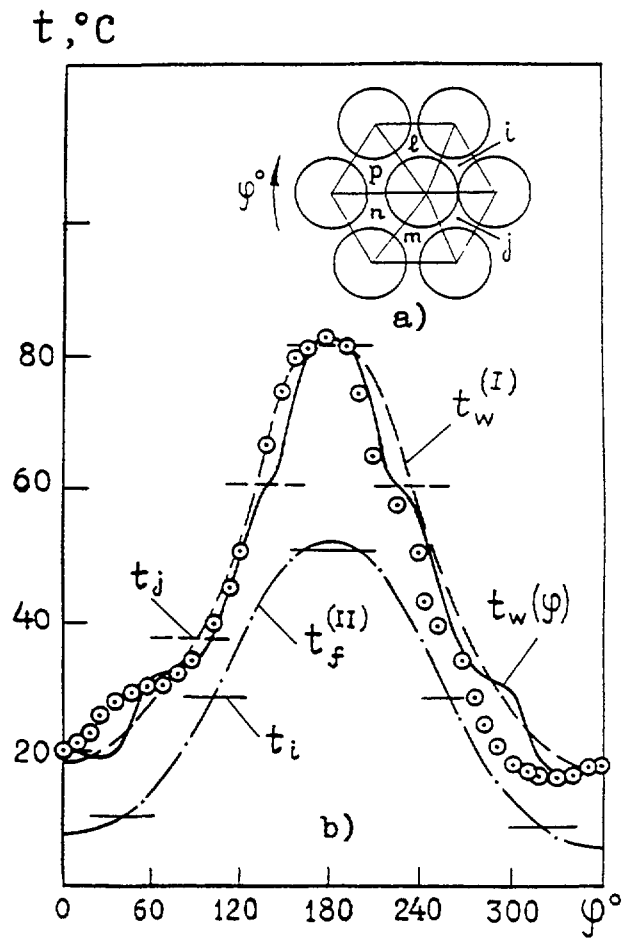
Fig. 4.37. Fragment of deformed bundle (a) and algorithm of .calculation of temperature distribution over the shifted pin (b):

t_i *- coolant temperature,* t_j *- wall temperature averaged over the separate parts of surface,* ⊙ *-experimental data,* ———— *- final distribution* $t_w(\varphi)$.
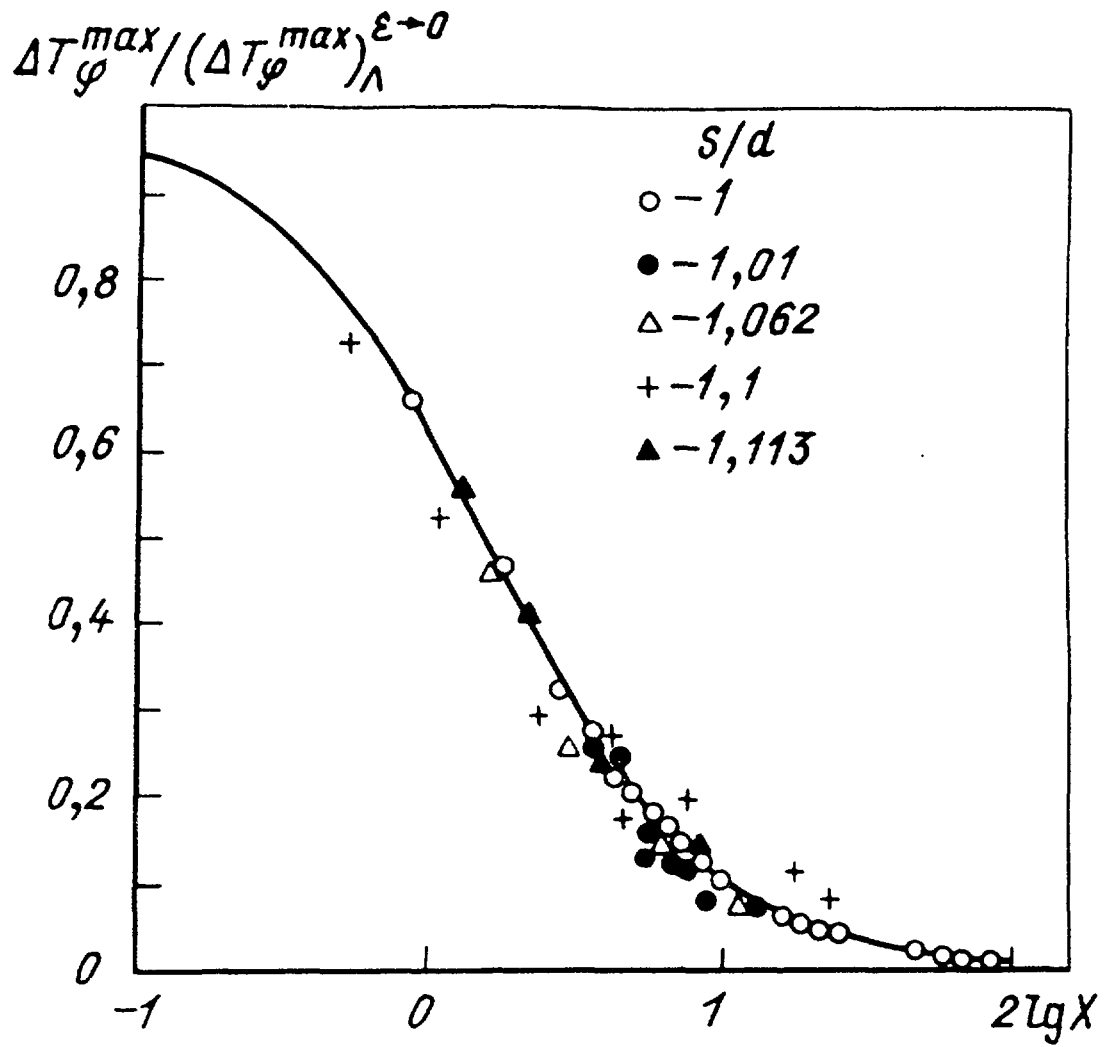
Fig. 4.38. Predictions of maximum temperature non-uniformity in the regular triangular pin bundle compared with experiments: $(\Delta T_\varphi^{max})_\Lambda^{\varepsilon \to 0}$ -laminar flow.
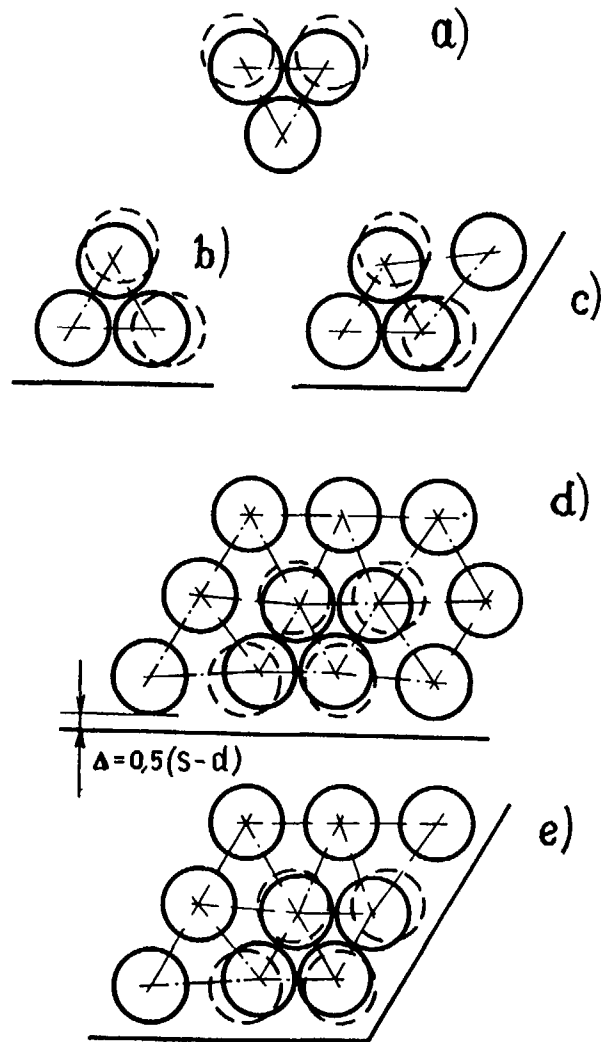
Fig. 4.39. Schematics of combined shift of non-wrapped pins in the internal (a), edge (b, d) and corner (c, e) areas.
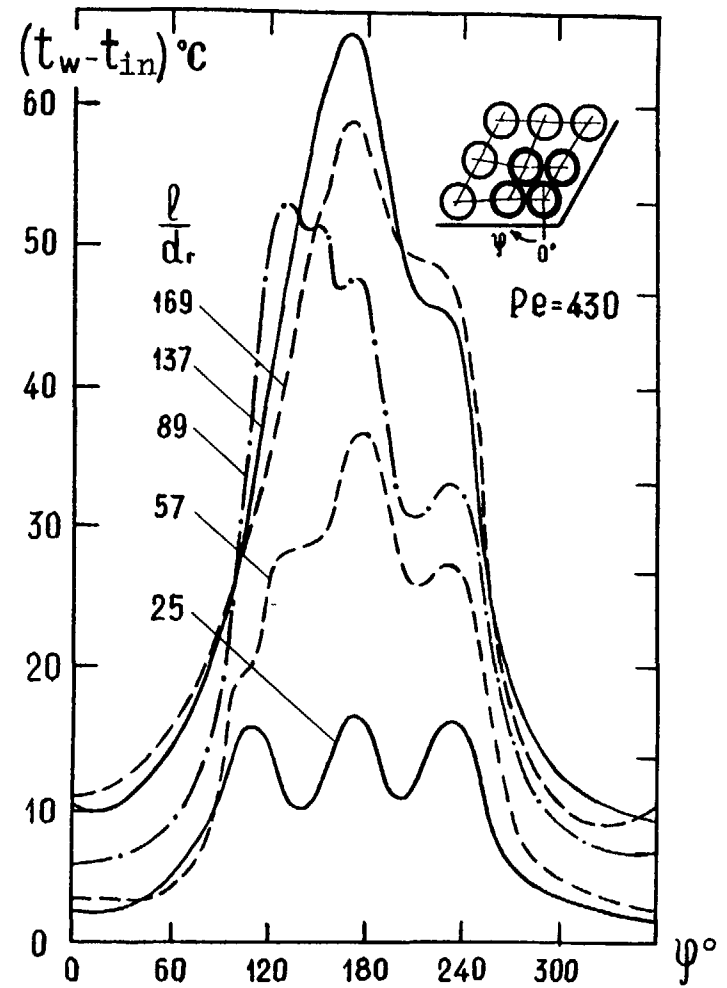
Fig. 4.40. Temperature around the smooth corner pin, when four pins are shifted until they touch one another.
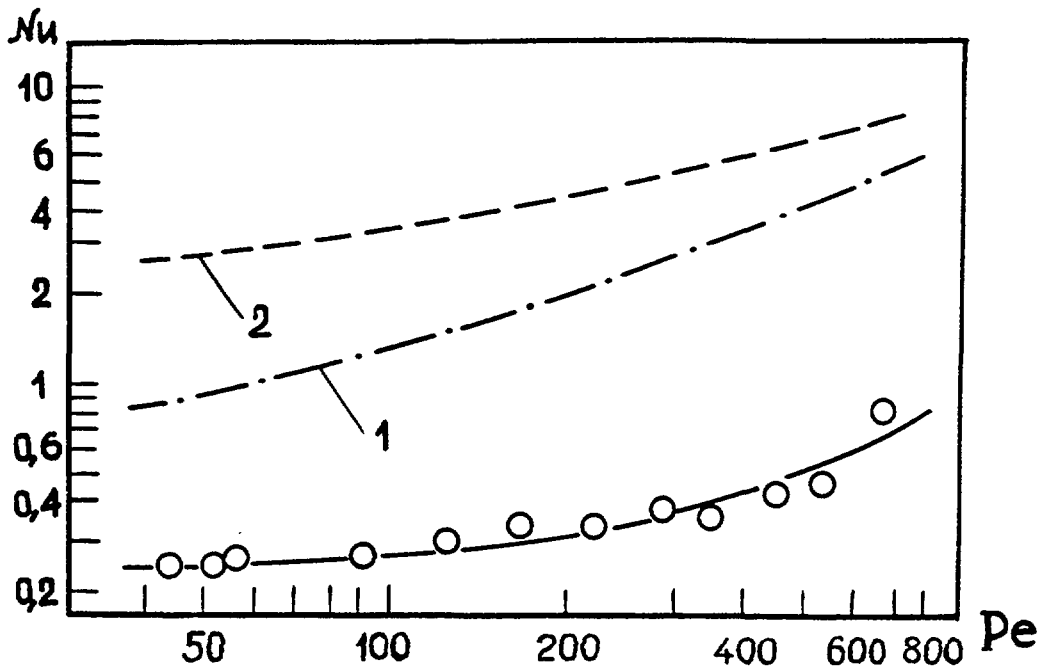
Fig. 4.41. Variation of edge pin heat transfer with Peclet number:
—○— - four pins are shifted, 1 -limiting shift of one pin, 2 - nominal geometry.

Predictions by (4.45) are in agreement with experimental data for various variants of pin shifting within a wide range of Peclet number (Fig.4.43,a-c).

4.4. PIN BENDING

Experimental investigations. Experiments have been carried out by the authors on measurements of the local pin wall temperature when the pin under investigation touches the six adjacent bended ones (one amplitude of bending), as it is shown in Fig, 4.44 - a,b. As the thermocouples are embedded at various levels, it allows temperature distribution to be found around the internal non-deformed) pin (Fig.4.44,b).

Geometry of the model is as follows:
Outer pin diameter, d, mm 16
Inter pin diameter, d_I, mm 13
Relative pitch, s/d, ... 1,185
Length of heated section, l_o, mm 1700
Distance between the end grids, L, mm 1820
Clearance between the wrapper and edge pins, Δ, mm 1,5
Relative clearance $\Delta / (s - d)$ 0,5
Thickness of the wrapper δ, mm 2,5
Wrapper size, b, mm 117,5
Heater .... stainless steel $\varnothing$ 2
Number of pins, n 37
Model cross section, w, cm^2 43,1
Hydraulic diameter, d_n mm 6,9

209
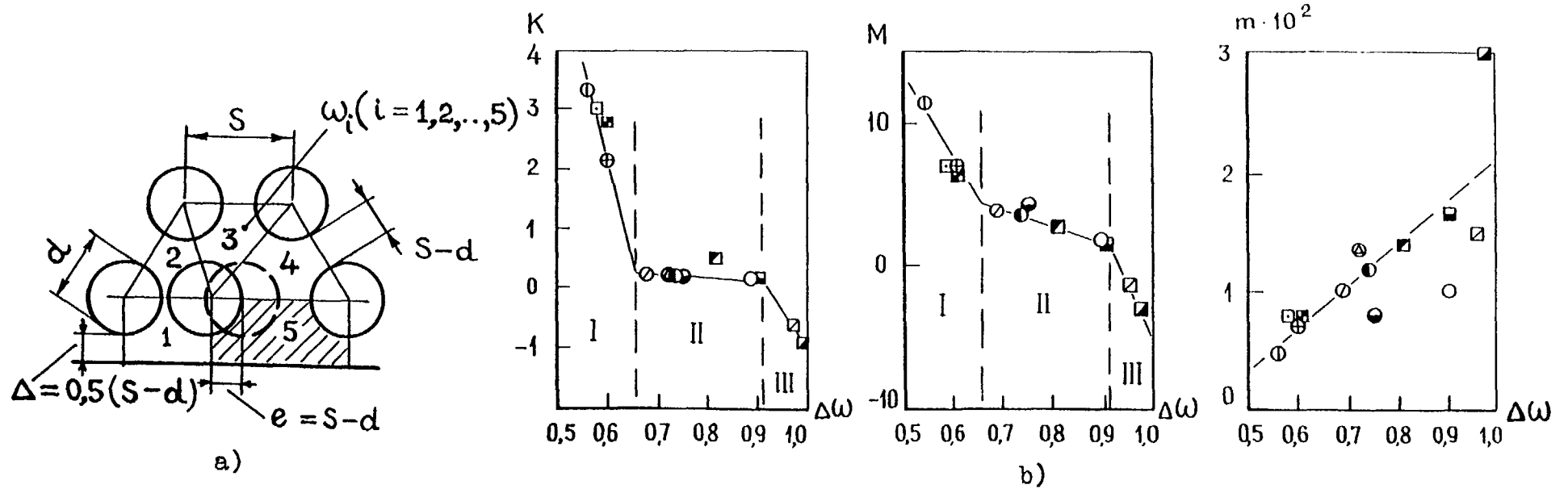
Fig. 4.42. Schematic view on the edge pins shift (a) and coefficients k, M and m ;
symbols - experimental data on various types of shifting.

$$\Delta T = \frac{t_w^{max} - t_w^{min}}{qR} \cdot \lambda_f$$

КАСАНИЕ 4ⁱ ИМИТАТОРОВ
модель без вытеснителей с
гладкими имитаторами

КАСАНИЕ 3ⁱ ИМИТАТОРОВ
модель без вытеснителей с
гладкими имитаторами

неоребренные имитат.
e=s-d
модель без вытеснителей

e=0,5(s-d)
оребренные имитаторы
модель без вытеснителей

e=0,5(s-d)
оребренные имитаторы
модель с вытеснителями

$$\Delta T = \frac{t_w^{max} - t_w^{min}}{qR} \cdot \lambda_f$$

номинальная геометрия
модель оребренных имитаторов

номинальная геометрия
модель неоребренных имитаторов

e=0,5(s-d)
смещение 2ⁱ гладких имитаторов

e=s-d
касание 2ⁱ гладких имитаторов

Fig. 4. 43-a, b.

211

$$\Delta T = \frac{t_w^{max} - t_w^{min}}{\bar{q}R} \cdot \lambda_f$$

Fig. 4.43. Maximal non-uniformity of pin temperature as internal (a) and edge (b, c) pins shifted in triangular bundle: O - experiments data, —— - prediction.

212
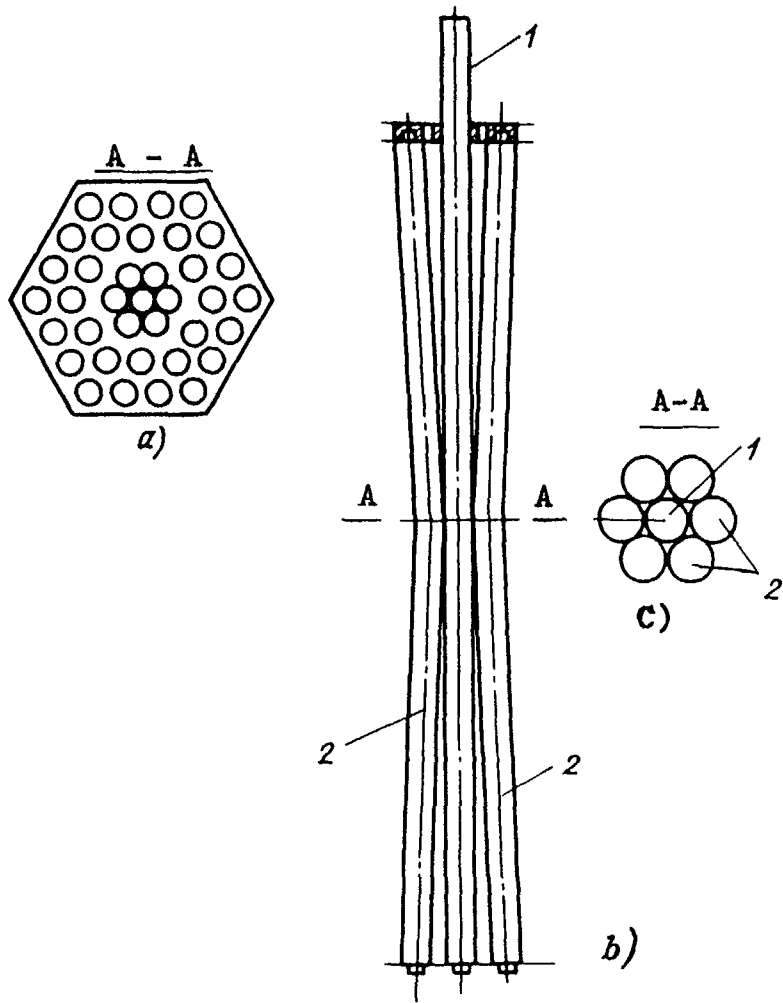
Fig. 4.44. Cross section (a) and axial view (b0 of the model with the pins banded in the middle zone (c).
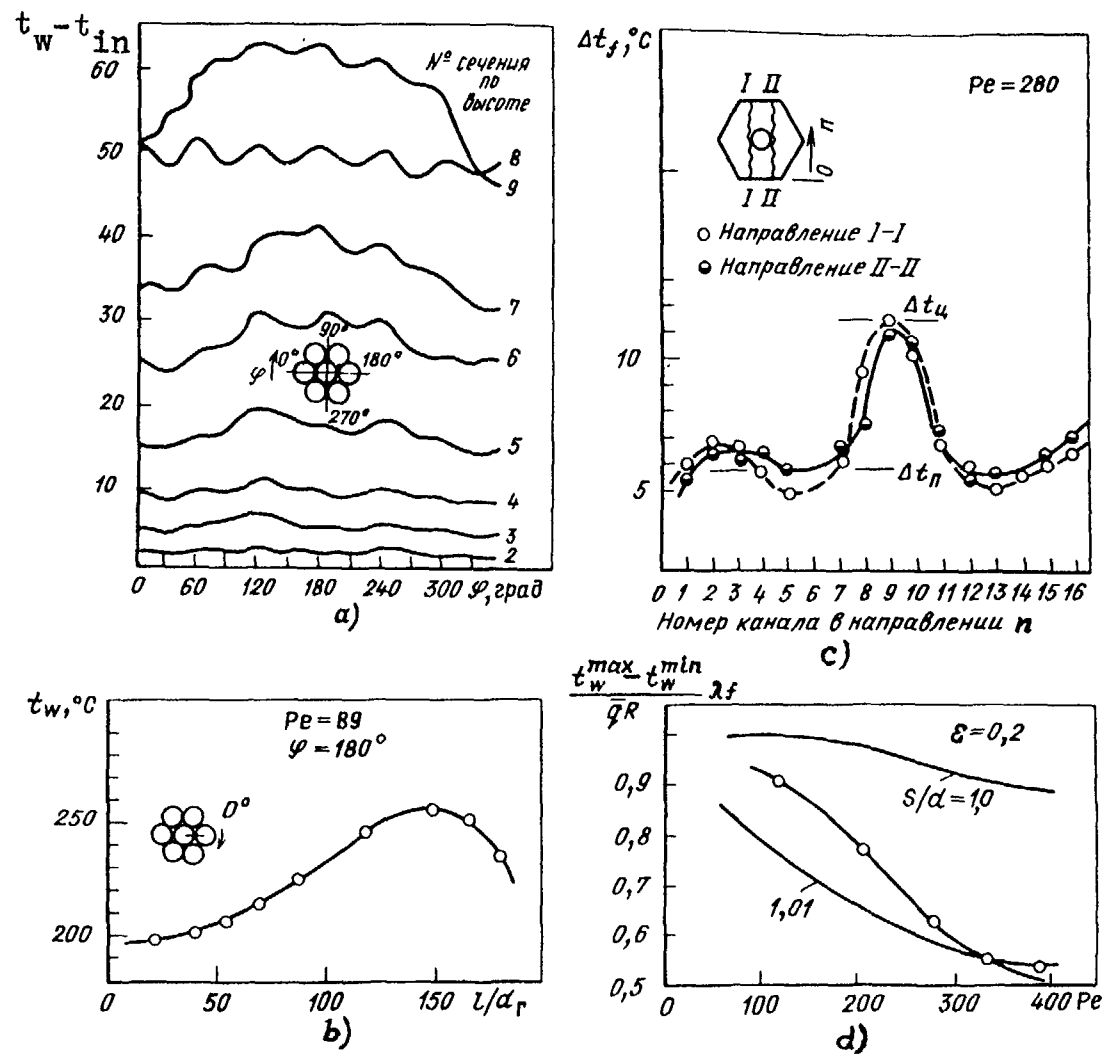
Fig. 4.45. Perimeter (a) and length (b) distributions of central pin temperature in such a model (see 4.44), coolant temperature (c) and relative temperature non-uniformities (d) (O - central pip) compared with those for pin bundles.

Against a background of the appreciate enhancement of temperature the periodic non-uniformity is observed in the contact point (Fig. 4.45a); temperature distribution along the pin has peak displaced along the coolant flow (Fig. 4.45b); coolant becomes highly heated in the compact channels and becomes subcooled in those of an enlarged section channels (Fig. 4.45c). Dimensionless periodic temperature non-uniformities at great Pe (Fig. 4.45d) is lesser than in compact bundles of the same equivalent thermal conductivity ($\varepsilon = 0.2$), but is practically coincident with those in the bundle with $s/d = 1.01$.

Analytical solutions. Equations and boundary conditions. Typical failure situation when pins bend till the compact channel is formed in the internal, edge or corner area of subassembly can be dscribed with the following equations:

Governing energy conservation equation:

$$\frac{d}{dz}\left(w_i\omega_i t_i\right) + w_{\Sigma_i} t^* = \frac{1}{\rho c_p} q_i \Pi_i +$$

$$+ \sum_{j=1}^{m} \mu_{ij}^m \frac{w_i + w_j}{2}\left(t_j - t_i\right)\varpi + \frac{\lambda_f + \lambda_t}{\rho c_p}\frac{d^2 t_i}{dz^2}\omega_i \qquad (4.46)$$

and using mass balance equation written for the channel

$$\frac{d}{dz}\left(w_i\omega_i\right) = -w_{\Sigma_i} \quad , \qquad (4.47)$$

we obtain

$$W_i\Omega_i\frac{d}{dZ}\left(T_i\right) + \left(T_i - T^*\right)\frac{d}{dZ}\left(W_i\Omega_i\right) =$$

$$= Q_i + \sum_{j=1y}^{m}\left(\mu_{ij}^T L\right)\frac{W_i + W_j}{2}\left(T_j - T_i\right) + \frac{1 + \dfrac{\lambda_t}{\lambda_f}}{Pe_L}\frac{d^2 T_i}{d Z^2}\Omega_i , \qquad (4.48)$$

where

$$W_i = \frac{w_i}{\overline{w}}; \quad \Omega_f = \frac{\omega_i}{\overline{\varpi}}; \quad Q_i = \frac{q_i\Pi_i}{\overline{q}\overline{\Pi}}; \quad Z = \frac{z}{L}; \quad T_i = \frac{t_i\lambda_f}{\overline{q}L}\frac{Pe}{4};$$

$Pe = \rho c_p \overline{w} L / \lambda_f$ -- Peclet number based on the heated length, $\overline{w}$ - - mean coolant velocity, ϖ - internal channel cross section, $\overline{q}$ - mean heat flux, Π - perimeter of the internal channel, Π_i - perimeter of the i-th channel, λ_f , λ_t - molecular and turbulent coolant thermal conductivity, $w_{\Sigma_i} = \sum\limits_{j=1}^{3} w_{ij}\Delta s_{ij}$ -- total transverse flows, w_{ij} - transverse velocity between the channels i and j, Δs_{ij} - clearance between the channels i and j.

Boundary conditions:

$$\left.\begin{array}{l} T_i(0) = 0; \\ T_i(1) = T_{out,} \end{array}\right\} \qquad (4.49)$$

214

Assuming, that change in temperature in the deformed channel does not influence on the temperature in adjacent nominal channels, we obtain:

$$T_j = \int_o^z Q_i dZ \ .$$

(4.50)

In the event of the constant in length power production we find that:

$$T^* = \begin{cases} Z, & if \ \dfrac{d}{dZ}\left(W_i\Omega_i\right) > 0 \ ; \\[2ex] T_i, & if \ \dfrac{d}{dZ}\left(W_i\Omega_i\right) \leq 0 \ . \end{cases}$$

(4.51)

Main features of temperature behaviour in deformed channels. An influence of the following factors on coolant overheating has been analyzed:

- axial thermal diffusion (term $d^2 T/ dz^2$)
- kind of deformation (extent and shape)
- power production distribution over the bundle length.

Variation in near wrapper clearance is given by the correlations:

$$J_i(Z) = \Delta_o \ \frac{1 + k \sin\left[\dfrac{\pi}{2}(2Z - 1)^n\right]}{1 + k} \ ;$$

(4.52)

$$J_2(Z) = \Delta_o\left(1 - \frac{k}{e^{n[2Z-1]^m}}\right)$$

(4.53)

where k, m, n - positive integers, Δ_0 - nominal clearance.

The features of the temperature behaviour are as follows (Fig. 4.46):

- the coolant temperature increases with the length of deformed section (curves 3 and 4 in Fig. 4.46) and as the minimum flow decreases;
- maximum temperature in deformed region does not exceed those under maximum allowable deformation (curve 2 in Fig. 4.46);
- the maximum coolant temperature is displaced up from the section of minimum flow,
- in the event of the pin bending is not so extend (about 10-20mm) a moderate rise in coolant temperature (less than 10% of the maximum allowable) takes place (curve 4, Fig. 4.46). If the pin is bended over the length 50-100mm, coolant temperature approaches the maximum value (curve 3, Fig. 4.46).

4.5. DEFORMATION OF BUNDLE AND SUBASSEMBLY WRAPPER TUBE

The great deformation of the bundle is observed at the end of campaign [23]. For example, in the middle cross section together with the bundle is shifted till touching two sides of the wrapper the pin displacement is observed (Fig. 4.35). In so doing, the compact channels can be formed in the internal and edge areas of subassembly.

Experimental results. One variant of the wrapper deformation is presented in Fig. 4.47a. The wrapper deflects in such a manner the pins touch one side, with the cavity being formed near the opposite side in the middle cross section. As to the performance of the experiment, it should be noted that the cavity can be approximately reproduced by the plate with the window inserted between the wrapper side and pins (Fig. 4.47b). The plate is made so, that displacers are regularly arranged (Fig. 4.47b, c). Wall clearance is bridged in the top and bottom parts. Other sides are under nominal conditions (Fig. 4.47c).

Geometry of the deformed region of the model defines the process of heat and mass transport in that region. Three inherent sections can be separated; they are the inlet ($l/d_h<70$), intermediate ($70>l/d_h>200$) and outlet ($l/d_h>200$). At the inlet section the maximum temperature of the corner pin (Fig.4.48) falls close to the wrapper ($\varphi \approx 0 \div 30^o$) and minimum temperature is observed at the opposite side ($\varphi \approx 180^o$). Within the central section temperature behavior becomes more smooth, but the region of regular channels $\left(\varphi \approx 180^o\right)$. At the outlet section the further enhancement of temperature non-uniformity occurs with the maximum at $\varphi \approx 0^o$. Thus, the temperature peaks change locations in various cross sections of the model.

Respective change in the maximum temperature non-uniformity along the corner pin is presented in Fig. 4.50. It is evident, that the corner pin produces the greatest temperature non-uniformity along the corner pin, the values of temperature non-uniformities around the specific pins (internal, intermediate, corner) at the same length are presented in Fig. 4.51. Under deformation the temperature behavior becomes non-symmetric (Fig. 4.51-4.53).

Prediction of temperature behavior in fast reactor subassembly. Calculations have shown [33, 42] that the temperature behavior in subassembly, defined having regard to stohastic deflections in geometry, differs essentially from those in regular geometry of the bundle. The compact channel formed in the edge or the corner area causes the intensity of inter-channel exchange to reduce, that is associated with the coolant temperature increases. The pin temperature peaks at the points of contact, with the temperature distribution around the pin increasing significantly.

These effects predicted for BN-800 are illustrated in Fig. 4.54 together with the general temperature non-uniformity induced by the wrapper bending, there are hot spots, where temperature is comparable with the mean outlet temperature. But there is no a high pin wall temperature observed at the reactor core outlet.

A great neutron flux in the middle of reactor core can cause the pins and wire to be twisted together (Fig. 4.35, 4.55). Joint twisting and bending effect results in the pins touching the subassembly wrapper. When swelling of the wrapper is more than swelling of the bundle, with the cavity being generated, the coolant flow is redistributed over the subassembly cross section, with the temperature non-uniformity increasing (Fig.4.56).

4.6 SUBASSEMBLY THERMAL INTERACTION

The periphery of reactor core incorporates a non-uniform power production, that cause the radiation deformation to proceed unevenly and finally it is responsible for the wrapper and bundle deformation, which can change in campaign.
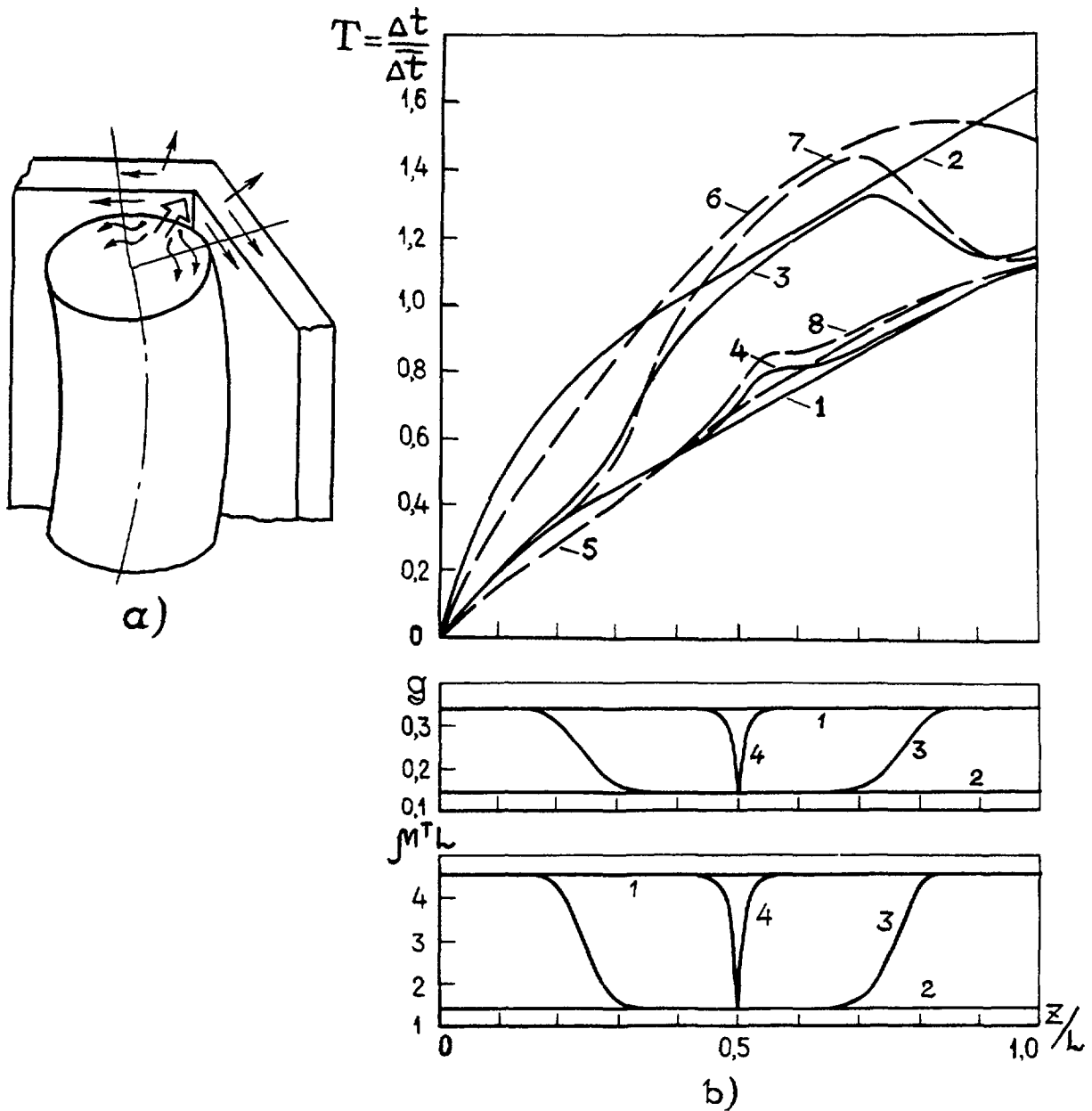
Fig. 4.46. Deformation of pip bundle when the corner pin bends (a) and variations in relative temperature T, coolant flow g in the corner channel and mixing factor with bundle length (b): 1 - nominal bundle, 2 -bundle retained against the cover, 3 - bending bundle, ———— - uniform equipped power production, ——— — - cosine power production.
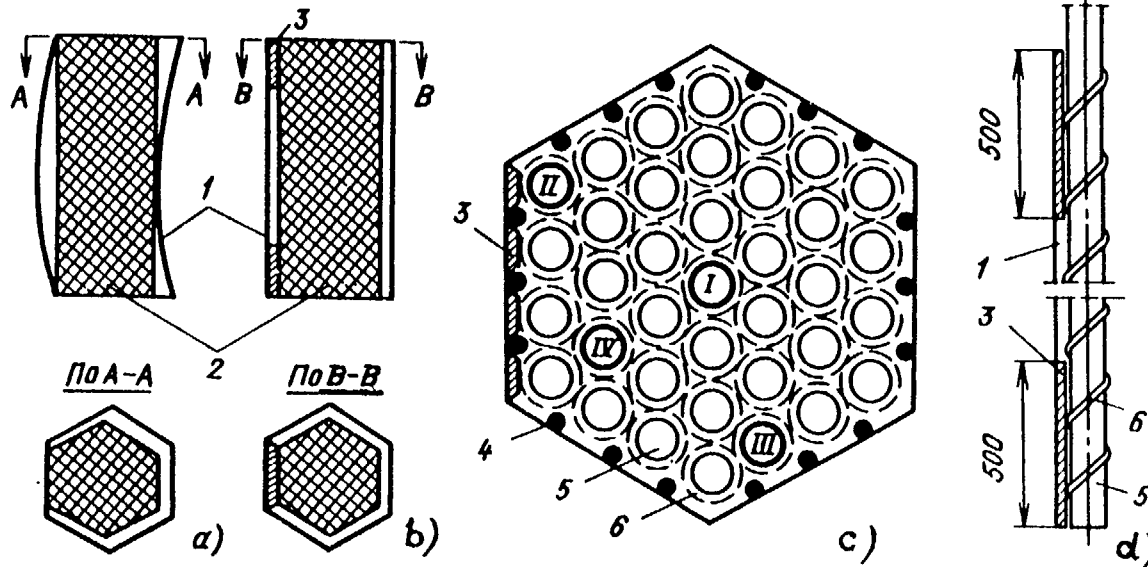
Fig. 4.47. Deformed cover (a) and the model axial (b, c, d).
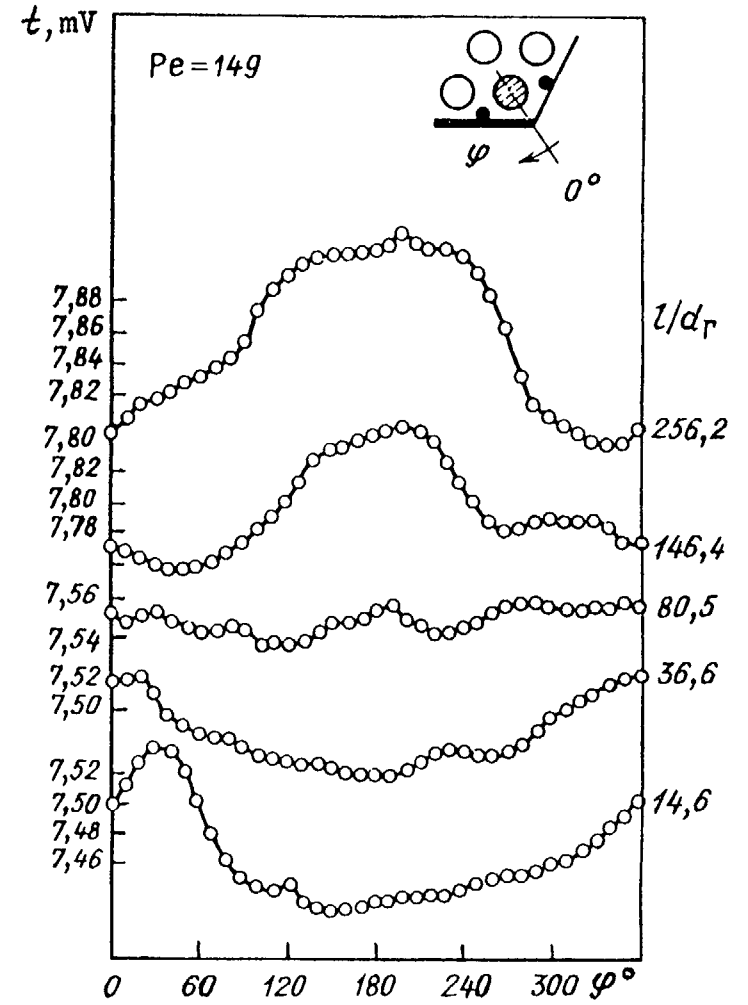
Fig. 4.48. Corner pin temperature in the model of deformed cover.
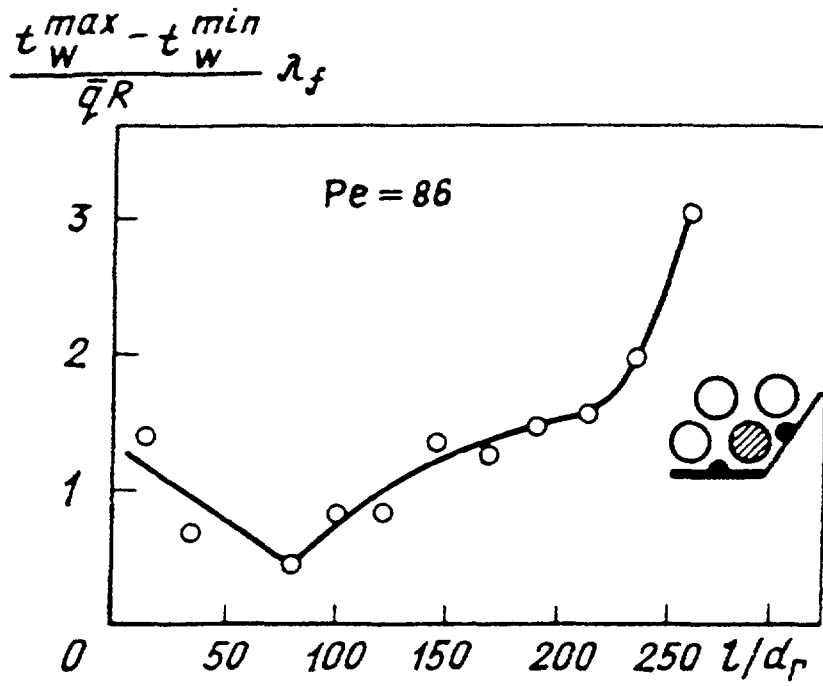
Fig. 4.49. Maximum temperature non-uniformity along the corner pin in the subassembly of deformed cover.
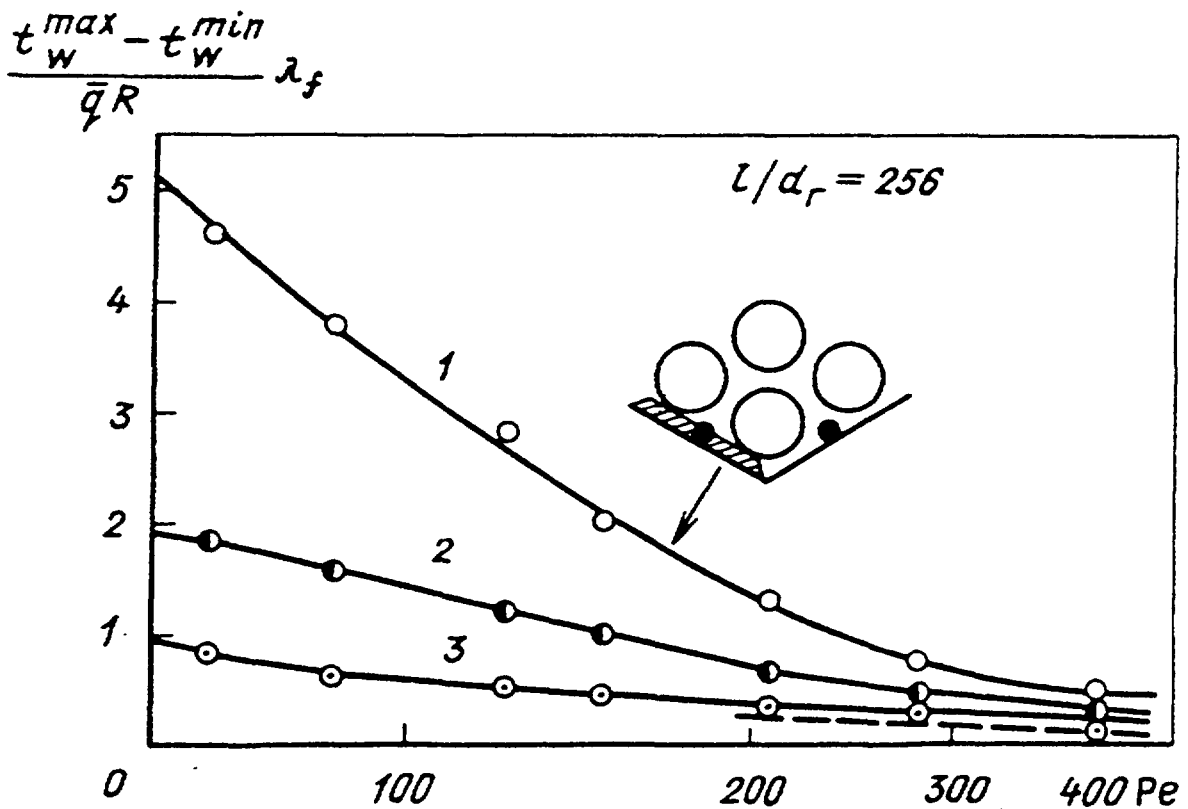
Fig. 4.50. Maximum temperature non-uniformity of the inherent pins at $1/d_h = 256$: 1 - corner, 2 - intermediate, 3 - internal pin; — — - corner pin in nominal geometry, O , ◑ , ⊙ - experimental data.
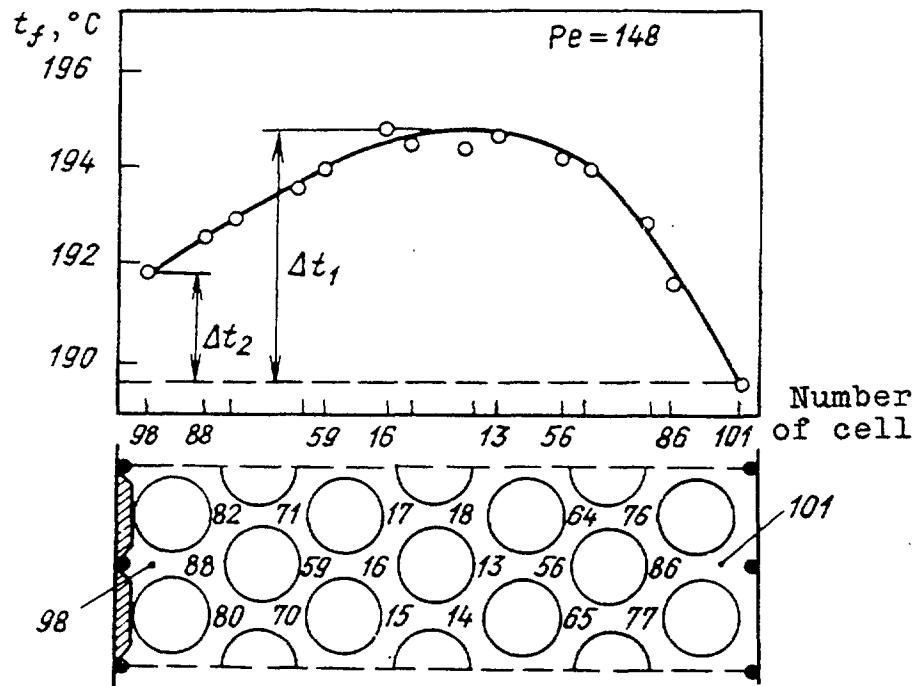
Fig. 4.51. Sodium temperature distribution in the outlet model cross section of deformed cover:

13÷101 - channel numbers, O - measurements,

—— - averaging line.
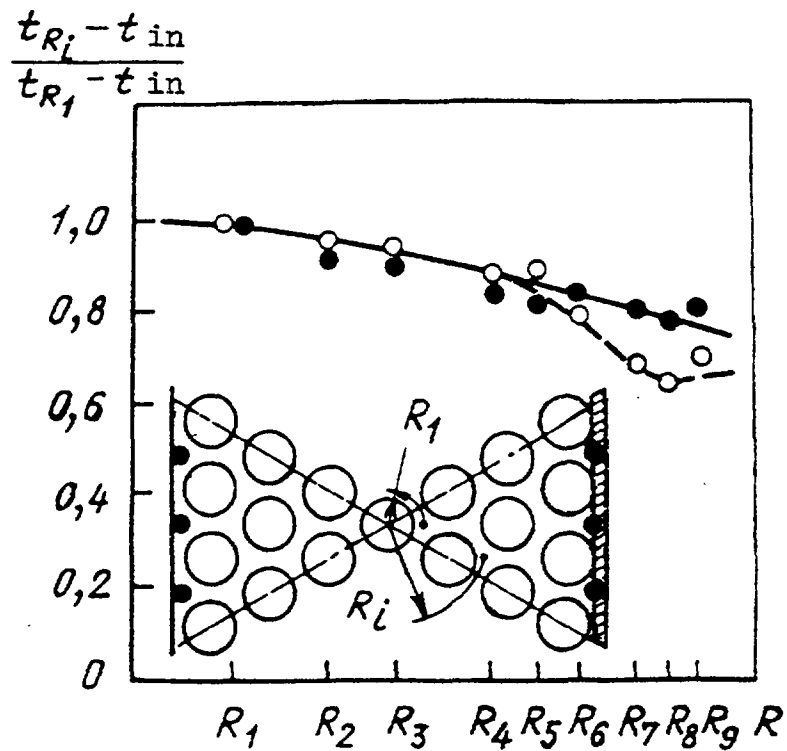
Fig. 4.52. Outlet coolant temperature in the model of deformed cover:

● - displacer is abundant, O - displacer is not abundant,

t_{in} - inlet coolant temperature.

220
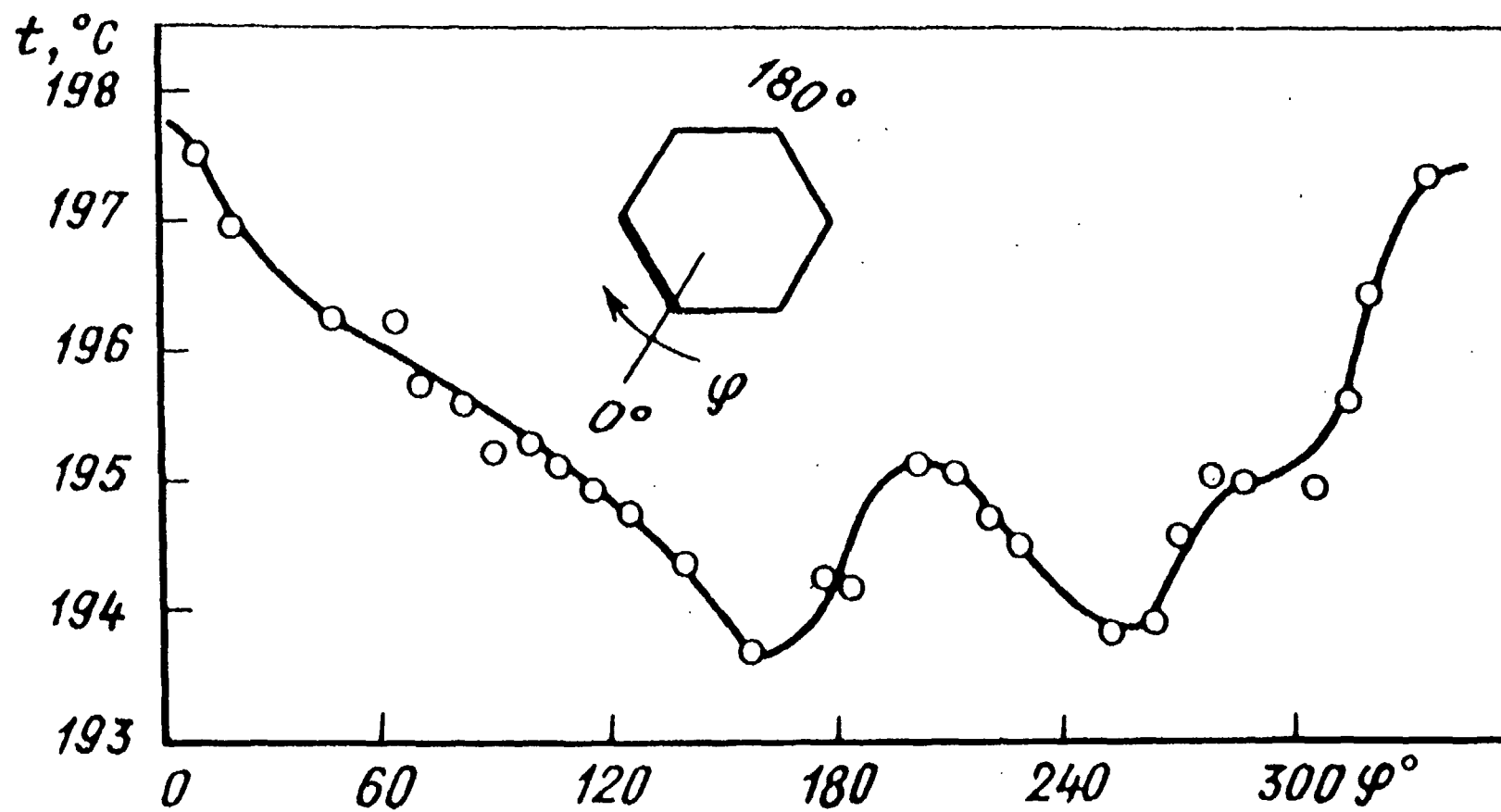
Fig. 4.53. Cover temperature measured in experiments.

q=const

$$t^{max}_{OBOЛ}$$

636 °C

741

560

557

555

639 555

636

870

630

557

560

550 666 546 550

$$\Delta t_\varphi$$

100 °C

106

206

12

10

100

15

93 7

18

7

106

20

7

322

103

19 12

10

17 28 140

11

18

b)

q=var

$$t^{max}_{OBOЛ}$$

590 °C

596

655

525

540

530

590

630

540

596

550

565 560 858

632

540

560

696 550

$$\Delta t_\varphi$$

86 °C

93

8 7 160

15 10

95 9

86

8

20 11

322

93

115 13

10

160 45

20

18

c)

a)

$$\frac{q}{\overline{q}}$$

q var

q const

1 3 5 7 9   № ТВЭЛА
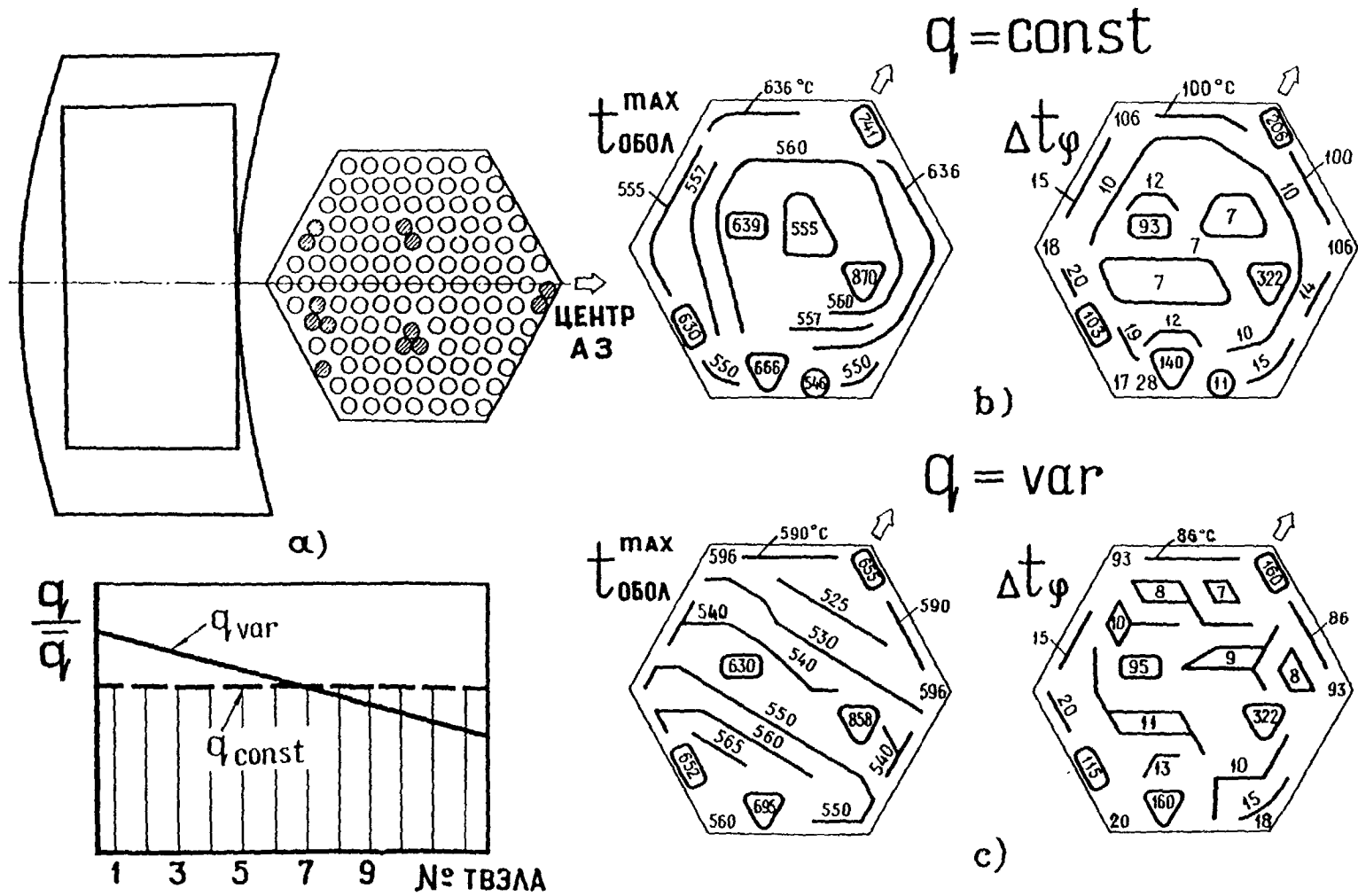
Fig. 4.54. Schematics of deformed bundle sections (a), maximum pin temperature and maximum temperature non-uniformity around the pin under conditions of uniform (b) and variable (c) power production.
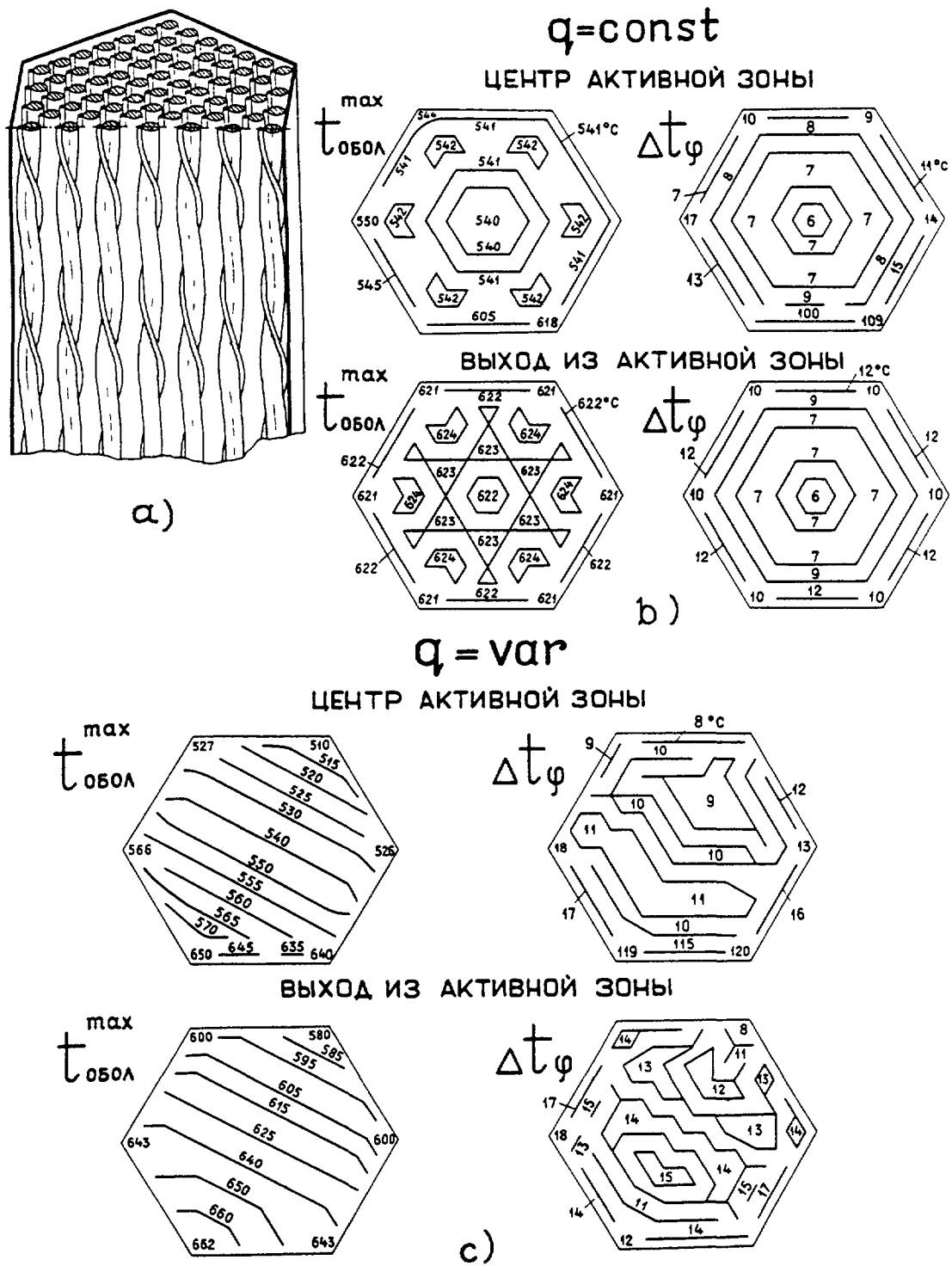
Fig. 4.55. Twisting wire wrapped pins (a), maximum pin temperature and maximum temperature non-uniformity under conditions of uniform (b) and variable power production (c).

223
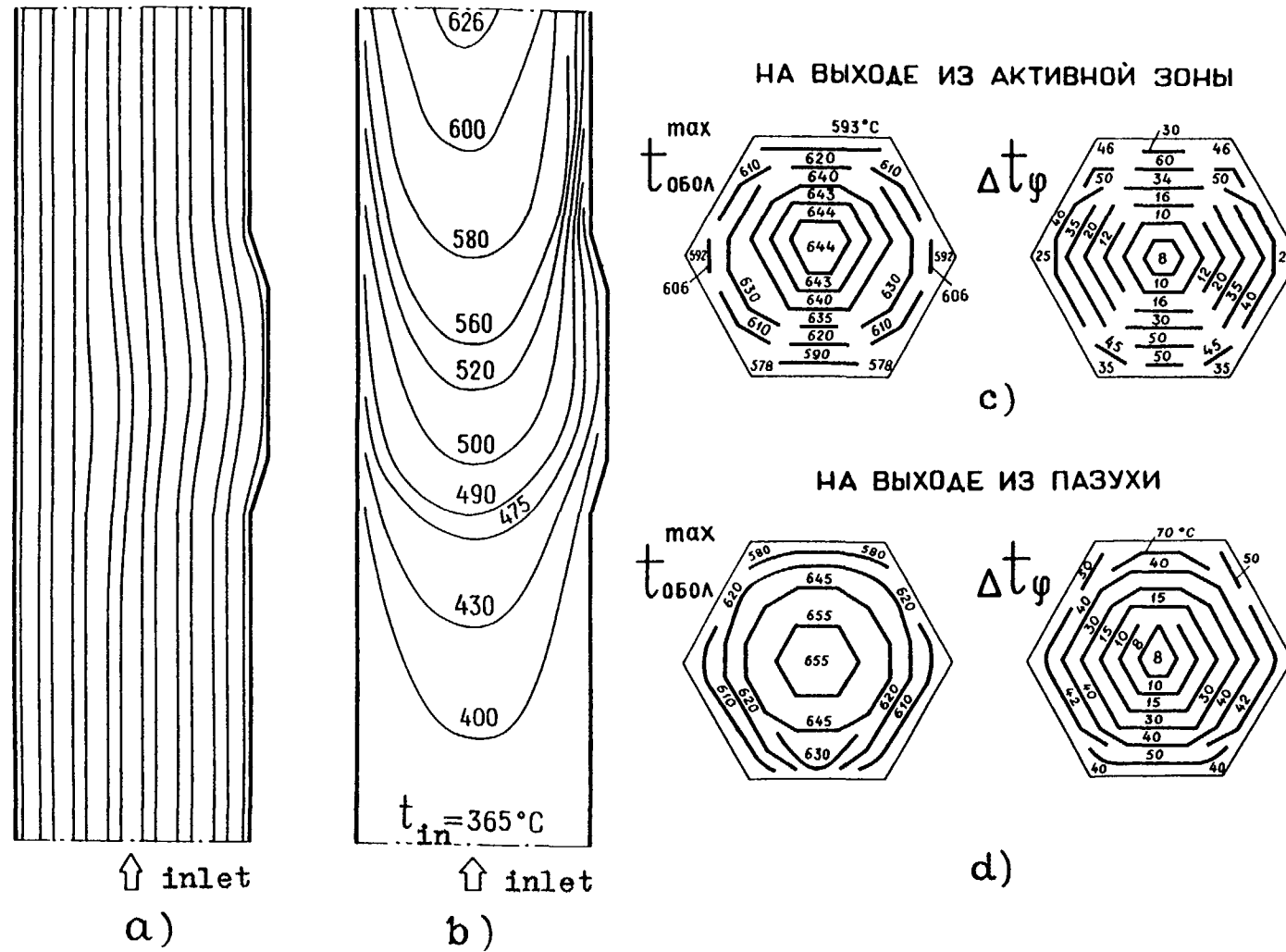
Fig. 4.56. Cover expansion (a), coolant temperature in axial cross section of the bundle (b), pin temperature and temperature non-uniformity at the core outlet (c) and in the top expanded section (d).
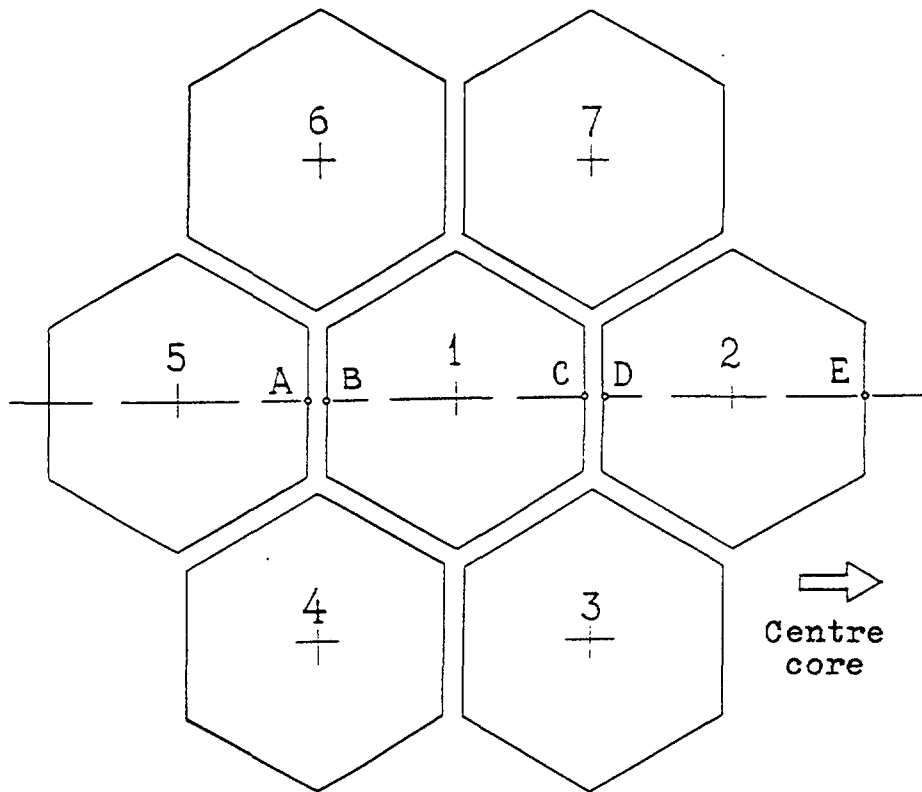
Fig. 4.57-a.
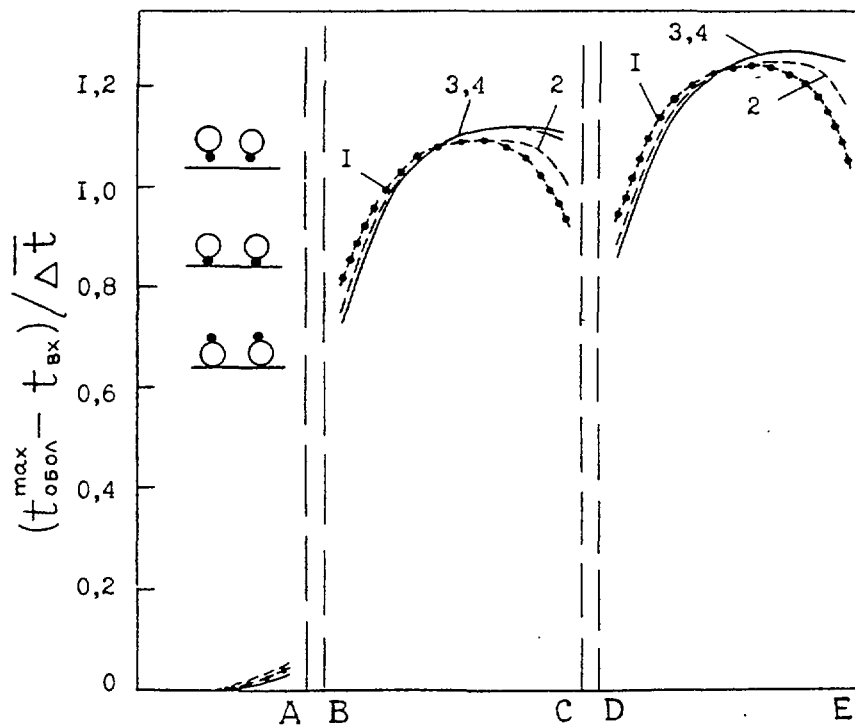
Fig. 4.57-b.
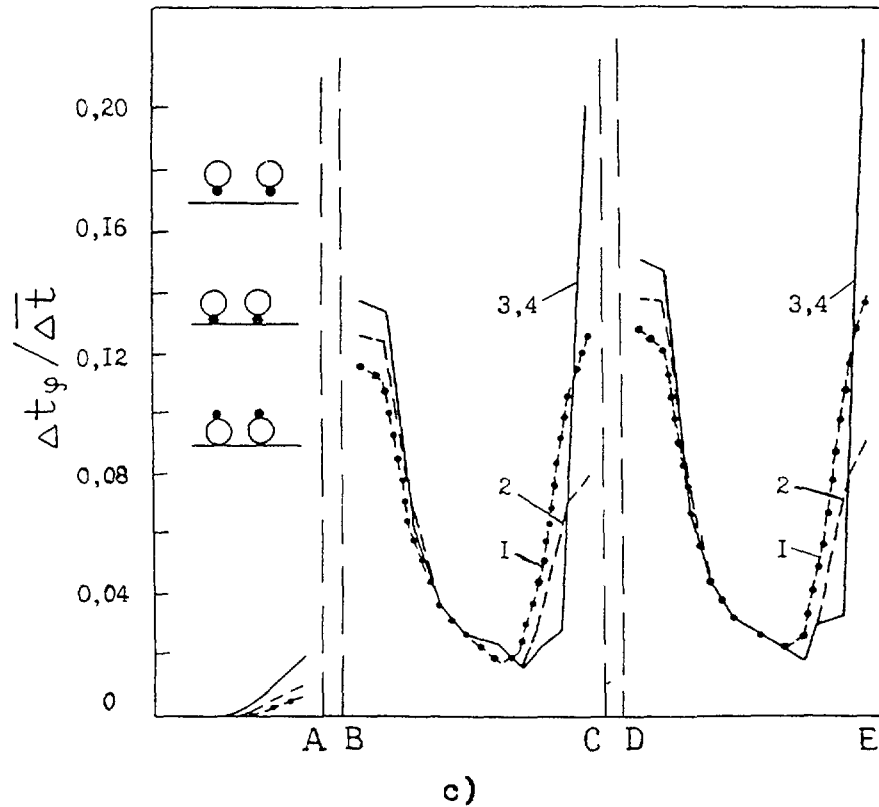
Fig. 4.57.   Schematic of the peripheral area of reactor core (a), predictions of maximum pin temperatures (b) , of maximum temperature non-uniformity (c) in deformed geometry:

1 - nominal geometry, 2 - bundle bending when the edge pin wires touch to one side of the cover, 3 - bundle bending when the edge pin claddings touch to the cover ,
4 - combined cover bending until it touch adjacent cover (A, B, C, D, E) -specific points at the cover sides).
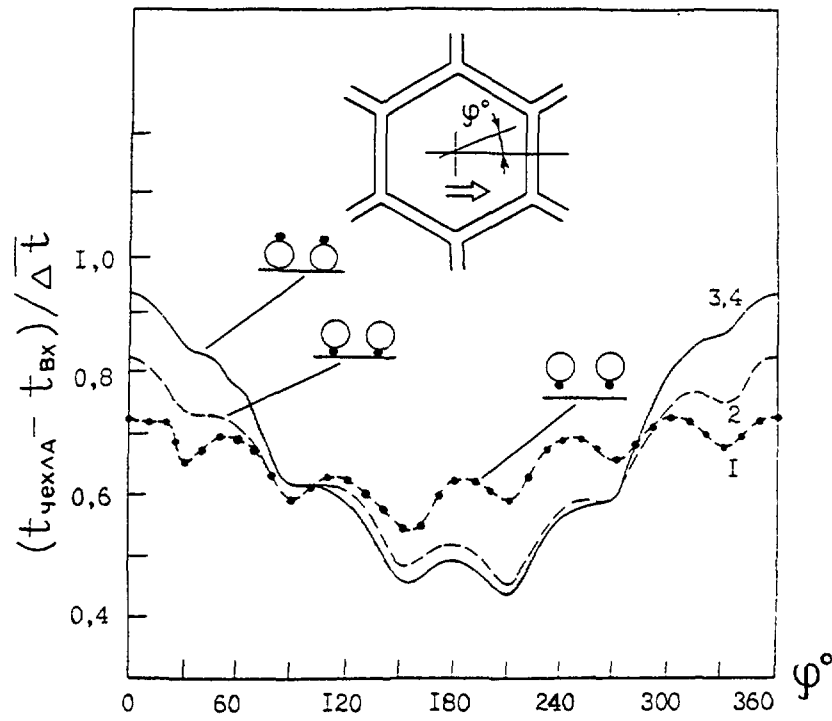
Fig. 4.58. Temperature distribution over the cover in various type of the bundle and cover deformation (symbols see in Fig. 4.57).
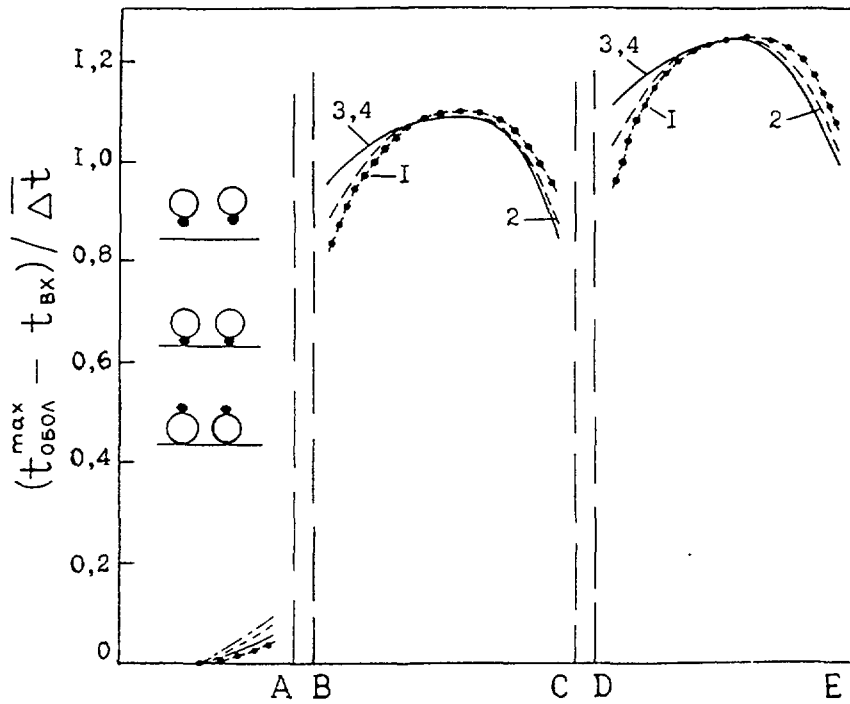
Fig. 4. 59-a.
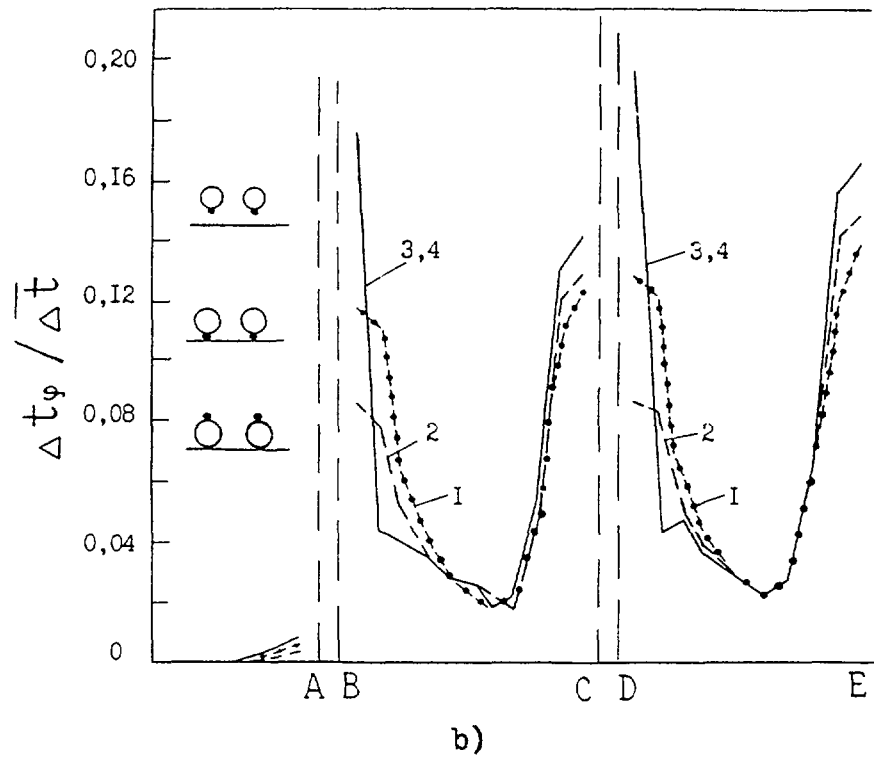
Fig. 4.59. Maximum pin temperature (a), maximum temperature non-uniformity (b) in the events of deformation.
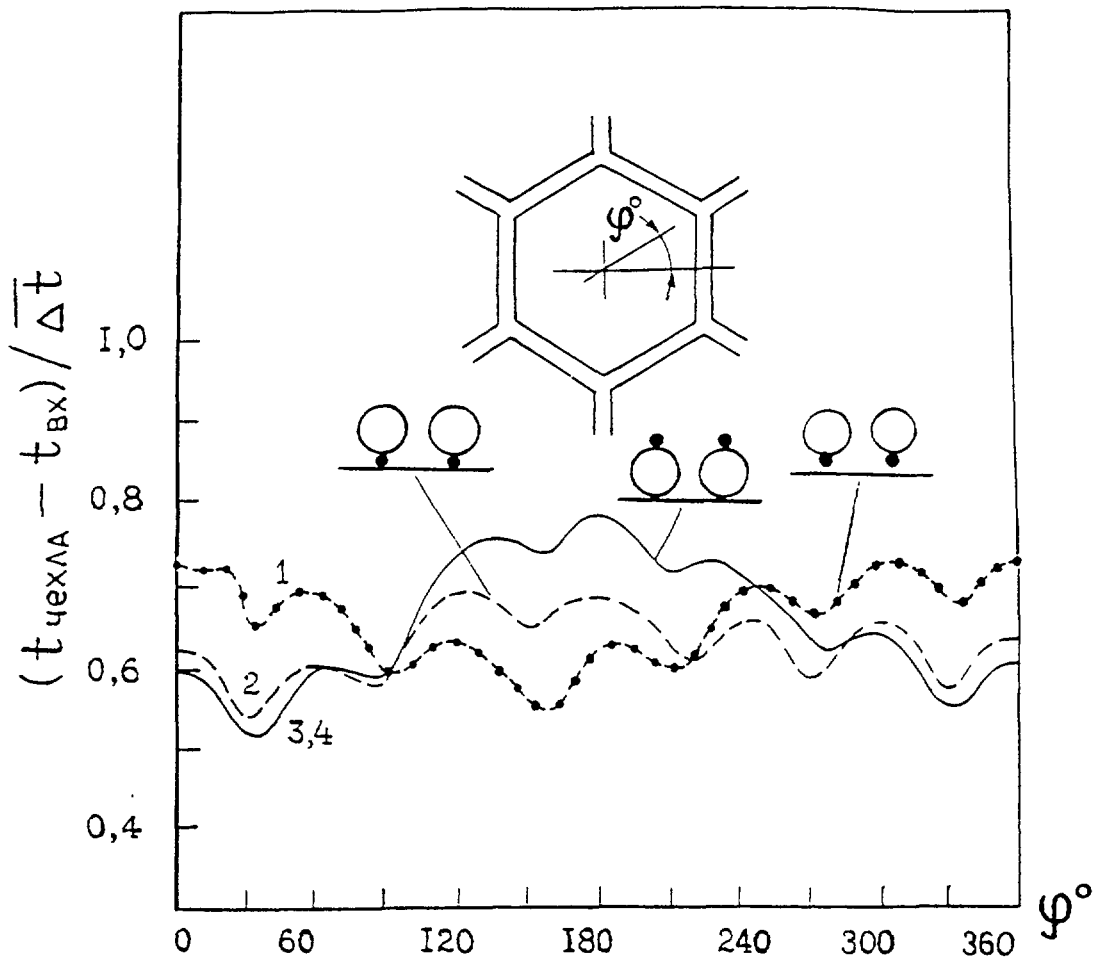

*.Fig. 4.60. Temperature around the cover (symbols see in fig. 4.47).*
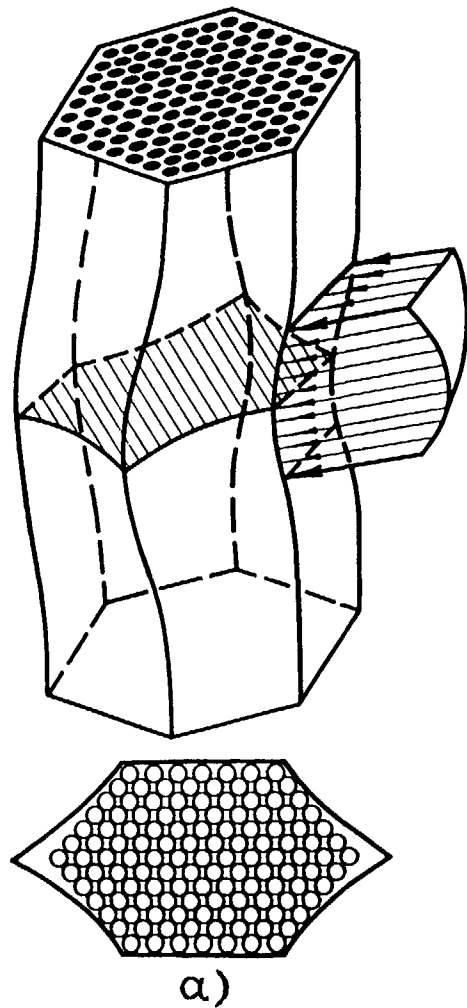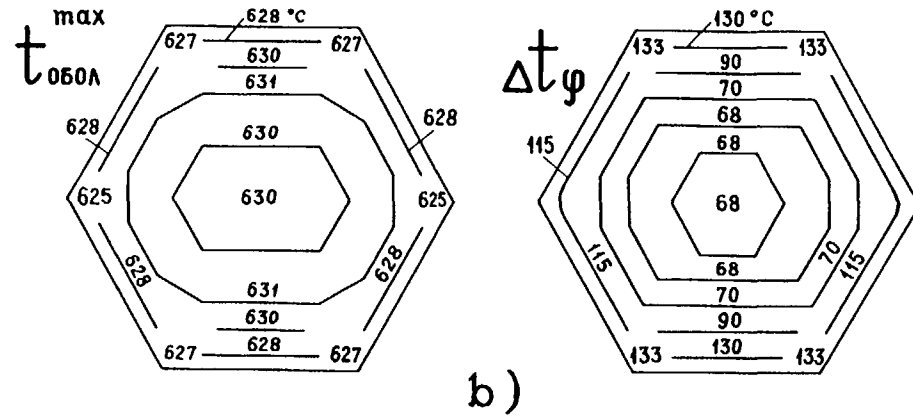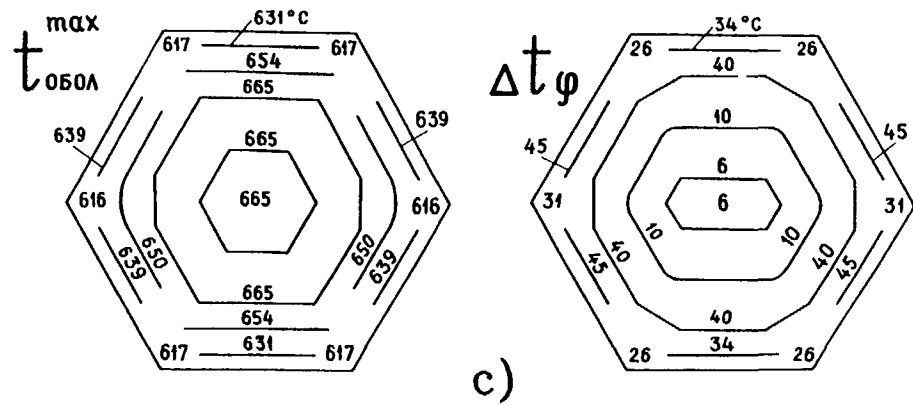
Fig. 4.61. *View of fast reactor subassembly in cover crushing (a), maximum pin temperature and maximum temperature non-uniformity in the middle cross section (b) and the core outlet (c).*

In the event of the bundle bended in the direction of the core center (Fig. 4.57 a) and the edge pins touching the cover, maximum pin temperature (Fig. 4.57 b), well as maximum azimuthal temperature non-uniformity (Fig. 4.57 c) increases.

The pin bundle deformation results in the distorted temperature behavior at the wrapper (Fig. 4.58). If the pin bundle is bended away from the core center, the lesser temperature non-uniformities are observed (Fig. 4.59, 4.60).

As for the crumpled cover, it should be noted that a force applied to the wrapper can amount up to some kiloNewtons. Under the effect of such a distributed load the deformation may be significant [43, 44] (Fig. 4.61): the bundle and wrapper are deformed, the bundle pitch changes in several directions, that results in variation in coolant flow through the subassembly. But, because the deformed area as usual covers not more than one third of the subassembly length, variation in pressure drop seems to be not more that 10-15%.

CONCLUSIONS

1. A joint analytical and experimental studies of fast reactor thermal hydraulics result in the data obtained on influence of various factors on distribution of local velocities (flow rates) of liquid metal coolant around and along the pins in the inherent areas of the subassembly (internal, edge and others), as well as across the subassembly. The relationships and graphical representation are needed to predict hydrodynamics in reactor core.
   The followings are among the most important results of hydraulic studies:
   - Channel-to-channel interaction of the coolant flows is the basic factor defining variation in hydraulic characteristics of the pin bundle, as whole and separate channels, as particular, that generates a need for performing analytical and experimental studies of multi-pin bundles simulating a fast reactor subassembly.
   - The hydraulics of fast reactor subassembly is to a large extent defined by a great non-uniformities of velocity around the edge pins and combined exchange within the subassembly due to wire wrap on the pins.
   - Contrary to the previous notion on the possibility for predicting subassembly hydrodynamics based on the coolant velocity averaged over the subassembly cross section or based on the hypothesis of isobaric cross section, it has been show that such an approaches, as a rule, do not ensure the wanted accuracy of results.
   - Hydrodynamic calculations taking into account channel-to-channel interaction of the coolant flows reflect realistically specific hydraulic features of interconnected channels and allows the prediction of velocity distribution over the subassembly to be defined reliably.
   - Flow parameters and geometry of the edge areas of subassembly, as well as data on the local hydraulic characteristics of the edge channels allow the optimal variants of the subassembly geometry to be chosen, as an important conditions for the uniform distribution of coolant temperature over the subassembly cross section.
   - An irregular field of velocity in the edge area of subassembly or deformed field due to shifting of one or several pins from nominal positions can serve as input data for gaining momentum mixing factor (smooth pins), velocity distribution in the bundle of wire wrapped pins is used to derive convective component of interchannel exchange, including those in the channels between pins and the subassembly wrapper.
   The parameters mentioned were gained and used in the code developed to validate thermal hydraulics of fast reactor core.

2. The study of deformed subassemblies (shifting, bending, swelling, creeping and so on) occupies a highly important place in the thermal hydraulic validation of reactor core. The following problems have been solved:

- Temperature behavior of pins in the various events of single or coupled shifting was studied during experiments, as limiting variants. The main effect were understood and the basic relationships were derived. Numerical procedures were developed that gave results being in agreement with experimental data.
- Universal relationship was derived which allows estimations of temperature non-uniformity under the real operating conditions taking into consideration statistical character of variation in the channel cross section during deformation.
- Experiments were carried out on the mock-up subassemblies to study temperature behavior in bending of pin bundle and wrapper tube. Analytical solution for different cases of pin and wrapper bending was obtained, with the following comparison predictions and experimental data.
- Subchannel code TEMP-MIF intended to predict thermal hydraulics of reactor core having regard to subassembly deformation allows validation of temperature behavior of fast reactor core performance with a high accuracy. This code is of high speed and can be used in the wider ranges of parameters than other known codes.

3. The temperature distribution in several adjacent subassemblies were analyzed having regard to variable power production over the core radius, that is responsible for non-uniform radioactive deformation in campaign.

In the event of the subassembly wrapper bends toward to the core center, the maximum pin temperature increases, as well as azimuthal temperature non-uniformity. At the same time the pin temperature decreases in the area close to opposite sides of the wrapper, that is connected with the enhancement of the width of clearance between the edge pins and wrapper tube.

The force exerted on the wrapper due to thermal interaction of subassemblies can be significant (some kiloNewtons), and as a result the wrapper deformation occurs: there observed variations in the mean pitch-to-diameter ratio, bundle cross section area, coolant flow through the subassembly. Effects are different and can be estimated using the codes developed.

REFERENCES

[1]   Subbotin V.I., Ushakov P.A., Levchenko Y.D.. Velocity Field in Turbulent Flow Passing through the Pin Bundle. Preprint IPPE-198, Obninsk, 1970 (in Russian).

[2]   Eifler W., Nijsing R. Experimental Investigation of Velocity Distribution and Flow Resistance in a Triangular Array of Parallel Rods. Nucl. Eng. and Des., 1967, v.5.

[3]   Ibragimov M.H., Yusoupov I.A., Kobzar L.L. et al. Calculation of Wall Shear Stresses and Turbulant Velocity Distribution. Atomic Energy, 1964, v.21.

[4]   Buleev N.I. Calculation of Velocity Field and Turbulence Thermal Conductivity in Combined Channels. Thermal Physics of High Temperature, 1971.

[5]   Subbotin V.I., Ushakov P.A. Calculation of Pin Bundle Hydrodynamics. Simulating of Thermodynamics in Fast Reactor Core, Prague, 1971, p.44-57.

[6]   Ushakov P.A., Zhukov A.V., et al. (USSR), Mantlik F., Heina J., et al. (CSFR. Investigation of Thermadynamics in Regular and Deformed Bundles of Pins. M., CEMR, 1978.

[7]   Subbotin V.I., Zhukov A.V., Ushakov P.A. Liquid Metal Velocity Distribution in Fast Reactor Subassembly Models. State and Trends of LMFBR, Obninsk, 1975, v.2, p.100-127.

[8]   Heina J., Chervenka J., Mantlik F. Results of Local Measurements of Hydraulic Chracteristics in Deformed Pin Bundle. UJV - 4156-T, part1. Rzez, Czech Republic, 1977.

[9]   Zhukov A.V., Sorokin A.P., et al. Thermal Physic Validation of Temperature Behavior in Fast Reactor Subassembly Having Regard to Hot Spot Factors. Preprint IPPE-1816, Obninsk, 1986 (in Russian).

[10]   Zhukov A.V., Sorokin A.P., Titov P.A. Turbulent Momentum Exchange in Pin Bundle. Preprint IPPE-2015, Obninsk, 1989 (in Russian).

[11]   Rowe D.S., Jonson B.M., Knudsen L.G. Implication Concerning Rod Bundle Mixing Based on Measurements of Turbulent Flow Structure. Int. J. Heat Mass. Transfer, 1974, v.17.

[12]   Rowe D.S. A Mechanism for Turbulent Mixing between Rod Bundle Subchannels. TANS, 1969, v.12.

[13]   Roidt, Pecherski, Markin et al. Determination of Turbulent Mixing Factor in Pin Bundles. Heat Transfer, 1972, v.96.

[14]   Rudzinski K.F. et.al. Turbulent Mixing for Air-Water Flow in Simulated Rod Bundle Geometries. Canadian J. Chemical Eng. , 1972, v.50.

[15]   Zhukov A.V., Sviridenko E.J., Matjukhin N.M., et al. Investigation of Combined Flow Hydrodynamics in Wire Wrapped Pin Bundles. Preprint IPPE-867, Obninsk, 1979 (in Russian).

[16]   Zhukov A.V., Sviridenko E.J., Matjukhin N.M., et al. Local Hydrodynamic Characteristics of Interchannel Exchange in Fast Reactor Subassembly. Preprint IPPE-665, Obninsk, 1976 (in Russian).

[17]   Zhukov A.V., Sviridenko E.J., Matjukhin N.M., et al. Study of Interchannel Exchange in pin Bundles of Small Relative Pitch. Preprint IPPE-799, Obninsk, 1977 (in Russian).

[18]   Zhukov A.V., Sorokin A.P., Titov P.A. Analysis of Data on Interchannel Exchange in Wire Wrapped Bundles. Part 1. Internal Area. Preprint IPPE-1574, Obninsk, 1984 (in Russian).

[19]   Bolle L. et. al. Experimental Determination of the Local Transverse Mixing in a Rod Bundle with Helical Wire Spacer / Rep. Int. Meeting on Reactor Heat Transfer. 1973. Karlsruhe, Germany.

[20]   Patch L. Experimental Studies of Flow Distribution in a Wire Wrapped LMFBR Blanket Assembly. Ibid. 1979. Karlsruhe, Germany.

[21]   Markley R.A. Status of Core Thermohydraulic Development in the USA. Thermodinamics of FBR Fuel Subassemblies under Nominal and Non-Nominal Operating Conditions, EWGFER / 29, 1979.

[22]   Proshkin A.A., Likhachev Yu.I., Touzov A.N. Analysis of Experimental Data on Fast Reactor Subassembly Deformation. Atomic Energy, 1981, v.50.

[23]   Marbach J. Comportement d'un Faisceau d'ajgulles Phenix Sour Irradiation *11* Irradiation Behavior of Metallic Materials for Fast Reactor Core Components.CEA-DMECH-B. P.N.2-91190, YJF-Sur-Yuette, France, 1979.

[24]   Zhukov A.V., Sviridenko E.J., Matjukhin N.M., et al. Temperature Fields and Heat Transfer in the Edge Areas of Hexahonal Bundles. Problems of Nucl. Science and Eng. Reactor Des., 1977, 4(18) (in Russian).

232

[25]   Zhukov A.V., Matjukhin N.M., Nomophilov E.V. Temperature Fields in Non-standard and Deformed Bundles. Thermal Physics and Hydrodynamics of Fast Reactor Core and Steam Generators, Prague, 1978.

[26]   Zhukov A.V., Sviridenko E.J., Matjukhin N.M., et al. Temperature Behavior in Deformed pin Bundles under Uniform and Non-uniform Thermal Loads. Preprint IPPE-909, Obninsk, 1979, Part 1 (in Russian).

[27]   Shulc V. Experimental Investigation of Temperature Fields in Deformed Pin Bundles. Hydrodynamics and Heat Transfer in Fast Reactor Core and Steam Generators, Prague, 1984, v.1.

[28]   Hishida H. Detailed Consideration on Wire-Spaced LMFBR Fuel Subassemblies Under the Effect of Unsertainties and Non-nominal Operating Conditions. IWGFR/29. Vienna: IAEA, 1979.

[29]   Miki K. Deformation Analysis of Fuel Pins Within the Wire-Wrap Assembly of an LMFBR. Nucl. Eng. and Des., 1979, v. 52.

[30]   Moller R., Tchoke H. Steady-State Local Temperature Fields with Turbulent Liquid Sodium Flow in Nominal Disturbed Bundle Geometries with Soacer Grids. Nucl. Eng. and Des., 1980, v. 62.

[31]   Zhukov A.V., Sviridenko E.J., Matjukhin N.M. Heat Removal in Fast Reactor Core. Atomic Energy, 1985, v.58.

[32]   Zhukov A.V., Sorokin A.P., Ushakov P.A., et al. Thermal Physic Validation of Temperature Behavior in Fast Reactor Subassembly Having Regard to Hot Spot Factors. Preprint IPPE-1778, Obninsk, 1986 (in Russian).

[33]   Kazachkovski O.D., Zhukov A.V., Sorokin A.P., et al. Temperature Behavior inDeformed Fast Reactor Subassemblies. Atomic Energy, 1988, v.65.

[34]   Recommendations on Thermal Hydraulic Calculation of Fast Reactor Core. PTM 1604. 008-88. State Committee on Nuclear Energy. M., ONTI IPPE, 1989.

[35]   Zhukov A.V., Kirillov P.L., Matjukhin N.M., et al. Thermal Hydraulic Analysis of LMFBR Subassembly, M., Energoatomizdat, 1985.

[36]   Zhukov A.V., Sorokin A.P., Khudasko V.V. Problems of Thermal Hydraulics in Non-Nominal LMFRB Operations, Textbook, ONPEI, Obninsk, 1990 (in Russian).

[37]   Zhukov A.V., Sorokin A.P., Matjukhin N.M.. Interchannel Exchange in Fast Reactor Subassembly: Codes and Applications, M., Energoatomizdat, 1991.

[38]   Zhukov A.V., Matjukhin N.M., Sviridenko E.J. Experimental Study of Influence of Deformation on Temperature Behavior of Edge Pins. Thermal Physical Investigations, IPPE, 1980, Part1, p.27-37 (in Russian).

[39]   Bobkov V.P., Savanin N.K. Local Heat Transfer Coefficient and Its Use in Temperature Calculations. Atomic Energy, 1981, v.51.

[40]   Zhukov A.V., Sviridenko E.J., Matjukhin N.M., et al. Influence of Deformation on Tempeature Behavior and Heat Transfer in Specific Areas of Fast Reactor Subassembly. Preprint IPPE-979, Obninsk, 1980 (in Russian).

[41]   Zhukov A.V., Sviridenko E.J., Matjukhin N.M., et al. Experimental Investigation of Liquid Metal Temperature Behavior and Heat Transfer in Triangular bundles. Preprint IPPE-800, Obninsk, 1978 (in Russian).

[42]   Kazachkovski O.D., Sorokin A.P., Zhukov A.V., et al. Stochastic Temperature Non-Uniformities in Deformed Subassemblies. Preprint IPPE-1678, Obninsk, 1985 (in Russian).

[43]   Zabudko L.M., Likhachev Yu.I., Proshkin A.A. Operation of Fast Reactor Subassemblies, M., Energoatomizdat, 1988.

[44]   Liebe R. Subassembly Experiments and a Computer Code to Analyze the Dynamic Code Deformation During Local Failure Propagation. Nucl. Eng. and Des., 1977, v.43.

Chapter 5

INTERMEDIATE HEAT EXCHANGER THERMAL HYDRAULICS

5.1. FEATURES OF LMFBR IHX THERMAL HYDRAULICS

Thermohydraulic processes in the inter-tube space of fast reactor intermediate heat exchangers (combined transversal-axial flow) were studied in the wide ranges of the main parameters' variation, including low-velocity and natural convection heat removal [1-3]. The studies were concerned with the validation of thermal hydraulic performance of heat exchangers, as under nominal and non-nominal operating conditions. Of particular value are experimental and calculation data on the local velocity and temperature behavior inside of the tubes and in the inter-tube space, allowing calculation of full-scale heat exchanger or developing numerical procedures and codes of IHX thermal hydraulic analysis. Thus, the case in point will be the combined approach to fast reactor IHX thermal hydraulics.

The main feature of such an investigations is detailed velocity and temperature measurements in the "hot" and "cold" coolants compromising a local (in each tube and in each channel) and an integral (in headers) techniques. Some of ideas on the modeling of fast reactor IHX thermal hydraulics have been considered in the chapter 1.3. The others are presented below. It will be recalled that transversal and axial components of liquid metal velocity are measured with the use of electromagnetic method, whereas the temperature behavior is controlled by the mobile thermocouples. It should be noted that only local modeling provides for gaining a plausible results and for their converting into the full-scale IHX performance, whereas the "global" measurements (when temperatures in the "hot" and "cold" flows are determined in the headers) produce particular results which are considered inappropriate to the actual design of the multi-tube IHX.

Doing it away to reproduce and study hydrodynamics and heat transfer in full scale, it should be noted that local thermal modeling mentioned above allows the experiments to be carried out on a simple tube bundles considering the main hydrodynamic and thermal effects of transversal-axial flow not associated with that the particular structure are reproduced in general terms, the data gained to be converted into "infinite" (regular) zones of full-scale heat exchangers and the most important effects involving one or another of heat exchanger's design reproduced in the model. However, in developing such a simple models the fundamental conditions of multi-tube heat exchangers should be accounted, such as the number and length of the tubes, their arrangement, coolant flow and so on. Under this performance the data gained in the experiments, as pointed above, are a great convenience to be applied as a reference data in the development of calculation procedure.

5.2. HYDRAULIC RESULTS

Triangular arrangement. Experiments were carried out on the "plane" models (Fig. 1.14 and 1.15 from the Chapter 1.3) involving one or three rows of the tubes, displacers attached to the wrapper (the models are justified in the Chapter 1.3).

Experimental one-row model with triangular arrangement of the tubes has the following geometrical parameters:

Outer diameter of the tube (displacers) d, mm 19
Inner diameter d_l, mm 18
Number of tubes n 7
Number of displacers N 16
Pitch-to-diameter ratio s/d 1.315
Tube length enclosed by the spacing grids L, mm 1000
Height of the inlet window l_0, mm .... 350(150)
Height of the outlet window L_0, mm 80
Depth of the wrapper h_0, mm 175
Thickness of the wrapper b, mm 43,5

Coolant (eutectic alloy NaK) comes from the "large volume" (bottom header) throughout the window into the tube bundle, with flowing to the top header, that simulates the inlet conditions (see Fig. 1.14).

Electromagnetic technique is used (see in detail Chapter 1.4) to measure the local velocity of liquid metal. The local electromagnetic sensor (Fig.1.16) is mounted inside of the measurement tube, which is introduced in turn in the various zones of the model cross section. At the tube surface, near the magnet, there are two normally posioned pairs of electrodes, which control the transversal and axial components of liquid metal velocity. Rotating and moving tube with the sensor inside allow the local velocity to be measured at a different level

The sensor's geometry is as follows: width (a), length (b) and height (c) of the magnet are 5:15:5 mm, respectively, the cooper wire diameter $d_l = 0.2$ mm, distance between the ends of electrodes $\delta_l = 1.7$ mm.

The use of the electromagnetic technique for measuring local velocity in the model of LMFBR IHX has permitted a study of the structure of transversal-axial flow, establishment of the laws that govern the variation in transversal and axial components of velocity with the length and depth of the tube bundle.

Experimental results. Transversal component of velocity

The azimuthal direction (Fig.5.2, 5.3). Maximum velocity was observed not in the narrow clearance between the tubes and displacers, but rotated by $\Delta\varphi \cong 15 \div 20$. This is revealed as during the sensor calibration (Fig. 5.2), and in experiments itself (Fig. 5.3). The maximum amplitude of velocity is observed to be at the first tube.

The axial direction (see Fig. 1.22). Distribution of transversal velocity in the clearance between the tube and displacer over the inlet window height is of the exponential form. Beyond the top edge of the window, velocity reduces to zero, with the increasing as approached to the outlet window. Relationships for the other tubes are the same, but velocity varies more smoothly. Maximum values reduce with the depth of the bundle.

Axial components of velocity. At the inlet (Fig. 5.4, a) and outlet (Fig. 5.4, b) sections of the model the distribution of axial velocity incorporate the great non-uniformity (especially for first and second tube), with the maximum velocity (flow rate) being observed in the after zone of tube ($\varphi \cong 180^0$ for the inlet window and $\varphi \cong 0^0$ for the outlet window).

Maximum for the ensuing (along the coolant pass) tube is the minimum for the preceding tube that is evident from the velocity distribution over the outlet window of the model bundle. There are reverse flows (of a weak intensity) at the corner of the rectangular wrapper as demonstrated by negative values of the signal at the last tube $170^0 \leq \varphi \leq 280^0$ (curve 7 in Fig. 5.4, b).

Hydrodynamics of various tube rows in heat exchanger. Distributions of coolant flows averaged around the tube perimeter (Fig. 5.5, a-d) are of considerable importance in reaching conclusion on the performance of various tube rows. The coolant flow is of irregular character: at the inlet section it rises gradually with the length and the depth of the model, at the outlet section it decreases with the model depth (c). In the top edge cross section flows level off in the inlet window, but stratify with increasing length, that is the flow enhances around the last tube (lag effect) and reduces around the first tube. Maximums appearing in the flow distribution around every tube are shifted along the length in dependence of the depth of the tube location. Thus, finally we have practically linear function (d).

A total flow rate through the area of «closed» cross section is constant (see relationship (b) in Fig. 5.5 and the flow balance is confirmed by the measurements with an accuracy ±1%.

$$(\sum v_n)_l / v = 1 \qquad\qquad (5.1)$$

Profiles of the coolant velocity (Fig. 5.5, a) allow gaining an impression about the coolant flow variation with the tube rows. The proper flow lines shown in Fig.5.5 differ in the percentage proportion of full flow that permits analyzing the tube performance.

It is evident, that an uniform distribution of the flow rate takes place in the cross section $l = 350$ and 800 mm. Between these sections the flow lines are shifted to the back wall of the cover. The following flow distributions are observed at the inlet and outlet of the model:

Inlet window (l_0 - height)
Length $0.4\,l_0$ - 25% of full axial flow
              $0.7\,l_0$ - 50%
              $0.9\,l_0$ - 75%
Outlet window (L_0 - height)
Length $0.5\,L_0$ - 25%
              $0.7\,L_0$ - 60%
              $0.8\,L_0$ - 75%

If the transversal and axial components of velocity are plotted along the horizontal and vertical axis, we can draw the vector diagram of resulting flows in the inlet and outlet sections of the model (Fig. 5.6). If the inlet window is involved, the slopes of the flow path reduce as the moved away from the bottom edge of the inlet window (Fig. 5.7). But the slopes at a distance $l = 380$ and 400 mm from the edge of the inlet window are abnormal. It should be noted that the flow around first tube is practically axial ($\varphi \cong 5 \div 10^0$), but those around second and third tubes have the slopes in the range $\varphi \cong 15 \div 20^0$ due to lap effect. Then the slopes reduce again with the maximums being observed in the relations.

It should be noted, that the rate of transversal flow drop with the depth of the inlet window is approximately equal to the rate of the axial flow rise with the height of the inlet window (Fig. 5.8). Equalization of the coolant flow over the tube rows can be achieved by the reduction of the inlet window size. So, if the inlet window is overlapped by 60%, flow non-uniformity reduces by a factor of 2, resulting in the more graduate flow variation with the bundle length (see Fig. 1.21, a, b). Practical value of the effect indicated is that the possibility appears to reduce heat transfer area in heat exchanger.

The model with the reduced inlet window ($l_0 = 150$ mm instead of $l_0 = 350$ mm) gives the more completed transversal velocity of a parabolic character with the blurred maximum falling on the 1/3 of the inlet window (Fig.5.9). Velocity distribution at the inlet section is also more $l_0 = 350$mm.

In the event of the reduced inlet window in parallel with the improved hydrodynamics there also has been some a rise in hydraulic resistance (Fig. 5.10) that is for the most part connected with the pressure drop over the inlet window. However, the rise in hydraulic resistance may be thought of as a small in comparison with the rather great and benefit effect of flow equalization.

The effect mentioned above was also observed in hydraulic experiments on the three-row models with the triangular and square arrangement of the tubes as shown in Fig. 5.11, c, d. Measurements performed in the three-row model with the triangular bundle have revealed, as a whole, the same relationshops as those in the one-row model, that has allowed drawing a conclusion that the one-row model with displacers readily simulates the multi-row bundle hydrodynamics.

Square bundle (low velocities). Experiments have been carried out on the three-row model of heat exchanger (Fig. 1.15, b) under conditions of low coolant velocities. We can follow the coolant flow direction, along which the lesser resistance takes place most likely. This is the clearance between the wrapper and first tube, where the maximum axial velocity is generated as demonstrated by the results presented in Fig. 5.12 and 5.13; whence it follows that maximum axial velocity falls within the first tube perimeter ($\Delta\varphi \approx 120^0$) adjacent to the plane wall of the model as at the inlet (Fig. 5.12) and at the outlet (Fig. 5.13)of coolant. As a result of the enhancement of velocity in the space between first tube and cover, velocity reduces in other parts of the model, in particular at a distance 90 mm from the bottom edge of the window (Fig. 5.14). Transversal velocity distributions around the tube in the area of inlet (Fig. 5.15) and outlet (Fig. 5.16) windows have maximums in the clearances between tubes and minimums (zeroth values of velocity) in the frontal and after areas of the tube.

Behavior of axial velocity averaged over the tube perimeter with the model height is as follow (Fig. 5.17):

- At the inlet section ($0< h \leq 130$ mm) velocity rises gradually as with the length and with the depth of the model;
- At a level $h \cong 130$ mm velocities coincide, near the top edge ($h = l_0 = 150$ mm they are little different from each other, except the tube 1 which has a jump of velocity that represents the coolant arriving under the window edge (Fig.5.12);
- The model outlet velocity increases if directed from the seventh to first tube, where there is the clearly defined velocity maximum. The maximum is due to flow "summing" over the channel in the outlet window (the whole coolant flows the tube 1).

The main hydrodynamic effect of the bundle under consideration is, as in the bundles previously investigated of a reduced inlet window, a relatively uniform distribution of subchannel flows over the depth and height of tube bundle. Thus, this effect revealed in the model with triangular bundle is validated in experiments with the square bundle. As mentioned above, it is of a great importance in possible decreasing of heat transfer surface in fast reactor heat exchanger.

Distributions of axial flows over the perimeter in various models (triangular, square bundles, one- , three-row models, with reduced or enhanced inlet window) are summed in Fig. 5.11, where it is evident an influence of the inlet window height, as well as the fact that data obtained on one-row and three-row model are identical.

Predictions of hydrodynamics of triangular heat exchangers. Macro-distribution of the coolant velocity in the inter-tube space of heat exchanger is calculated on the basic of the porous body model (code RAPORT-1). Theoretical approach presented in [4-8] and prediction procedure is included into the Governing Technical Materials [9].

Later the procedure was essentially improved, since the mathematical model, numerical procedure, constants were verified and tested using experimental data on velocity distribution over the inter-tube space. Electromagnetic technique of velocity measurement, as well as information gained with the use of the technique has a great advantages over an other measurements. The velocity fields were predicted for the one-row and three-row models with the triangular and square arrangement of the tubes in a wide range of Reynolds numbers ($10^4 \leq Re \leq 10^6$) under various boundary conditions. Basically, three types of boundary conditions on the given velocity at the inlet and outlet of the model:

    A) uniform distribution (considerable resistance of the inlet grid),
    B) non-uniform distribution (answering experimental velocity around first tube in the model),
    C) non-uniform distribution given by the definite laws (relationships)

Pressure drop in the events of axial and lateral flows were taken from the [10] after the processing and data generalization. When analyzing the one-row model, consideration must be given to the following features of the problem under discussion. The model has one row of seven tubes. It means that within one pitch the transverse and axial velocities can noticeably vary.

A porous body model assumes that the averaged velocity is of "smooth" profile and varies only slightly within the one pitch. Thus, calculation of low-tube bundle by using the porous body model furnish insights into the nature of the process and helps in answering the questions: how the model can be applicable to the low-tube bundles and what discordance can be appeared in the process.

In calculating of the one-row bundle enclosed in the box with the displacers, the porous body model uses friction factors in transverse and axial flows deduced from experiments on multi-row ("infinite") bundles. Comparison analysis of calculation allows the following conclusion to be reached:

- wide variation of Reynolds number ($10^4 \le Re \le 10^6$) causes the velocity behavior to change only weakly, which is to say that flow pattern depends almost not at all on the Reynolds number;

- it is evident that an inertia is enhanced with Reynolds number: inlet non-uniformity in the header increases, its dying down is retarded, flow rearrangement begins later;

- boundary conditions are of great importance. Uniform inlet velocity gives more regular flow pattern across the bundle. Non-uniform (experimentally revealed) behavior causes the flow pattern to vary significantly as at the inlet section as over the bundle cross section;

- calculations conducted under the boundary condition determined in the variant "C" show the results which are sufficiently close to those obtained in the variant "B";

- a comparison between predictions and experimental data show that they are in good qualitative and partly quantitative agreement.

Calculations have been conducted for the square tube bundle under boundary conditions A, B, C at $Re = 10^4$ and $2*10^4$. In the event A, inlet hydraulic non-uniformity is revealed to be $u_z^{max} / u_z^{min} = 2.7$, and outlet one is 4.5. Variation of Reynolds number within the range $10^4 \div 2*10^4$ does not practically influence on the solution, but inlet non-uniformity increases with the Reynolds number and outlet one reduces. In the event B the hydraulic non-uniformity falls to 2.0 (inlet) and 4.3 (outlet). Variant C gives the theoretical inlet and outlet profiles being close to predictions based on experimental profiles.

Fig. 5.18 presents experimental and calculated curves for axial velocity distribution along the first and seventh tube of the model. Calculations have allowed improvement of the inlet section hydrodynamics in the model with the square tube arrangement. By hydrodynamic improvement is meant that coolant axial velocity becomes of uniform character at the inlet section, more exactly in the edge of the inlet window. Hydraulic non-uniformity varies in a wide ranges in dependence of the inlet window height and relative pitch of the bundle. In the compact bundle with the small windows maximum velocity is observed to be at the first tube. In the free bundles with the large windows maximum velocity takes place on the internal tubes.

Three models of heat exchanger were calculated. Here relative pitch was $s/d = 1.06$; 1.2; 1.3; 1.4 and relative height of the inlet window $H/B = 0.55$; 1.0; 2.0; 3.0, where B - the width of the tube bundle. It is evident from Fig. 5.19, that if windows are small a free bundle is optimum, and a compact bundle - for the large windows. The model tested is near the optimum.

5.3 THERMAL RESULTS

On technique of the local thermal modeling. Experiments were carried out on the three-row model of a triangular and square tube arrangement (Fig. 1.14, 1.15) using NaK alloy as a hot (inter-tube space) and a cold (inside of tubes) coolant. Every tube and every channel is equipped by the capillaries inside of which the mobile thermocouples are moved (Fig. 5.20).

Essentially, the local technique of thermal measurements is as follows:
Temperature variation of every tested tube with the height (Fig. 5.21) is determined for the purpose of analyzing temperature difference "maximum temperature of the hot coolant" - "minimum temperature of the cold coolant".
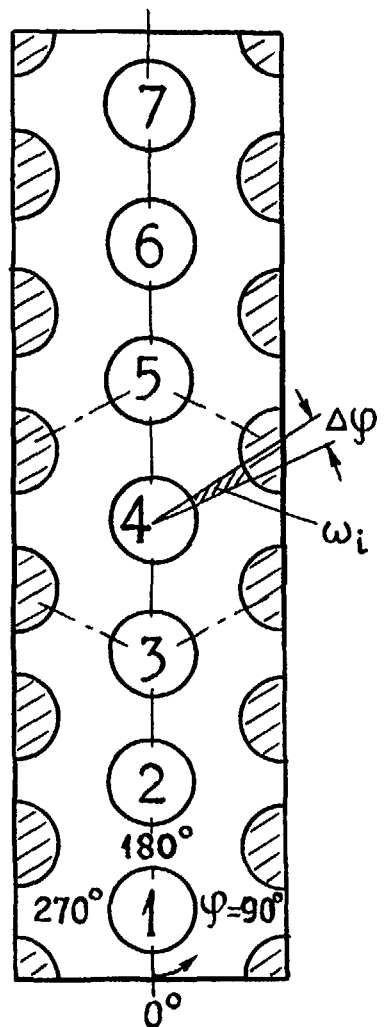
Fig. 5.1. Single-row assembly cross section.
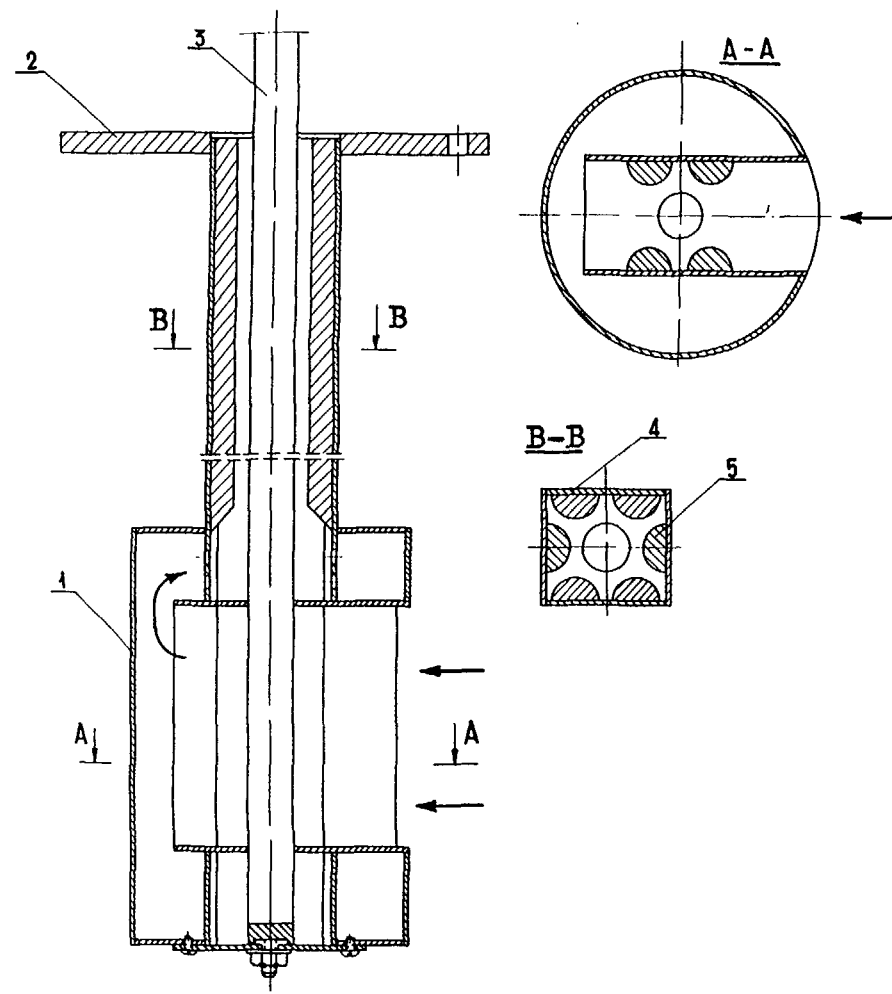
Fig. 5.2. Calibration model and the transverse velocity behaviour
1 - header, 2 - support plate, 3 - pipe
*4 - wrapper, 5 - displacer.*
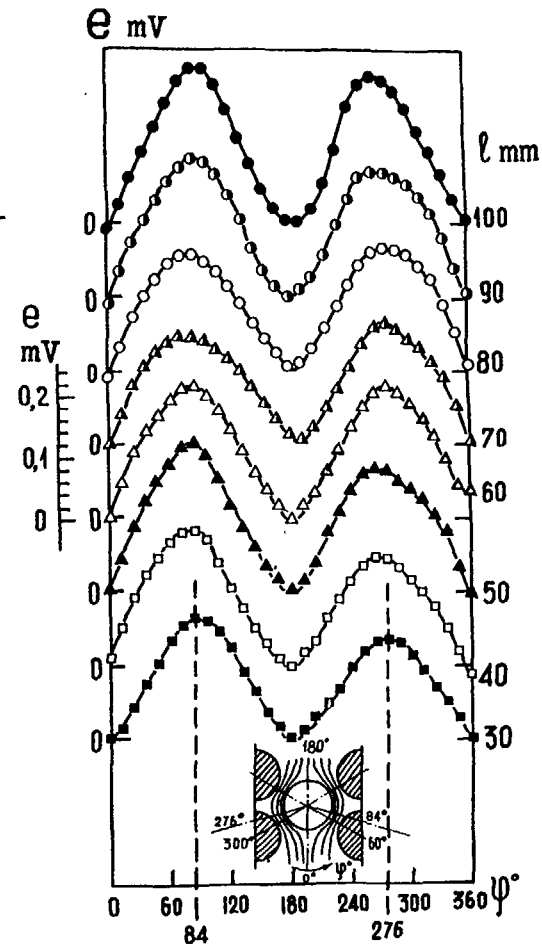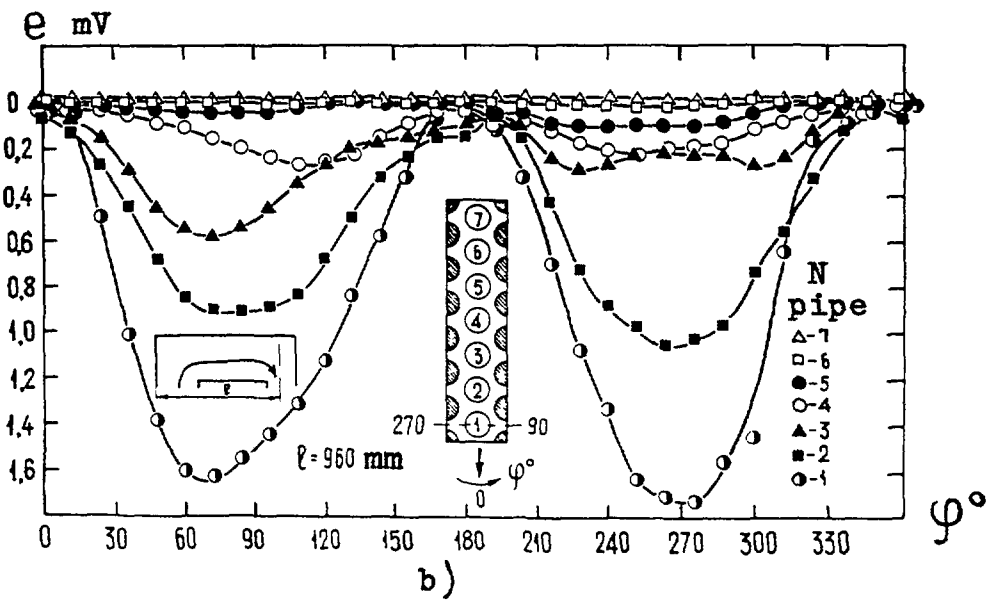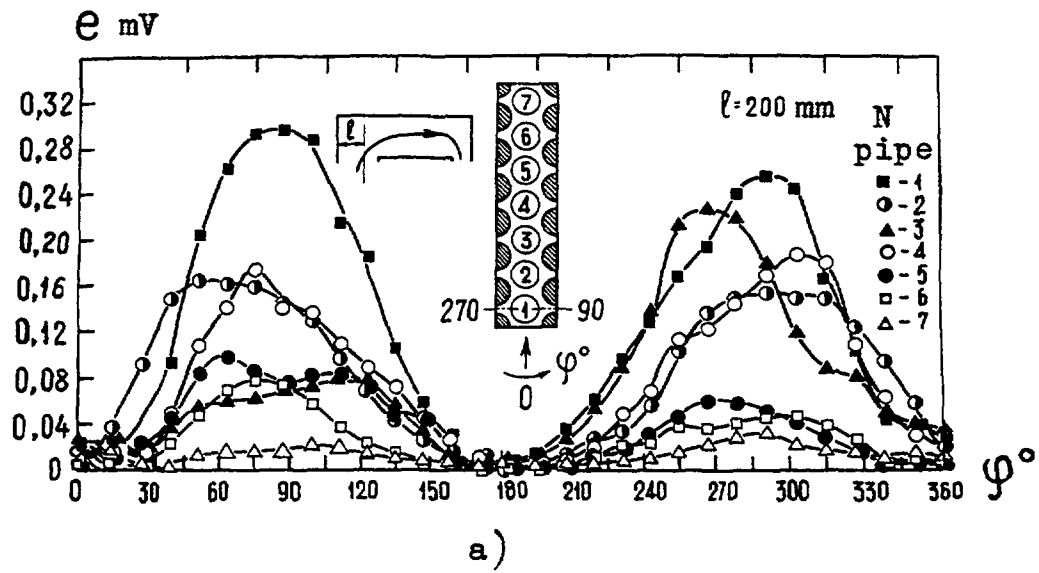
Fig. 5.3. Transverse component of velocity around pipe in inlet (a) and outlet (b) windows of the model assembly.

242
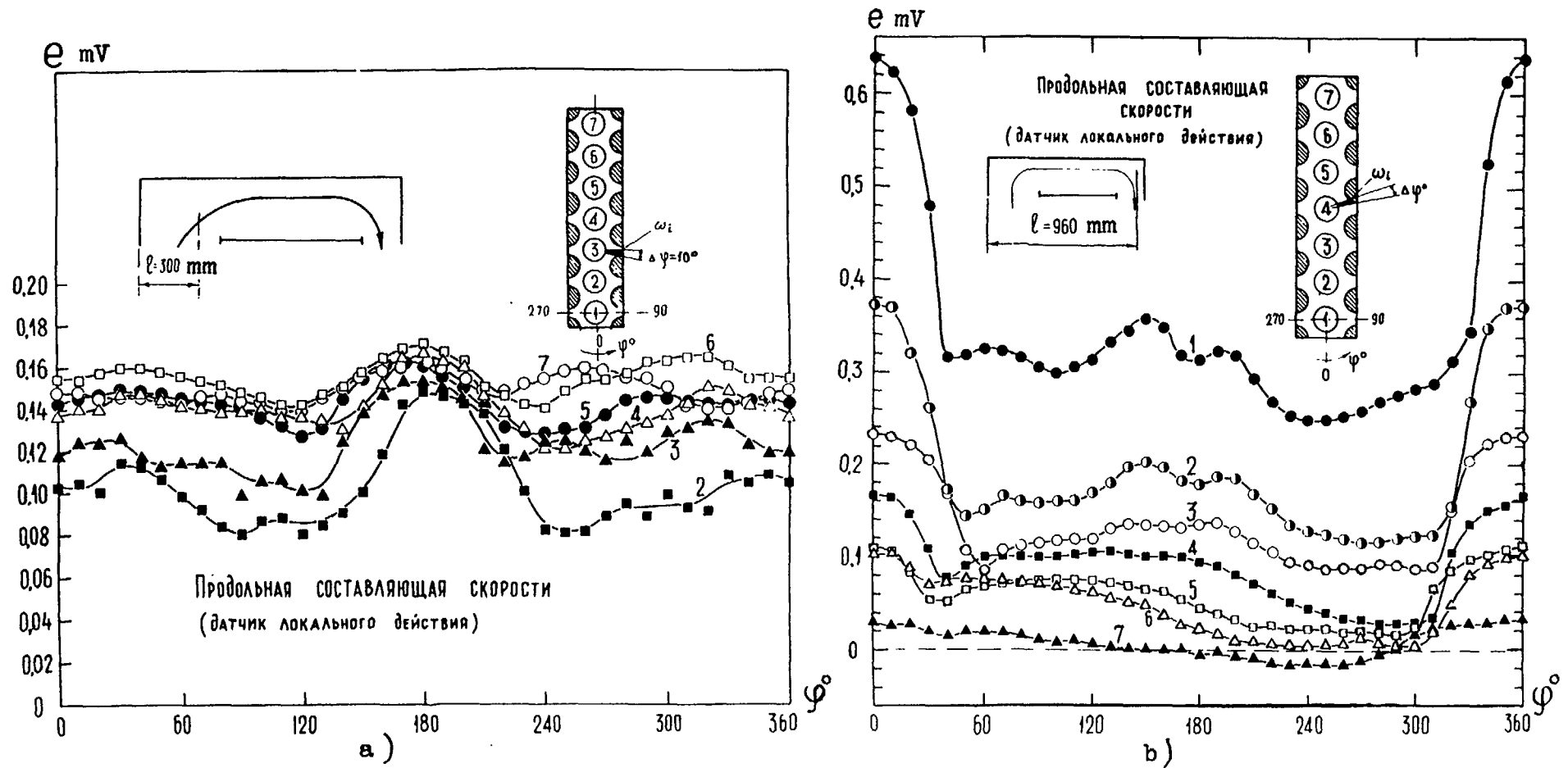
Fig. 5.4. Axial component of velocity around pipe in inlet (a) and outlet (b) windows.
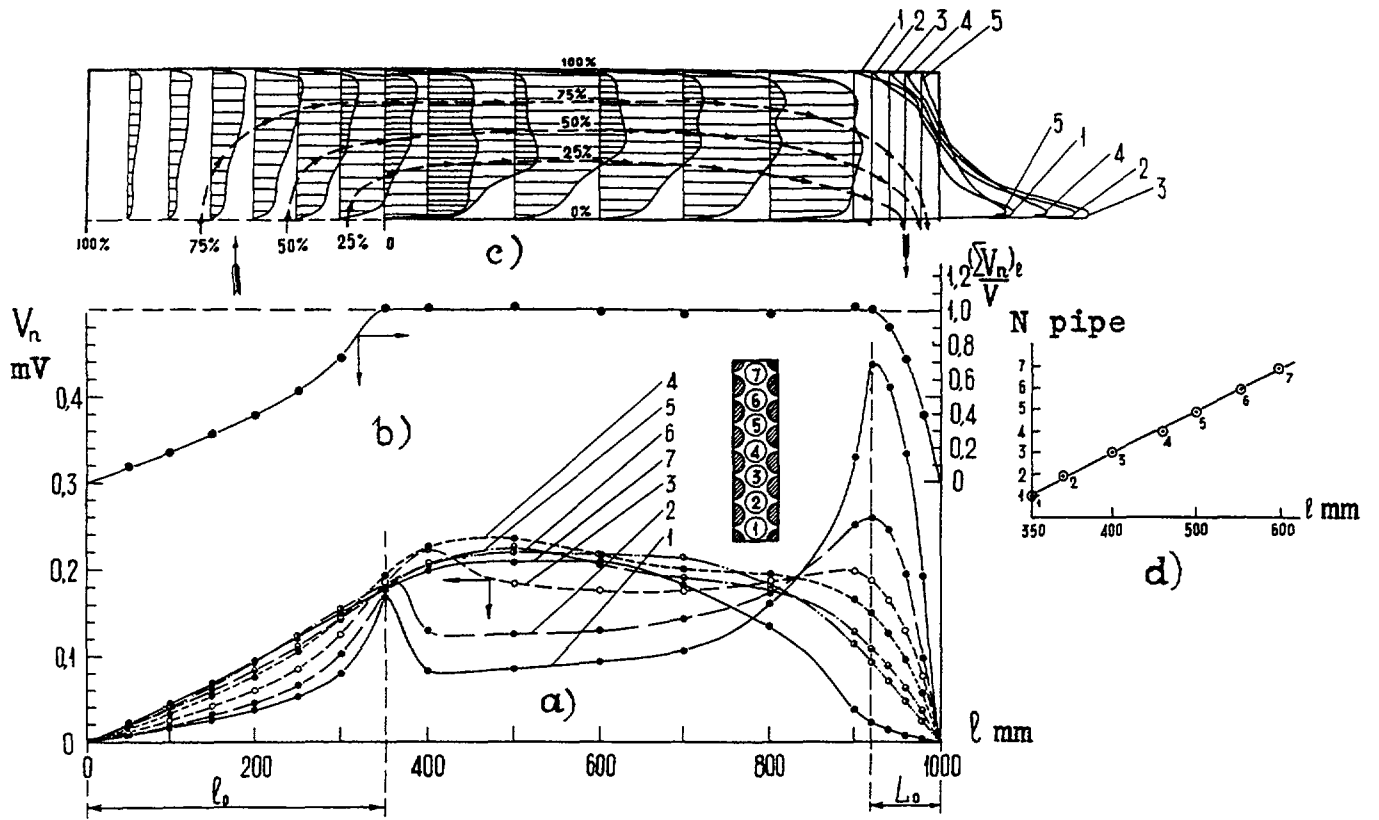
Fig. 5.5 Axial velocity (a); axial flow rate with the model length (b); with the
height and deepness (c); maximum axial velocity for a different pipes (d).
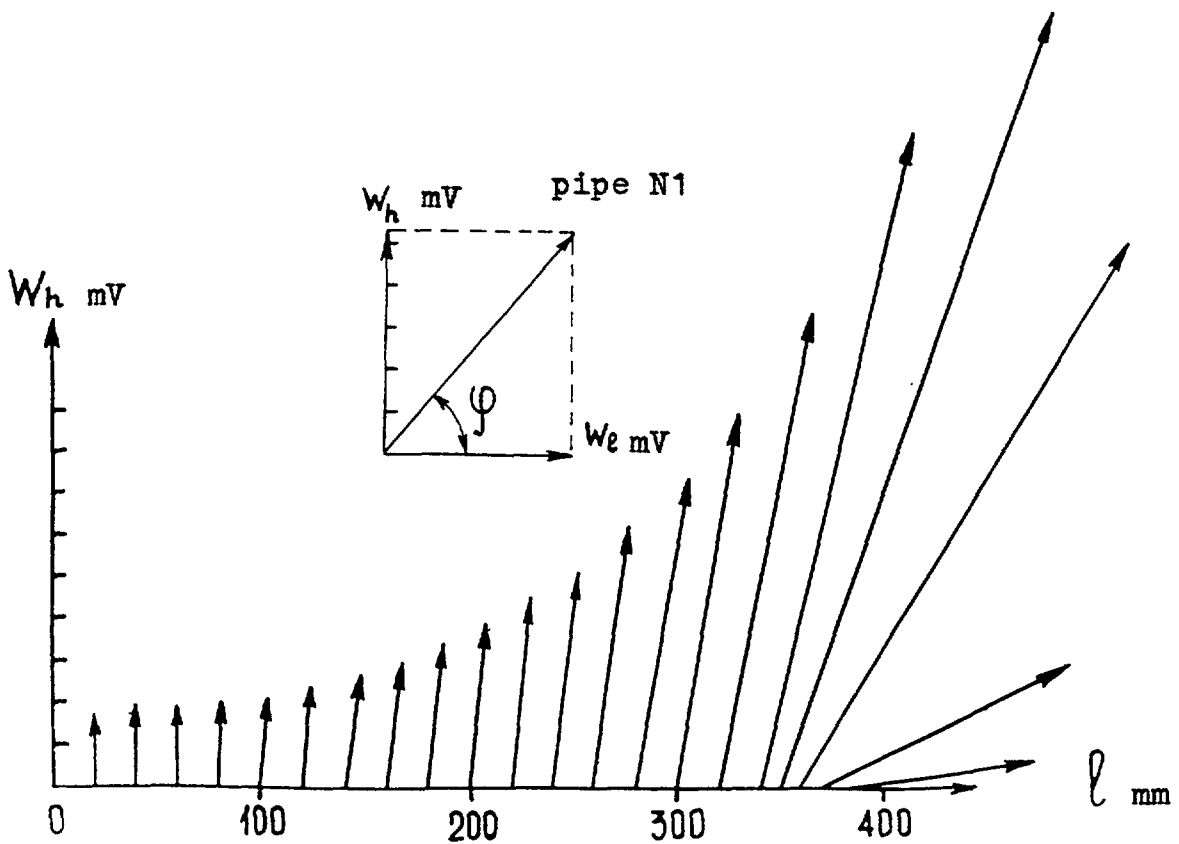
Fig. 5.6 Inherent vector diagram for inlet window of the model.
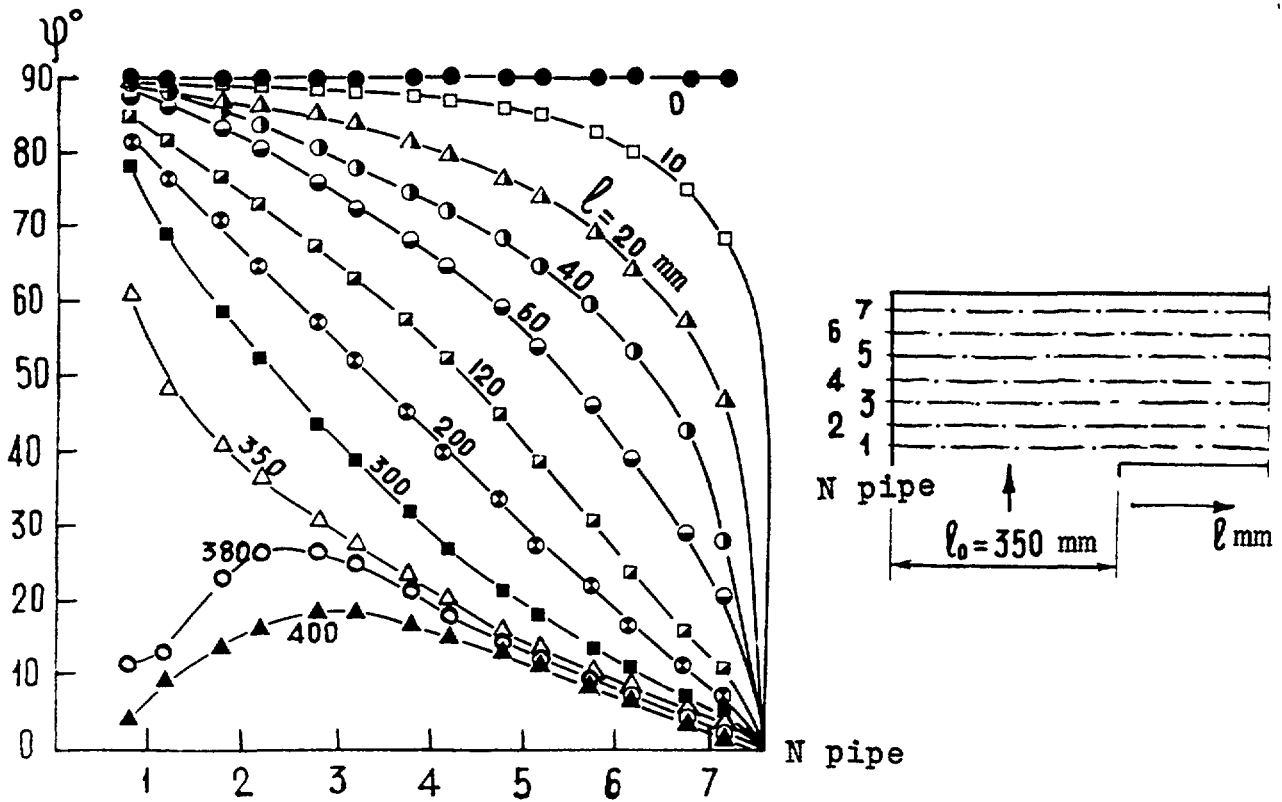
Fig. 5.7. Change in the slope of the flow with the deepness of the inlet window.
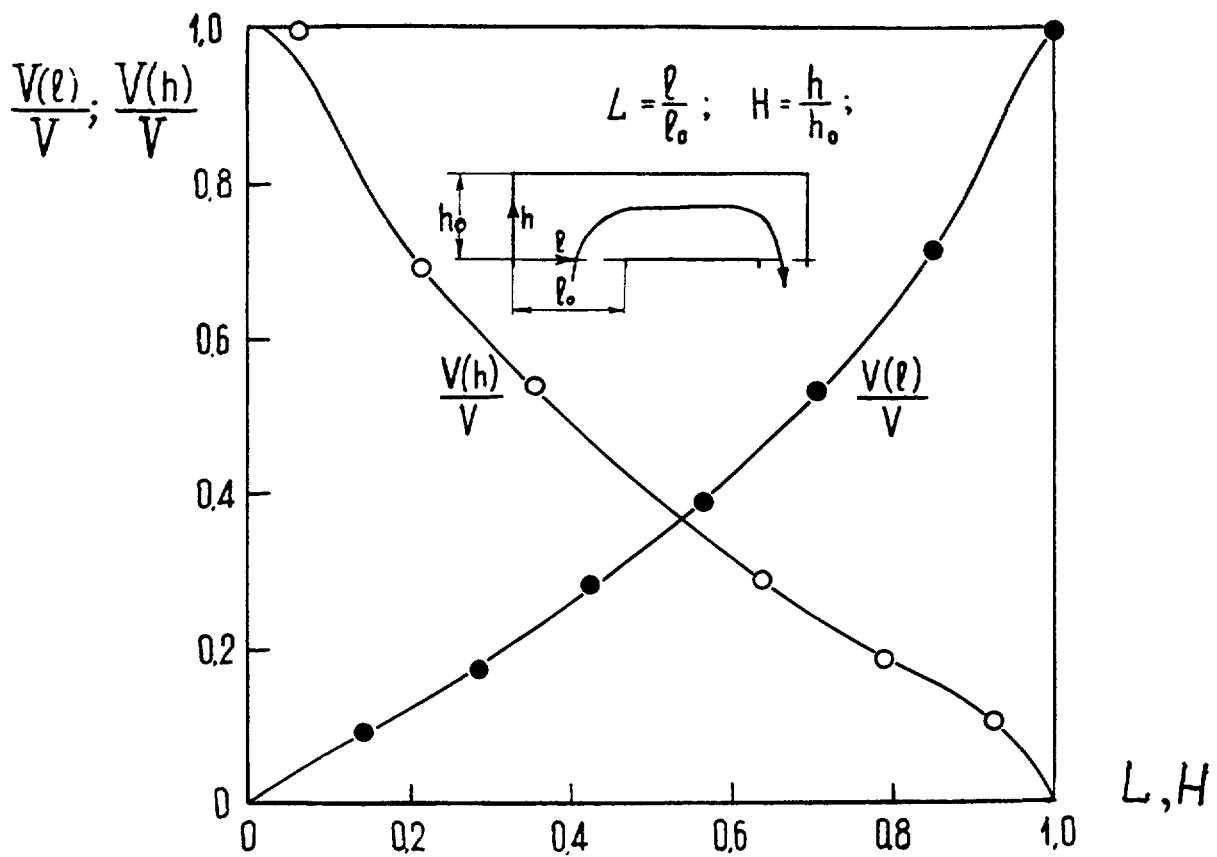
Fig. 5.8. Transverse and axial flow in the inlet window.

245
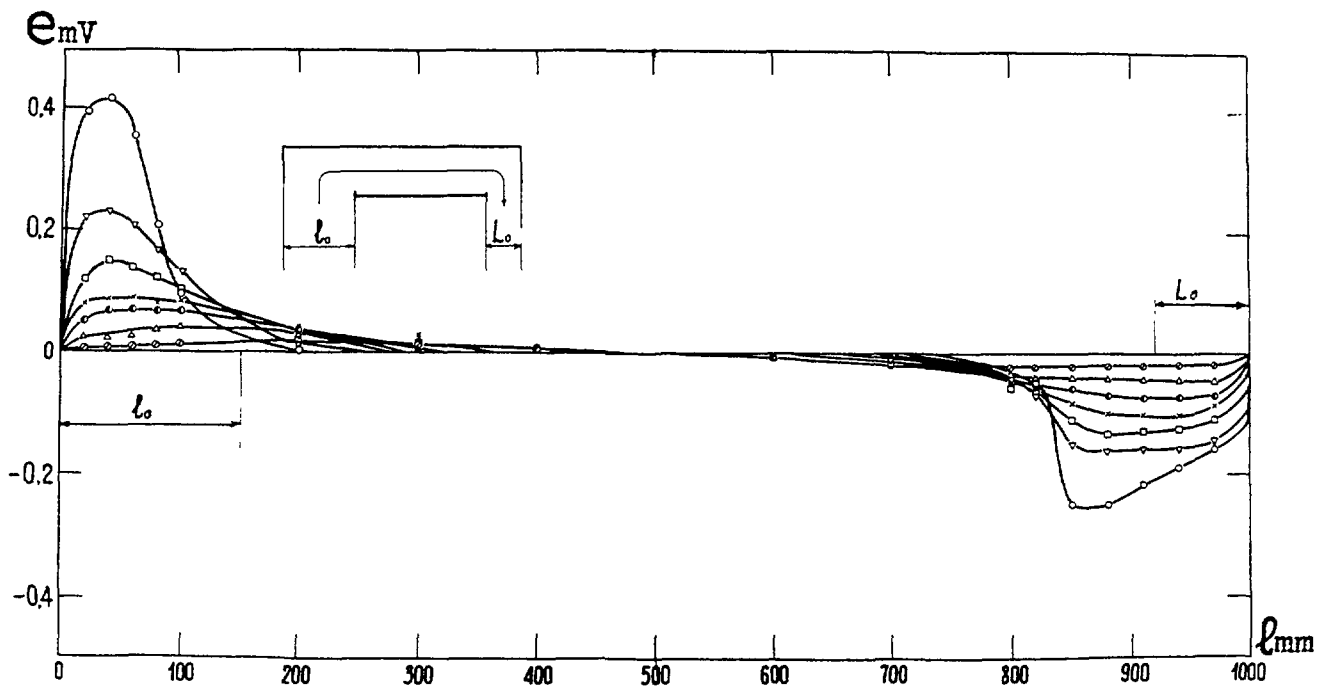
Fig. 5.9. Transverse velocity with the model height in the event of the reduced
size of the inlet window.
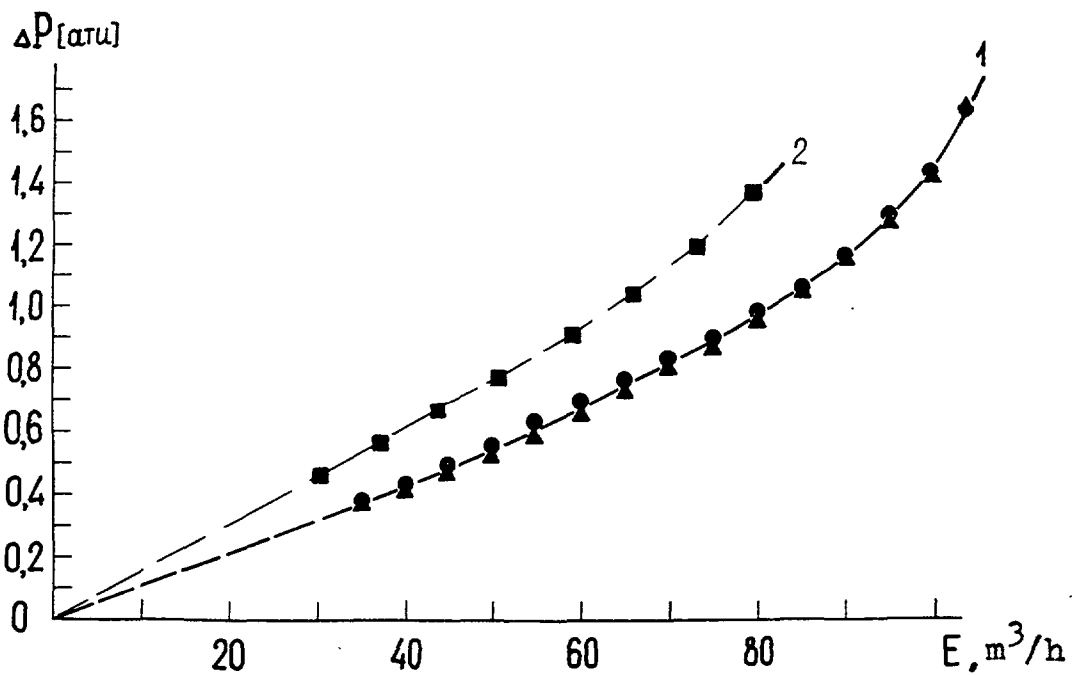
Fig. 5.10. Hydraulic losses with the flow through the model assemblies in the
inlet windows.

246
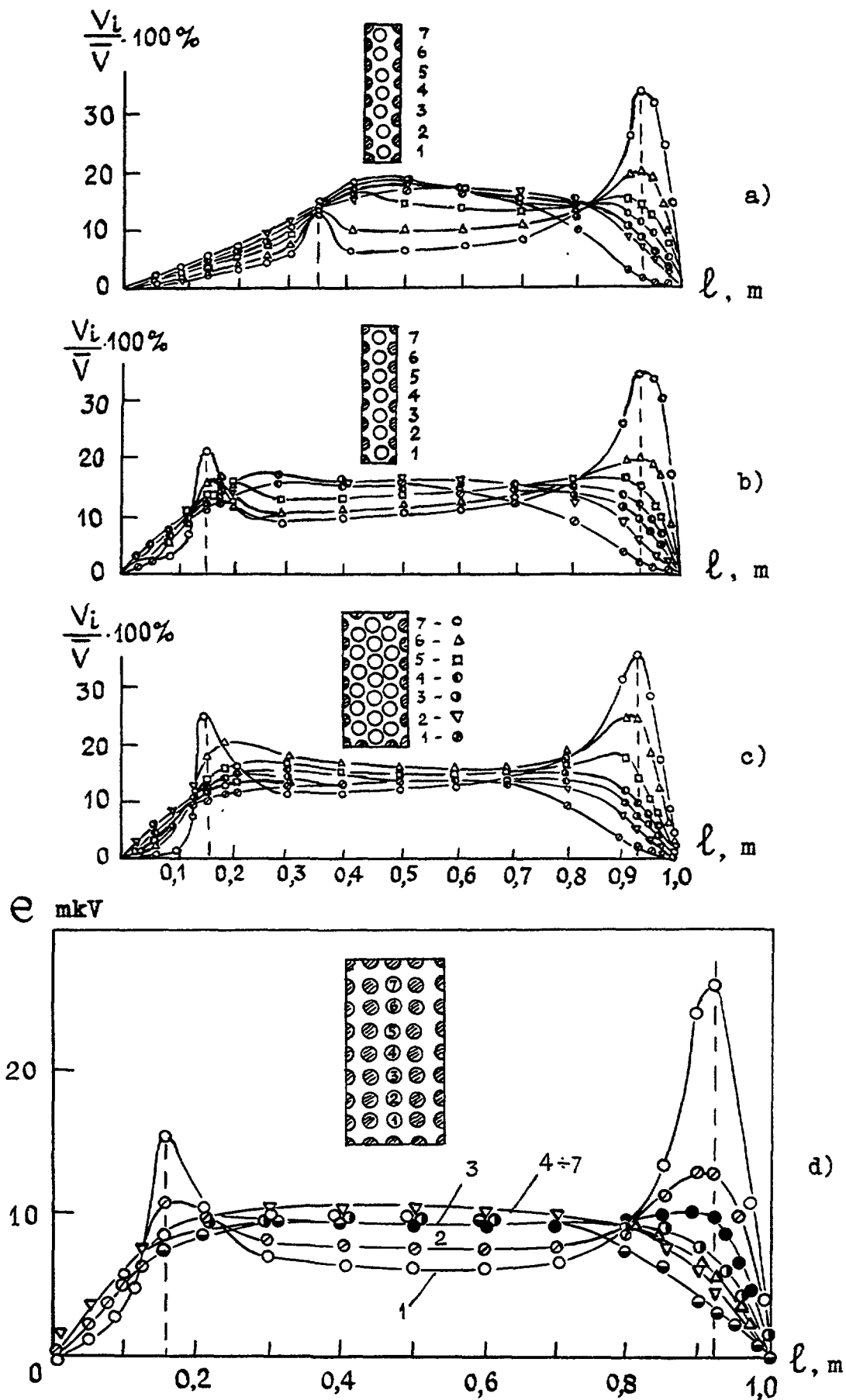
Fig. 5.11. Coolant flow with the model sizes at various height of inlet window (a, b, c - triangular arrangement of pipes, d - square arrangement).
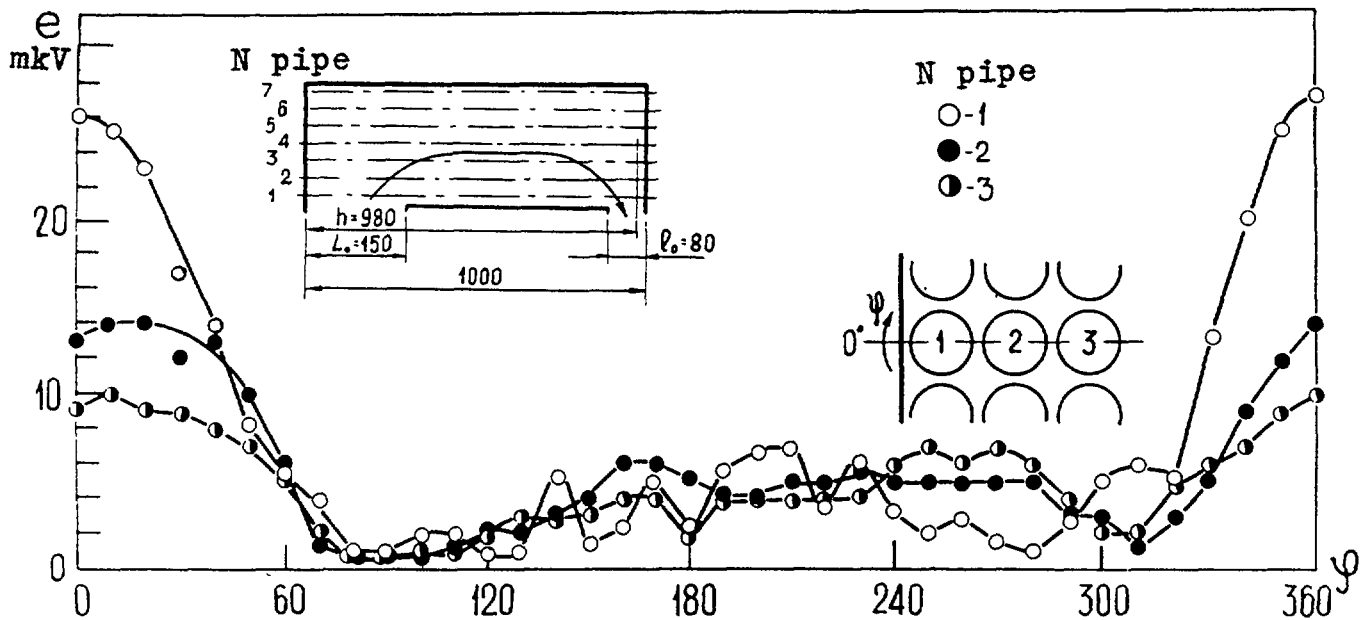
Fig. 5.12. Axial velocity around pipe in the outlet window at a level 150mm.
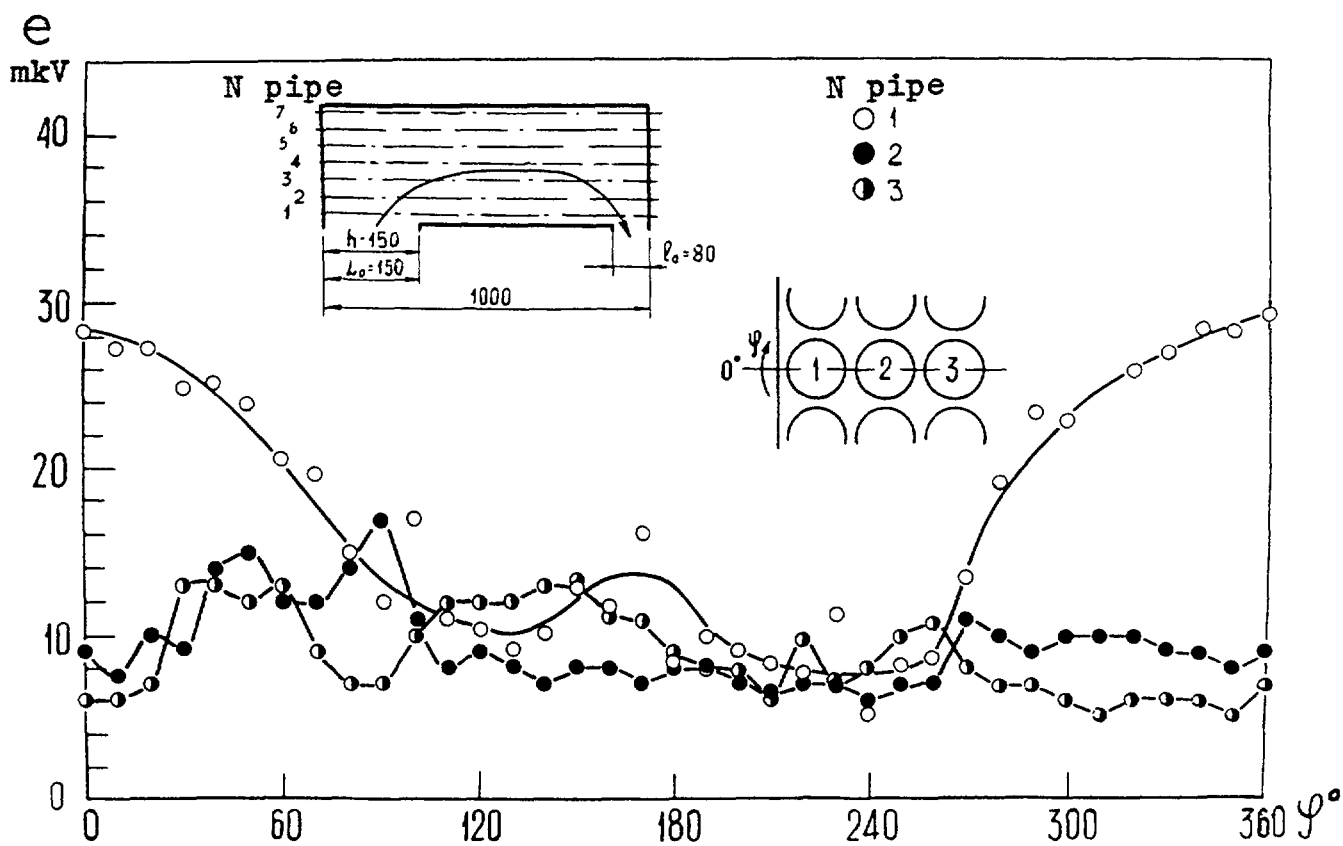
Fig. 5.13. Axial velocity around pipe in the outlet window at a level 980mm.

248
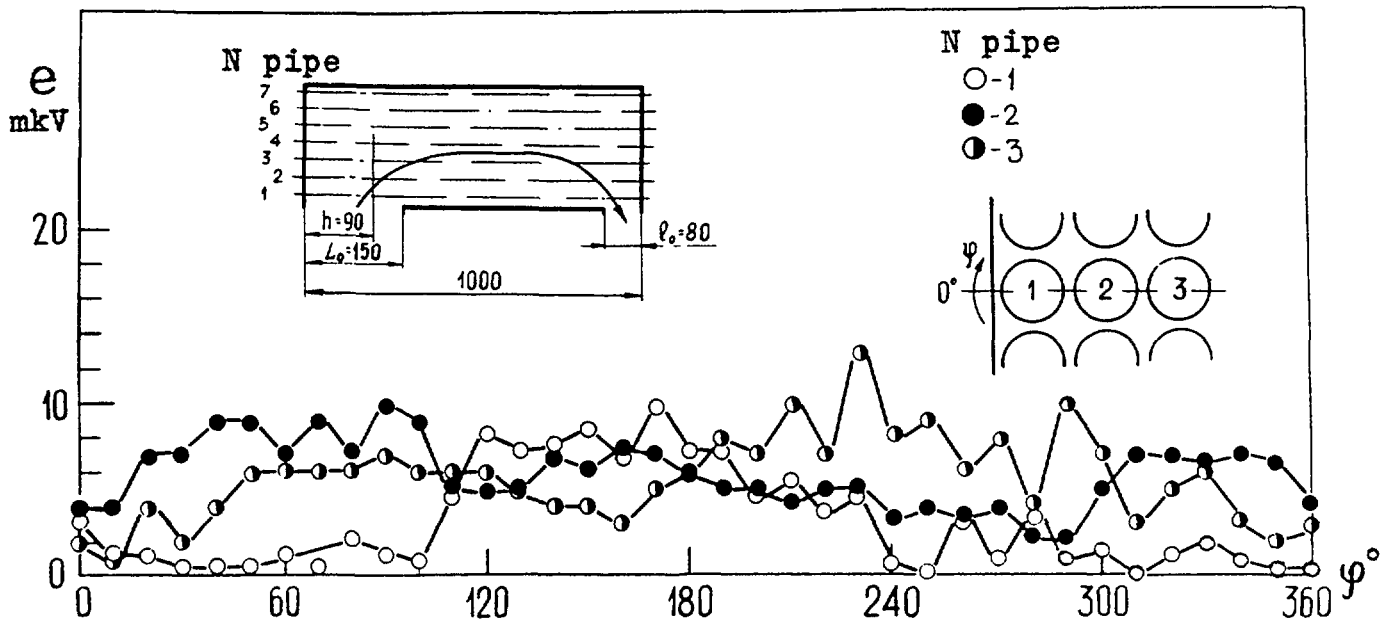
Fig. 5.14. Axial velocity around pipe in the inlet window at level 90mm.
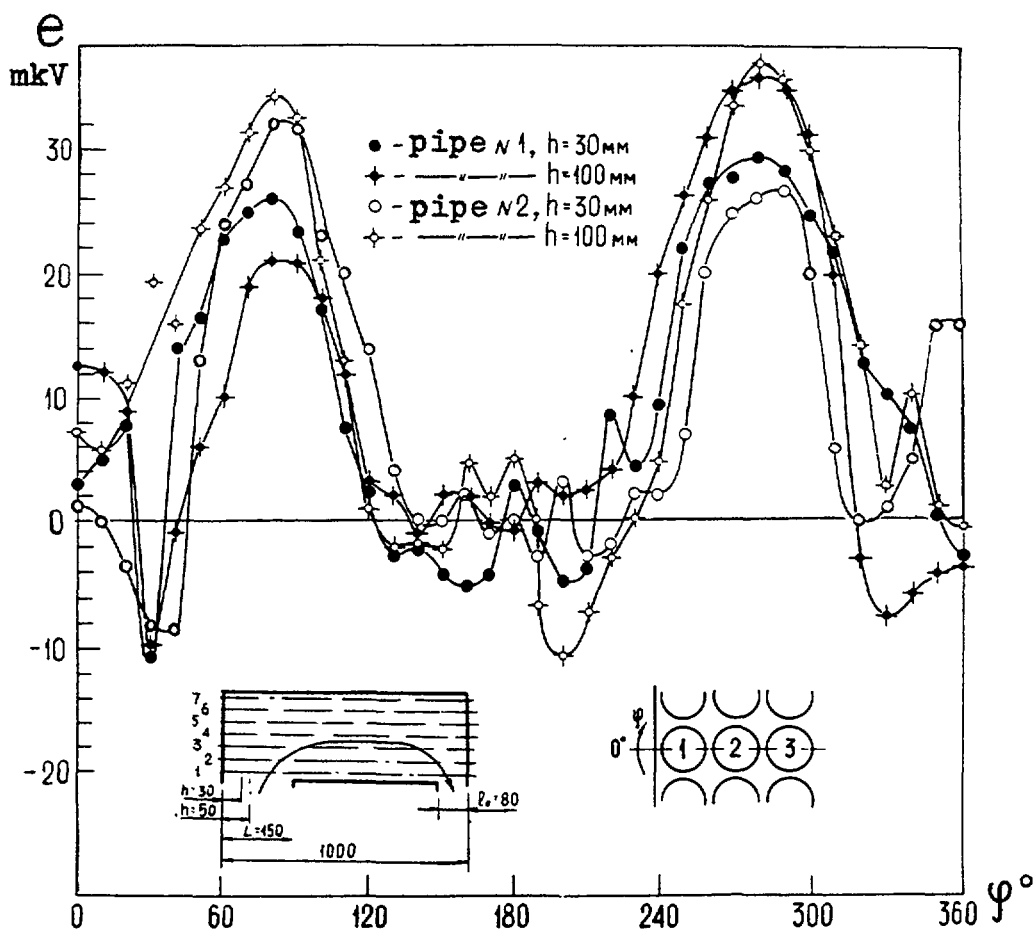
Fig. 5.15. Transverse velocity around square arranged pipes at h =30 and 100mm.

249
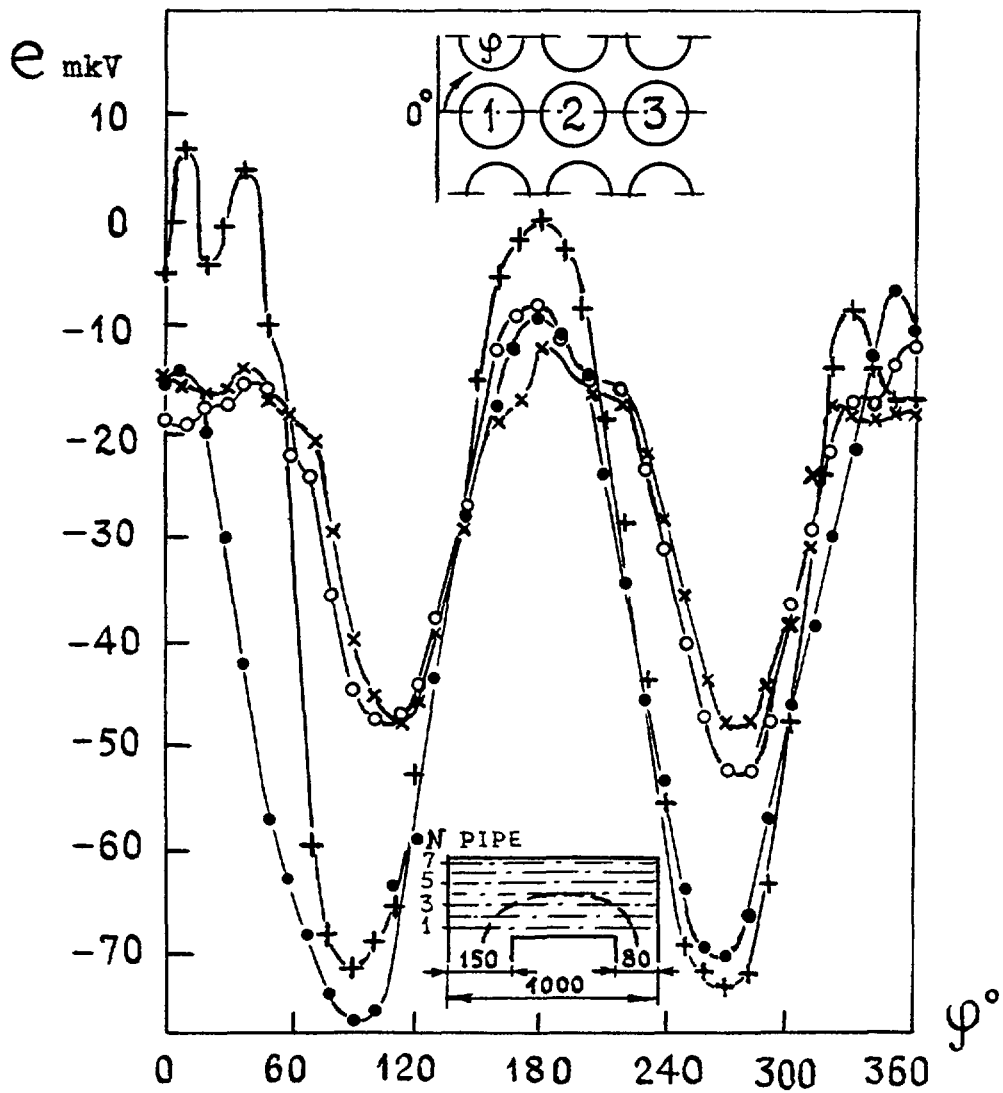
Fig. 5.16. Transverse velocity around pipes (square arrangement) in the outlet window of the model:

● , + , - *pipe 1 and* O , × - *pipe 2 for* h = 950 *and* 970mm, *respectively.*
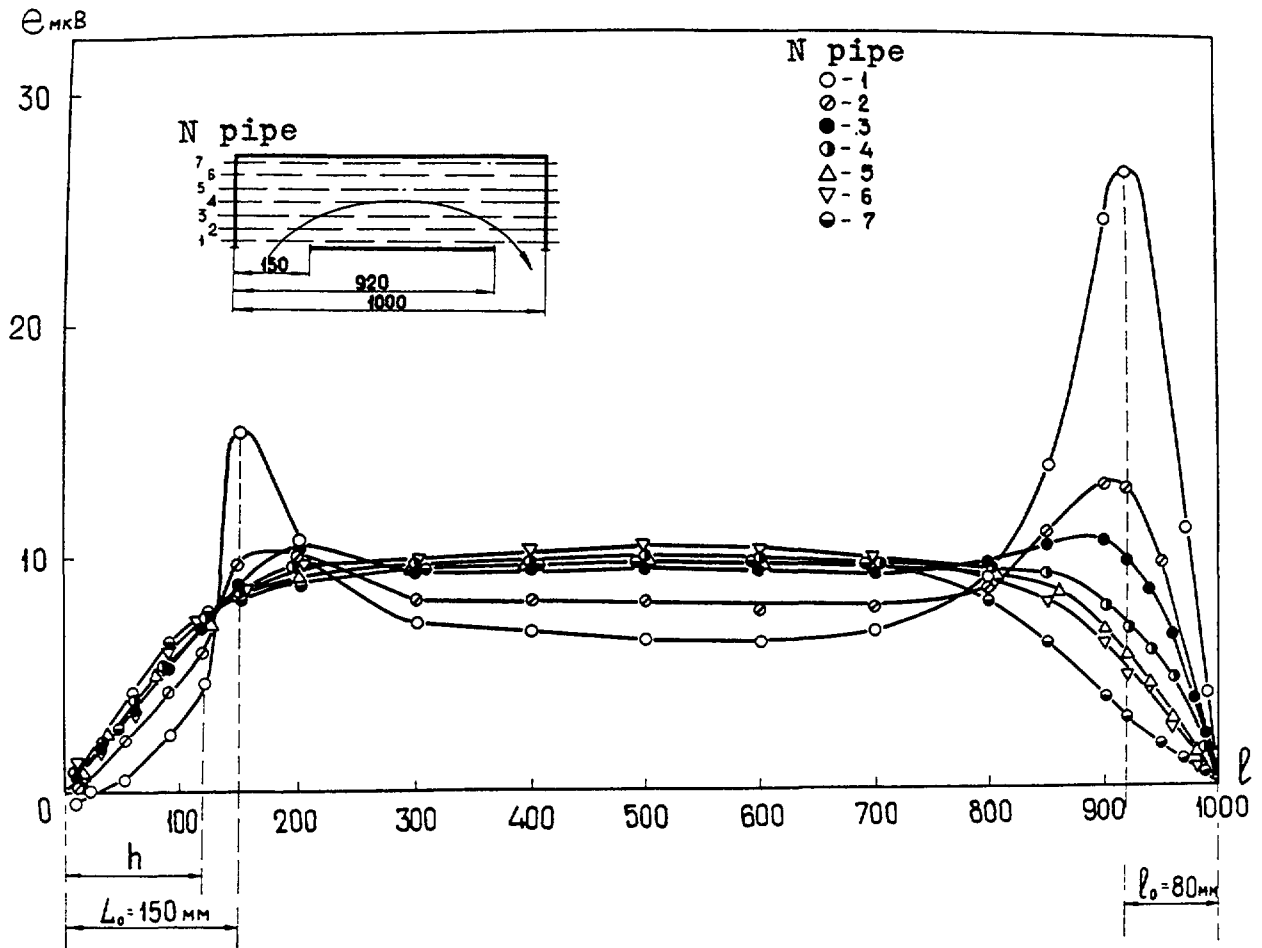
Fig. 5.17. Axial flows with length for the pipe 1÷7.
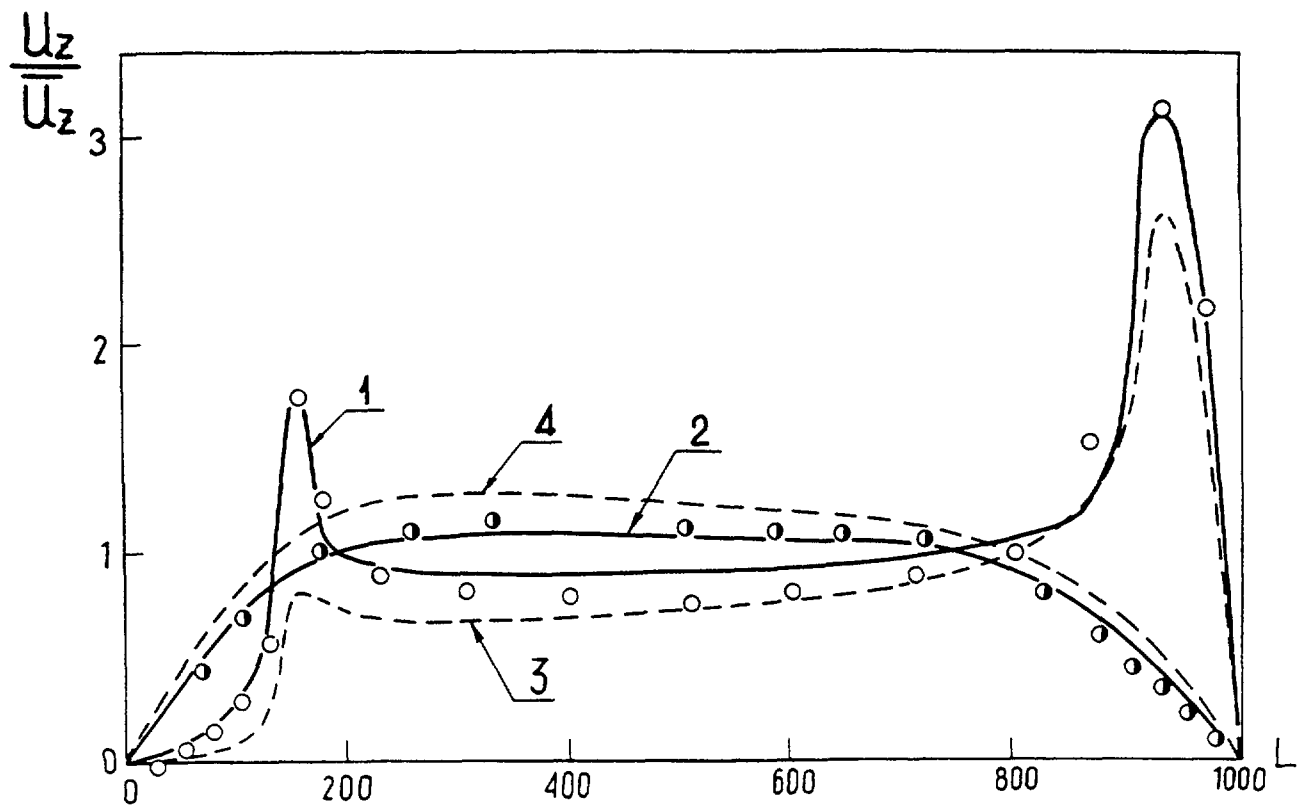
Fig. 5.18. Dimensionless velocity around the pipes № 7:
1, 2 - prediction at the inclined inlet;
3, 4 - prediction at the direct inlet; O , ◑ - experiments, respectively.
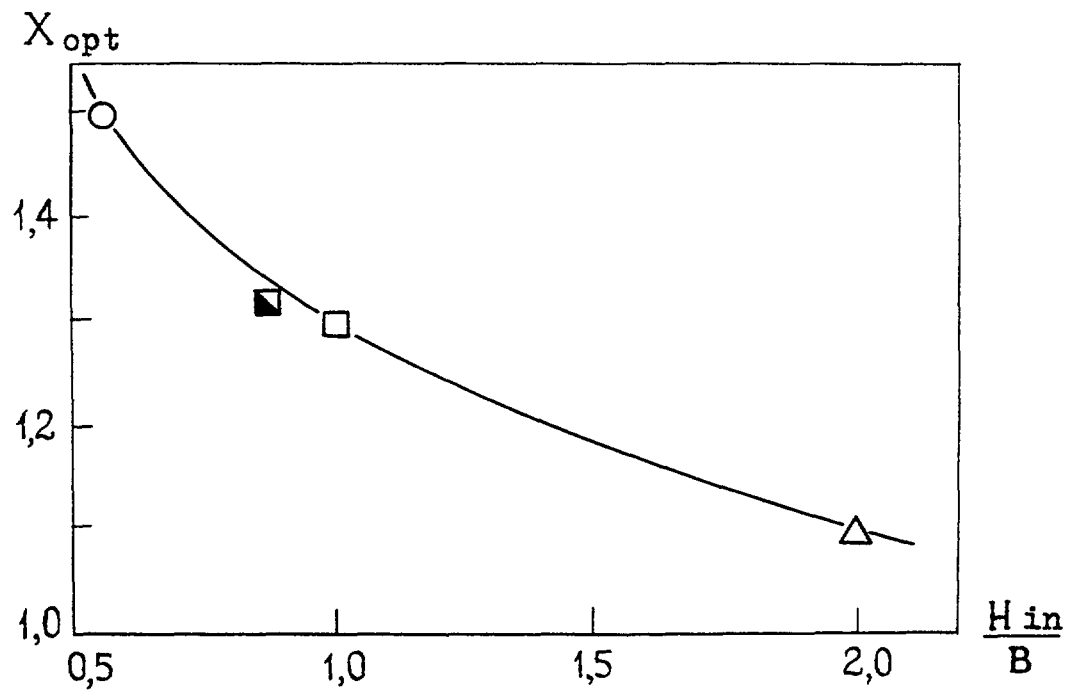
Fig. 5.19. Optimal pipe bundle pith with the outlet window height; ◨ -model.
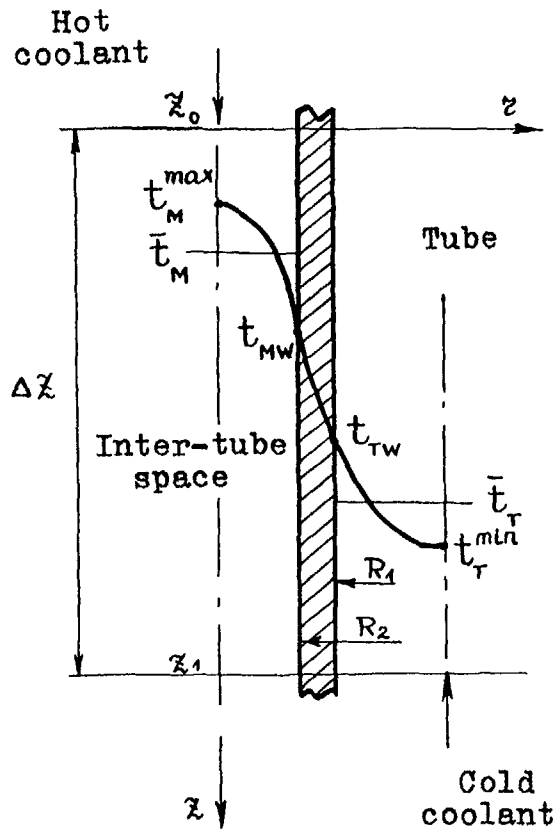
Fig. 5.20. To heat transfer calculation.
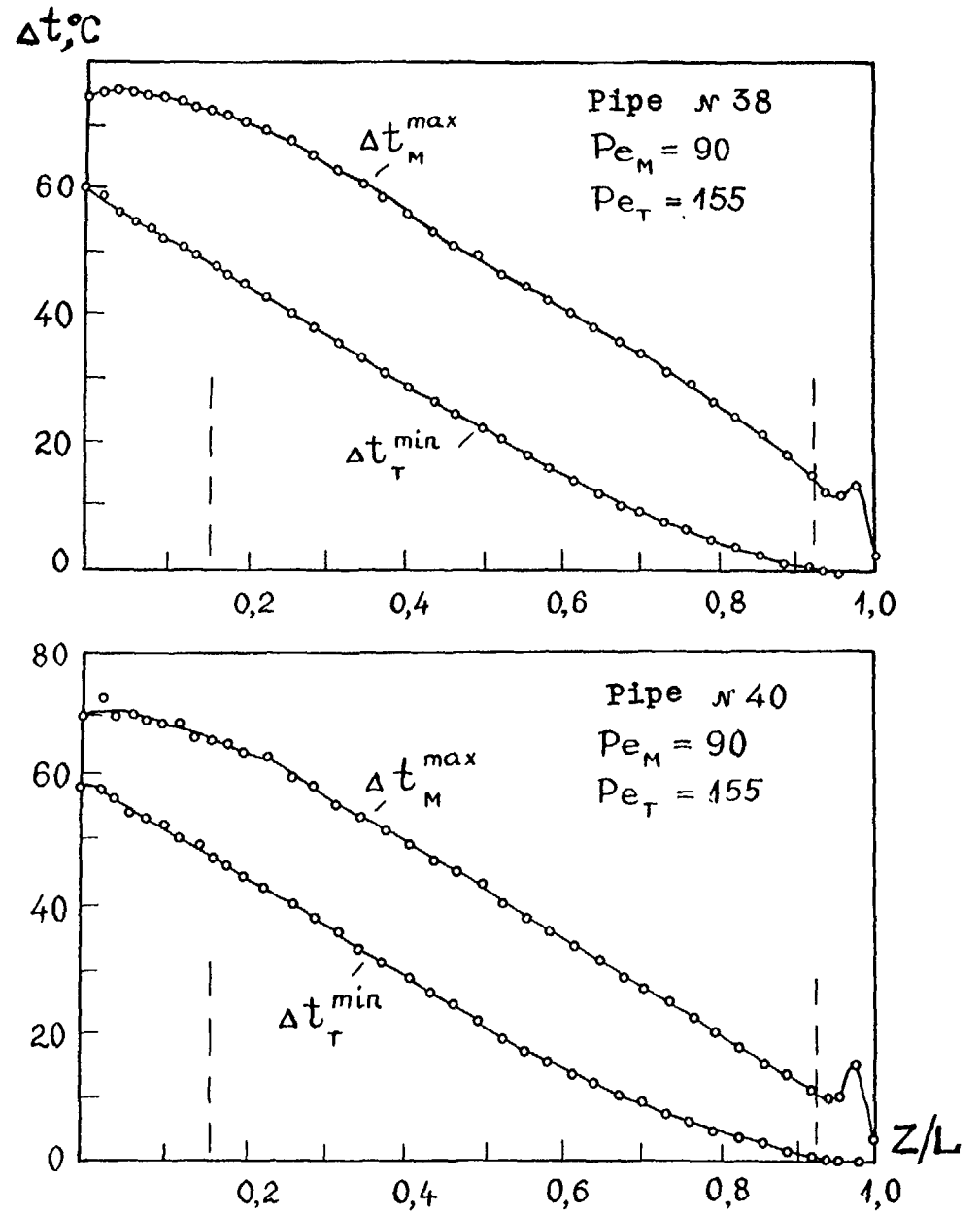
Fig. 5.21. Internet coolant temperature fields inside (T) and outside (M).
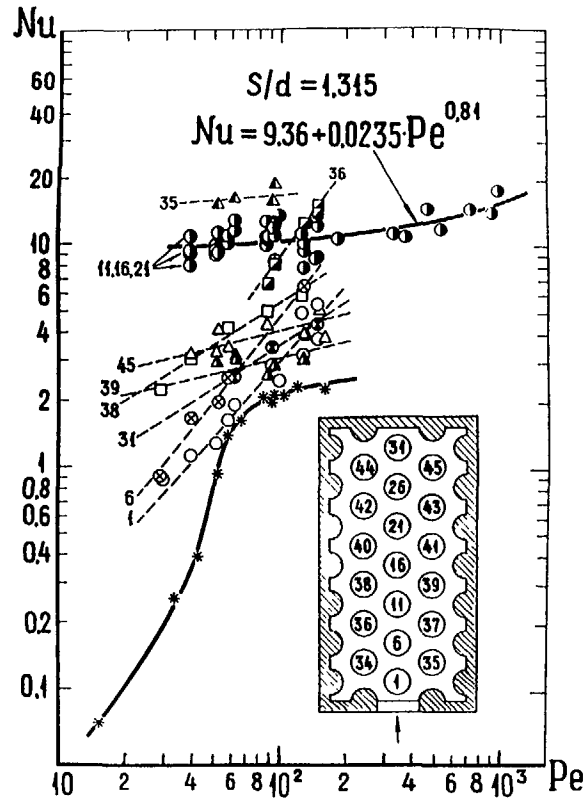
Fig. 5.22. Nusselt -Peclet numbers relation:
- local modelling of internal area of the model,
- processing with averaged temperature in headers,
other subscripts - near wall pipes.
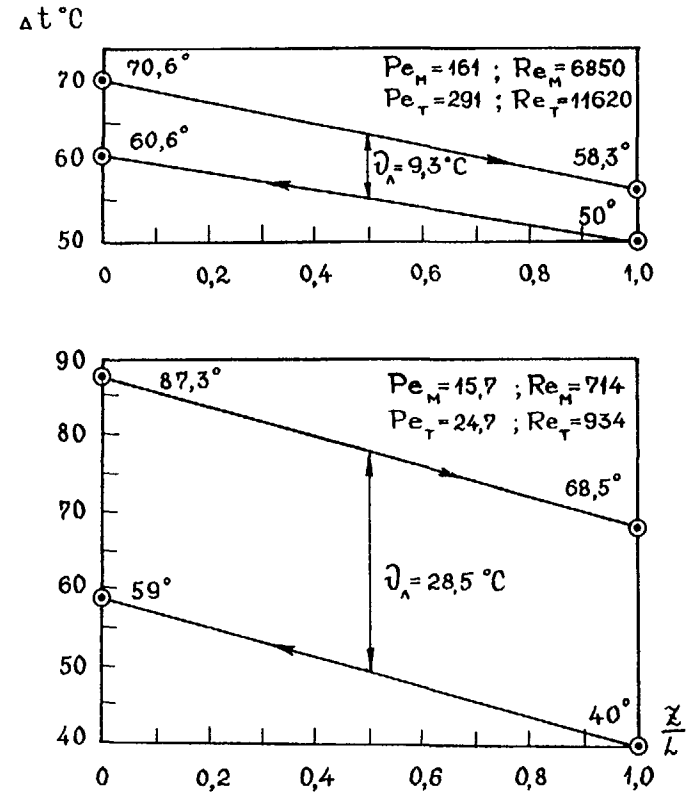

Fig. 5.23. Measurement scheme for coolant temperature:
υ_Λ - mean logarithmic temperature difference,
⊙ - temperature in the header.
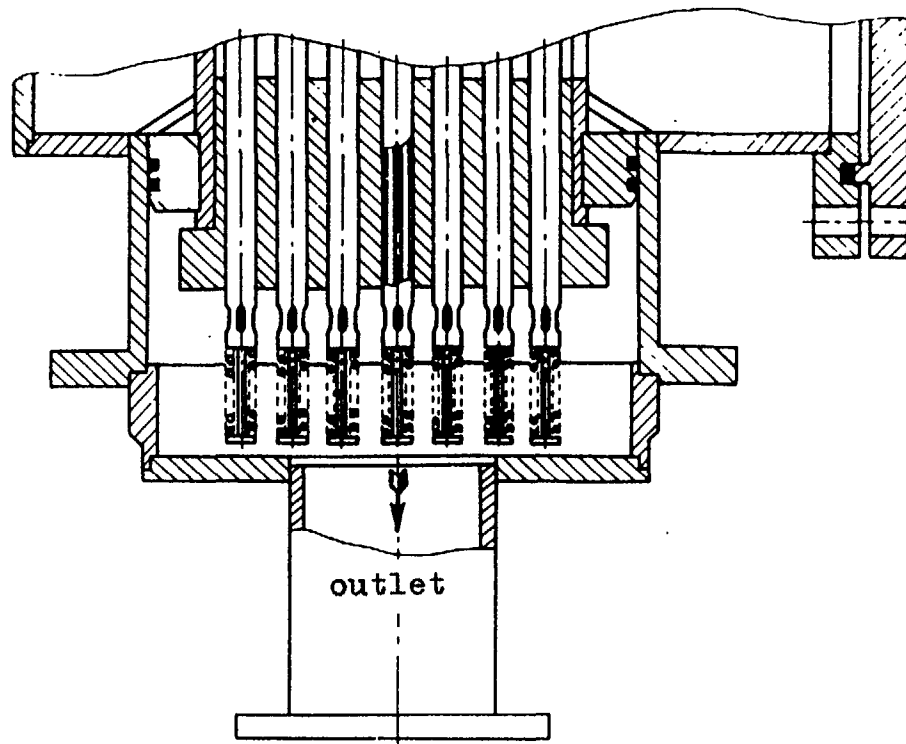
Fig. 5.24. *The outlet chamber design in downward flow of «cold» coolant.*
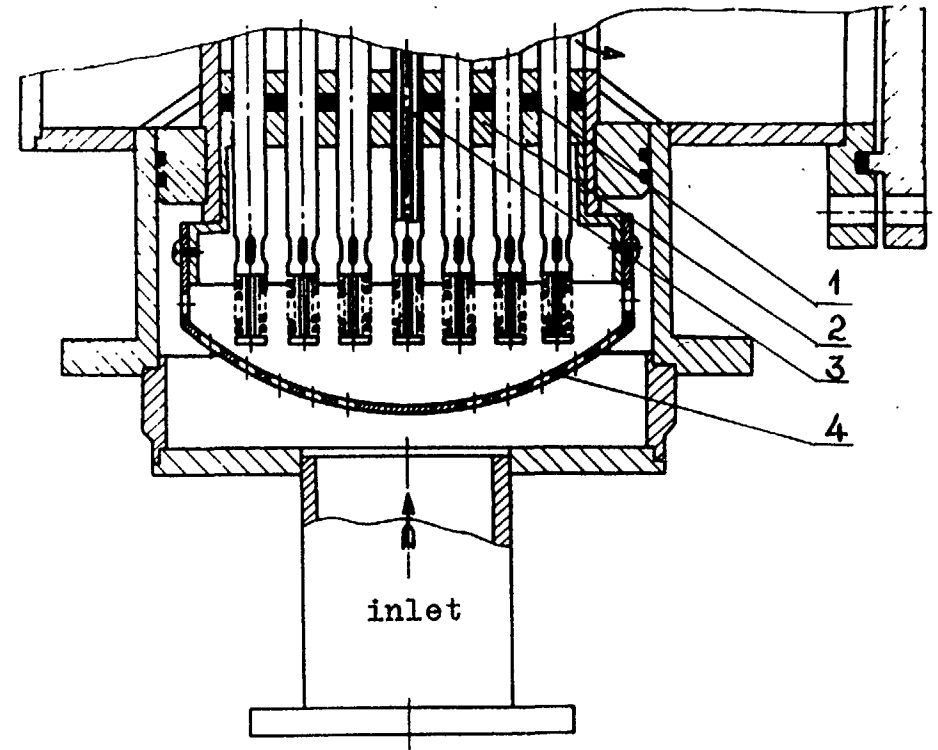
Fig. 5.25. *The outlet chamber design in forward flow of the «cold» coolant:*

1 - insulation, 2- pipe plate,
3 - operating pipes instrumented by thermocouples
4 - fabric body.,
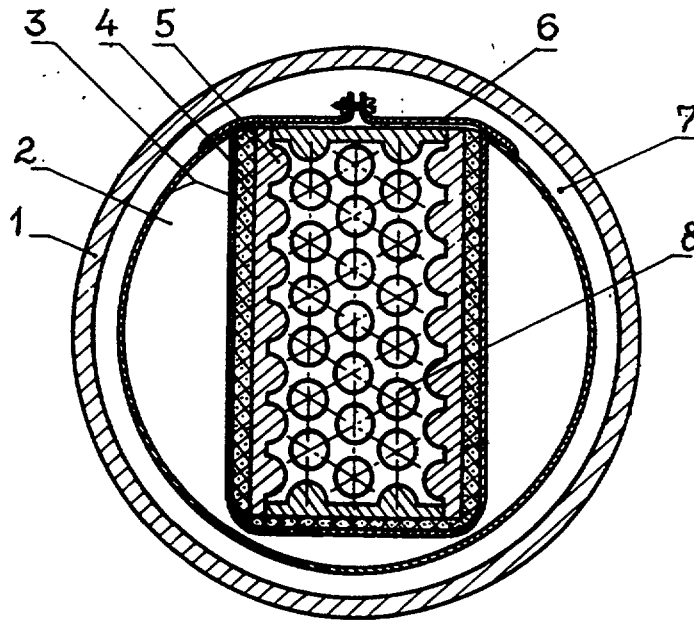
Fig.5.26. Cross-sectional diagram
1 - model case, 2 - air layer,
3 - empty displaces, 4- insulation,
5 - wrapper tube, 6- clamping band,
7 - coolant-filled cavity, 8 - pipe.
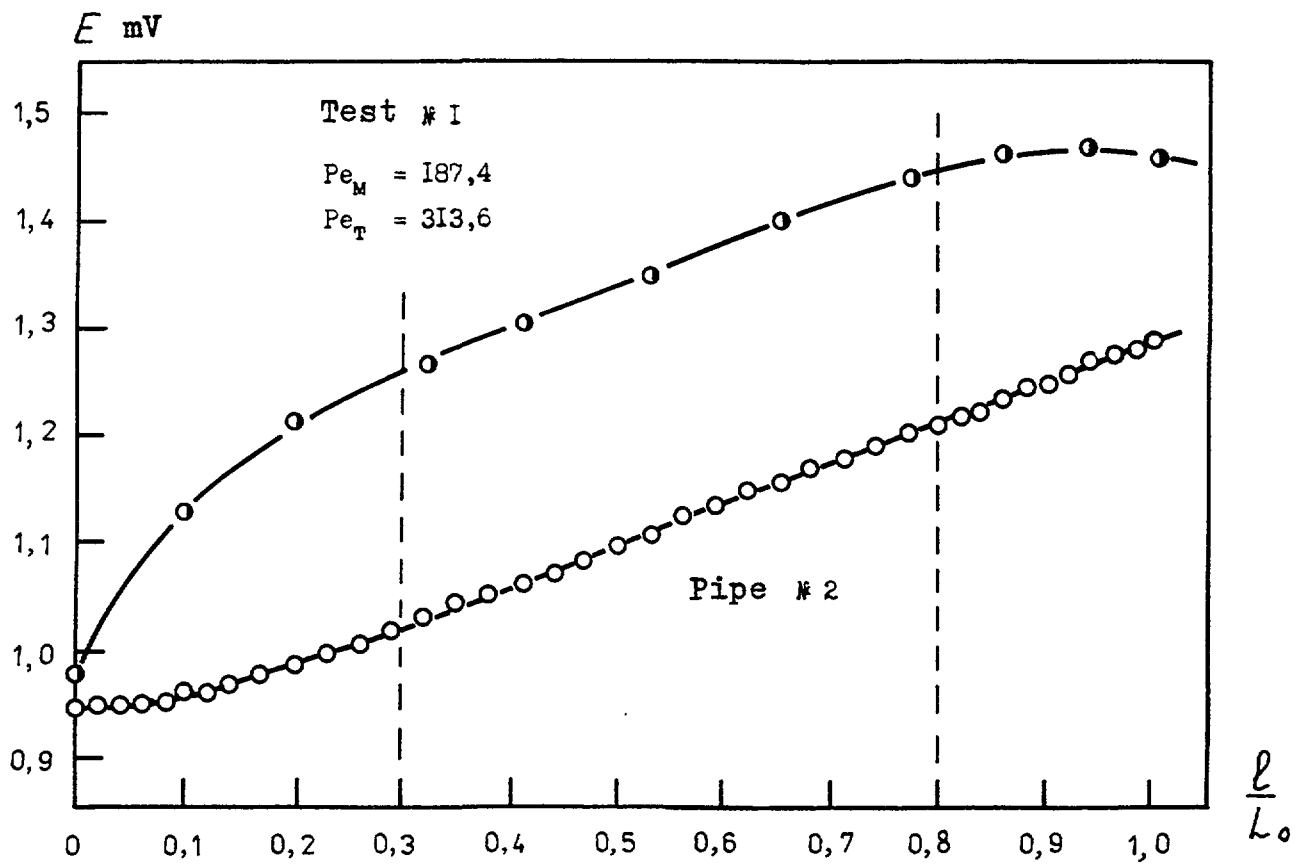
Fig. 5.27. Temperature field in downward flow of coolant (moderate low velocities)
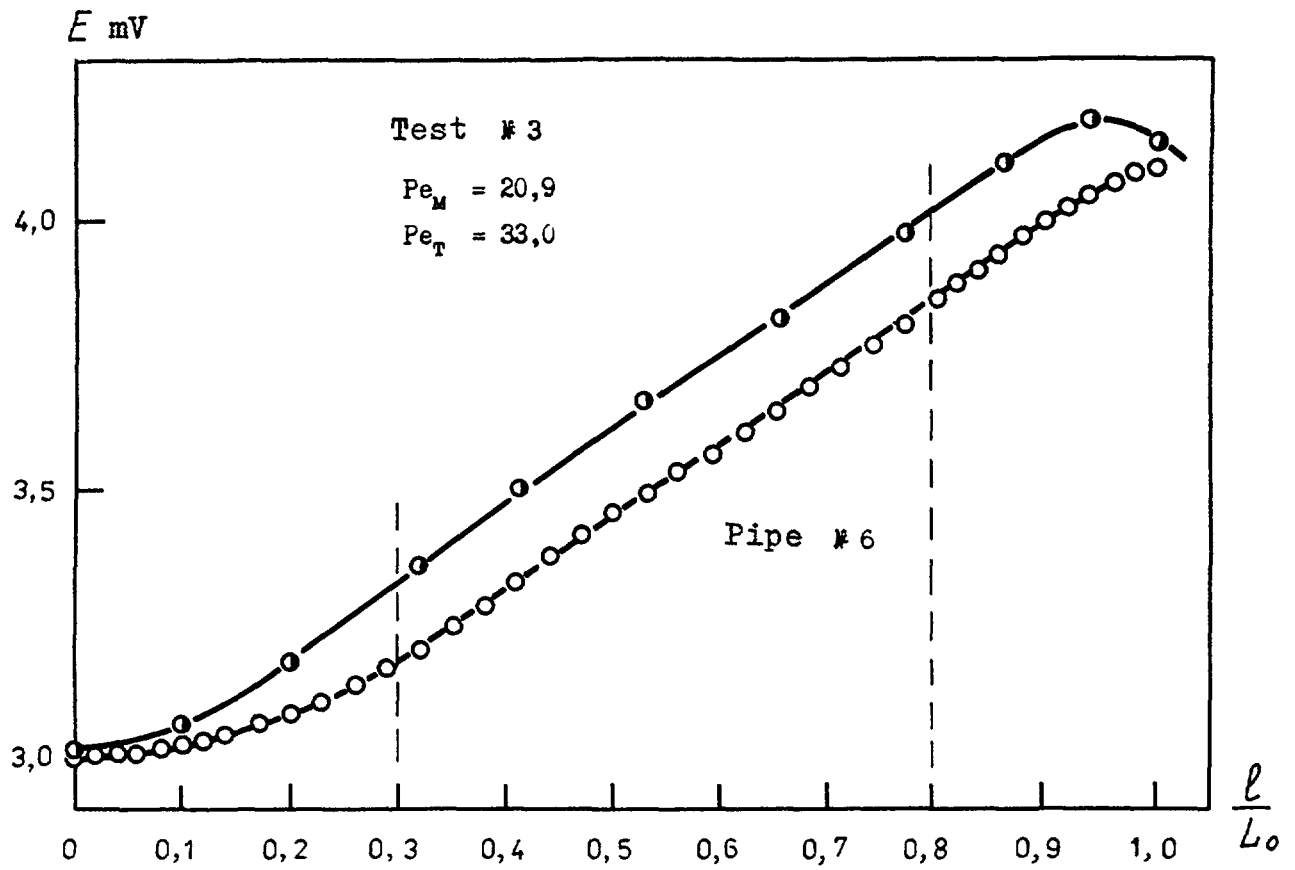
Fig. 5.28. Temperature field in downward flow of coolant (very low velocities).
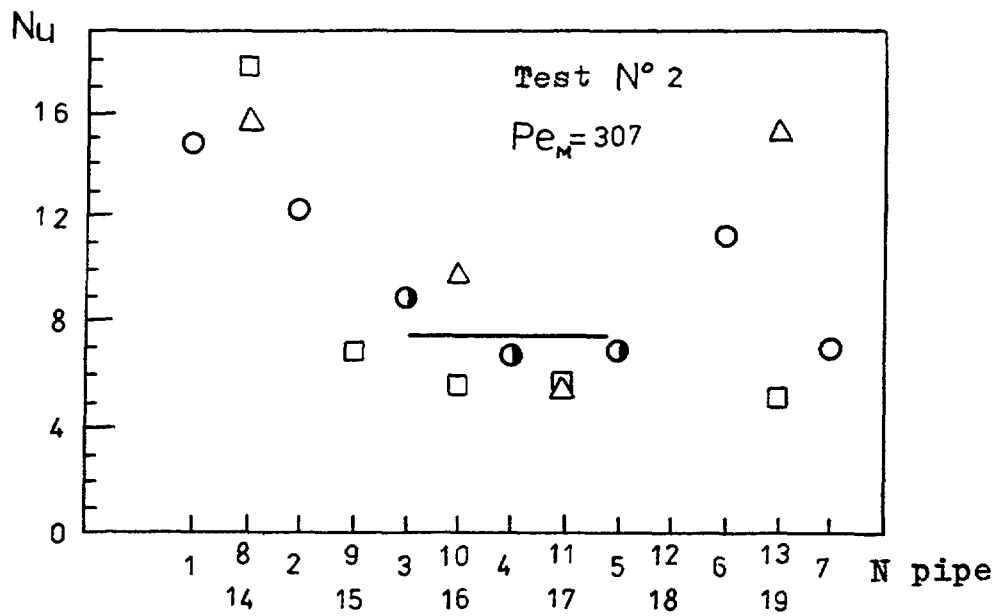
Fig. 5.29. Nusselt number for various pipes.
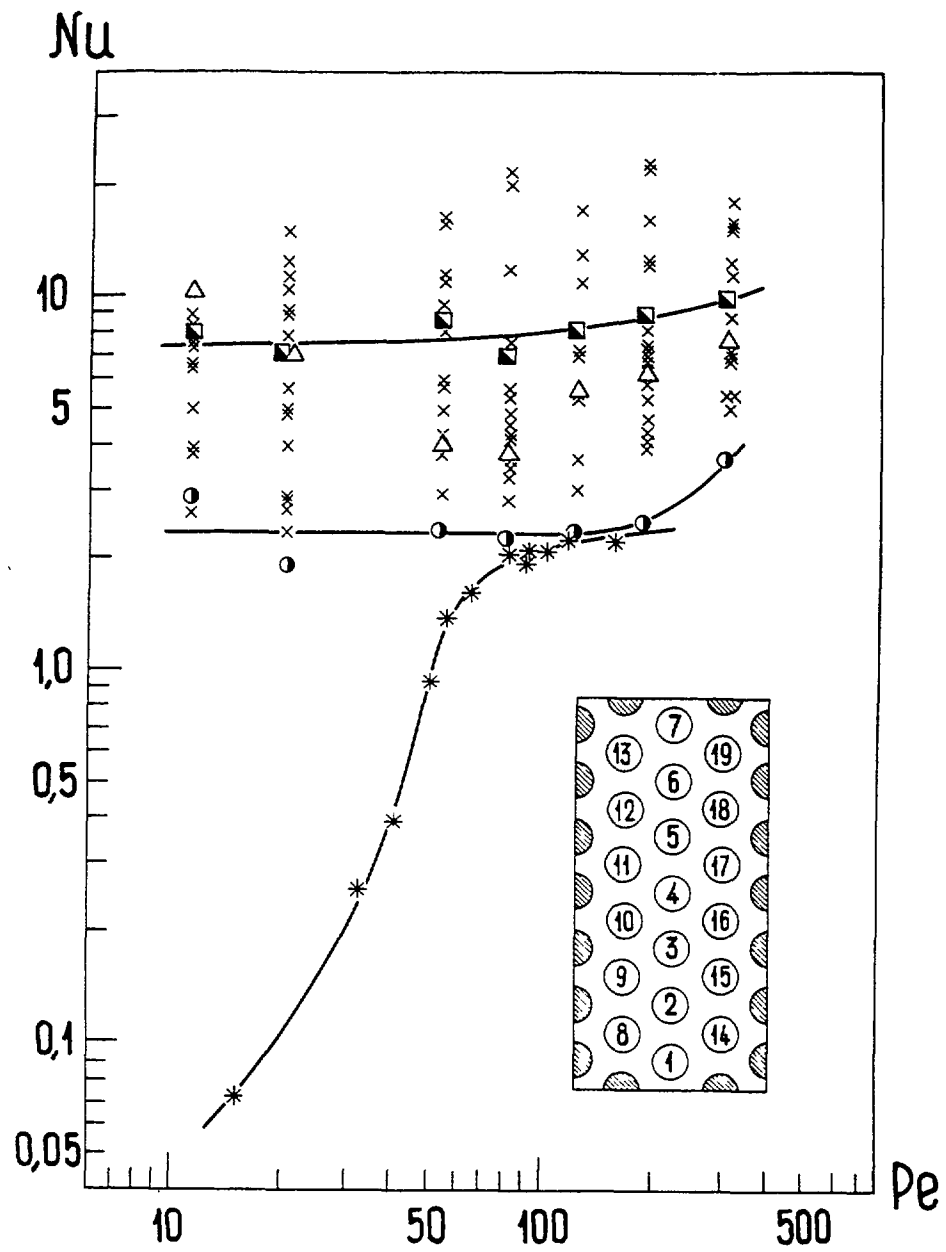
Fig. 5.30. Nusselt number as a function Peclet number:
■ - *internal area (local modelling)*
◖ , * - *data processing based on average*
header temperature.
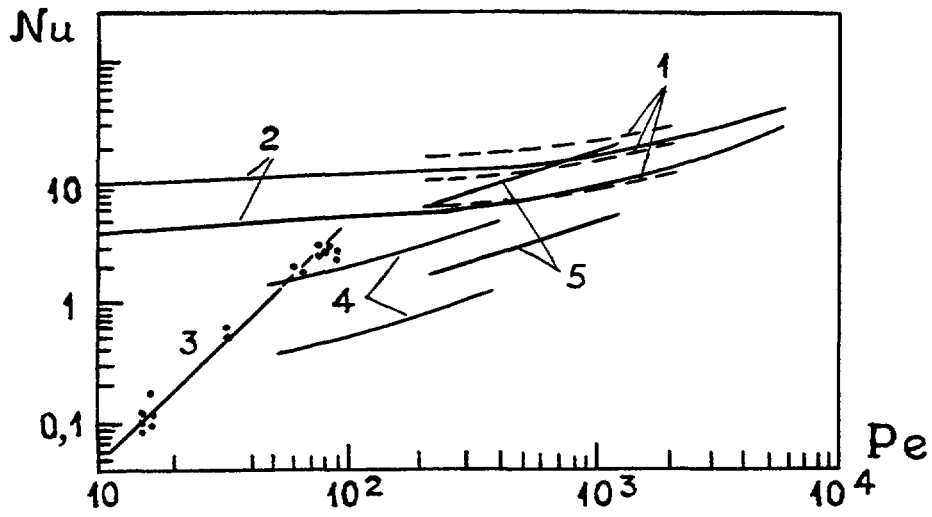
Fig. 5.31 Comparison the different authors data on Nu =f(Re) for heat exchangers:

1 - [15], 2 - [16], 3 - [17], 4 - [19],5 - [18].
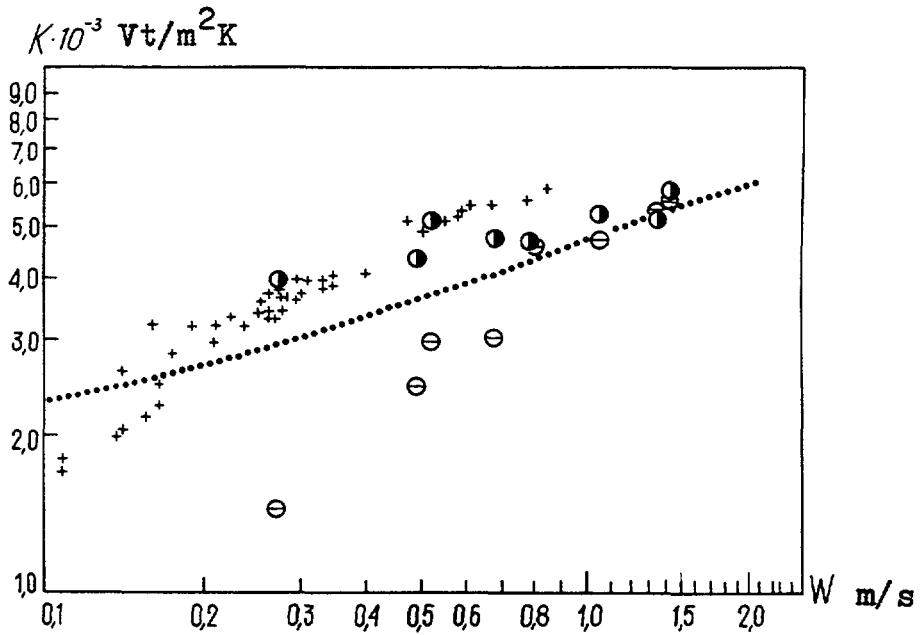
Fig. 5.32. Heat transfer coefficient K with the heating coolant velocity:

⊖ - *using average temperature in headers*

⦿ - *local modelling*

········ - *using universal profile of temperature*

+ - *data [22].*

$(t - t_{in}), °C$

70

60

50

40

30

20

10

0

Pipe № 34
$Pe_м = 30,7$
$Pe_r = 201,7$

2

$t_м^{max}$

3

10

11

t_r^{min}

0   0,2   0,4   0,6   0,8   1,0 Z/L
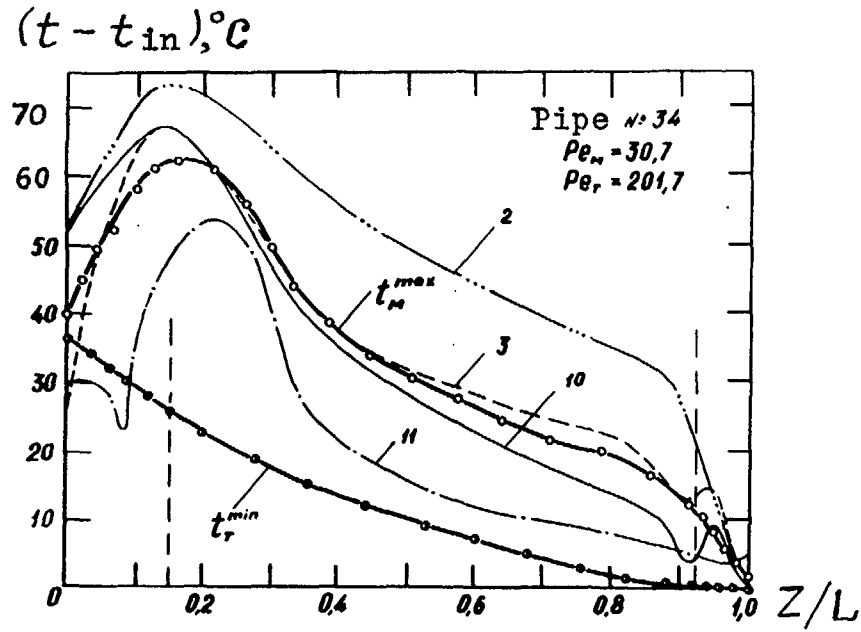
Fig. 5.33.   Inherent temperature distribution in square arrangement.

$\mathcal{N}u$

10

1,0

0,1

0,01

8   10   20   30   40   50 60 70 Pe

53 52 51 50 49 48 47

46 45 44 43 42 41 40

39 38 37 36 35 34 33
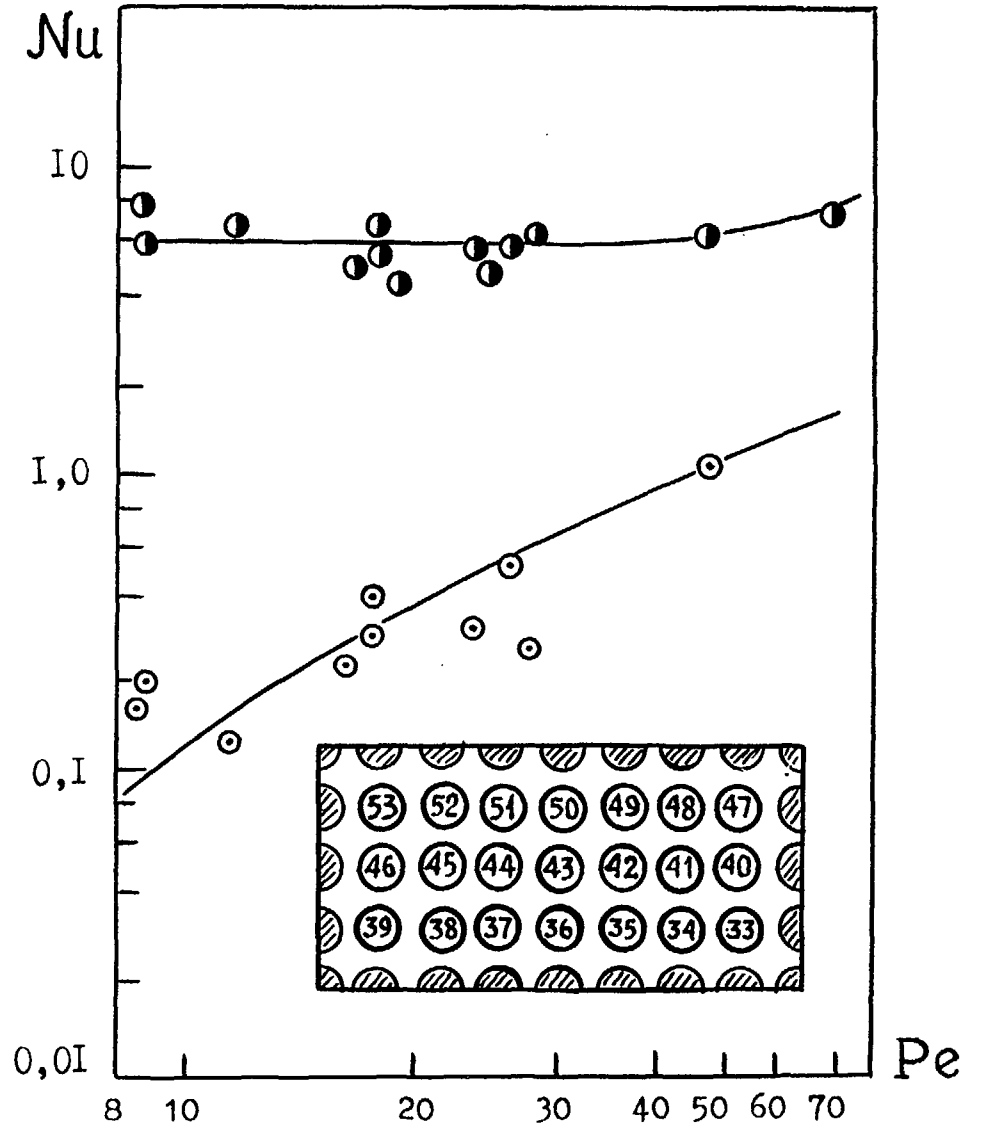
Fig. 5.34.   Nusselt-Peclet numbers relation in square arrangement of pipes:
◑ - internal area (local modelling), ⊙ - processing with average temperatures.
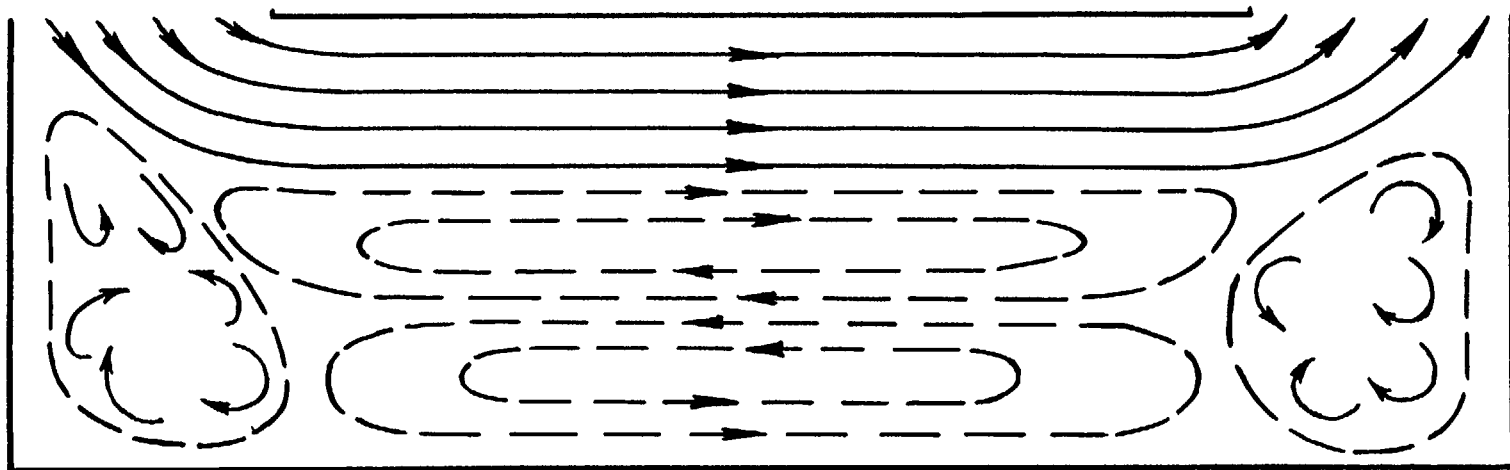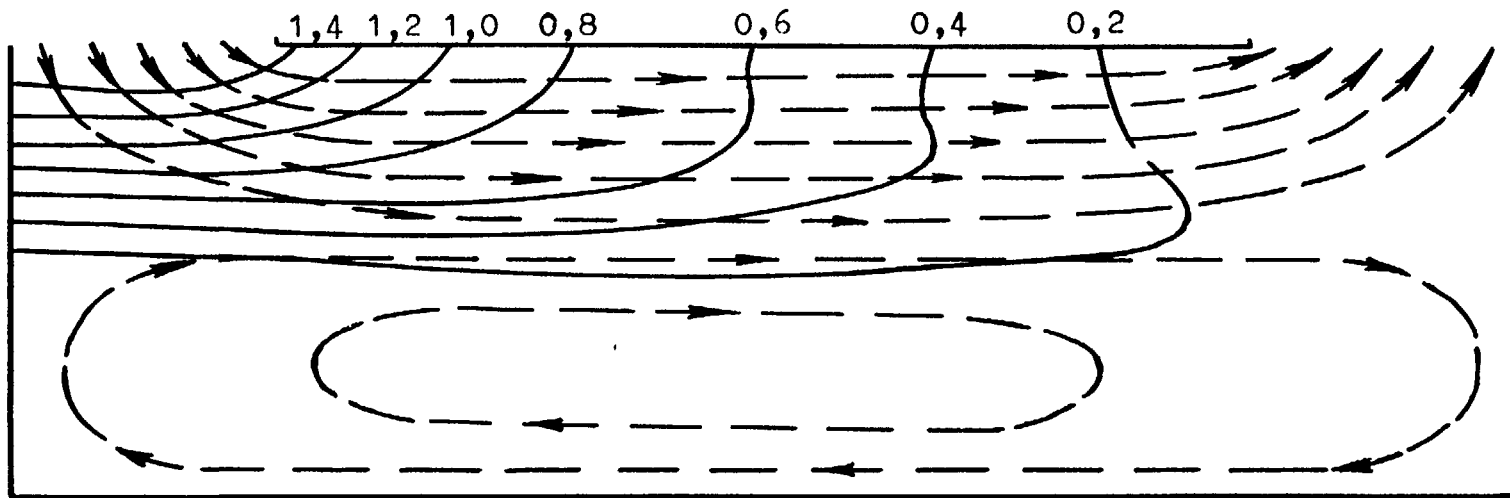
Fig. 5.35. Schemes of reverse circulation.
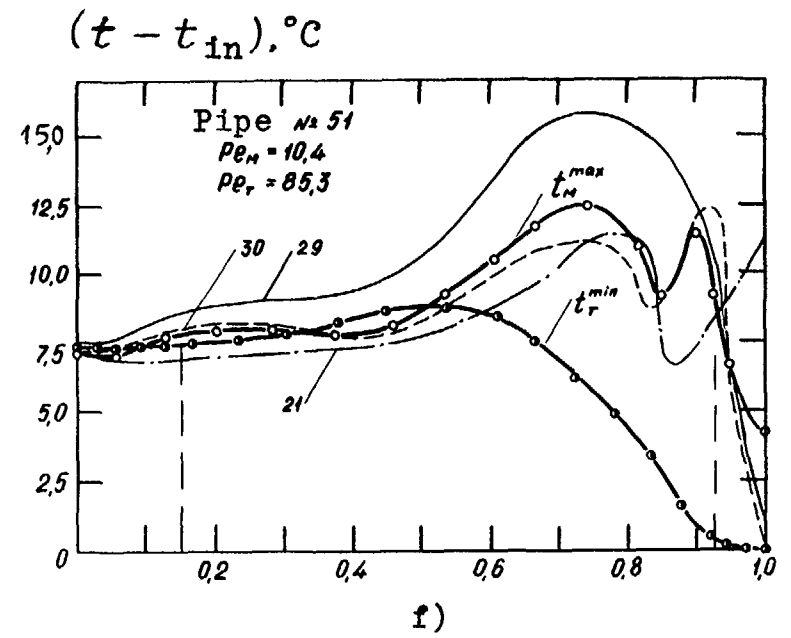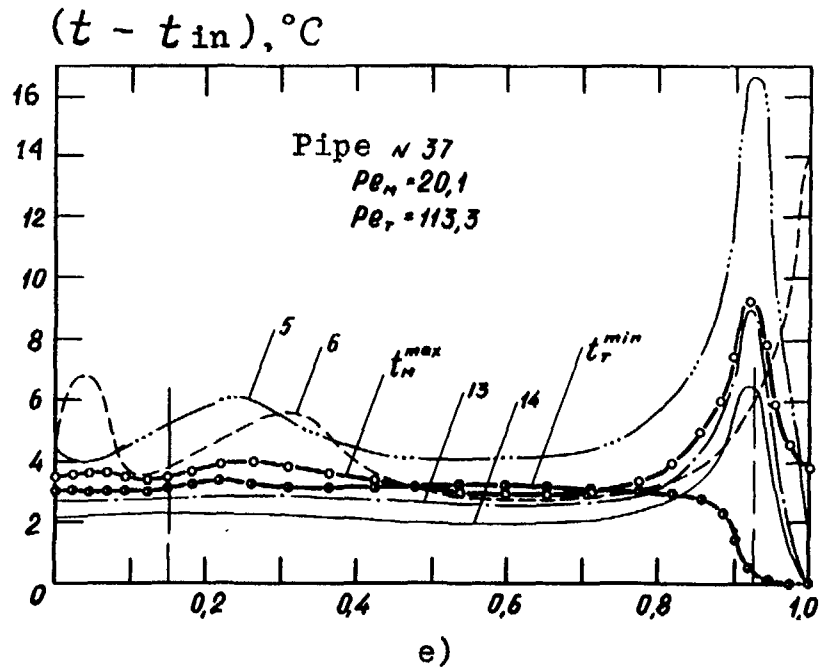
Fig. 5.36. Temperature fields with reflooding flows;
a, b - forward row; c, d - middle row; f, e - deep row of pipes.

Fig. 5.36-a, b, c, d

263

Fig. 5.37. Part of model section enclosed by a natural eddy with the main criterion (evaluated by Yuriev Yu. S.) O , ⊕, ⊖ , ⊕ , ⊗ , ⬤ , ⬤ , ⊖ , ⊕ , ⬤ , ⬤ , ⊙ , ⬤ , ✖ - experimental data, - - - - - formula(5.3.35)

Fig. 5.38. Boundaries of non-stable flow in heat exchanger model (1) and in BN full size heat exchanger (2) (evaluated by Yuriev Yu. S.) ⊖ , ⊕, ⊕ , ⊗ , ⬤ , ⬤ , ⬤ , ⊖ , ⊕ , ⬤ , ⊙ , ⬤ , ✖ , - experimental data.

Fig. 5.39. Prediction of velocity (a) and temperature (b) in BN heat exchanger taking into account natural convection (data by Oefanov A.D. et. al.)

264

- Heat transfer is defined on the section $\Delta z = 500$ mm between $z = 300$ mm and $z = 800$ mm measured from the bottom edge of the box (this section is selected in the middle part of the model for the end effects connected with the inlet and outlet windows to be excluded).

The following simple transformations are used:
- Balance of heat is written for the length d_z using temperature difference ($t^{max} - t^{min}$) found in experiments (Fig.5.20):

$$\rho\, C_p \frac{\pi d_T^2}{4} w_T \frac{dt_T}{dz} = \pi\, dk(z)(t_M^{max} - t_T^{min}) \tag{5.2}$$

where $k(z)$ - local heat transfer coefficient relative to the temperature difference ($t^{max} - t^{min}$); w_T - coolant velocity inside of the tube; temperature t_{max} is taken as the arithmetic mean of the thermocouple readings in the enclosing channels.
- Thermal resistance between the channels' centers determined in experiments is presented as:

$$\left(\frac{\lambda_f}{k}\right)_{exp} = \frac{4}{Pe_T} \cdot \frac{d}{d_I} \cdot \frac{\Delta z}{\Delta t_T} \overline{\vartheta} \quad [\text{мм}] \tag{5.3}$$

Here we deal with the thermal resistance related to the liquid thermal conductivity λ_f chosen as a scale k is the averaged over the length Δz heat transfer coefficient related to the external temperature difference:

$$\overline{\vartheta} = \Delta z^{-1} \int_{Z \in \Delta Z} \vartheta(z)dz \tag{5.4}$$

and Δt_T - coolant heating on the length Δz ; $Pe_T = \dfrac{w_T d_I \rho c_p}{\lambda_f}$ - cold coolant Peclet number. Thermal resistance (λ_f / k) incorporates thermal resistance of the inter-tube space (dh / Nu_M'), thermal resistance inside of the tube (d_I / Nu_T') and thermal resistance of the tube wall $\dfrac{\lambda_f d}{2\lambda_W} \ln \dfrac{d}{d_I}$, that is

$$\left(\frac{\lambda_f}{k}\right)_{exp} = \frac{d_h}{Nu_M'} + \frac{d_I}{Nu_T'} + \frac{\lambda_f d}{\lambda_W 2} \ln \frac{d}{d_I} \tag{5.5}$$

Here Nusselt numbers in the inter-tube space (Nu_M') and inside of the tube (Nu_T') are based on the external temperature difference ($t^{max} - t_w$) and ($t_w - t^{min}$), respectively.

Since the Nusselt numbers, thus defined, form only a part (β) of the Nusselt number relative to the averaged temperature, that is $Nu' = \beta Nu$, relationship (5.5) can be written as

$$\left(\frac{\lambda_f}{k}\right)_{exp} = \frac{d_h}{\beta Nu_M} + \frac{d}{\beta Nu_T} + \frac{\lambda_f d}{\lambda_W 2} \ln \frac{d}{d_I} \tag{5.6}$$

Required criteria is

$$Nu_M = \frac{d_h\big/\beta}{(\frac{\lambda_f}{k})_{exp.} - \frac{d}{\beta \, Nu_T} - \frac{\lambda_f d}{\lambda_W 2} \ln \frac{d}{d_I}} \qquad (5.7)$$

Factor β is taken to be equal $0.65 \div 0.7$ [11-13].

Nusselt number for a round tube is calculated according to [4]:

$$Nu_T = 5 + 0.025 Pe^{0.8} \qquad (5.8)$$

We are reminded that an essence of the universally accepted " integral" measurement technique for the heat transfer coefficient in the inter-tube space is as follow:

1. General (integral) over the model heat transfer coefficient is determined with the logarithmic temperature difference:

$$K_M = \frac{\overline{Q}}{F \cdot \vartheta_l} \qquad (5.9)$$

where $Q = (Q_i + Q_\delta)/2$ - arithmetic mean between the heat lost to the inter-tube space by the "hot" coolant (Q_i) and the heat perceived by the "cold" coolant inside of the tubes (Q_δ), F - heat transfer area based on the mean diameter $d = (d_I + d_j) / 2$ and the length $L = 1$ m,

$$\vartheta_l = \frac{\Delta t_{max} - \Delta t_{min}}{\ln\big(\Delta t_{max} - \Delta t_{min}\big)} \qquad (5.10)$$

is the logarithmic mean difference of temperatures, Δt_{max} and Δt_{min} - maximum and minimum temperature difference between "hot" and "cold" coolant in the model headers.

2. From the integral heat transfer coefficient the Nusselt number in the inter-tube space is determined as:

$$\overline{Nu_M} = \frac{d_h}{\lambda_f\left(\dfrac{1}{K_M} - \dfrac{1}{\alpha_T} - \dfrac{\delta}{\lambda_w}\right)} \qquad (5.11)$$

3. Nusselt numbers in the inter-tube space found by the local thermal modeling are compared with those found by the "integral" method.

Results in the triangular bundle of tubes. There are some types of the points in Fig. 5.22:

A) For the tubes positioned in the central row (tubes 11, 16, 21) experimental data are given by the equation:

$$Nu = 9.36 + 0.023 Pe^{0.81} \tag{5.12}$$
$$(20 \leq Pe \leq 1200, \ s/d = 1.315)$$

which can be derived, when substituting relative pitch of the tube arrangement in heat exchanger $s/d = 1.315$ in the generalized relationship for the pin bundles (see Chapter 3.3). Thus, heat transfer processes going on near the tubes 11, 16, 21 simulate those in the internal zones of multi-tube fast reactor heat exchanger, and the local technique allows studding full scale heat transfer in the models with relatively small number of tubes. Relationship (5.12) is proposed to predict Nusselt numbers in the internal area of fast reactor heat exchanger of a triangular arrangement of the tubes.

B) For the model as a whole a logarithmic mean temperature difference is used. Fig. 5.23 presents variation in the integral flows inside of tubes and through the inter-tube space for the maximum and minimum Peclet (Reynolds) numbers achievable during experiments. Inlet and outlet temperatures here are the mean temperatures (for every flow) in the model headers. Experimental data available on Nusselt number fall on the most low-lying curve in the Fig.5.22, that demonstrates the Nusselt numbers are underestimated as compared with the relationship (5.12): they are 3.5 times lover at Pe=200 and ~140 times at Pe $\cong$ 15. Thus, the commonly used approach to study heat transfer on the basic of measurements of mean temperatures in the model headers gives a particular results (being time only for the model under consideration) which can not be extended to the multi-tube heat exchangers.

C) Data for the tubes adjacent to the wrapper lie, as a rule, below than those gained in local measurements for the internal tubes, but higher than those in integral measurements in the model headers. In this event, results are observed to stratify in dependence of the tube number, that is connected with the different hydraulic and thermal conditions.

Thus, some limiting (boundary) values of Nusselt number can be separated, which are inherent for the different thermal hydraulic conditions: maximum values for the internal region of heat exchanger (local measurements) and minimum value for the whole of model, including influence of the headers.

Nusselt numbers for the edge tubes fall within the range between the limiting values. In the average, they are described as:

$$lg \, Nu = -0.734 + 0.632 \, lg \, Pe \tag{5.13}$$
$$20 \leq Pe \leq 250 ; \ s/d = 1.315$$

This relationship can be advised to carry out the estimated calculations of the edge tubes of fast reactor heat exchanger, assuming that the edge tubes compose noticeable part of the tube bundle and individual approach is required in calculating.

Various flow directions in the inter-tube space (modeling, experiments, results). Results mentioned above were obtained when hot coolant flows from bottom upwards (due to construction), whereas in fast reactor heat exchangers coolant flows from top to bottom. Special experiments have shown that flow direction does not have a pronounced effect on thermal hydraulic performance, as at relative great and low coolant velocity. Let us enlarge on the experiments mentioned here.

The model bundle presented in Fig. 1.14 was modified, as applied to new problem (flow from top to bottom). In addition, the model was improved for the purpose of equalizing temperature fields. Fig.5.24 presents the unit through which the coolant leaves for the inter-tube space when flowing from bottom upwards.

When reversing flow the inlet chamber (Fig.5.25) was formed from the unit. To distribute coolant flow over the tubes more uniformity an extra pool was made by reducing size of the bottom tube plate. Originally tubes were sealed in the tube plate, with the gap between tube and hole in the plate being 0.02 mm. Big thickness of the tube plate reduced the flow through the gap to zero. Possibility of such a flow increases as the tube plate thickness is reduced. To eliminate flow a layer of special rubber was introduced in the plate which had no direct contact with the coolant and by this means it was safe against mechanical destruction's. Also this layer reduces heat flux through the tube plate from hot coolant to cold one.

An extra pool, formed because a thickness of the tube plate was decreased, as well as working tubes were lifted, is covered by the oval frame. In order to prevent the possible pollution penetrates into the inlet chamber from the coolant, the oval form is surrounded by the stainless steel net.

The model wrapper (Fig.5.26) is a rectangular box positioned inside of the test section, which contains working tubes arranged in three rows across the width and 6-7 rows across the depth by a triangular manner with the relative pitch s/d = 1.315. Tubes are spaced and sealed by the plates and their upper ends are supported by the special plate made fast to the cover. Thus, tubes are fixed relative to the wrapper while they can move about the tube plates, that keeps they away from possible deformations during experiments.

Modeling hydrodynamics of a full-scale heat exchanger using the model with the lesser number of tubes is validated by the following ideas [1]:

• To choose one or three rows of tubes and two rows of displacers at the wrapper provides the measurements of transverse and axial components of liquid metal velocity are the same as in one-row and three-rows model;

• To choose seven rows across the depth of the model is justified by the flow stabilization beyond from the third-fourth row;

• To choose length of the test section L_0 = 1000 mm and the size of the inlet window - 150 mm and the outlet window - 80 mm is reasonable relying on the fact that transverse supply and removal of the hot coolant have an effect on temperature behavior over a distance that is not more than twice window size, and as a result more than half height of the model (section between windows) operates under self-similar conditions.

As to a compatibility between an in-pile and out-of-pile thermal processes, the lesser heat losses in the model wrapper the more strict is modeling.

268

In order to eliminate such a losses three sides of the rectangular box are covered by thermal insulation - quartz textile (Fig. 5.26), which has no contact with liquid metal. All described above serves to provide adiabatic conditions at the test section.

Quality data (temperature fields) were obtained practically for all tubes of the model. Fig. 5.27 and 5.28 illustrate, as an example, data for internal tube at the relative great ($Pe \cong$ 187) and small ($Pe \cong 20.9$) coolant velocities, respectively. Nusselt numbers were predicted to a good accuracy. They are shown in Fig. 5.29 for one of the flow along the internal row (tubes $1 \div 7$) and the edge row (tubes $8 \div 19$). See Numbers of tubes in Fig. 5.30.

Although Nusselt numbers at separate tubes are differ noticeably (due to different geometry and hydrodynamics), experimental data on the other rows are approximately the same, that arises from the uniform temperature distribution over the front and depth of hot flow Fig. 5.30 presents experimental data as a function $Nu = f(Pe)$.

Mean value falls within a small range (not more than ±10%) on the relationship:

$$Nu = 7.2 + 0.0235 Pe^{0.81} \tag{5.14}$$
$$10 \le Pe \le 350$$

Calculation results by this relationship lie some below than (5.12) gained provided the coolant flows in the internal space from bottom upwards. But discrepancy is not so great to notice effect of flow direction within the range under discussion. It should be noted that (5.12) and (5.14) wrapper a wide range of Peclet number ($10 \le Pe \le 1200$), with the range of small Peclet number enclosed by (5.14) that is of great practical importance (region of possible natural convection).

Combination of (5.12) and (5.14) gives very simple average relationship:

$$Nu = 8.4 + 0.0235 Pe^{0.81} \tag{5.15}$$
$$10 \le Pe \le 1200$$

which can be applied in calculating heat transfer in the inter-tube space of heat exchanger when hot coolant flows from top to bottom or from bottom upwards in an indicated range of Pe. The last formula differs from (5.12) and (5.14) by no more than 10%.

As to experimental data on integral heat transfer (predictions based on the average temperatures in the headers), heat transfer coefficients are rather high, but are expected to be much less than those for " infinite" of tube bundle determined by local measurements.

It is evident that at low coolant velocity "integral" Nusselt number does not depend on Peclet number (as in laminar flow) being approximately equal to 2.5, that indicates that temperature field is uniform at small Pe. Value $Nu \cong 2.5$ is about three times as less than those for "infinite" bundle ($Pe < 120$). Of course, in this event, also heat transfer coefficient is some lesser due to the average temperatures in the headers differ from the tube bundle temperature in spite of absence of the wrapper effect on the temperature behavior in tube bundle.

A correlation between the data available and (5.14) testifies that results are in agreement in the range $70 \le Pe \le 200$ and differ widely at small Peclet number ($Pe < 70$), with

the discrepancy increasing with the Pe reduction. All this suggests that heat transfer coefficient based on the mean temperatures measured in the headers are of partial character. Notice that the data obtained in other well known studies on heat transfer in the intertube space using mean temperatures in the headers not only lie below, but reduce shortly with the Pe reduction (5.31).

Predictions in a triangular tube bundle . Here we consider numerical procedure on defining heat transfer coefficients based on the universal profile of liquid temperature.

It was shown in [20] that under stable heat removal conditions the relative temperature is approximated by the universal relationship:

$$T^+ = \begin{cases} y^{++} & 0 \le y^{++} \le 1 \\ 1.87\ln(y^{++}-1) + 0.065y^{++} - 0.36 & 1 < y^{++} << 11.7 \\ 2.5\ln y^{++} - 1 & y^{++} > 11.7 \end{cases}$$ (5.16)

where

$$T^+ = \frac{(t-t_w)\lambda_w}{aq_M}\sqrt{\frac{\tau_w}{\rho}}, \quad y^{++} = \frac{y}{a}\sqrt{\frac{\tau_w}{\rho}};$$

t_w - local wall temperature, t - coolant temperature at a distance y from the wall, $a = \lambda_f / (\rho c_p)$ - thermal diffusivity, τ_M and q_M - shear stress and heat flux at the wall (local values). Much of what follows is connected with Fig. 5.20 which is used for the making that clear.

We consider an internal channel of heat exchanger and with (5.16) we can obtain:

$$t_{WM}^{max} - t_{WM} = \beta_M f(y_M^{++})q_M,$$ (5.17)

$$t_{TM} - t_T^{min} = \beta_T f(y_T^{++})q_T$$ (5.18)

where

$$\beta_M = \frac{a}{\lambda_f \sqrt{\tau_{WM}/\rho}}, \qquad \beta_T = \frac{a}{\lambda_f \sqrt{\tau_{WT}/\rho}}$$

τ_{WM} and τ_{WT} - shear stress at the outer and inner wall of the tube, respectively.

From the heat conduction equation written for the tube wall follows that:

$$q_M 2\pi R_2 = q_T 2\pi R_1 = \frac{\pi(t_{WM} - t_{WT})}{\frac{1}{2\lambda_W}\ln\frac{R_2}{R_1}}$$

or

$$q_M = \frac{\lambda_w (t_{WM} - t_{WT})}{R_2 \ln \frac{R_2}{R_1}} = q_1 \frac{R_1}{R_2}$$

(5.19)

System of equations (5.16) - (5.18) allows the connection between temperature difference wall-coolant and heat flux to be found at the outer surface of the tube:

$$t_M^{max} - t_T^{min} = q_M \left[\frac{R_2}{R_1} \beta_T f(y^{++}) + \beta_M f(y^{++}) + \frac{R_2 \ln \frac{R_2}{R_1}}{\lambda_w} \right]$$

(5.20)

If the Blasius relationship for hydraulic resistance is used:

$$\xi = 0.3164 \, Re^{-0.25},$$

(5.21)

So will:

$$\beta = 5.14 \frac{d_\Gamma}{\lambda_f \sqrt{\Psi} \, Pr \, Re^{0.875}}$$

(5.22)

$$y^{++} = 0.199 \sqrt{\Psi} \, Pr \, Re^{0.875} \frac{y}{d_h}$$

(5.23)

where $\psi = \tau_W / \tau_W$ - relative shear stress at the wall.

Let y_T^{++} and y_M^{++} be maximum values of dimensionless coordinates inside of the tube and in the inter-tube channel, respectively. Relation (5.20) may be written as:

$$q_M = k(t_M^{max} - t_T^{min})$$

(5.24)

where heat transfer coefficient is defined by the following expressions:

$$\frac{\lambda_f}{k} = \Delta_W + \Delta_T + \Delta_M$$

(5.25)

$$\Delta_W = \frac{\lambda_f}{\lambda_W} R_2 \ln \frac{R_2}{R_1}$$

(5.26)

$$\Delta_T = 5.14 \frac{d_h}{Pr \, Re^{0.875}} \cdot \frac{R_2}{R_1} f(y^{++})$$

(5.27)

$$\Delta_M = 5.14 \frac{d_h}{\sqrt{\Psi} \, Pr \, Re^{0.875}} f(y^{++})$$

(5.28)

271

Here Δ_W, Δ_T, Δ_M mean the thickness of the thermal resistances in the wall, inside of the tube and in the inter-tube space, respectively.

It follows from the (5.24) that q_M refers to heat flux appearing in the point at the outer wall of the tube answering the maximum temperature difference $(t_M^{max} - t_T^{min})$, while in processing experimental data heat transfer between coolant in the inter-tube space and those inside of the tube is defined by (5.24) implying that q_M - averaged over perimeter heat flux at the outer wall of the tube, that is:

$$\overline{q}_M = k(t_M^{max} - t_T^{min}) \tag{5.29}$$

In the tube bundles with $s/d > 1.2$ shear stress does not vary around the tube [21] and because of this, we can consider $\psi = 1$ in (5.27). By assuming also that heat flux is invariant with the tube perimeter, we obtain the procedures for calculating heat transfer coefficients with the formulas (5.24) and (5.29) are the same.

When evaluating the heat transfer coefficients based on the averaged temperature, we resort to the fact that relative temperature (as relative velocity) depend only slightly on Peclet number. From the universal temperature profile it follows that:

$$\frac{\overline{t}_M - t_{WM}}{t_M^{max} - t_{WM}} \cong 0.65 \tag{5.30}$$

$$\frac{\overline{t}_T - t_{WT}}{t_T^{min} - t_{WT}} \cong 0.65 \tag{5.31}$$

Having indicated the thickness of the thermal resistances as Δ_T', Δ_M' and Δ' and taking into account in (5.30) and (5.31) we obtain

$\Delta'_{T,M} = 0.65 \, \Delta_{T,M}$

$\Delta' = \Delta_W + 0.65 \, (\Delta_T + \Delta_M)$

Fig. 5.32 presents comparison of experimental data with those predicted with (5.25) - (5.28).

Thermal studies of square tube bundle (low coolant velocity). Experiments were carried out in the range of low liquid metal velocity (NaK), including natural convection($90 \le Re \le 3650$; $2 \le Pe \le 70$). The model bundle schematic is presented in Fig. 1.15b. Below is given specific features of thermal hydraulics and data on heat transfer coefficients in square bundle with relative pitch $s/d = 1.315$.

Heat transfer coefficients. Inherent temperature behavior is presented in Fig. 5.33 (as mentioned above, measurements have been conducted by the use of the local thermal modeling technique).

Experimental data on Nusselt numbers (Fig. 5.34) are clustered close to value $Nu \cong 5.9$ and remained practically constant as Peclet number varies, only at $Pe > 50$ heat transfer is observed to rise somewhat with Peclet number, but it is beyond reason to say about

dependence $Nu = f(Pe)$ (Nu and Pe are calculated with the hydraulic equivalent diameter of "infinite" square bundle as a reference size and mean coolant velocity in the inter-tube space is used as reference velocity).

The value $Nu \cong 5.9$ is distinctly smaller than those in triangular bundle ($Nu \cong 9.36$ -see Fig. 5.22 or (5.12)). As hydraulic diameter in square bundle is more than in triangular bundle, heat transfer coefficients in the inter-tube space of the square bundle under discussion fall far short of those in triangular bundle, all other factors being the same.

Nusselt number in the form of

$$Nu = 5.9 \tag{5.32}$$
$$(2 \leq Pe \leq 70, \ s/d = 1.315)$$

can be recommended for calculating heat transfer in the internal zone of the square tube bundle within indicated range in parallel with relations (5.12) or (5.15) for triangular bundle. As intermediate channels located between the regular rectangular and triangular channels are calculated, the heat transfer coefficients fall within the range of values predicted with (5.12), (5.15) and (5.32). Nusselt numbers predicted with (5.32) being the limiting one (low coolant velocity) have of course to be supplemented by experimental data at $Pe > 70$.

For the model as a whole experimental data (as in triangular bundle) lie along a lowest curve in Fig. 5.34 presenting a conservative results as compared with (5.32): as a factor of 6 at $Pe \cong 70$, and of 120 at $Pe \cong 2$.

Thus, the next evidence has been provided in support of that the traditional technique of studing heat transfer based on the measurements of mean temperatures in the headers causes (as in the event of triangular bundle) the particular results to be gained, which are inherent only in the model bundle under consideration and which can not be converted into multi-tube heat exchangers.

Specific features of thermal hydraulics at low velocity of the hot coolant (reversal circulation). In the most designs of heat exchanger the hot coolant runs from top to bottom, with density increasing, that ensures stability of its circulation. Otherwise, when the hot coolant moves from bottom upwards, an increase of density cause the flow to become non-stable and the possibility for reversal circulation in the inter-tube space appears. This is most likely to be in the square bundle, because of the greater coolant porosity than those in triangular bundle.

Heat transfer coefficient in the heat exchanger as a whole reduces not only due to hydraulic and temperature non-uniformities, but due to actual blockage of the part of heat exchanger by natural circulation eddy, which forms a lessened temperature area ("cold" eddy) in the inter-tube space.

Fig. 5.36-a, b, c, d, f, e shows one of the typical performance of the model bundle with the formation of recirculation loop deep inside bundle (Fig. 5.36-c, d, f, e) and with the common coolant recirculation near the first rows of tubes (Fig. 5.36-a, b). Prof. Yu. S. Yuriev performed analysis of the flows indicated above that allows the conditions of such a flows occurrence to be revealed and some criteria for estimating to be derived.

Let us indicate the flow fraction blocked by the eddy as f_{NC} and mark that velocity in the rising part of recirculation loop increases: $U_Z \sim 1/(1-f_{NC})$.

If a balance of forces acting on the liquid within the recirculation loop is states as the hydraulic resistance between the weights of «hot» and «cold» half-loops», we can derive relationship to define the blockage fraction:

$$f_{NC} = \frac{1 - \frac{1 - \frac{C_1}{R^2(Re_{ef} A_z)}}{C_2(\frac{k_\beta}{A_z})(\frac{1+0.5p}{1+p})}}{1 + a_{rz}R}$$

(5.33)

Here C_1 and C_2 - empirical factors, $Re_{ef} = \frac{U_{z_0}L}{V_{ef}}$ - effective Reynolds number including the length of the tube bundle L and nominal velocity in the inter-tube space (U_{z_0}); V_{ef} - effective viscosity; p - heat transfer parameter (see (5.39)); other parameters will be further explained.

Putting $f_{NC} = 0$, we obtain boundary equation for the non-stable flows:

$$\left[(\frac{k_\beta}{A_Z}) \cdot (\frac{1+0.5p}{1+p}) \right]_0 = \frac{1}{C_2} - \frac{\frac{C_1}{C_2}}{R^2 (Re_{ef} A_Z)_0}$$

(5.34)

Condition $k_\beta \to \infty$ gives the limiting blockage fraction (see 5.33)

$$f_{NC\,max} = \frac{1}{1 + a_{rz}R}$$

(5.35)

Taking into consideration a small contribution of viscous forces, we can derive a simple formula:

$$\frac{f_{NC}}{f_{NC\,max}} = 1 - \frac{\kappa^0_{NC}}{\kappa_{NC}}$$

(5.36)

where

$$\kappa_{NC} = \frac{\kappa_\beta}{A_Z} \frac{1+0.5p}{1+p}$$

(5.37)

is the main combined similarity criterion for the velocity and temperature with the availability of natural circulation in the inter-tube space. Let us indicate K_{NC}^0 as minimum, critical value of the criterion setting the boundary of the natural circulation existence. If $K_{NC} >$

K_{NC}^0 - natural circulation exists, if $K_{NC} \leq K_{NC}^0$, so will be no. Value of K_{NC}^0 was determined in experiments described above.

The main combined similarity criterion can be written in the expanded form:

$$k_{NC} = \frac{Gr_M}{Re_M} \frac{1}{32\kappa} \frac{Pe_M + 2\Lambda}{Pe_M + 4\Lambda}$$ (5.38)

if remembering that

$$\kappa_\beta = \frac{\beta \Delta T g L}{u_{cp}^2} ; \quad A_z = \xi \frac{L}{2d_h} = \frac{32\nu k}{u_{cp}d_h^2} \frac{L}{} ;$$

$$k = 0.406 + 1.9\sqrt{x-1} \quad \text{is the space factor (square bundle, laminar flow)}$$

$$p = \frac{4\bar{k}L}{u_{cp}\rho c_p d_\Gamma} ; \quad \bar{k} = \frac{1}{\dfrac{d_h}{Nu_M \lambda_f} + \dfrac{\delta_w}{\lambda_w} + \dfrac{d}{Nu_T \lambda_f}} ;$$

or

$$p = \frac{1}{Pe_M} \frac{4\dfrac{L}{d_h}}{\dfrac{1}{Nu_M} + \dfrac{\lambda_f}{\lambda_w}\dfrac{\delta_w}{d_\Gamma} + \dfrac{d}{Nu_T d_\Gamma}} = \frac{\Lambda}{Pe_M}$$ (5.39)

$$a_{rz} = \frac{5.53}{(x-1)^{0.135}k} \quad \text{- anisotropic factor}$$

$$Re_M = \frac{u_{cp}d_h}{\nu} ;$$

$$Gr_M = \frac{g\beta \Delta T d_h^3}{\nu^2}$$

Let us define parameters:

$$\frac{\kappa_\beta}{A_z} = \frac{Gr_M}{Re_M} \frac{1}{47.7} ; \quad \Lambda = 54; \quad \delta = \frac{215}{Pe_M} ; \quad à_{rz} = 4.3 ; \quad k = 1.49 ; f_{NC\,max} = 0.57$$

and as a result we can have

$$f_{NC} = 0.57 \left[1 - \frac{\left(\dfrac{Pe_M + 107}{Pe_M + 215} \cdot \dfrac{Gr_M}{Re_M} \right)_0}{\dfrac{Pe_M + 107}{Pe_M + 215} \cdot \dfrac{Gr_M}{Re_M}} \right]$$ (5.40)

Blockage factor was defined in experiments through analysis of the tube temperature behavior: first of all, numbers of "cold" tubes N_C close to which the coolant runs from top to bottom and the value of f_{NC} was calculated as follows: $f_{NC} = N_x / N$, where $N = 21$ total number of the tubes in the model.

Experimental data are evident from Fig. 5.37 to be in satisfactory agreement with the analytical main similarity criterion which as was found in experiments to be $K_{NC} = 26$, that has allowed to set the boundary of recirculation flow, as well an order of power reduction. An absolute ΔT - U_M plot yields (where ΔT - inlet temperature difference between hot and cold streams, U_M- mean velocity) the boundary of stability as:

$$\Delta T = \frac{8.32 \cdot 10^2 \, vk}{\beta g d_h^2} \left(\frac{\dfrac{u_M d_h}{a} + \dfrac{4\dfrac{L}{d_h}}{\dfrac{1}{Nu_M} + \dfrac{\lambda_f}{\lambda_w}\dfrac{\delta_w}{d_h} + \dfrac{d}{Nu_T d_h}}}{\dfrac{u_M d_h}{a} + \dfrac{2\dfrac{L}{d_h}}{\dfrac{1}{Nu_M} + \dfrac{\lambda_f}{\lambda_w}\dfrac{\delta_w}{d_h} + \dfrac{d}{Nu_T d_h}}} \right) \tag{5.41}$$

It is show in Fig. 5.38 for the model bundle and in-pile heat exchanger with the following parameters:

$v = 3.14 *10^{-7}$ m^2/s; $k_l = 1.49$; $\beta = 3.14 *10^{-4}$ 1/k; $h = 1.56 *10^{-2}$ m;
$a = 6.5 *10^{-5}$ m^2/s; $Nu_M = 6$; $Nu_T = 5$; $d = 19 *10^{-3}$ m

An area being over the curve represents a non-stable flows resulting in the power reduction.

2-D calculation of IHX taking into account natural convection. The basis for the procedure is an anisotropic porous body model with the momentum and energy conservation equations [8]. For the numerical solution of the equation system written for the fast reactor heat exchanger the code TAKT has been developed. Predictions were compared with the experimental data indicated above on the liquid metal model, as well as on the air model [23]. Thermal hydraulic analysis of Super PHENIX IHX conducted with the code was in a good agreement with the predicted outlet temperatures.

The next step in improving code TAKT was the development of the 2-D block with natural convection [24]. To reveal natural convection effects the following assumptions were accepted:

• transient flow is not considered;
• coolant in the inter-tube space is accepted to have no contact with reactor body, that is boundary conditions on velocity and temperature are given;
• only turbulent flow through the inter-tube space is considered.

The first assumption facilitates significantly numerical procedure and the two last permit analyzing, in the pure state, natural convection effects.

Mathematical formulation of the problem. Momentum, mass and energy conservation equations written for the coolant in the inter-tube space are analyzed and discussed in [8].

Boundary conditions are given in the following forms:

- *for velocity*: conditions of impermeability and sliding are given at the solid borders; uniform distribution is given at the inlet and outlet;
- *for temperature*: conditions of insulation are given at the solid surface; hot coolant inlet- uniform or linear distribution, hot coolant outlet - the same heat flux; cold coolant inlet - fixed temperature, cold coolant outlet - the same heat flux [8].

Numerical procedure is presented in detail in [25]. The problem is solved by the sequential approximations, that is : velocity is determined without considering natural convection, then the temperature distribution is calculated through the use of which a new velocity distribution is found even taking into account natural convection and so on. Sequential approximations are performed till the attainment of velocity will be determined with the needed accuracy . In debugging the convergence problems are investigated, test checking is performed and coefficients are found [24].

LMFBR IHX performance was predicted provided the following parameters:

- Tube bundle length, L = 7.3 m,
- Outer wrapper radius, R = 1.147 m,
- Inner wrapper radius, R_0 = 0.467 m,
- Height of the inlet and outlet windows, H = 1.0 m,
- Relative pitch of the bundle, s/d = 1.34,
- Outer diameter of the tube, d = 0.016 m,
- Mean velocity in the inter-tube space, U = 0.74 m/s,
- Mean velocity of the hot coolant (inside of tubes), w = 0.728 m/s,
- Inlet temperature of hot coolant , T_{in} = 547 °C,
- Inlet temperature of cold coolant , Θ_{in} = 309 °C.

Predicted distribution of the axial velocity has shown that the side inlet and outlet of the coolant cause the hydraulic irregularities to occur (Fig.5.39-a). They initiate the temperature non-uniformities with the maximum value attained at the cold coolant outlet. It may be as much as ~ 60 ° C (Fig. 5.39-b) and realized in the hot area of heat exchanger, that is the possibility of thermal stresses occurring can be greatly enhanced. In changing ratio between the full specific heat capacities the maximum temperature gradient can replace to the cold part of heat exchanger.

CONCLUSIONS

1. The study of intermediate heat exchanger thermal hydraulics was performed on the mock-up tube bundles with the limited number of tube rows (one-, three-row bundle with displacers at the wrapper). Hydraulic and thermal modeling has allowed obtaining an experimental data on multi-tube system. Thermohydraulic investigations were carried out in triangular and square tube bundles as applied to nominal performance and during low-velocity transients, including natural convection and reversal circulation. Experimental data can be used both to predict temperature behavior in the full scale heat exchangers and to verify computer codes.

2. Investigations of hydrodynamic parameters are based on the electromagnetic measurements which is found to be very effective in studying combined (axial-transverse) flow; whereas thermal investigations use the local modeling technique, that allows the data obtained to be extended to the full-scale fast reactor heat exchanger. In addition, it is shown that traditional integral measurements of the mean temperature in the model headers causes the particular results to be obtained, which are unsuitable for using in multi-tube system such as BN heat exchangers.
3. Among the constants needed to validate BN heat exchanger thermal hydraulics there are:
   • heat transfer coefficients in triangular and square tube bundle (regular area of heat exchanger) in nominal coolant flows, as well as under low velocity conditions, including natural convection;
   • heat transfer coefficients for the edge areas of heat exchangers which differ noticeably from those in regular tube bundle;
   • values and laws of variation in axial and transverse components of velocity with the height and depth of the tube bundle, as an input information for verification of computer codes;
   • formation of temperature field in the inter-tube space in various coolant flows, including low velocities;
   • criteria of flow stability and their values as applied to the mock-up bundles and in-pile heat exchangers.
4. The most important effect observed during experiments on mock-up bundles is an equalization of coolant flow over the depth of tube bundle when the inlet window reduces in height. This effect appears in different arrangement of the tubes in bundle (triangular, square), in different number of tubes and so on, varies in its value and allow the heat transfer surface to be optimized. It also shows a significant reserve of the heat transfer surface in the BN heat exchanger under operation.
   The data gained on velocity and temperature behavior in mock-up tube bundles when the inlet window varies in size are widely used to improve computer codes on fast reactor heat exchanger thermal hydraulics. Codes PROTVA, UGRA, TAKT, RAPORT and others built on a porous body model are successfully employed in practice.

REFERENCES

[1]   Zhukov A.V., Sorokin A.P., Sviridenko E.J., et al. Experimental and Numerical Modelling of Heat Exchanger Thermal Hydraulics. Models, Sensors, Measurement Techniques, Liquid Metal Facility. Textbook, Obninsk, ONPEI, 1992 (in Russian).

[2]   Zhukov A.V., Sorokin A.P., Sviridenko E.J., et al. Experimental and Numerical Modelling of Nuclear Power Plants Thermal Hydraulics. Overview IPPE-0270M, CNIIAtominform, 1995.

[3]   Zhukov A.V., Sorokin A.P., Sviridenko E.J., et. al. Experimental and Numerical Modelling of Heat Exchanger Thermal Hydraulics. Overview IPPE-0269M, CNIIAtominform, 1995.

[4]   Subbotin V.I., Ibragimov M.H., et al. Hydrodynamics and Heat Transfer in Nuclear Power Plants, M., Atomizdat, 1975.

[5]   Kolmakov A.P., Yuriev Yu.S. Application of a Porous Body Model to Calculate Velocity and Temperature Fields in Reactor Core. Preprint IPPE-249, Obninsk, 1971 (in Russian).

[6]   Gorchakov M.K., Kolmakov A.P., Yuriev Yu.S. Friction Factor Anizotropy in Porous Body Representing Pin Bundle. Preprint IPPE-446, Obninsk, 1973 (in Russian).

[7] Gorchakov M.K., et al. Application of a Porous Body Model to Reactor and Heat Exchanger Thermal Hydraulics. Thermal Physics of High Temperature, 1976, v.14, p.866-870.

[8] Subbotin V.I., et al. Computations of Problems of Reactor Thermal Physics. M., Atomizdat, 1979.

[9] Trojanov M.F.et al. Recommendation on Computation and Design of Intermediate Liquid Metal Heat Exchangers. NPO CKTI, L., 47, 1982 (in Russian).

[10] Zhukauskas A.A. Convective Heat Transport in Heat Exchangers., M., Nauka, 1982.

[11] Kirillov P.L., Subbotin V.I., et al. Round Tube Heat Transfer to Na-K Alloy and to Mercury. Atomic Energy, 1959, v.6, p.382-390.

[12] Kaliaskin V.I., Kudriavtseva L.K., Ushakov P.A. Forced Convection Heat Transfer to NaK Alloy in Compact Bundle. Thermal Physics of High Temperature, 1973, v.11, p.781.

[13] Ushakov P.A., Zhukov A.V., Matjukhin N.M. Liquid Metal Turbulent Azimuthal Temperature Non-Uniformities in Regular Bundles. Thermal Physics of High Temperature, 1977, v.15, p.76-83.

[14] Subbotin V.I., Ushakov P.A., Gabrianovich B.N., et al. Round Tube Liquid Metal Heat Transfer. Engineering & Physics J., 1969, v.4, p.16-21.

[15] Graber H., Rieger M. Experimentelle Untersuchunge der Wärmeübergangs an Flüssigmetalle (Na-K) in parallel durchströmten Rohrbündeln bei exponentieller Wärmefluss − Verteilung in erzwungener laminarer oder Turbulenter Strömung. International J. Heat and Mass Transfer, 1970, p. 1645-1703.

[16] Zhukov A.V., Sviridenko E.J., Matjukhin N.M. Experimental Investigations of Liquid Metal Heat Transfer in Triangular Pin Bundles. Preprint IPPE-800, Obninsk, 1978 (in Russian).

[17] Kondratiev V., Krupkin L.K., et al. Heat Transfer in the Inter-Tube Space of BOR-60 Heat Exchanger. Atomic Energy, 1974, v.36, p.305-306.

[18] Broks R.D., Rosenblatt A.L. Mech. World and Engng. Rec., 1953, vol. 75, p. 363.

[19] Kirillov P.L., Suvorov M.J. Liquid Metal Heat Transfer in the Inter-Tube Space of Heat Exchanger. Liquid Metals, M., Atomizdat, 1967, p.194-203.

[20] Kirillov P.L. Generalisation of Experimental Data on Liquid Metal Heat Transfer. Atomic Energy, 1962, v.13, p.481-483.

[21] Subbotin V.I., Ushakov P.A., Levchenko Yu.D. et al. Turbulent Velocity Field in Longitudinal Flow in Pin Bundle. Preprint IPPE-198, Obninsk, 1970 (in Russian).

[22] Boudov V.M., Golovko V.F. Intermediate Heat Exchangers in Fast Reactors (Analytical Overview). OKBM, Nizni Novgorod, 1976.

[23] Boudov V.M., et al. Predictions & Experiments on Combined Axial-Transverse Flow in Fast Reactor Heat Exchangers. Heat Transfer and Hydrodynamics of Single-Phase Flow in Pin Bundle, L., Nauka, 1979, p.56-68.

[24] Yefanov A.D., Vlasova V.N., et al. Forced Convection in Liquid Metal Heat Exhcanger. Preprint IPPE-1257, Obninsk, 1982 (in Russian).

[25] Gosman A.D., et al. Numerical Methods in Viscous Liquid Flow, M., 1972.

Chapter 6

THERMAL HYDRAULIC ANALYSIS OF TRANSIENT AND ACCIDENT PROCESSES. LIQUID METAL BOILING IN LMFBR CORE

In recent years the necessity of analysing flow and temperature behaviour in pin bundles arises from the study of as transient operation of reactor and analysis of accidents associated with circulation contour failures. Thermo hydraulic analysis calls for the problem of combined heat removal in the «liquid-pins» system to be resolved, it should be noted that it is the more complex problem than a steady-state calculations.

Specific problems arise in studying the coolant boiling. Vapour generation in any part of subassembly, taking into account the great difference between specific volumes of vapour and liquid, is a strong disturbing factor responsible for a realignment of hydrodynamics, causing the flow to become instable. Study of possible failures covers an events of fuel pin cooling under conditions of low flow rate or natural circulation.

6.1 TRANSIENT THERMAL HYDRAULICS MODELLING

Subchannel approach to transient thermohydraulics was realized in the code MID . Numerous verification tests have been performed with the experimental data IPPE and others [1,2]. Fig.6.1 and 6.2 show the pin temperature predicted by the use of Duhamel integral.

Temperature relaxation parameters. Numerical solution of heat transport equations and inherent transient distribution of temperature in fuel and coolant is presented in [3]. Predictions were carried out in turbulent flow at various Reynolds numbers, with the convective heat transport , molecular and turbulent diffusion in radial and axial directions taken into account. Different coolants (Na, H_2O, Pb) and fuels (U, UO_2) were studied. Results of numerical analysis were supported by experimental data gained in momentary switching-off the heater of the model.

Data analysis has shown that in power step input the pin temperature (or coolant overtemperature) is pproximately described by exponential correlation:

$$\theta = \theta_\infty \left[1 - \exp(-\tau / \tau_r) \right] \tag{6.1}$$

where τ - time, τ_r - parameter of temperature relaxation.

In order to derive explicit correlation of τ_r on the bundle parameters an analytical solution of transient heat conduction problem was considered under isothermal boundary condition at the pin surface. This solution holds that the time it takes for the pin temperature to be established is defined by the following parameter:

$$\tau_{pin} = \frac{d^2}{4a_0} \left[0.1729 + 0.9452 \left(\frac{\Delta_l}{\lambda_l} + \frac{\Delta_k}{\lambda_k} \right) \frac{\lambda_0}{d_0} \right], \tag{6.2}$$

where d- pin diameter, d_o - fuel diameter, Δ_l - thickness of cladding, Δ_c- thickness of the contact sublayer between fuel and cladding, λ_0, λ_l, λ_c - thermal conductivity of fuel, cladding and contact sublayer, a_o - thermal diffusivity.

Analysis of data at $Re \leq 10^4$ has shown that dynamics of fuel temperature change essentially depends on the coolant flow. It is primarily due to coolant overtemperature ΔT, which is comparable to radial non-uniformity of the fuel temperature at relatively small Reynolds number. Then, to the parameter τ_{pin} must be added the time $\tau_q = (\rho c_p)_o \cdot \Delta T / q_v$ needed to increase fuel temperature by ΔT. From the energy balance we obtain:

$$\tau_q = \frac{\pi d_o^2}{4\omega} \cdot \frac{(\rho c_p)_o}{(\rho c_p)_f} \cdot \frac{h_q}{\overline{W}} \tag{6.3}$$

where ρ - density, kg/m^3; c_p - specific heat capacity, J/kgK; q_v - volumetric heat production, W/m^3; h_q - length of power production section, m; $\overline{W}$ - mean coolant velocity, m/s; ω - flow cross section, m^2. Subscripts «o» and «f» mean fuel and fluid, respectively.

Transient heat conduction in fuel pin cooled by the plane coolant flow (uniform velocity distribution) suggests that the time it takes for the coolant passes through the power production section h_q / w must be taken into account, influence of which on temperature relaxation is essential. As a result, we have $\tau_r = (2/\pi) \cdot (\tau_{pin} + \tau_q + h_q / \overline{W})$.

Having presented the pin temperature or coolant overtemperature as a function of time in the form of unified dependence (6.1) shows that parameter τ_r is the generalised dynamic characteristic. Fig.6.3 presents correlation (6.1) in $(\theta / \theta_\infty - \tau / \tau_r)$ coordinates. Geometry of subassembly and annular channel for which these data were calculated is presented in the Table 6.1. Fig. 6.4. presents the same data in the $(\theta / \theta_\infty - \tau / \tau_o)$ coordinates, where τ_o is the pin constant. Correlation is presented in the form: $\theta = \theta_\infty [1 - \exp(-\tau / \tau_o)]$

It is evident that the pin constant can not be considered as generalised dynamic characteristic. The following nomenclature is used:

$$R_o = d_o / d, \quad R = (d - 2\Delta_I) / d, \quad H = 2h_q / d,$$

$$\Lambda_o = \lambda_o / \lambda, \quad \Lambda_I = \lambda_I / \lambda_f, \quad A_o = a_o / a_f, \quad , A_I = a_I / a_f,$$

$$R_T = (\Delta_c / \lambda_c) \cdot (2\lambda_f / d),$$

Re - Reynolds number, Pr - Prandtl number, x - relative pitch of the bundle, R_a - the outer radius to inner one ratio, $\lambda_f \cdot a_f$ - coolant thermal conductivity and thermal diffusivity, a_o - pin thermal diffusivity.

Parameter τ_o contains an empirical variable being the heat transfer coefficient which takes into account thermal resistance, as the temperature establishes inside of the pin [4]. Other parameter τ_r does not contain a similar variable. Thus, it can be concluded that relaxation temperature in subassembly of fast and water reactors is scarcely affected by the

thermal resistance. It can be explained by the fact that coolant overtemperature is in excess of the temperature difference «wall-liquid»

In modeling steady state heat removal the tubes heated from the inside by electrical helix are used. The layer of silicon organic insulates the electrical helix from the tube wall. The condition for approximate modeling is that the equivalent thermal conductivity of experimental tube is equal to that in fuel pin [5]. Experiments and predictions have shown that under conditions of power step the tube wall temperature is also governed by the relationship (6.1.

Thus, parameter τ_r is a generalised dynamic characteristic of the subassembly or the model . It allows the conditions for approximate modeling as an equality of dimensionless values of relaxation parameters in nature and in the model to be established. If the time it takes for coolant to transported through the heated section is chosen as the time scale, that condition for approximate modeling is: $\left(\tau_r W / h_q\right)_{model} = \left(\tau_r W / h_q\right)_{nature}$.

6.2. EXPERIMENTAL STUDY OF CRITICAL HEAT FLUX IN LIQUID METAL NATURAL CIRCULATION CONTOUR

Having regard to physical and thermal dynamic properties of liquid metal coolants, to choose sodium as a coolant in fast breeder reactors was to be an ideal decision. In nominal performance the outlet sodium temperature is much less than sodium boiling temperature. However, boiling is possible in improbable severe accident. Among the consequences of such a process may be the pin superheating, loss of pressure. Furthermore, it can cause the reactivity to enhance due to positive void reactivity factor of sodium.

That is why, liquid metal boiling was given much attention over the last three decades. Heat transfer, flow patterns, hydraulic resistance, heat transfer crisis, mechanism of boiling, problems of stability were being discussed. Results of studies presented for example in [6-15] have shown that boiling in liquid metal has some specific features in comparison with water boiling, among these are:
- the growth of liquid metal vapour bubble is of explosion character, with the rate of the bubble growth being in order of 10 m/s;
- two-phase patterns in liquid metal are the same as those in common liquids, with the disperse-annular flow dominating at the pressure close to atmospheric;
- two-phase friction with the energy supplied is lesser than those in adiabatic flows, that is connected with the vapour pushes the interface out of the main flow;
- phase transition in disperse-annular liquid metal flow is, as a rule, performed by evaporation of near-wall film provided bubbles are not generated at the wall (boiling is lacking), heat transfer coefficient is as great as hundreds of kW/m^2, an influence of mass velocity and quality appears to be moderate.

Attention in studying the pin bundle liquid metal boiling focuses on the analysis of transient and emergency performance caused by the drastic changes in power, by the various kindes of blockages, by the pump shut-down.

Experimental facility. Fig.6.5 presents test section containing 7-pin bundle to study boiling of eutectic alloy NaK. Pin-displacers are used to reproduce «infinite» pin bundle,

283

pins are spaced with the spacer grids positioned in four cross sections, two in each section, with the cross sections being placed *130 mm* apart and two grids in every section being *5 mm* apart. Two grids together form a peculiar kind of chamber-header, from where thermocouple readings come and pressure is extracted.

The length of heated section is *420 mm*, with the section of hydrodynamic stabilisation *165 mm* long being upstream from the heated section. Mobile 7-pin bundle *200 mm* in length is mounted next, which can be moved to a distance up to *300 mm* directly during boiling. In the first experimental set the tubes with the roughness *0.15 mkm* were used as an elements, in the second set the tube of roughness *1.25 ÷ 0.63 mkm* were used.

Circulation contour AR-1 and test section. Fig.6.6 shows the contour with the test section to study liquid metal boiling. As it is clear from Fig.6.6, the electromagnetic pump, coolant heater, equipment to calibrate magnetic flow meters, as well as cold catcher are inserted in the contour.

Before testing, liquid metal coolant was purified during three days steadily. In that time the cold catcher maintained at the temperature $80°C$ (thermocouple N 7), with oxide concentration being $5÷10\%$ weight.

Experimental results. Readings of flow-meter and four potentiometers to measure coolant quality are presented in Fig.6.7 At pressure *p=0.06 MPa* the boiling onset is observed at the heat flux $q=117$ kW/m^2. Local boiling (sensor N 5) extends for all heated section, as the power supplied to the test section increases. In doing so, the inlet flow rate was kept practically constant at a level established before boiling. Such a behaviour was conserved until the boiling covers all heated section. By convention the mode of boiling with invariant flow rate and heat flux to the value $q= 133$ kW/m^2 was named the mode 1. On further heating, transition to pulsating mode was observed, named the mode 2.

The mode 2 of boiling appears as periodic process: At the beginning the heated section is steamed, then the developed vapour plug floats up, but the area being freed from the plug was filled with «cold» liquid. As it is visible from Fig.6.7, during the vapour plug generation the coolant flow rate failed to zero and at the instant the plug floats up it rises steeply.

Thus, experiment have shown that at heat flux q being from *100* and *133 kW/m²* and flow rate *G=0.75 m³/h* the stable heat removal due to coolant boiling was observed. As the heat flux increases up to 150 w/m^2, the boiling becomes pulsating, flow rate reduces periodically to zero and then drastically grows. Temperature characteristics are shown in Fig. 6.8. As it is visible from the figure, under condition of the mode 1 the outlet wall temperature remained constant and was equal to $740°C$. In the mode 2 (pulsating) a drastic increases in wall temperature with amplitude $~90°C$ were observed. It should be noted that the outlet coolant temperature behavior presented in Fig. 6.8 has some specific features. In the first (stable) mode of boiling the coolant temperature did not vary and was $730°C$, that was practically equal to saturation temperature at the pressure *0.06 MPa.*

The sensor signals were recorded and processed by computer in order to define the correlation relationships between the individual parameters, the wall temperature, and quality being correlated with the inlet flow rate.
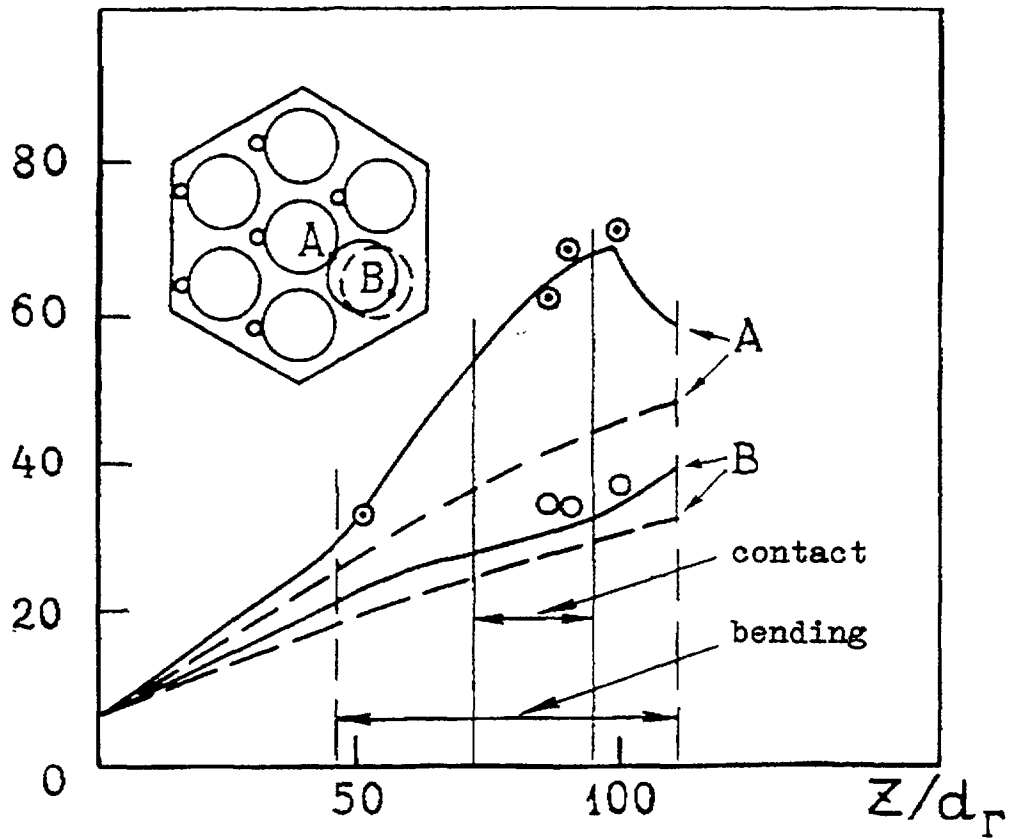
Fig. 6.1. Temperature variation with the form lines A and B in the event of the edge pin bending:

⊙, ○, - *experiment,* —— - *prediction taking into account the pin bending,*
——— - *prediction without regard bending.*
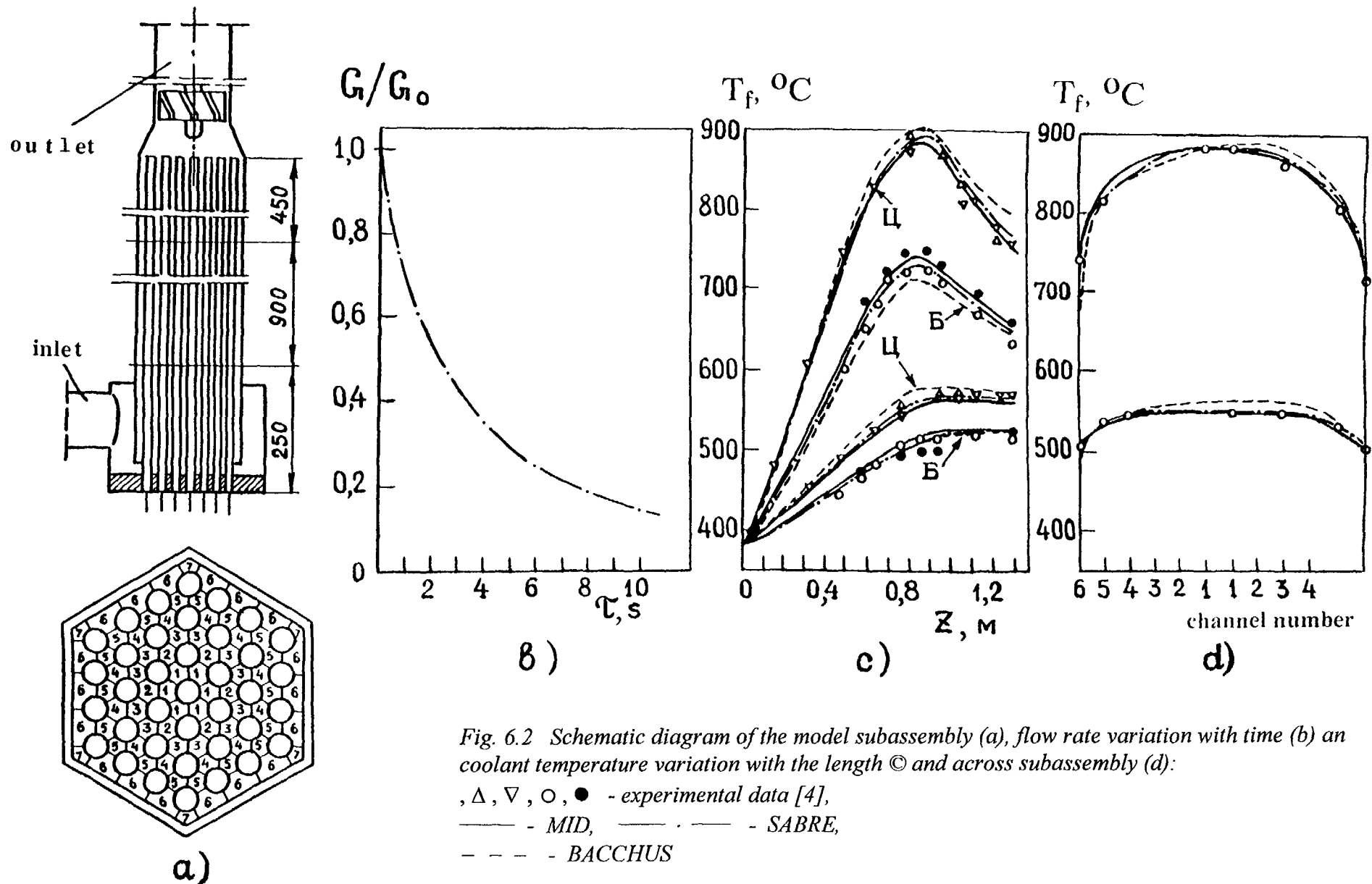
Fig. 6.2 Schematic diagram of the model subassembly (a), flow rate variation with time (b) an coolant temperature variation with the length © and across subassembly (d):

, Δ, ∇, ○, ● - experimental data [4],

————— - MID, ——— · ——— - SABRE,

— — — - BACCHUS
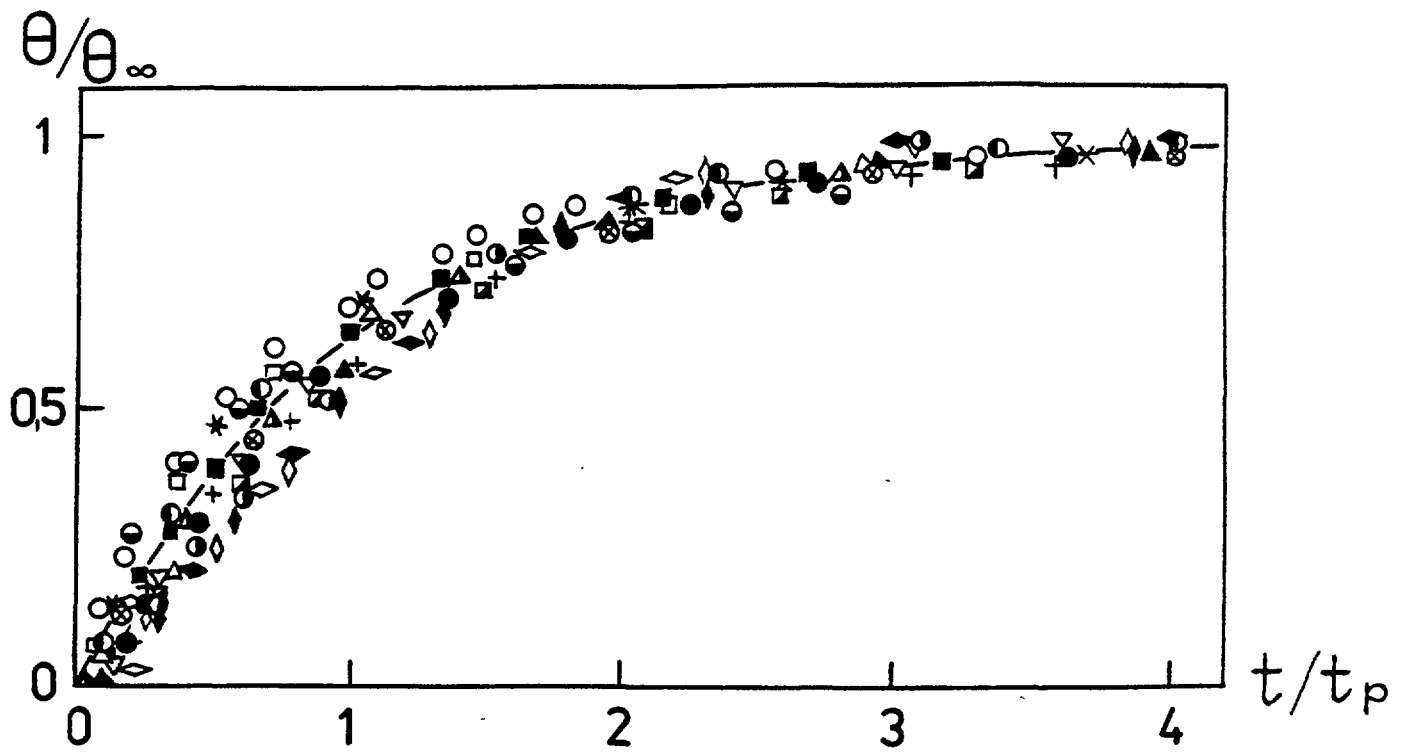
Fig. 6.3. Dimensionless temperature at the pin surface as a function of
parameter t/t_p .
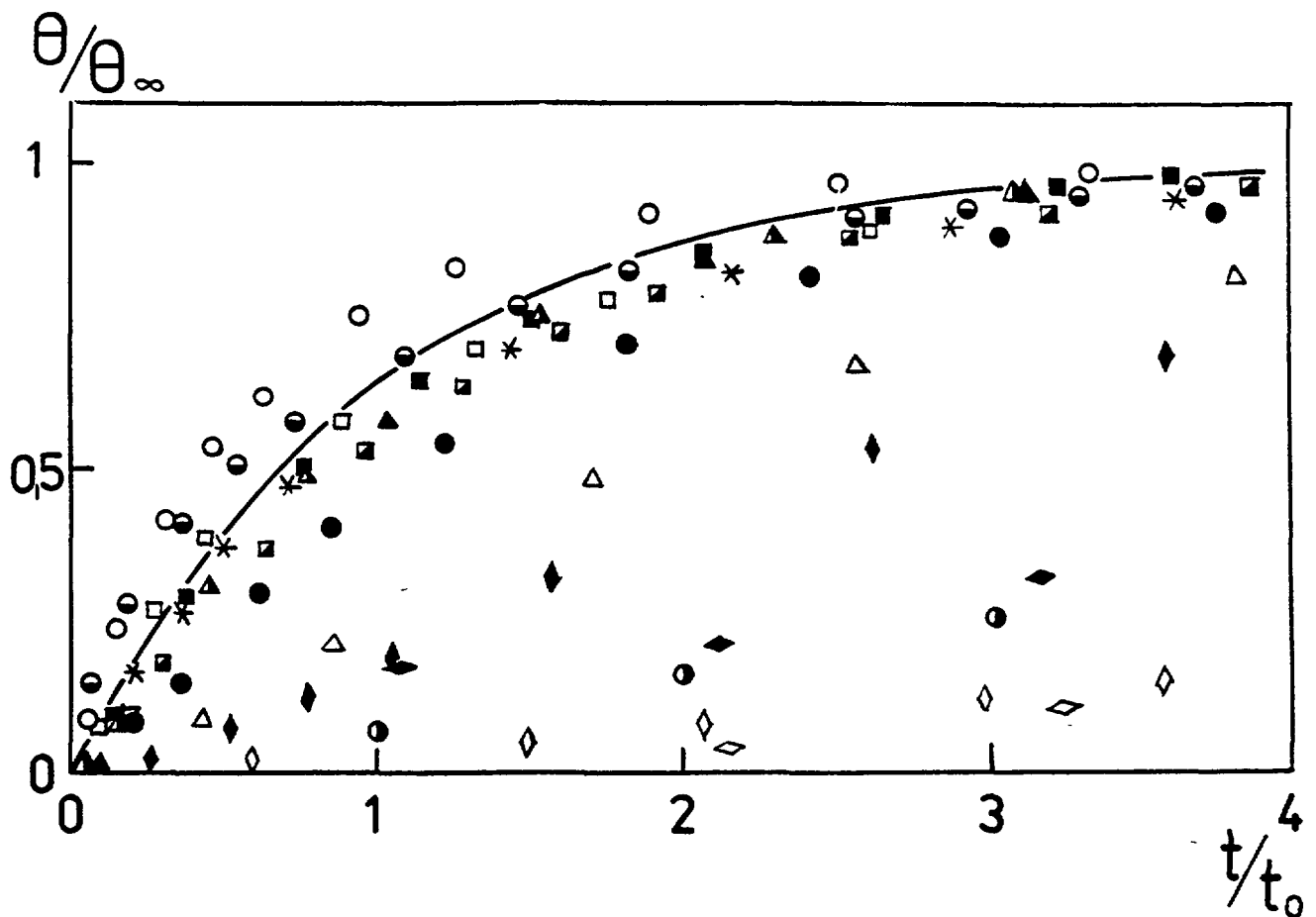
Fig. 6.4. Dimensionless temperature at the pin surface as a function of
parameter t/t_o .
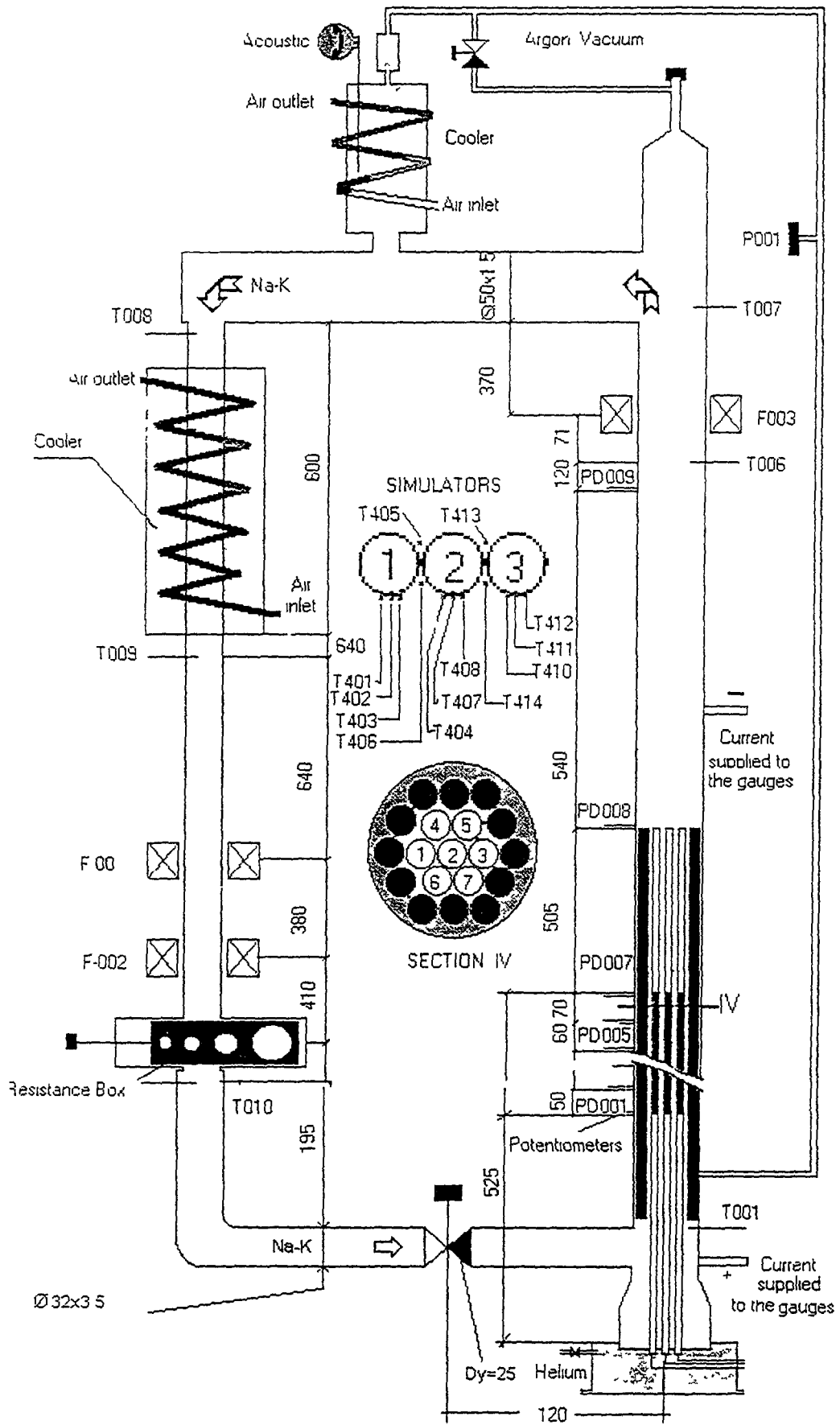
Fig. 6 5   Schematic of the contour
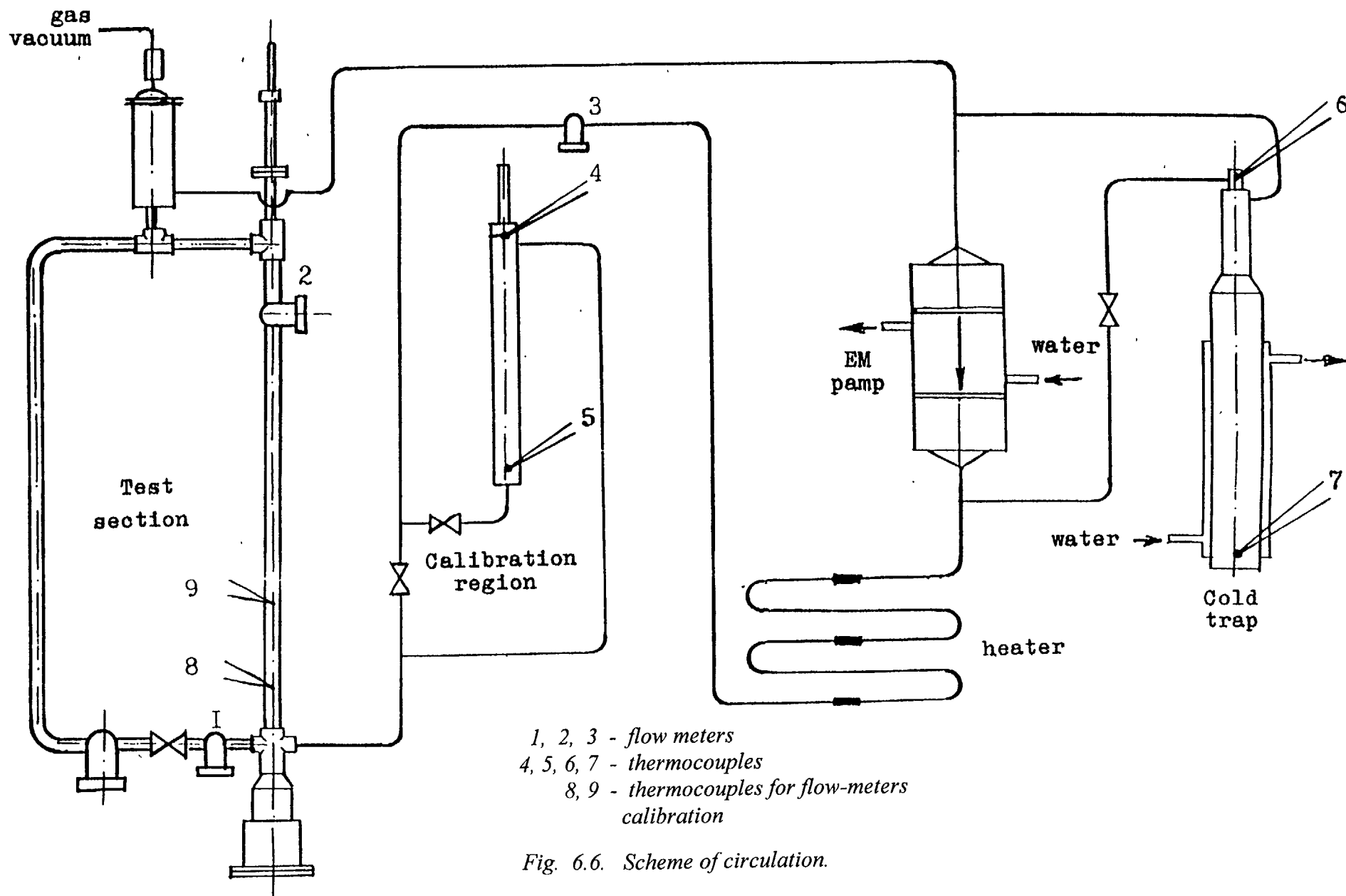
Fig. 6.6. Scheme of circulation.

1, 2, 3 - *flow meters*
4, 5, 6, 7 - *thermocouples*
8, 9 - *thermocouples for flow-meters calibration*

q 10^5 W /m^2

2,0

I,0

τ,

Flow rate at test section inlet

U V/cm

G_{BX} = 0,75 m^3/ h

G_{BX} =I,9 m^3/h

10

τ,min

UV/cm.

void fraction

potentiometer 4

10

τ,min

I stage of boiling
(2I min)

II stage of boiling
(I3 min)

U V/cm

10

τ,min

potentiometer 3
(389 mm from beginning of heating)

U V/cm

10

τ,min

potentiometer 2
(194 mm from beginning of heating)

U V/cm

10

τ,min

potentiometer 1
(68 mm from beginning of heating)

*Fig. 6.7 Characteristics of the first (1) and second (II) stages of boiling in model subassembly.*
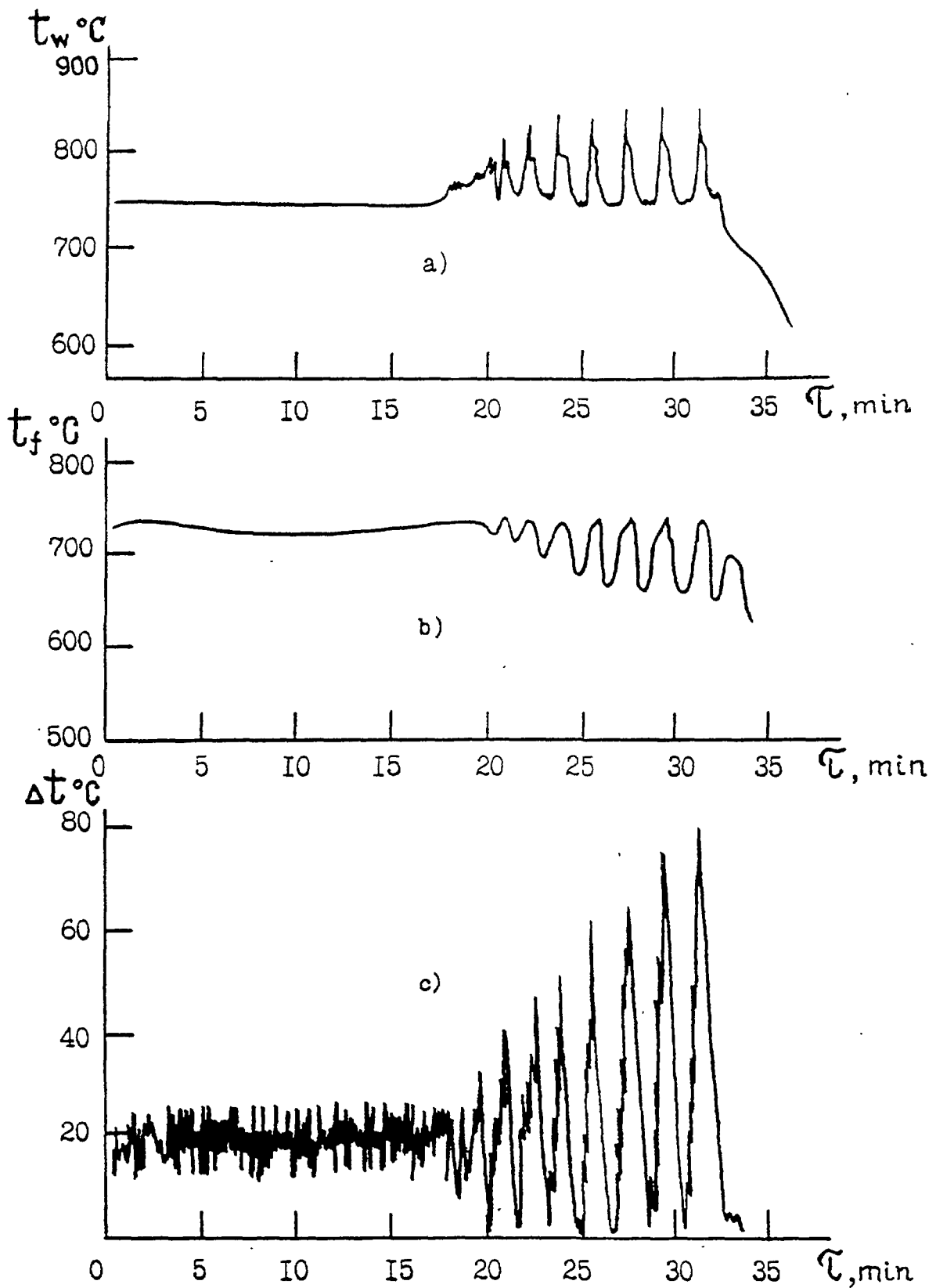
Fig. 6.8. Temperatures of simulator wall (a), coolant temperature at heating region outlet (gross-section IV) (b) and temperature difference «wall-fluid» cross-section III (c).
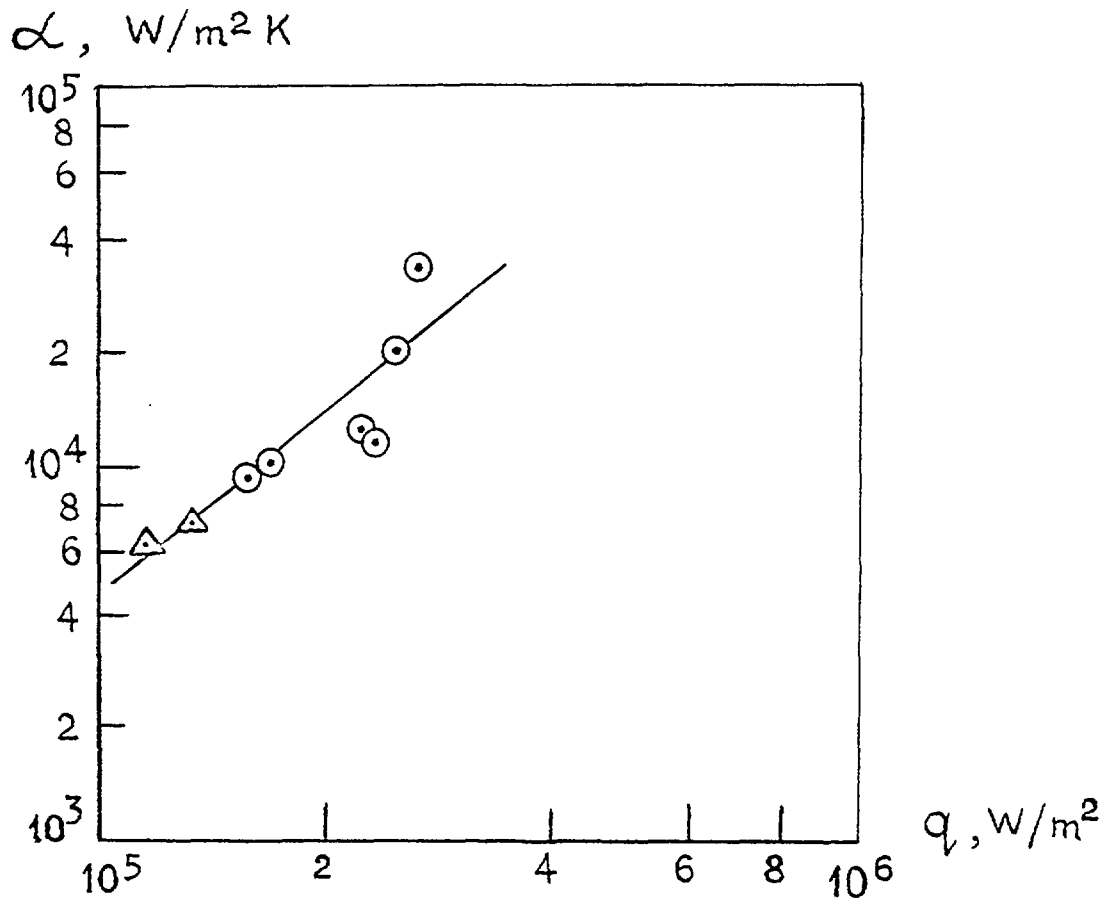
Fig. 6.9. *Heat transfer variation with the surface heat flux density:* △ - *first experimental set,* ☉ - *second experimental set.*
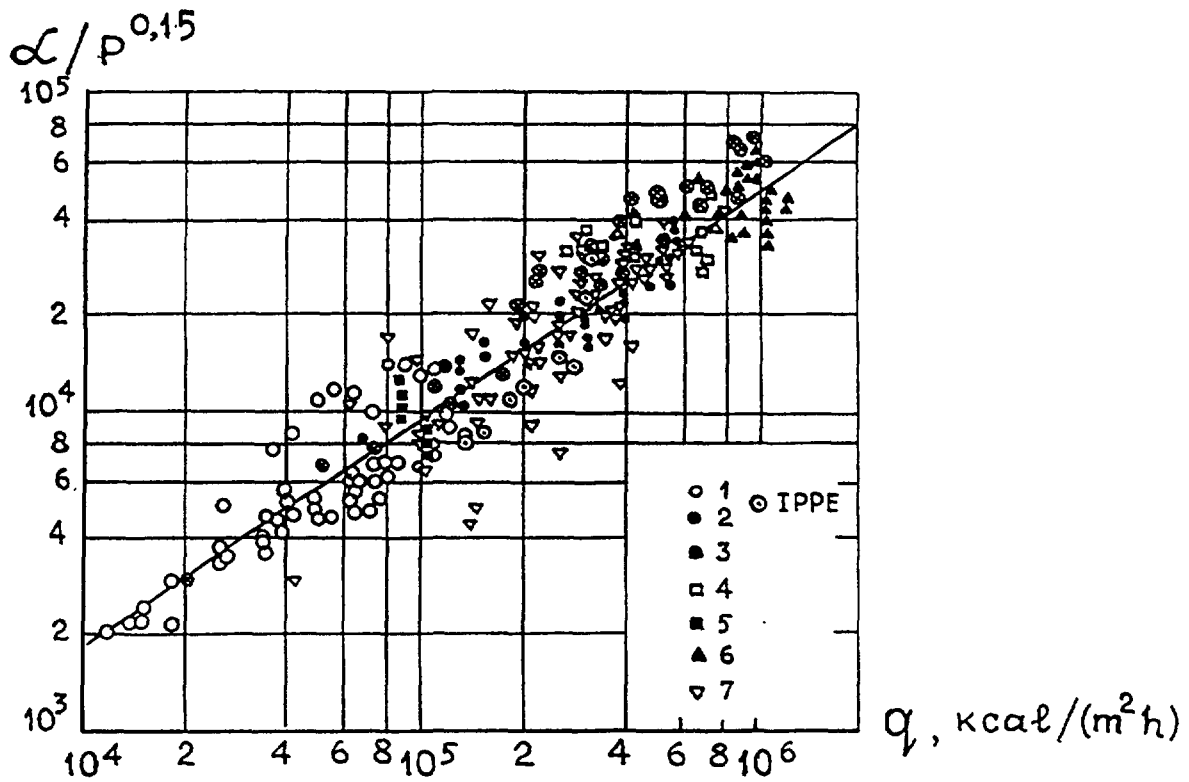
Fig. 6.10. Comparison of external data on liquid metal boiling heat transfer potassium [15]:

1 - large volume $(3q^{0.7})$

2 - tube, d = 10mm (electrical heating)

3 - tube, d = 10mm (heat electrical)

4 - tube, d = 8.3mm⎤

5 - tube, d = 22mm | *electrical*

6 - tube, d = 4mm | *heating*

7 - tube, d = 6mm ⎦

eutectic sodium - potassium alloy [IPPE]

⊙ - 7-pin bundle

$d_e = 3.52mm$ *(electrical heating)*

$$q_{cr}(\ell/d)^{0,8}/[(1-2X_{in})z]$$
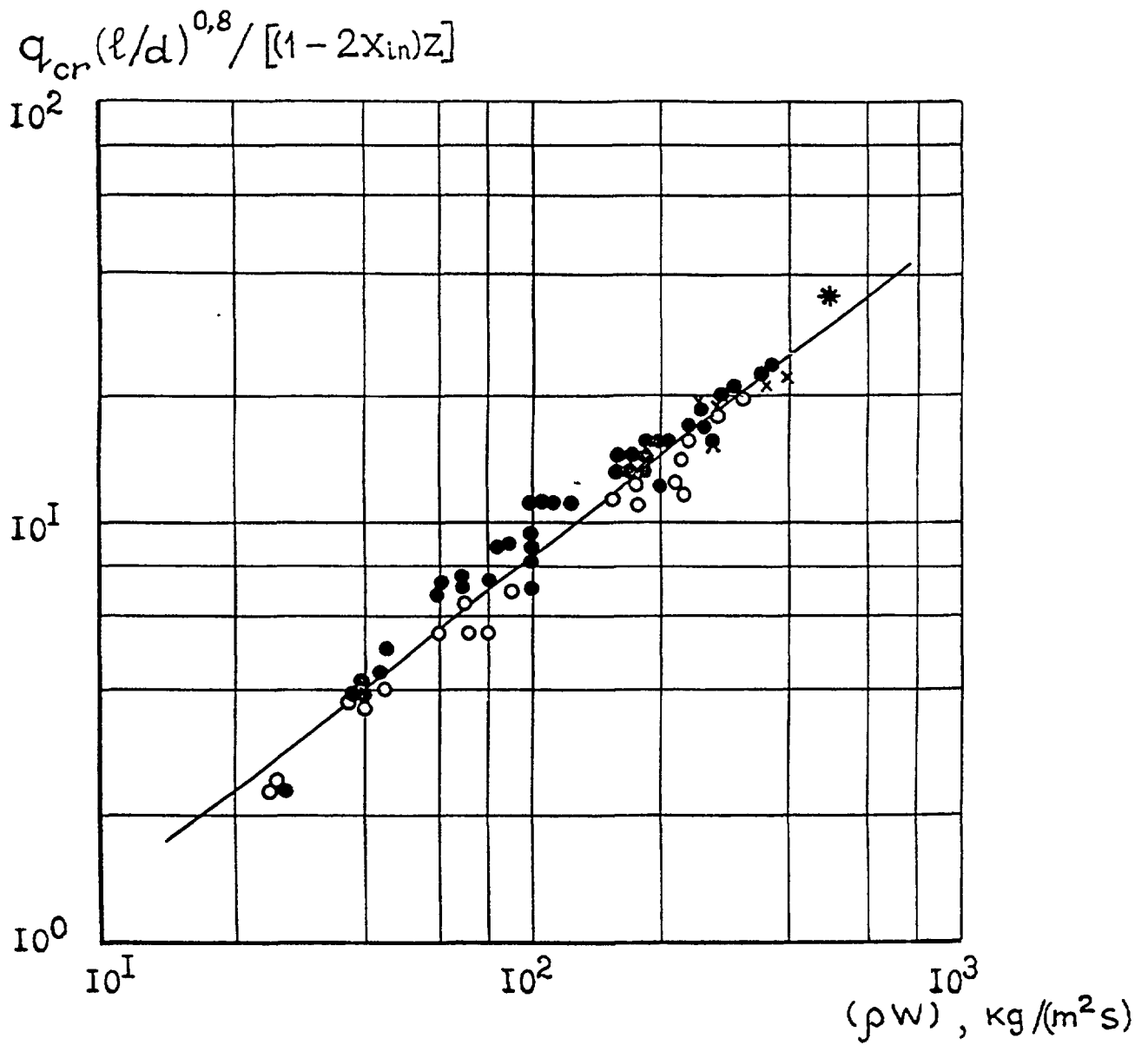
Fig. 6.11.   CHF value with coolant mass velocity on tube:
sodium (●), potassium (○), annuli: sodium (×) [2],
experiments IPPE on 7-pin bundle, eutectic sodium-potassium
alloy (*).

294
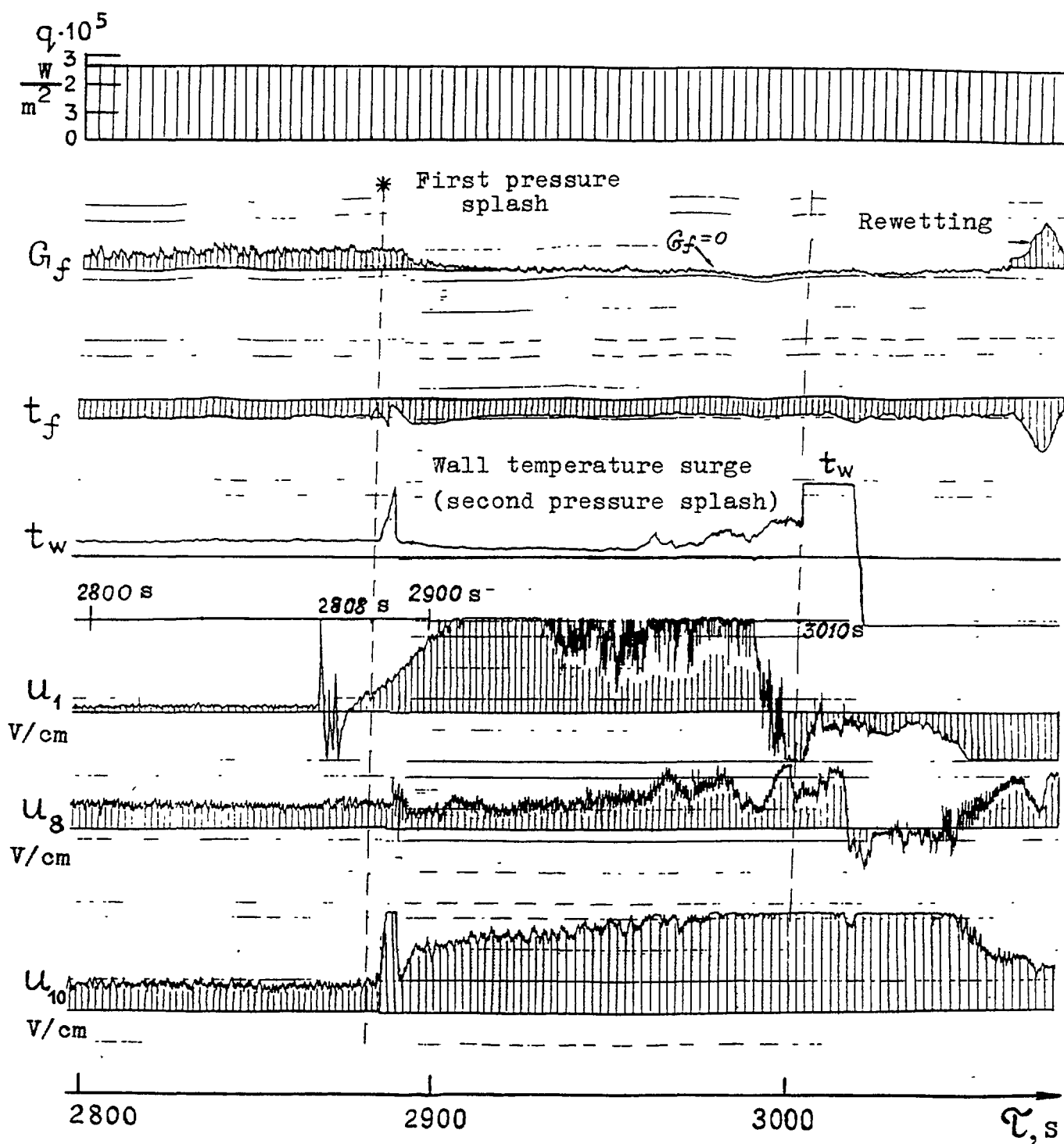
Fig. 6.12. Time - variation of boiling characteristics.

Boiling heat transfer coefficient. The main factor influencing heat trasfer coefficient value is the heat flux value (Fig.6.9) Due to small variation in circulation velocity a direct relationship between heat transfer coefficient and velocity failed to be revealed.

Fig.6.10 shows a good correlation between experimental data and data on potassium boiling in tubes *4 ÷10 mm* in diameter in the rages *0.2-4 bar, x= 0.04 -0.8,* ρW=*22-1490 kg/ (m².s), q=10⁵-1.4. 10⁶W/m².*

Thus, the boiling heat transfer coefficient for eutectic NaK alloy in pin bundle can be followed to relationship for tube potassium boiling:

$$\alpha = 3 \cdot q^{0.7} p^{0.15} \tag{6.4}$$

where $[q] = W/m^2$, $\{[p] = bar$.

Analysis performed by Kottowski [15] and other authors (Borishanski [9], Subbotin [8], Shah [11]) has shown that the round tube boiling in liquid metals - Na, Km Hg, Cs and others – is described by unified function that is close to the relationship for liquid metal pool boiling.

To predict boiling heat transfer in sodium bundle with pitch-to-diameter ratio *s/d = 1.18* the following relationships are recommended:

for $p/p_{cr} = 4 \cdot 10^{-5} \div 10^{-3}$

$$\alpha = 9.28 \left(q^2 \lambda' r \rho' / \sigma T_s^2 \right)^{1/3} \left(p/p_{cr} \right)^{0.45} \tag{6.5}$$

for $p/p_{cr} = 10^{-3} \div 2 \cdot 10^{-3}$

$$\alpha = 1.16 \left(q^2 \lambda' r \rho' / \sigma T_s^2 \right)^{1/3} \left(p/p_{cr} \right)^{0.15} \tag{6.6}$$

Here, q in MW/m^2; r - specific evaporation heat, J/kg; σ- surface tension, N/m^2; λ in $W/(m . k)$; ρ in kg/m^3, saturation temperature T_s in K. As well as in criterion form [16]

$$Nu = 8.7 \cdot 10^4 \cdot Pe^{0.7} \cdot K_p^{0.7} \tag{6.7}$$

where $Nu = \alpha l / \lambda$; $Pe = \left(q/r\rho'' \right) c_p' \rho' \left(l/\lambda' \right)$

Critical heat flux. During experiments at heat flux ~*151 kW/m²* an amplitudes of wall temperature pulsations and coolant temperature rises sharply, that is a forerunner of heat transfer crisis.

Thus, the only approximate data on critical heat flux were get under conditions of natural circulation. The value obtained is in a good agreement with relationship presented in [15] (Fig.6.11):

$$q_{cr} = 0.216 \ r \left(1 - 2x_{in} \right) \left(\rho W \right)^{0.807} \left(d/l \right)^{0.8} \tag{6.8}$$

Based on the unique point there is no way of recommending the reliable relationship to predict q_{cr} in pin bundle, additional experiments must be called on to analyze results in-depth.

Some results on liquid metal boiling presented here were get when pressure was released by *0.06-0.05 MPa* after *2800* s experimental performance. At first, during more than *100 s* this pressure release was not bringing about any obvious changes in boiling, but as time passes the first pressure jump occurred which was attended with the wall temperature rise, fast change in all sensors' signals and ejection of some amount of the coolant from the test section (Fig.6.12). In this case the inlet flow rate dropped to zero and amplitude of the magnetic flow meter signal was coming under reduction at the test section outlet flow meter dropped to zero that indicated that the test section is filled with vapour and liquid is absent.

Liquid evaporation finished after 3000 s. In that moment the process was coming to be hard controlled and to be of explosion character. Second, more strong pressure jump was observed. Wall temperature exceeded 1100°C (registration limit) and pin wall section of 50 mm in length was melted Heaters itself were not destroyed. Thus, experimental results indicate that pressure release brings the threat to fast reactor core performance.

CONCLUSIONS

The following features of liquid metal boiling in the pin bundle under natural circulation conditions has emerged from the experiments:

- the stable boiling takes place only within the limited range of heat flux variation, its boundaries and conditions of transition to the unstable boiling are defined by a number of factors;
- development of unstable boiling being attended with the great temperature and flow pulsations can lead to the heat transfer crises, with the safety margin is lacking in essence;
- wall-liquid temperature differences in stable boiling is 15-20°C, those in unstable boiling - 25-50°C;
- in the event of dryout the pin wall temperature achieves the melting temperature very rapidly;
- data on heat transfer are in a good agreement with experimental data on liquid metal tube and pool boiling;
- the unified relationship for critical heat flux in liquid metal pin bundle is in a satisfactory agreement with boiling in tube and annuli.

Technical base generated to perform boiling experiments permit carrying out a future researches with the following purposes:

- to define the borders of the stable boiling in dependence of different parameters and factors;
- to develop criterion analysis of liquid metal boiling heat removal;
- to study conditions of pin wall integrity.

REFERENCES

[1]   Zhukov A.V., Sorokin A.P., Matjukhin N.M. Interchannel Exchange in Fast Reactor Subassemblies. Codes and Applications, M., Energoatomizdat, 1991 (in Russian).
[2]   Huber F., Mattes K., Peppler W., et. al. Loss of Flow Experiments in Sodium in an Electrically Heated 37-Pin Bundle with Sinusoidal Axial Heat Flux Distribution.. Proc. of the LMFBR Safety Topical Meeting, Lion, France 1982, v.1V, p.341-349.

[3] Mikhin V.I., Fetisova L.N. Numerical Analysis of Transient Temperature Behavior in Central Areas of Subassembly. Preprint IPPE-2240, 1992 (in Russian).

[4] Kuznetsov I.A. Accident and Transition Processes in Fast Reactors, M., Energoatomizdat, 1987 (in Russian).

[5] Subbotin V.I., et al. Hydrodynamics and Heat Transfer in Nuclear Power Plants, M., Atomizdat, 1975.

[6] Zeigarnick Yu., Litvinov V.D. Heat Transfer and Pressure Drop in Sodium Boiling in Tubes. Nucl. Science and Des., v.72.

[7] Dwyer O., Hsu C. Evaporation of the Microlayer in Hemispherical Bubble Growth in Nucleate Boiling of Liquid Metals. Intern. J. of Heat and mass Transfer, 1976, v. 19, p. 185.

[8] Subbotin V.I., Sorokin D.N., et al. Heat Transfer in Liquid Metal Natural Convection Boiling, M., Nauka, 1969.

[9] Borishanski V.M., Kutateladze S.S., et al. Liquid Metal Coolants, M., Atomizdat, 1976.

[10] Kirillov P.L. Heat Transfer in Liquid Metal Flows in Round Tube (Single- and Two-Phase Flows. Doctor of Science Thesisis, IVTAN, Moscow, 1968.

[11] Shah M.M. A Survey of Experimental Heat Transfer Data for Nucleate and Poll Boiling of Liquid Metals and New Correlations. International J. of Heat and Fluid Flow, 1992, v. 13, p. 370-379.

[12] Chang S.H., Lee Y.B. A New Critical Heat Flux Model for Liquid Metals under Low Heat Flux-Low Flow Conditions. Nucl. Eng. and Des., 1994, v. 148, p. 487-498.

[13] Kaizer A., Huber F. Sodium Boiling Experimental A Low Power under Natural Convection. Nucl. Eng. an Des. 1987, v.100, p. 367-376.

[14] Yamaguchi K. Flow Pattern and Dryout under Sodium Boiling Conditions. Nucl. Eng. and Des., 1987, v. 9, p. 247-263.

[15] Kottowski H.M., Savateri C. Evaluation of Sodium Incident Overheat Measurements with Regard to the Importance of Experimental and Physical Parameters. International J. of Heat and Mass Transfer, 1977, v. 20, p. 1281-1300.

[16] Kirillov P.L., Yuriev Y.S., Bobkov V.P.. Hand-Book on Thermal Hydraulics (Nuclear Reactorts, Heat Exchangers, Steam Generators), M., Energoatomizdat, 1988 (in Russian).

OVERALL CONCLUSIONS

1. The validity of thermohydraulics in fast reactor core and heat exchanger is largely influences by the accuracy of the system of correlations written for the friction factors, heat transfer coefficients, mixing factors and so on. The development of the complete and accurate system is critical in nuclear power engineering. Method of thermohydraulic analysis, features of thermohydraulic phenomena, computer codes developed with the use of closing relations are based on the experimental results and numerical modeling of the processes in nuclear reactor units.

2. Two computation procedures form the basis for prediction of reactor core and heat exchanger thermal hydraulics: subchannel approach (subassembly) and a porous body model (intermediate heat exchanger). In working out the codes much attention has been given in the IPPE to the non-nominal reactor operation being caused by diabatic conditions at the wrapper, by the random departure of parameters from nominal values in campaign, by the transients associated with liquid metal boiling. In all instances the inter-channel exchange is of primary importance in the computations.

3. Analysis of the process and performance of experiments with the ensuing development of computer codes are based on the following principles:
   - thermal modeling of fuel pins (heat flux up to 1.2 MW/m^2) with the distributed power production;
   - modeling of reactor core and heat exchanger thermal hydraulics;
   - local measurement technique, including electromagnetic flow meters, miniature thermocouples, with the ensuing correlation between hydraulic and thermal data, that gives sufficient information on fast reactor subassembly performance;
   - high-power liquid metal facilities operating in a wide range of working temperatures with sodium or sodium-potassium alloy used as a coolant, which allow the large-scale out-of-pile experiments to be carried out.

4. Electromagnetic technique allows the local hydraulic characteristics of axial, transverse and combined (axial-transverse) flows through the models simulating subassembly and heat exchanger to be measured. The advantages and possibilities of the technique are as follows:
   - experiments may be performed with the same coolants as those in reactor;
   - small-sized sensors meet reactor technological standards;
   - local flow rate can be defined around and along the pins;
   - local hydrodynamic features in deformed systems (bending and shifting of pins, blockages, manufactoring tolerances and others) can be revealed;
   - Measurements remain precise due to sensors' sensitivity as well as due to the lack of any elements inserted into the flow which can distort the hydrodynamics.
   - The technique is easy to realize, low in cost, advantageous for reading information. It can be convenient means for studying physics of combined transverse-axial flow.

5. Features of thermohydraulics in reactor core and heat exchangers are as follows:
   - Among the main factors defining hydraulic behavior in fast reactor core subassembly are large velocity non-uniformities around the edge pins and intensive inter-channel exchange due to wire wrap;
   - Inter-channel exchange is one of the most important reasons for the hydraulic characteristics in pin bundle to differ from those in insulated channels;
   - Combined prediction and experiment researches have yielded information on the influence of various factors on liquid metal flow behavior;

- As distinct from the previous hypothesis on the possibility to predict hydrodynamics using the averaged, across the subassembly, coolant velocity or hypothesis of isobaric section, it has been shown that such a prediction does not provide the wanted accuracy. Feasibility of the hypothesis of isobaric section should be limited by the bundles of smooth pins being free from displacers;

- Hydraulic features in mutually relative channels are properly reflected by the subchannel analysis accompaning for inter-channel exchange, which allows predicting reliable velocity distributions over the pin bundles;

- Subassembly hydrodynamics, as a whole, depends, to a large measure, on the features of the edge areas of the pin bundle. Predictions and experimental data on local hydrodynamic characteristics in the edge channels allow the optimal geometrical variants to be chosen;

- Local hydrodynamic measurements, as applied to fast reactor heat exchangers, permit gaining the experimental data needed for predicting combined flow. Appropriate codes have been developed and verified on the experimental data available.

6. On the subject of inter-channel exchange in fast reactor subassembly the following remarks are in order:
- Study of inter-channel exchange was performed by the use of the electromagnetic technique which permits probing deeper into the finer details of the process with the ensuing correlations derived for the local and integral mixing factors within a wide ranges of defining parameters;

- Physical picture of the inter-channel exchange in the bundle of wire wrapped pins is as follows;
    - convective component of inter-channel exchange intensity distribution along the bundle follows sine law;
    - the exchange intensity depends on the relative pitch of the bundle, on the kind and pitch of wire wrap, on Reynolds number;
    - directed coolant flow is observed around the subassembly wrapper.

- Modified thermal track technique allows investigation of the local and integrated mixing factors. Using this technique the data on the total thermal mixing factor have been obtained;

- Joint application of electromagnetic and thermal track technique allow the total mixing factor to be divided into separate components, the non-equivalence factor between heat and mass transfer to be determined;

- The main component of inter-channel exchange in fast reactor core subassembly is convective component due to the wire wrapped on the pins, whereas in reactors with high conductive pins an exchange due to pin heat conduction dominates;

- The equivalence factor is found in liquid metal experiments to be equal to about 0.7;

- To evaluate mixing factors due to turbulent, molecular diffusion and convective transport the empirical and analytical correlations have been derived within the pitch-to-diameter ratio range $0.1 < s/d < 2.0$;

- Experimental data on inter-channel exchange are at the basis of procedures developed to predict velocity and temperature behavior in reactor core and heat exchangers. A knowledge of thermal mixing factors allows an influence of a number of the factors resulting in campaign to be estimated, such as: pin bundle deformation, non-uniform power production, blockages, thermal interaction of the subassemblies, low coolant velocity including natural convection and so on. The

300

subchannel approach and the porous body model are straightforward and reliable procedures;

- Theoretical analysis of liquid metal heat removal supplements experimental investigations. The notions of inter-channel exchange (mass, momentum, energy mixing factors, non-equivalence factor between heat and mass transport, "effective" mixing factor and so on) allow the numerical procedure to be developed and the system of thermal hydraulic governing equations to be reduced to single equation of convective heat transfer (using the concept of equivalent thermal conductivity of pin bundle).

7. Generalized relations derived from the experiments form the basis for most calculations of steady state heat removal in any axi-symmetric system cooled by liquid metal;

8. Analytical procedures and experimental techniques have been successfully combined in considering an irregular processes (variable power production, entrance section). The main physical features are as follows:

- Relative length of entrance section reduces with the pitch-to-diameter ratio and equivalent thermal conductivity of pins. In laminar flow the entrance section length is in direct proportion to Peclet number (heat transfer due to molecular heat conduction), in turbulent flow it has a peak;

- Universal formula describing variations in temperature and heat transfer at the entrance section has been proposed;

- It is Duhamel's integral that allows the experimental data gained under hydraulically unstable conditions being converted into those under variable power production (at least in fast reactors).

9. Due attention should be given to the thermophysical validation of the edge (wall) pins as the most dangerous area of subassembly in terms of temperature non-uniformity. The main features of the edge pins performance are as follows;

- Temperature non-uniformity at the edge pins far exceed those at the inner pins;

- Heat transfer coefficients in the edge area of fast reactor subassembly are lesser than expected in the internal area by a factor of 1.5-2.0. The relations presented take into account the availability of displacers within the edge channels;

- Maximum temperature non-uniformity at low Peclet numbers (transition region) can present a severe hazard to emergency cooling of reactor core provided that power is kept at sufficiently high level;

- Heat removal in the edge channels is, as a rule, of unstable character, that depends on equivalent thermal conductivity, relative pitch, shape and size of displacers and other factors;

- Pin bundle deformation causes the temperature non-uniformity to increase and the heat transfer coefficient to reduce at the edge pins;

- As coolant passes through the gap between subassemblies, it reduces coolant temperature in the edge channels, so temperature non-uniformity increases by ~50% in the event of the ratio between flow through the inter-subassembly space and those through the subassembly is ~5-6%;

10. Transient reactor core and heat exchanger behavior is the key problem of fast reactor thermal hydraulics:

- During operation subassembly is subject to the combined action of various factors, with the temperature non-uniformity being among the most important one.

- The combined subchannel codes TEMP involving solution of macro-transport equations, having regard to inter-channel exchange, has been verified on the extensive experimental data that allows predicting to a high accuracy nominal and

non-nominal temperature behavior in fast reactor core. The code TEMP is of high-performance and has gained widespread acceptance.
- Thermal mechanical analysis performed having regard to subassembly deformation indicates the enhancement of maximum temperature of the pins, as well as maximum temperature non-uniformity.

11. Combined experimental & analytical investigations of intermediate heat exchanger thermal hydraulics have presented a basic information on velocity and temperature behavior. The main results are as follows:

in the field of hydrodynamics:
- The use of electromagnetic technique has allowed the physics of axial-transverse flow to be studied, as well as characteristics of triangular and square arrangement of the tubes in a wide range of Reynolds number;
- From the local measurements of transverse and axial components of velocity we can conclude whether the given design of heat exchanger is optimum;
- Equalization of coolant flow over the tube bundle reduces heat transfer surface area and, in doing so, its economic feasibility is enhanced;
- Experimental data have been used as a closing constants in the code development.

in the field of thermal behavior:
- Data on heat transfer coefficients and temperature behavior can be used in the validation of heat exchanger equipment and in the development of optimization methods;
- The local thermal modeling allows the processes going on in the multi-tube heat exchanger to be studied on the small-scale models (19 tubes);
- Computer codes verified on the experimental data are profitably employed in thermal hydraulic validation of fast reactor heat exchangers.

12. For the purpose of developing procedure of transient data generalization and to derive approximate criteria, the transient temperature behavior has been investigated in the bundle with various kinds of fuel. It has been shown that pin wall temperature dynamics can be expressed in the form of universal time-dependence;

13. The objectives of experimental and analytical validation of reactor core performance under accident conditions to be pursued by extensive researches into sodium boiling. Experiments have been concerned with the investigations:
- onset and development of the coolant boiling under various flow and power productions;
- critical heat flux;

possible destruction of pins and inherent phenomena.

Predictions have been concerned with the analysis of the following processes:
- molten fuel/coolant interaction;
- drastic increase in the fragment surfaces within the system under consideration;
- vapor explosion;
- aerodynamical effects;
- the process propagation.

Up to now the following researches have been performed:
- Experimental base has been built up (high temperature facility, equipment and measurement technique);
- Experiments have been carried out to study liquid metal boiling dynamics;
- The model two-phase flow has been stated;

- The system of macro-transport governing equations has been analyzed in the framework of subchannel approach;
- Inter-channel characteristics have been analyzed, as applied to two-phase flow.

14. The foregoing shows that the complete system of closing relations and constants required in thermal hydraulic analysis of fast reactor core and heat exchangers have beenderived for the following :

- prediction of coolant flow distribution over the channel having regard to inter-channel exchange;
- prediction of coolant temperature distribution over the channel;
- definition of temperature difference "wall-liquid" and maximum temperature non-uniformity;
- consideration of variable power production;
- inclusion of various factor defining temperature behaviour;
- definition of maximum pin temperatures.

The most advanced thermohydraulic codes are the codes GID, TEMP, MIF, MID developed for the LMFBR core, and those for intermediate heat exchanger are PROTVA, UGRA, TAKT and others.

Authors consider that the material presented fulfill the modern thermal hydraulic requirements.

NEXT PAGE(S)
left BLANK

CONTRIBUTORS TO DRAFTING AND REVIEW

Bogoslovskaya, G.P.	Institute of Physics and Power Engineering, Russian Federation
Cevolani, S.	Institute of Nuclear and Alternative Energy, Italy
Ninokata, H.	Tokyo Institute of Technology, Japan
Rinejski, A.A.	International Atomic Energy Agency
Sorokin, A.P.	Institute of Physics and Power Engineering, Russian Federation
Zhukov, A.V.	Institute of Physics and Power Engineering, Russian Federation